SAND2011-6463P

4th Workshop on Ramp Compression held 18-19 January 2011

Jean-Paul Davis (host/organizer)
Dawn Flicker (hosting manager)

ICE workshop series revived (after 4-year hiatus) as Ramp-Compression Workshop

- June 2004 – SNL hosted in Albuquerque
- December 2004 – LLNL hosted in Livermore
- October 2006 – SNL hosted in Albuquerque

- January 2011 – SNL hosted in Albuquerque
- From the announcement:

  "The workshop is envisioned as an opportunity for unclassified discussion and presentation of current work in […] areas of research on ramp compression experiments."

Sandia National Laboratories

Attendance at the 4th Workshop was larger and broader than previous meetings

- Approximately 55 attendees
- Academia (CIW, WSU, Caltech, NPS, Imperial College)
- International (AWE, CEA, Imperial College)
- National Labs (LLNL, LANL, SNL)

- 21 presentations in the areas of Techniques, Facilities, Diagnostics, Standards, Analysis, Strength, Computation

- Official tour of the refurbished Z Machine

- Feedback from one participant:

  "… the workshop was very good, and a significant step forward over the last one in terms of breadth of content and the institutions represented. The talks were good and stimulated a lot of discussion. At any time during the breaks, one could see several side discussions quickly forming."

Some high-level observations

- **Significant developments of new techniques & diagnostics**
  - **Magnetically Applied Pressure-Shear (MAPS)**
  - **EOS measurements using radiography of cylindrical converging geometry**
  - **2-D “plane-VISAR” velocity interferometry**
  - **Frequency-conversion PDV**
  - **XRD and EXAFS used routinely at laser platforms**
  - **Two presentations on temperature measurement**

- **Ramp-compression experiment capability becoming ubiquitous**
  - **Imperial College using older MAGPIE pulser, building new MACH pulser**
  - **CEA/Valduc developing HE-PWG driven ramp compression**
  - **Ramp compression demonstrated on LANL’s NHMFL single-turn machine**
  - **Also represented were:**
    - **GEPI (CEA/Gramat)**
    - **Veloce, Z (SNL)**
    - **Omega (LLE)**
    - **tape-cast GDI, Janus, NIF (LLNL)**

More high-level observations

- **Serious thought being put into analysis of ramp-compression data**
  - **Estimate dissipation from evolution of ramp toward shock**
  - **Reciprocal acceleration analysis to find simple-wave regions**
  - **Orientation-dependent rate effects in plasticity of tantalum recovered by dislocation density based model with anisotropic dislocation nucleation**
  - **Generalized wave analysis to extract strength with minimal assumptions**
  - **Methods to mimic ramp compression in atomic-scale MD simulations**

- **Computational emphasis on MHD and optimization**
  - **New semi-relativistic correction improves performance of Alegra-MHD**
  - **Dakota optimization and UQ accessed from within Alegra input deck**
  - **New general 1-D Lagrangian code “Laslo” available**
    - **Simple to modify/extend (either model equations or material models)**
    - **Already includes MHD and optimization**
    - **Ideal for experiment design/analysis**

4th Workshop on Ramp Compression
18-19 January 2011 at Sandia National Laboratories
Computer Science Research Institute, Room 90
1450 Innovation Pkwy SE, Albuquerque, NM

Tuesday, January 18, 2011

	CHAIR	TOPIC	SPEAKER(S)	AFFILIATION	TITLE
8:00	**SIGN-IN & COFFEE**				
9:00	**INTRODUCTION**		Jean-Paul Davis & Dawn Flicker	SNL	
9:10	Rob Hixson	*Techniques*	Jon Eggert	LLNL	***Laser-Based Ramp-Compression: Wave-Profile Analysis and X-Ray Diffraction***
9:40		*Techniques*	Ray Lemke & Matt Martin	SNL	***Isentropic Compression Experiments Using a Cylindrical Liner Z-Pinch*** ***Determination of Material Equation of State from Multi-Frame Monochromatic X-Ray Backlighting***
10:25	**BREAK**				
10:45	Frank Cherne	*Techniques*	Scott Alexander & Tom Haill	SNL	***Magnetically Applied Pressure-Shear (MAPS): A New Method for Direct Measurement of Strength at High Pressures***
11:30		*Standards*	Carl Greeff	LANL	***EOS Standards***
12:00	**LUNCH**				
13:20	Dan Dolan	*Diagnostics*	Neil Holmes	LLNL	***Making Pyrometric Measurements in Ramp Loading Experiments***
13:40		*Diagnostics*	Camille Chauvin	CEA	***Investigation of Temperature Measurement of Material under Dynamic Loading Using Infrared Optical Pyrometry***
14:10		*Diagnostics*	Ray Smith	LLNL	***New 2-D Interferometry Results for Laser-Driven Compression of Si and Al***
14:40		*Diagnostics*	Tommy Ao	SNL	***Measuring Ramp Compression with PDV***
15:10	**BREAK**				
15:30	**BUS LEAVES FOR TOUR OF Z**		24 guests maximum		***(workshop room available for informal meetings)***
17:00	**END**				

Wednesday, January 19, 2011

	CHAIR	TOPIC	SPEAKER(S)	AFFILIATION	TITLE
8:00	**SIGN-IN & COFFEE**				
8:30	Seth Root	*Facilities*	Simon Bland	Imperial	***Initial Ramp-Wave Experiments at Imperial College***
8:50		*Facilities*	Christophe Voltz	CEA	***Isentropic Compression Driven by High Explosives: Application to Experiments on Tin and Aluminum 6061-T6***
9:10		*Facilities*	Doug Tasker	LANL	***Adaptation of Existing Facilities to Isentropic Compression Experiments***
9:40		*Facilities*	Pierre-Yves Chanal	CEA	***Recent Developments on the GEPI Facility for Isentropic Compression Experiments***
10:10	**BREAK**				
10:30	Matt Martin	*Analysis*	Roger Minich	LLNL	***Estimating the Energy Dissipation and Entropy in a Ramp Wave***
11:00		*Analysis*	Roger Minich for Daniel Orlikowski	LLNL	***Dissecting Lagrangian Velocities and Ramp Waves***
11:30		*Analysis*	Josh Robbins	SNL	***Sensitivity Analysis and Parameter Optimization Using 1-D MHD Simulations of Magnetic Drive Experiments***
12:00	**LUNCH**				
13:20	Scott Alexander	*Strength*	Jow Ding	WSU	***Modeling of the Dynamic Inelasticity of Poly- and Single-Crystal Tantalum Under Ramp Wave Loading***
13:50		*Techniques*	Jeff Nguyen	LLNL	***Review of Tailored Loading Effort at LLNL Gas Gun Facility***
14:20		*Strength*	Bryan Reed	LLNL	***Fundamental Thermodynamic Approaches to Extracting Strength from Velocimetry***
14:50	**BREAK**				
15:10	John Heidrich	*Computation*	Matt Lane	SNL	***Characteristic Curves and Scaling in Shockless Compression Using Molecular Dynamics***
15:40		*Computation*	Allen Robinson	SNL	***Recent ALEGRA-MHD Developments Applicable to Magnetically Driven Ramp Compression***
16:10		*Computation*	Greg Weirs	SNL	***Visualizing Material Model Data Using Prism***
16:30	**DISCUSSION & WRAP-UP**		Jean-Paul Davis & Dawn Flicker	SNL	***(open discussion, next workshop)***
17:00	**END**				

Ramp Compression Workshop

Albuquerque, January 18, 2011

Jon Eggert

Ray Smith, Ryan Rygg, Jim Hawreliak, Dylan Spaulding, Damien Hicks, Yuan Ping, Rip Collins

LLNL

Outline

1) Wave-profile analyses for EOS:
   - A) Review of Omega data
   - B) Plans for the NIF

2) *Extreme Chemistry*
   - A) Sodium
   - B) Aluminum

3) Beyond wave-profile experiments
   - A) X-ray diffraction
   - B) EXAFS
   - C) Transmission / Reflectivity
   - D) Spectroscopy

Ramp compression experiments on the OMEGA laser have enabled peak pressures of 1500 GPa

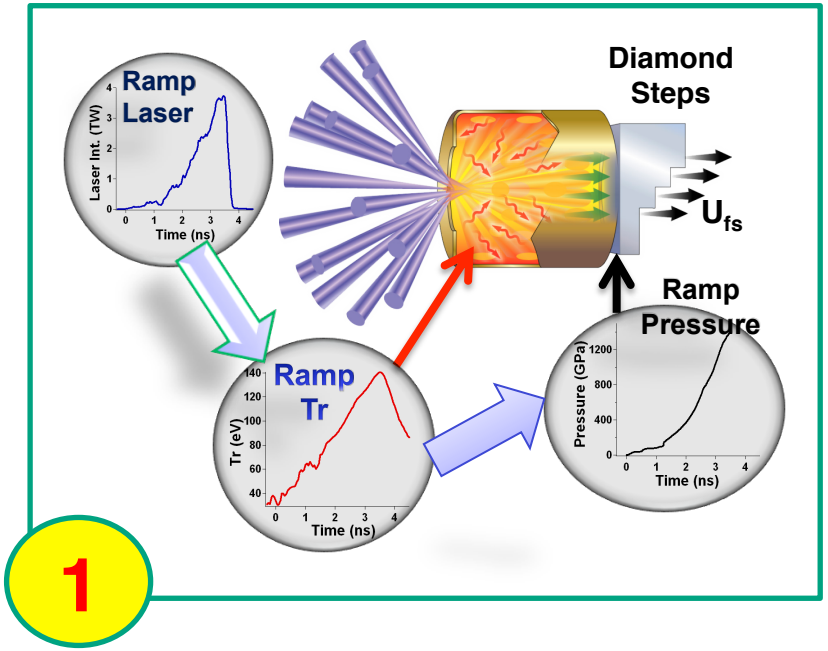

VISAR

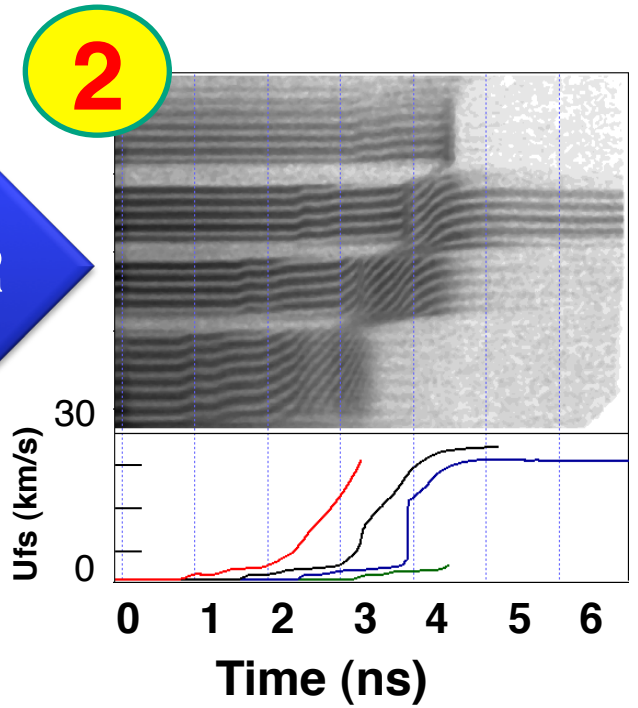

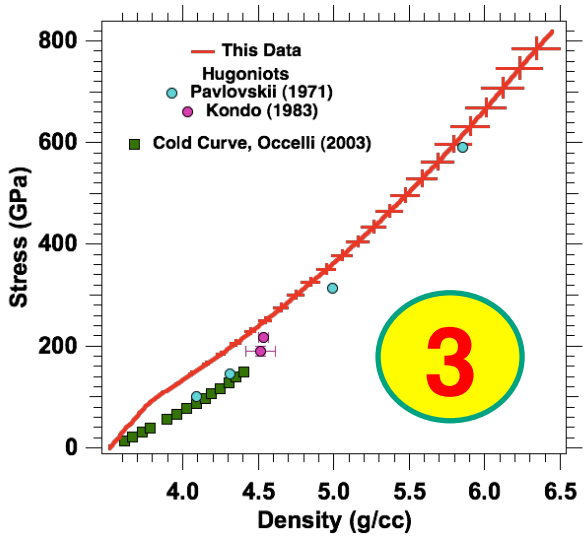

EOS

Stress-Density

EOS results for diamond up to 800 Gpa and Ta up to 300 GPa

Diamond

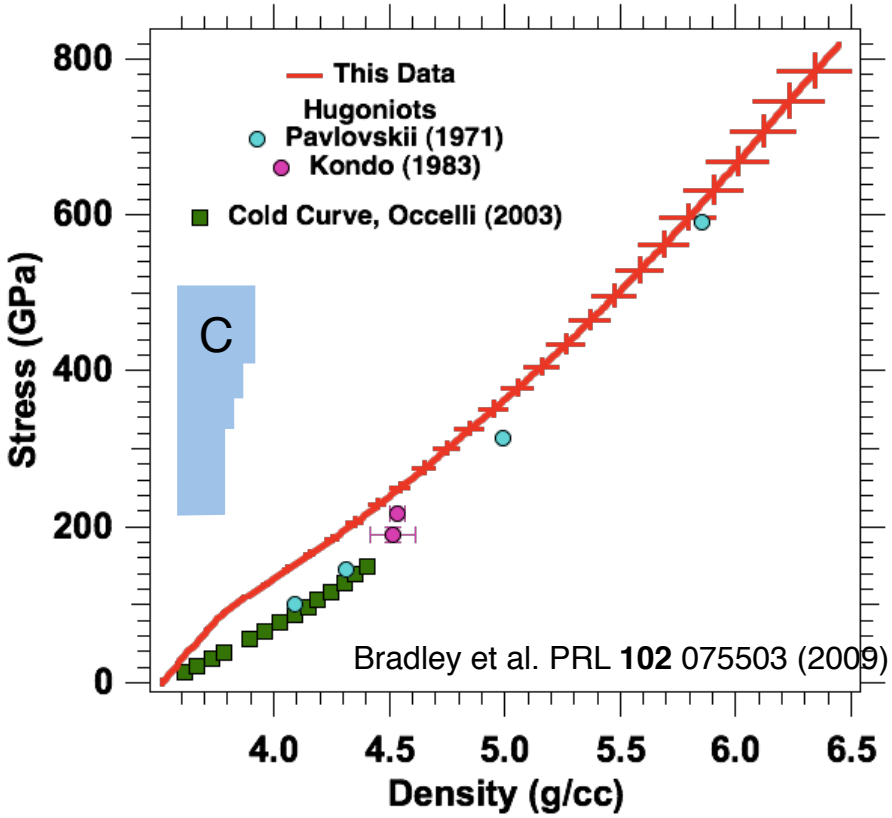

Tantalum

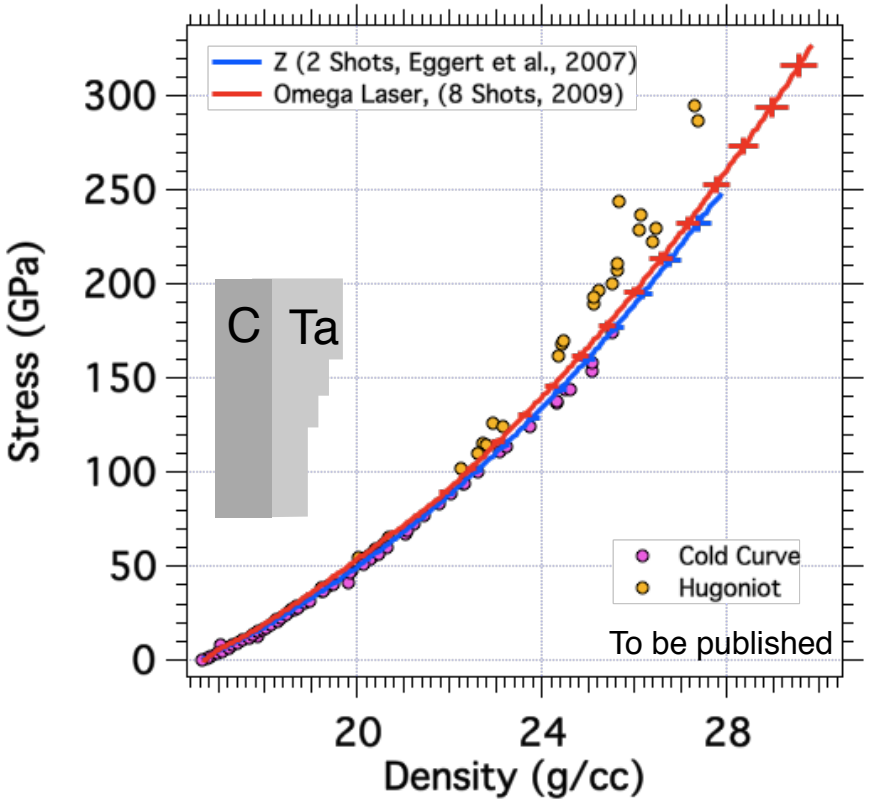

Preliminary data on iron

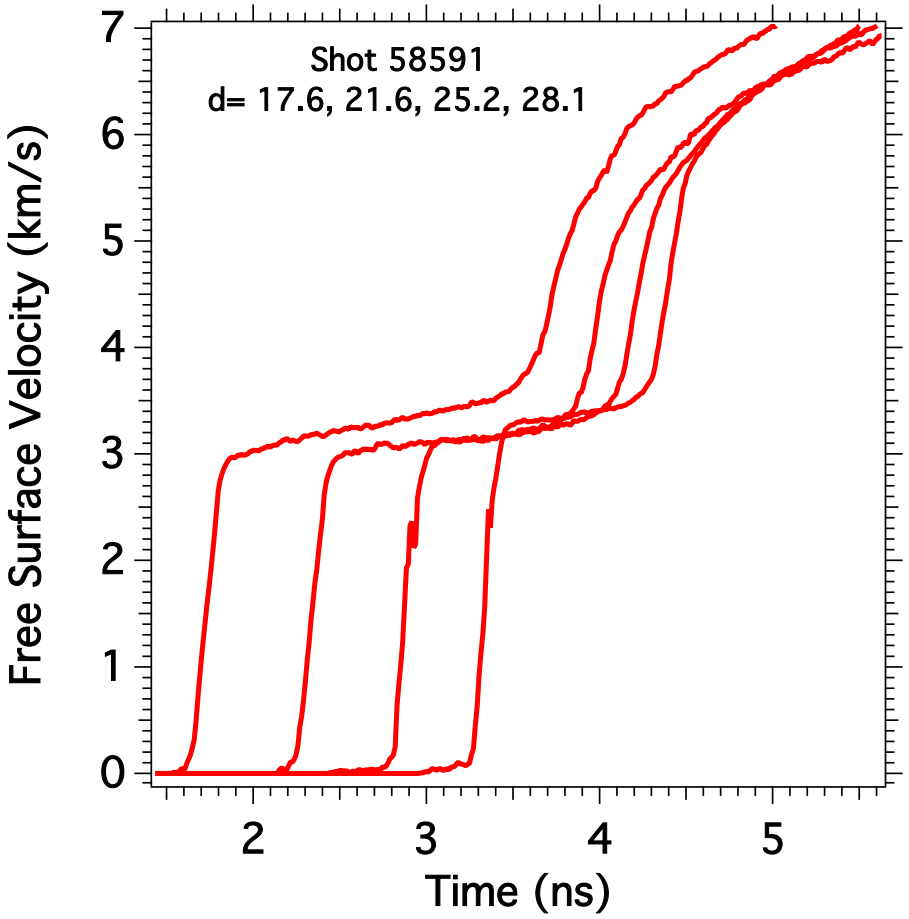

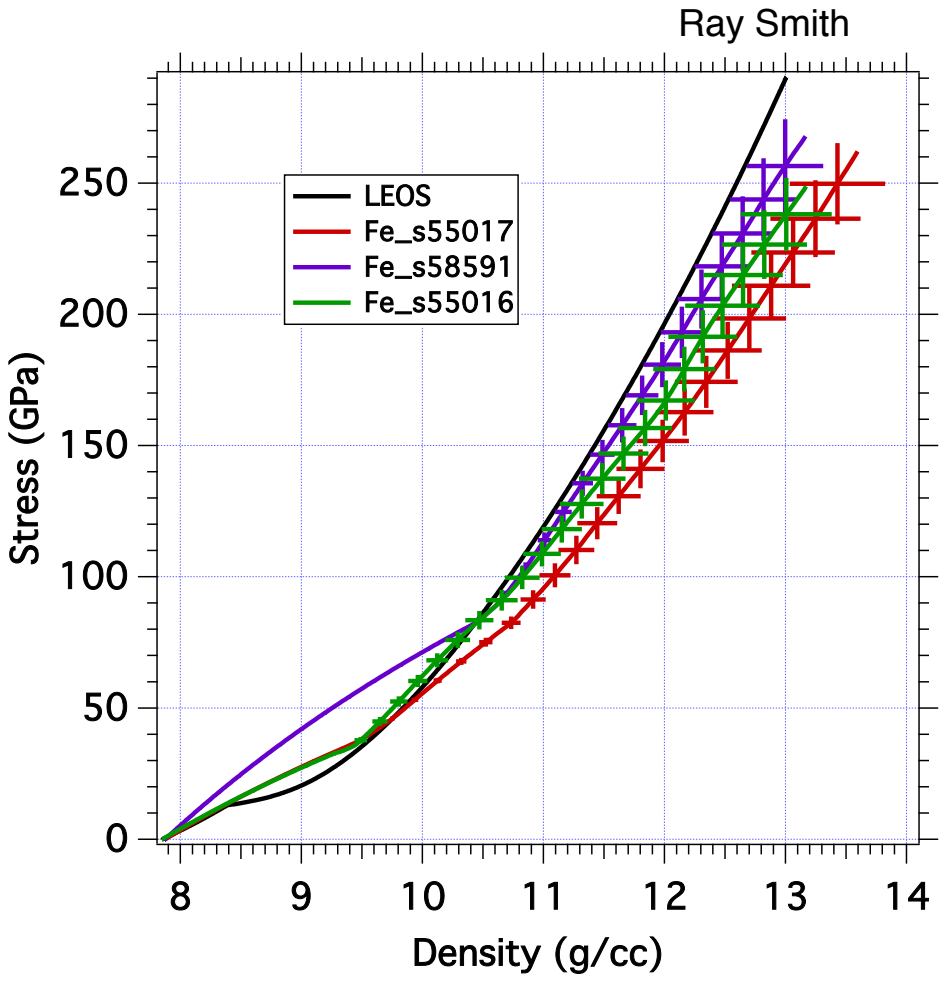

We are working to find the ramp EOS on Iron

1. Need a steady shock into epsilon-iron
2. Pulse shaping is a challenge

The NIF EOS platform is an ignition-scale hohlraum with a side-mounted package

- The basic target package will consist of a diamond ablator/ramp generator coupled to the Ta sample
- A series of preliminary experiments are required to characterize the ramp response of the diamond and Ta samples

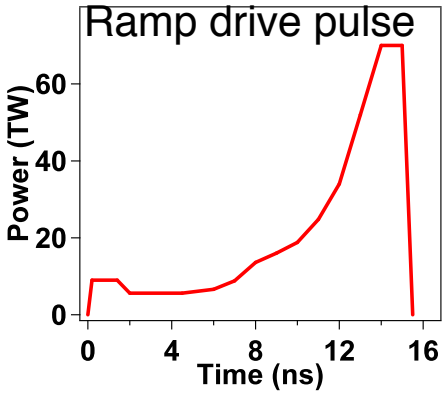

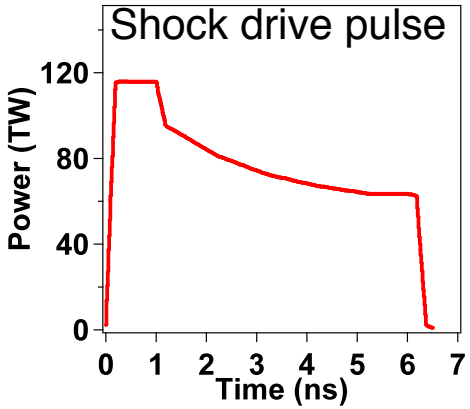

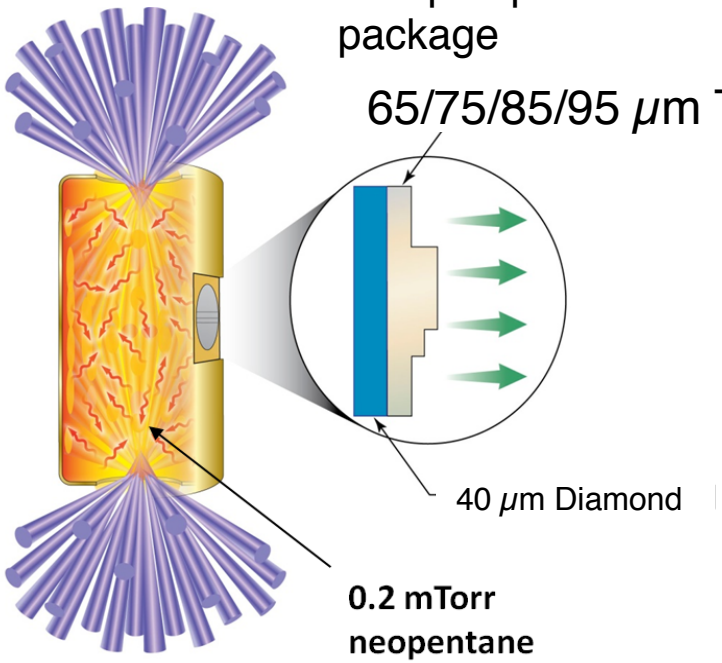

Primary diagnostics:

(1) VISAR/SOP – measures free surface velocity; also reflectivity & temperature in the sample

(2) DANTE – measures radiation temperature in hohlraum and will help to optimize the drive by comparing with rad-hydro simulations

8 Mbar Ta simulation and analysis (nif_8Mb_24h)

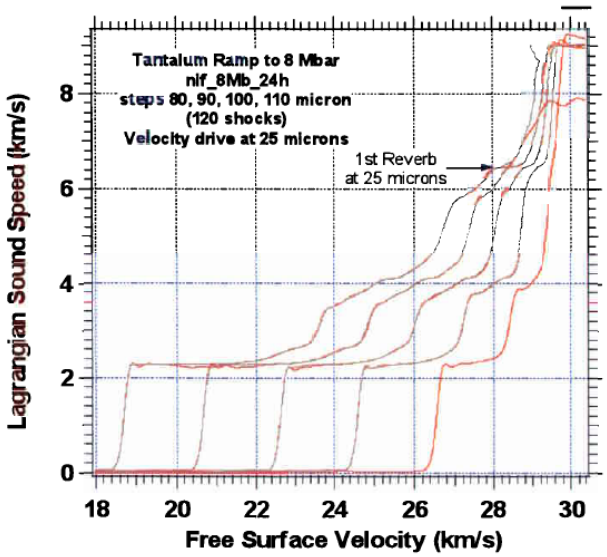

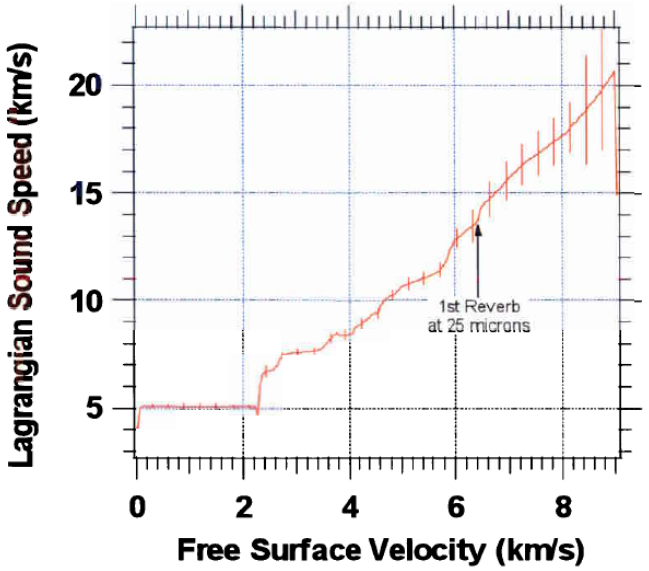

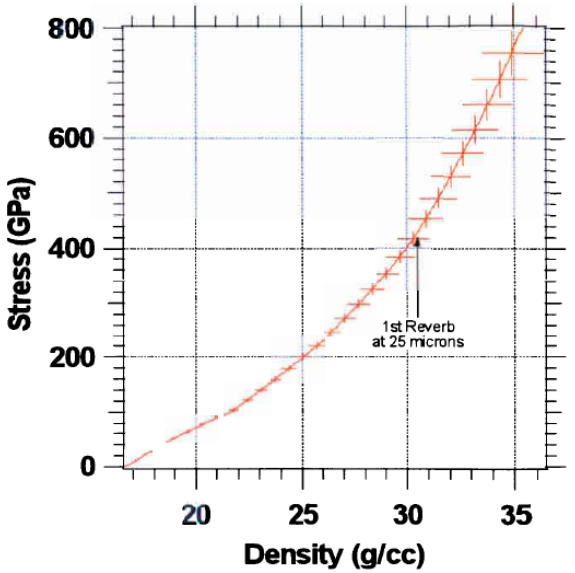

Results expected for Ta assuming ΔL = 100 nm, Δt = 50 ps, VPF = 0.03 km/s.

::

Parameter	Error in Parameter	$\Delta\rho/(\rho-\rho_0)$ at 6 Mbar	$\Delta P/P$ at 6 Mbar
Step height, ΔL	100 nm	0.7%	0.6%
Time, t	50 ps	3.8%	3.5%
Velocity, U_{FS}	.03 km/s	1.9%	1.3%
Total per shot		5%	4%

Uncertainties are directly related to experimental observables

We plan to shoot 7 Ta and 5 diamond shots on NIF this spring.

Shot	Purpose and Scope	Pulse Shape	Total Energy	Target Name	Result
1	20 Mbar Materials EOS Planarity and Drive	26 ns EOS Ramp	287 kJ	MD_EOSPlan -A-01	Demonstrate Planarity, and Drive on Diamond Target.
2	8 Mbar Materials EOS Preheat	26 ns EOS Ramp	287 kJ	MD_EOSPreheat-A-01	Measure thin-sample pre-heat and drive.
3,4	8 Mbar EOS Drive	26 ns EOS Ramp	177 kJ	MD_TaEOS-A-01 MD_TaEOS-B-01	Measure drive for 8 Mbar tantalum.
5,6	8 Mbar EOS Measurement	26 ns EOS Ramp	177 kJ	MD_TaEOS-C-01 MD_TaEOS-D-01	Measure EOS tp 8 Mbar tantalum.
7	8 Mbar EOS Measurement, taken on classified Visar	26 ns EOS Ramp	177 kJ	MD_TaEOS-E-01	Measure EOS tp 8 Mbar tantalum.

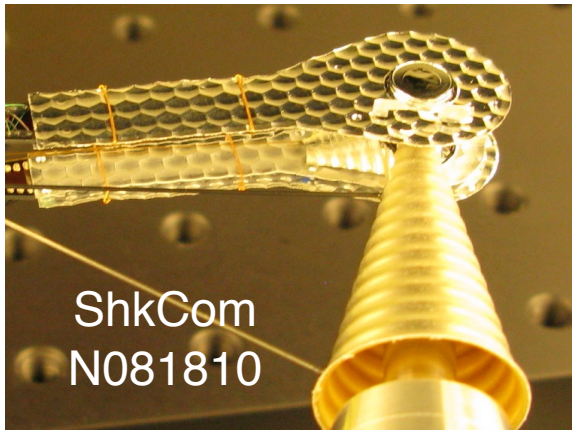

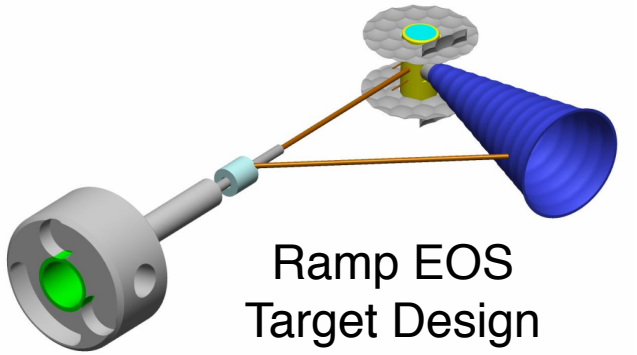

Ramp EOS
Target Design

Our EOS targets are very similar to the successful ShkCom targets

Extreme Chemistry

Extreme Chemistry is an old idea, but is just now beginning to become reality

Examples from sodium and aluminum

New platforms are driving a paradigm shift in condensed-matter science (physics, chemistry, materials)

Traditional view: materials become simple at high pressure appears to be completely wrong!

". . . what the present results most assuredly demonstrate is the importance of pressure in revealing the limitations of previously hallowed models of solids"
–Neil Ashcroft (2009).

FCC, 65 GPa

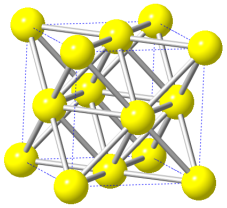

cI16, 108 GPa

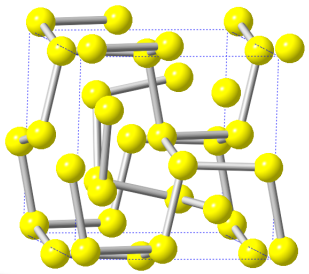

oP8, 119 GPa

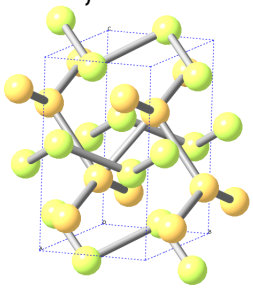

tI19, 147 GPa
Incommensurate

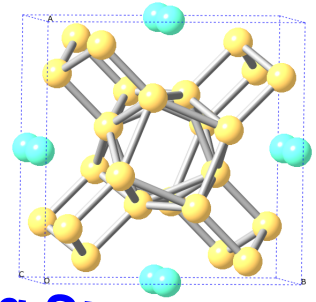

hP4, 190 GPa
Insulating, Transparent Electride

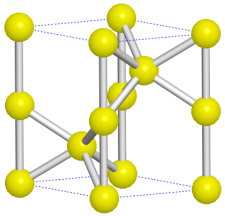

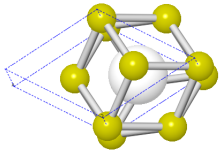

Increasing Structural Complexity

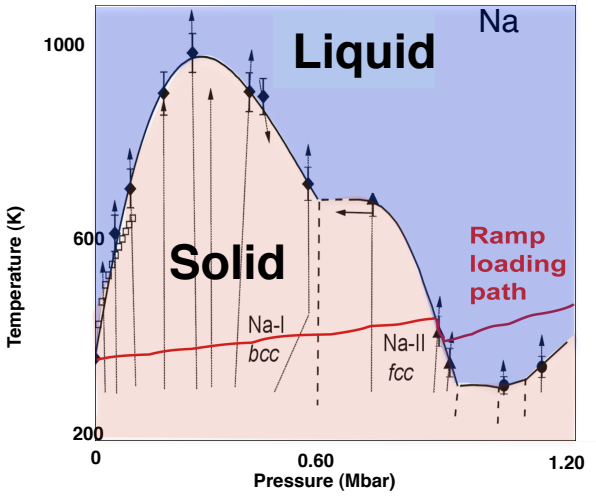

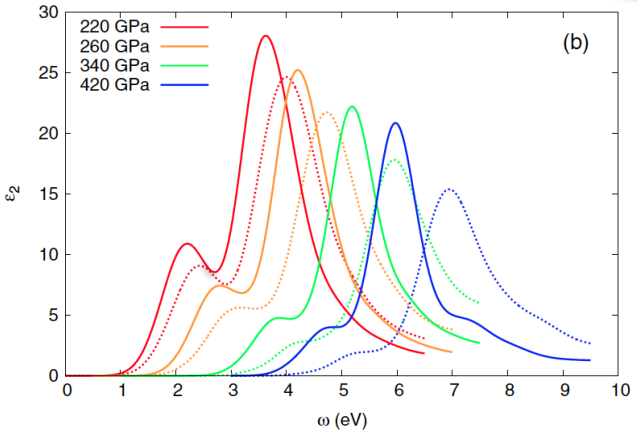

Band-gap predictions increase to 420 GPa

Aluminum is predicted to have at least 3 new phase transitions up to 10 Tpa.

Pickard and Needs, Nature Materials (2010).

Traditional view: materials become simple at high pressure appears to be completely wrong!

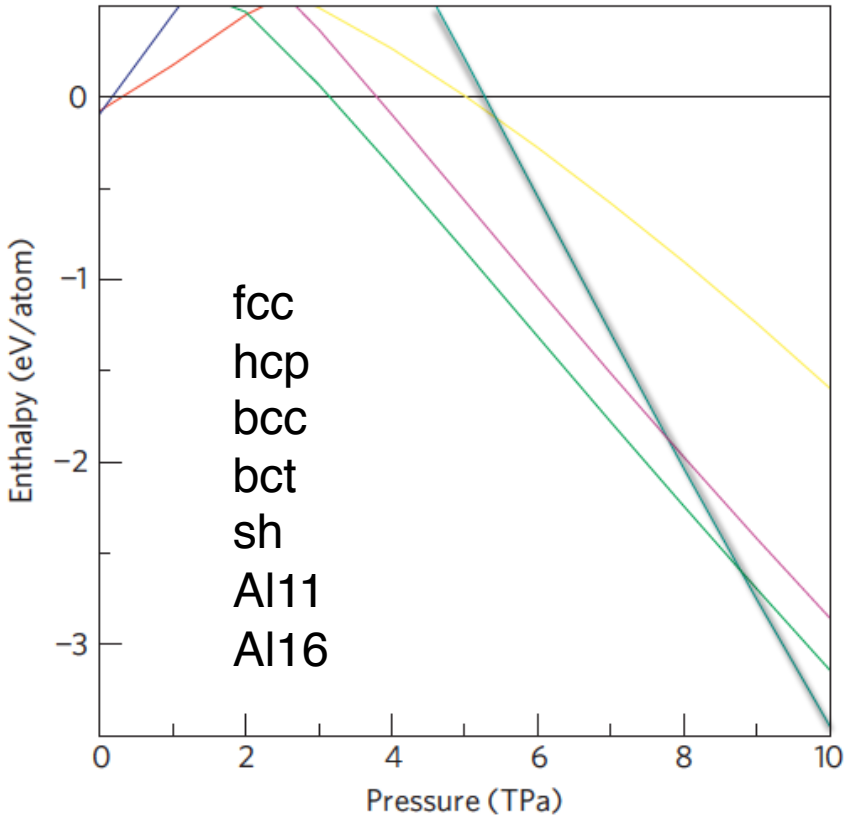

Figure 1 | Enthalpy–pressure relationships for Al phases. Enthalpy differences from the bcc phase are shown. The slopes of the curves give the volume differences from the bcc structure. The host–guest and simple hexagonal structures are favoured at high pressures because they are denser than the close-packed structures.

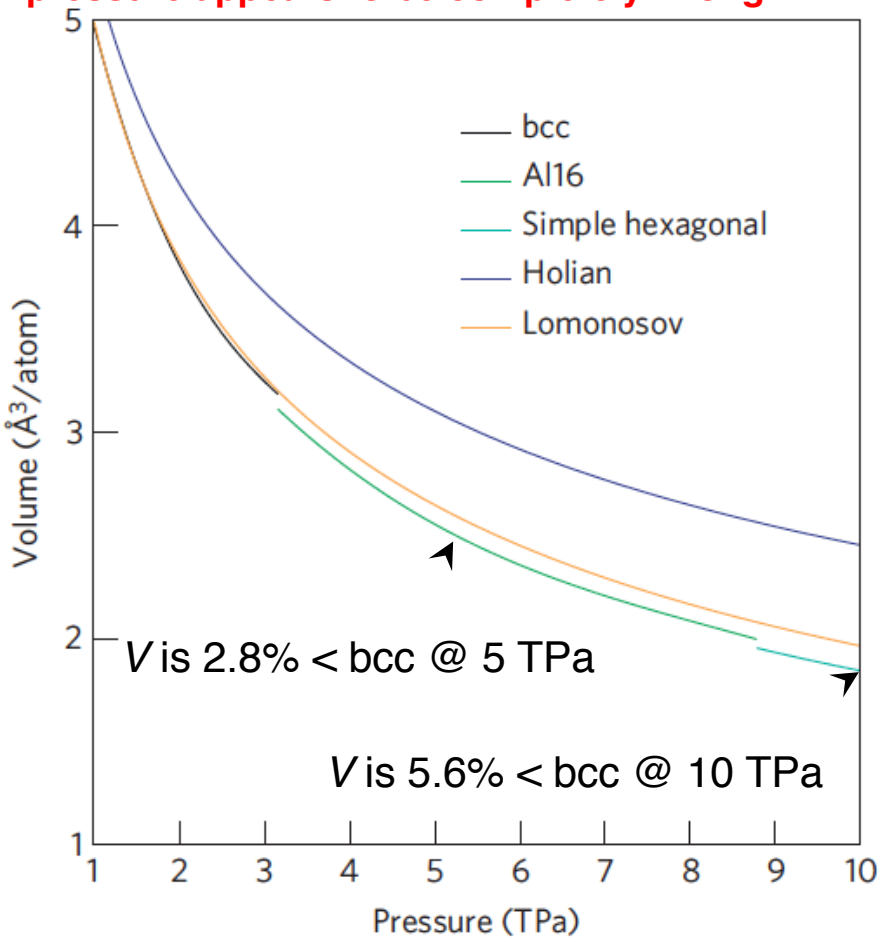

Figure 3 | Equation of state of Al. The volume–pressure relationship calculated in this work and from the EoSs of Lomonosov[4,5] and Holian[18].

High pressures phases of aluminum are also predicted to be complex

Pickard and Needs, Nature Materials (2010).

FCC

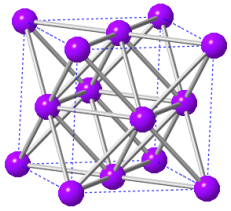

HCP
0.217 TPa

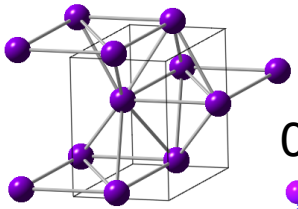

BCC
0.38 TPa

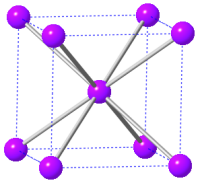

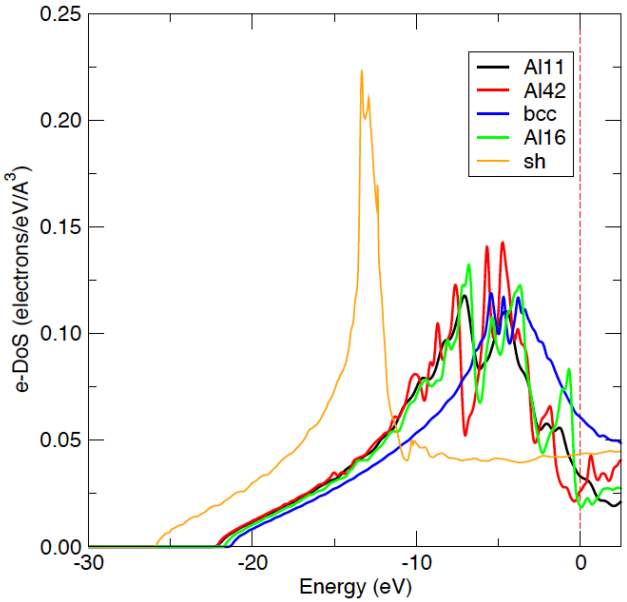

Host-Guest structure of Ba-IVa (Incommensurate Electride)
3.2-8.8 TPa

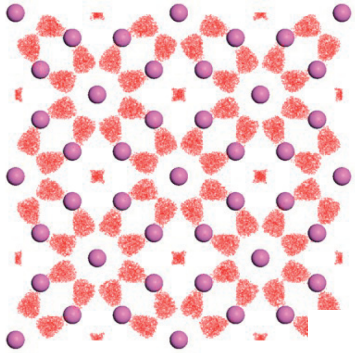

Up to 10 TPa aluminum is still metallic

Electrides form above about 3.2 TPa

Simple Hexagonal Electride
8.8 – 10 TPa

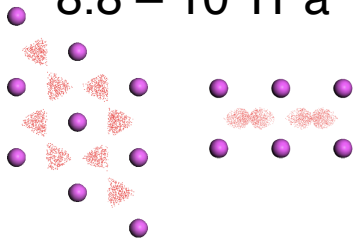

CMMA Electride
> 10 TPa

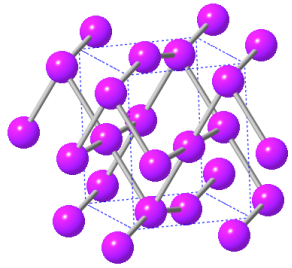

"all structures near 30 TPa are far from close packed"

$MgSiO_3$ shows a large discontinuity in decay

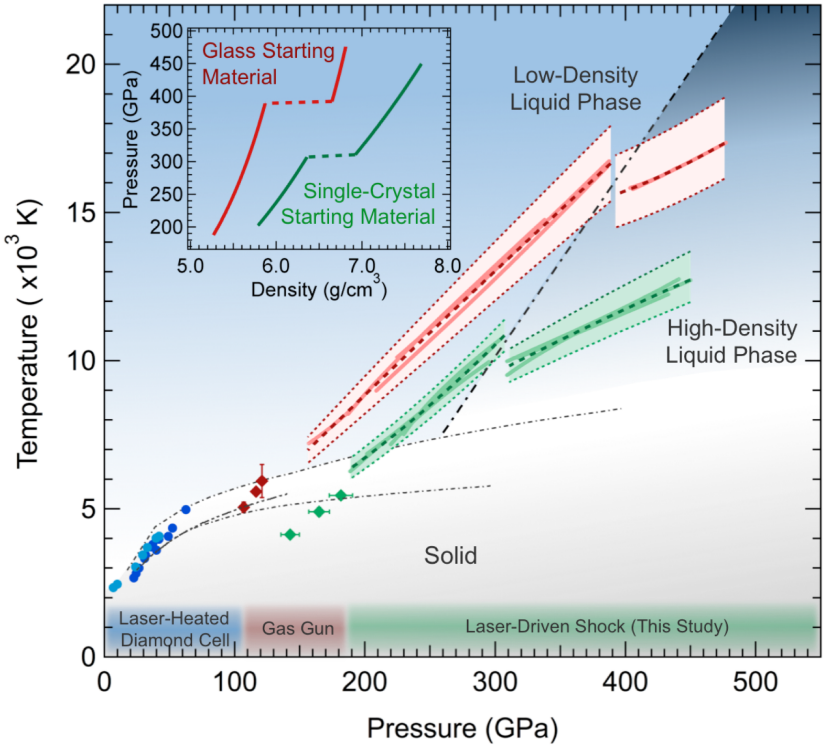

Dylan Spaulding

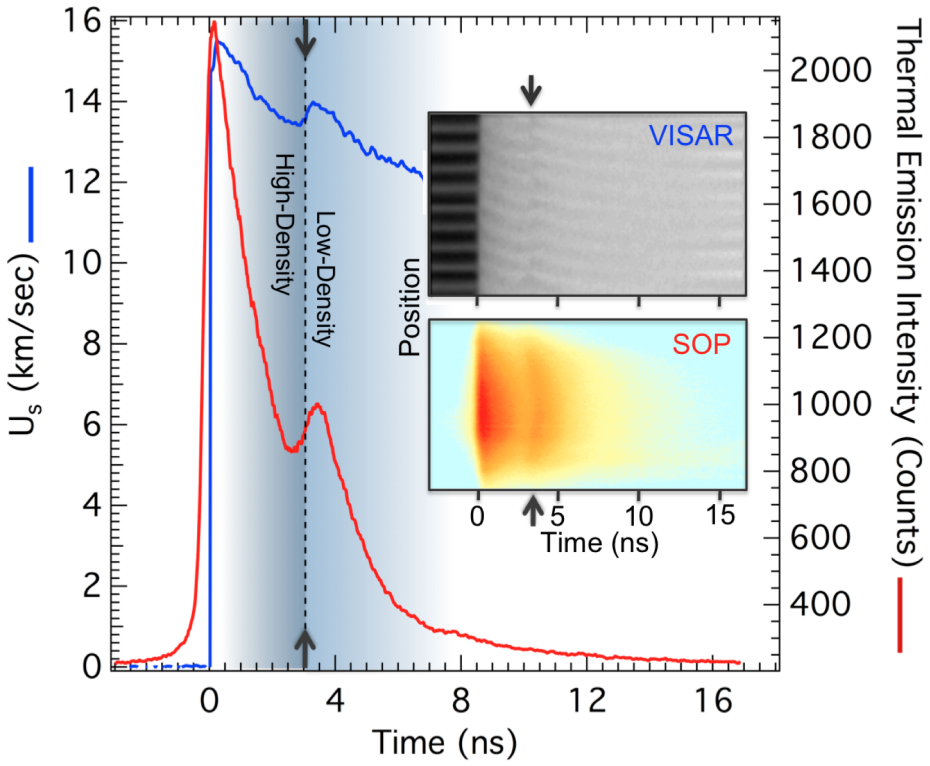

Discontinuity both in VISAR and in SOP. Is this a liquid-liquid transition? Is it possible that we are observing a refreeze transtion?

Beyond Wave-Profile Analyses

- To really explore this new extreme chemistry experiments must be done in the TPa regime.

- We need new diagnostics that go beyond wave-profile analyses

Sandwich Ramp-Compression

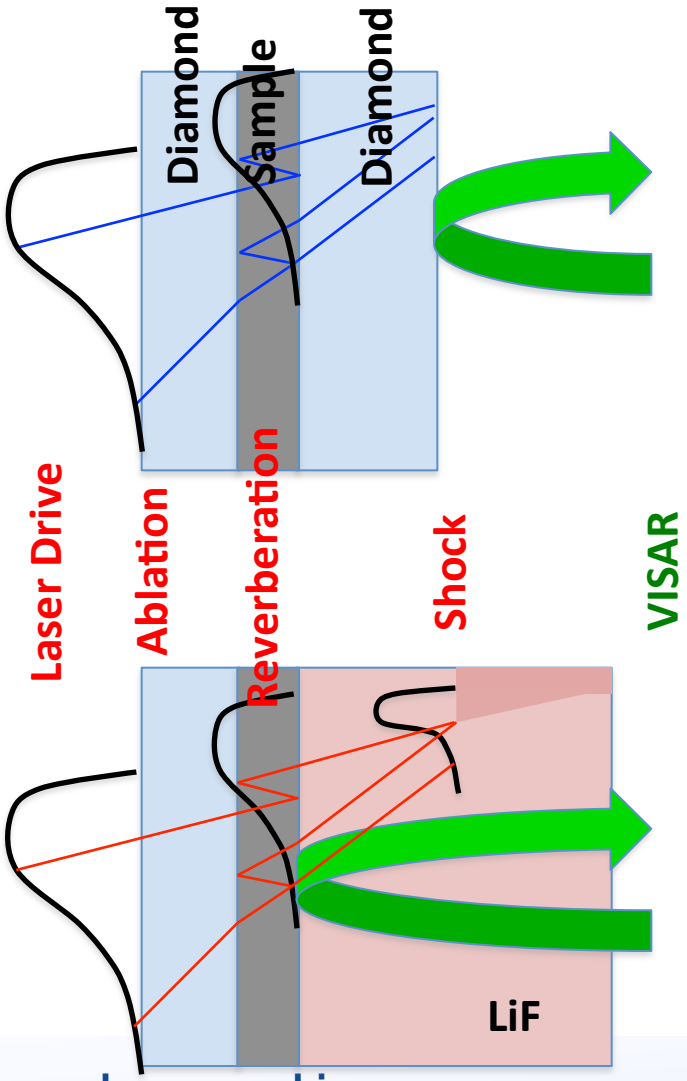

the LiF or Diamond interfacial pressure is the same as in sample

If we know the EOS of LiF or Diamond we can find the Pressure in the sample using the VISAR diagnostic

Using this target design, we believe we can ramp compress samples to ~30 Mbar, Hold the state for several ns, Determine the pressure, and Make a measurement.

XRD, XAFS, XANES, Reflectivity, ... Temperature remains the most important parameter that we do not know how to measure.

In addition to wave profiles we measure x-ray diffraction to determine structure, stress, strain, and texture

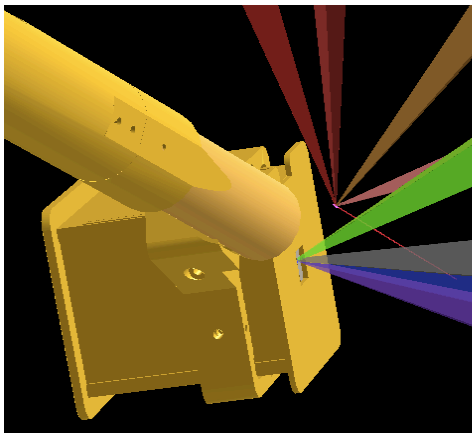

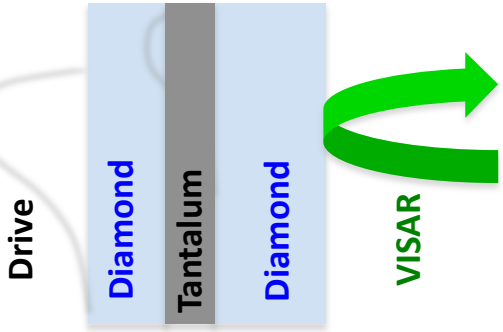

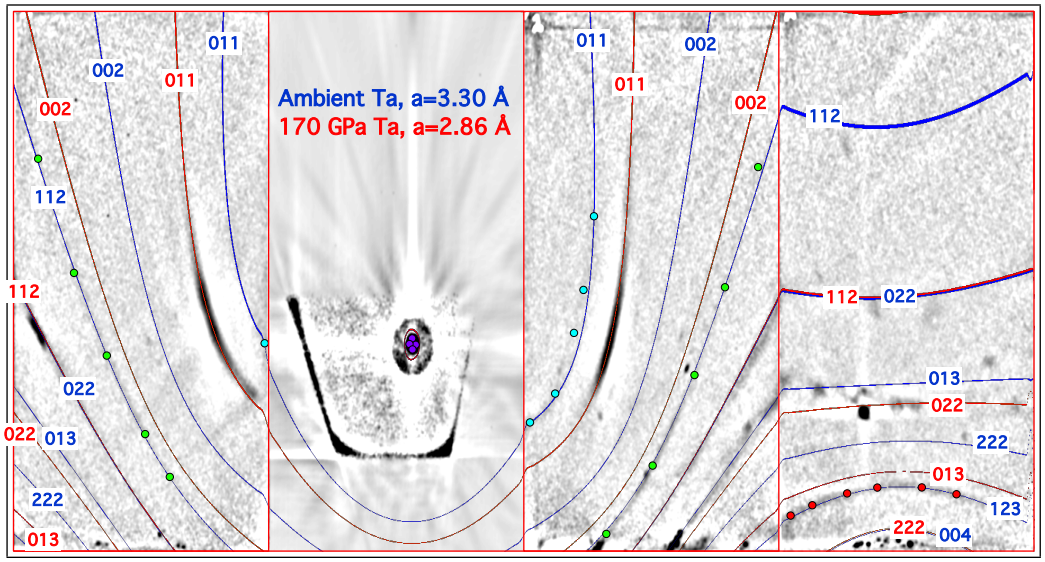

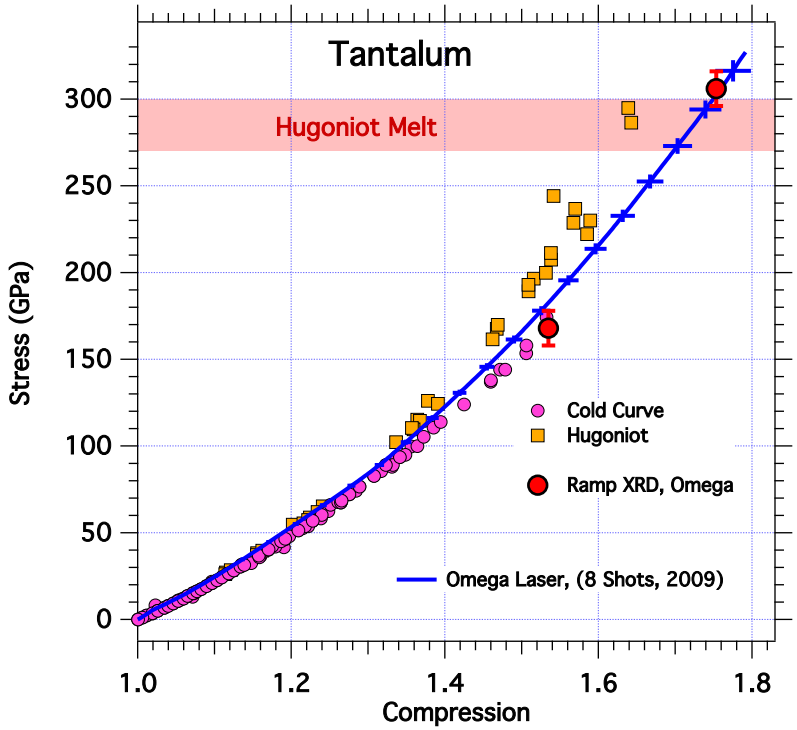

Tantalum remains BCC until 300 GPa. No sign of FCC phase. Some evidence of texture change.

Ryan Rygg
Jim Hawreliak

Diffraction, Hugoniot, Ramp wave-profile, and DAC data are consistent and give P-rho-T and structure

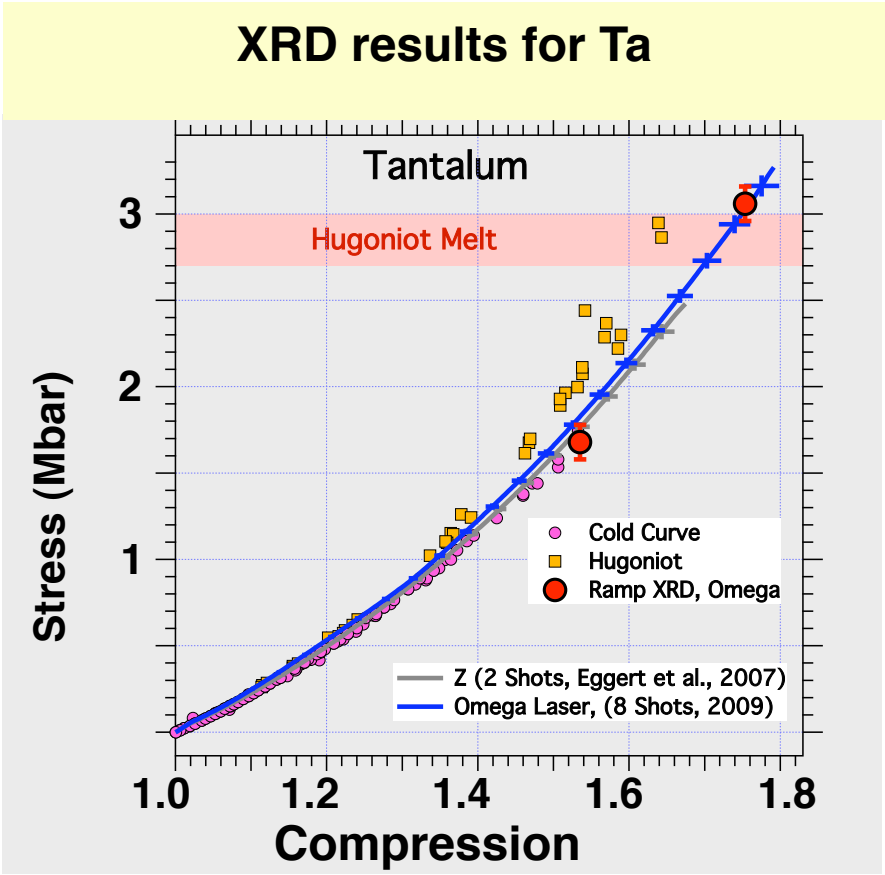

Ryan Rygg
Jim Hawreliak

Diffraction, Hugoniot, Ramp wave-profile, and DAC data are consistent and give P-rho-T and structure

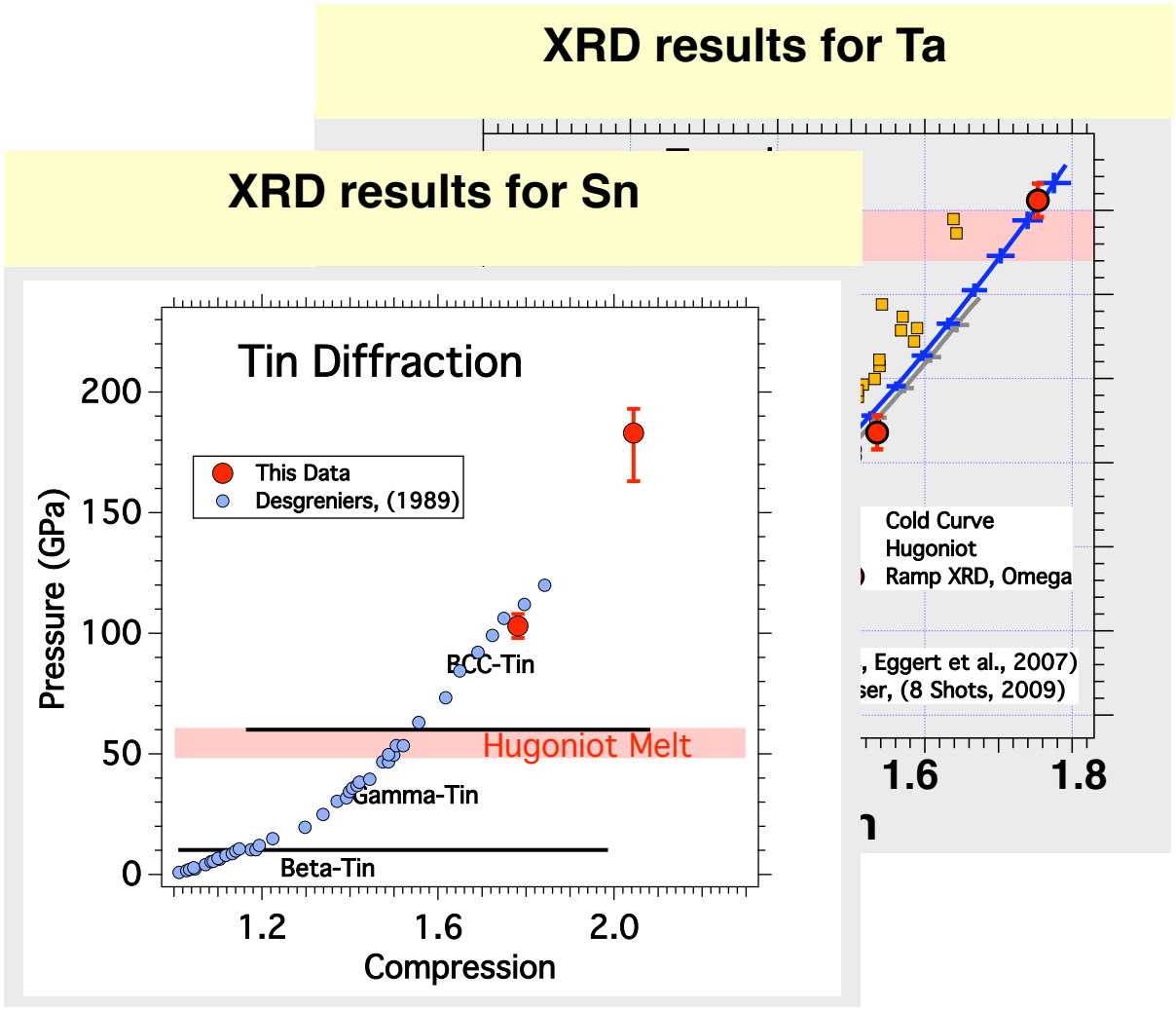

Ryan Rygg
Jim Hawreliak

Diffraction, Hugoniot, Ramp wave-profile, and DAC data are consistent and give P-rho-T and structure

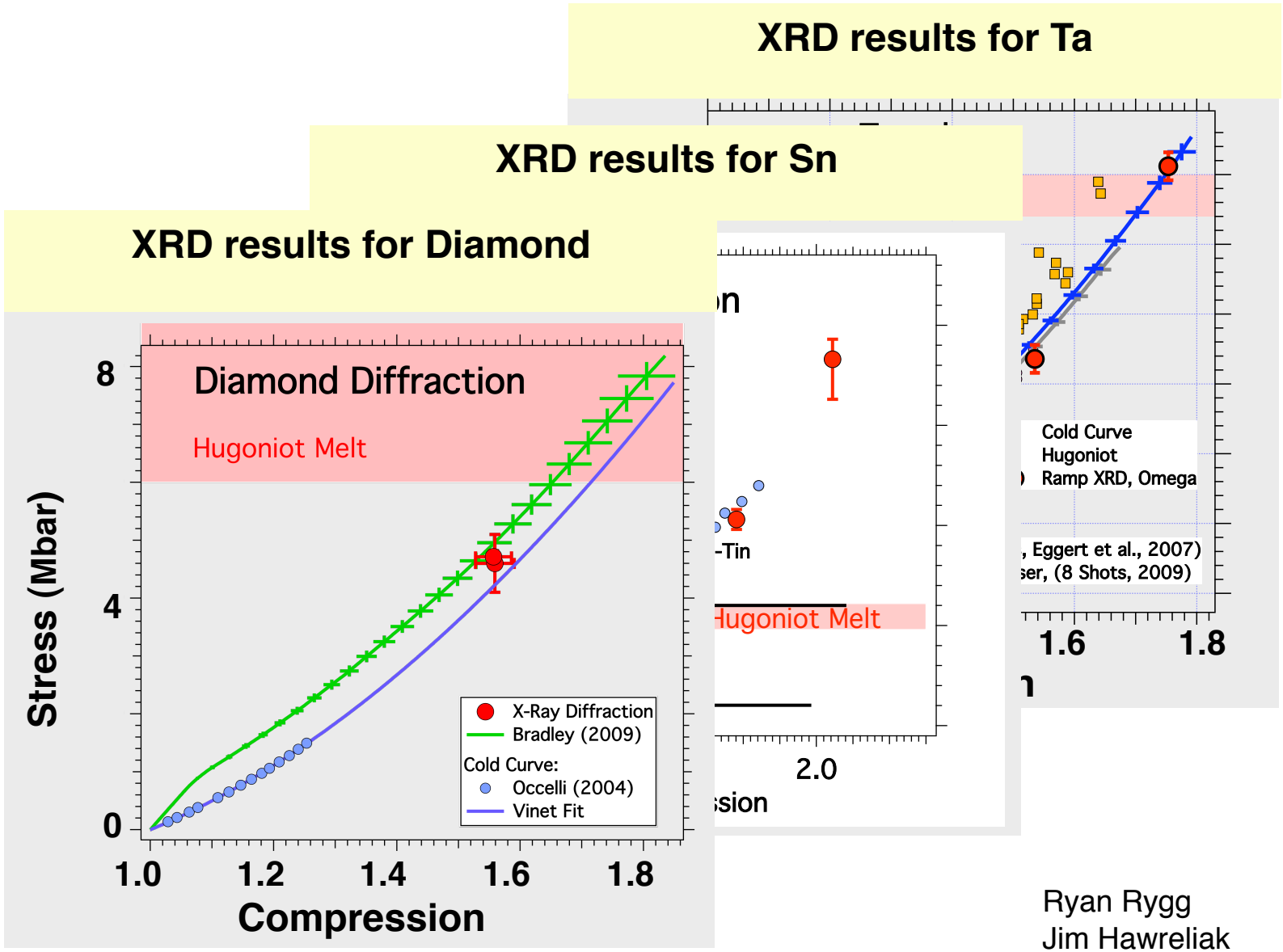

Ryan Rygg
Jim Hawreliak

Diffraction, Hugoniot, Ramp wave-profile, and DAC data are consistent and give P-rho-T and structure

XRD results for Ta

XRD results for Sn

XRD results for Diamond

XRD results for Fe

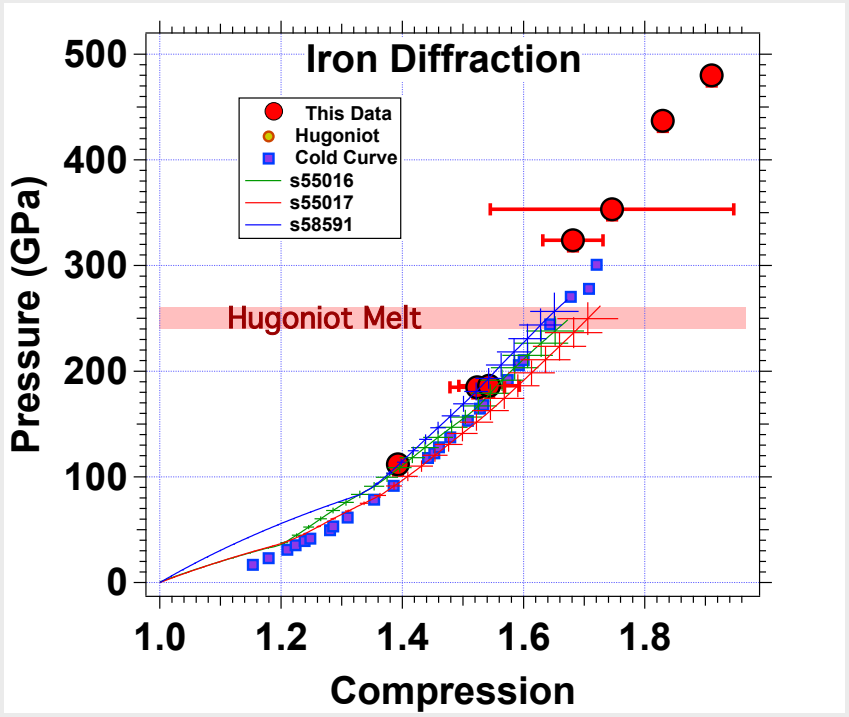

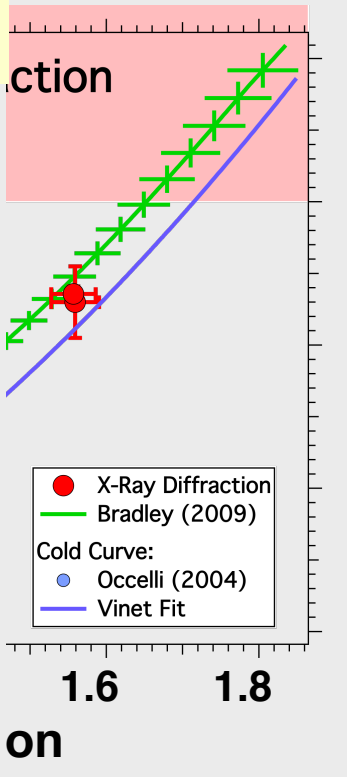

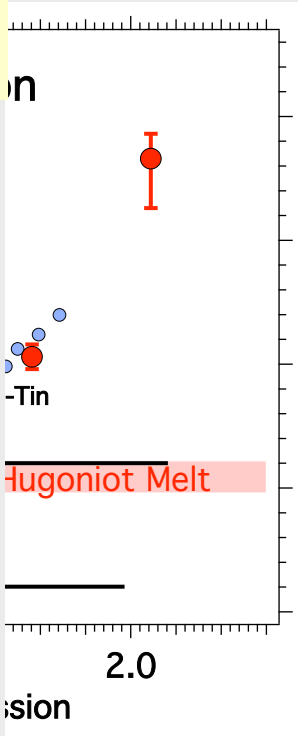

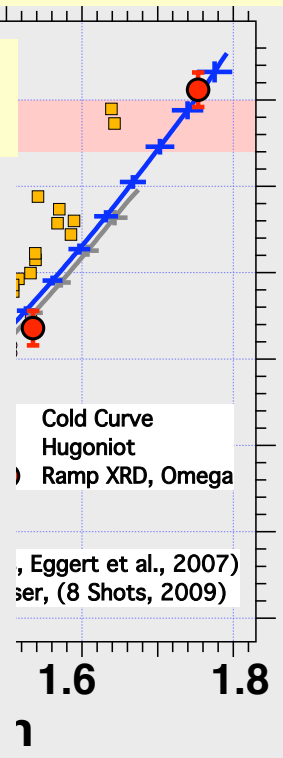

Ryan Rygg
Jim Hawreliak

EXAFS data is used to determine local order, structure, temperature in a 50 ps snapshot

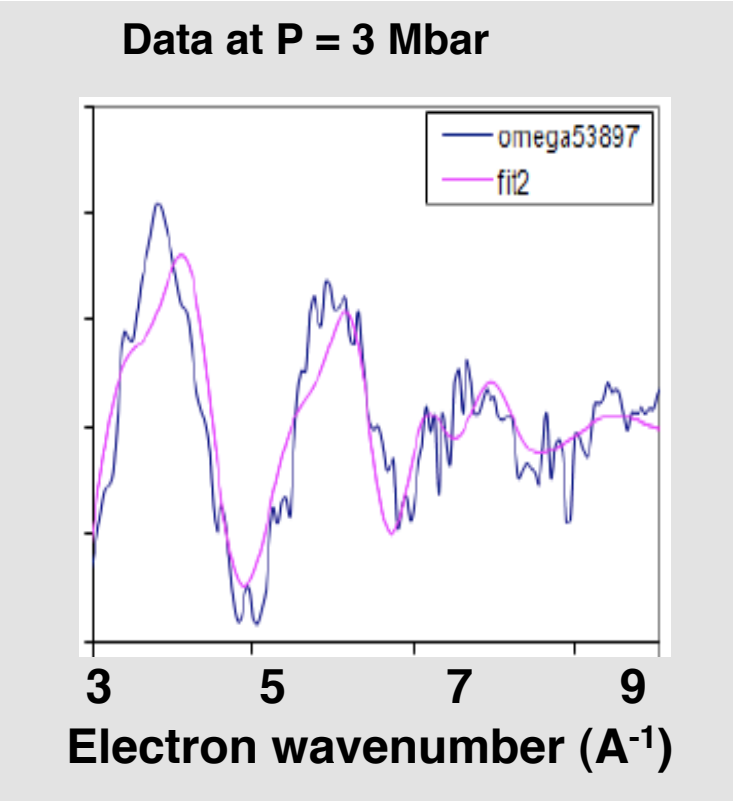

X-ray Scattering/absorption shows local structure in Fe to 3 Mbar (Hicks)

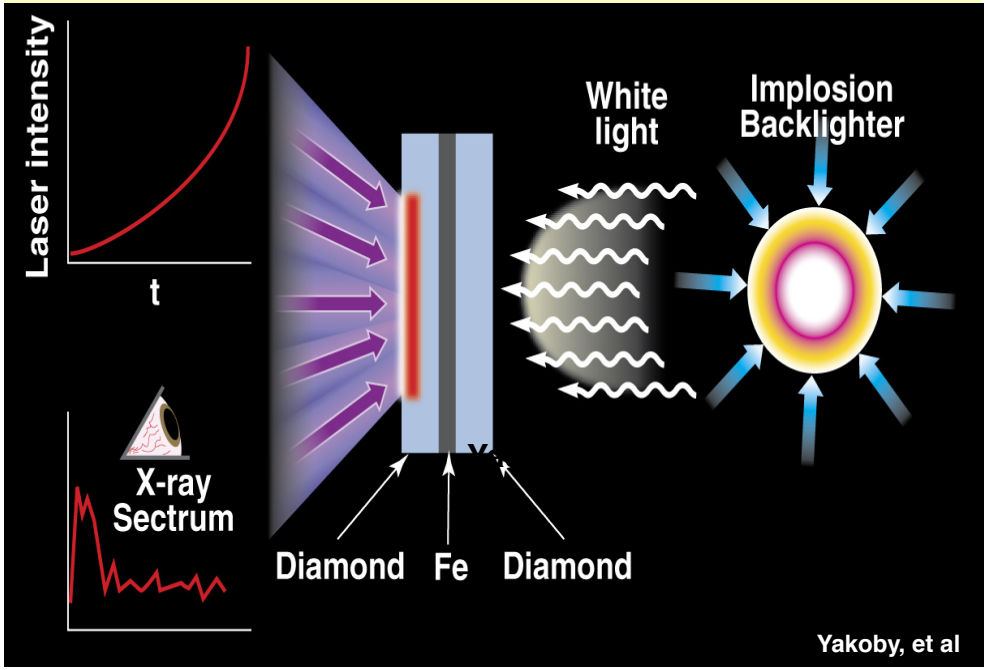

Damien Hicks
Yuan Ping

Best fit to EXAFS data at 3 Mbar shows HCP structure, compression =1.55, T=6000 K

Input from simulations aids EXAFS analysis

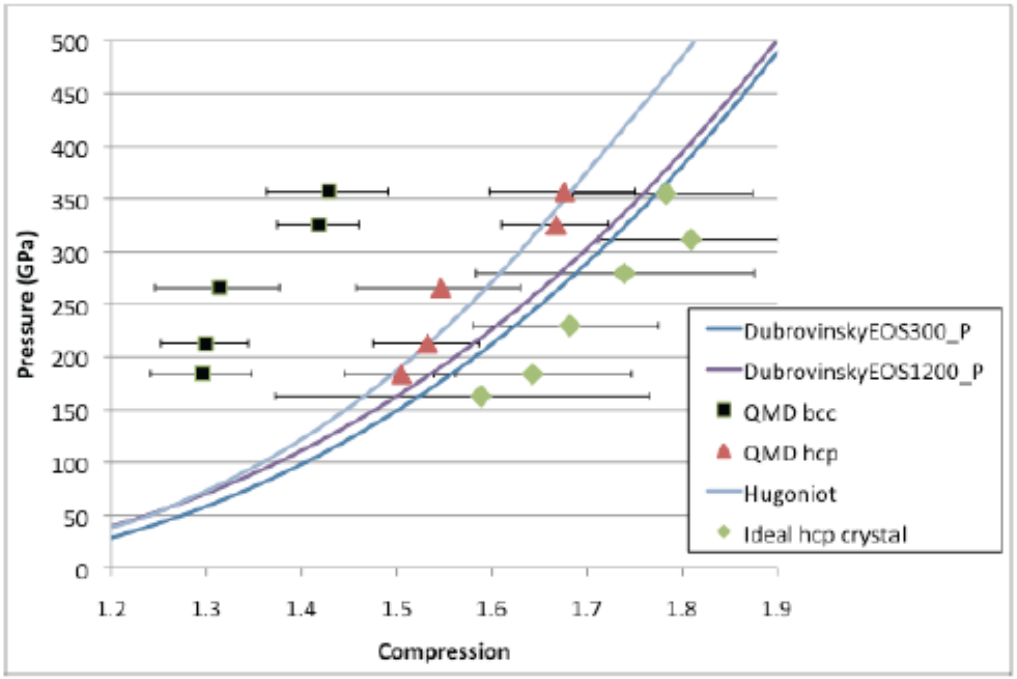

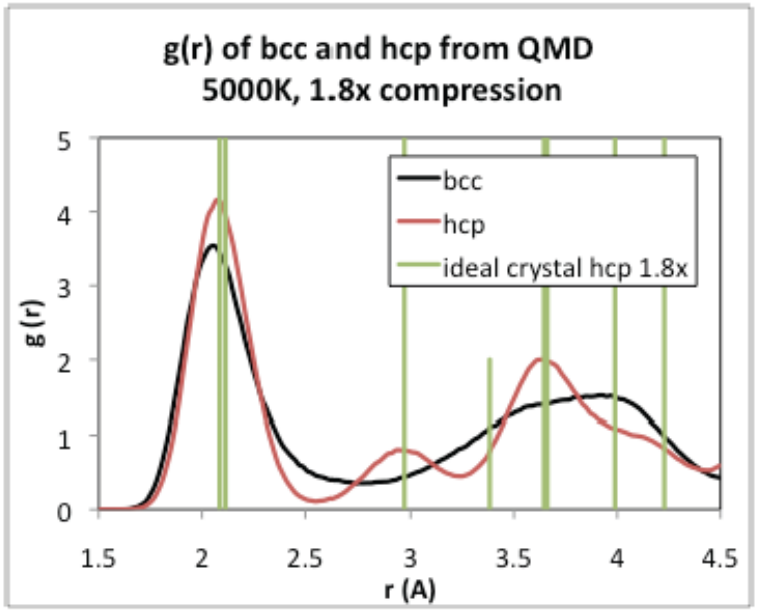

- Best fit of exafs data with different phases gives slightly different densities due to different g(r).
- Fitting with hcp shows the most reasonable density, which is along Fe hugoniot.

Temperature by EXAFS and XRD agree

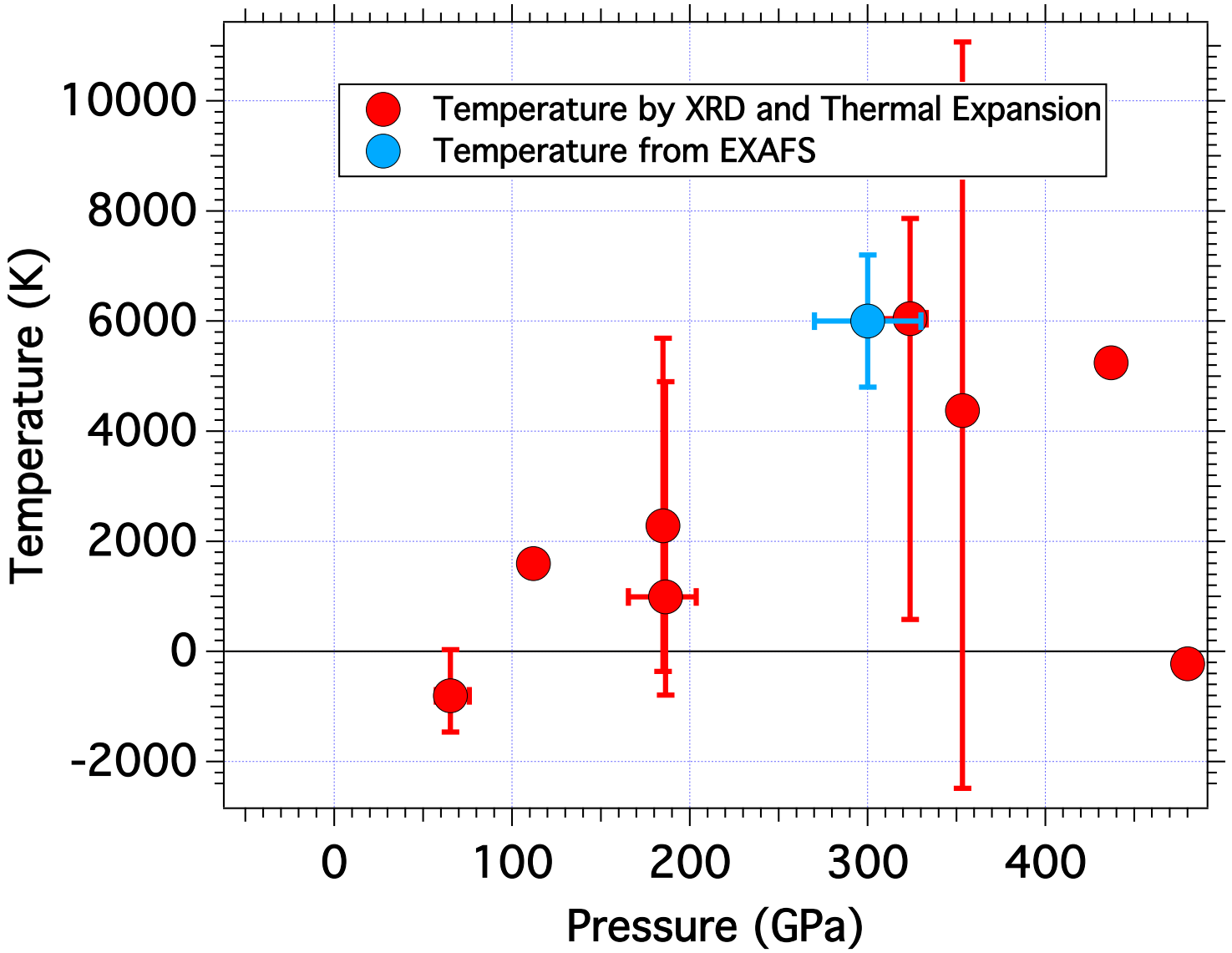

LiF remains transparent to over 8 Mbar under ramp compression

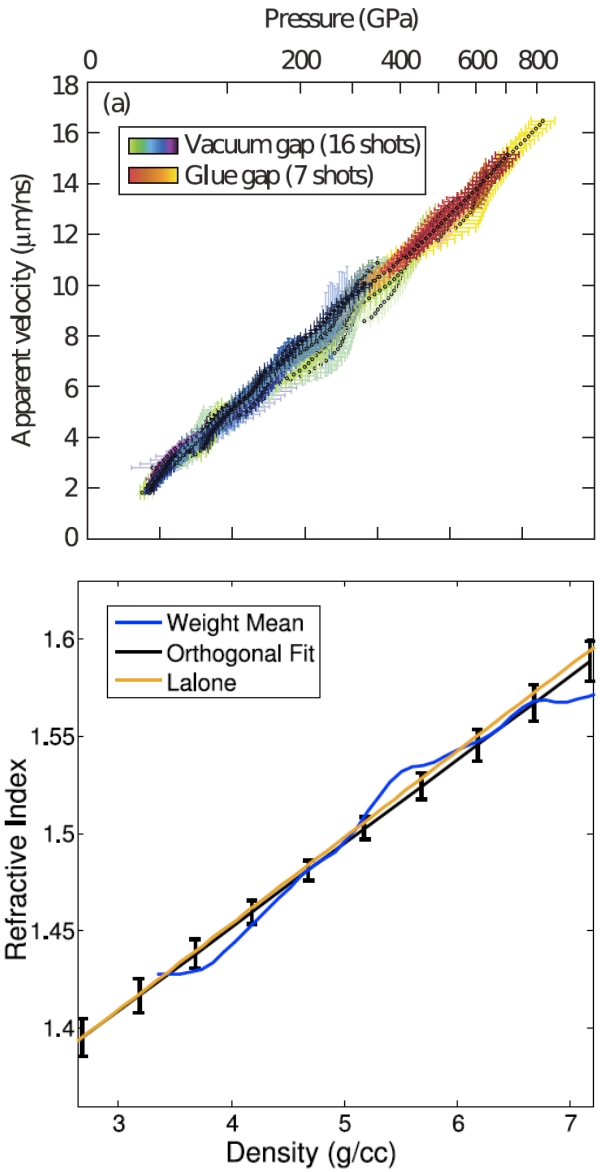

Hayes (2001)

$$\left.\frac{dU_A}{dU_T}\right|_{U_T} = \left.\left(n - \rho\frac{dn}{d\rho}\right)\right|_{U_T} \qquad n^2 - 1 = \frac{E_d E_o}{E_0^2 - \hbar^2\omega^2}$$

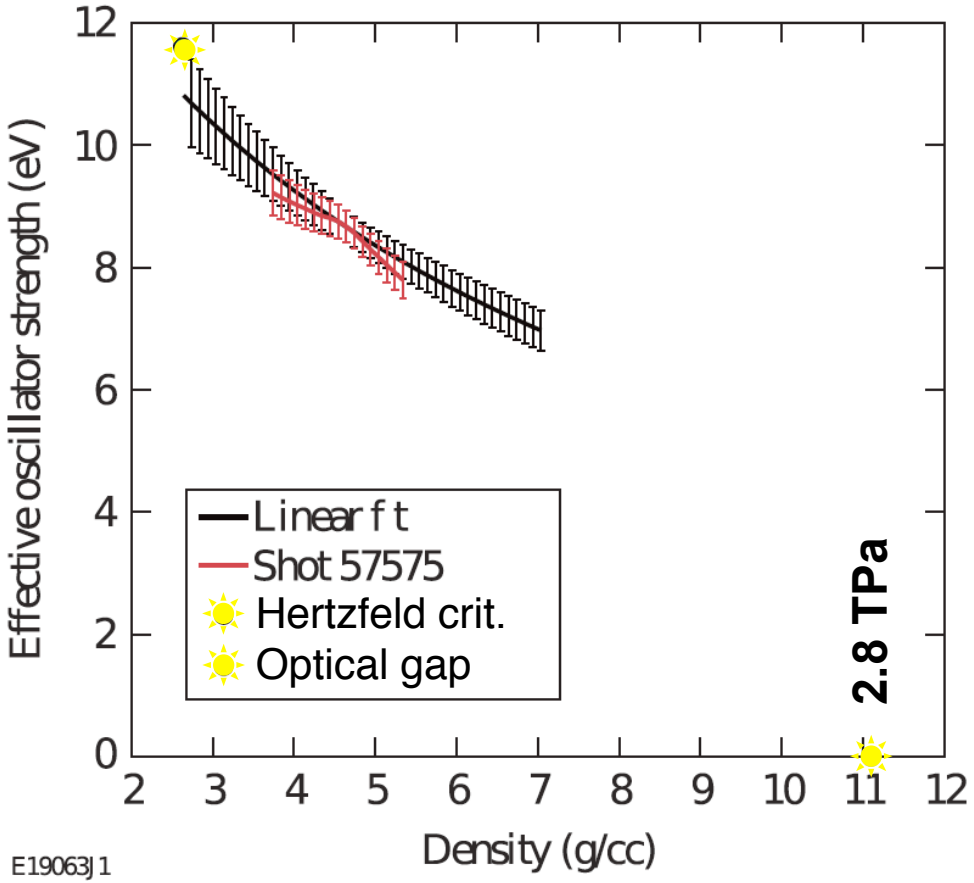

We need a complex suite of drivers

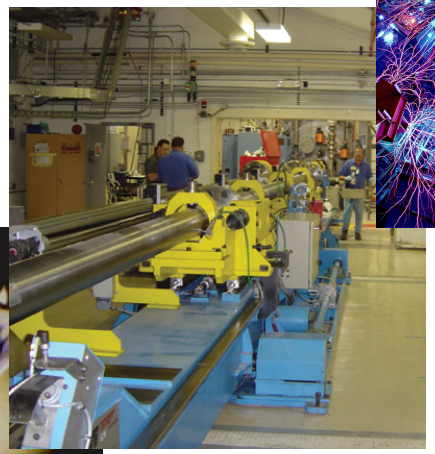

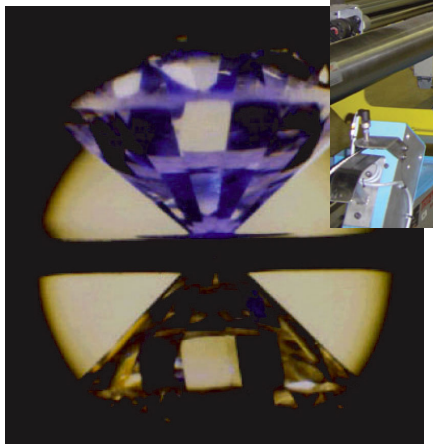

DACs

Jasper

Z

Omega

HEPP

NIF

Pressure, Strain Rate

Isentropic Compression Experiments Using a Cylindrical Liner Z-Pinch

Ray Lemke

R. D. McBride, M. R. Martin, J-P Davis and M. D. Knudson

4th Workshop on Ramp Compression

18-19 January 2011; SNL; Albuquerque, NM

We developed a technique for obtaining off Hugoniot EOS data via magnetically driven liner implosions on Z

- **Large pressures possible in cylindrical geometry [$P \alpha (I / R)^2$]: *I=20 MA, R=0.25 cm, P~10.2 Mbar*.**
- **Magnetically driven liner implosions for HEDP studies demonstrated at LANL (Pegasus & Atlas), AFRL (Shiva Star), and in Russia (VNIIEF).**
  - **I = 12-30 MA implodes 10-100 g liner in 10-20 μs; velocity < 20 km/s.**
  - **X-ray radiography key diagnostic.**
- **Magnetically driven liner experiments on Z quasi-isentropically compress solid beryllium to P ~ 3 Mbar.**
  - **I = 20 MA implodes 0.169 g liner in ~0.1 μs; velocity ≤ 54 km/s.**
  - **Cylindrical ICE (*isentropic compression experiment*).**

Sandia National Laboratories

Abel inverting multiple x-ray images of imploding liner yields time sequence of density profiles

Be Liner Z-Pinch Implosion

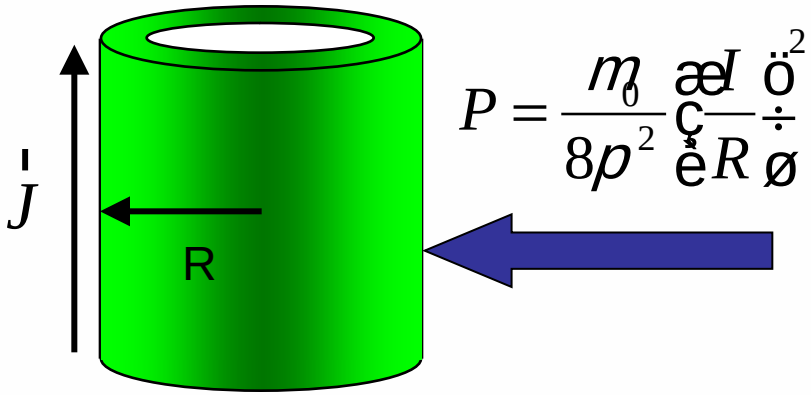

Two-frame 6151 eV x-ray radiography

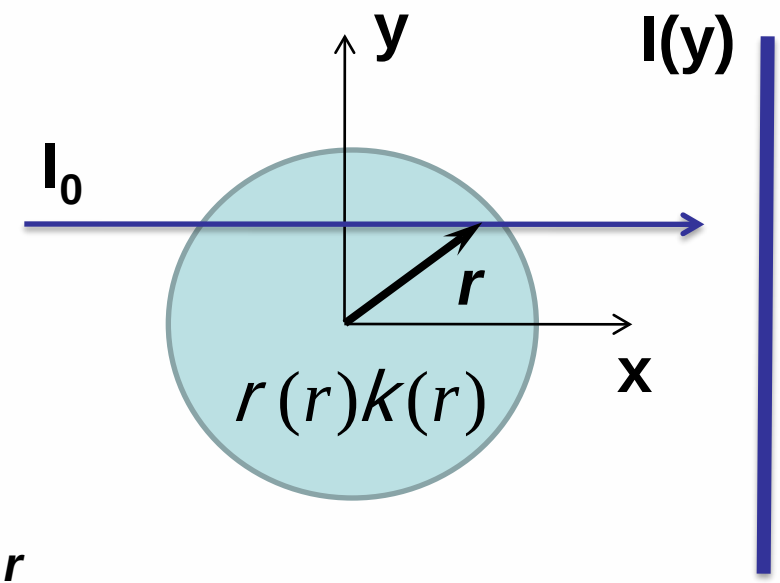

Abel inversion yields liner density vs. r

$$r(r)k(r) = -\frac{1}{\pi}\int_r^1 \frac{d\ln[I(y)/I_0]}{dy}\frac{dy}{\sqrt{y^2 - r^2}}$$

Sandia National Laboratories

Discrete equations for pressure & velocity obtained by mapping Abel inverted densities to mass coordinates

Liner Density vs. R (m_i = 10 mg)

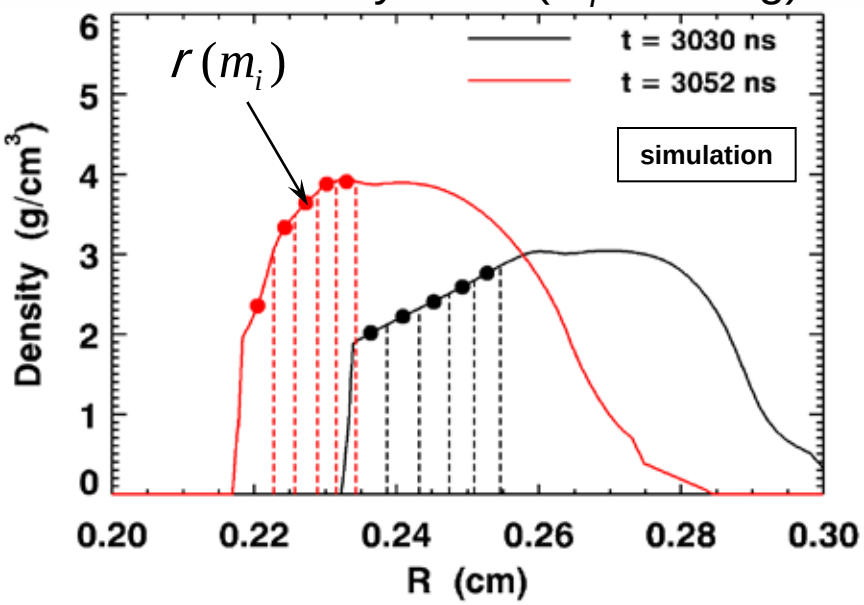

Hydro Equations

$$\frac{D\rho}{Dt} = -\rho\nabla\cdot\mathbf{u} \Longrightarrow u_r(m_{i+1}) = \int_{m_i}^{m_{i+1}} \frac{1}{2\pi L_z r}\frac{\partial V}{\partial t}dm + u_r(m_i)$$

$$\frac{D\mathbf{u}}{Dt} = -\frac{1}{\rho}\nabla P \Longrightarrow P(m_{i+1}) = -\int_{m_i}^{m_{i+1}} \frac{1}{2\pi L_z r}\frac{\partial u_r}{\partial t}dm + P(m_i)$$

Algorithm developed by Matt Martin.

Sandia National Laboratories

Simulated cylindrical Be ICE determines current shape, radiograph timing, and self-consistency of pressure unfold

- **ALEGRA resistive MHD code.**
- **Liner: R_i=0.24 cm; R_o=0.32 cm.**
- **Current shape based on Sesame EOS Be 2020 isentrope.**
- **Four radiographs in 22 ns window.**
- **Verifies quasi-isentropic compression of solid Be.**
- **Determines uncertainty propagation.**

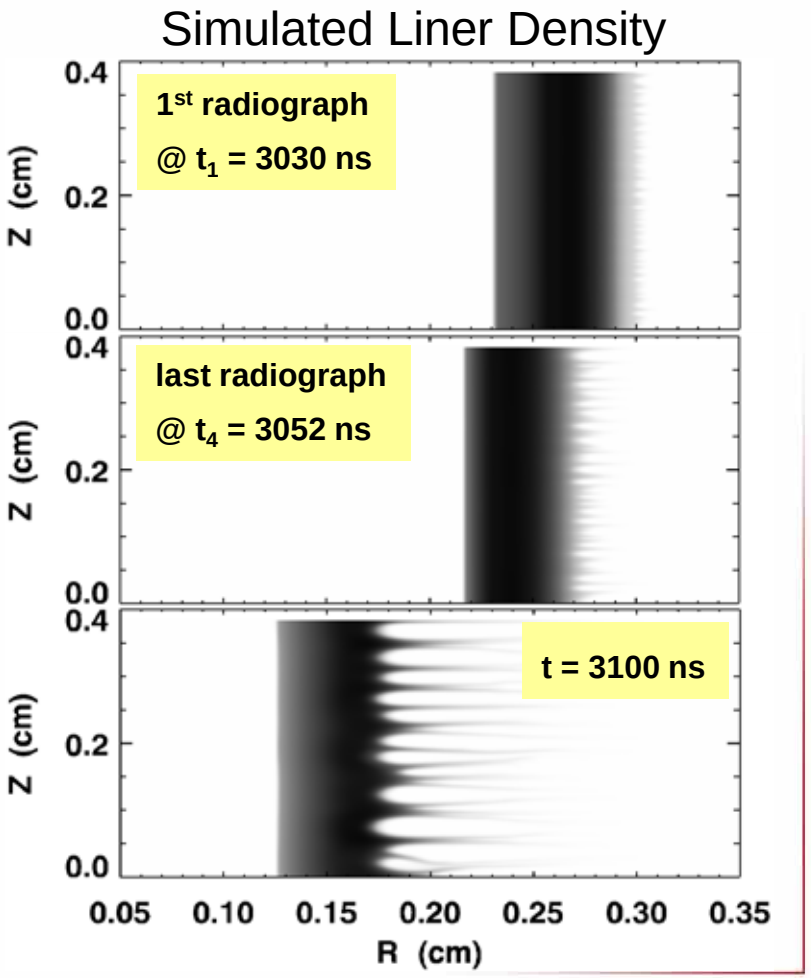

Sandia National Laboratories

Simulated cylindrical ICE shows effect of +/- 4% uncertainty in Abel inverted density on pressure

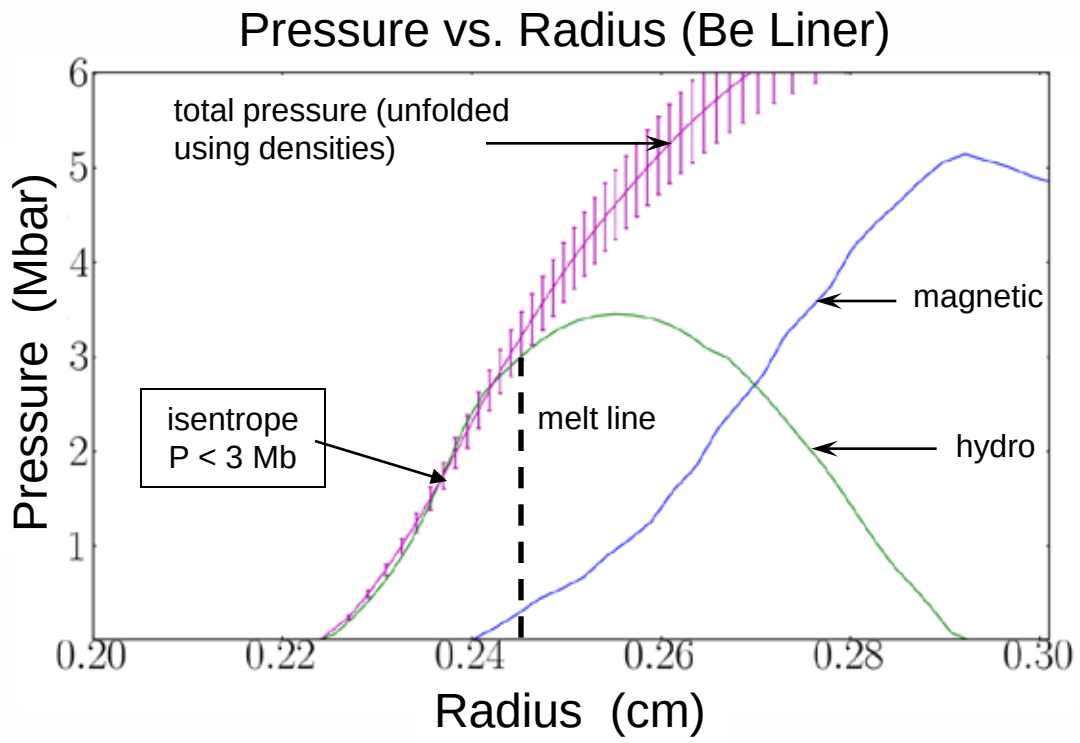

Magnetic diffusion reduces maximum pressure of unfolded isentrope.

Sandia National Laboratories

Simulated cylindrical ICE verifies solid Be compressed along isentrope of Sesame EOS 2020

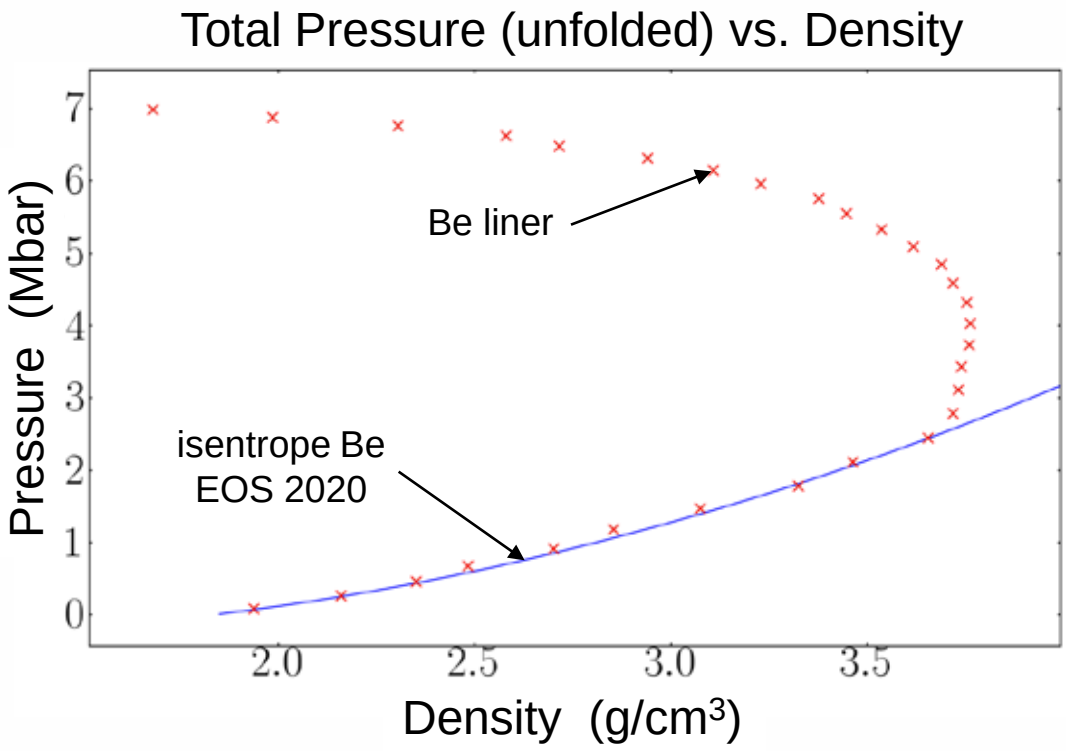

Sandia National Laboratories

For quasi-isentropic compression the current waveform is based on the material EOS

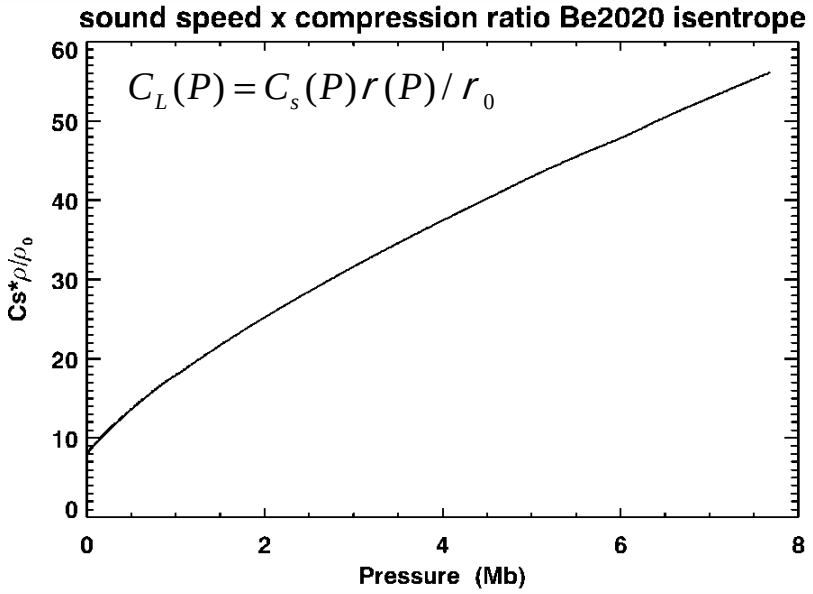

Liner thickness < shock up distance X_S.

$$X_S = t_R C_{LN} C_{L0} / (C_{LN} - C_{L0})$$

Pressure at time t_n.

$$t_n = t_R - X_S [C_{LN}(P_{\max}) - C_{Ln}(P_n)] / C_{LN}(P_{\max}) C_{Ln}(P_n)$$

Sandia National Laboratories

Be liner ICE produces required shaped current drive and 4 radiographs at desired times

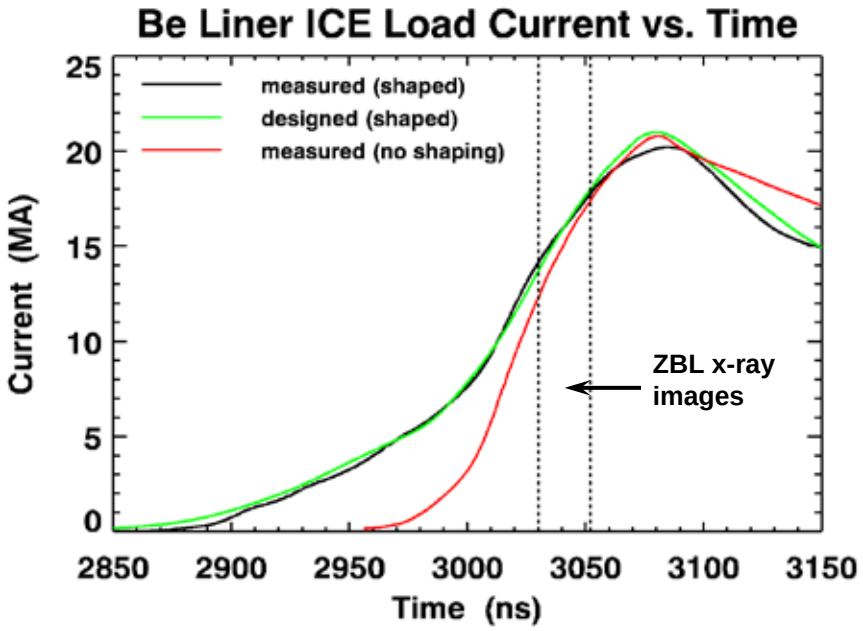

6151 eV Backlight Images

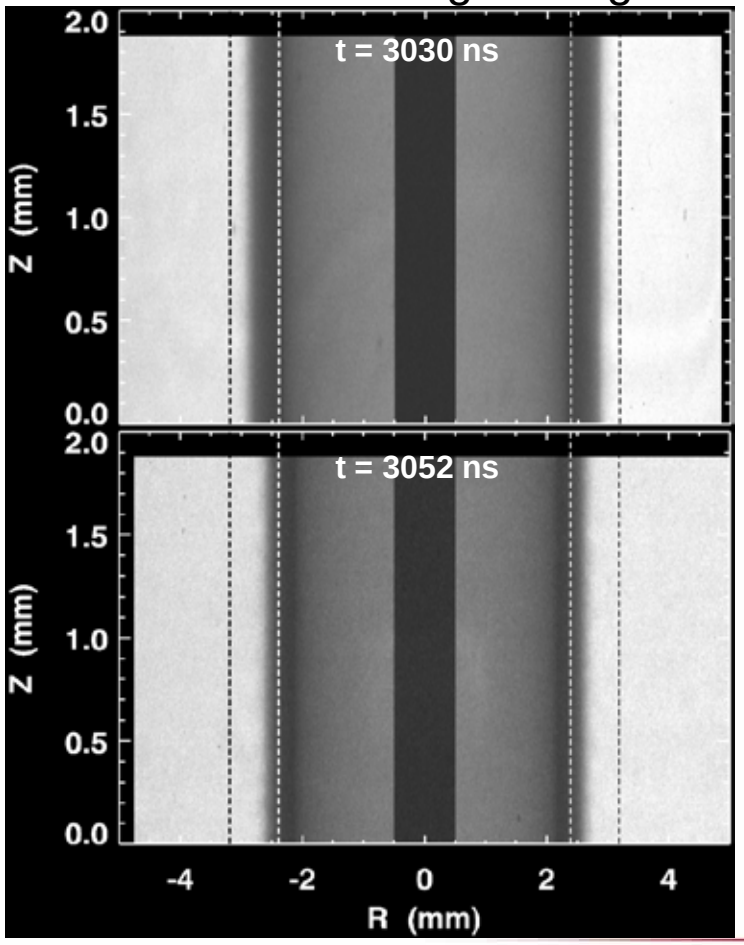

Sandia National Laboratories

Abel inverted densities in good agreement with MHD simulation indicating quasi-isentropic compression achieved

Abel inversion of transmission for R > 0 yields density profiles.

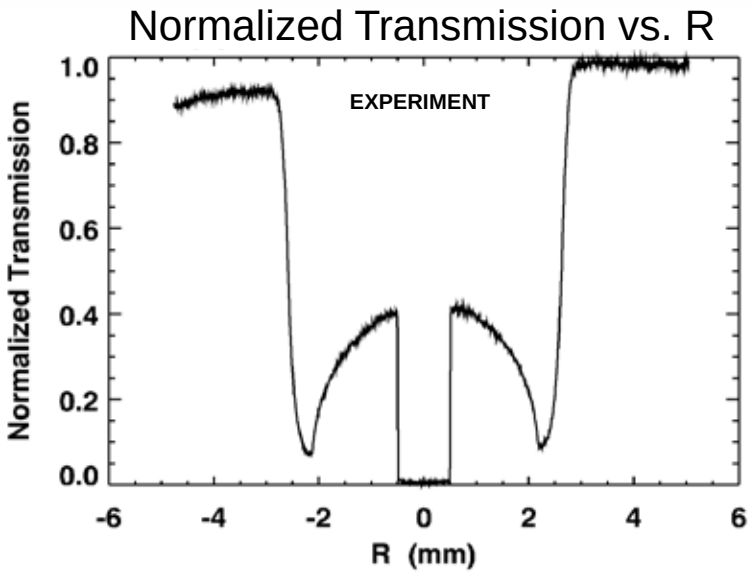

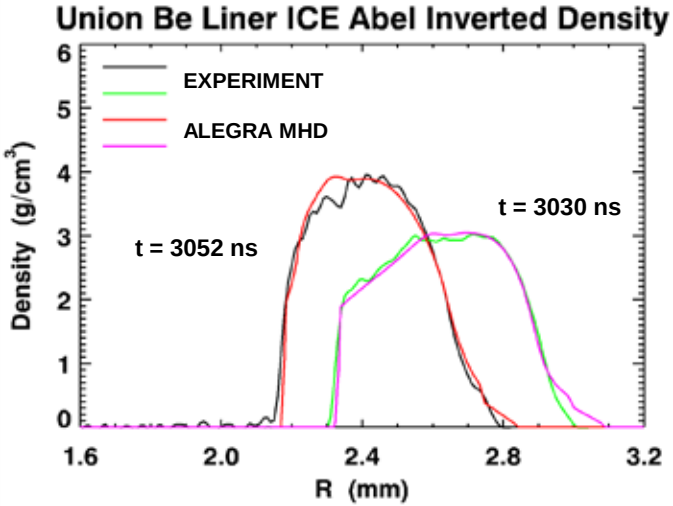

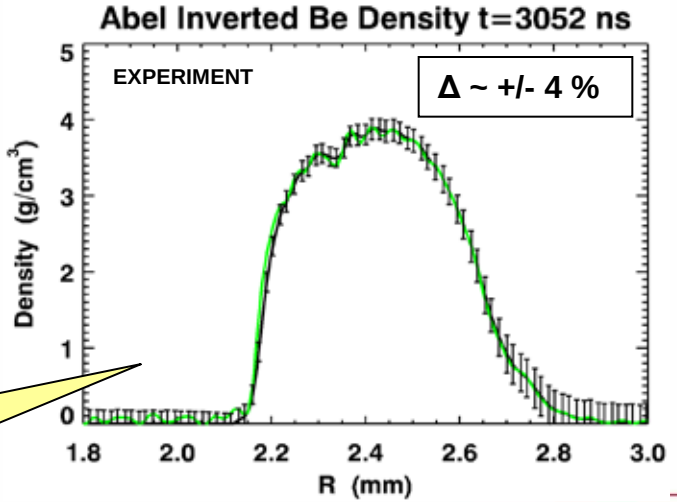

Error bars established assuming noise in x-ray transmission is random.

Sandia National Laboratories

Cylindrical ICE on Z produces Be isentrope to ~3 Mbar

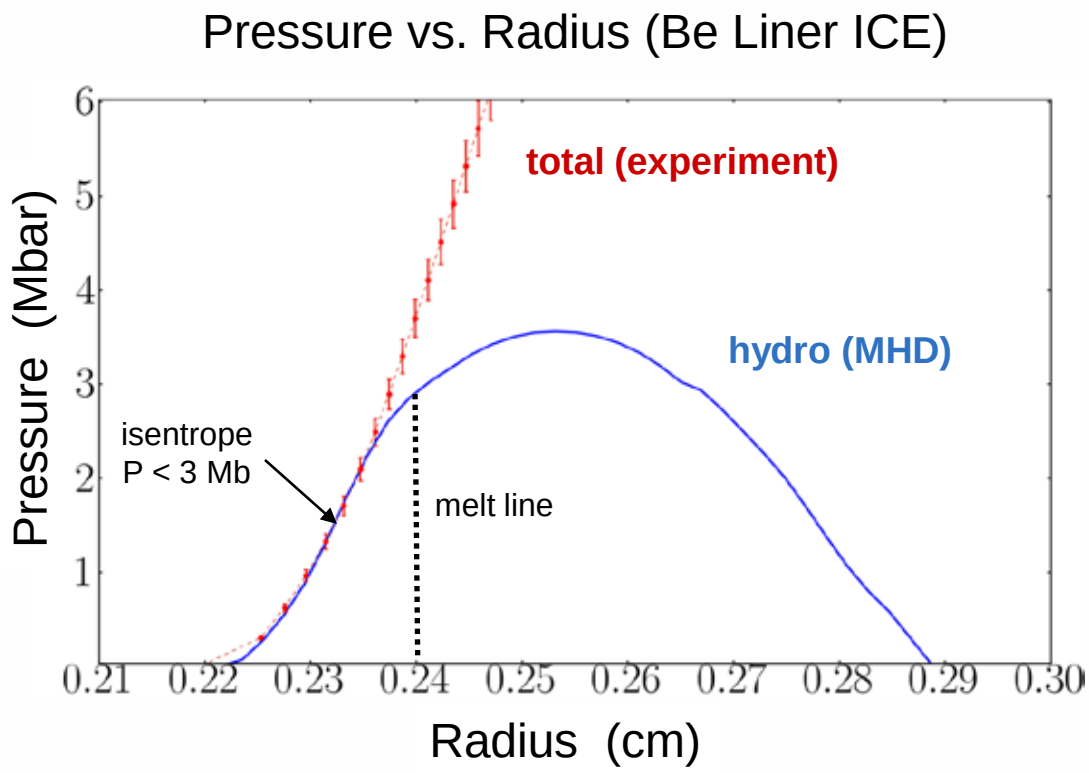

MHD simulation: *at peak compression inner 156 μm Be solid (116 μm field free); P = 3.2 Mbar; ρ = 3.9 g/cc.*

Sandia National Laboratories

The unshaped standard short current pulse produces a ~4 Mbar shock in the Be liner in excellent agreement with simulation

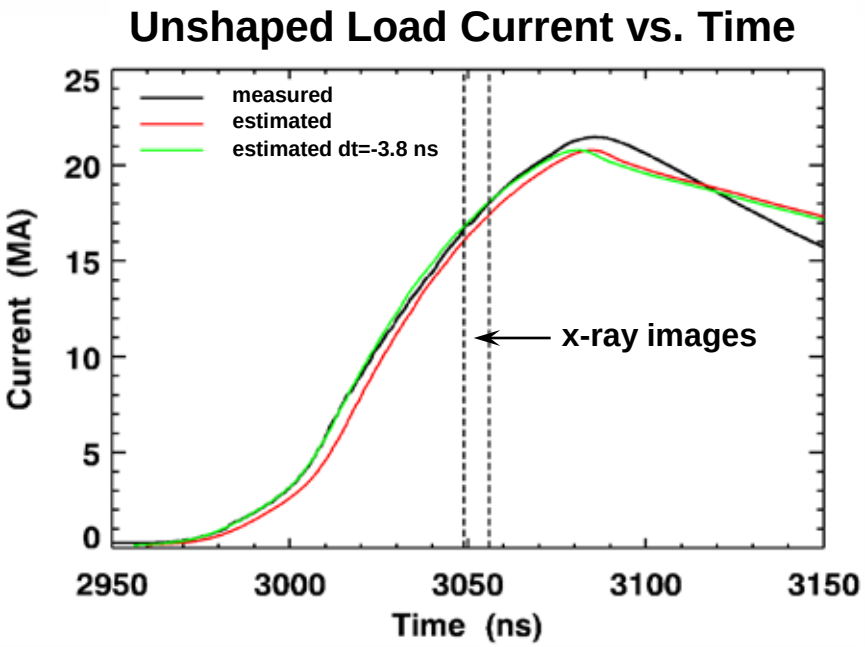

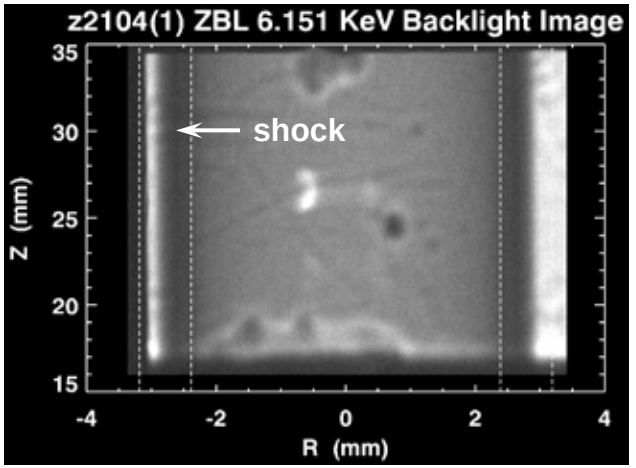

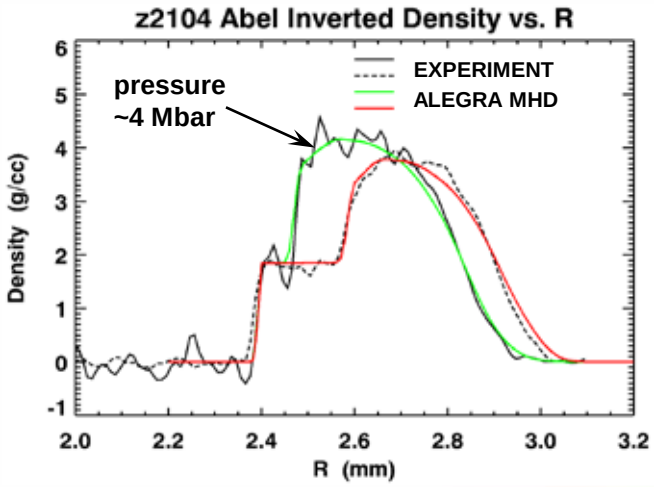

Results are further evidence of quasi-isentropic compression using shaped pulse.

Sandia National Laboratories

Conclusions

- ***Demonstrated that off Hugoniot data can be obtained from x-ray radiographs of an imploding liner.***
  - **Accuracy of results depends on signal-to-noise ratio of radiographs.**
  - **With ZBL 6.151 KeV backlighter limited to pressures < 6 Mbar.**
  - **Method practical on Z for pressures > 6 Mbar depending on backlighter.**
- ***Current shaping for quasi-isentropic compression reduces MRT.***
  - **Liner stays solid longer; large bubble formation delayed.**

Determination of Material Equation of State from Multi-Frame Monochromatic X-Ray Backlighting

Matthew R. Martin

R. W. Lemke, R. D. McBride, M.D. Knudson, and J-P. Davis
Sandia National Laboratories

Sandia is a multiprogram laboratory operated by Sandia Corporation, a Lockheed Martin Company, for the United States Department of Energy's National Nuclear Security Administration under contract DE-AC04-94AL85000.

What information can we infer from high spatial resolution multi-frame monochromatic backlighting?

Radiographs from Liner Experiment

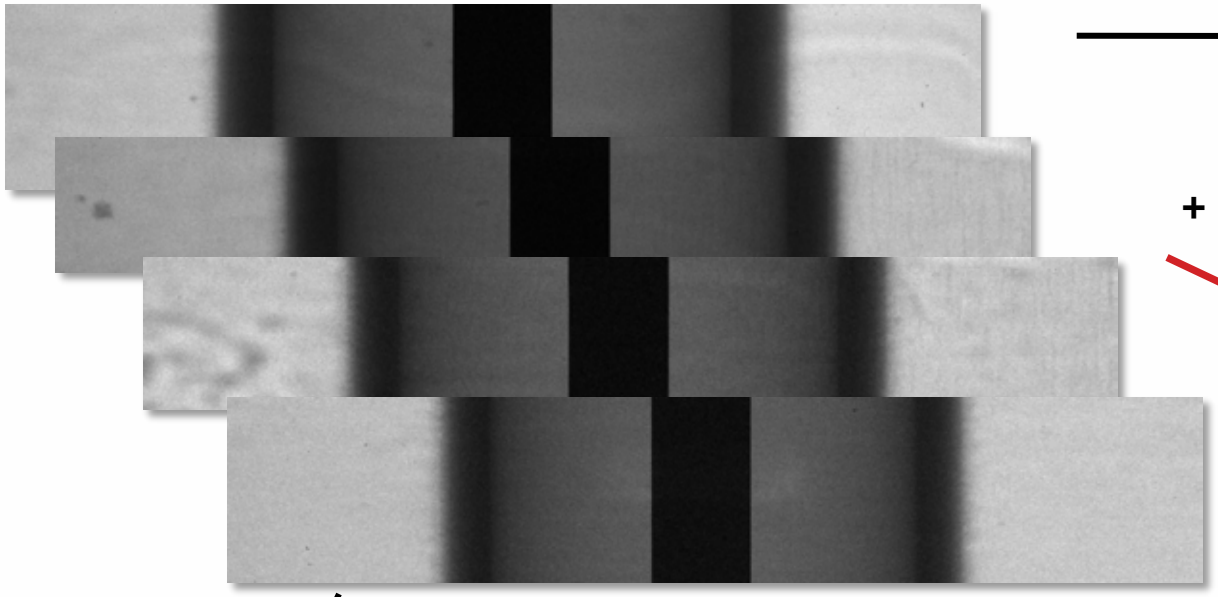

Density

+ Constitutive Relations

- **Magnetic Field?**
- **Phase?**
- **Strength?**

Velocity Profiles

Pressure Profiles

Equation of State

Sandia National Laboratories

Radial Intensity Profile for Backlit Cylinder

- Noise is distributed in two dimensions over image plane
- Linear (but not unique) transformation to density depends locally on the derivative of the intensity
- Assume local symmetry along Z axis and repeatedly sample to reduce spatial variation

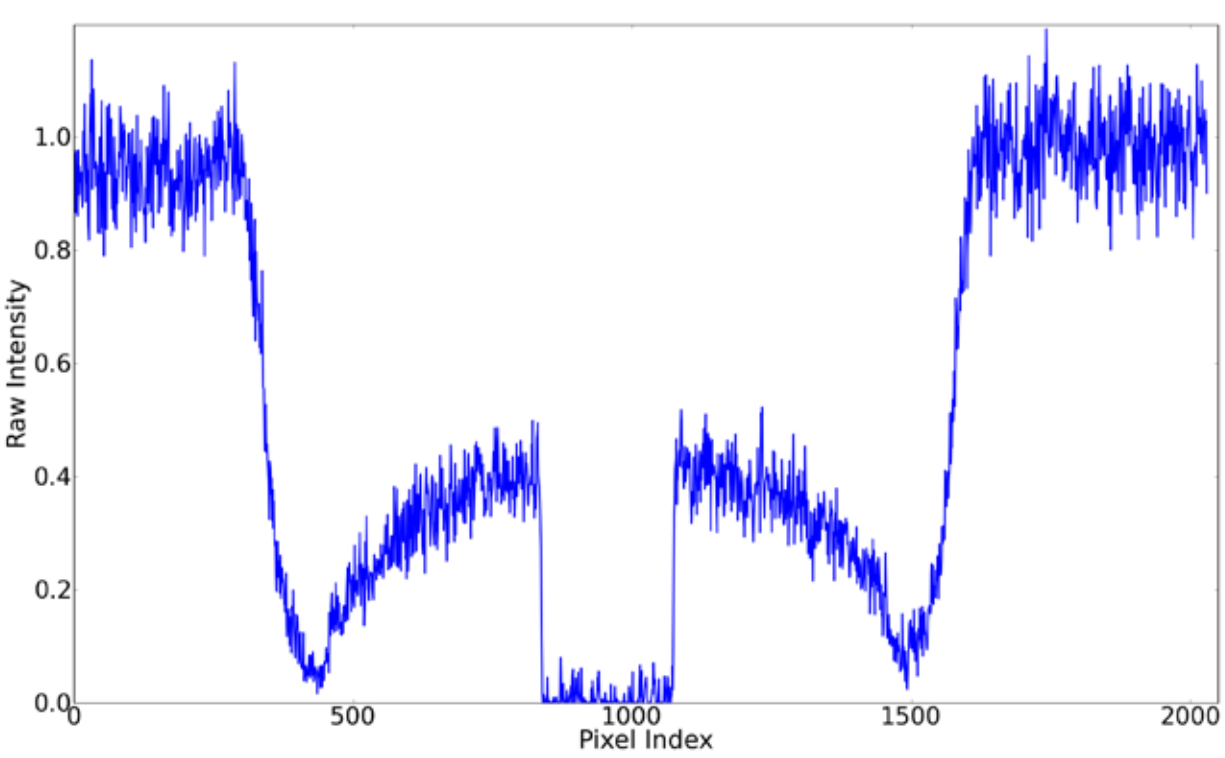

Sandia National Laboratories

Average Intensity(r) for Compressed Cylinder

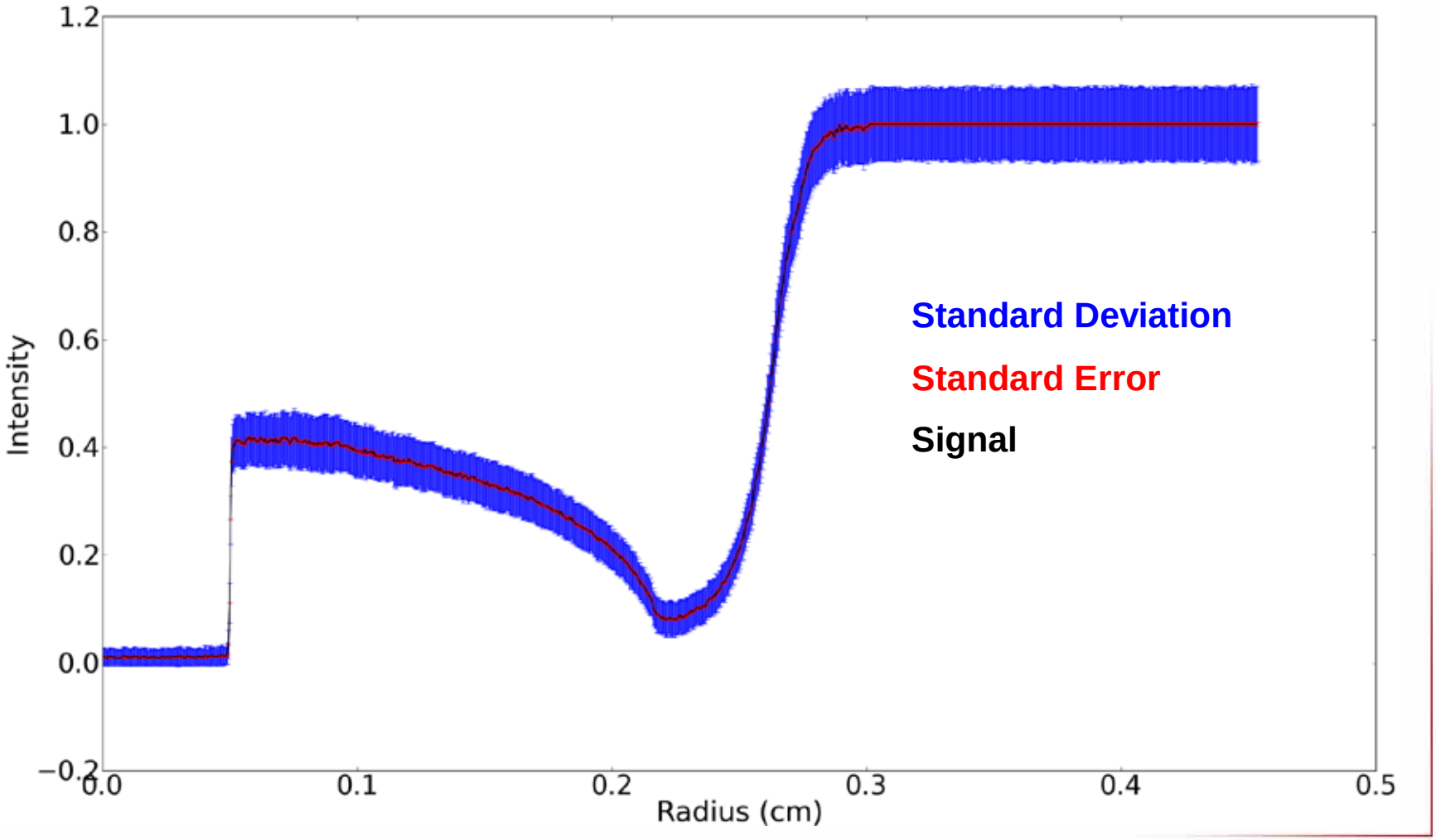

Sandia National Laboratories

Fully Discrete Abel Transform Implementation

- **Two-point Abel deconvolution based on:**
  C.J. Dasch, "One-dimensional tomography: a comparison of Abel, onion-peeling, and filtered back-projection methods", Applied Optics 1992

$$F(r_i) = \frac{1}{\Delta r} \sum_{j=0}^{\infty} \mathbf{D}_{ij} P(r_j)$$

$$\mathbf{D}_{ij} = 0 : j < i$$

$$\mathbf{D}_{ij} \propto j^{-2} : j \gg i$$

- **D is defined by two point interpolation method**

- **F(r) gives κ(r) (cm^-1)**

- **Apply known total mass of the system and monochromatic assumption to solve for mass absorption coefficient (cm^2/g):**

$$\mu = \frac{1}{M_{liner}} \int \kappa(r) dV$$

Sandia National Laboratories

Density Profile for Liner Experiment at Machine Time: 3.030e-06s

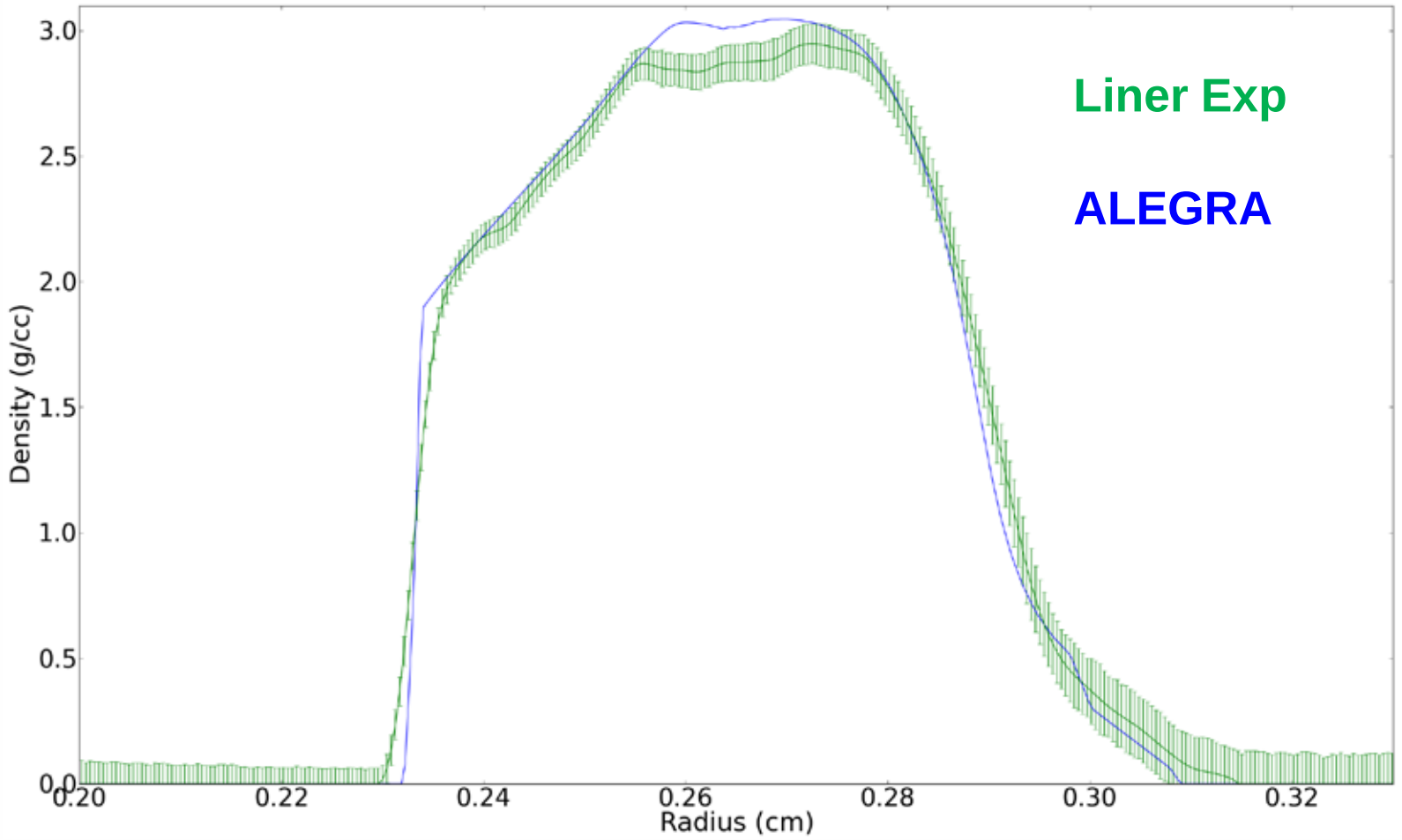

Sandia National Laboratories

Surface Fitting Method for Determination of Isentrope from Multi-Frame Radiography

- **Given a set of continuous density profiles at discrete times t^n**
  - **Assume compressible fluid model in mass coordinates**
  - **Map continuous density profile to discrete particles of constant mass**
  - **Integrate fluid equations to determine radial velocity and total pressure as a function of mass and time**
  - **Use MHD simulation to determine magnetic pressure contribution in the solid material**

$$\frac{D\rho}{Dt} = -\rho\nabla\cdot\mathbf{u}$$

$$\frac{D\mathbf{u}}{Dt} = -\frac{1}{\rho}\nabla P$$

$$m = 2\pi\ L_z \int_0^r \rho r dr$$

$$dm = 2\pi L_z \rho r dr$$

1-D Cylindrical

$$\frac{\partial V}{\partial t} = 2\pi L_z r \frac{\partial u_r}{\partial m}$$

$$\frac{\partial u_r}{\partial t} = -2\pi L_z r \frac{\partial P}{\partial m}$$

Semi-Discrete Equations in Mass Coordinate System

$$\int dP = -\int \frac{1}{2\pi L_z r}\frac{\partial u_r}{\partial t} dm$$

$$\int du_r = \int \frac{1}{2\pi L_z r}\frac{\partial V}{\partial t} dm$$

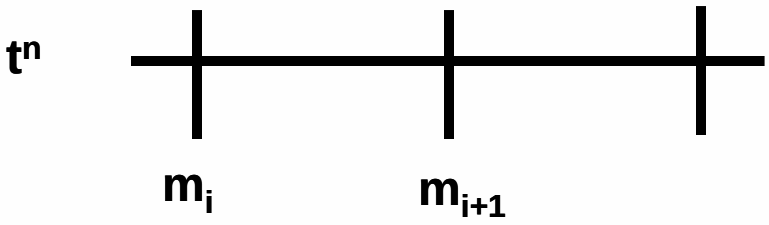

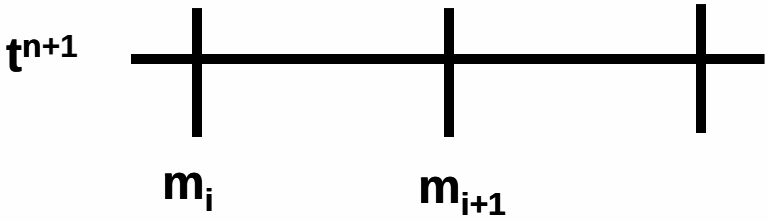

$$u_r(m_{i+1}) = \int_{m_i}^{m_{i+1}} \frac{1}{2\pi L_z r}\frac{\partial V}{\partial t} dm + u_r(m_i)$$

$$P(m_{i+1}) = -\int_{m_i}^{m_{i+1}} \frac{1}{2\pi L_z r}\frac{\partial u_r}{\partial t} dm + P(m_i)$$

Tracking the Trajectory of a Fluid Particle Between Backlighter Frames

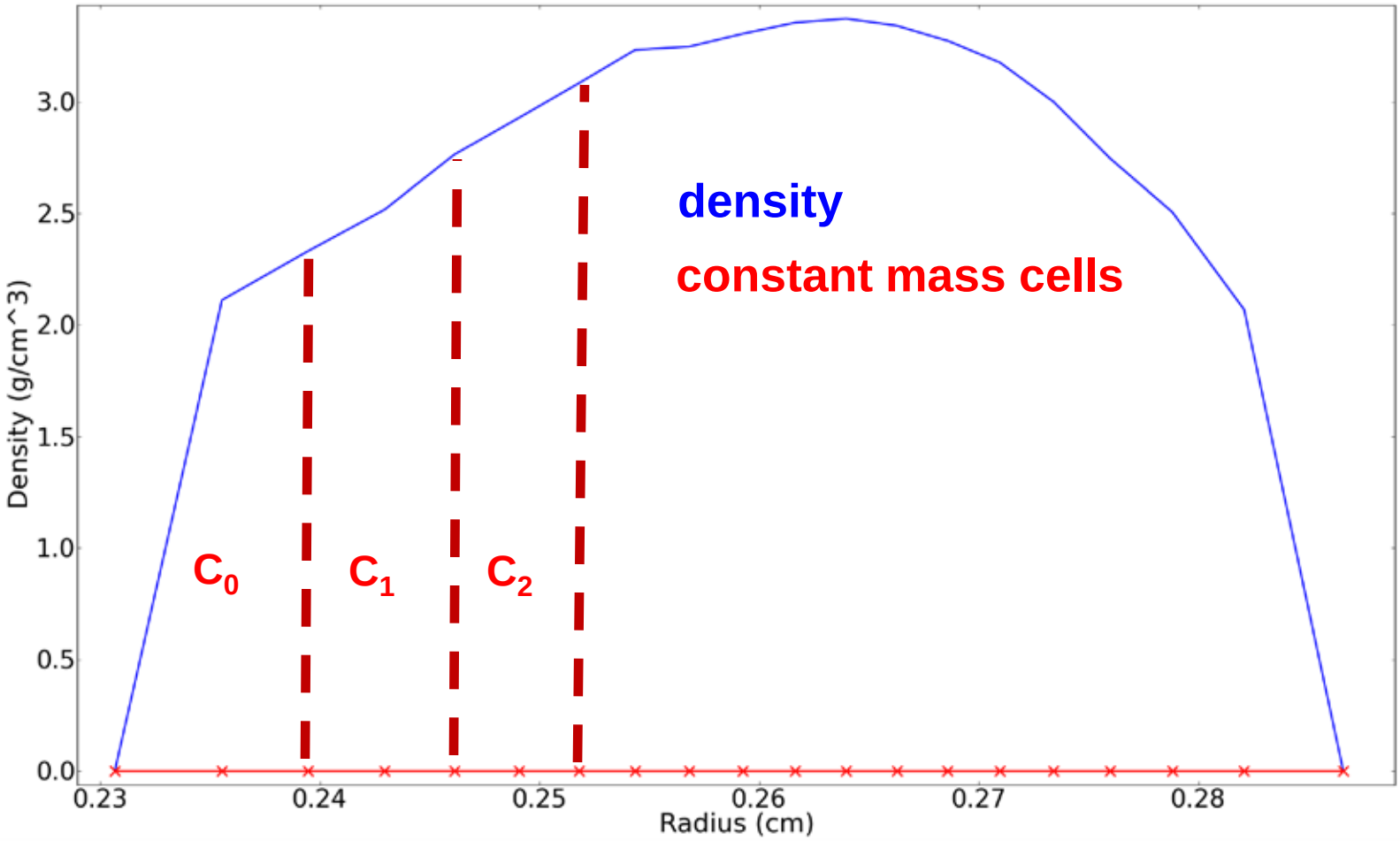

Sandia National Laboratories

Numerical Evaluation of the Discrete Equations

- Map Abel inverted density to mass coordinates
- Time differentiation by uncertainty propagating smoothing spline
- Low order integration over discrete mass cells
- Inner surface velocity boundary condition interpolated from spline fit
- Assumed P=0 inner surface for pressure boundary conditions
- ALEGRA simulation used to determine position of melt boundary

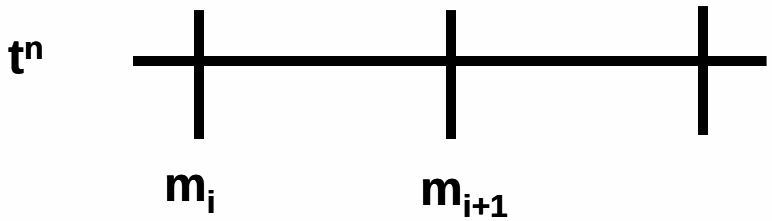

$$u_r(m_{i+1}) = \int_{m_i}^{m_{i+1}} \frac{1}{2\pi L_z r}\frac{\partial V}{\partial t}dm + u_r(m_i)$$

$$P(m_{i+1}) = -\int_{m_i}^{m_{i+1}} \frac{1}{2\pi L_z r}\frac{\partial u_r}{\partial t}dm + P(m_i)$$

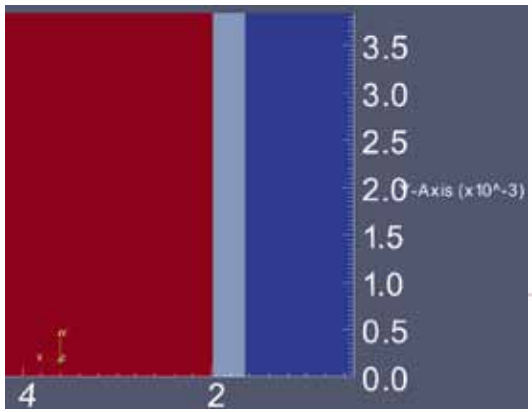

Sandia National Laboratories

The Unfolded Total Pressure Diverges from the Isentrope due to Melt and Magnetic Pressure

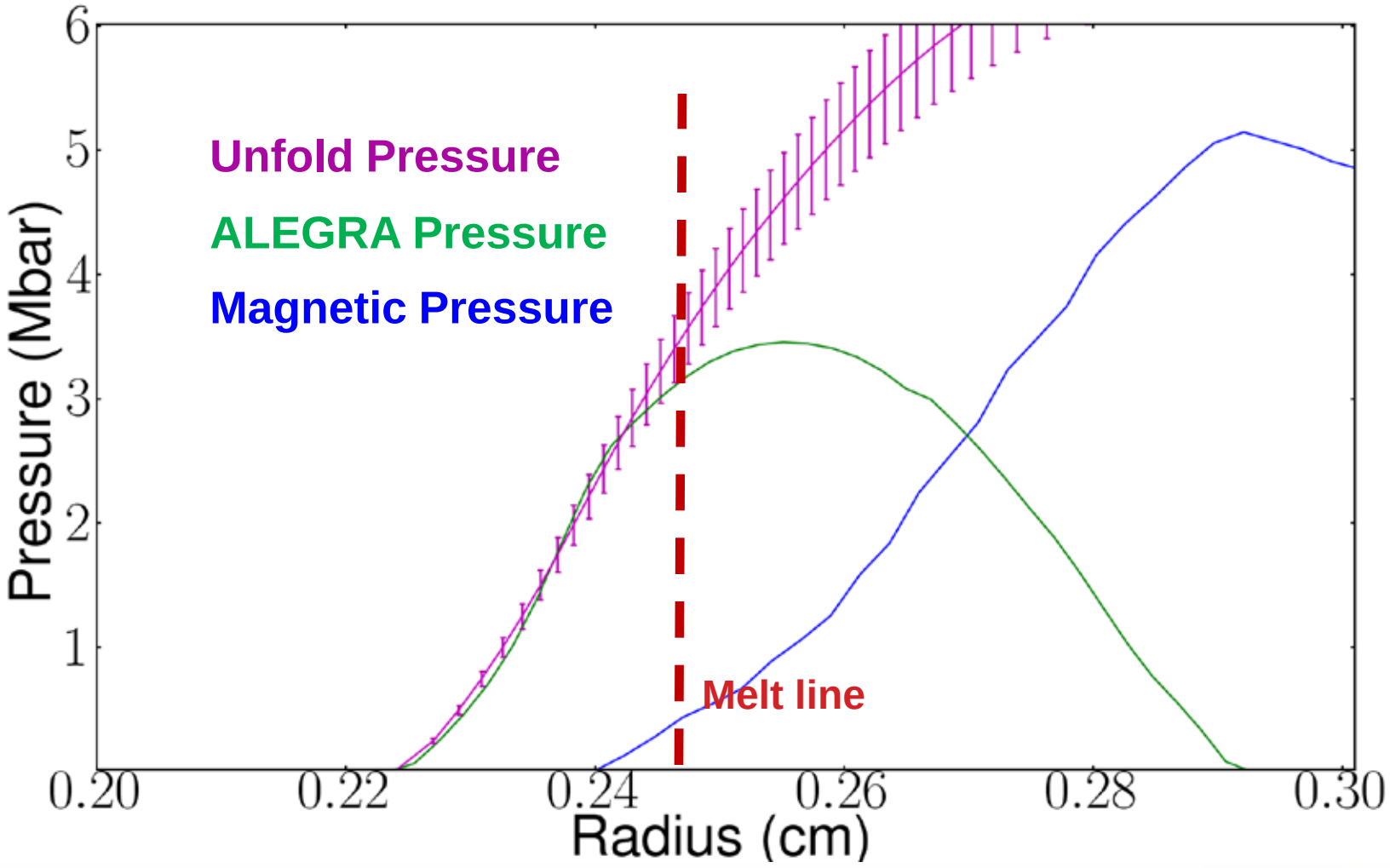

Sandia National Laboratories

Isentrope Determined from Five Frame Unfold of ALEGRA Simulated Density Profiles

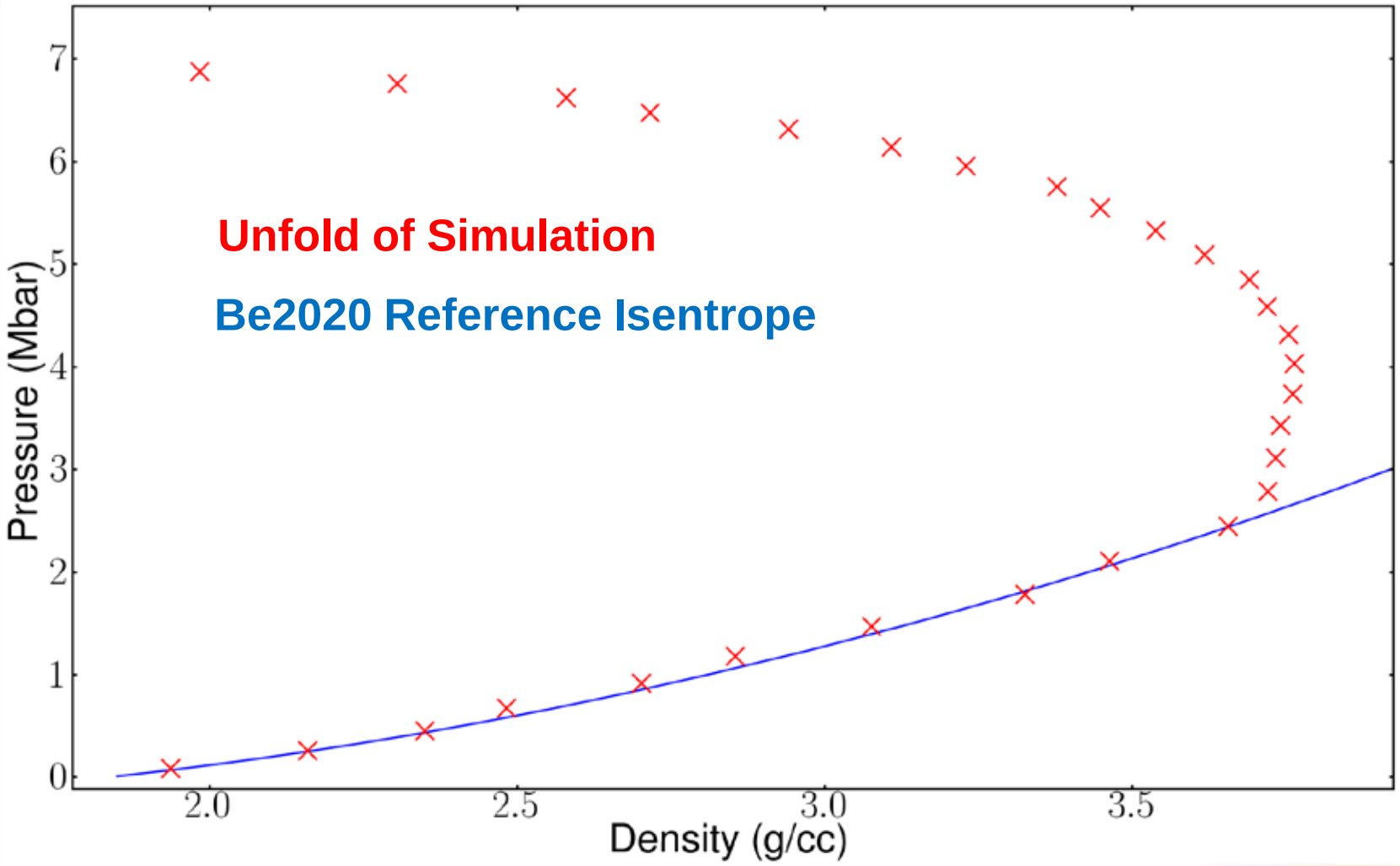

Sandia National Laboratories

Unfolded Isentrope for Liner Experiment

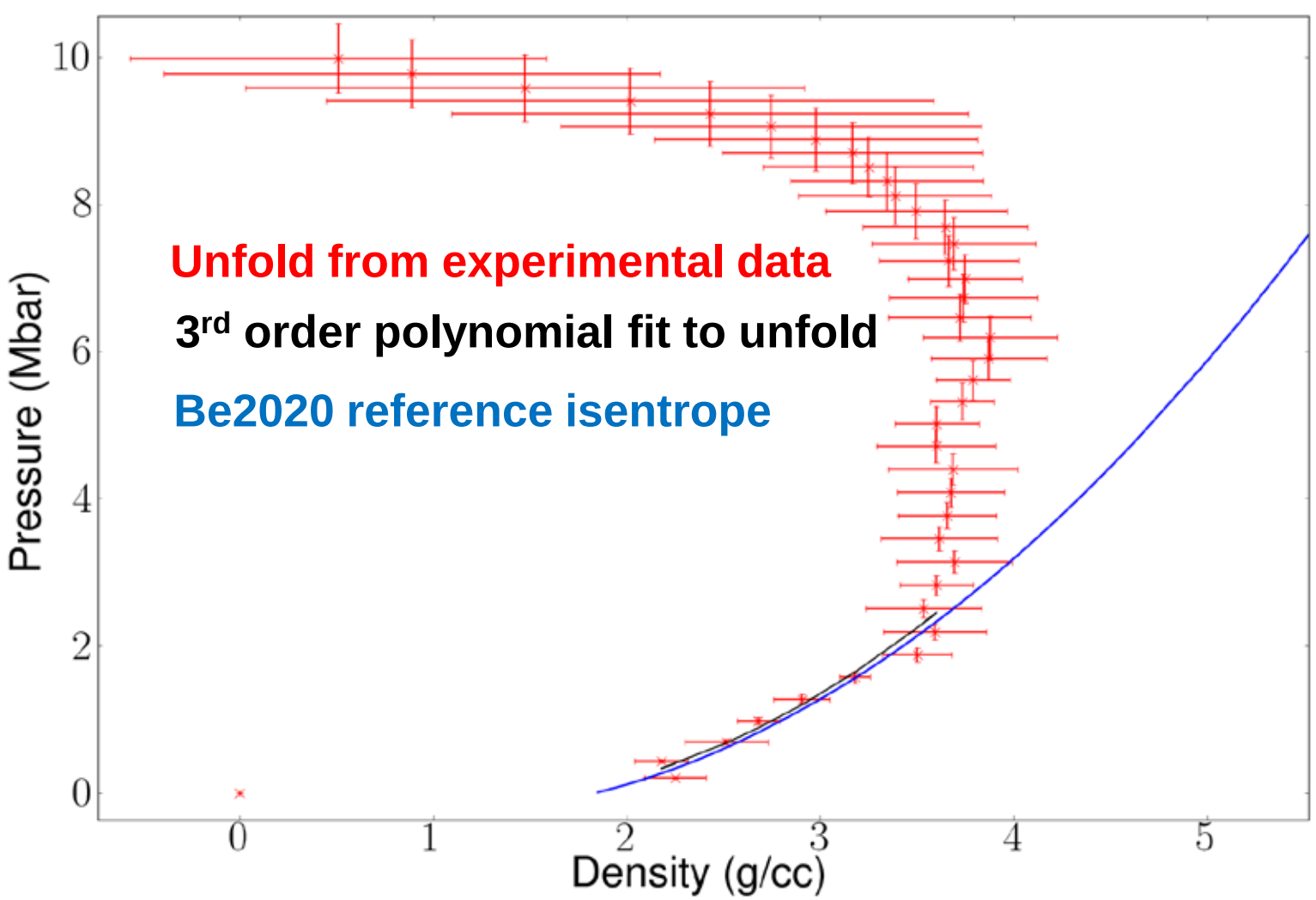

Sandia National Laboratories

Unfolded Isentrope for Liner Experiment

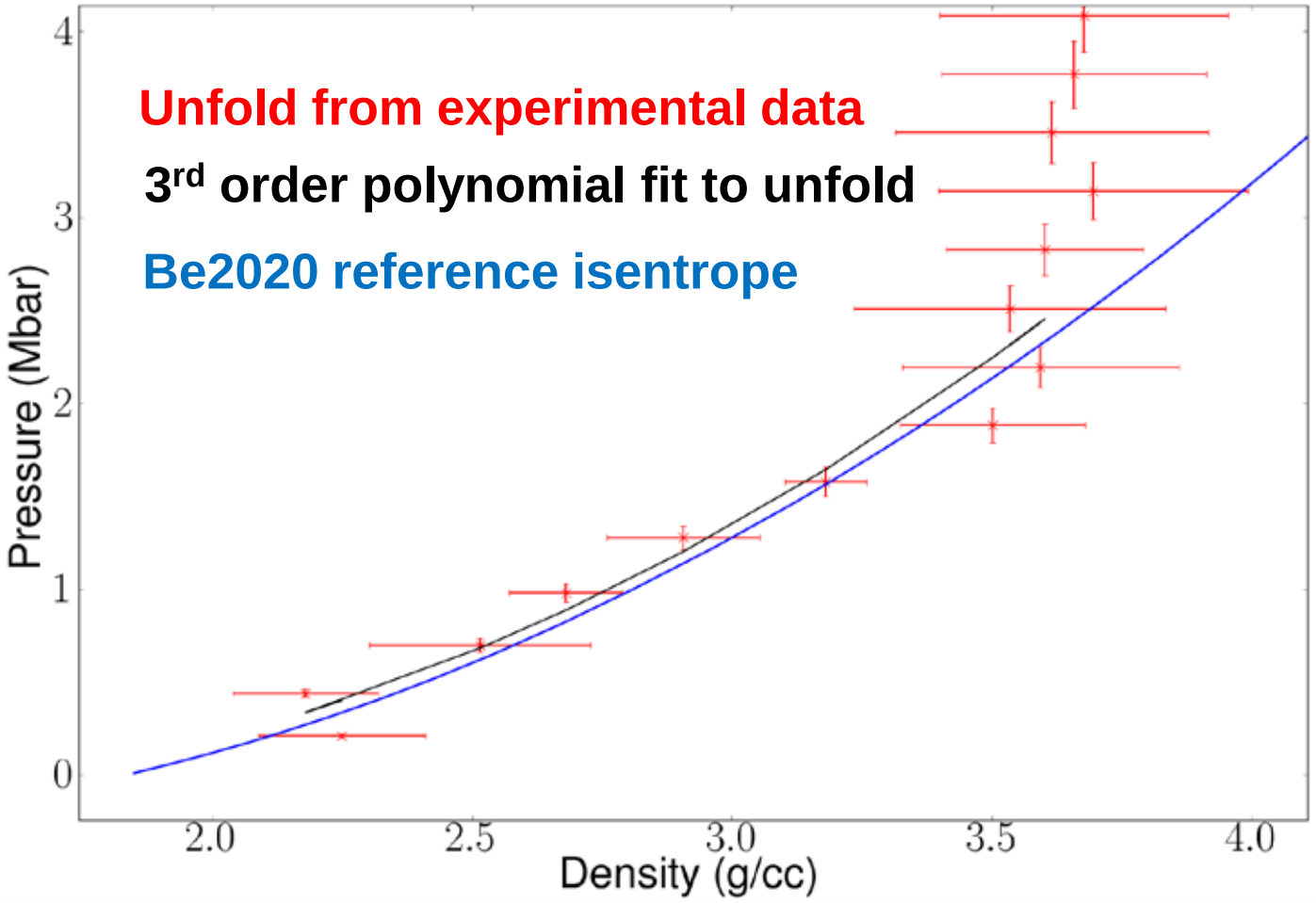

Sandia National Laboratories

ALEGRA Simulation is Used to Design a Cylinder that Implodes while Maintaining a Solid Inner Core

t ~3.046E-6s

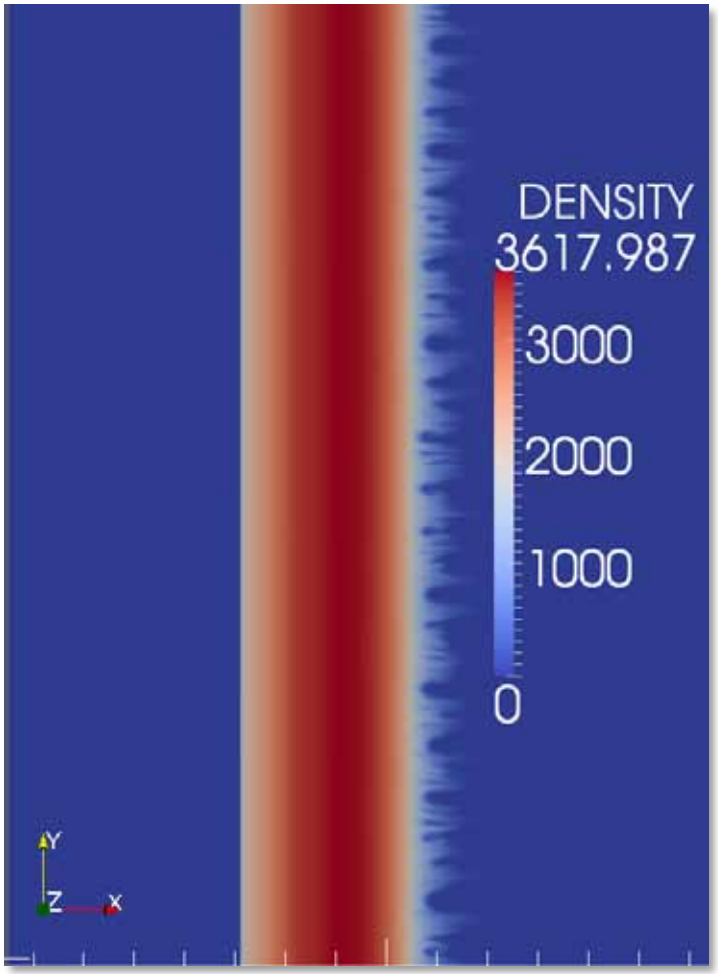

2 mm

t ~3.069E-6s

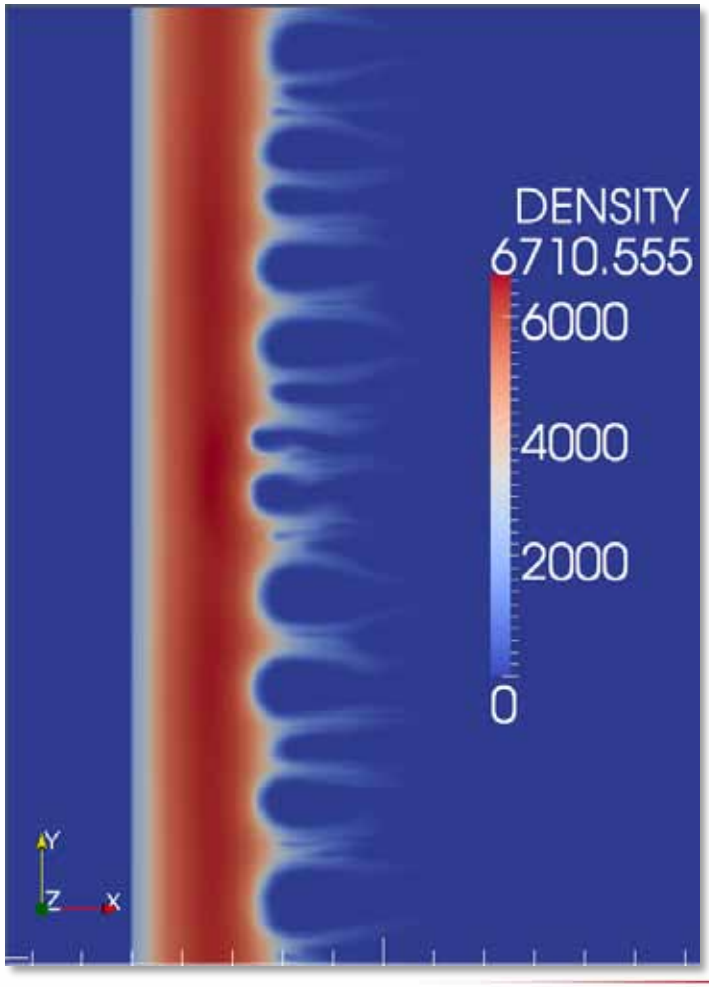

2 mm

Sandia National Laboratories

Synthetic Radiography of 2D ALEGRA Simulation Shows the Impact of MRT Instability on the Intensity Profiles

P* ~ 4Mbar

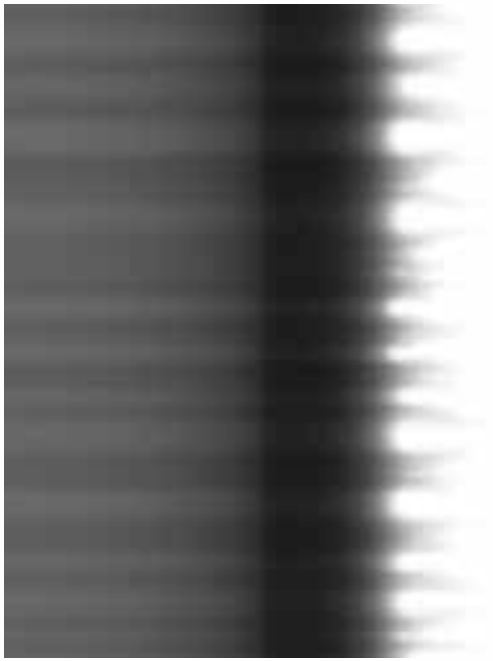

t ~3.060E-6s

P* ~ 8Mbar

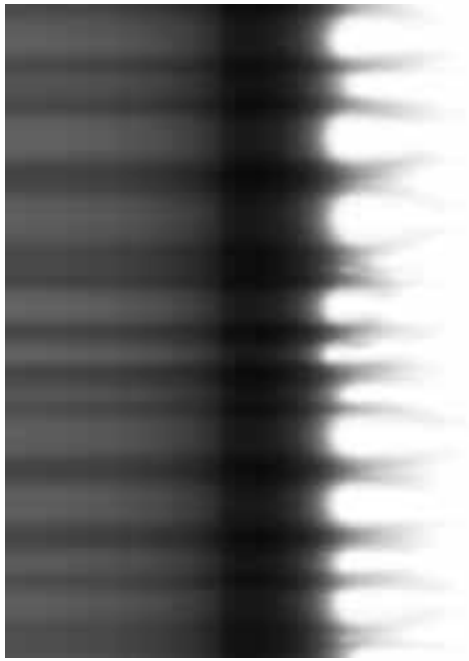

t ~3.069E-6s

P* ~ 12Mbar

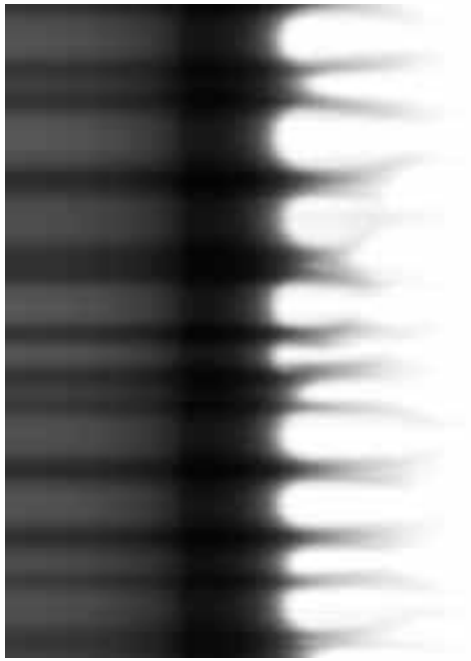

t ~3.075E-6s

P* -> Peak Pressure in Solid Phase

Sandia National Laboratories

Background Noise is Applied to Synthetic Radiographs

Intensity

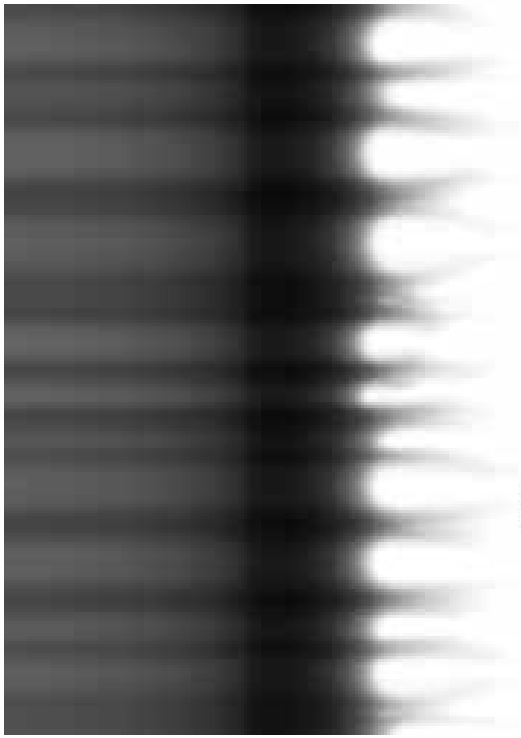

Sampled Noise

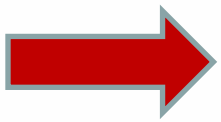

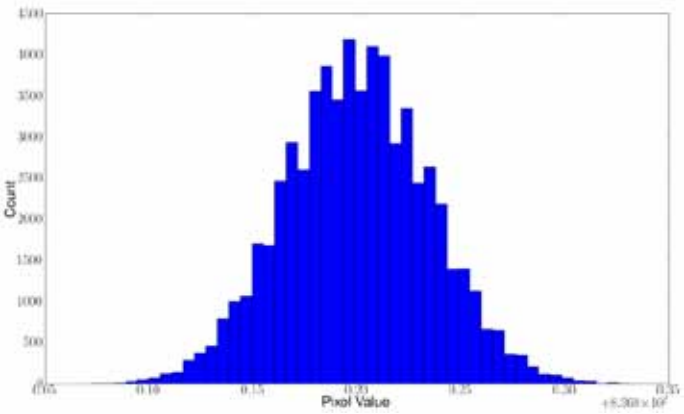

Intensity

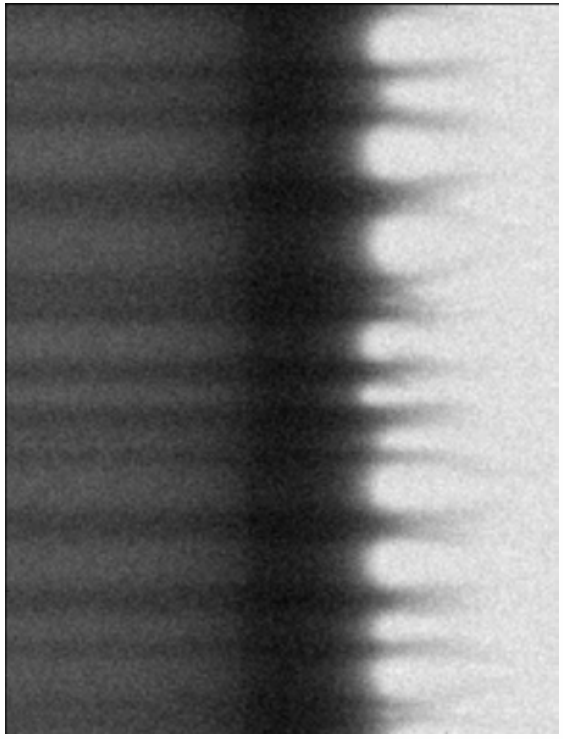

t ~3.069E-6s

t ~3.069E-6s

Sandia National Laboratories

Abel Inversion of Synthetic Radiograph

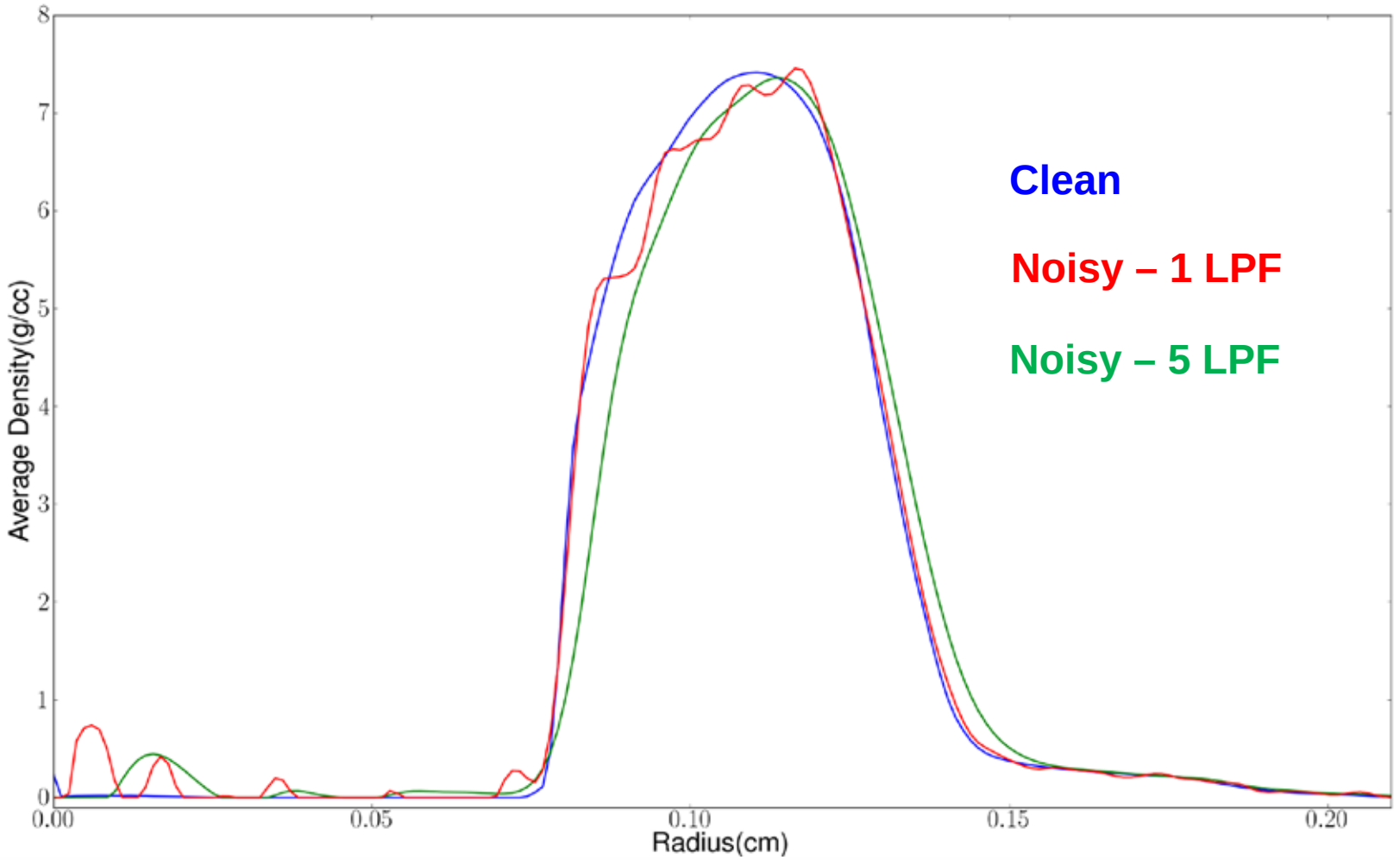

Sandia National Laboratories

Liner Unfolded Pressure at Fifth Frame in Sequence

Synthetic 2D frames with Liner Exp 1 noise at machine times: 3us+[60,63,65,67,69,71,73,74,75]ns

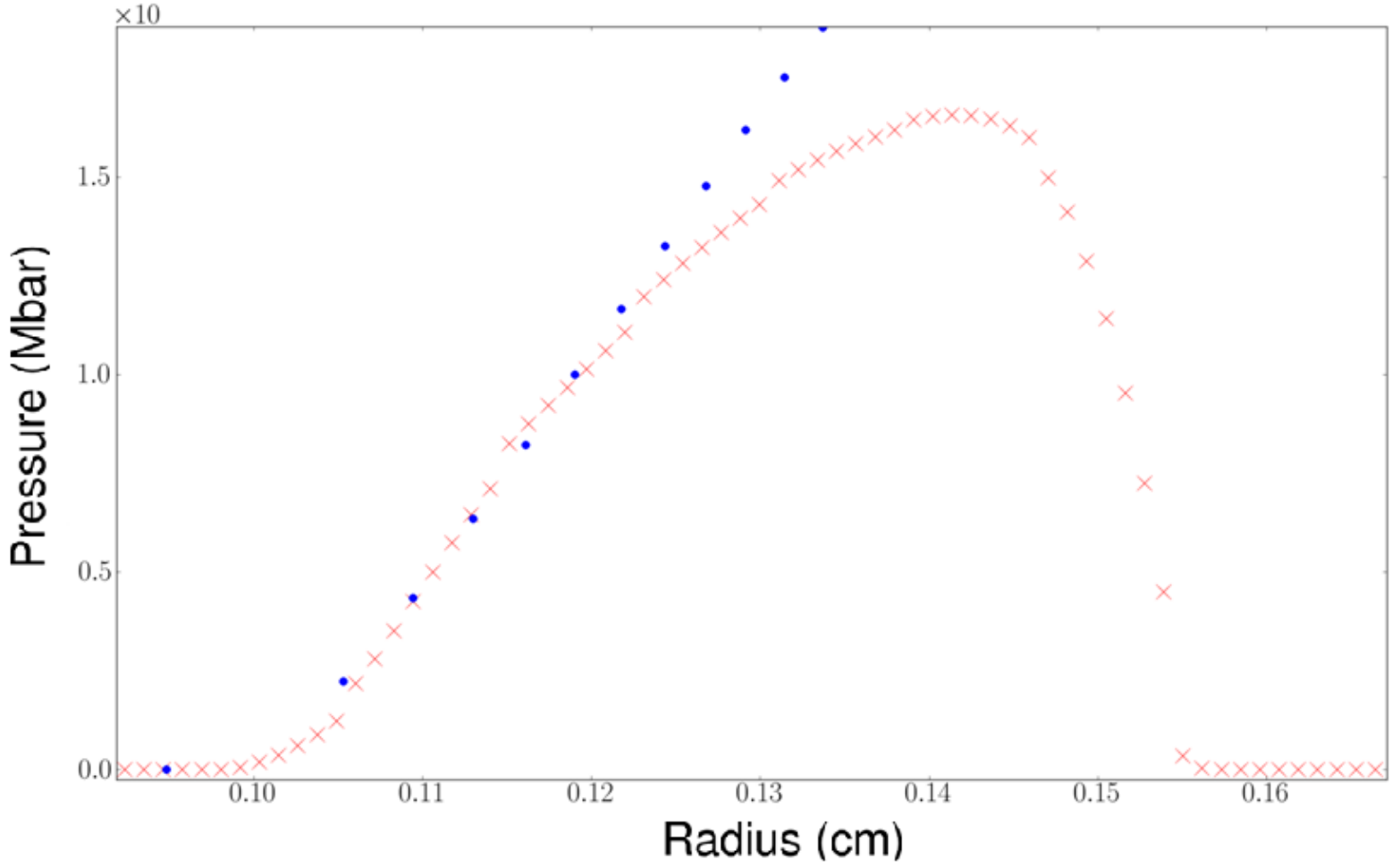

t~3.069E-6s

Sandia National Laboratories

Conclusions

- Monochromatic x-ray backlighting in conjunction with surface fitting analysis yields information on the total pressure in the system
- The dominant mechanisms for determining uncertainty in pressure profile with this method are:
  - Signal to noise ratio of the measured intensity profile
  - Diffusion of the magnetic field into the solid
  - Location of the melt transition
  - Spacing of radiographs in time
- Cylindrical convergence allows for larger pressures than flyer-plate experiments at the cost of limited diagnostic access and larger uncertainty in the unfolded equation of state
- Evidence of highly magnetized solid beryllium at multi-megabar pressures

Sandia National Laboratories

Magnetically Applied Pressure-Shear (MAPS):

A New Method for Direct Measurement of Strength at High Pressures

C. Scott Alexander,

Thomas A. Haill,

and James R. Asay

Dynamic Material Properties &

HEDP Theory Departments

Sandia National Laboratories

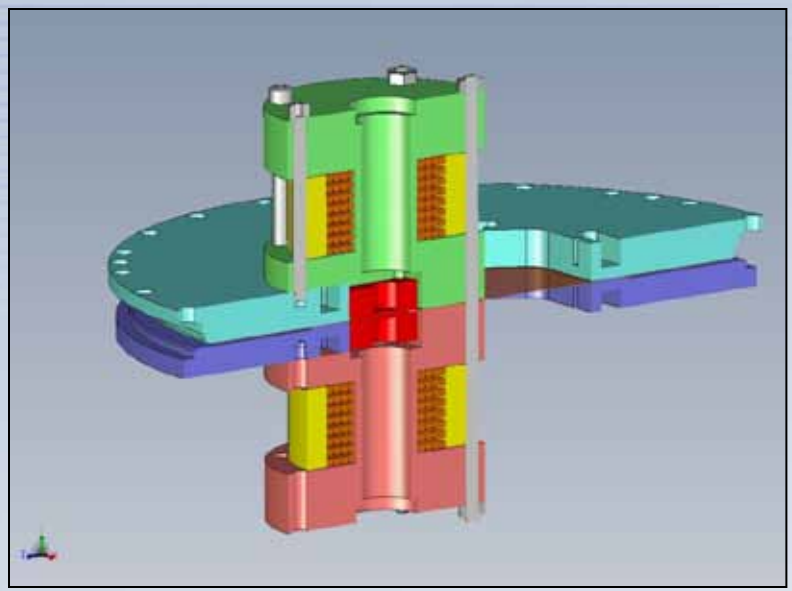

Presented at the 4th Workshop on Ramp Compression

Sandia National Laboratories, Albuquerque, NM

January 18-19, 2011

Outline

- **Motivation**
- **Overview of the MAPS approach to strength measurement**
  - Principles of operation
  - Implementation on the Veloce Small Pulser
  - Design considerations
- **ALEGRA simulations of the experimental configuration**
  - Simulation parameters
  - Predicted experimental results
  - Stress coupling
- **Experimental results**
  - Initial measurements on aluminum
  - 2D material response of zirconia
- **Summary**

Motivation for MAPS

- **Measure strength of materials at high pressures**
  - Ability of a material to sustain deviatoric (shear) stresses
  - Critical aspect of material behavior
- **MAPS is:**
  - New experimental approach
  - Crossed magnetic fields simultaneously produce both longitudinal and shear stresses
  - Higher pressures possible than with traditional methods
  - Data reduction does not rely on computer models as in Rayleigh-Taylor techniques
- **Applications:**
  - Armor
  - Weapons design
  - Inertial Confinement Fusion
  - Planetary science

C. S. Alexander, J. R. Asay and T. A. Haill, Magnetically applied pressure-shear: A new method for direct measurement of strength at high pressure, JAP, 108, 126101 (Dec 2010).

Operating principles behind the MAPS technique

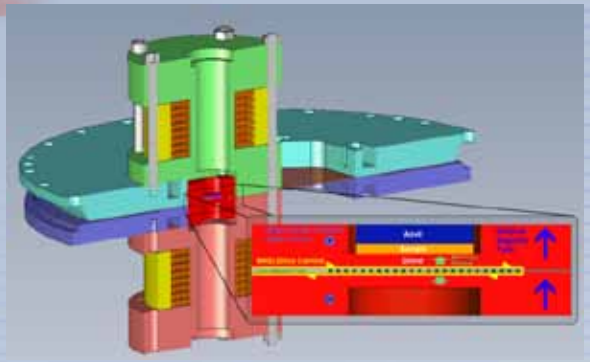

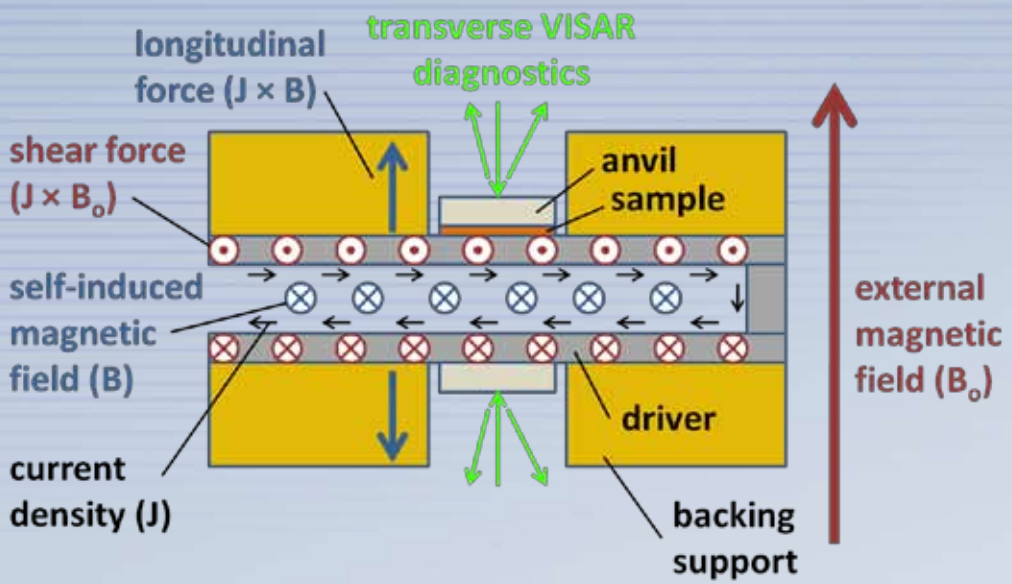

1. A pulsed power drive generates current (J) in parallel panels and induces a magnetic field (B) between the panels
2. The interaction J×B produces a pressure wave which compresses the material
3. A large (10T, ~10^5 times Earth's field) external magnetic field (B_o) is applied
4. The interaction J×B_o produces a shear wave in the driver (panel)
5. The generated shear wave propagates through the sample material where it is truncated to a level determined by the sample strength
6. Specialized VISAR interferometry is used to record both longitudinal and transverse particle velocities
7. Pressure and strength are calculated from the measured particle velocities

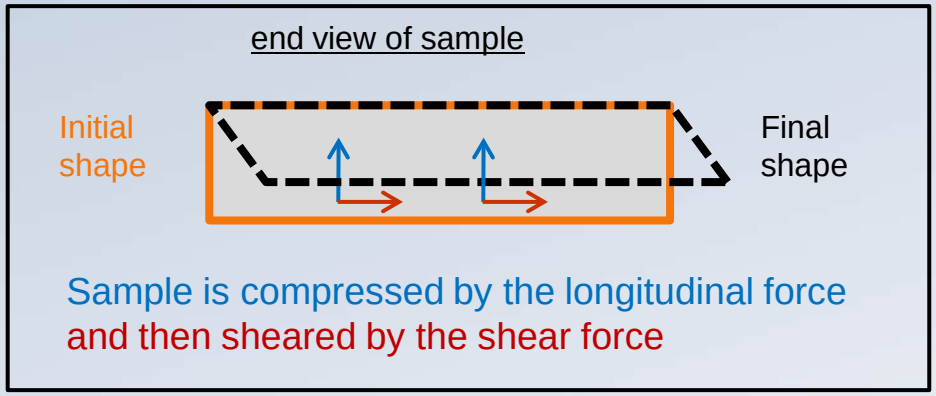

MAPS: a novel method to measure shear strength at high pressure

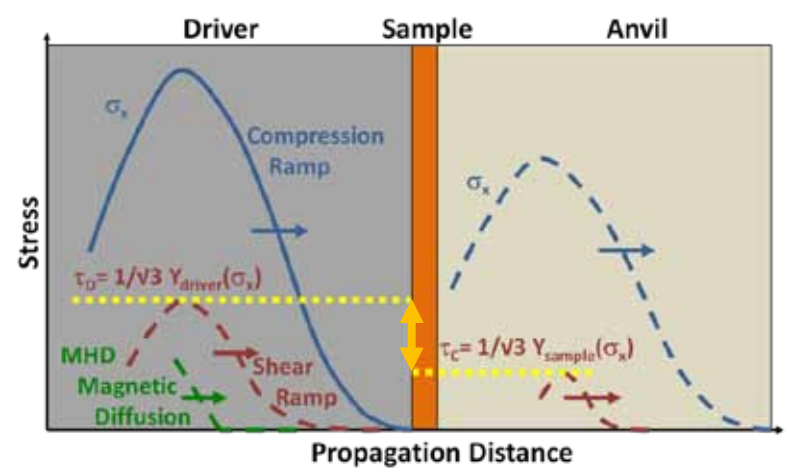

- Sample is compressed by longitudinal wave to high pressure
- Shear wave is produced in driver by interaction of drive current and an external magnetic field
- Maximum shear that can be transmitted through sample limited by von Mises yield criterion

$$\tau \leq 1 / \sqrt{3}\, Y(\sigma_x)$$

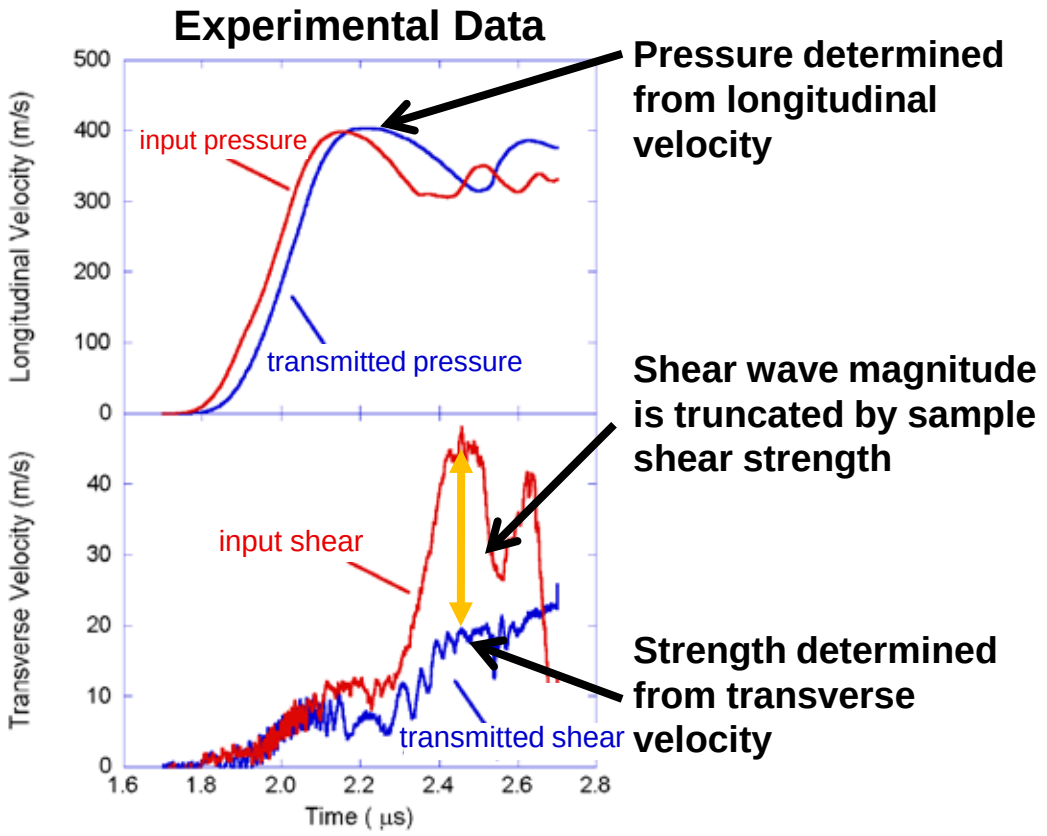

- Strength determined directly from longitudinal and shear particle velocities measured at anvil free surface using VISAR

LDRD LABORATORY DIRECTED RESEARCH & DEVELOPMENT

Sandia National Laboratories

Notional View of the MAPS Experimental Implementation

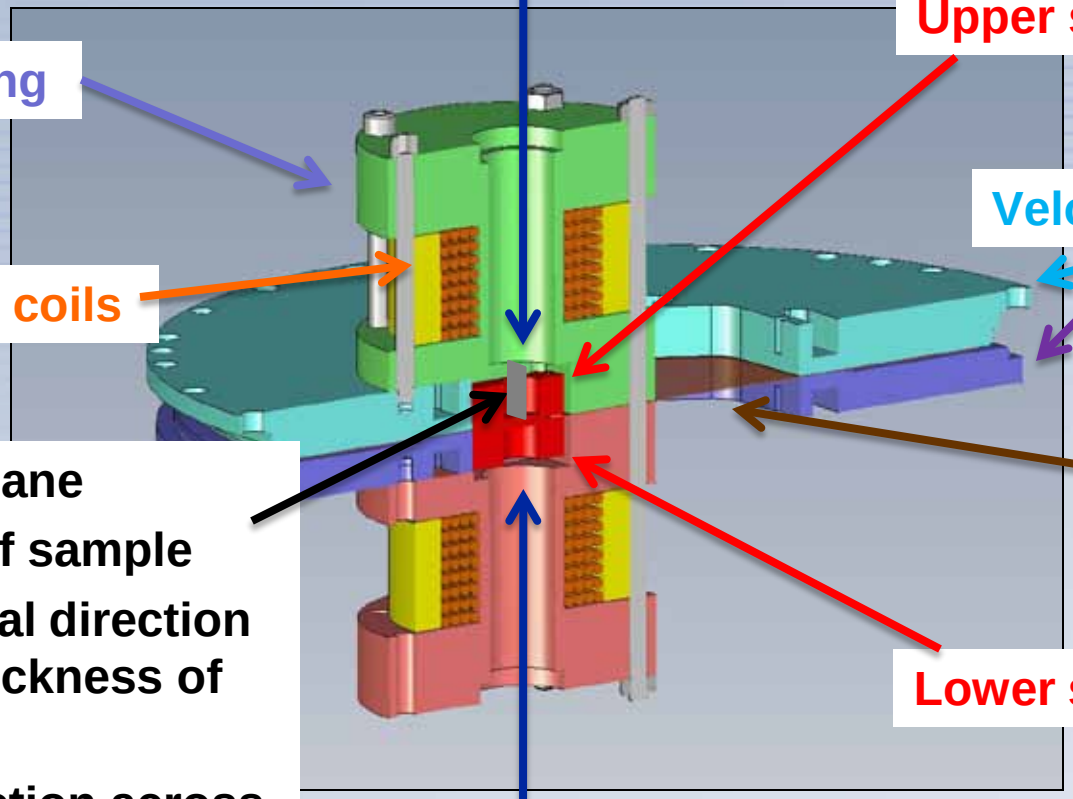

- Simulation plane
  - At center of sample
  - Longitudinal direction through thickness of panel (x)
  - Shear direction across width of panel (y)

MAPS Experiments on the Veloce Small Pulser

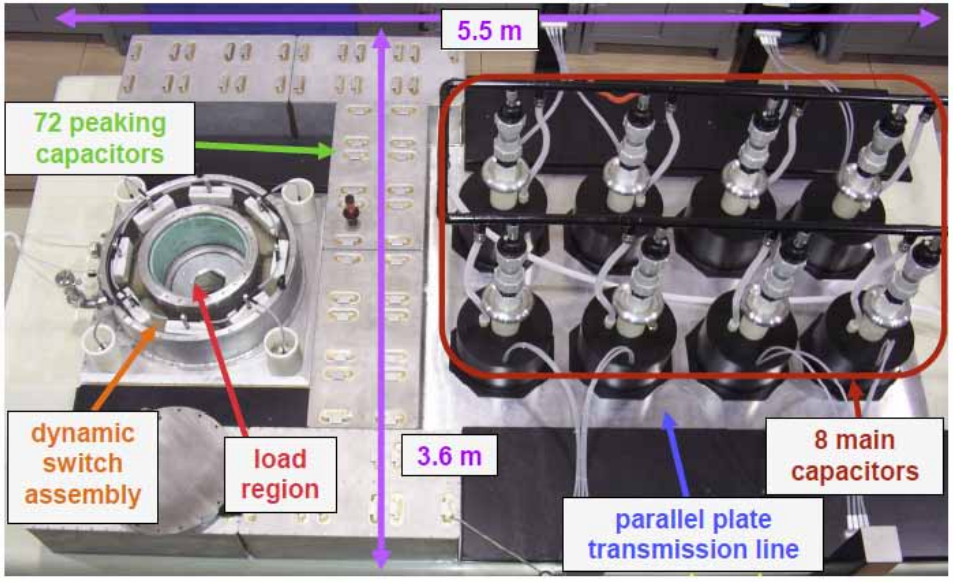

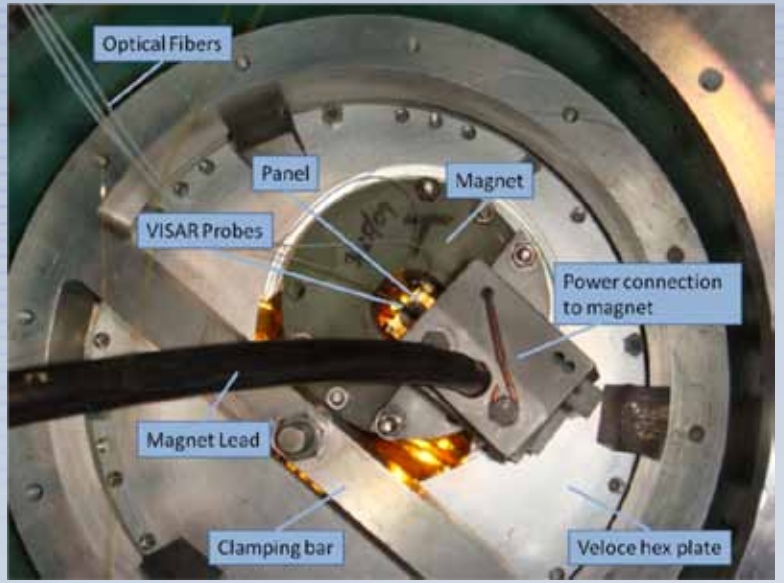

- **MAPS developed on SNL's Veloce pulser**
  - 2.5 MA, 2 μs current pulse
  - ~10 GPa sample pressures
  - 10 mm diameter, 50-100 μm thick sample sizes

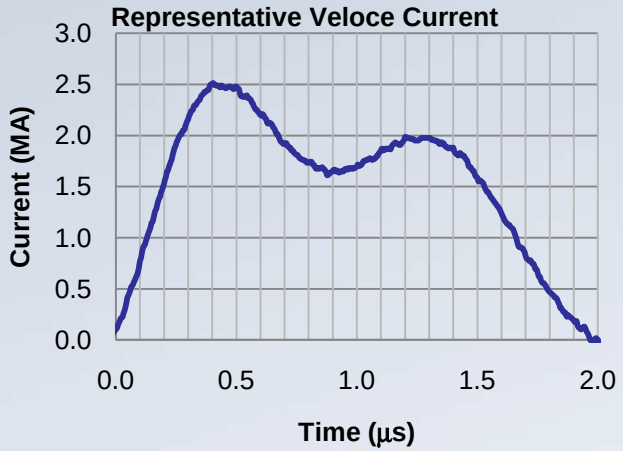

T. Ao, et al., A compact strip-line pulse power generator for isentropic compression experiments, RSI, 79, 013903 (2008).

LDRD LABORATORY DIRECTED RESEARCH & DEVELOPMENT

Sandia National Laboratories

Design of Driver Panel: Desired Properties of Driver Material

- **High Yield Stress**
  - Shear stress generated by $J \times B_o$ limited by driver yield stress
- **High Melt Temperature**
  - Remain solid
  - Efficiently couple magnetic forces into driver
- **High Conductivity (Low Resistivity)**
  - Increase drive current for given capacitor bank charge
  - Inhibit magnetic diffusion (MHD drive) into driver
- **Low Density**
  - Magnetic forces able to accelerate panels

Design of Anvil Panel: Desired Properties of Anvil Material

- **High Yield Stress**
  - Do not limit material stresses received from test sample
    - Anvil strength must exceed sample strength at measurement pressures
  - Propagate high longitudinal and shear stresses (velocities) to free surface with little attenuation
  - Avoid spall
- **High Melt Temperature**
  - Remain solid
- **Low Conductivity (High Resistivity)**
  - Allow faster permeation of external B_o field
  - Inhibit current flow into anvil

Materials of Interest: Initial Material Parameters

sample

driver

anvils

Z	Material	Density (g/cm^3)	Melt Temperature (K)	Yield Stress (GPa)	Poisson Ratio	Conductivity $(\mu\Omega*cm)^{-1}$
13	Aluminum	2.7	933	0.29	0.33	0.377
22	Titanium	4.54	1933	0.85	0.30	0.024
26	Iron (304 SS) (V-250 SS)	7.87	1808	(0.34) (1.56)	(0.283) (0.283)	0.103
29	Copper	8.96	1356	0.12	0.33	0.598
42	Molybdenum	10.22	2890	1.6	0.375	0.192
47	Silver	10.50	1235	0.05	0.37	0.629
73	Tantalum	16.65	3269	0.77	0.30	0.080
74	Tungsten	19.3	3683	2.20	0.30	0.177
79	Gold (Cu)	19.32	1338	0.02 (0.63)	0.42	0.425
92	Uranium	18.95	1405	0.40	0.30	0.033
	Diamond	3.52	~ 3820	35 - 91	0.104	$< 10^{-8}$
	Sapphire	3.97	~ 2326	14 - 18	0.18 – 0.29	$< 10^{-1}$
	Zirconia (YTZP)	6.026	~ 2988	8.5	0.3124	$< 10^{-8}$

Physics Models in ALEGRA - a 3D/2D Radiation Magneto-Hydrodyanmics code

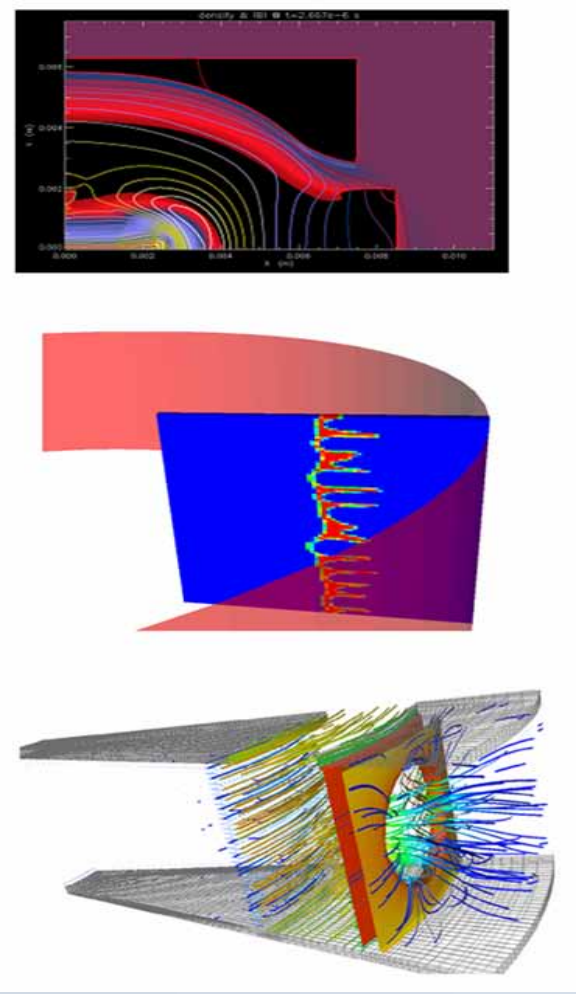

- **2D (RZ & XY) and 3D (XYZ)**
- **Unstructured Finite-Element Based**
- **Eulerian/Lagrangian/ALE**
- **Object Oriented**
- **Massively Parallel**
- **Isentropic Multi-Material**
- **Coupled Physics**
  - Hydrodynamics
  - Magnetics
  - Thermal Conduction
  - Radiation (Multi-Group Diffusion & IMC)
- **Material Models**
  - LANL Sesame & other EOS
  - Lee-More-Desjarlais (LMD) Conductivity
  - XSN & Propaceos Opacities

A. C. Robinson, et al., "ALEGRA: An Arbitrary Lagrangian-Eulerian Multimaterial, Multiphysics Code," AIAA 2008-1235, 46th AIAA aerospace Science Meeting and Exhibit, Reno, NV, Jan. 2008.

ALEGRA Material Models

Material	Equation of State	Strength Model	Conductivity Model
Molybdenum	KEOS Sesame ANEOS 2984	CTH Elastic-Plastic Steinberg-Guinan	Lee-More-Desjarlais (LMD)
Aluminum	SNL Sesame 3720	CTH Elastic-Plastic Steinberg-Guinan	Lee-More-Deslarlais (LMD)
Zirconia	Mie-Gruneisen Us-Up EOS	CTH Elastic-Plastic High Yield Strength	Constant Electric & Thermal Conductivity

Notional View of the MAPS Experimental Implementation

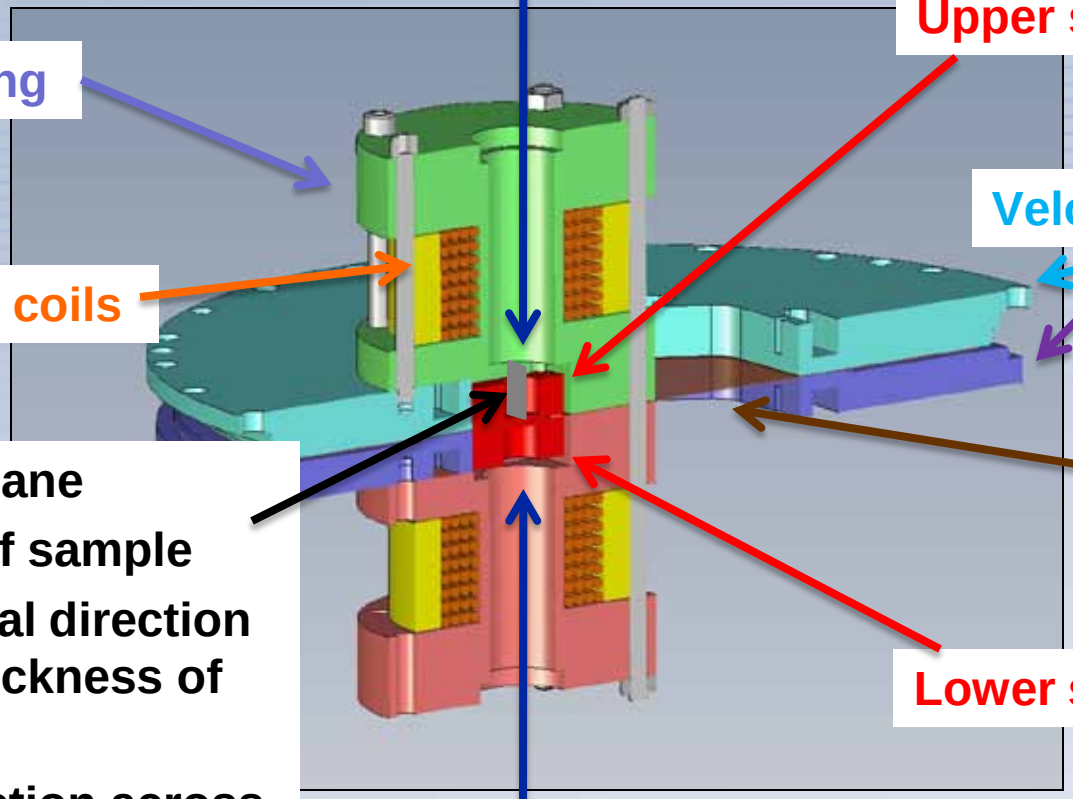

- Simulation plane
  - At center of sample
  - Longitudinal direction through thickness of panel (x)
  - Shear direction across width of panel (y)

ALEGRA Modeling of MAPS Experiments

$$B(t) = f(t)\,\frac{\mu_0\, I(t)}{W + G}$$

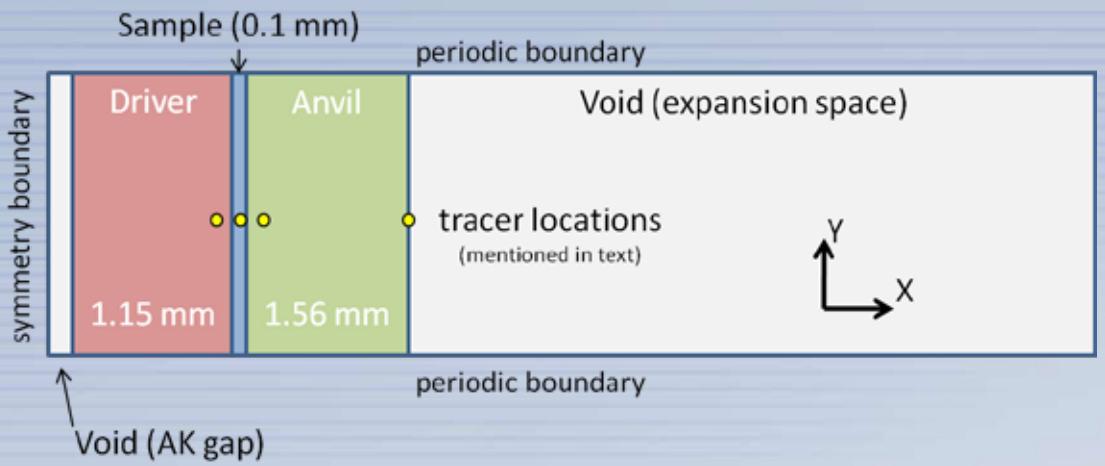

- Assume sufficient uniformity near center of sample
- 2D Cartesian Eulerian mesh
  - 5 - 10 μm cell size
- Periodic mesh in transverse or shear direction (Y)
- Uniform, static B_0 magnetic field in longitudinal direction (X)
- Current driven tangent magnetic field applied at AK gap

- Stripline BC
  - *W* = panel width
  - *G* = AK gap
- Current density out of the plane of mesh
- Lagrangian tracers throughout
  - Most significant tracers shown

Stress Coupling

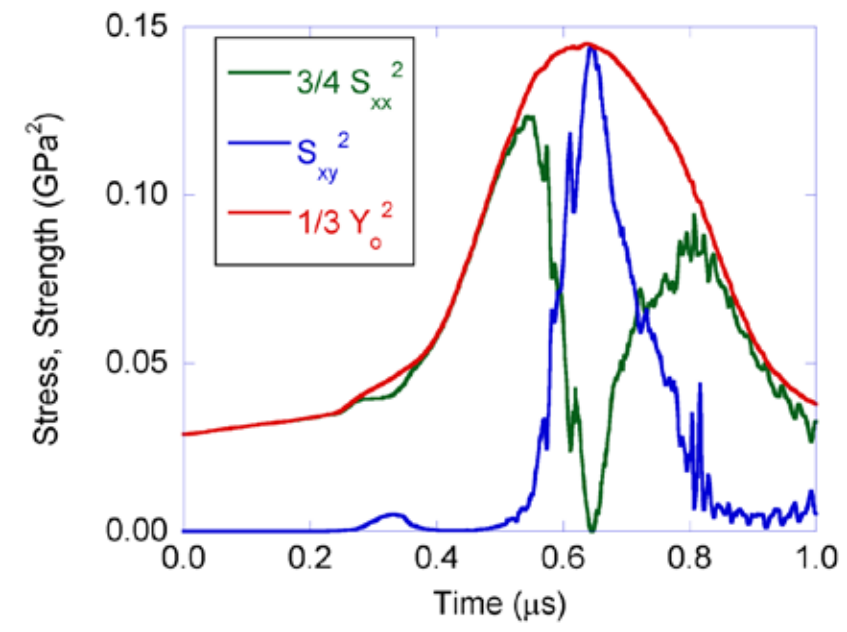

- **For inelastic materials, deviatoric longitudinal and shear stress are:**
  - Coupled through yield function
  - Limited by maximum yield stress
- **Sample probed at peak yield stress**
  - Forward shear wave arrives at sample during peak compression
- **Due to coupling, S_{xx} reduced to zero at yielding**

$$\frac{1}{3} Y_0^2 = \frac{3}{4} S_{xx}^2 + S_{xy}^2$$

Y_0 = Yield Stress

S_{xx} = Longitudinal stress deviator

S_{xy} = Shear stress deviator

J.W. Swegle and L.C. Chhabildas, “Chapter 25: A Technique for the Generation of Pressure-Shear Loading Using Anisotropic Crystalls,” pp. 401-415, in M.A. Meyers and L.E. Murr, Shock Waves and High Strain Rate Phenomena in Metals, Plenum Press, NY, 1981.

Transmission of shear at interface

- **We conducted an investigation of surface roughness on shear transmission at a boundary**
- **Geometry**
  - Molybdenum driver – (partial)
  - Glue layer – 1 μm thick
  - Aluminum sample – (partial)
  - Mesh cell size – 0.05 μm
- **Interface**
  - 1, 2 or 3 μm peak-to-valley roughness
  - 2 μm wavelength
- **Traction boundary condition**
  - Determined from MHD simulation

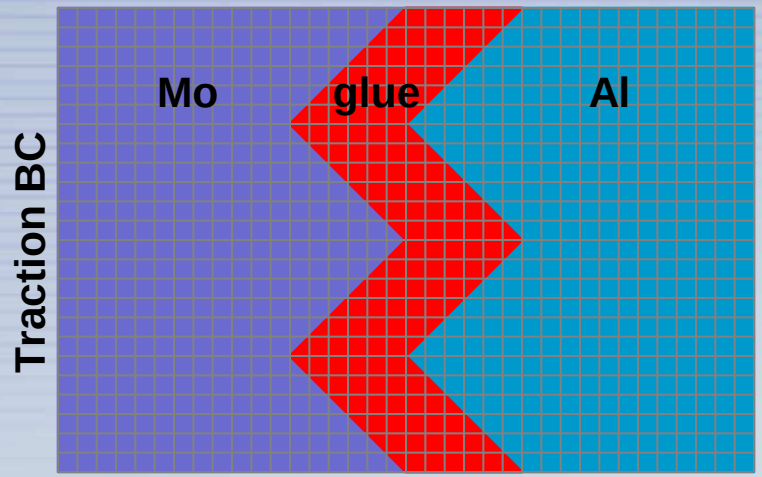

- **Results**
  - No reduction in shear through this range of parameters
  - Glue compressed by longitudinal stress
  - Shear transmitted by interlocking peaks and valleys of surface roughness

MHD Simulation Results: Free Surface Velocity

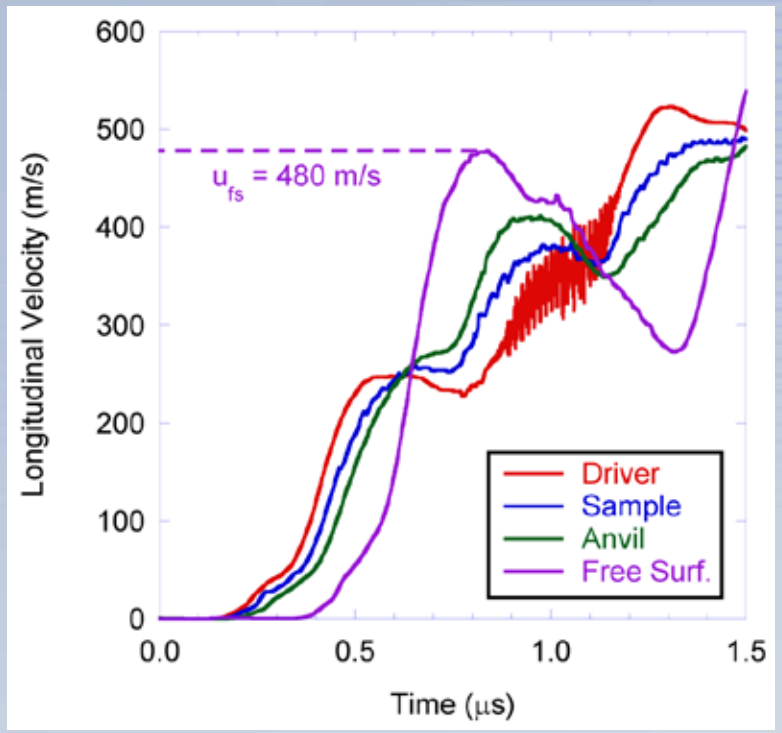

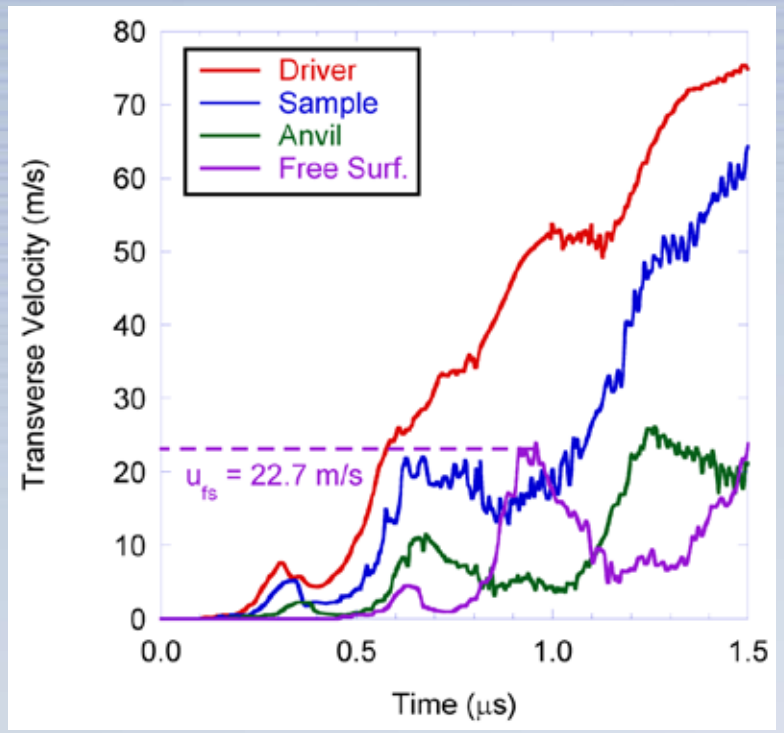

Longitudinal Free Surface Velocity

u_L = 0.480 km/s

C_L = 7.99 km/s

Shear Free Surface Velocity

u_S = 0.0227 km/s

C_S = 5.56 km/s

LDRD LABORATORY DIRECTED RESEARCH & DEVELOPMENT

Sandia National Laboratories

MHD Simulation Results: Tracer Longitudinal and Shear Stresses

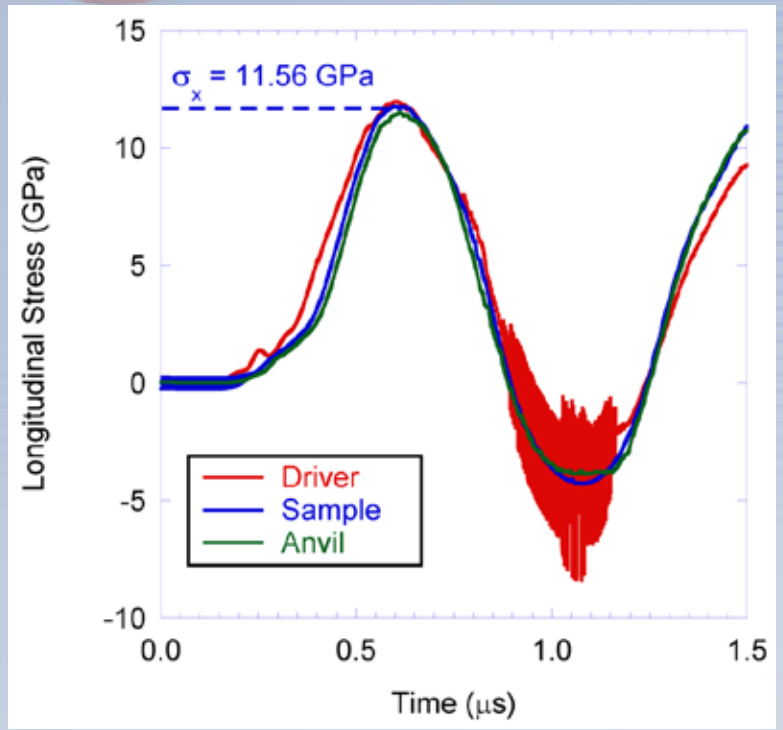

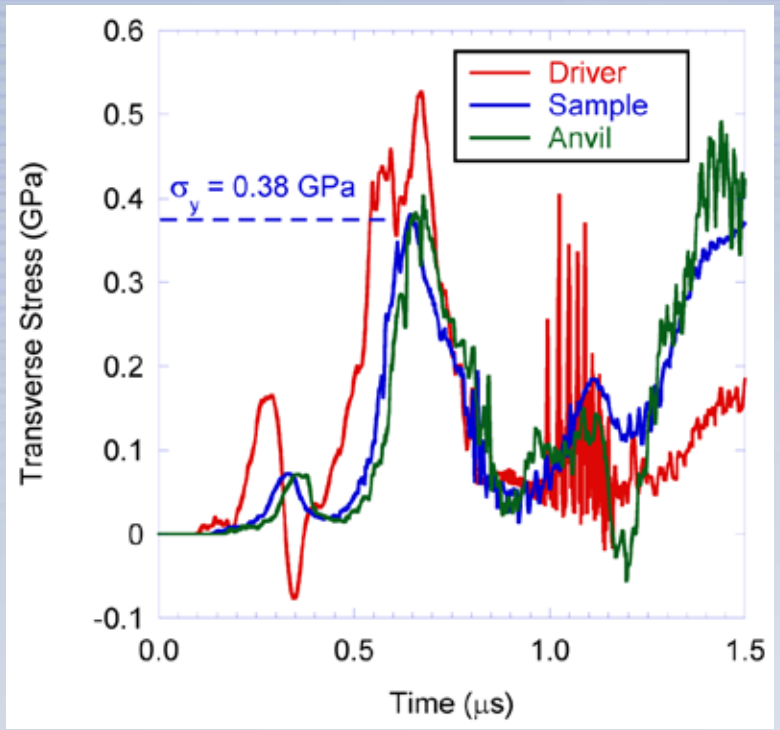

Simulated Longitudinal Stress

$\sigma = \rho C_L U_{PL} = \frac{1}{2} \rho C_L V_L$

σ = 11.56 GPa

Simulated Shear Stress

$\tau = \rho C_S U_{PS} = \frac{1}{2} \rho C_S V_S$

τ = 0.38 GPa

$Y = \sqrt{3}\,\tau = 0.661$ GPa

$Y_{SGL} = 0.660$ GPa

Self-consistent

LDRD Laboratory Directed Research & Development

Sandia National Laboratories

Initial MAPS experiments measure aluminum strength at 8.85 GPa

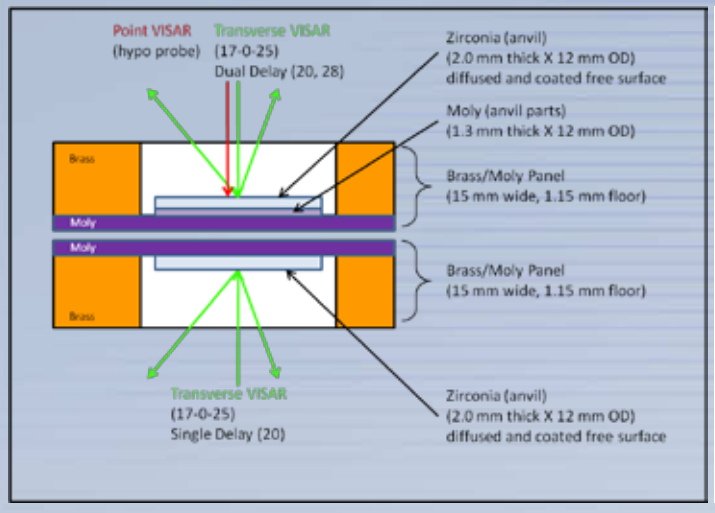

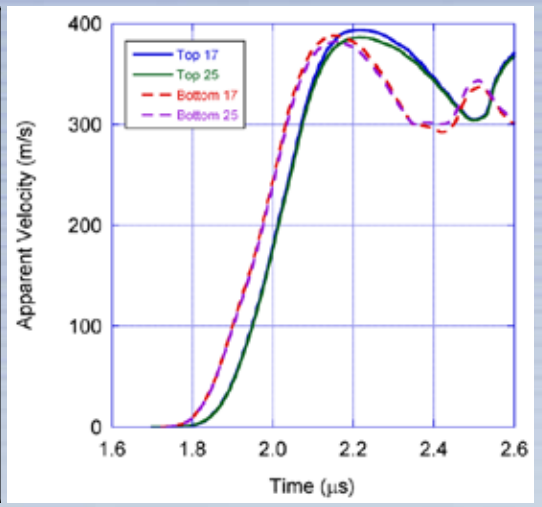

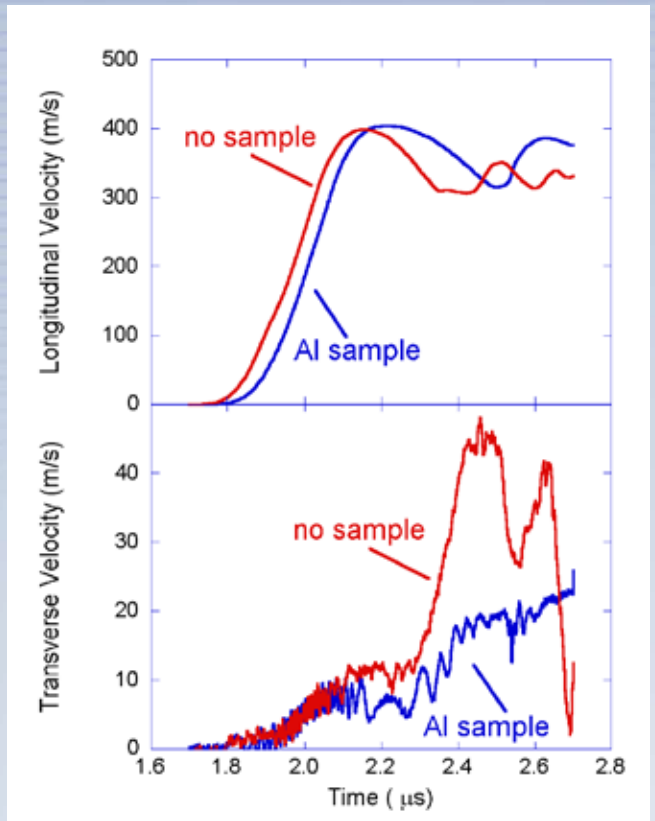

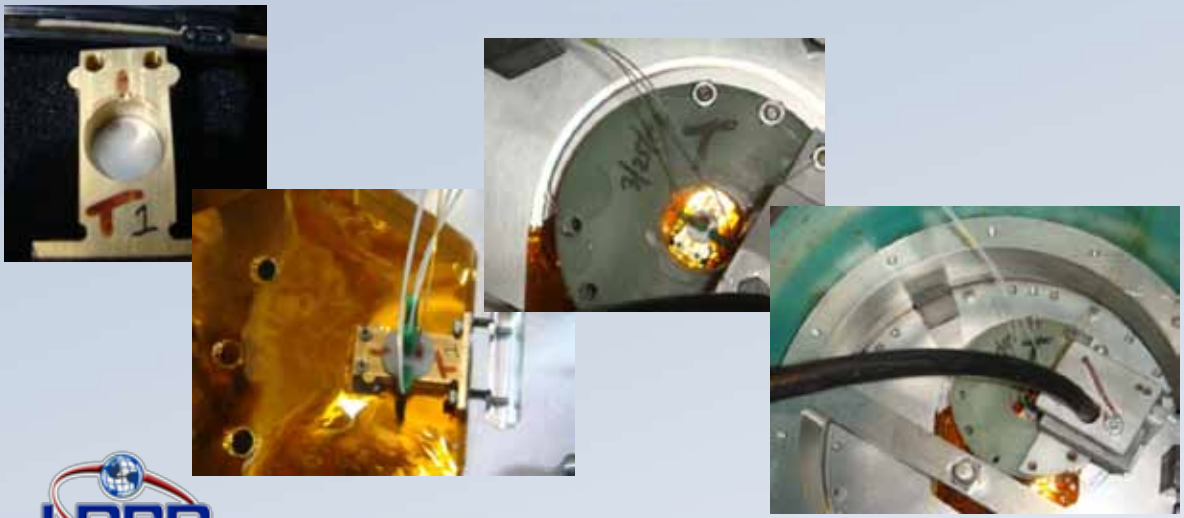

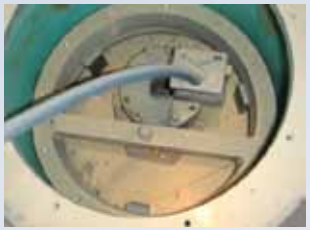

LDRD
LABORATORY DIRECTED RESEARCH & DEVELOPMENT

Sandia National Laboratories

Transverse VISAR velocity determination

$$v_1^* = \frac{\cos(\theta_1)+1}{2} v_x - \frac{\sin(\theta_1)}{2} v_y$$
$$v_2^* = \frac{\cos(\theta_2)+1}{2} v_x + \frac{\sin(\theta_2)}{2} v_y$$

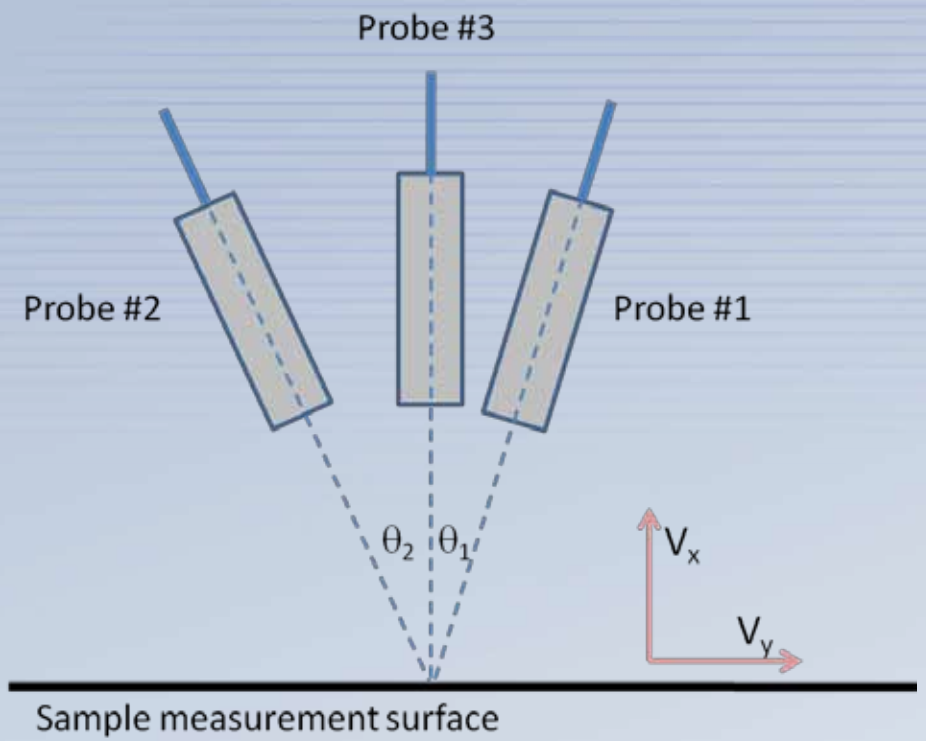

$$G_1 = \frac{1}{2}(\cos\theta_1 + 1)$$
$$G_2 = \frac{1}{2}(\sin\theta_1)$$
$$G_3 = \frac{1}{2}(\cos\theta_2 + 1)$$
$$G_4 = -\frac{1}{2}(\sin\theta_2)$$
$$F_1 = G_1 - \left(\frac{G_1 G_3}{G_4}\right)$$
$$F_2 = \left(\frac{G_3}{G_1 G_4 - G_2 G_3}\right)$$
$$v_x = \left(\frac{v_1^* - F_2 v_2}{F_1}\right)$$
$$v_y = \left(\frac{v_2^* - F_3 v_x}{G_4}\right)$$

Initial MAPS experiments measure aluminum strength at 8.85 GPa

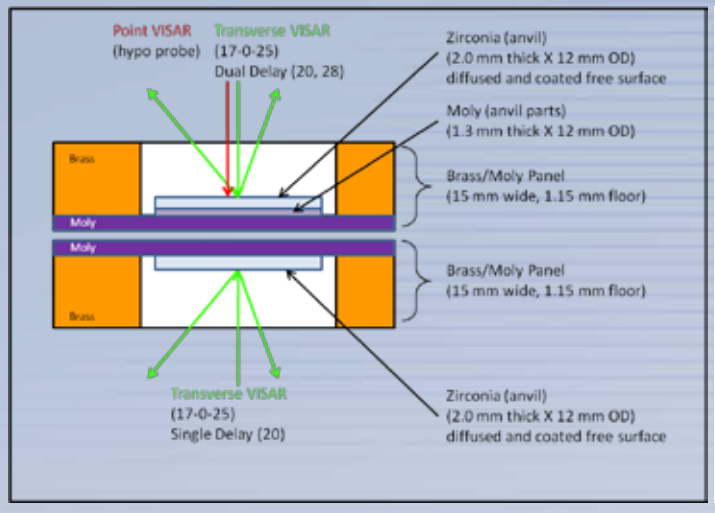

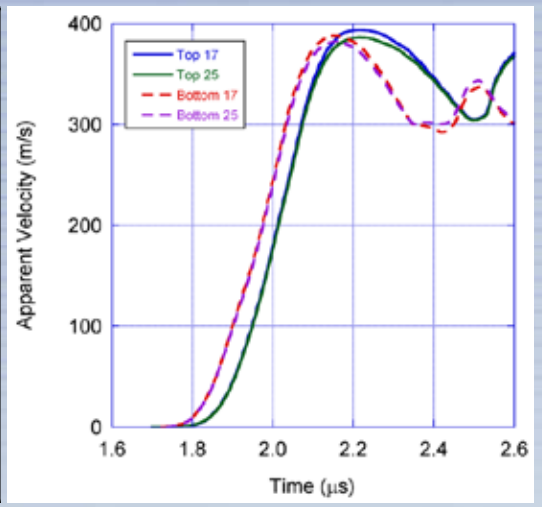

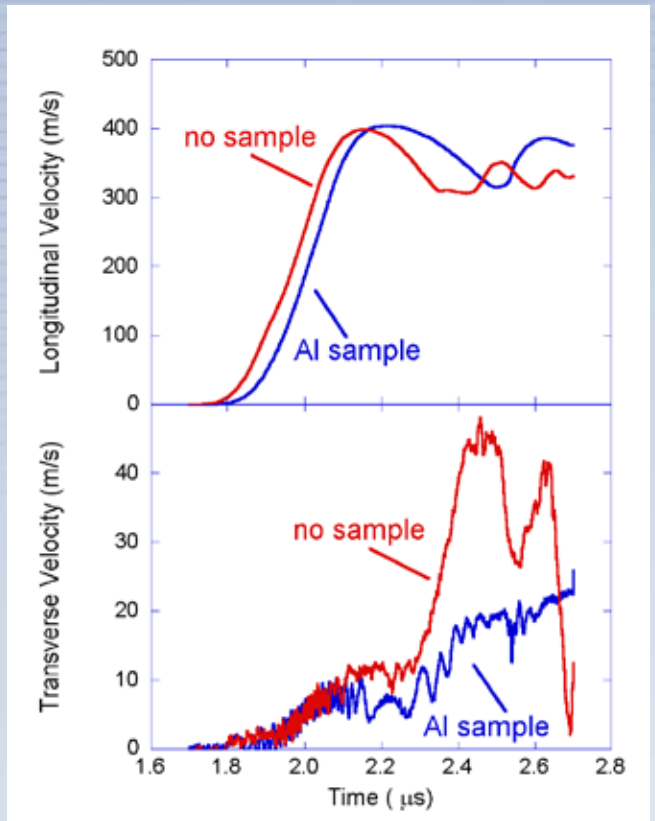

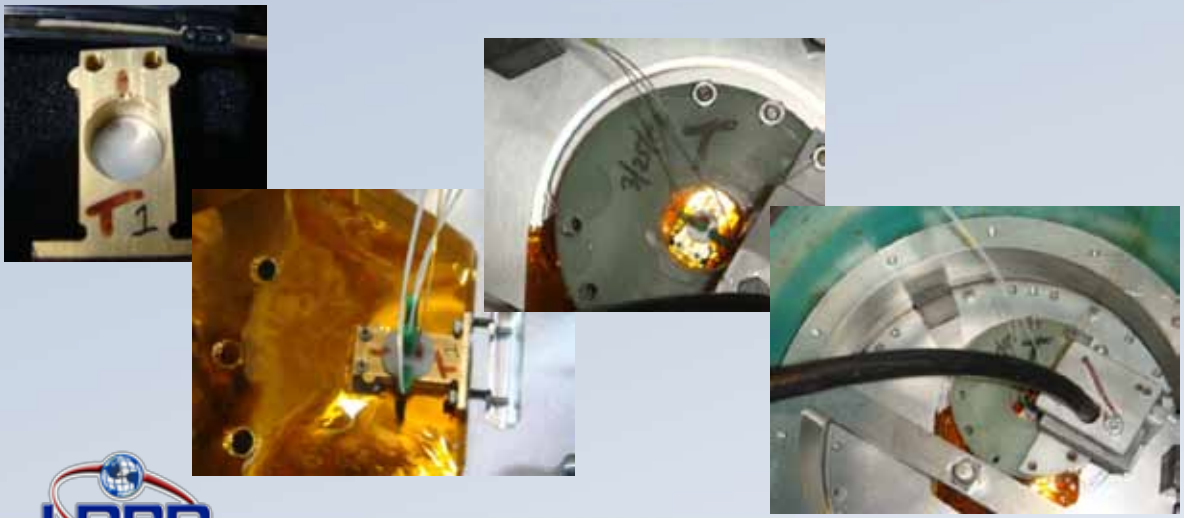

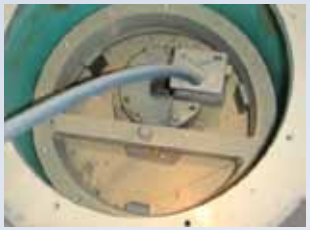

LDRD
LABORATORY DIRECTED RESEARCH & DEVELOPMENT

Sandia National Laboratories

Pressure and shear are calculated directly from measured free surface velocities

$\sigma = \rho_o C_L u_p$

σ = (6.07 g/cc) (7.33 km/s) ½(0.398 km/s)

σ = 8.85 GPa

$\tau = \rho_o C_\tau u_p$

τ = (6.07 g/cc) (4.105 km/s) ½(0.0187 km/s)

τ = 0.233 GPa

$Y = \sqrt{3}\,\tau$ = 0.404 GPa

±0.065 (16%)

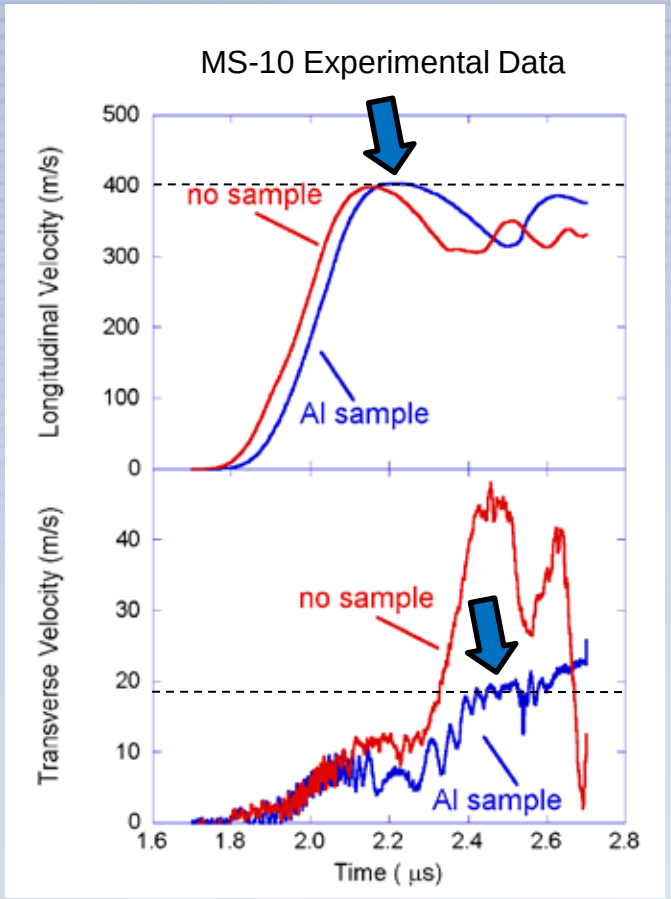

Initial MAPS data comparison with established strength data is excellent

Aluminum

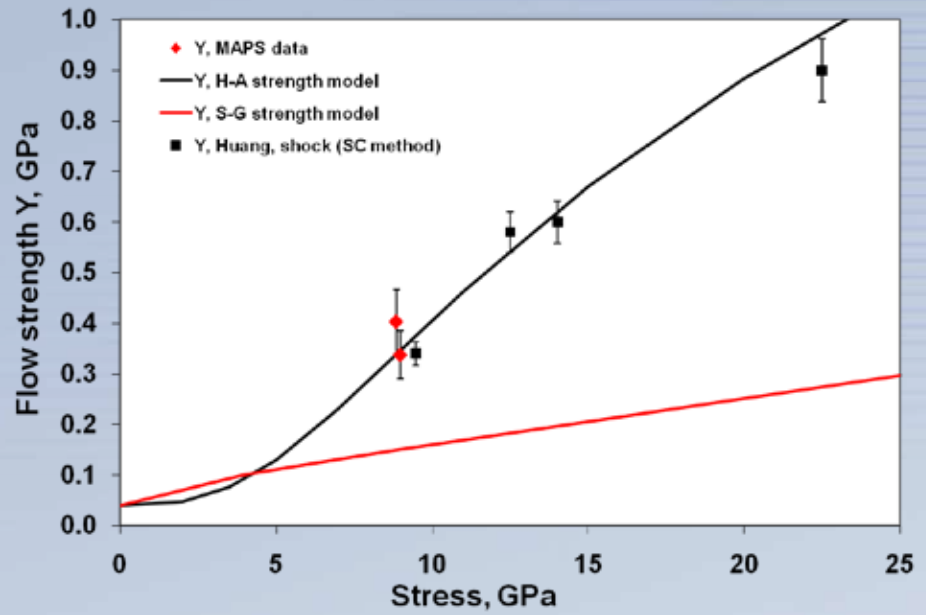

- **Accuracy and configuration being improved – goal is $\delta Y \leq 5\%$ at Mbar pressures**
- **Technique easily discriminates between strength models**

H. Huang and J.R. Asay, *J. Appl. Phys.* **98**, 033524 (2005)
D.J. Steinberg, S.G. Cochran, and M.W. Guinan, *J. Appl. Phys.* **51**, 1498 (1980)

Additional utility of the MAPS experimental configuration: 2D model validation data

New multi-dimensional capability for enhanced model validation!

•Has been applied to verify elastic response of zirconia anvil material to ~9 GPa

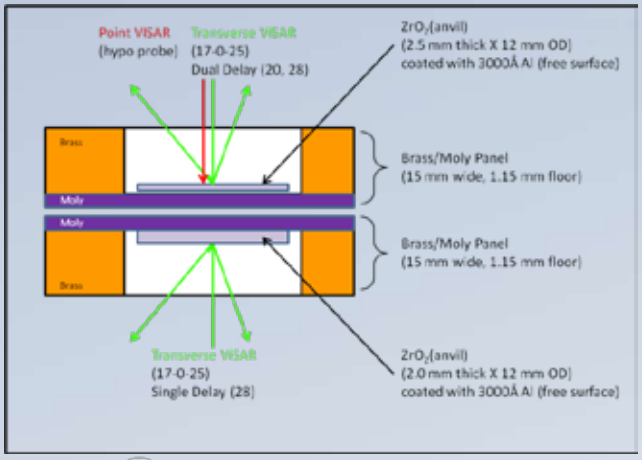

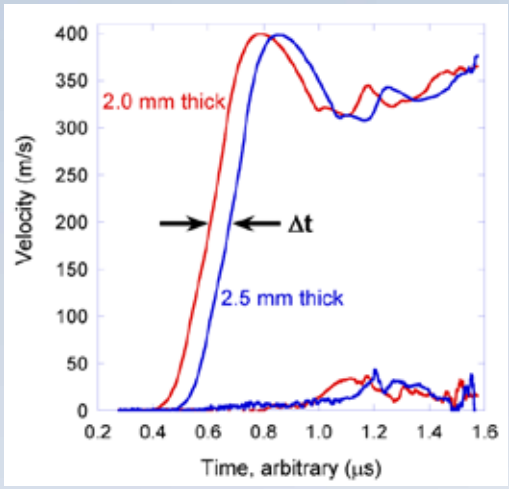

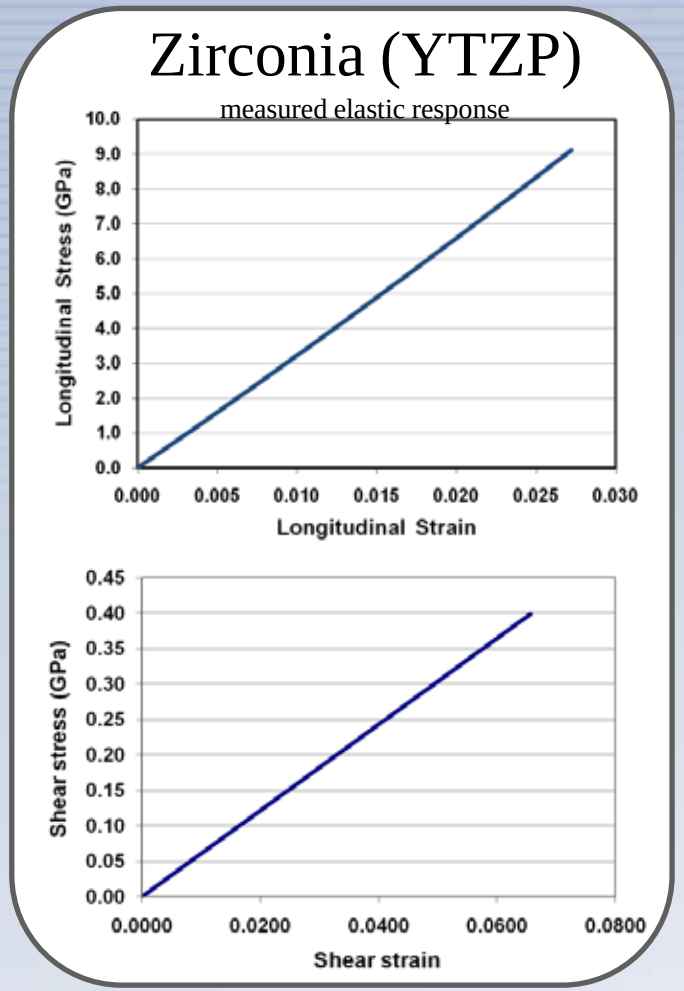

LDRD
LABORATORY DIRECTED RESEARCH & DEVELOPMENT

Sandia National Laboratories

Summary

- MAPS is a novel technique to directly measure material strength at high pressure
- Extensive MHD simulation was used to guide experimental development
- MAPS capability has been demonstrated through three successful shots
  - 2 Al strength
  - 1 ZrO_2
- Work is ongoing to demonstrate MAPS on additional materials at modest pressures
- Transition to Z is in progress (expected CY2012)

EOS Standards

Carl Greeff

Collaborators:

Jon Boettger, Matthias Graf, J. D. Johnson, Scott Crockett, Sven Rudin, John Wills

Thomas Mattsson, Luke Shulenburger, J.-P. Davis

Abstract

An approach to creating accurate EOS for pressure standards is described.

Applications to Cu, Au, and Ta are shown.

Extension of the method to high compressions using DFT is illustrated.

Comparisons with modern functionals show promise.

Motivation, Illustrated by Ta

Want to refine and extend pressure standards P(V,T) in multi-Mbar regime.

At several Mbar, Hugoniot and isentrope strongly separate.

Difference is 1 Mbar at P_i=3 Mbar.

High P isentrope is dominated by cold curve.

Isentropic compression experiments (ICE) allow in principle to separate thermal and cold contributions.

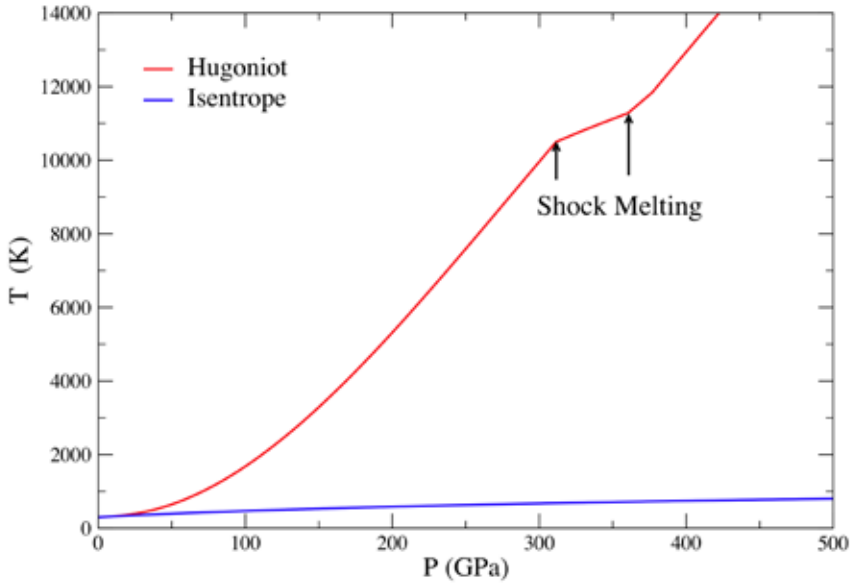

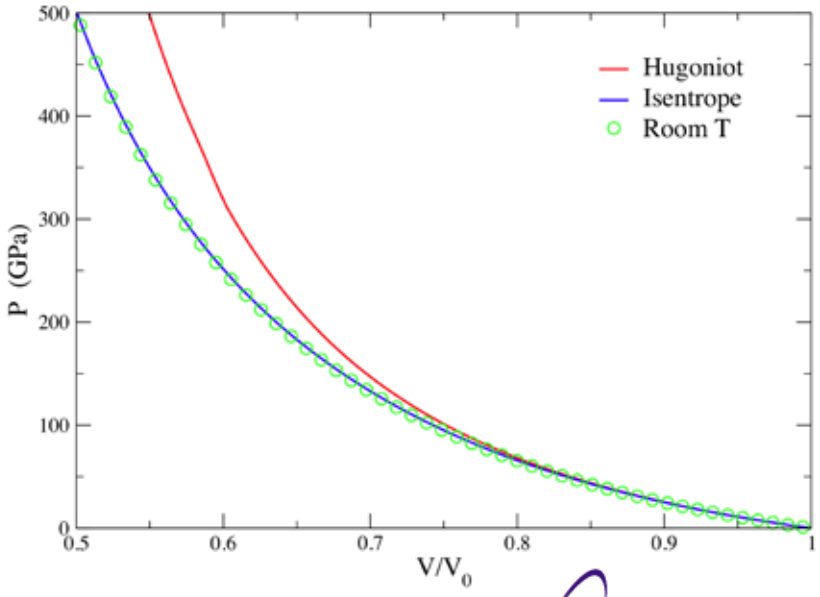

NNSA

Los Alamos

EOS Strategy

Data: lattice parameter, ultrasonic bulk modulus, Hugoniot, strongly constrain cold curve.

Not very tight experimental constraints on thermal excitation part of EOS under compression.

Strategy: combine empirical cold energy with DFT-based thermal excitations.

This strategy breaks down beyond compressions of V/V_0~0.6, and must be supplemented.

Experimentally, ICE dominated by the cold curve.

Theoretically, DFT can be used.

EOS Formulation

We take the Helmholtz free energy for each phase to be

$$F(V,T) = \phi_0(V) + F_n(V,T) + F_{el}(V,T)$$

where

ϕ_0 - static lattice energy

F_n - nuclear motion - approximated by quasi-harmonic

F_{el} - electronic excitation - independent electrons

EAM simulations indicate that for Cu, anharmonicity is very small, Lindemann melting is very accurate. We expect this to be true for other noble metals.

Nuclear motion and electronic excitation parts from DFT.

Φ_0 empirical, from density, B, Hugoniot, DFT at high P

Ab Initio Theory for Lattice Vibrations

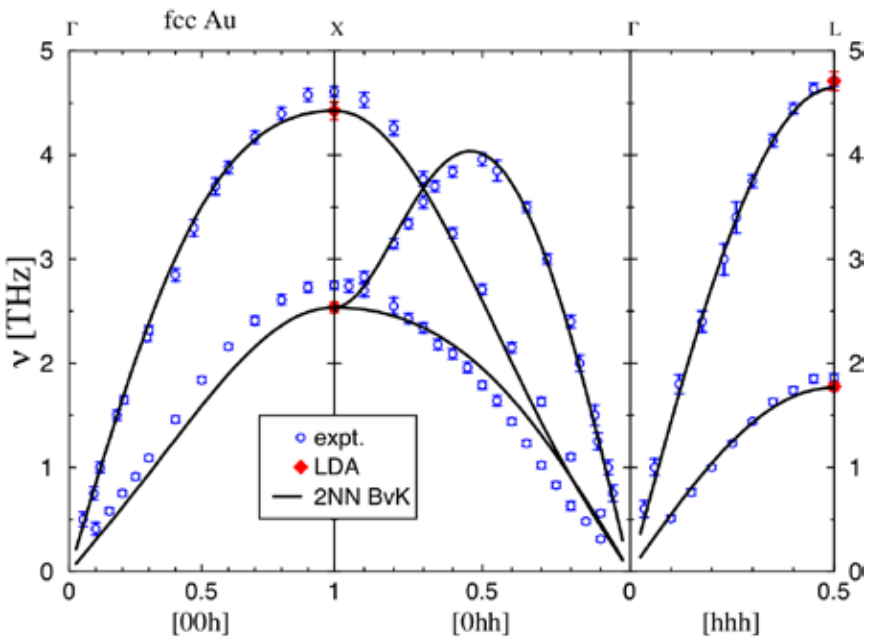

DFT calculations give phonon frequency moments to few %.

Sufficient to discriminate between Gruneisen parameter models.

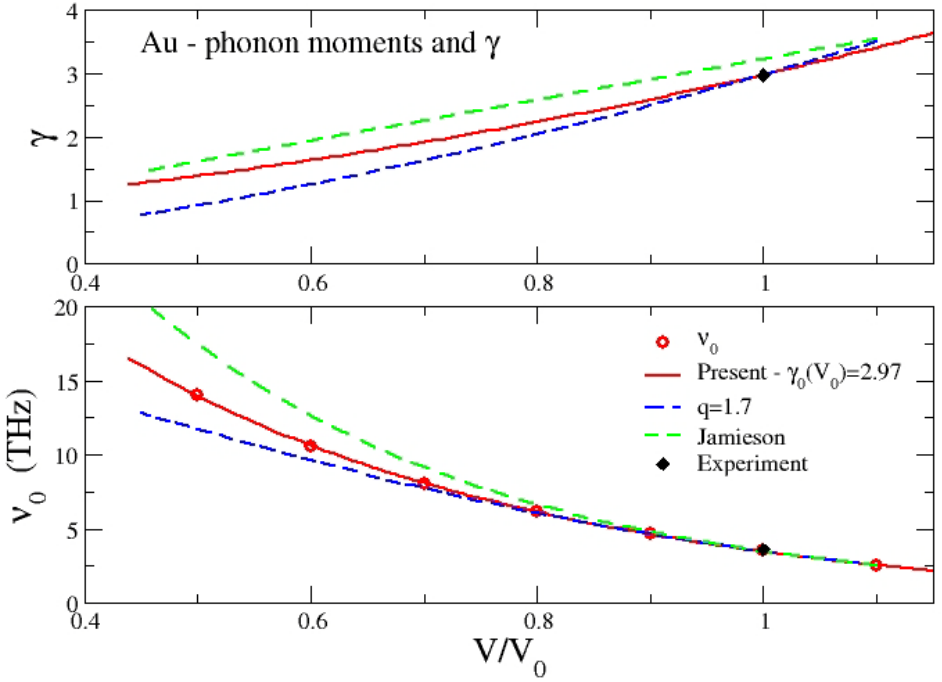

Application to Gold EOS

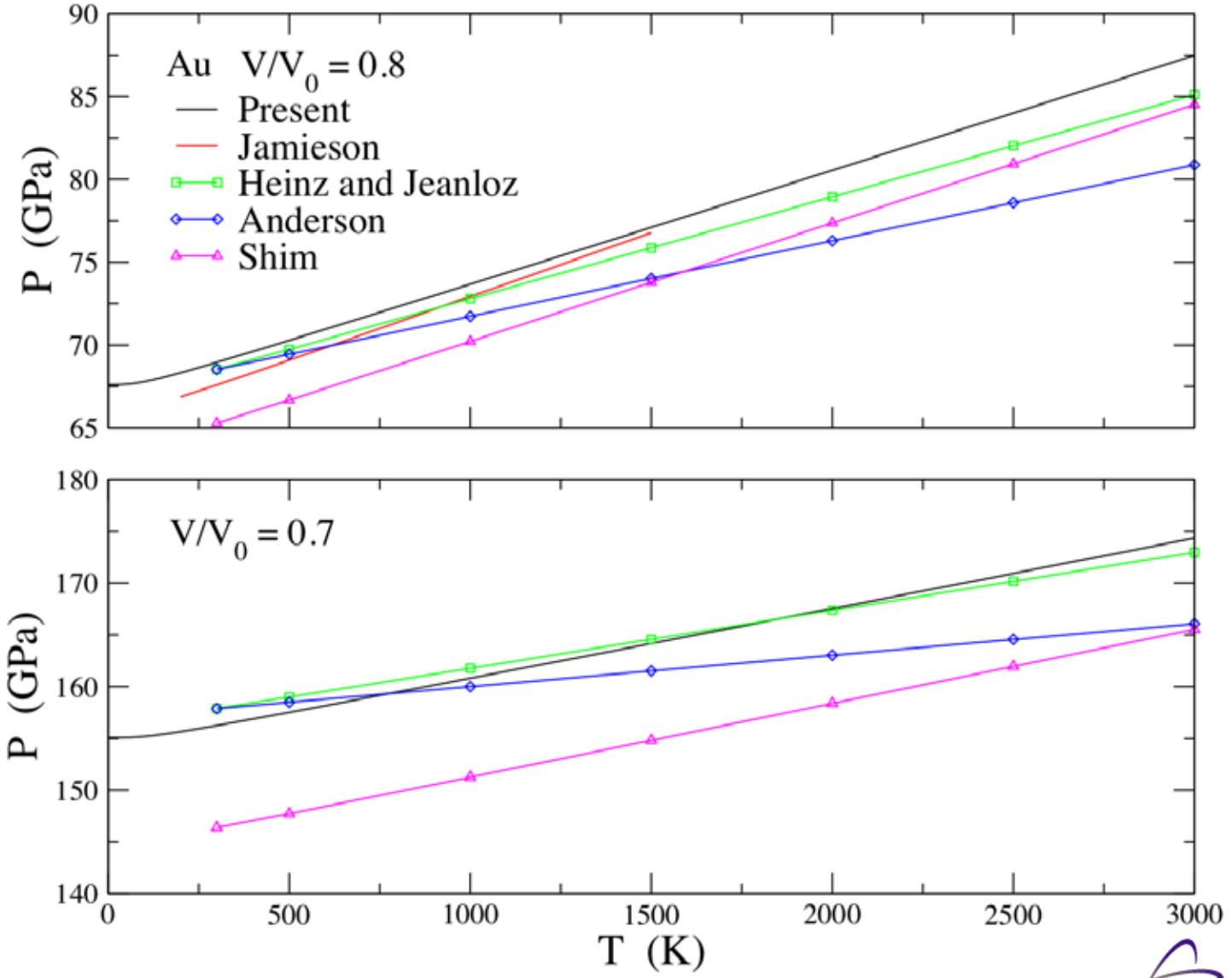

Application to Gold EOS

Data from Fei et al., Phys. Earth and Planetary Interiors, 143-144, 515 (04).

Au EOS of Greeff and Graf , PRB 69 (2004) predicts high T pressures in good agreement with MgO standard.

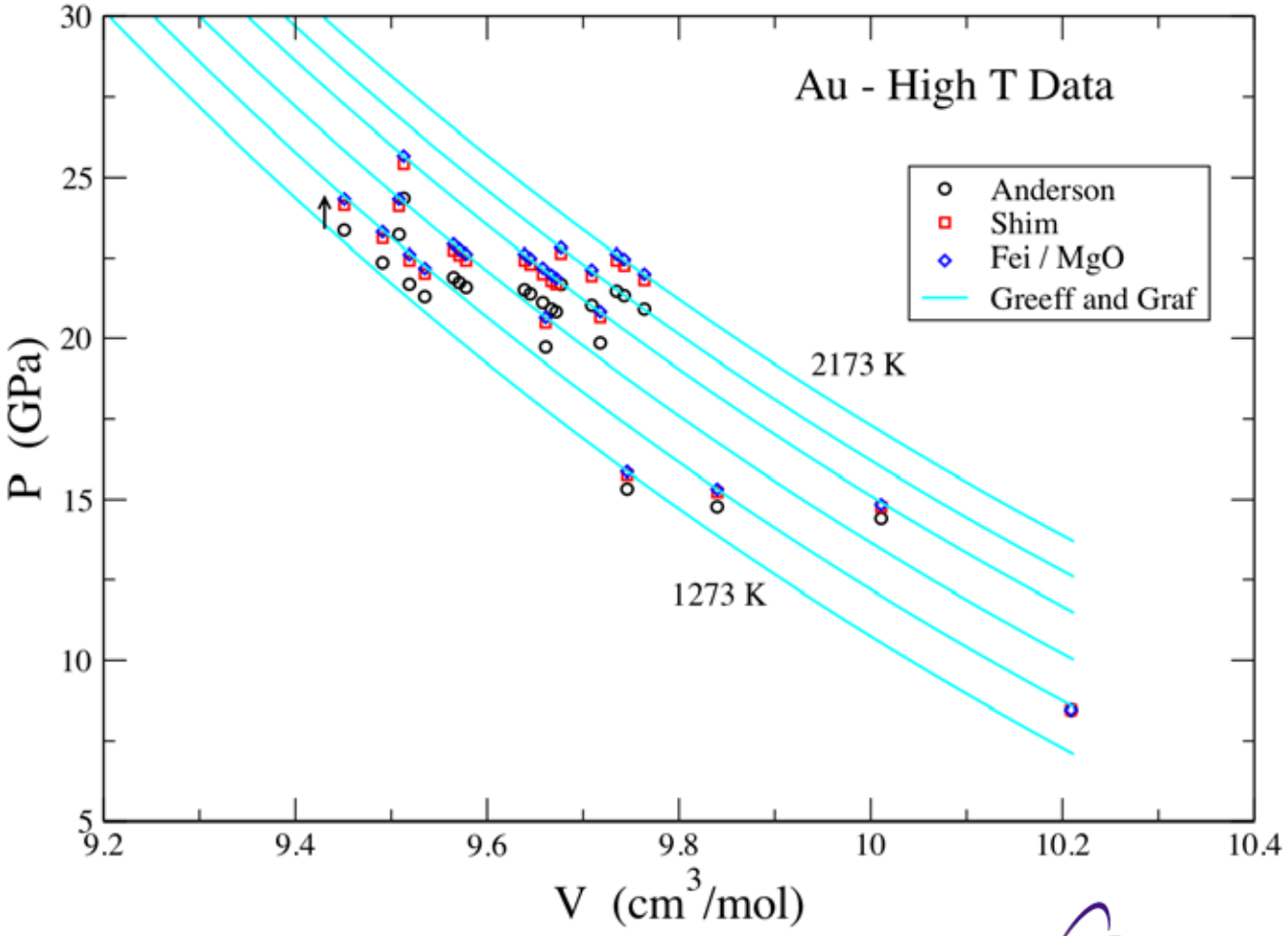

Application to Copper EOS

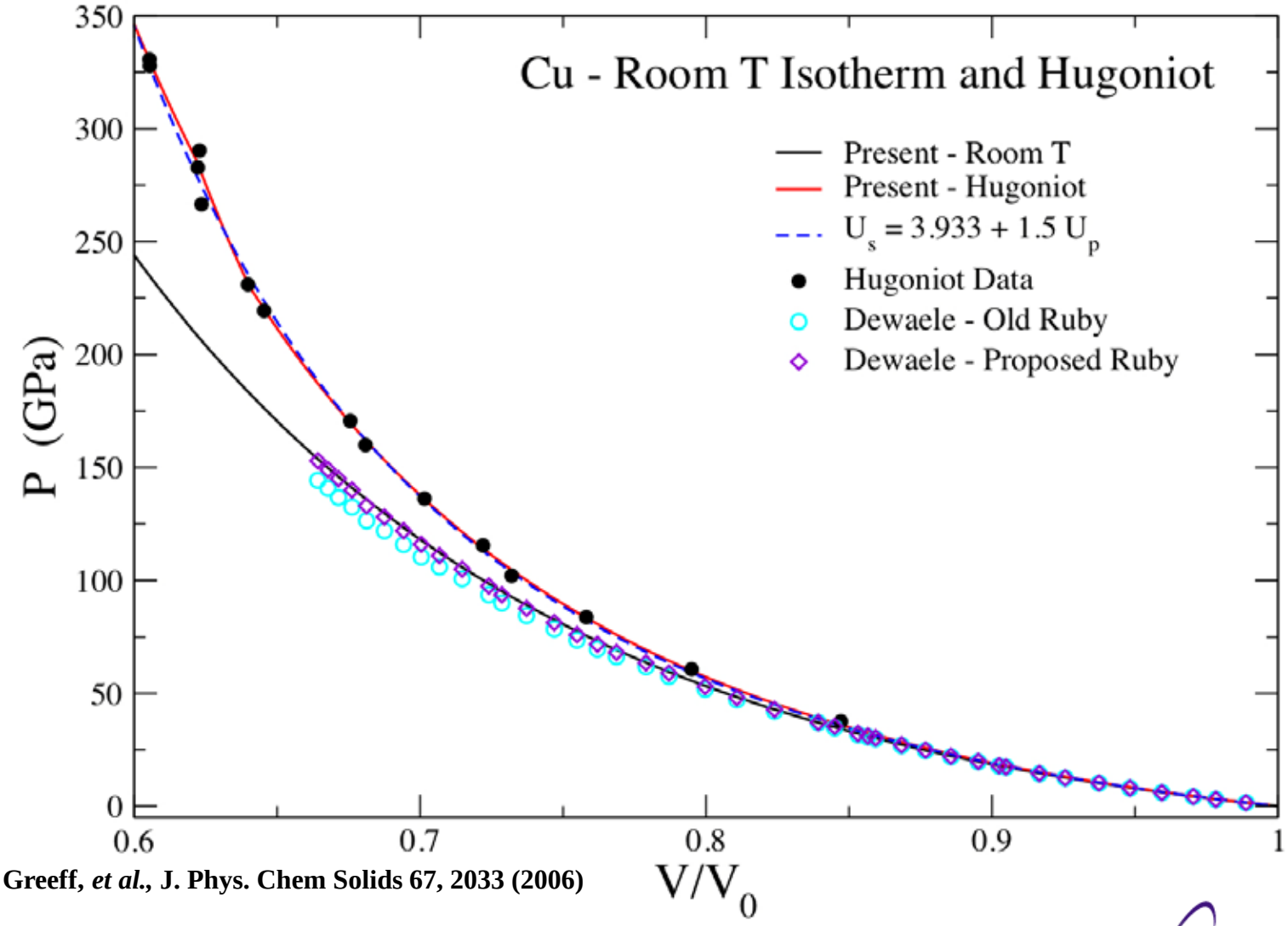

C. W. Greeff, *et al.*, J. Phys. Chem Solids 67, 2033 (2006)

Cu: Extension to High Compression

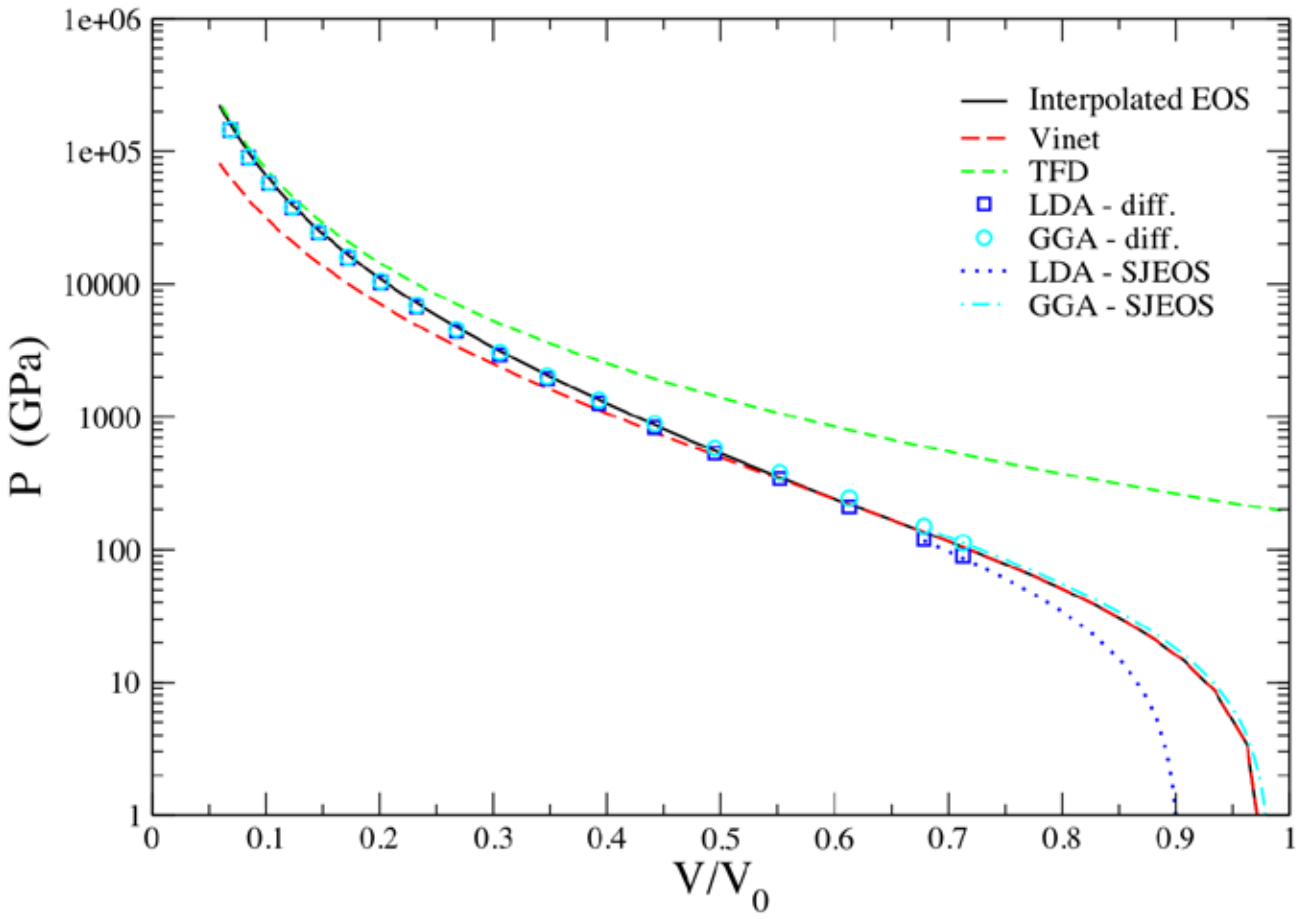

At very high P, 3 parameter ϕ_0 loses accuracy.

Extrapolating from Hug becomes more uncertain.

Fractional uncertainty in DFT gets smaller.

C. W. Greeff, *et al.*, J. Phys. Chem Solids 67, 2033 (2006)

Ta Room T Isotherm

Hugoniot data: Mitchell and Nellis, JAP 52 (81), DAC data:
Dewaele et al., PRB 70 (04), Cynn and Yoo, PRB 59 (99).

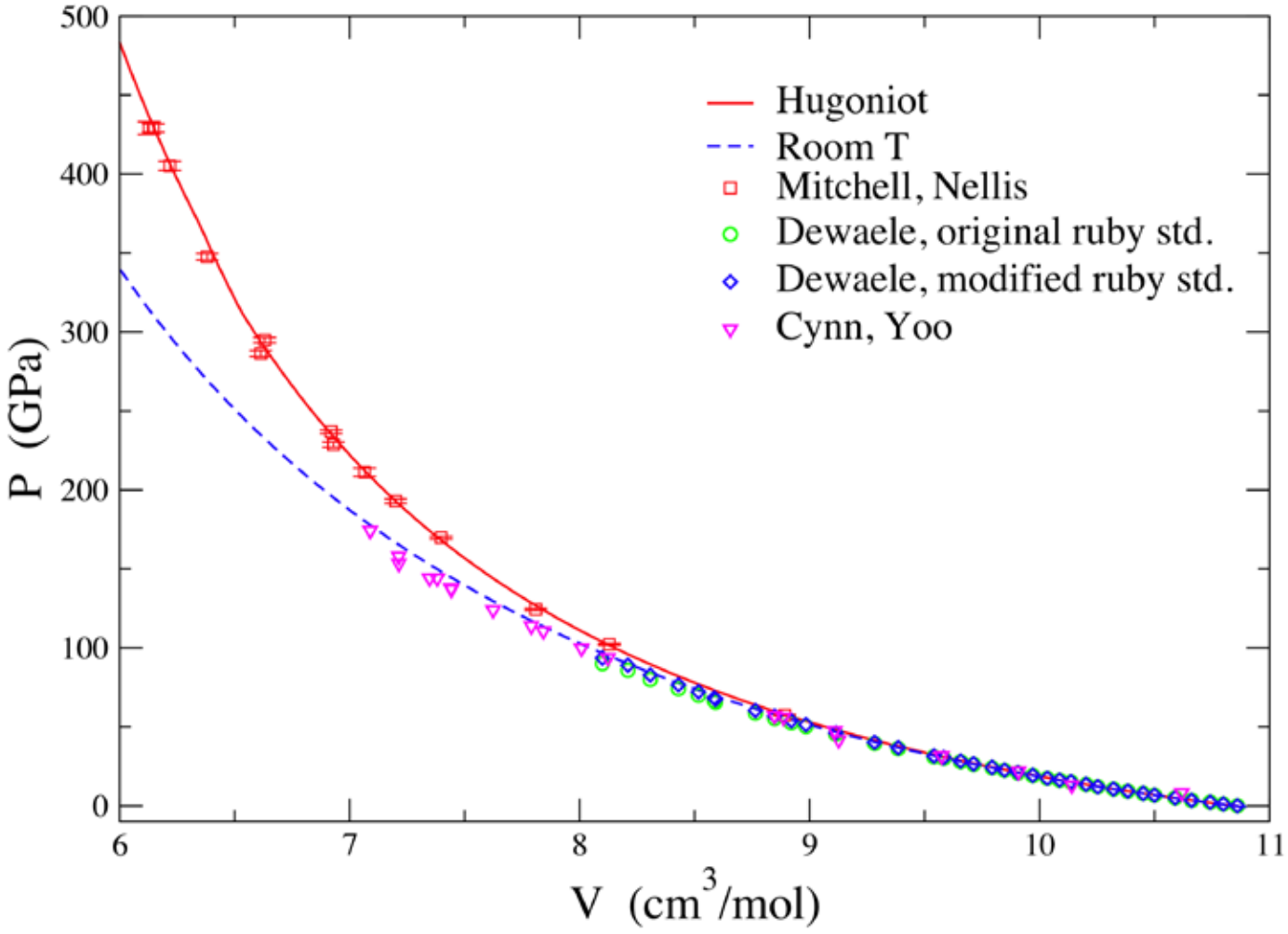

Present EOS gives room T isotherm systematically above DAC. About 10 GPa at 150 GPa.

Modified ruby std. improves agreement.

P above Cynn and Yoo. I think this is right.

Ta Cold Curve

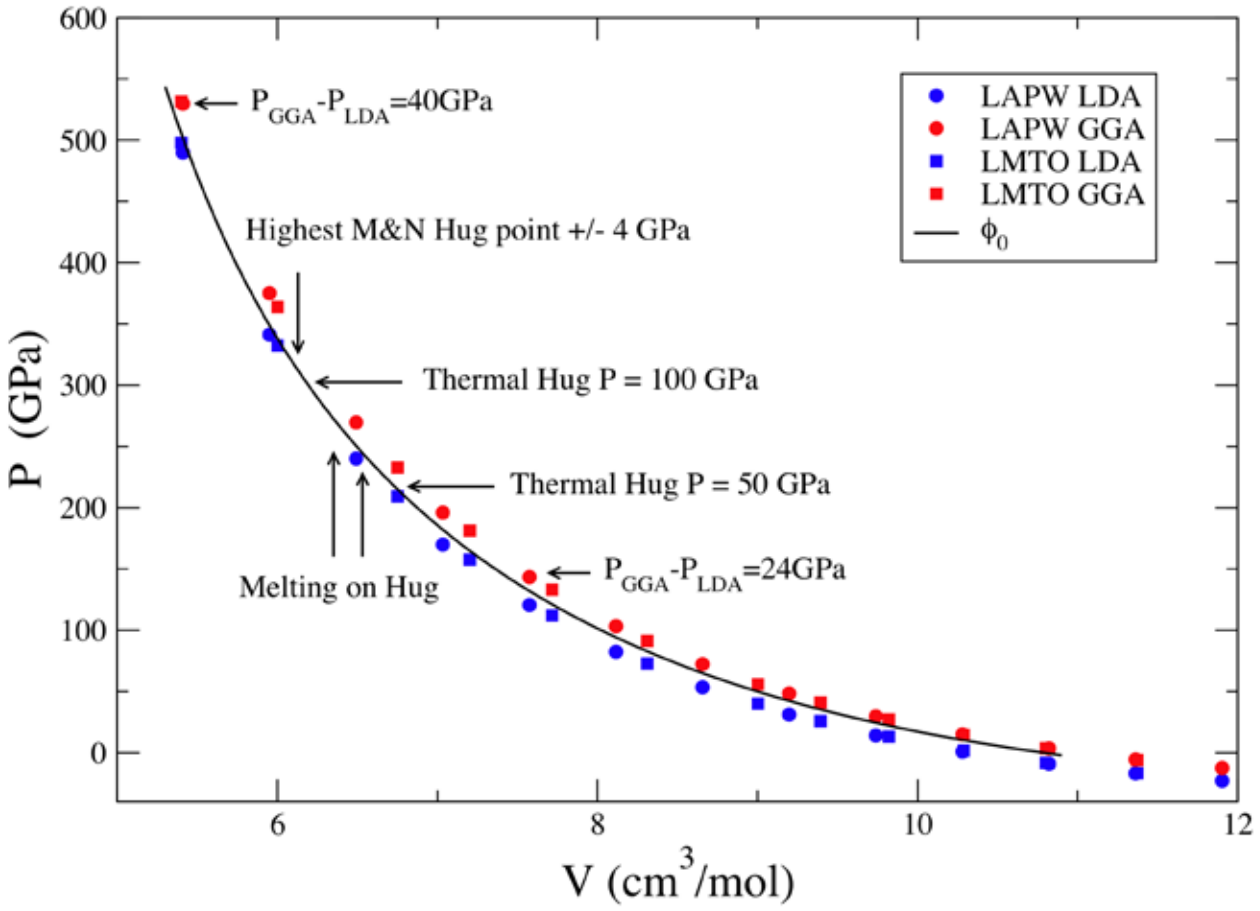

C. W. Greeff, *et al.*, SCCM 2009

Higher orders in strain expansion cold curve are adjusted to lie between LDA and GGA.

Melting gives ~10 GPa increase to Hugoniot P.

Tends toward LDA at higher density.

This trend seems to be significant, compared with likely sources of error.

Ta ICE Data

ICE experiments potentially allow for absolute pressure measurements in the multi-Mbar, cold regime.

Ta measurements in good agreement with EOS.

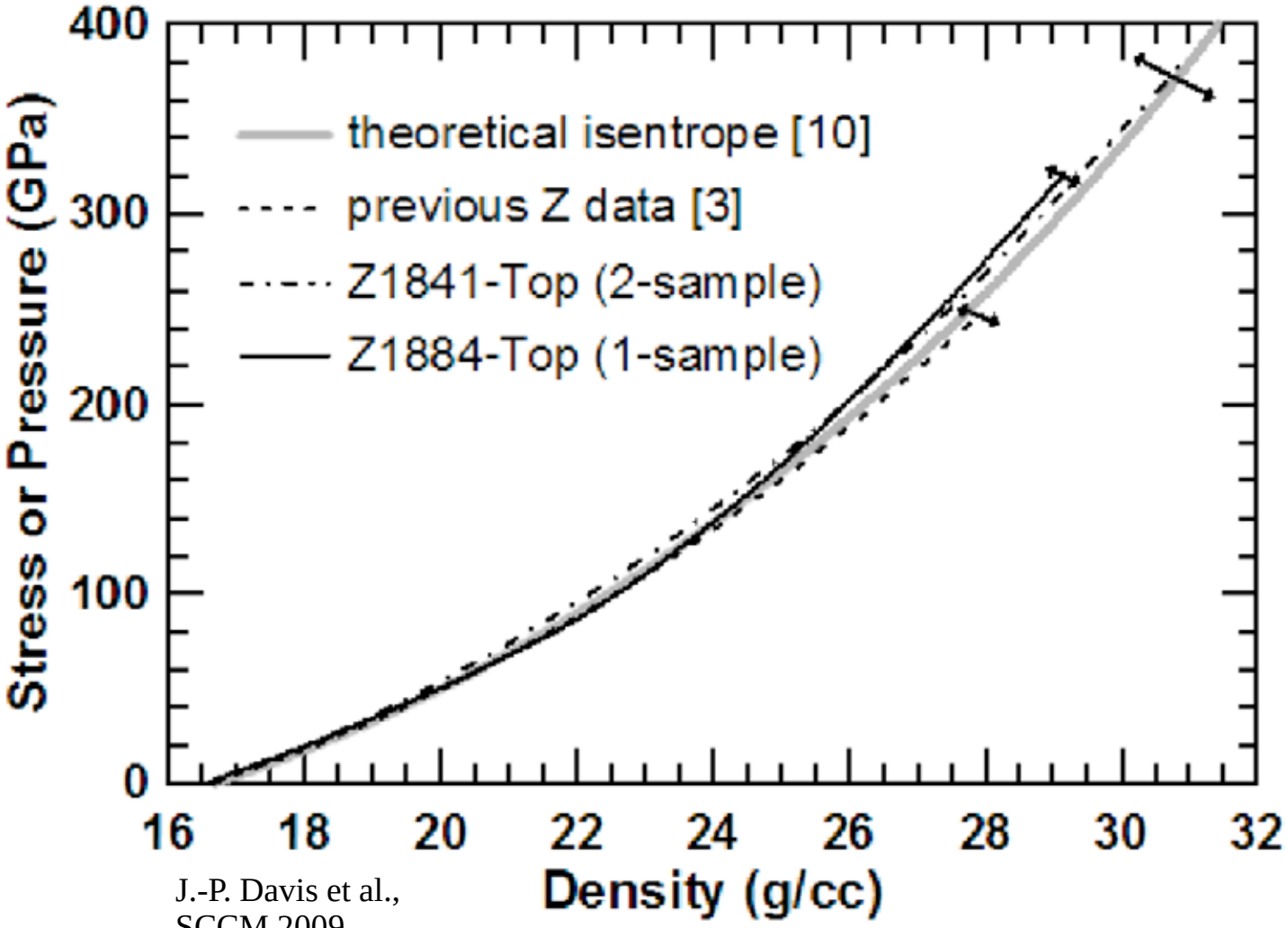

J.-P. Davis et al., SCCM 2009

Proposed Ta Phase Diagram

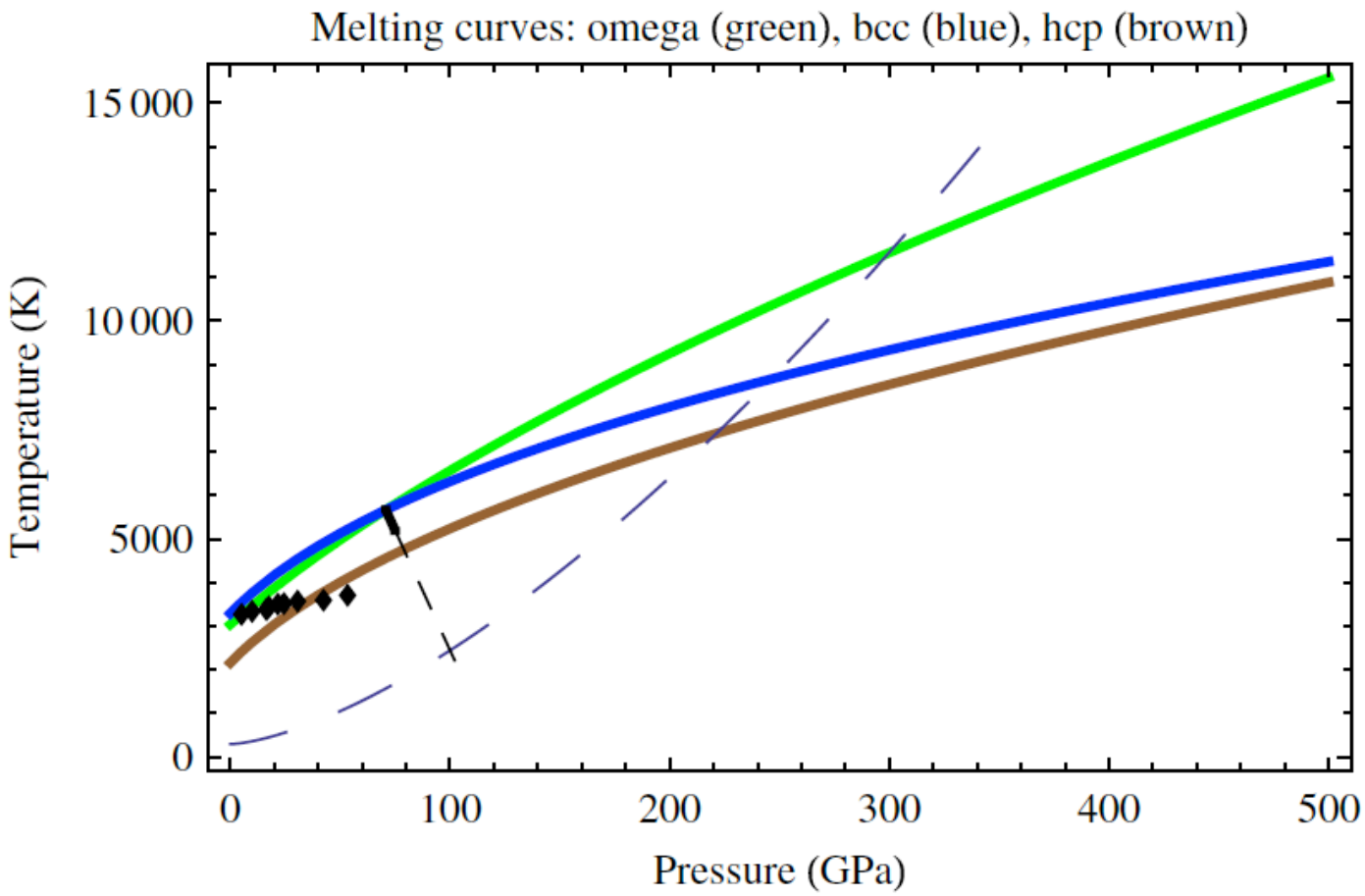

Burakovsky et al., PRL 104 2010 find evidence of a bcc-omega-liquid triple point in Ta.

This calls for further investigation, and will modify interpretation of Hugoniot.

Cu Cold Curve

DFT Calculations by Luke Shulenburger and Thomas Mattsson

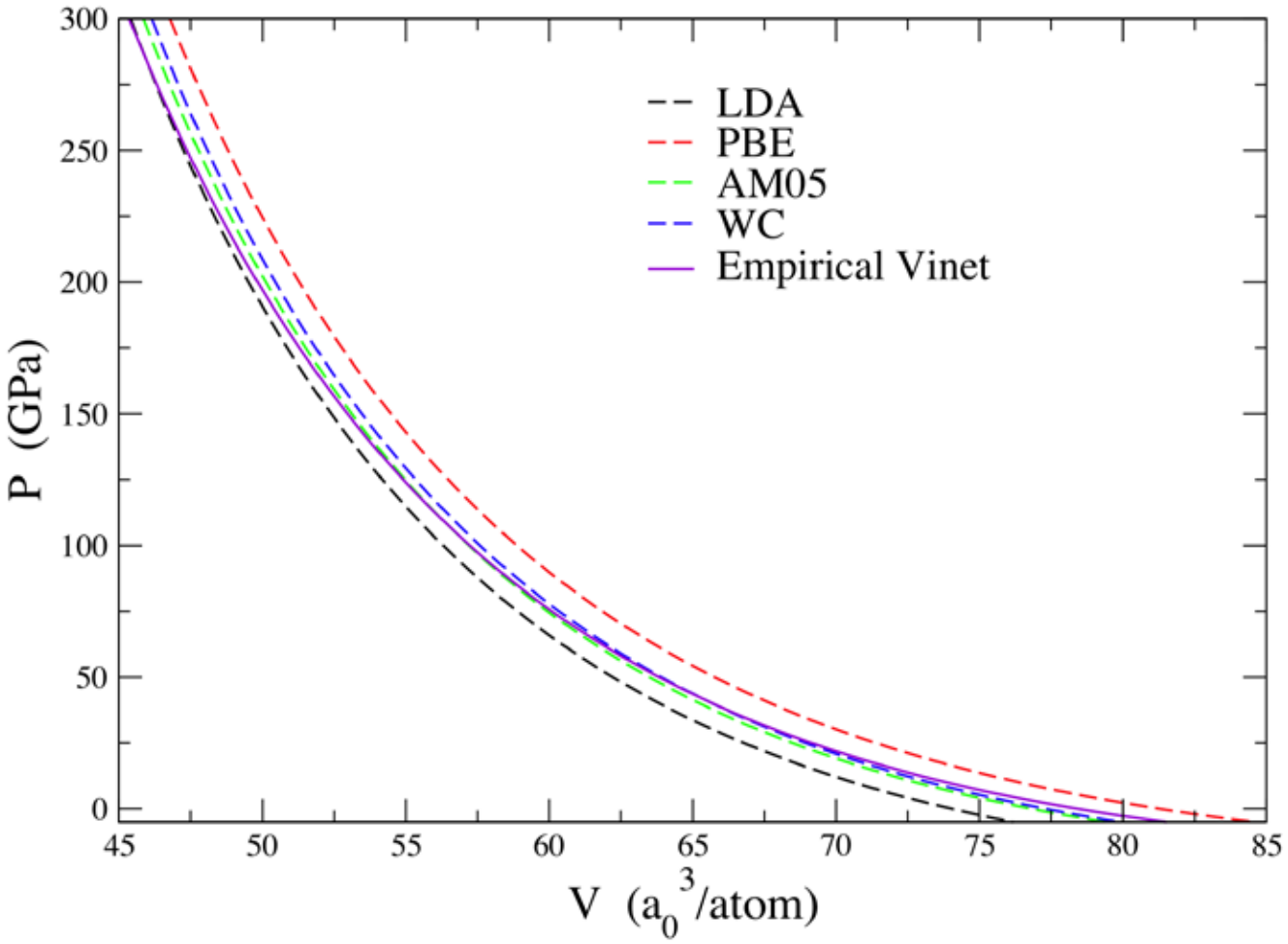

More modern exchange-correlation functionals reduce errors in equilibrium volume from ~3-4% to ~1-2%.

3-parameter Vinet form is too soft at high P.

Cu Cold Curve

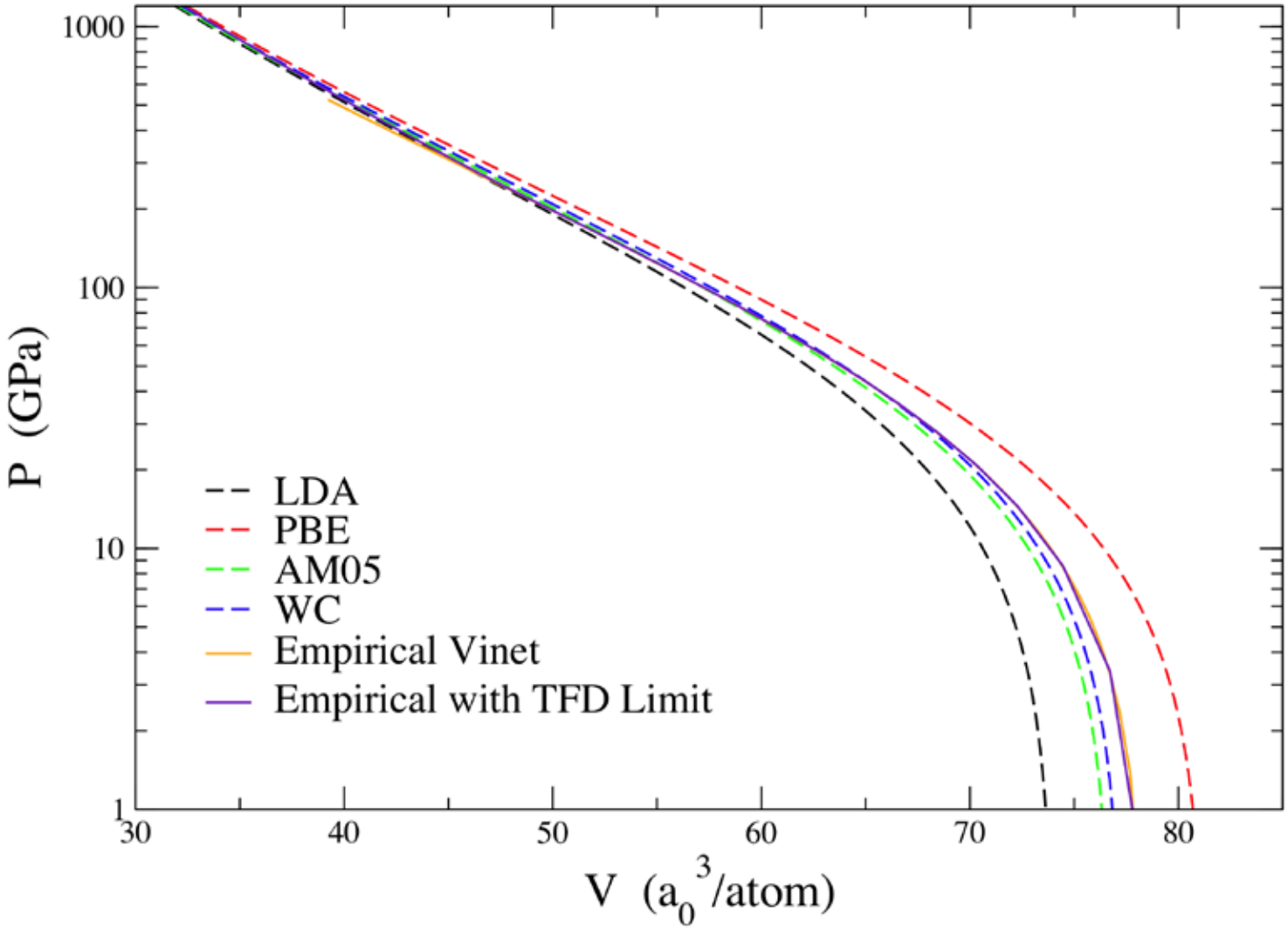

Ag Cold Curve

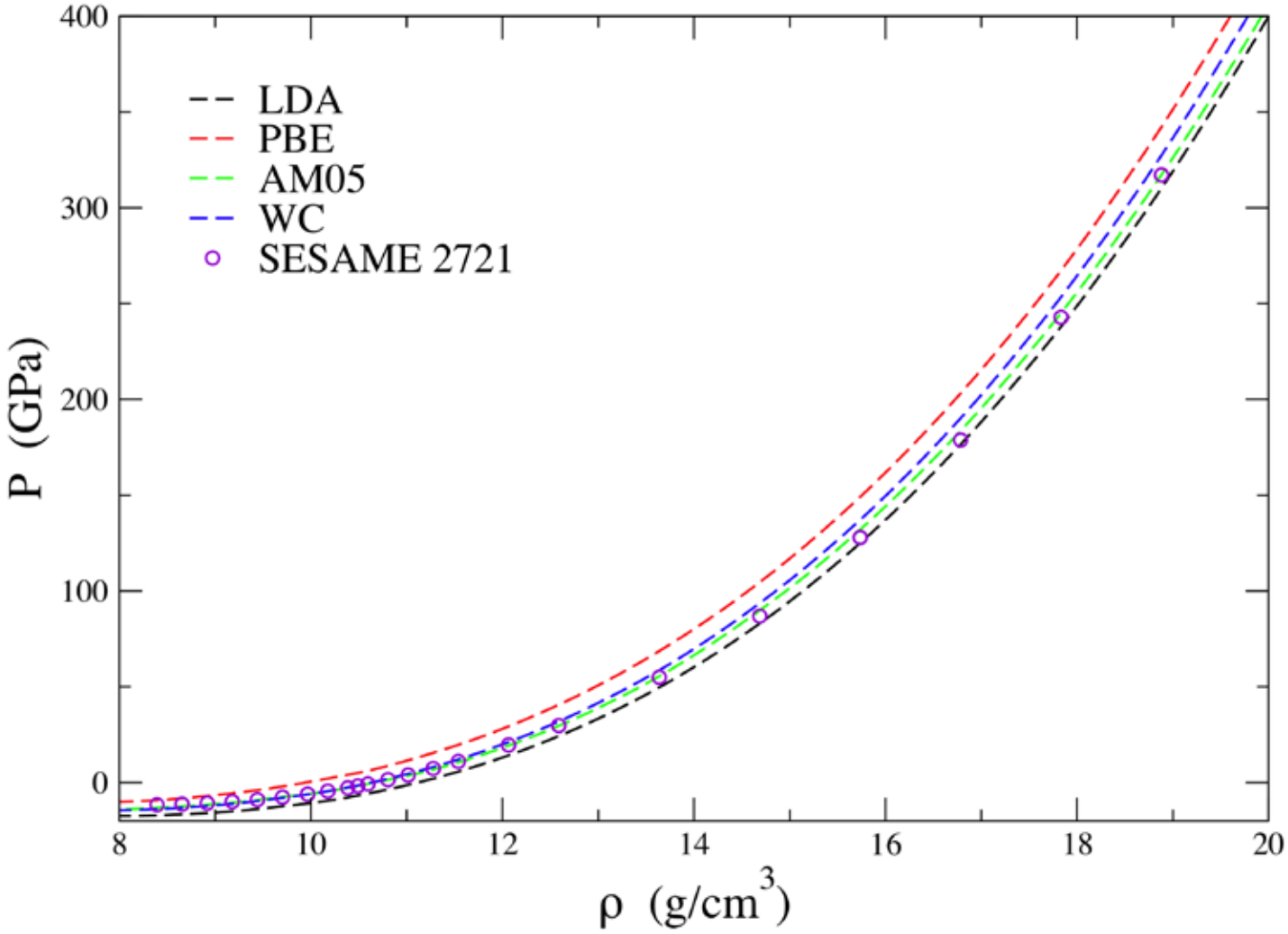

Summary

- DFT excitations + empirical (Hugoniot-based) cold energy gives good EOS to moderate compression ($V/V_0 \sim 0.6$).
- At higher compression, various factors conspire to make this less accurate.
    - Large Hugoniot thermal pressure.
    - Shock melting gives substantial pressure.
    - 3-parameter cold curve is becoming inadequate.
- We have used linear combination of LDA and GGA in this regime.
- This is problematic for multi-phase, because errors are phase dependent.
- New functionals are promising. Minimal need to “correct” DFT.
- ICE is only technique I know of to measure multi-Mbar cold EOS.
- We need a better parameterization of cold curve.

Application to Gold, Copper EOS

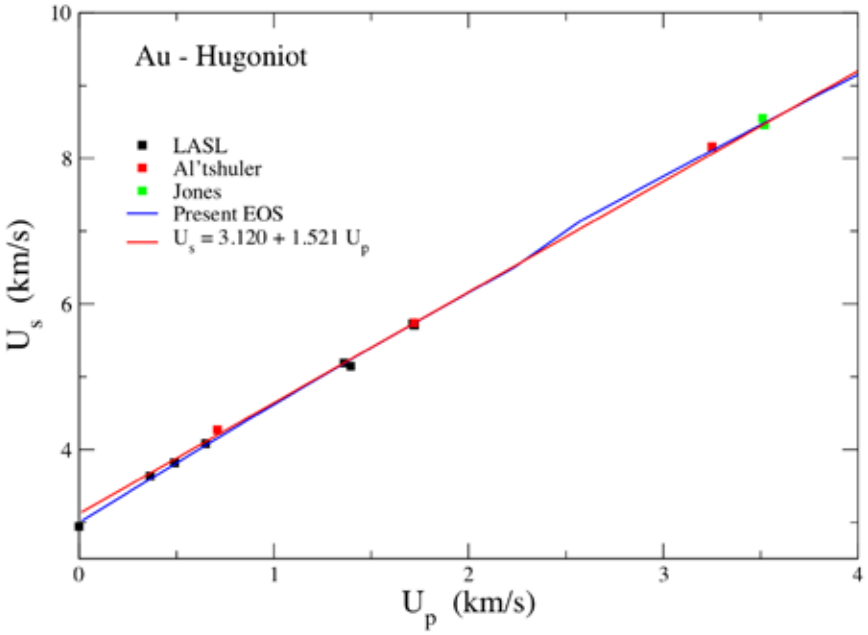

Note Au data are sparse, linear fit not consistent with bulk sound speed.

Cu data are abundant and consistent.

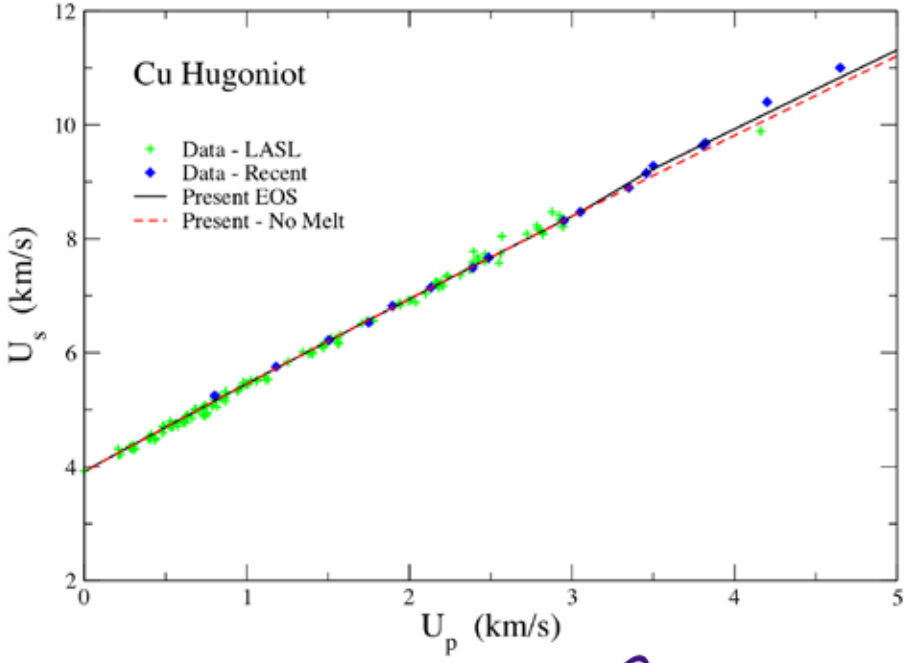

NNSA

Los Alamos

Application to Copper EOS

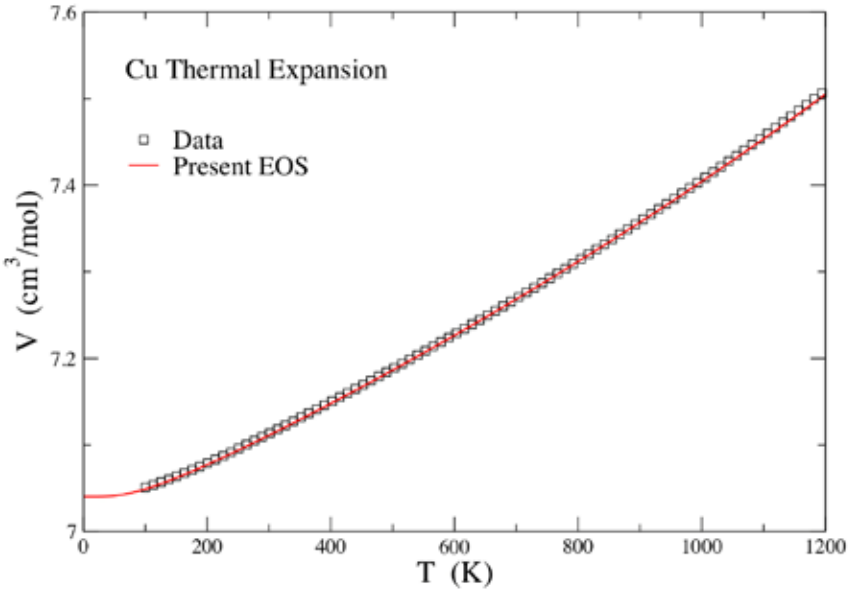

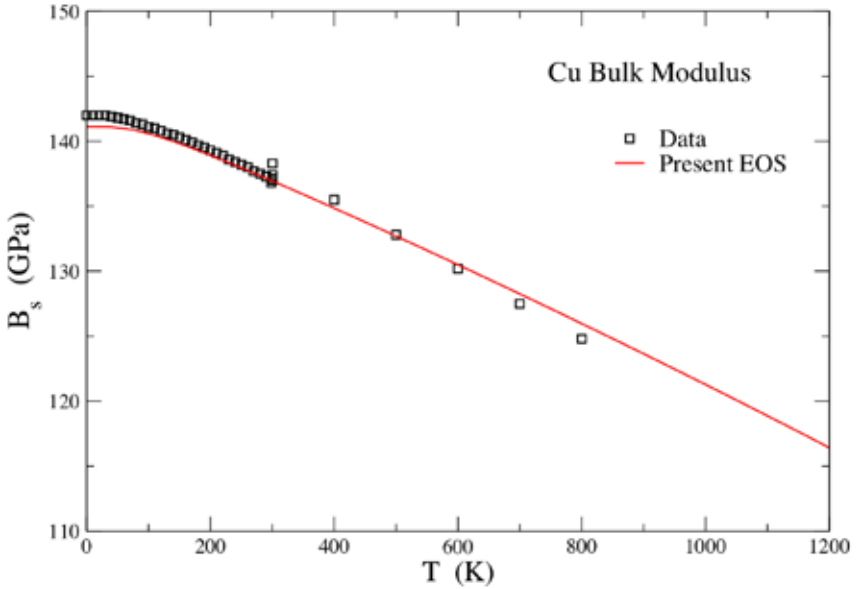

NNSA

Los Alamos

Nuclear Motion

For solid, effective Debye T is taken to be log moment of phonon frequencies.

$$\ln(k\theta_0) = \langle \ln(\hbar\omega) \rangle_{BZ} + 1/3$$

$$\gamma_0 = -\frac{d\ln\theta_0}{d\ln V} = A(V/V_0) + B(V/V_0)^2 + 2/3$$

Assumed V-dependence fits calculated moments well, allows for analytic derivatives.

Liquid uses 'standard' model: c_v=3Nk, ΔS_v=0.8Nk, Lindemann melting.

Nuclear Motion

Phonon frequencies determined as function of V using direct force method with VASP/PAW.

Moments interpolated using assumed V-dependence of γ.

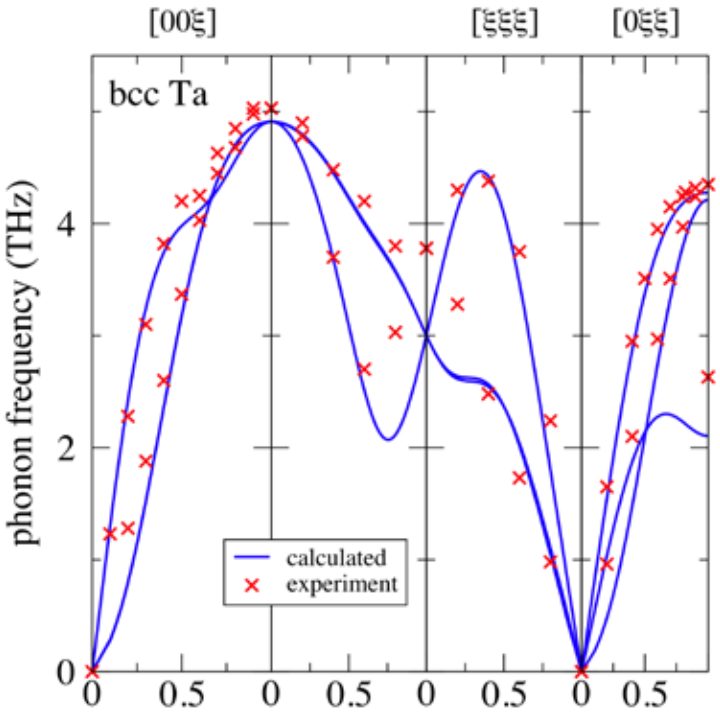

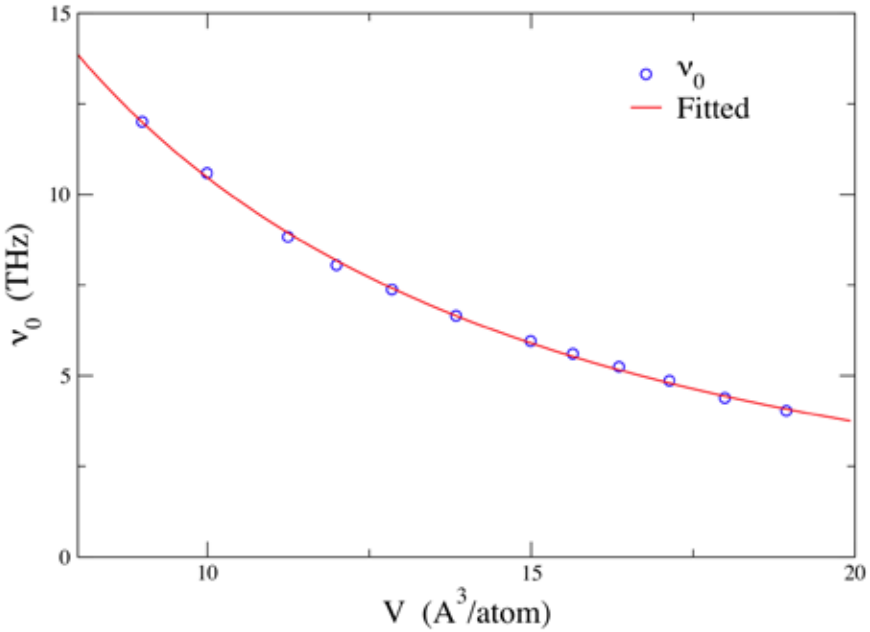

Making Pyrometric Measurements in Ramp Loading Experiments

UCRL-PRES-465651

Neil Holmes

LLNL

Presented at 4th Workshop on Ramp Compression

January 18, 2011

This work was performed under the auspices of the U.S. Department of Energy by Lawrence Livermore National Laboratory under Contract DE-AC52-07NA27344.

physical and life sciences

Acknowledgements

- Don Fujino
- Jeff Nguyen
- Daniel Orlikowski

Temperature measurements are essential

- In Hugoniot experiments, we can determine *P, ρ, E*. Measuring temperature helps determine energy partition, and lets us compare with static compression data, *e.g.* phase diagrams.
- When using ramp compression, with simple assumptions you can calculate *P, ρ* from velocimetry. Temperature is needed for EOS. And also for the same reasons above.
- Optical pyrometry is the most general method, and ought to work well in systems that have rear access only, or optically thick samples. For T > 1000 K, should have adequate time response.

The problem

- It's tricky to make temperature measurements at the back of a thick sample under ramp loading.
  - As the ramp steepens, rate-dependent effects could be important
  - If a phase transition is encountered under compression, a shock could form
- If any of these things happen, the relationship of the ramp compression at the front of the target to the conditions at the rear of the target is broken or, at least, suspect.
- For the ramp-loading problem, no analytic solution to the thermal transport problem exists

An example

- **When H_2O solidifies under ramp compression, a plateau is followed by a shock. This illustrates a general behavior.**

VISAR: Solidification Signature

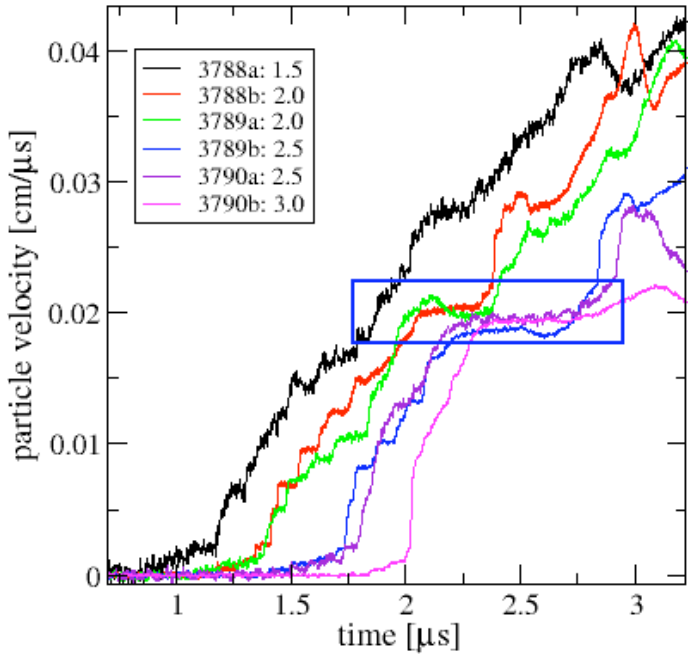

Thermodynamic path of experiment

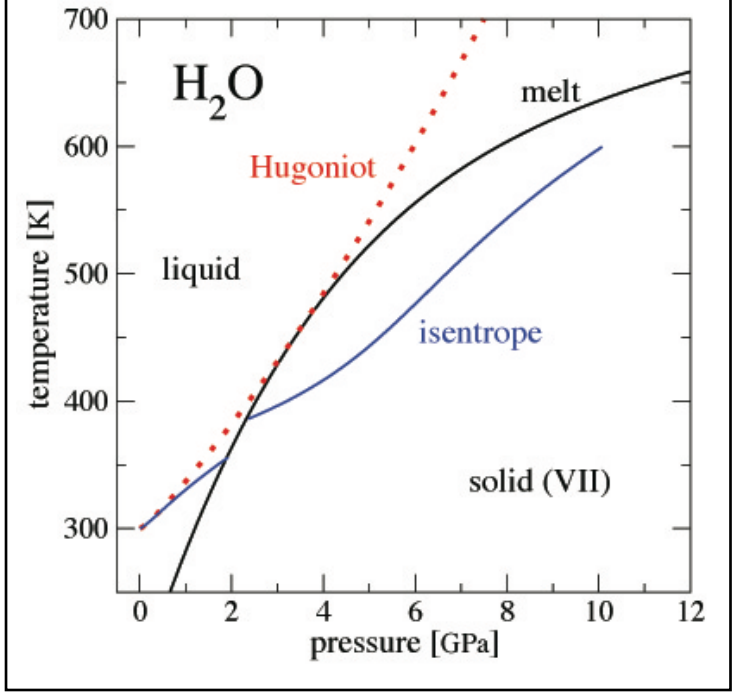

physical and life sciences

The solution is simple: make the sample thin

- If it's thin, characteristics won't cross: no shock formation
- If it's thin, there is not enough space for dispersion to steepen the wave, and no shock formation
- How thin is thin?

$$\Delta x = \frac{c}{20}\frac{P}{\dot{P}}$$

- *i.e.* the acoustic round-trip time is small compared to the normalized rate of change of pressure

Sample is surrounded, front and back, with windows.

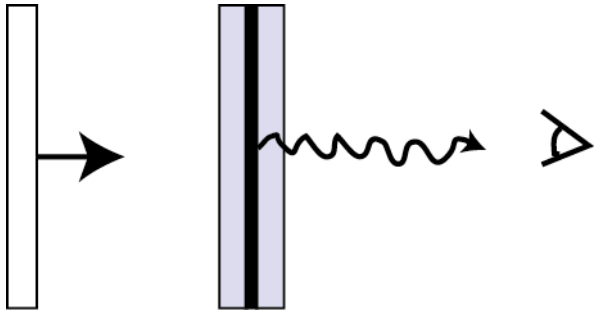

Simple simulations prove it out

- Sandwich a thin metal sample between windows—3 cases:
  - $Al_2O_3/Cu/Al_2O_3$
  - $Al_2O_3/Al/Al_2O_3$
  - LiF/Cu/LiF
- Simple ramp wave
- Ramp to 200 GPa

Simulation results.

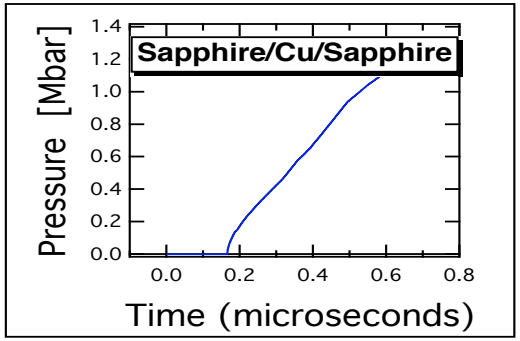

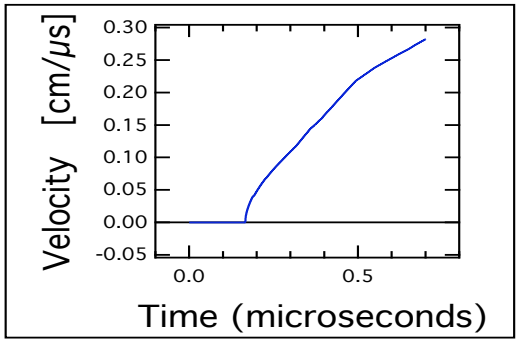

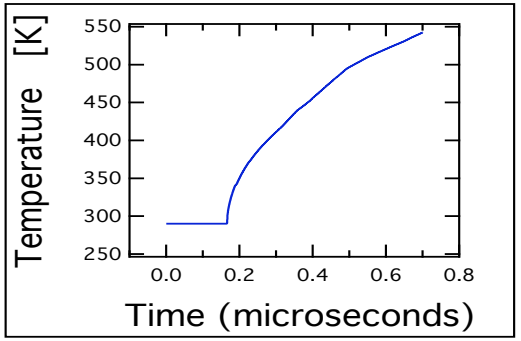

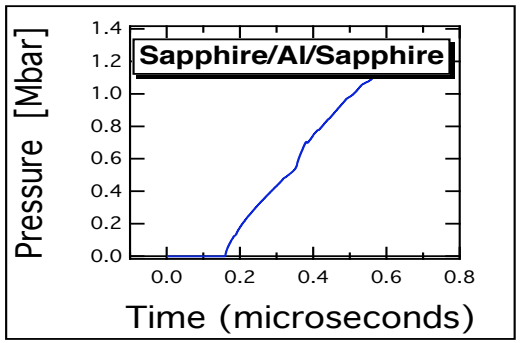

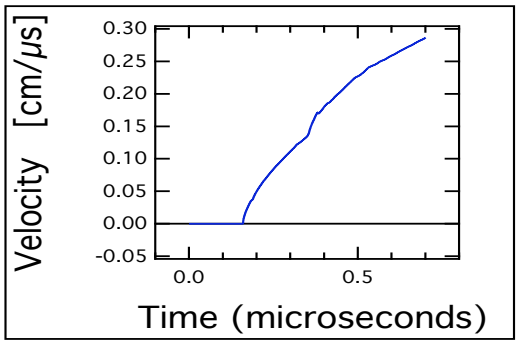

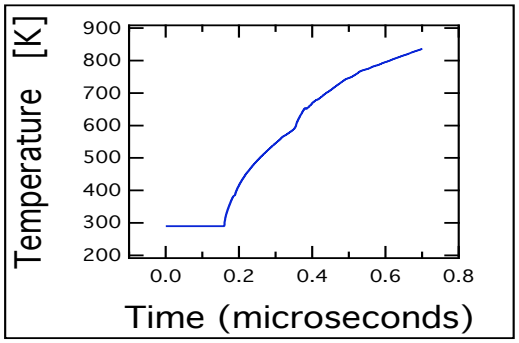

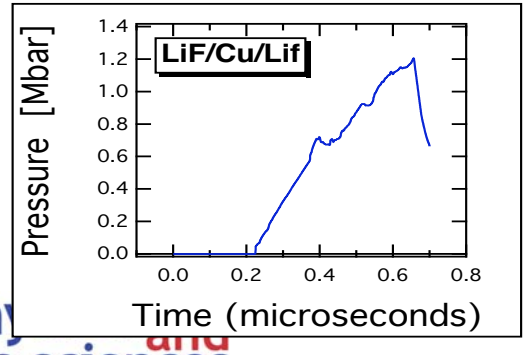

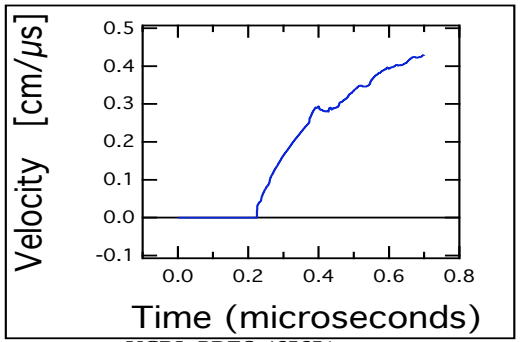

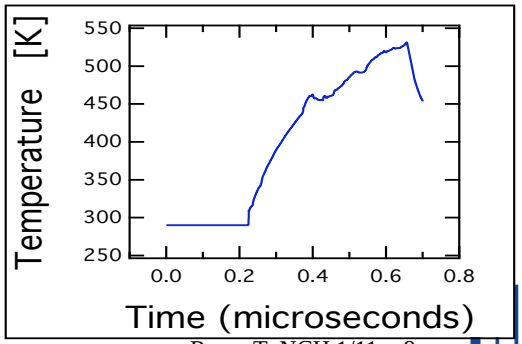

summary

- Thin is in!
- A thin sample may make temperature measurements under ramp, or combined shock/ramp loading practical
- The window thickness must be designed as part of the experiment

Investigation of temperature measurement of material under dynamic loadings using infrared optical pyrometry

Camille Chauvin, Jacques Petit

Summary

Introduction

Temperature measurement by optical pyrometry

Target design

Conclusion / Outlooks

Interest of temperature measurement

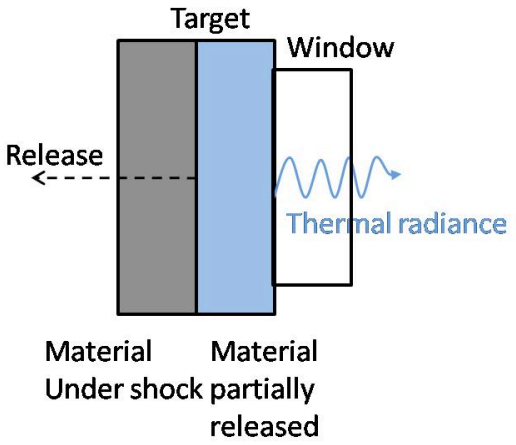

Objectives:

To define, to model and to understand the behavior of material under dynamic loading.

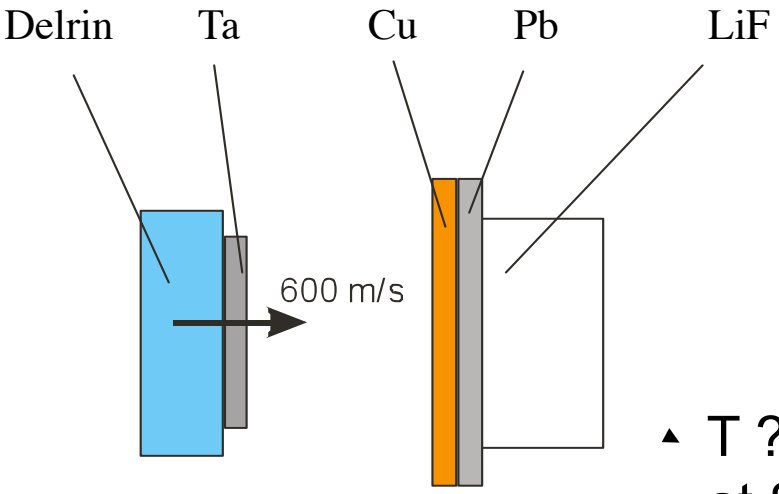

- T ?
  at 8 GPa

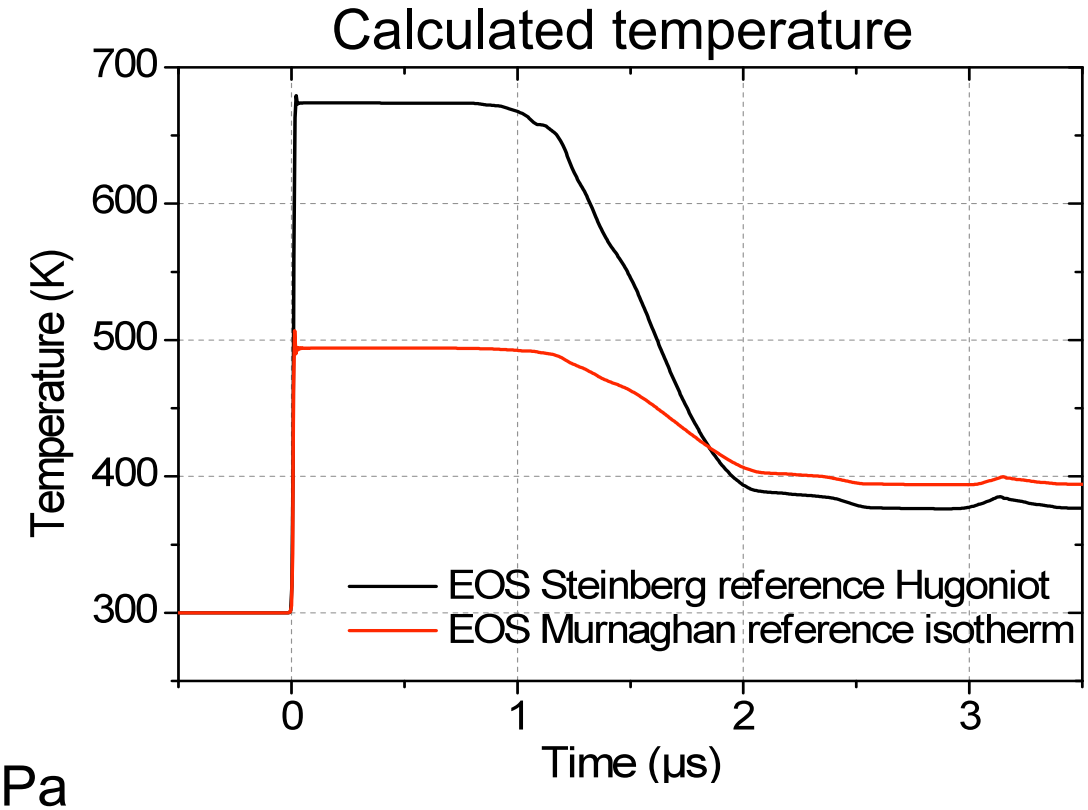

Goals of this work

Determination of the material temperature under shock wave or ramp compression from the thermal radiance of the surface.

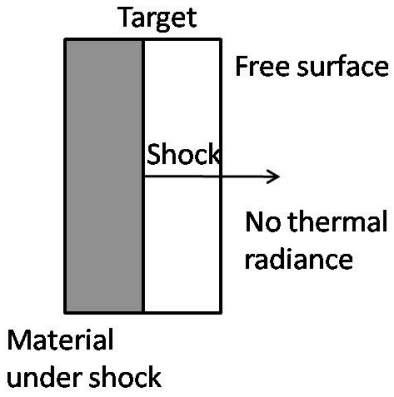

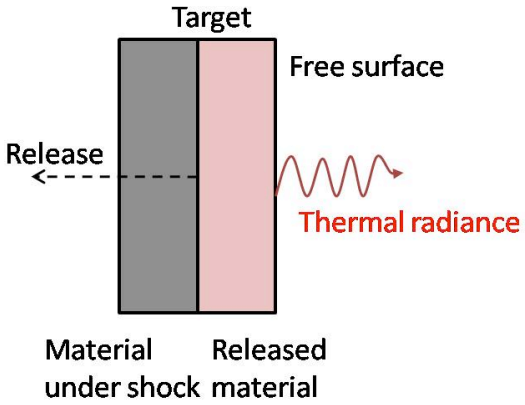

Managing to detect surface radiance at moderate shock amplitude (below 20 GPa, below 600 K)

- while improving the accuracy of the material temperature measurement,
- while understanding the origin of the detected radiances (thermal transfer).

Summary

Measurement of radiance

Main difficulty : Planck's law links the detected thermal radiance to the temperature only for blackbody.

The detected radiance emitted by a real object depends on its temperature and its emissivity.

$$L(\lambda,T) = \varepsilon(\lambda,T).L^{0}(\lambda,T)$$

1 measurement **but** 2 unknowns

→radiance L → emissivity ε

→ temperature T

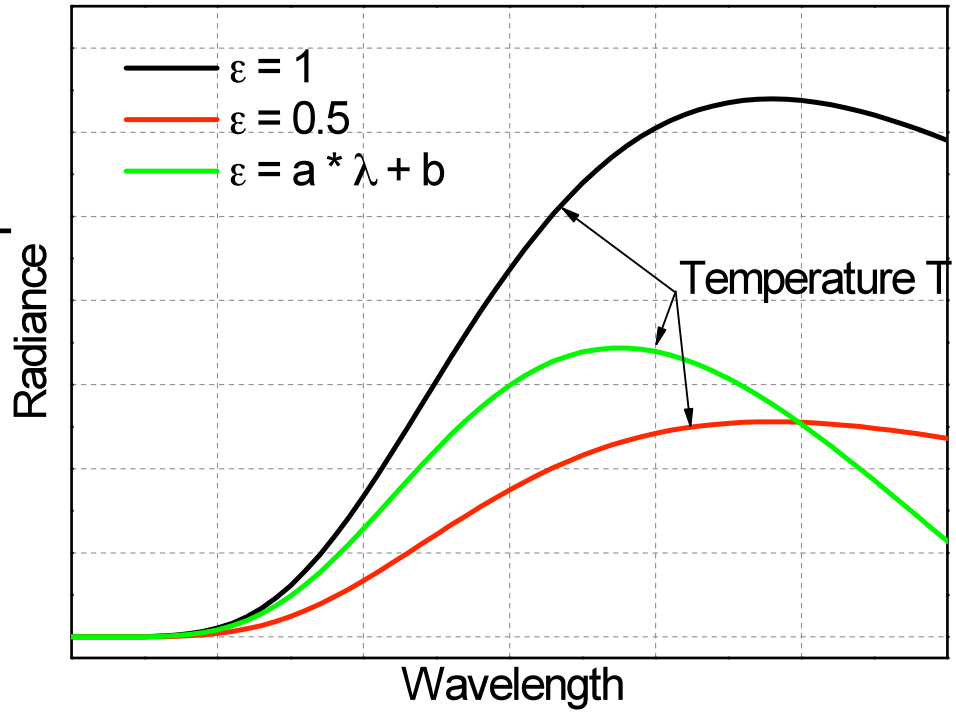

Lowering the influence of emissivity

- Emissivity boundaries

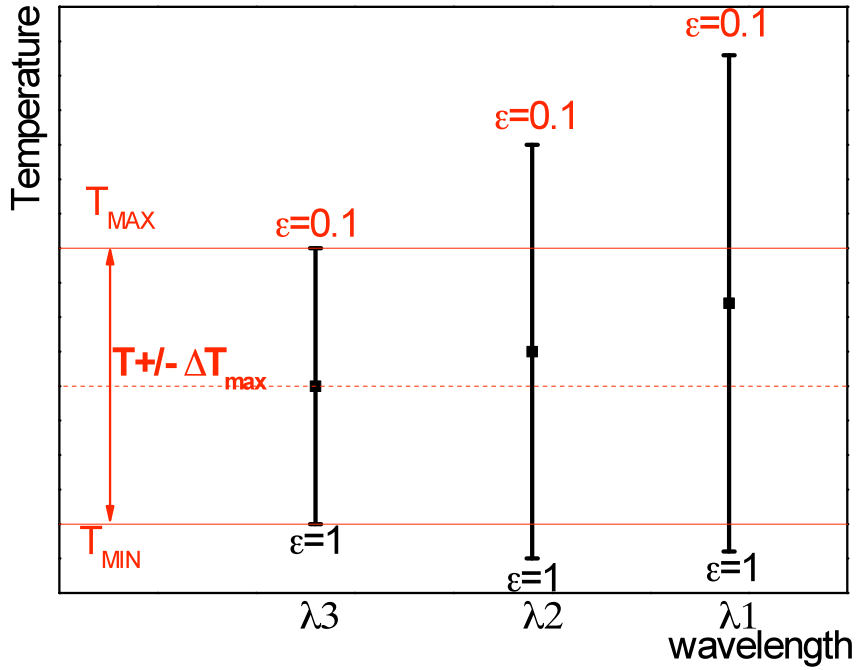

-The lower and upper boundaries of emissivity give the upper and lower boundaries of temperature on each temperature channel.
-The true temperature is where the temperature range overlap.

Lowering the influence of emissivity

- Analytical law for emissivity (well-adapted for multi-wavelength pyrometer)

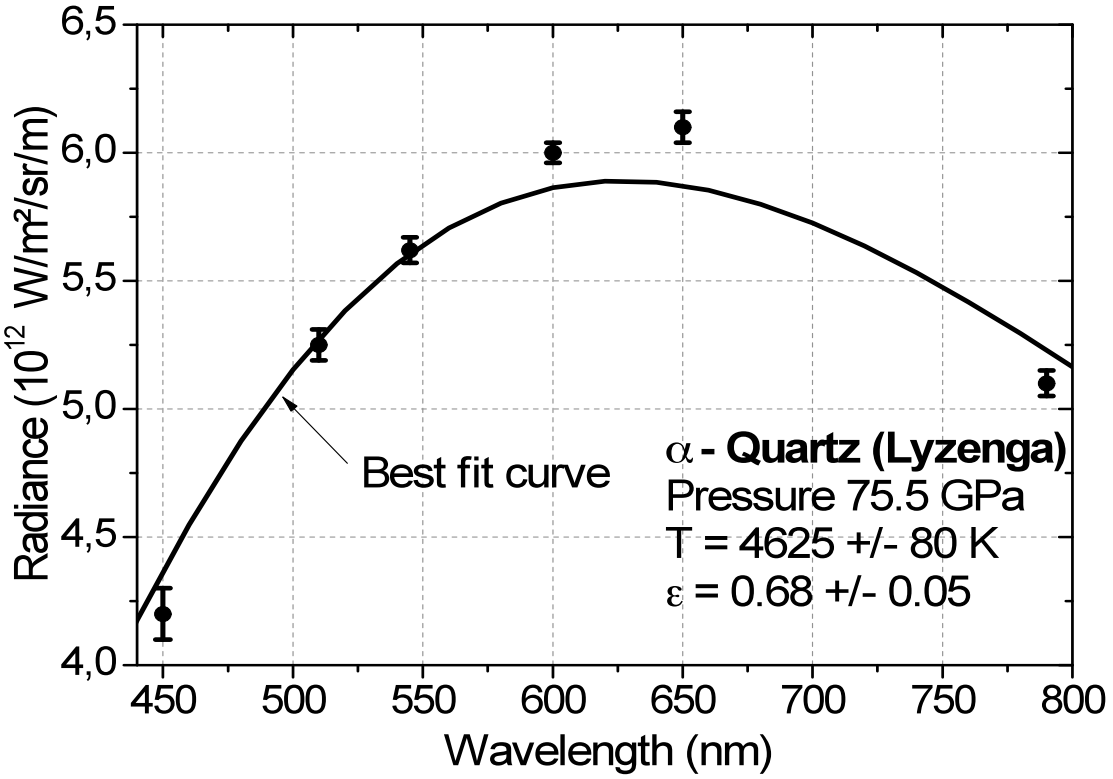

Infrared optical pyrometer

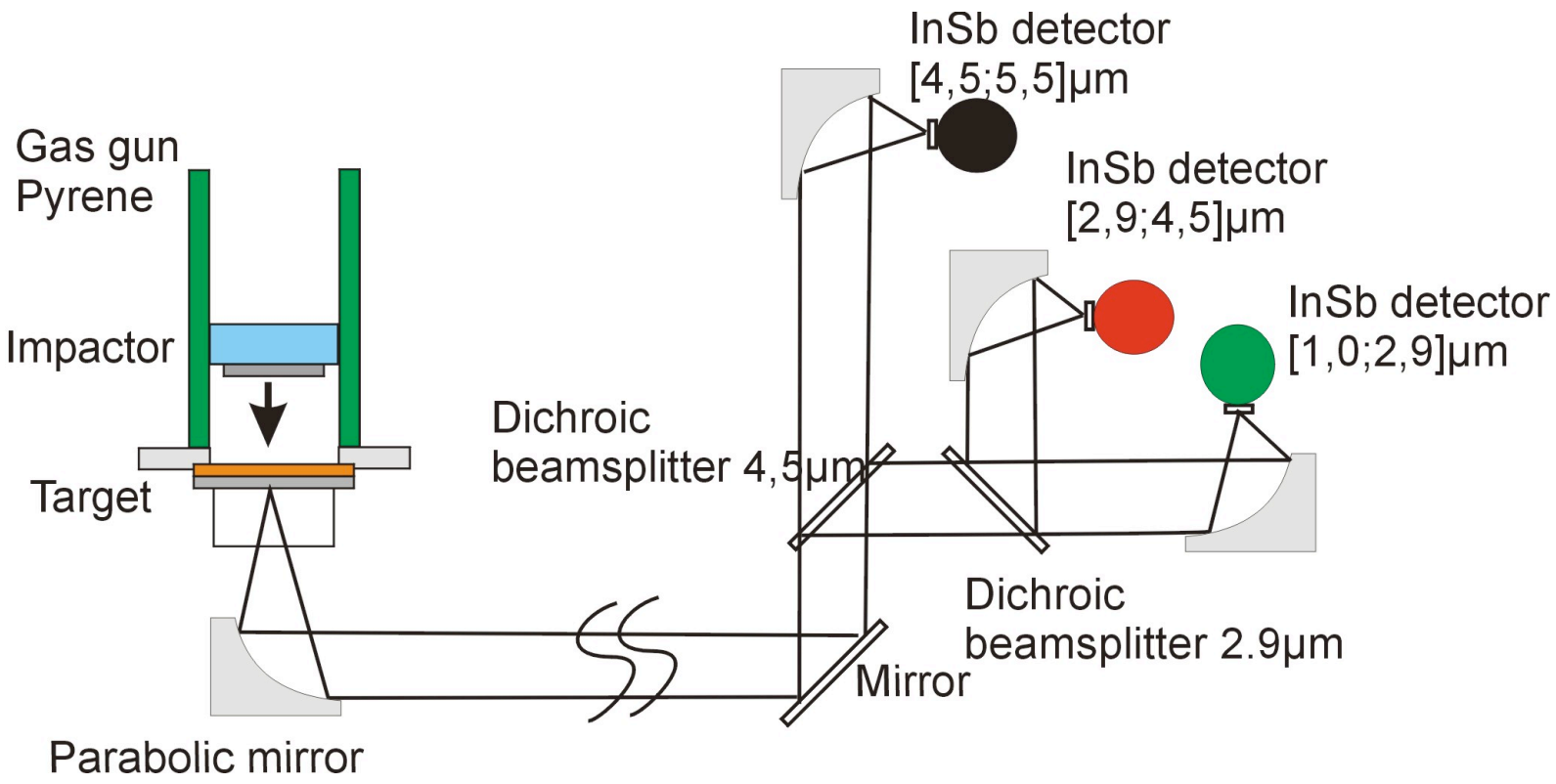

Minimal temperature: 350 K
Response time: 70 ns

Optical pyrometer design

Application:
shock wave compression

Pyrène Launcher

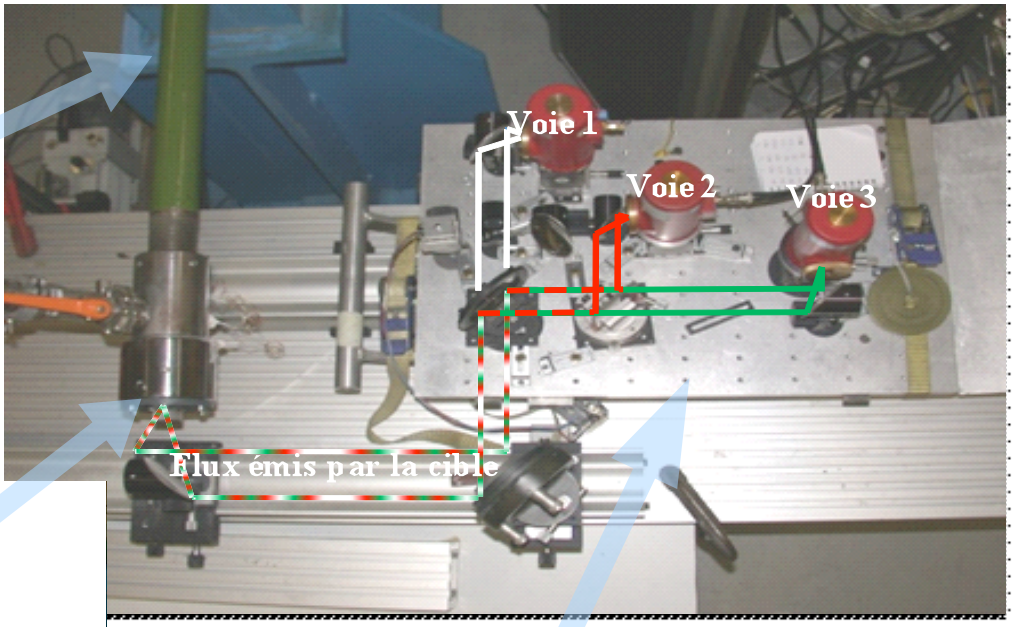

Parabolic mirror

Target

Debris protection

Pyrometer

Optical pyrometer design

Application:
ramp compression

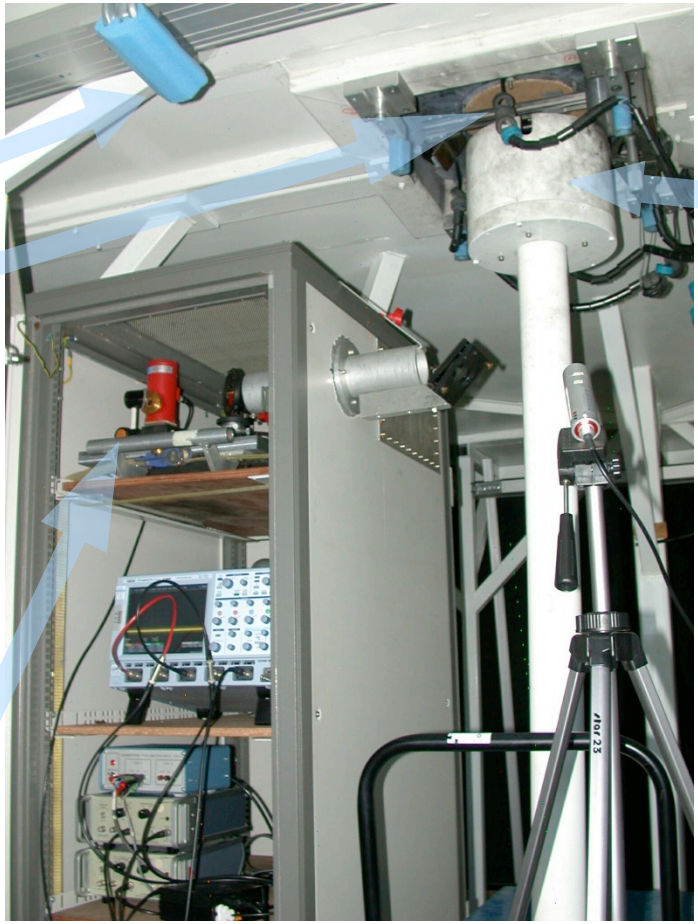

Unfolding method

The temperature of the material under shock is obtained in three stages:

1. Measuring the radiance temperature based on the radiance of each pyrometer channel.

2. Getting the true temperature:

   ⇒ hypothesis on emissivity.

3. Determining the temperature of the material from the true temperature:

   ⇒ choice of the target design

   ⇒ analysis of the thermal transfer phenomena at the interface.

Summary

Introduction

Temperature measurement by optical pyrometry

Target design

- residual or interface temperature?
- presence of glue
- use of an emissive layer and its compromise

Conclusion / Outlooks

Target design

Radiance emitted by the free surface of the shocked material.

- At the free surface

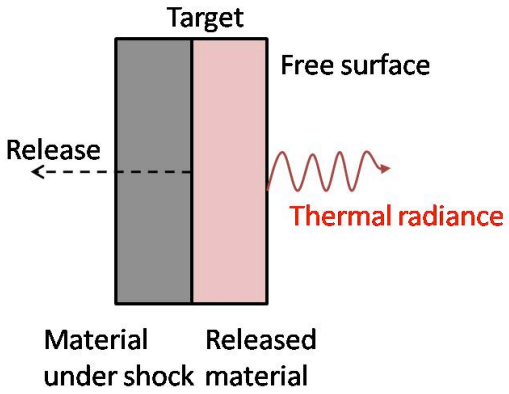

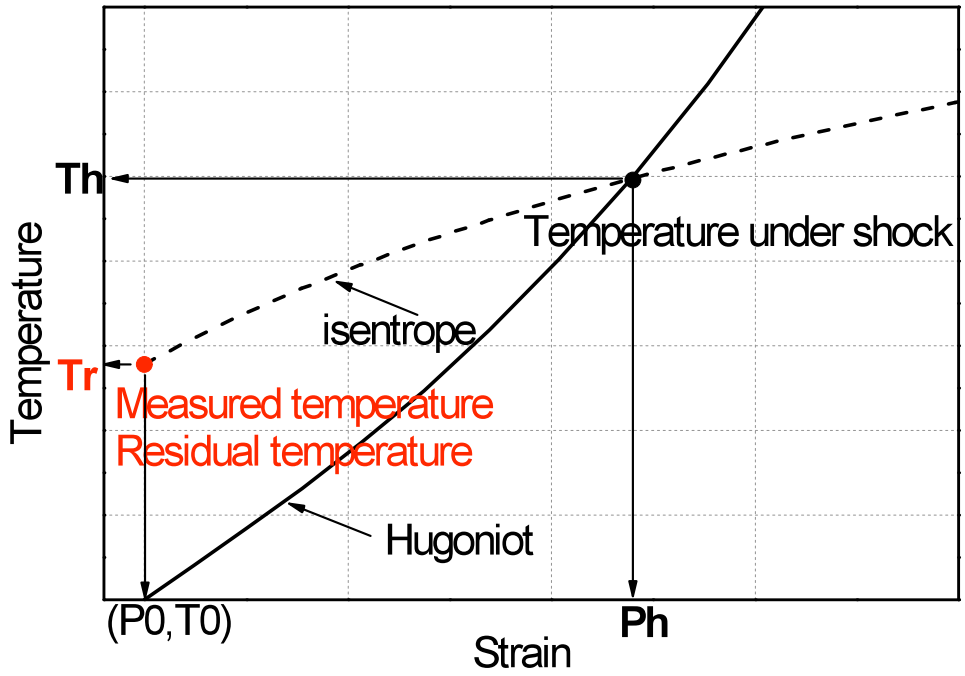

Advantage: measurement of the residual temperature,
→ follows the compression path of the material,
→ an emissive layer can be applied.
Drawback: temperature is sensitive on surface roughness
→ need a polished surface to prevent hot spots and ejecta,
→ low emissivity and so low radiance.

Target design

Radiance emitted by the interface of the shocked material.

- <u>At the interface between a material and a window</u>

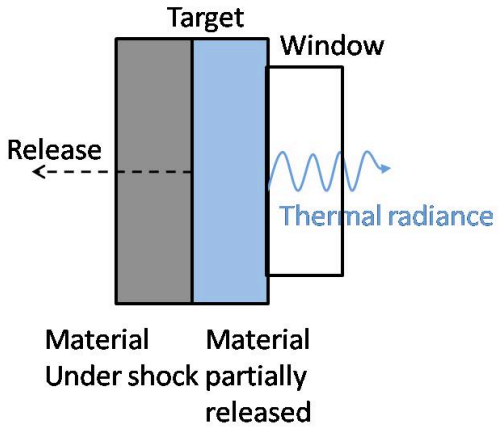

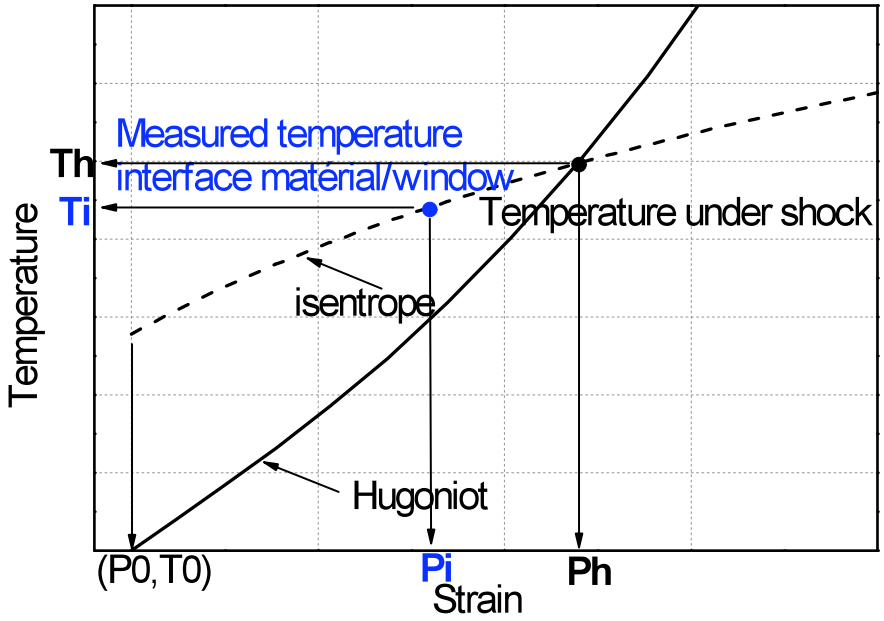

Advantage: interface and material temperatures are close,

→ more radiance,

→ presence of glue,

→ an emissive layer can be applied.

Interface temperature

The interface temperature is defined by the Fourier's Law:

$$T_I = T_1 - \frac{T_1 - T_2}{1 + \alpha} \quad \text{avec} \quad \alpha = \frac{\sqrt{(k\rho C_V)_1}}{\sqrt{(k\rho C_V)_2}}$$

α = 18

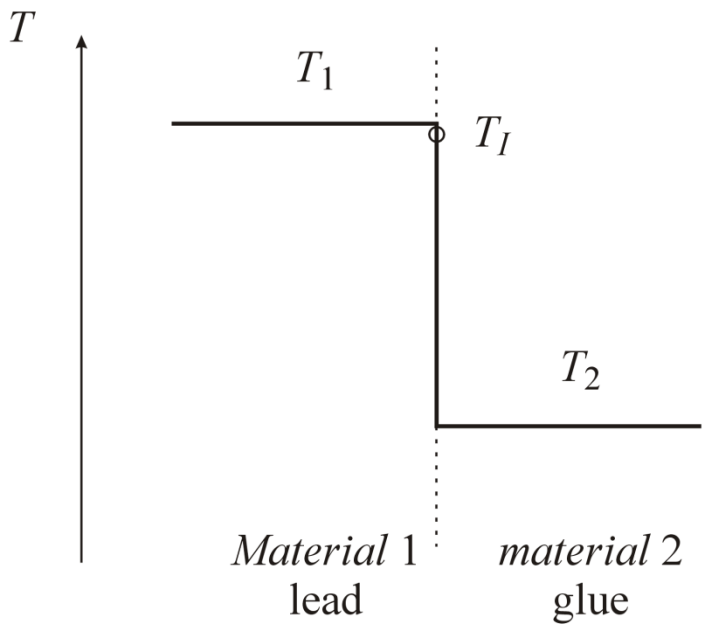

α = 0.9

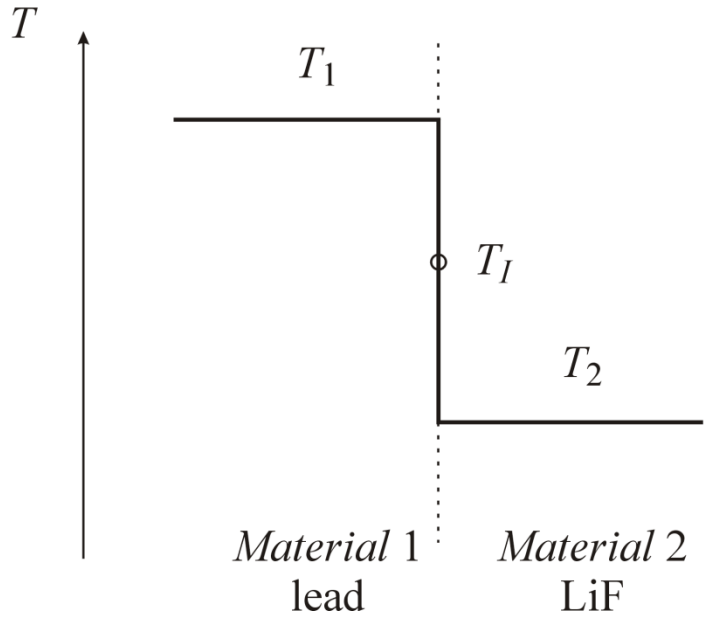

Presence of glue

The presence of the glue is essential to:
- realize a perfect contact between the material and the window,
- measure an interface temperature closest to the material temperature thanks to a thermal isolation and a low effusivity.

But, its transparency must be verified.

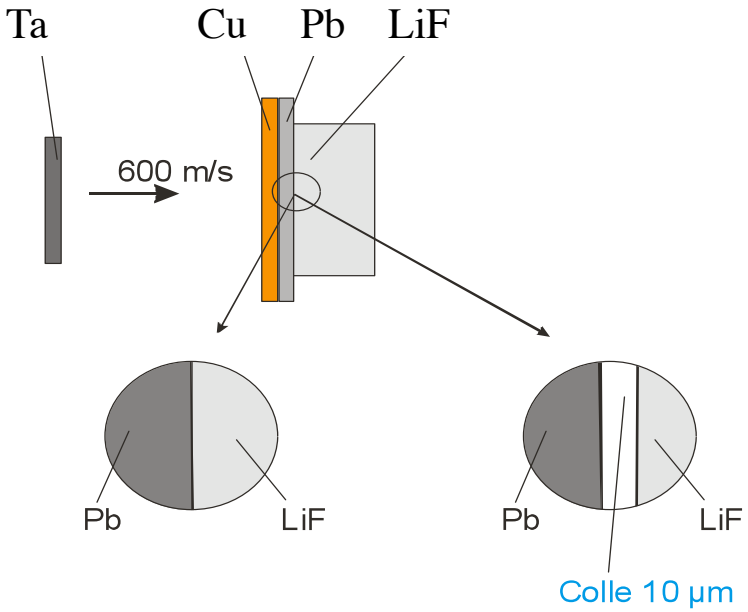

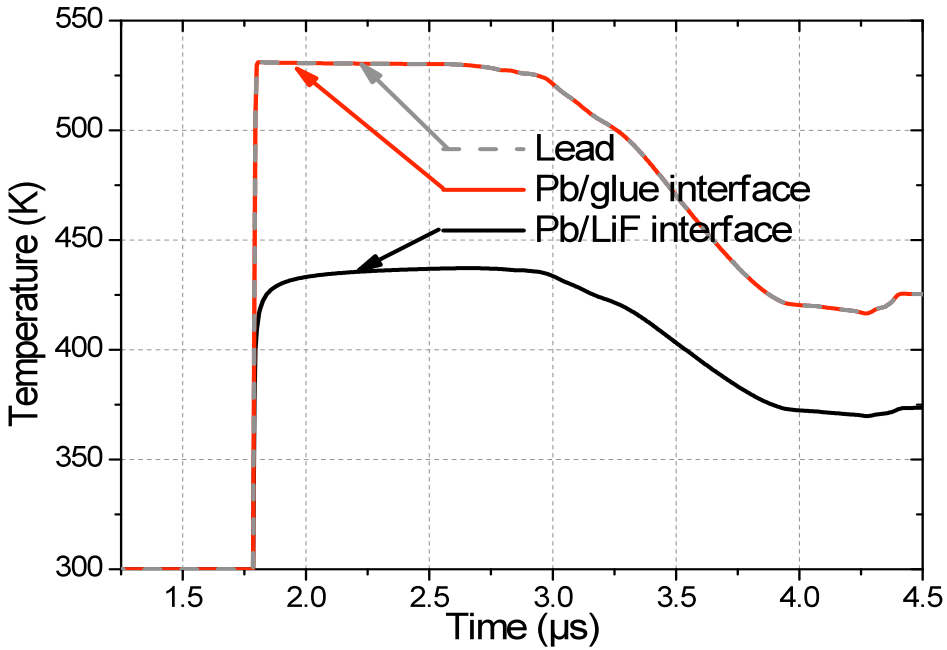

Interface only made of glue

The copper material emits a lower thermal flux than that of the lead.
The transparency of the glue is checked.

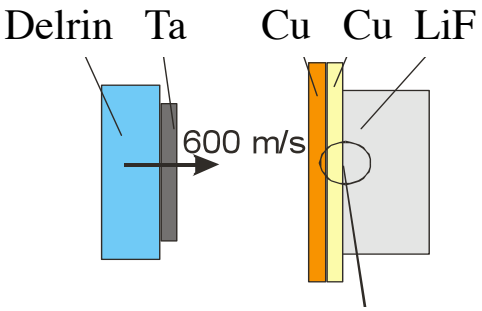

Impact on copper

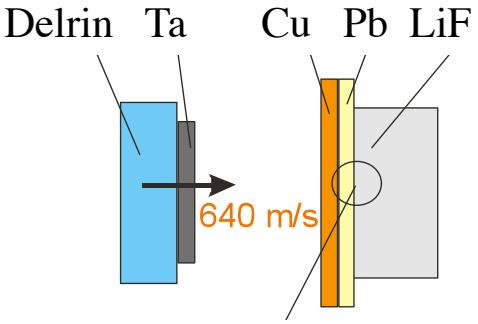

Impact on lead

Strain:
- in copper: 14,8 GPa.
- in glue: 8 GPa.

Strain :
- in lead: 12,5 GPa.
- in glue: 8 GPa.

Interface only made of glue

Cu / glue / LiF interface **Pb / glue / LiF interface**

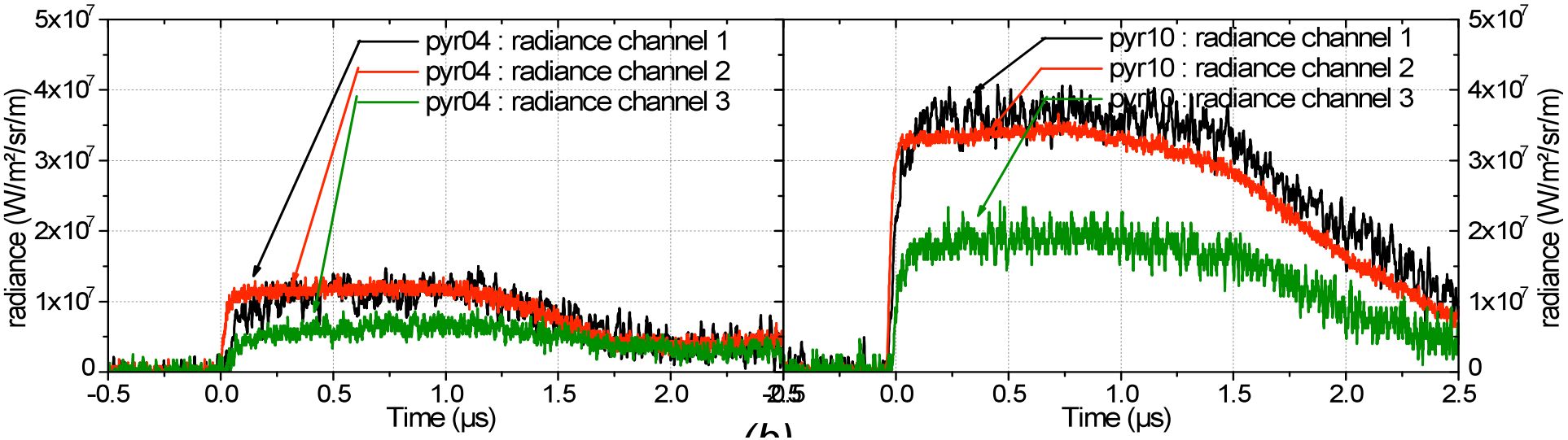

T = 422 ± 47 K
ε = 0.55 ± 0.45

T = 480 ± 25 K
ε = 0.70 ± 0.30

The collected radiances are different ➔ the glue remains transparent under shock wave compression.
The collected thermal flux is emitted by the material surface.

Interface only made of glue

Advantages:

The interface and material temperature are almost similar.

The interface temperature allows to investigate material behavior and polymorphic transition.

Nevertheless, the interface temperature is sensitive to the emissivity. So, the measured temperature accuracy is directly linked to the accuracy of the aimed surface emissivity.

$$\frac{\Delta T}{T} \approx \frac{\lambda k T}{h c_O} \frac{\Delta \varepsilon}{\varepsilon}$$

This interface temperature is also sensitive to the surface roughness and needs a polished surface.

Use of an emissive layer

The use of an emissive layer allows:

- to reduce the emissivity boundaries,
- to increase the collected flux → and so to improve the detection of low thermal flux.

The heat transfer in the different layers at the interface is only explained by thermal conduction.

This layer has to satisfy the following features to play the role of an emissive layer:

- an emissivity close to unity,
- an efficient thermal conductivity,
- a small thickness but guarantying opacity,
- a good adhesion between emissive layer and material.

Lowering the influence of emissivity

Use of emissive layer to improve apparent emissivity of the surface.

→The boundaries of the emissivity are more restricted,

→The deducted temperature accuracy is improved.

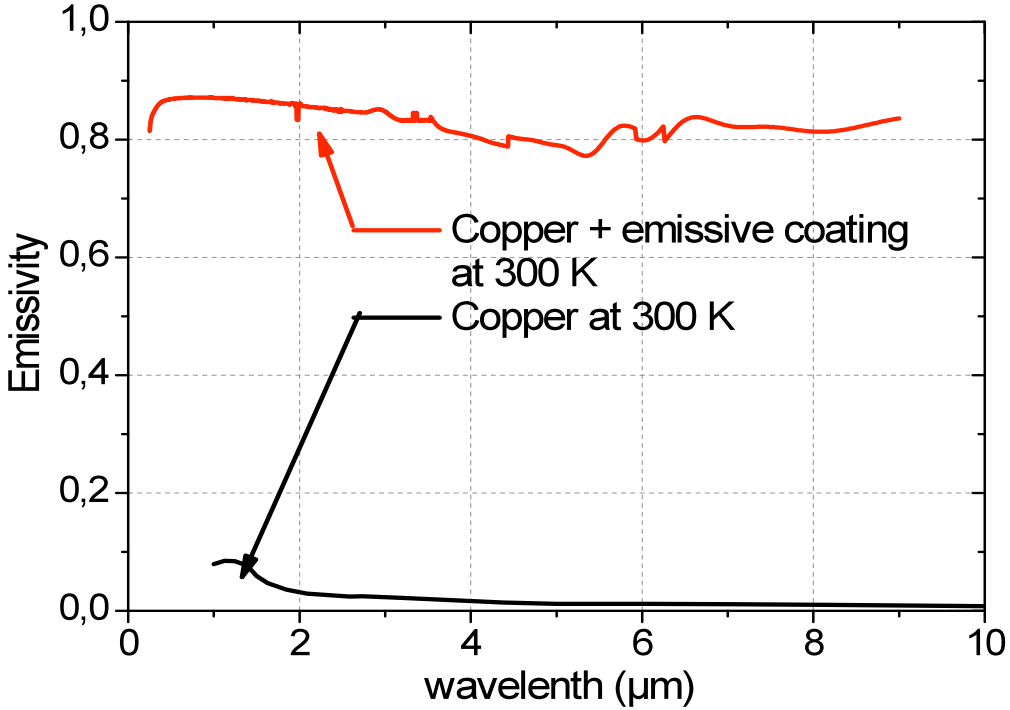

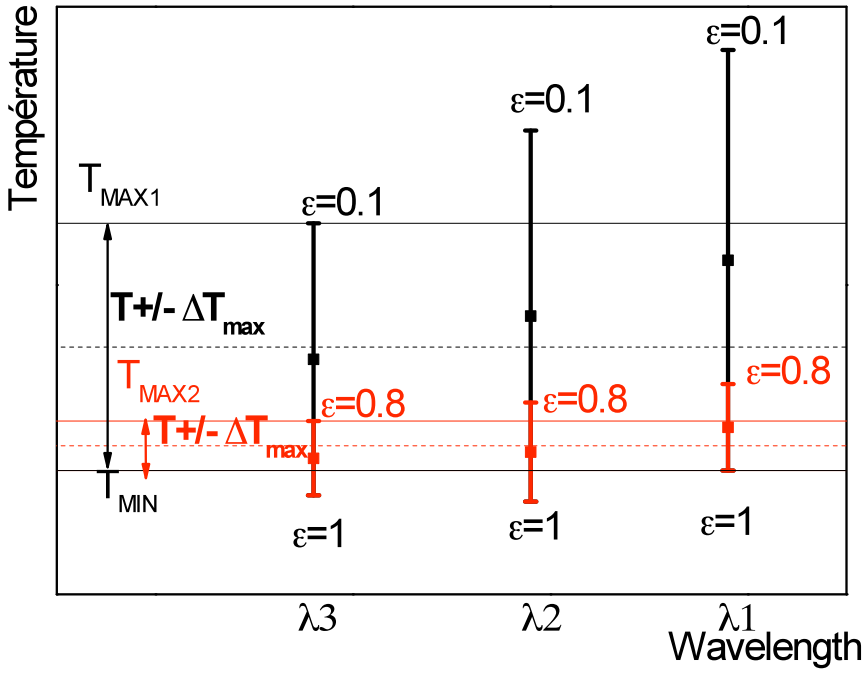

Emissive layer of $ReSi_2$ selected by numerical study

Pb / $ReSi_2$ / glue / LiF

thickness : 1 µm

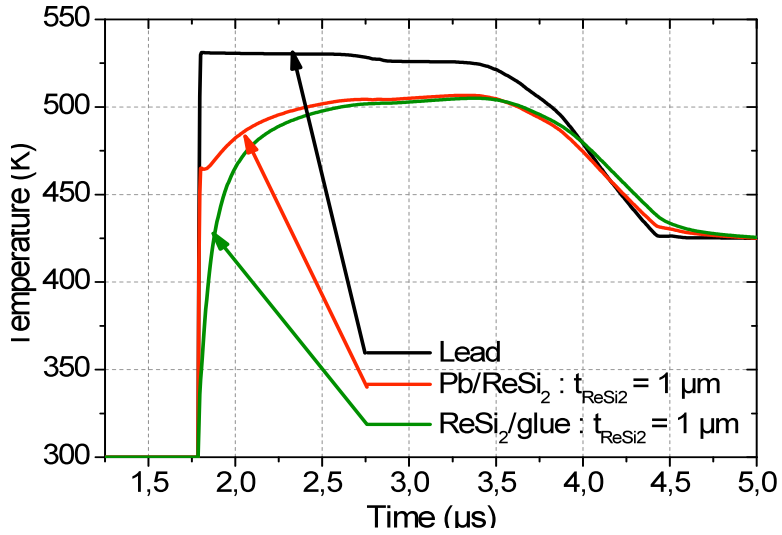

thickness : 0,5 µm

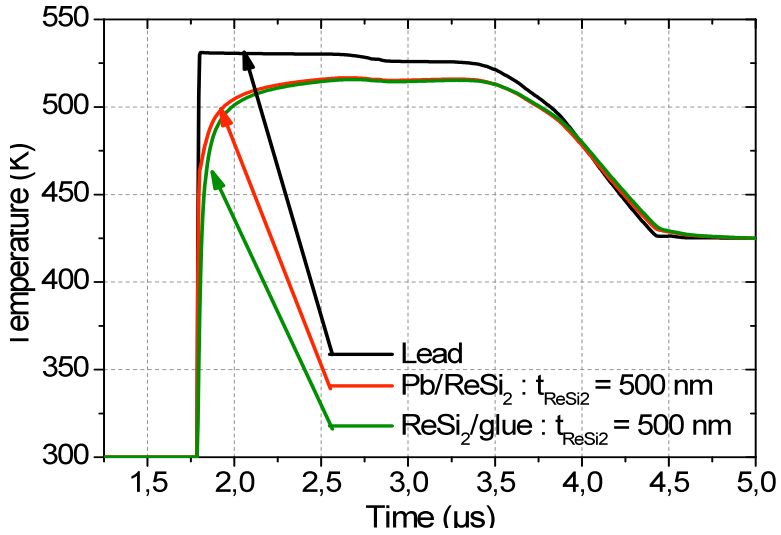

The interface temperature attains quickly a stable temperature.

Emissive layer of $ReSi_2$ selected by experimental study

Pb / glue / LiF

thickness : 1 µm
Pb / $ReSi_2$ / glue / LiF

thickness : 0,5 µm
Pb / $ReSi_2$ / glue / LiF

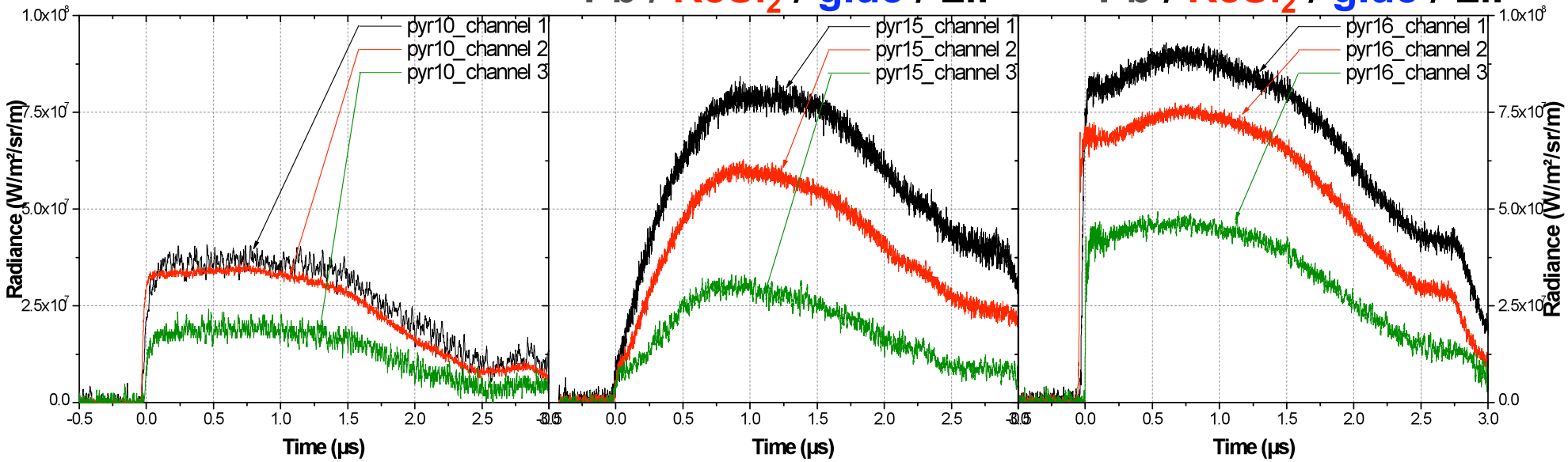

T = 480 ± 25 K
ε = 0.70 ± 0.30

T = 500 ± 10 K
ε = 0.85 ± 0.15

T = 515 ± 10 K
ε = 0.85 ± 0.15

This emissive layer increases the collected radiance of each channel.

Emissive layer of $ReSi_2$ selected by experimental study

Pb / glue / LiF

thickness : 1 µm
Cu / $ReSi_2$ / glue / LiF

thickness : 0,5 µm
Cu / $ReSi_2$ / glue / LiF

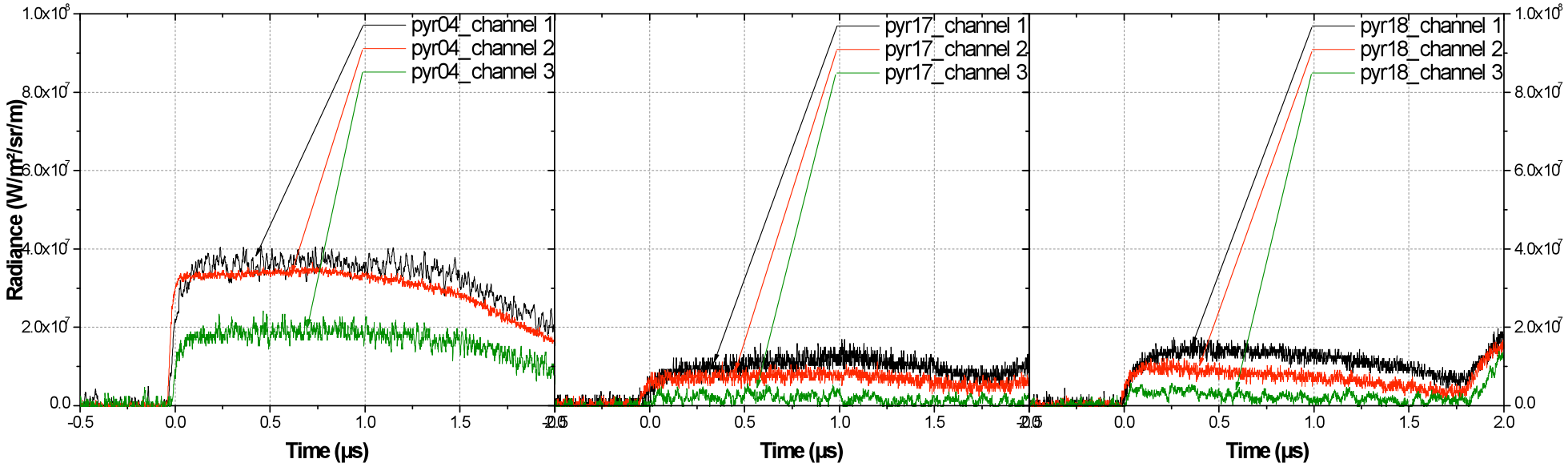

T = 480 ± 25 K
ε = 0.7 ± 0.30

T = 360 ± 10 K
ε = 0.85 ± 0.15

T = 370 ± 10 K
ε = 0.85 ± 0.15

Emissive layer of $ReSi_2$ selected by experimental study

Pb/$ReSi_2$ 1 µm/glue/LiF

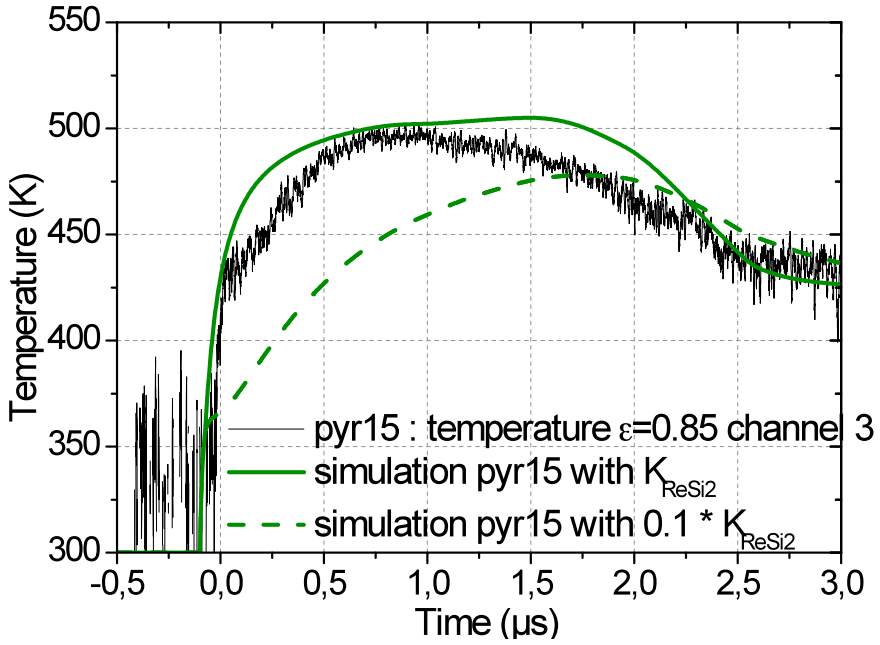

Pb/$ReSi_2$ 0,5 µm/glue/LiF

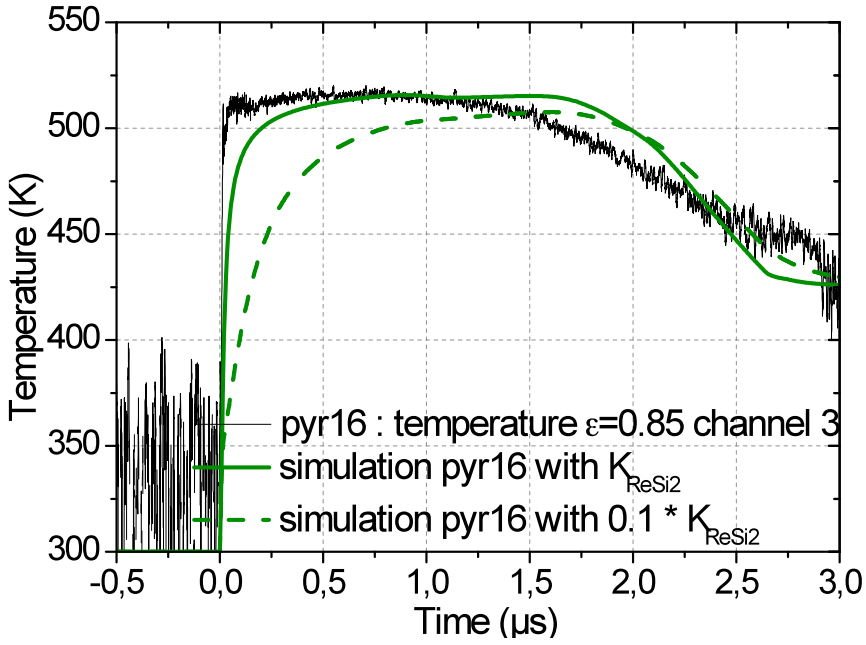

This emissive layer must be exactly defined to be used as a performant emissive layer (for example : thermal conductivity K).

Use of emissive layer

Advantages:

- The emissivity boundaries are restricted so the interface temperature is precisely determined.
- The collected flux is increased → and so the detection of low thermal flux is improved.
- The interface temperature is independent of the material emissivity and its possible variation.
- This layer avoids ejecta and hot spots.

However,

- The interface and material temperature are different,
- This layer must be perfectly known to obtain the material temperature,
- This layer could be adequate to observe polymorphic transition if its thermal conductivity and thickness are appropriate or if the ramp compression is enough softened.

Summary

A performant optical pyrometer

An infrared three-wavelength optical pyrometer has been developped allowing the low radiance temperature detection (from 350 to 1000 K) with a time response appropriate for shock experimentations.

Two independent methods to unfold the true interface temperature can be applied : short wavelength or analytical law for emissivity.

Both velocity and temperature measurements can be obtained and allow to temporally compare the wave propagation and the heat transfer.

Target design:

Temperature measurement is a compromise for the target design:

- a window is used to measure an interface temperature as close as possible to that of the material temperature,
- an emissive layer is applied at the interface to specify the value of the emissivity and so the interface temperature.

The emissive layer manages to increase the accuracy of the interface temperature (accuracy better than 5%). But, it is not the material temperature. This approach is appropriate for experimentations with supported wave compression to allow the thermal equilibrium.

Nevertheless, with a single glue layer, the interface temperature is that of the material temperature but with an unsatisfactory accuracy (< 10%).

Outlooks

An accurate measurement at low temperature with this three-wavelength infrared optical pyrometer associated to an effective emissive layer could provide some interesting information:

- for the study of material under other kinds of dynamic loadings (isentropic compression , laser shock compression),

- for evaluating the heating by plastic work,

- for detecting the polymorphic transition of the material under loading and for deducing a kinetic transition model.

New 2-D Interferometry Results for Laser-Driven Compression of Si (and Al)

Raymond F. Smith

Lawrence Livermore National Laboratory

Original concept developed by Dave Erskine in 1995

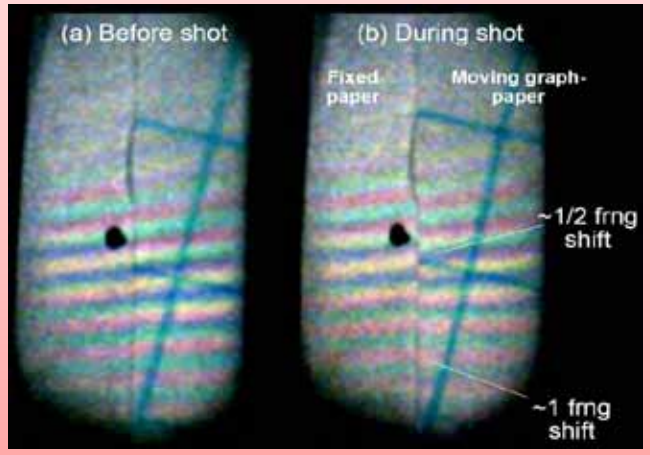

D.J. Erskine, Nature, 377, 317 (1995)

Recently developed by Peter Celliers to study shock planarity for NIC campaign

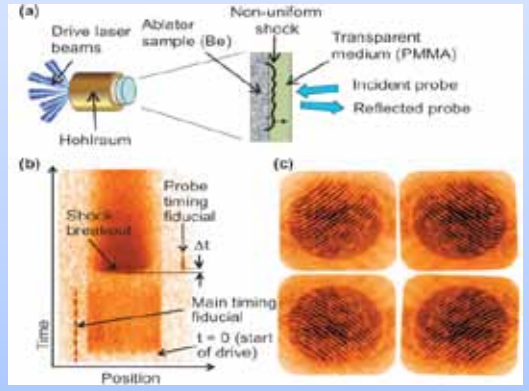

P.M. Celliers et al., RSI (2010)

New 2-D Interferometry Results for Laser-Driven Compression of Si (and Al)

Raymond F. Smith

Lawrence Livermore National Laboratory

Thanks to Collaborators

Dave Erskine, Cindy Bolme (LANL) , Peter Celliers, Jon Eggert, Gilbert Collins (LLNL)

Previous Silicon Data shows a large discrepancy between free surface and insitu measurements

Si Free Surface
(Gust and Royce JAP '71, Goto JJAP '82)

Si/LiF
(Turneaure APL '07)

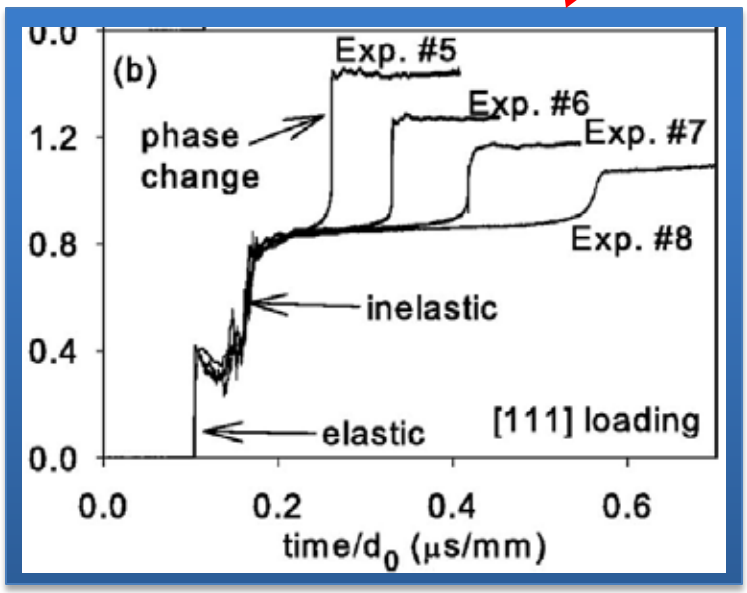

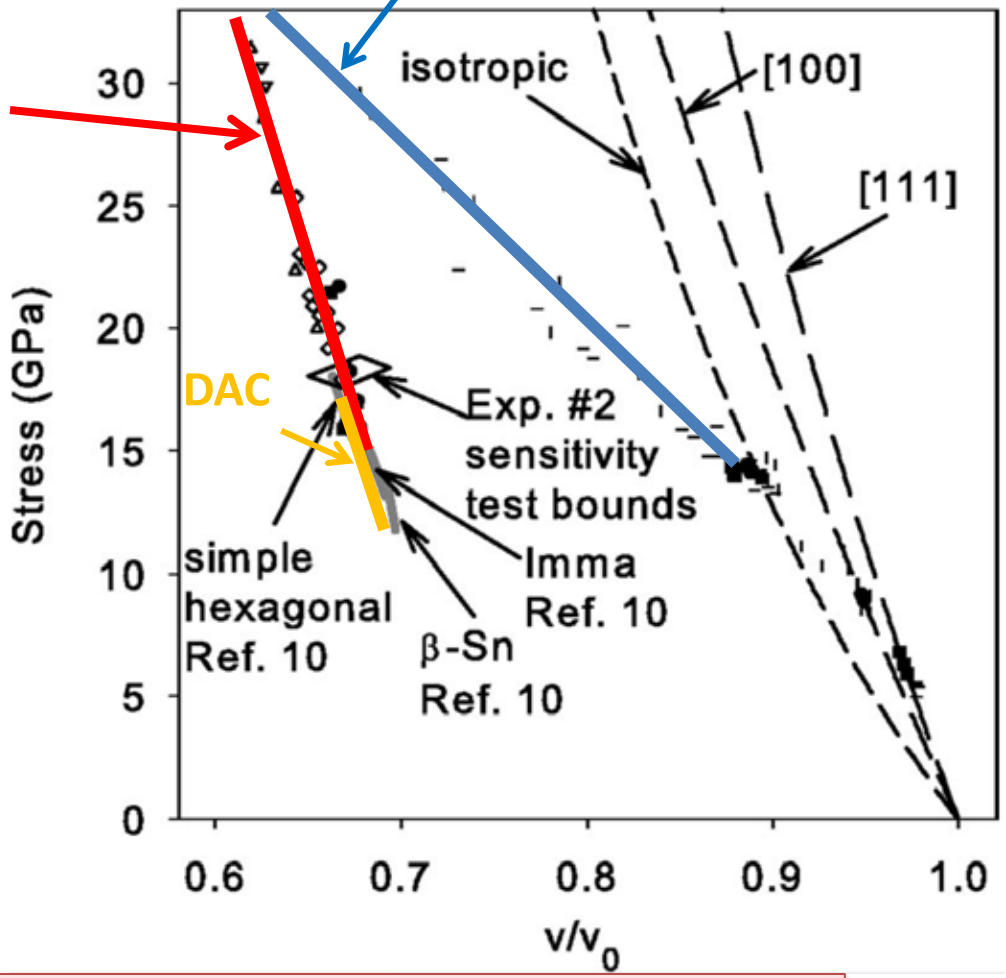

Larger Plastic Wave Speeds were measured for the free surface experiments

When does the onset of significant plasticity occur? ….a, b, c?

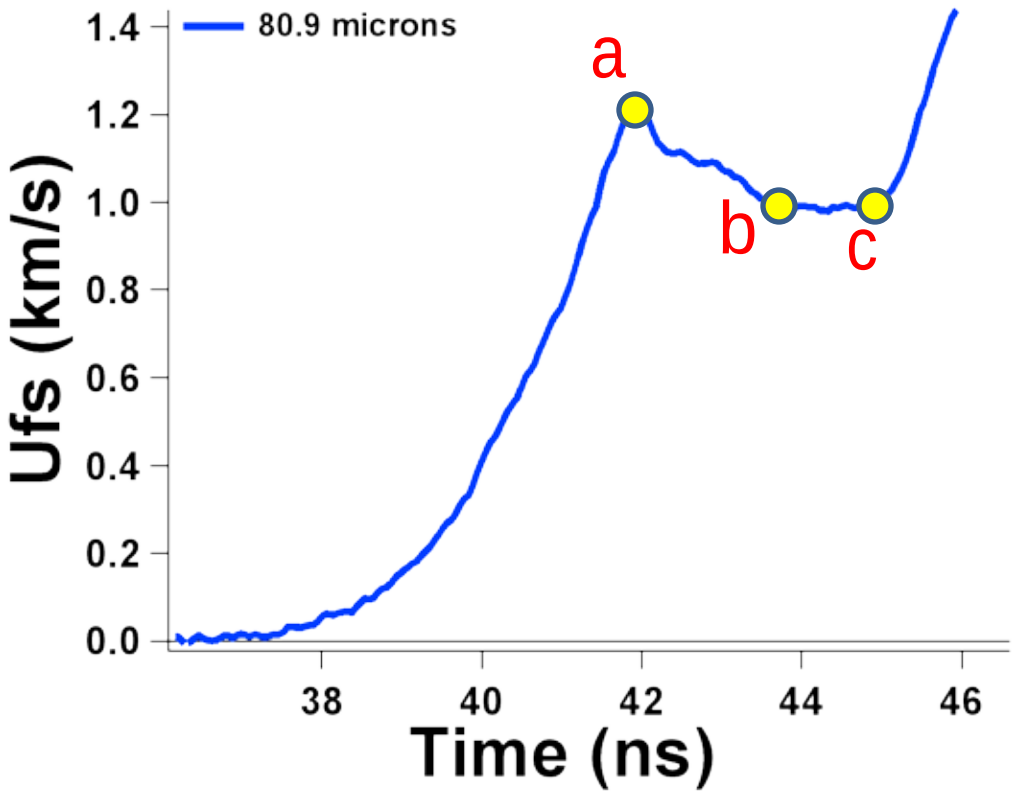

JAVELIN Setup on the Janus Laser Facility

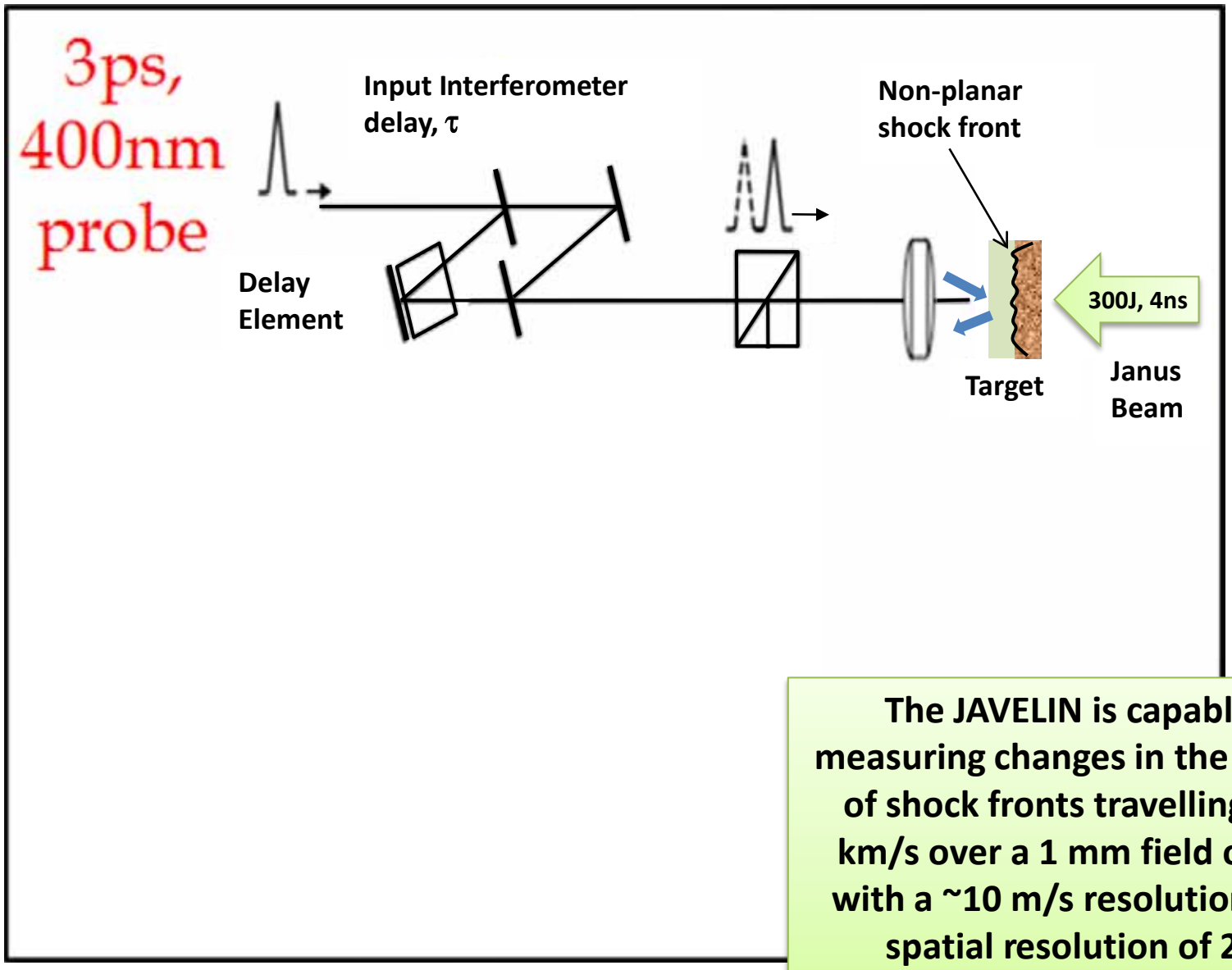

The JAVELIN is capable of measuring changes in the velocity of shock fronts travelling at 20 km/s over a 1 mm field of view with a ~10 m/s resolution and a spatial resolution of 2μm

JAVELIN Setup on the Janus Laser Facility

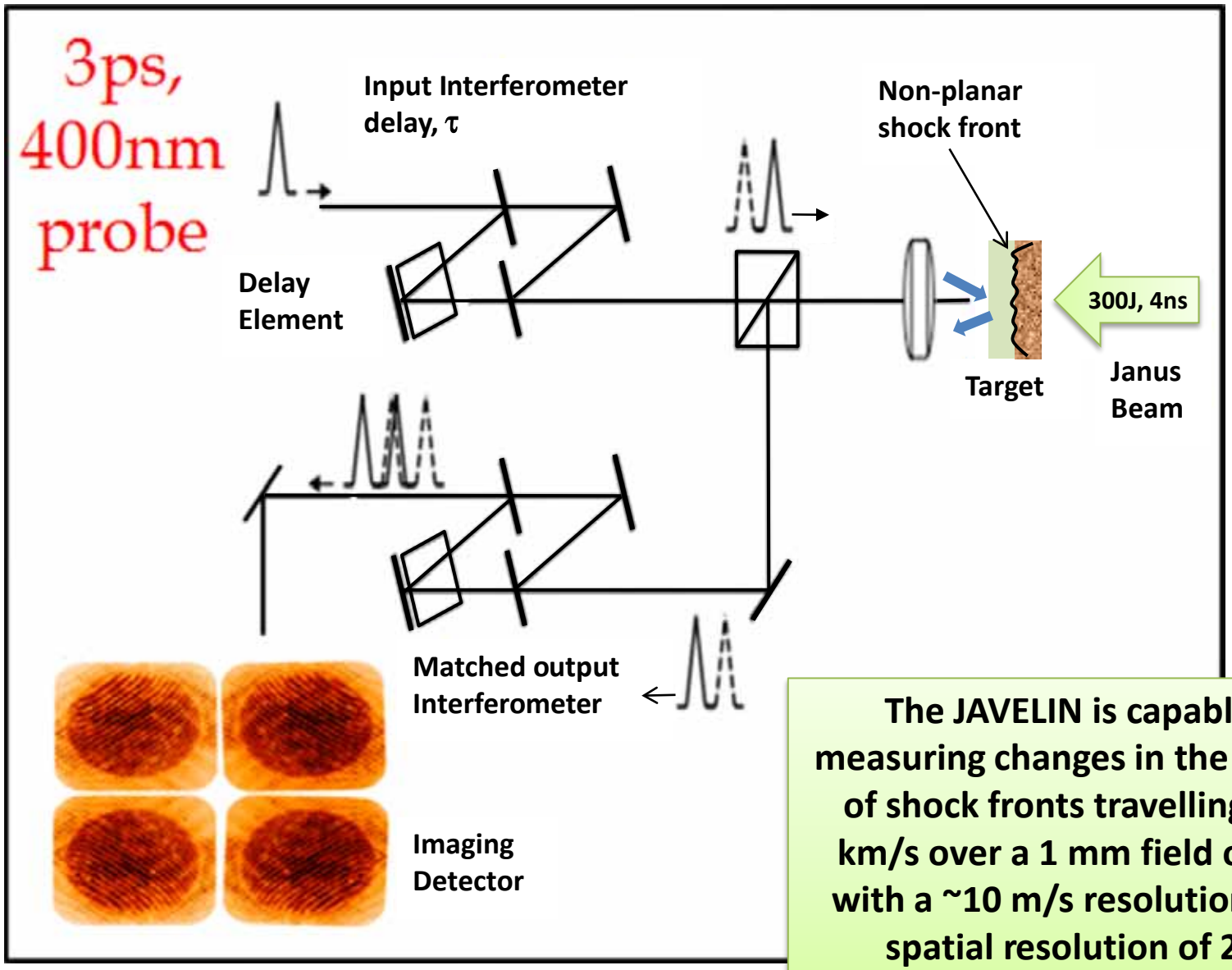

The JAVELIN is capable of measuring changes in the velocity of shock fronts travelling at 20 km/s over a 1 mm field of view with a ~10 m/s resolution and a spatial resolution of 2μm

Analysis

Grid aligns 4 images --> each target pixel has 4 input intensities
S_0, S_{90}, S_{180}, S_{270}

4-channel quadrature push-pull math used, analogous to point-VISAR

Summing complementary signals NF=(S_0+S_{180}) or (S_{90}+S_{270}) yields “ordinary” nonfringing image. Fringes cancelled.

Push-pull summing yields complex output. “Ordinary” image cancelled.
$F = (S_0 - S_{180}) + i(S_{90} - S_{270})$
Convert to polar coordinates
Phase proportional to velocity --> image of phase is output

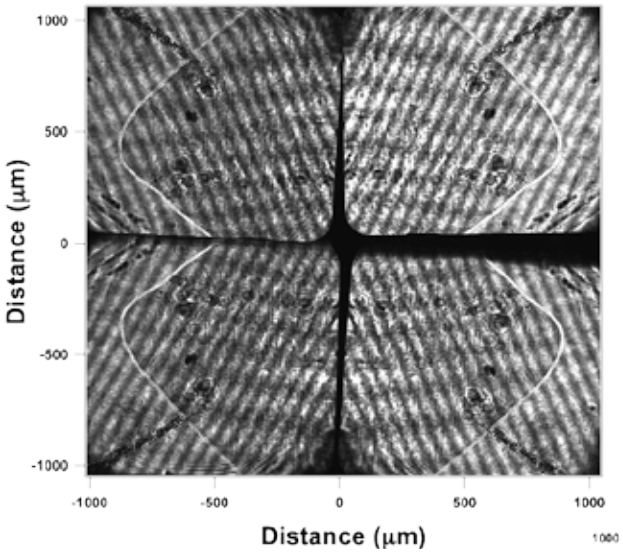

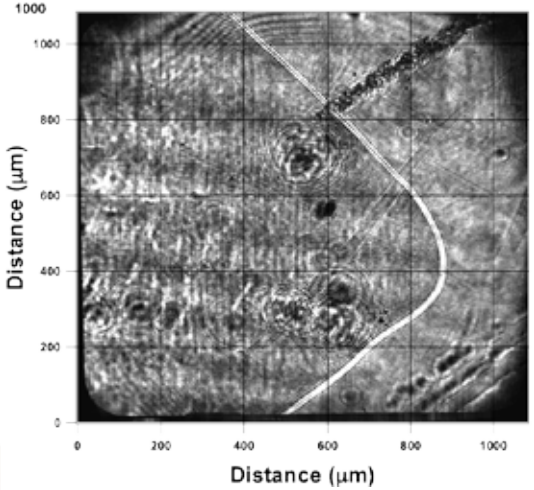

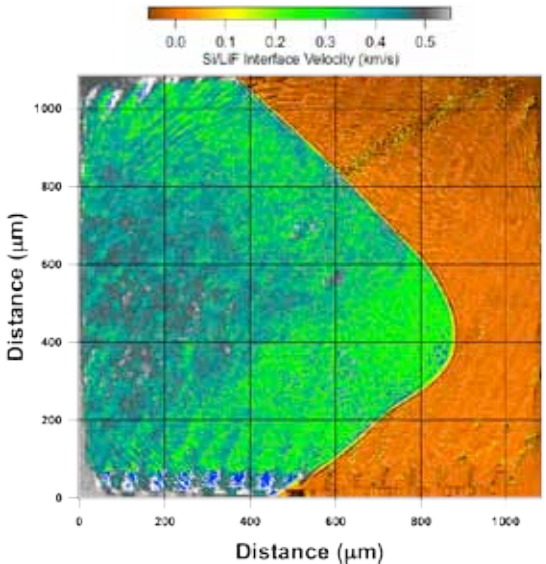

Goal of Experiment:

- Measure changes in reflectivity and velocity related to different deformation mechanisms:
  - Elastic to Plastic
  - Polymorphic phase transformation
  - Surface Fracture of free surface samples.

Target Design

Janus Laser focused down to 1mm focal spot

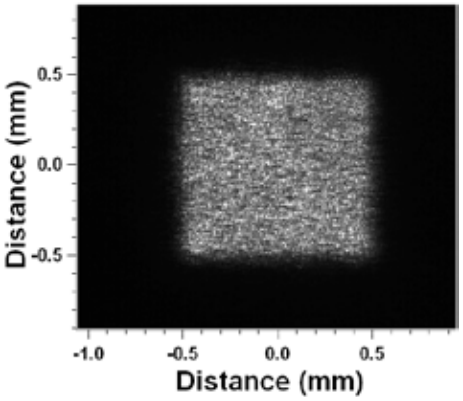

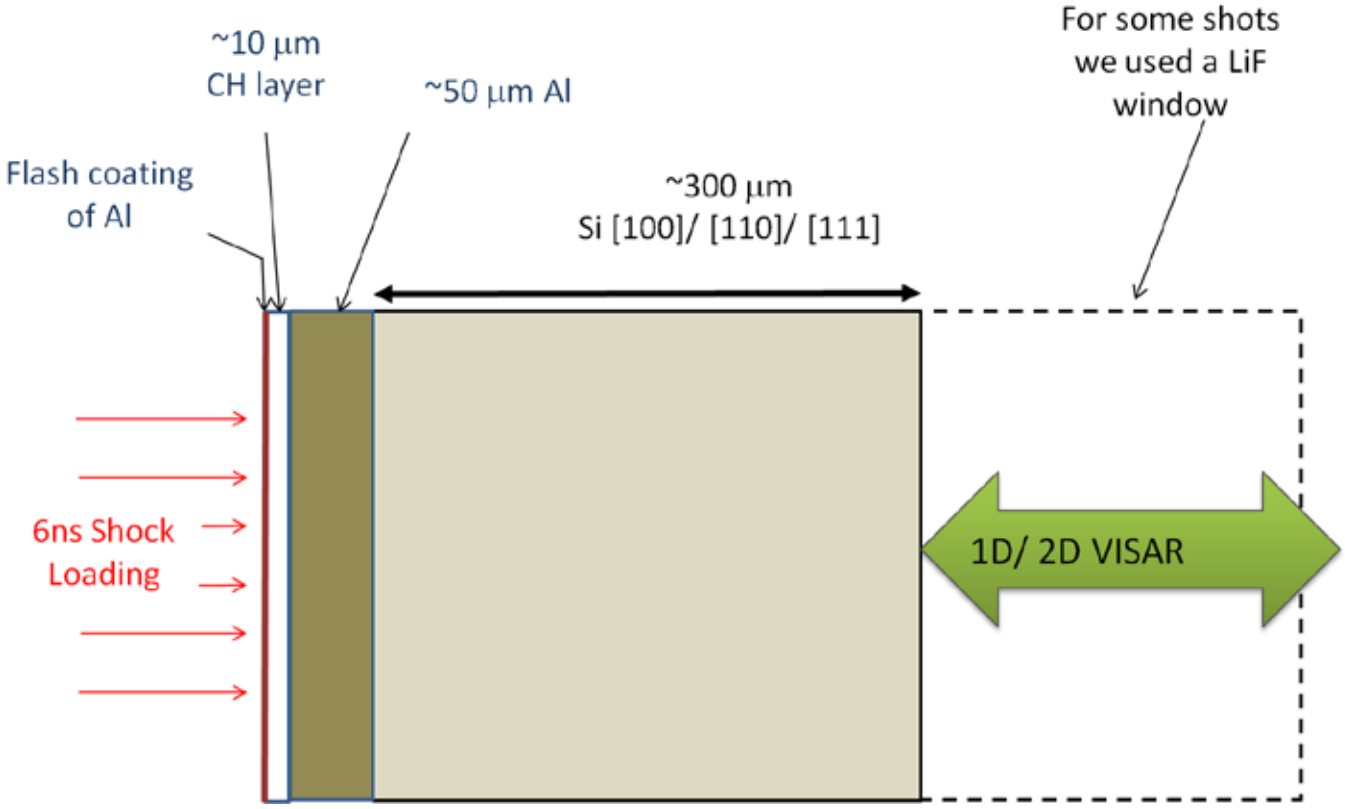

Combined use of 1D and 2D VISARs allow us to diagnose evolution of deformation

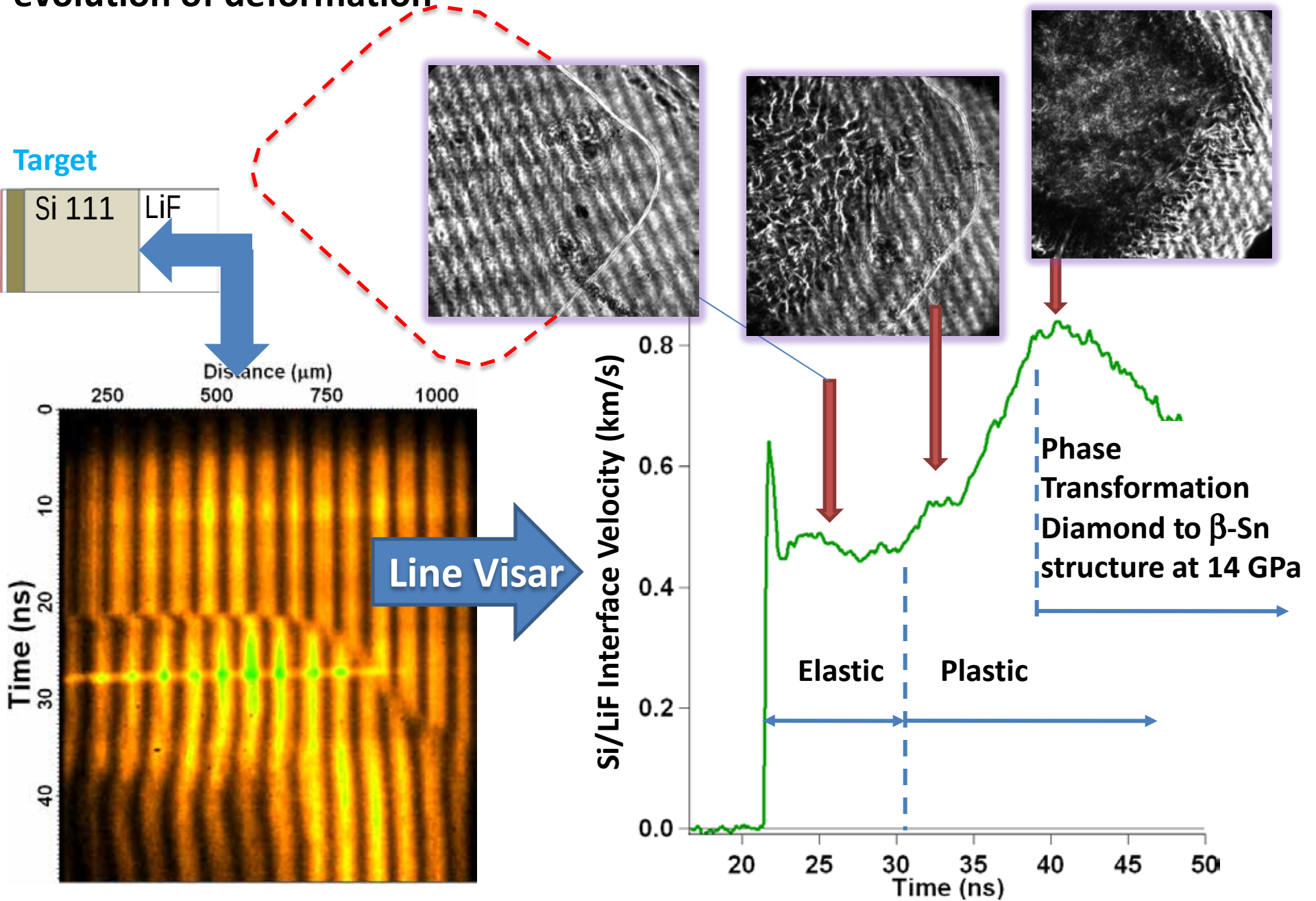

Velocity and Reflectivity changes are relatively smooth within Elastic precursor

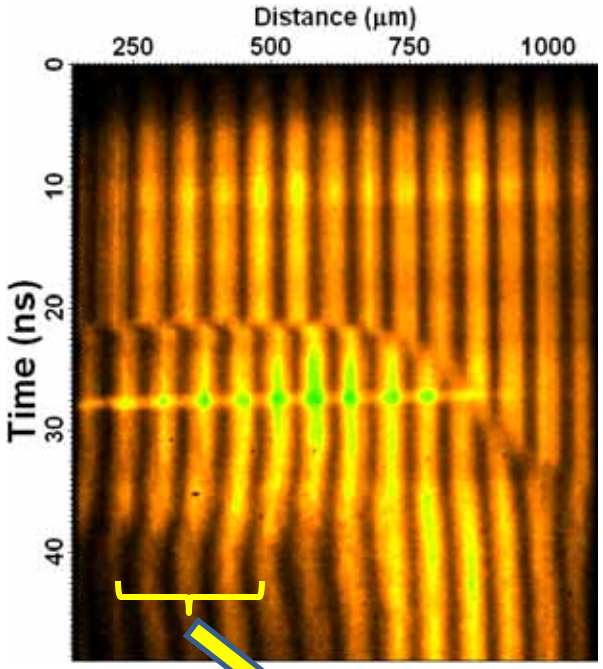

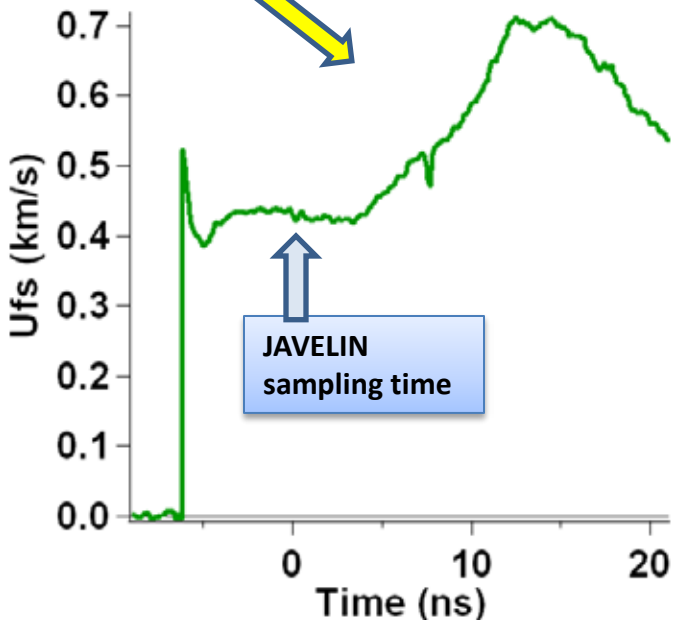

1mm Drive spot

Si 111/LiF

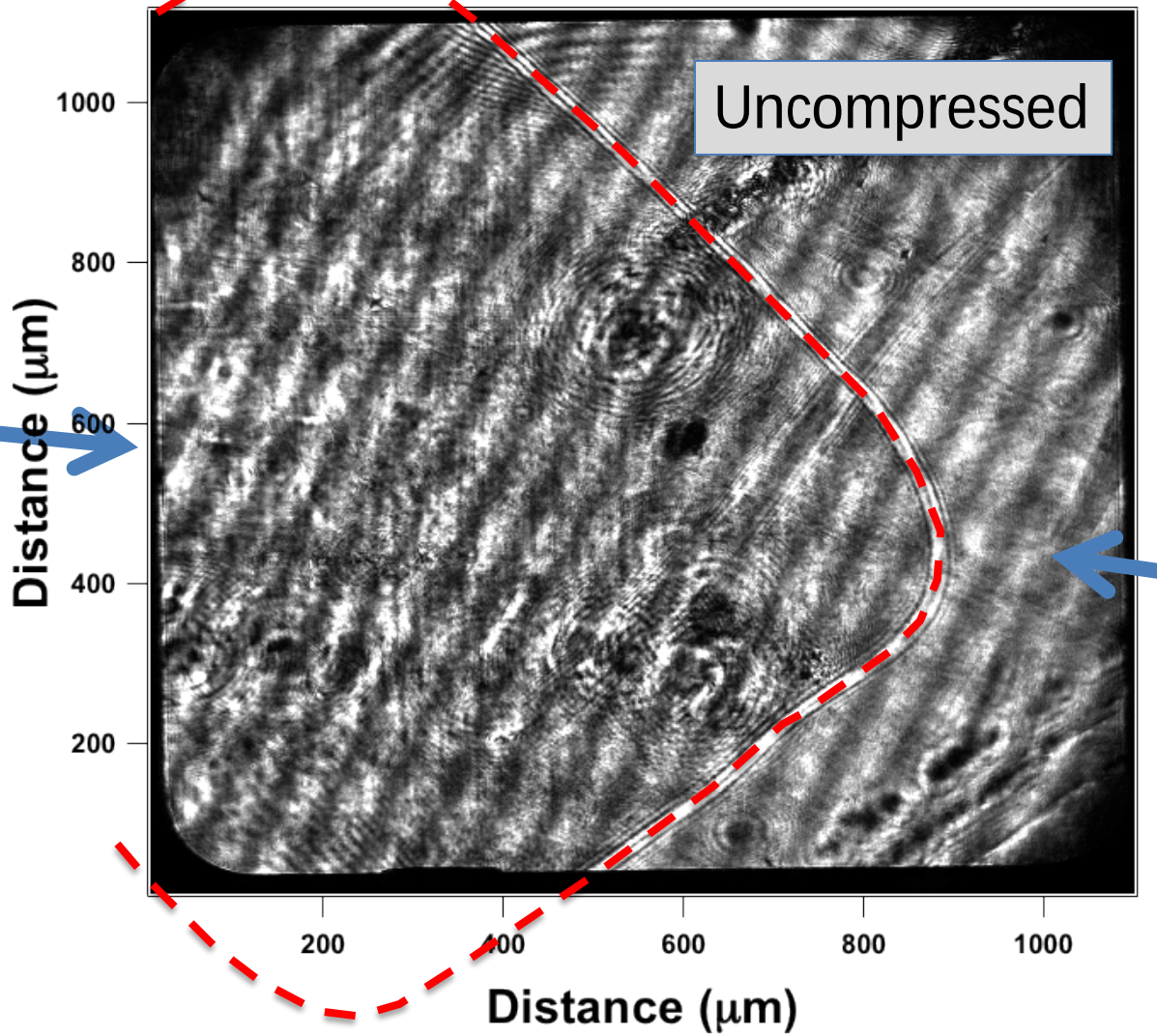

Velocity and Reflectivity changes are relatively smooth within Elastic precursor

Velocity Map

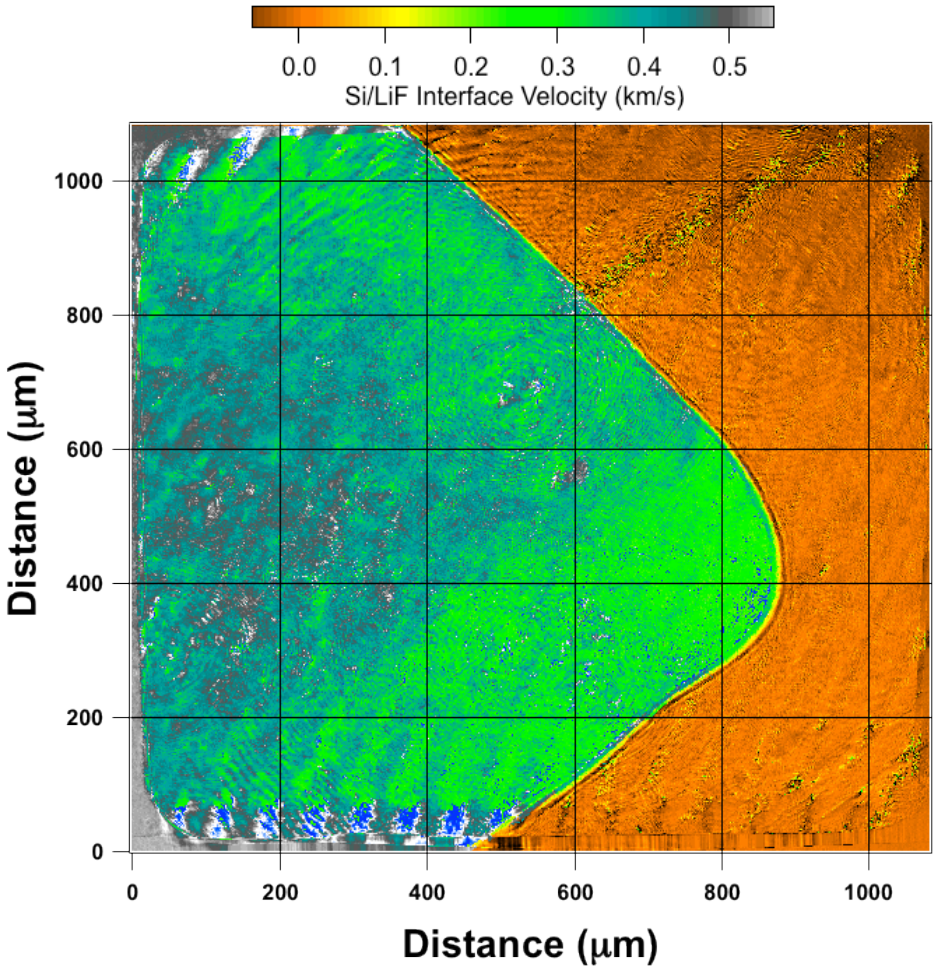

Non-fringing Image

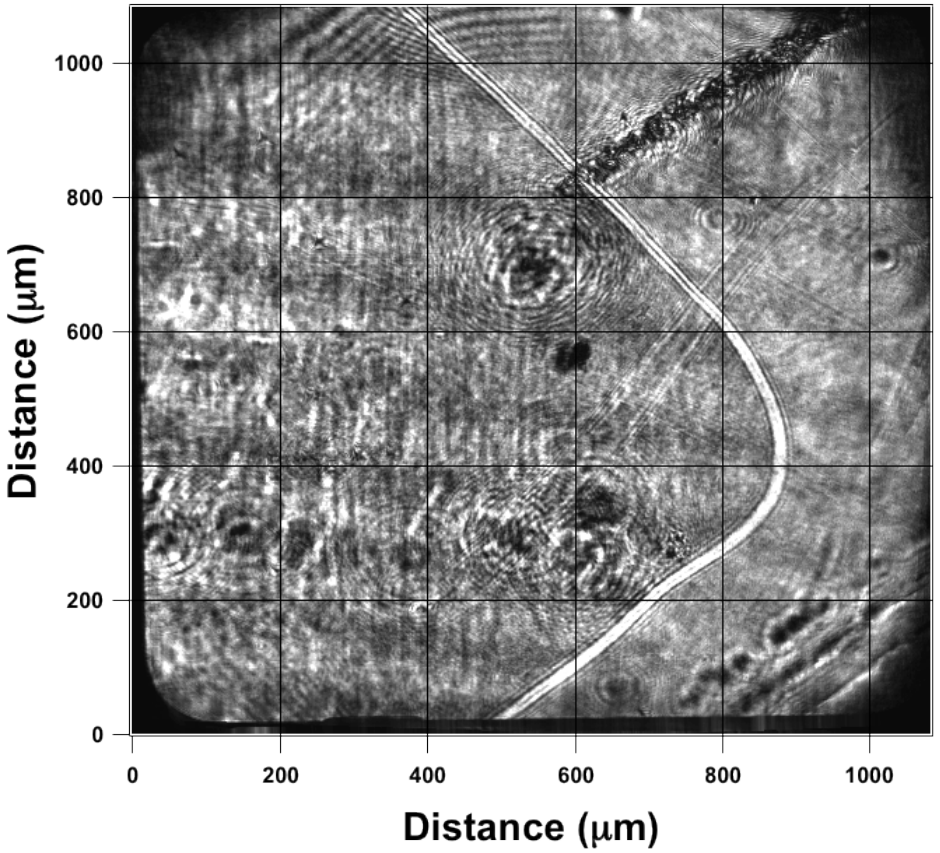

Velocity and Reflectivity changes are relatively smooth within Elastic precursor

Si 111/LiF

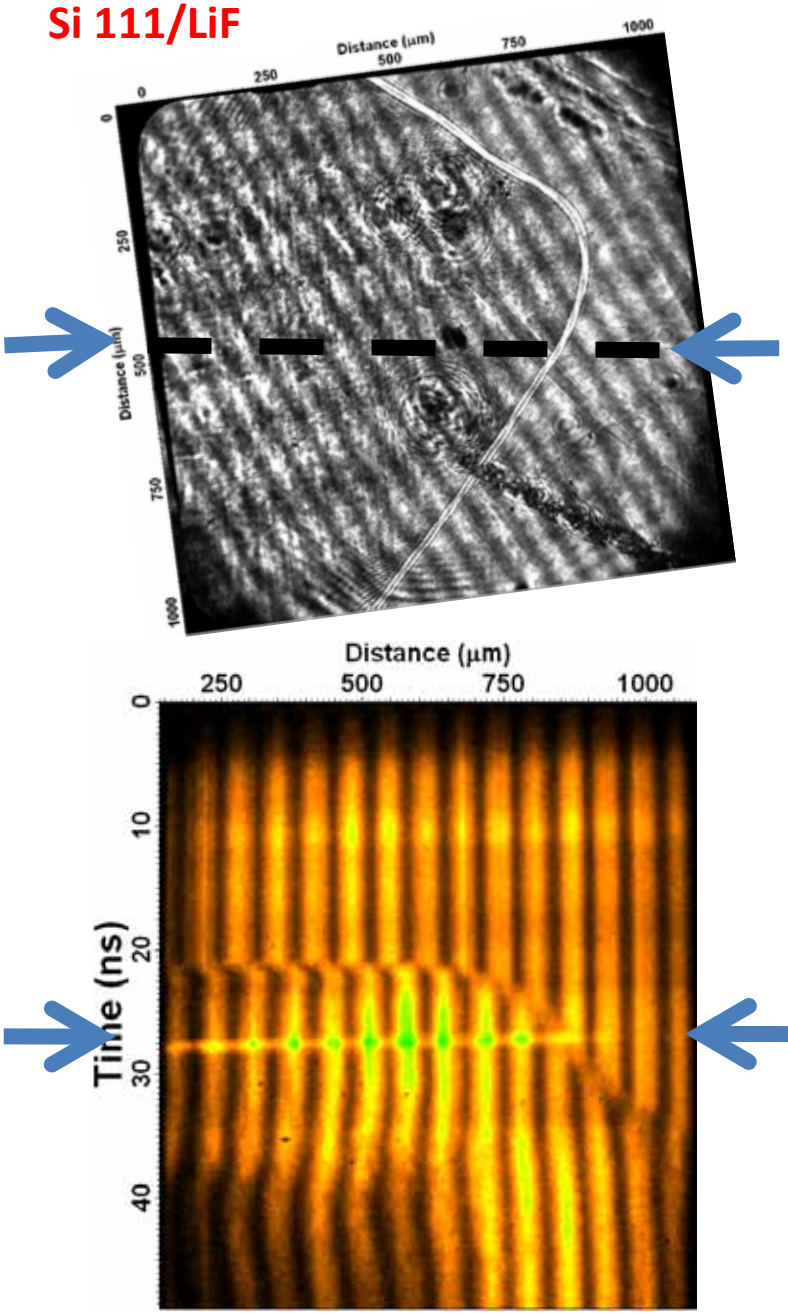

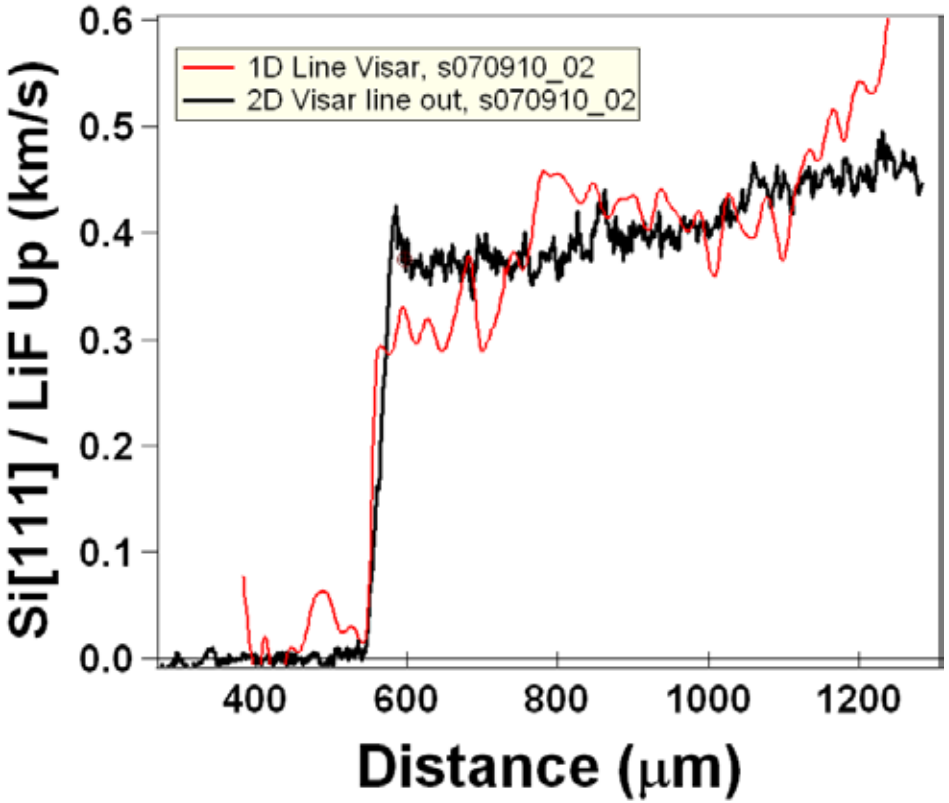

s070902

30μm Median filter applied to surface plots

Si/LiF,
u_p (km/s)

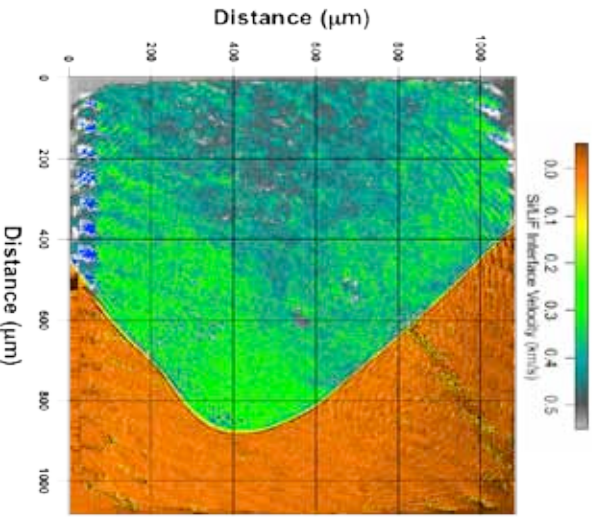

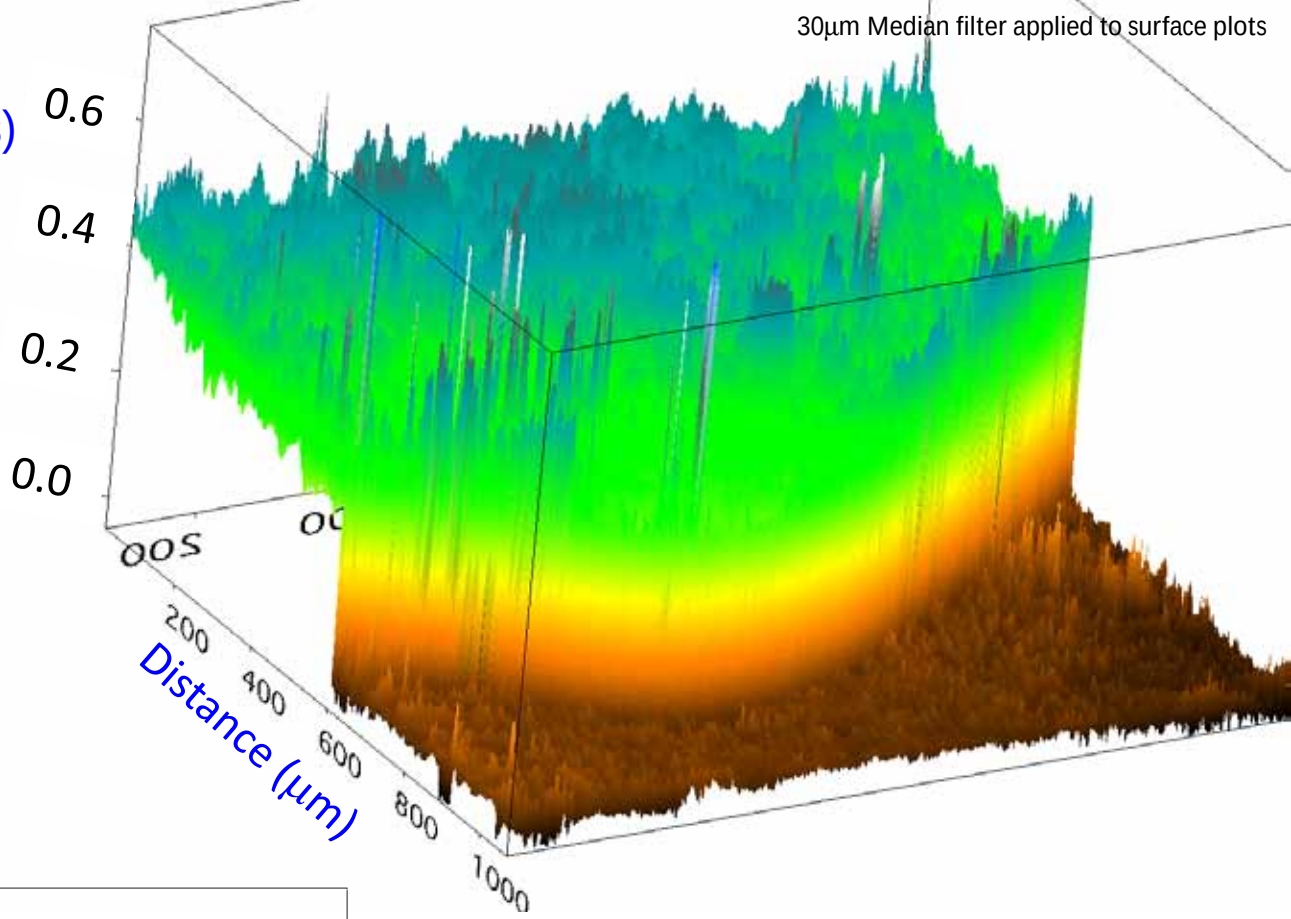

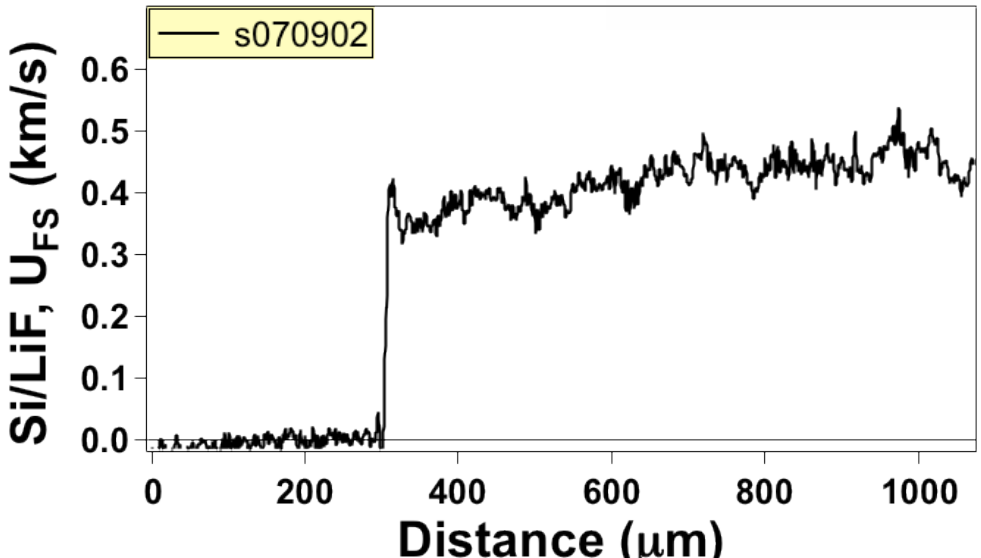

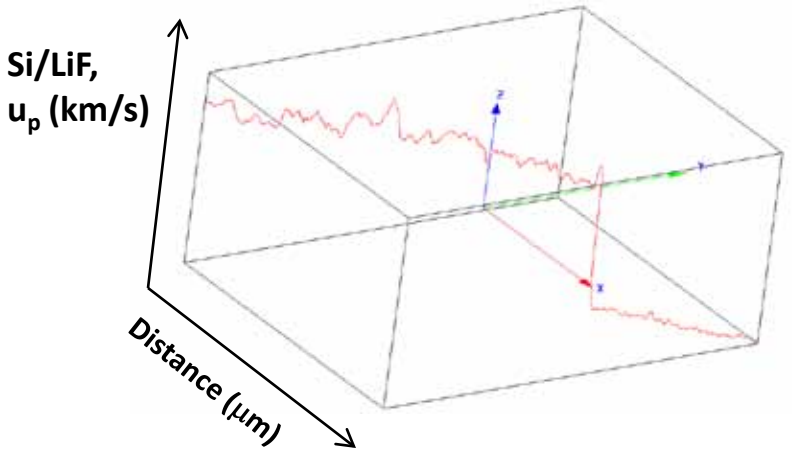

The onset of plasticity is marked by clear changes in the surface morphology

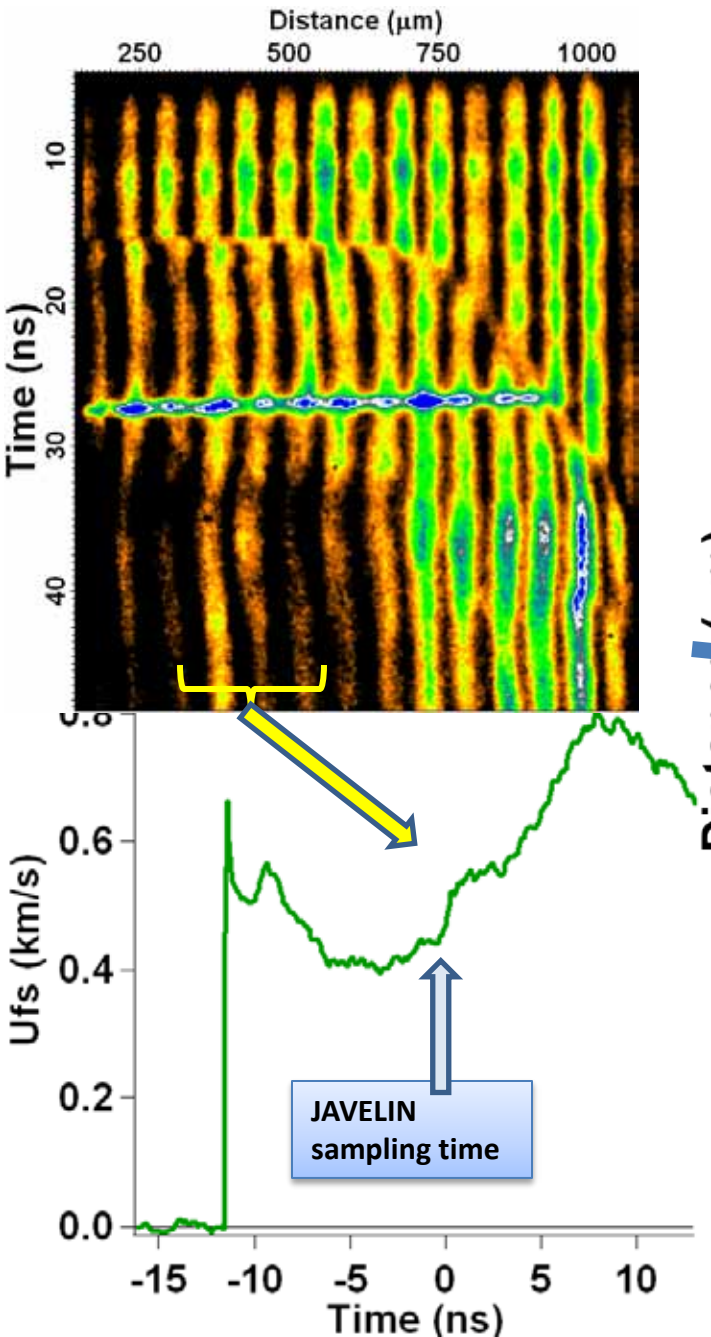

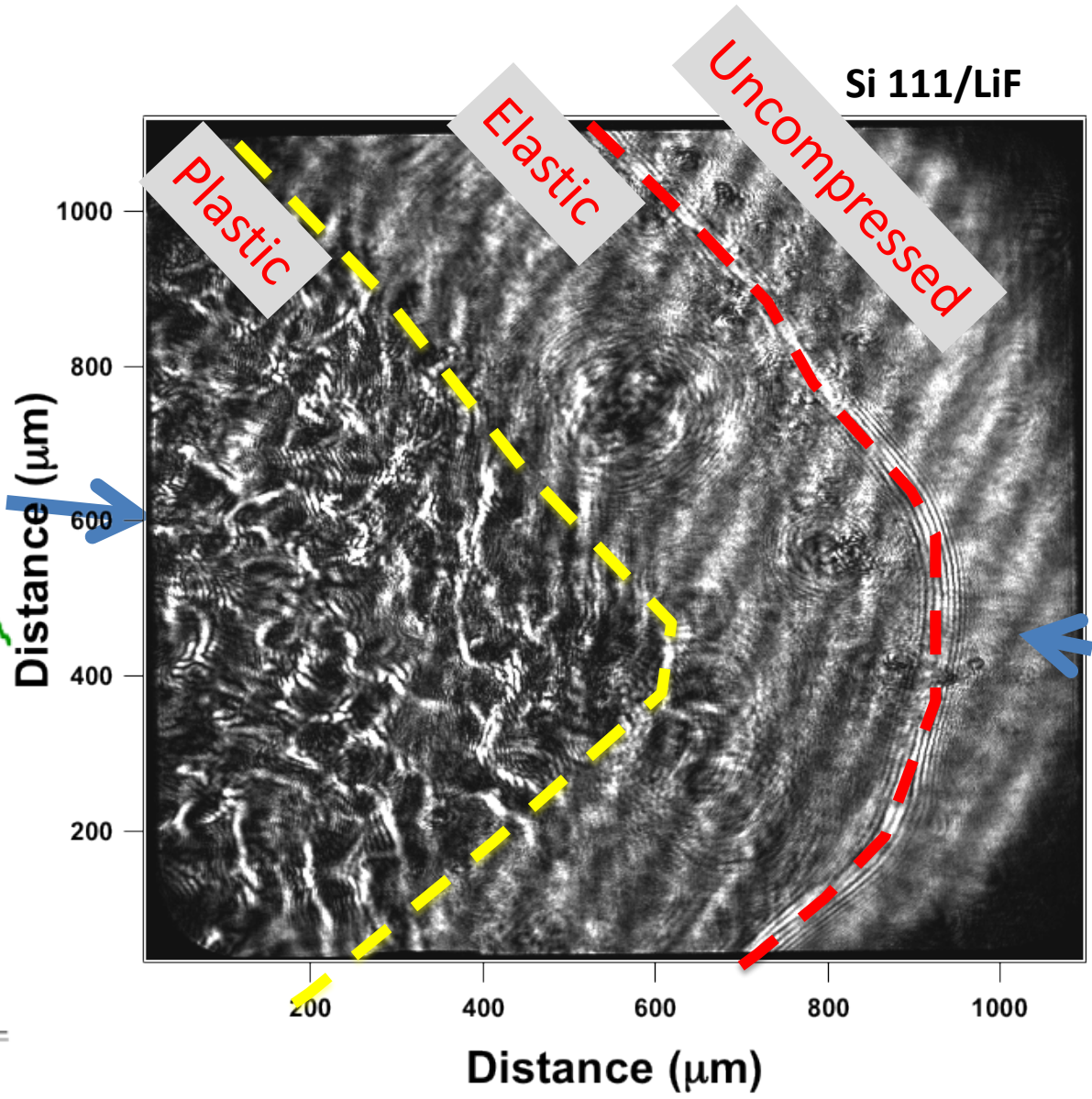

The onset of plasticity is marked by clear changes in the surface morphology

Velocity Map

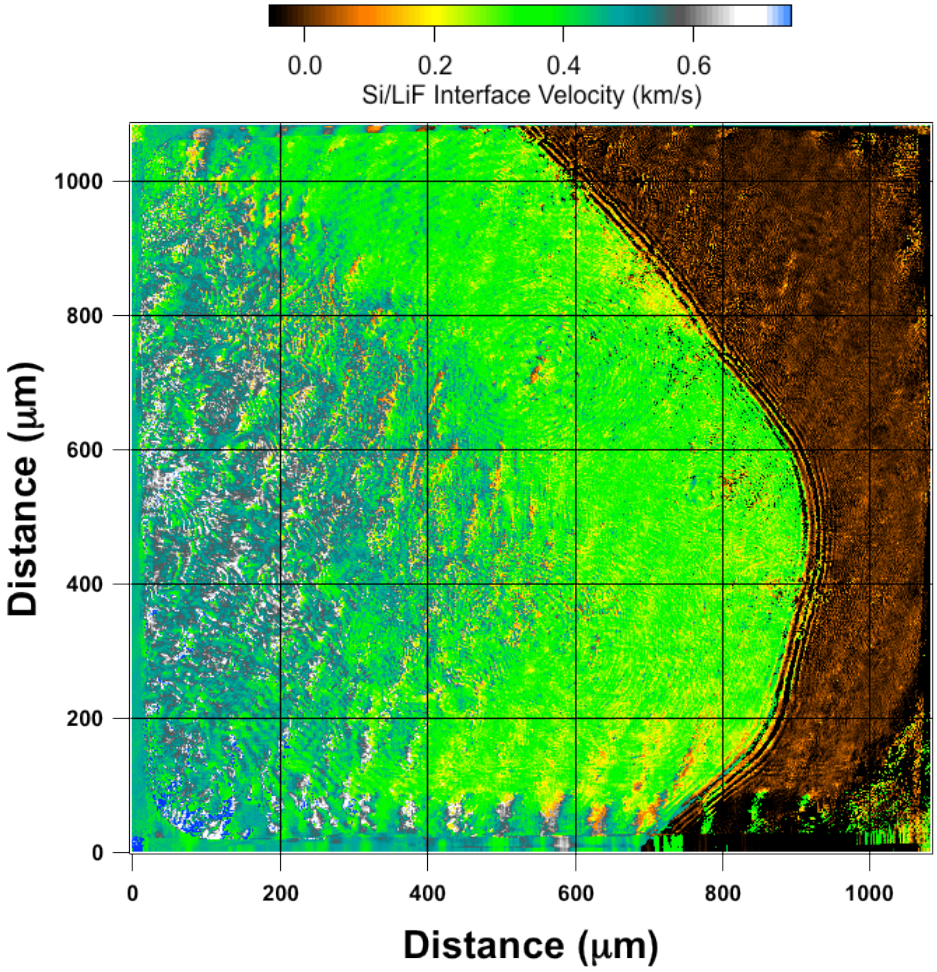

Non-fringing Image

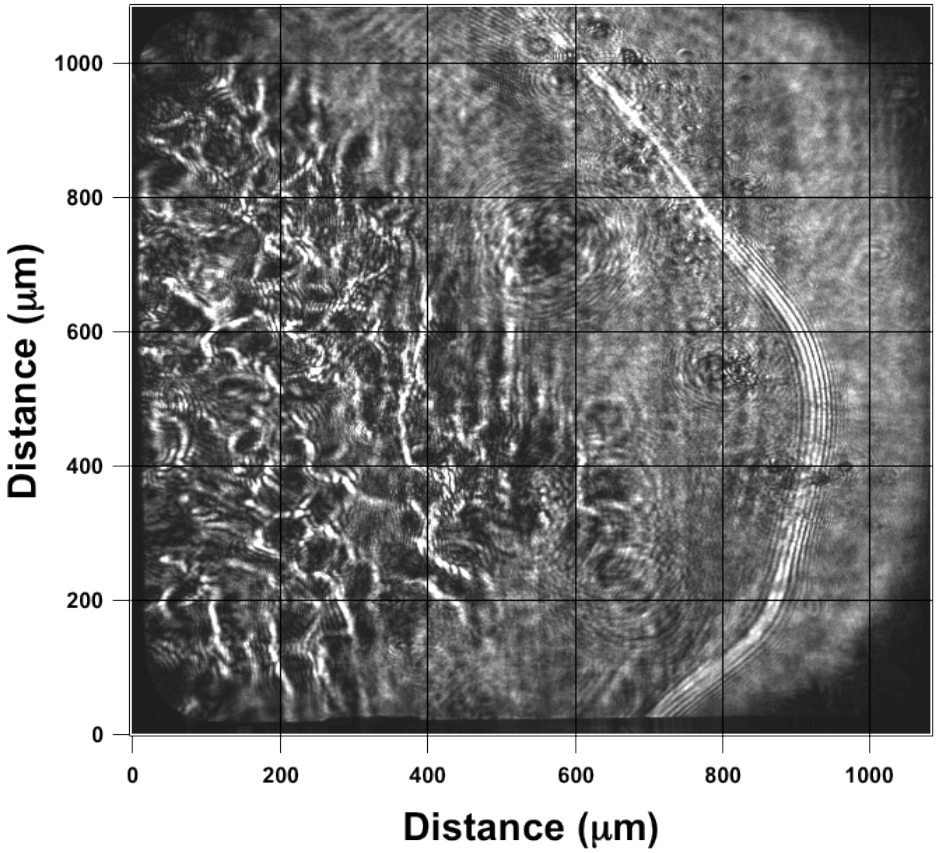

The onset of plasticity is marked by clear changes in the surface morphology

Si 111/LiF

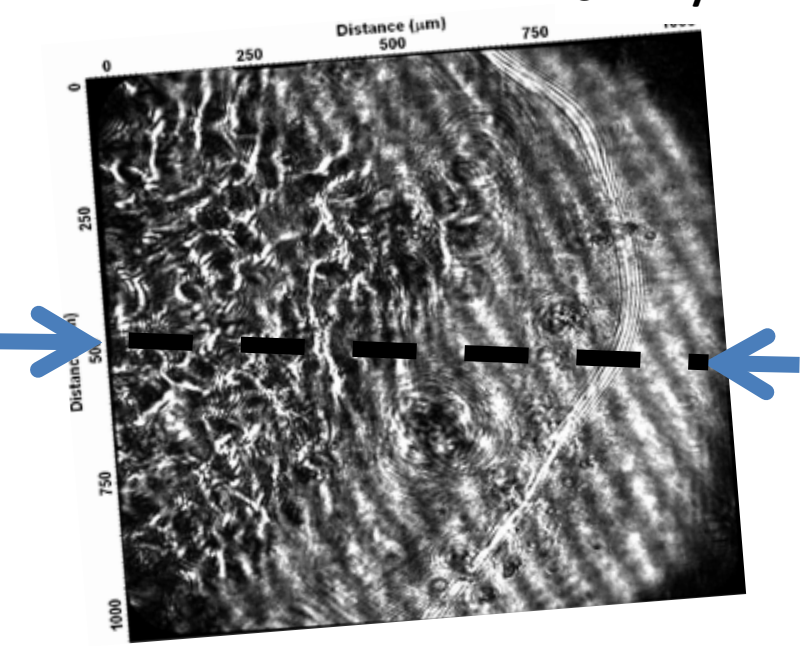

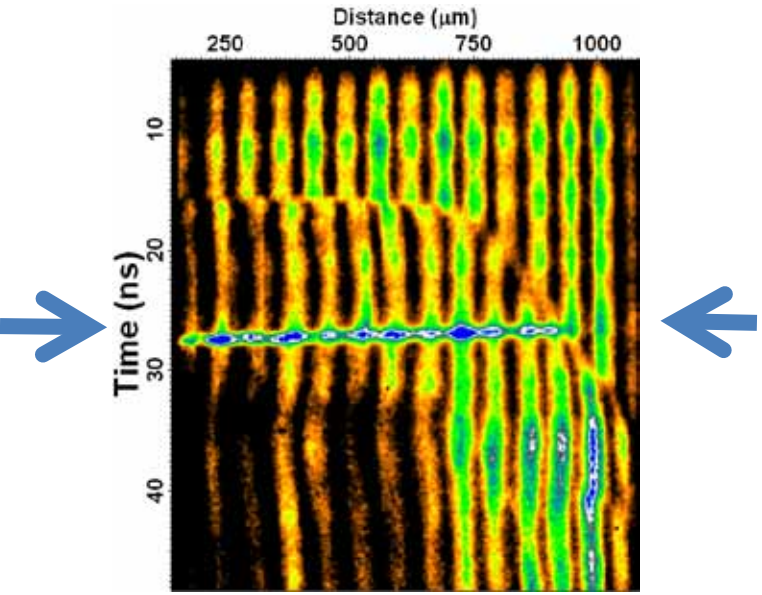

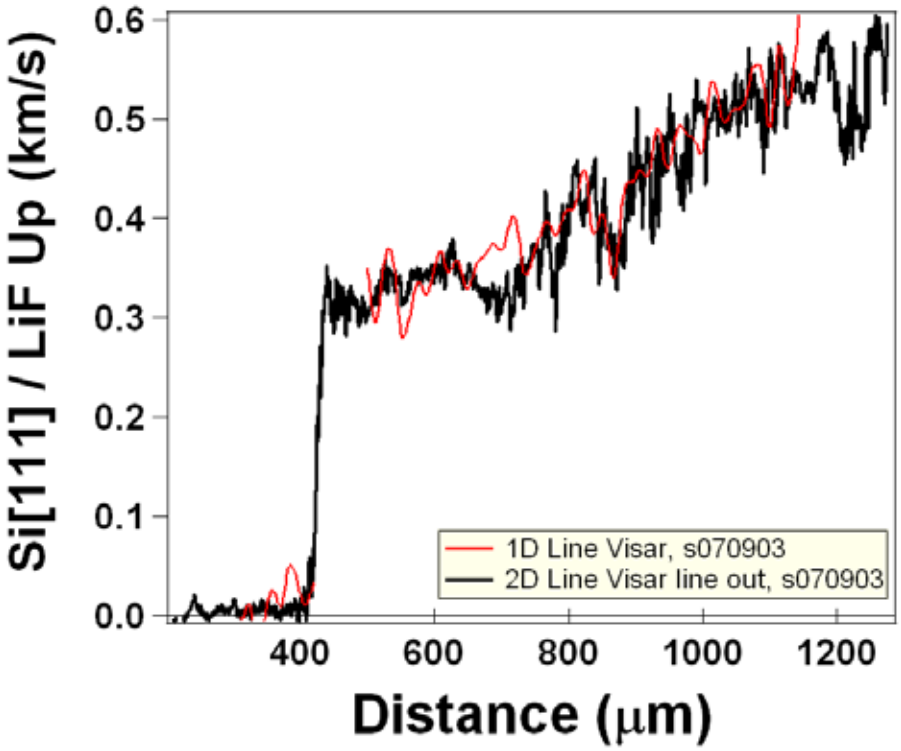

s070903

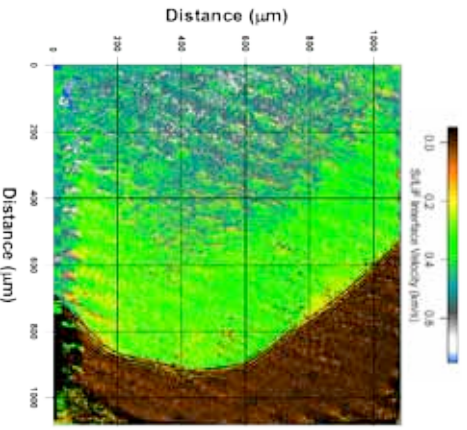

Si/LiF,
u_p (km/s)

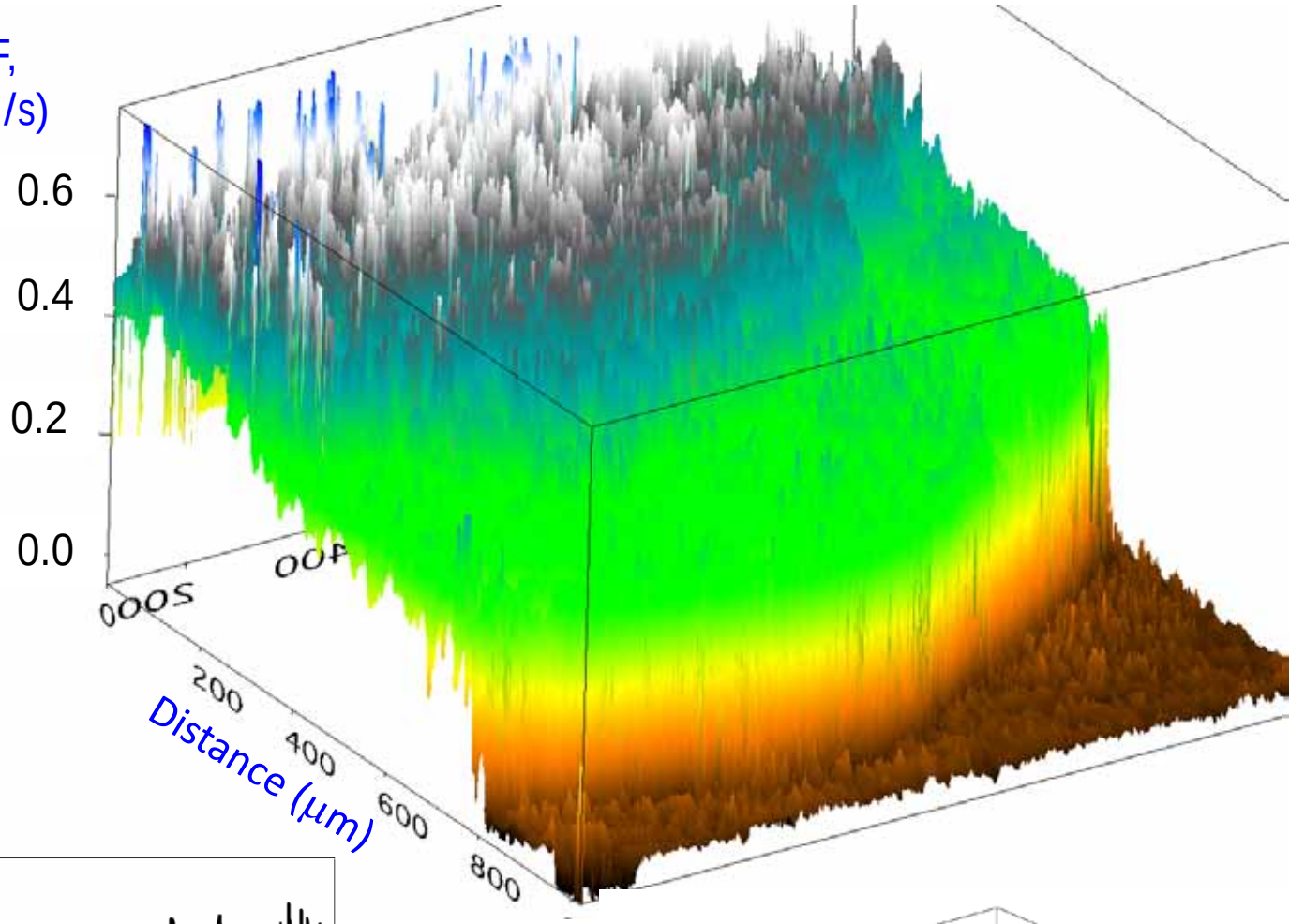

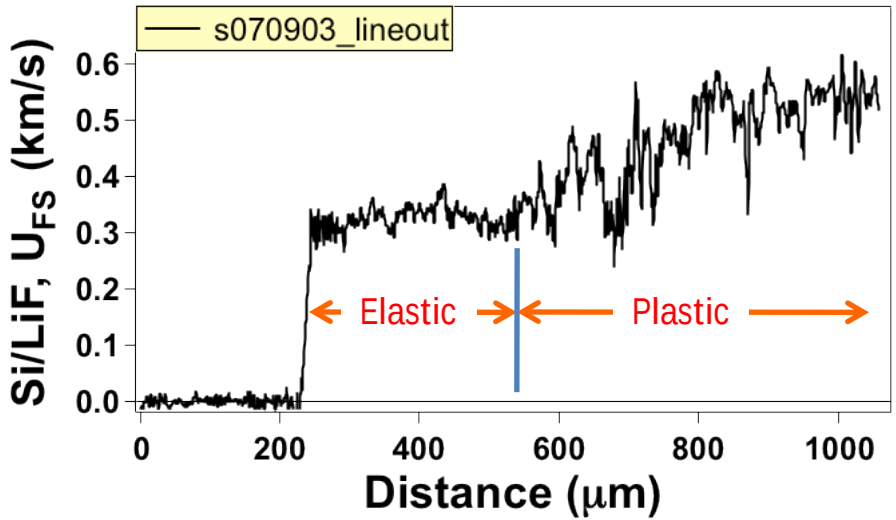

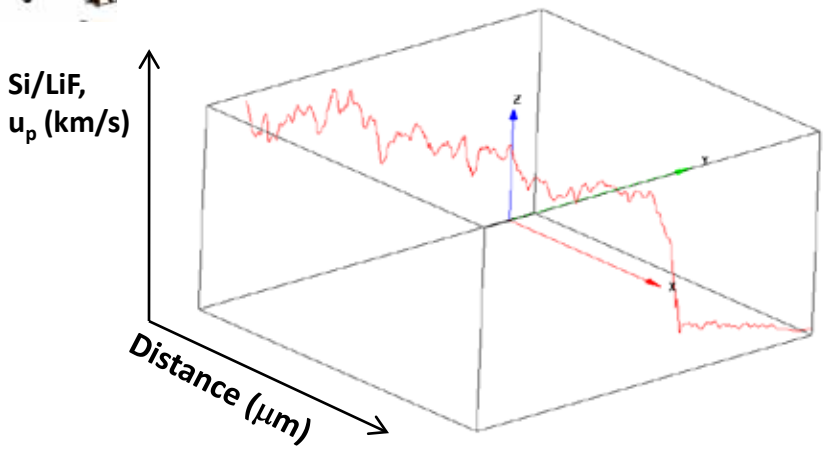

The transformation to the β-Sn phase coincides with the emergence of ~2μm scale structure

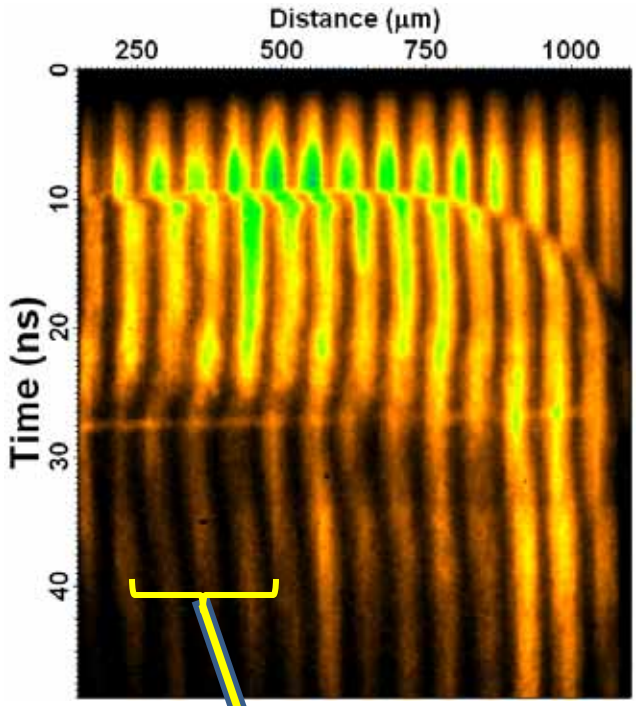

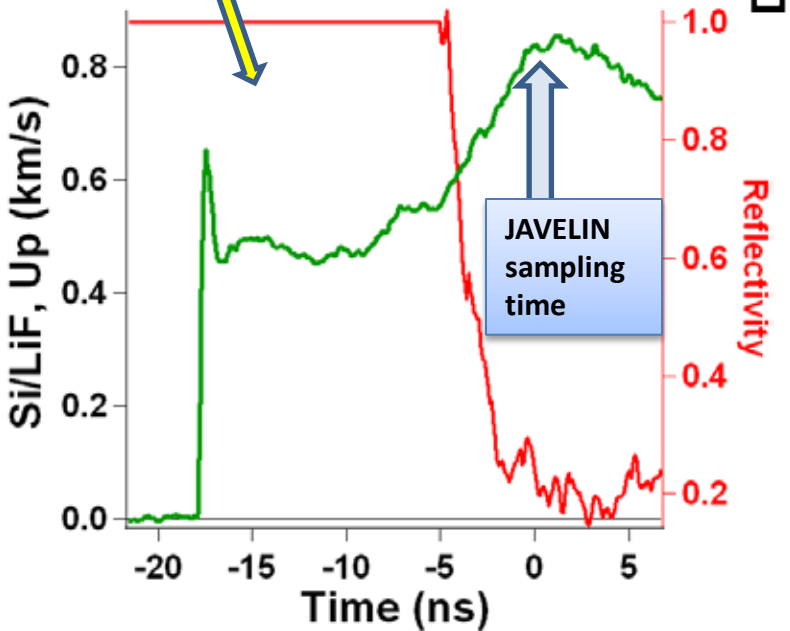

Transition from ambient to new phase

090704 – Si 111/LiF

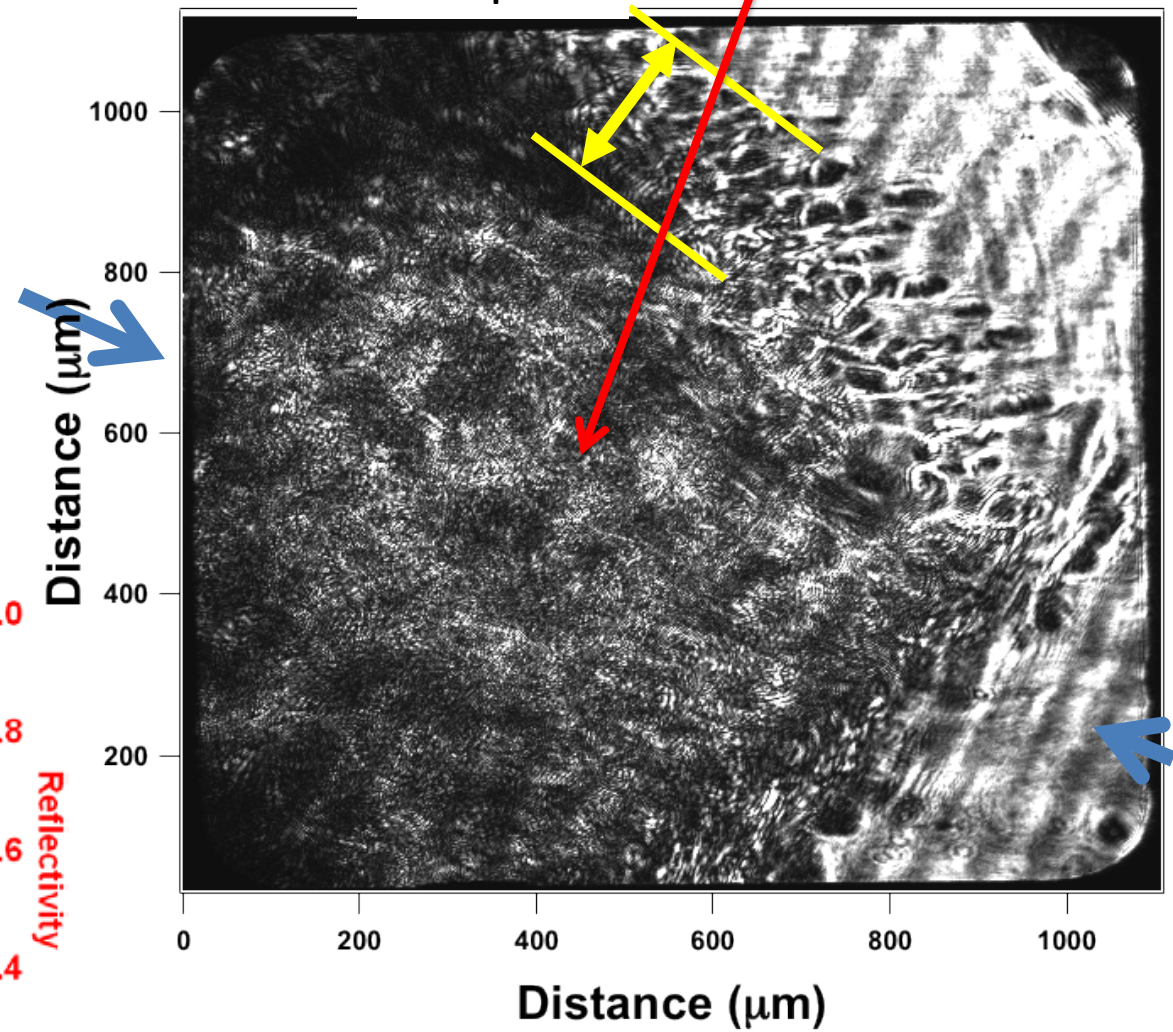

Onset of phase transformation witnessed by fall in reflectivity on 1D visar and emergence of very small scale grains in the 2D VISAR

The transformation to the β-Sn phase coincides with the emergence of ~2μm scale structure

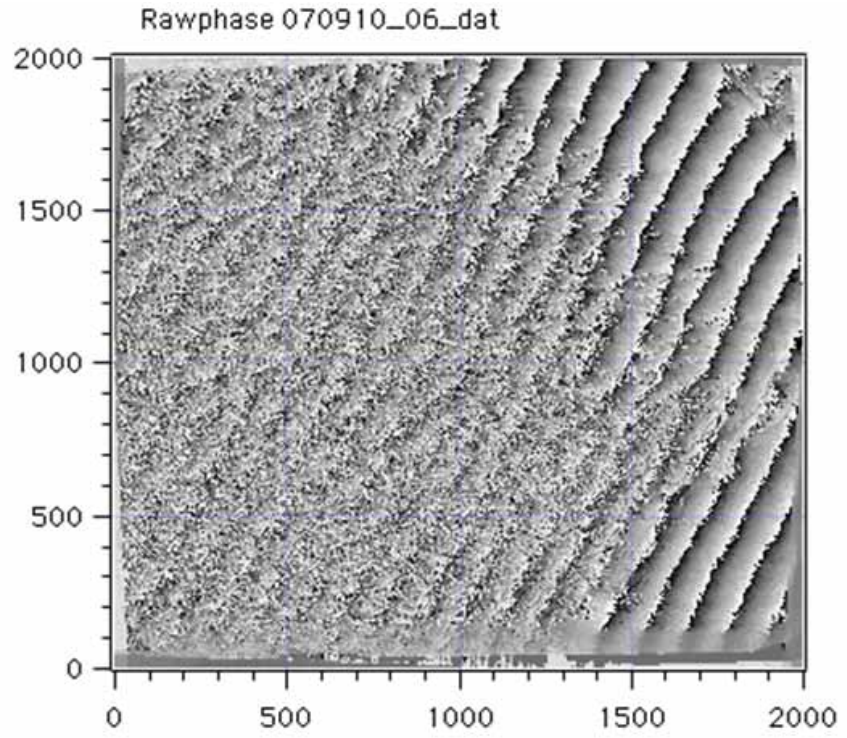

Non-fringing Image

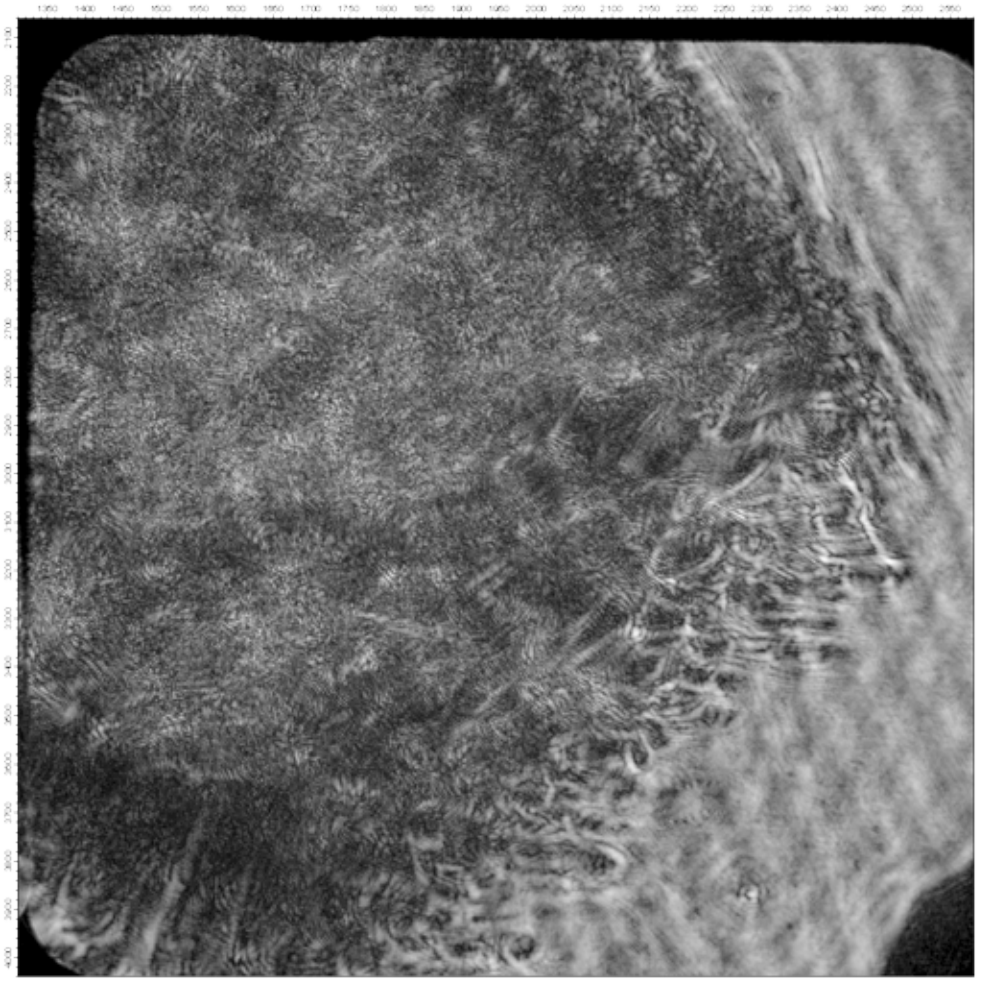

Free-Surface measurements show evolution of possible fracture networks

Si 111

Target

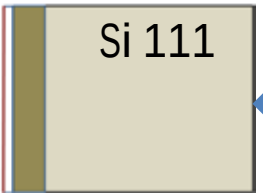

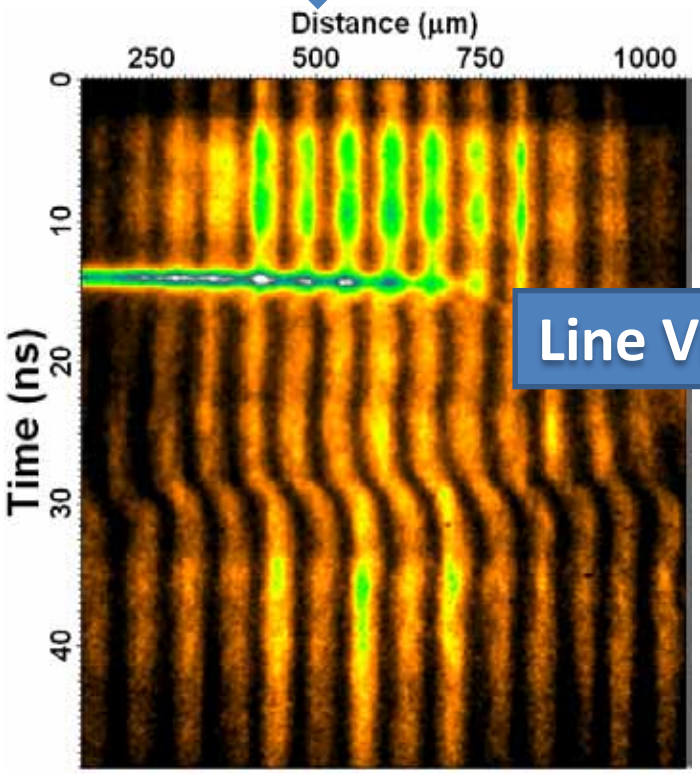

Line Visar

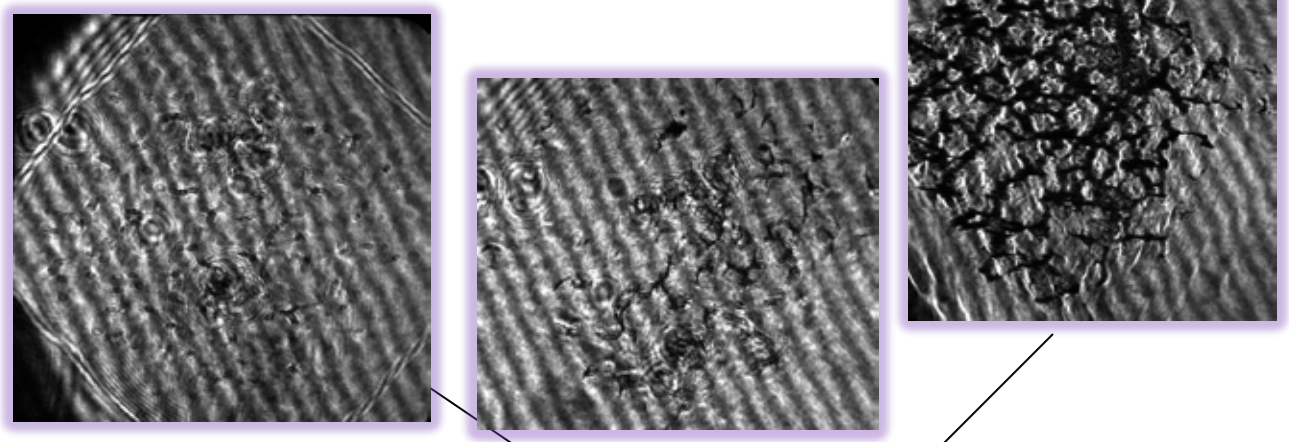

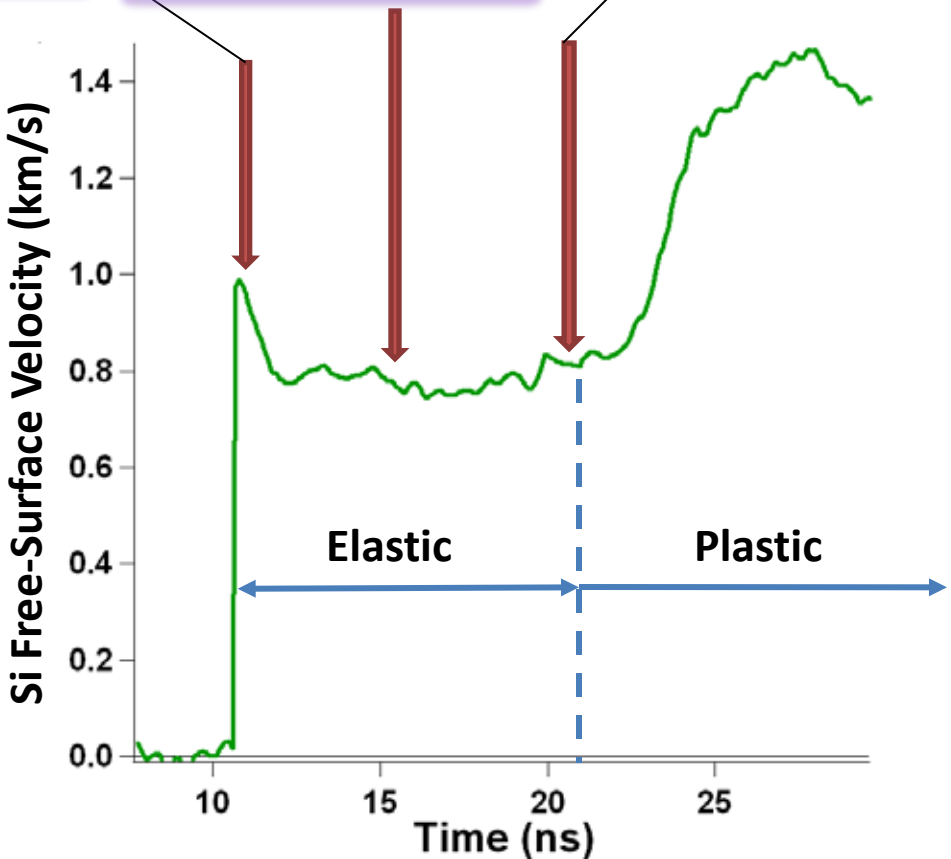

In the absence of a tamping LiF window, free-surface shows defects consistent with fracture

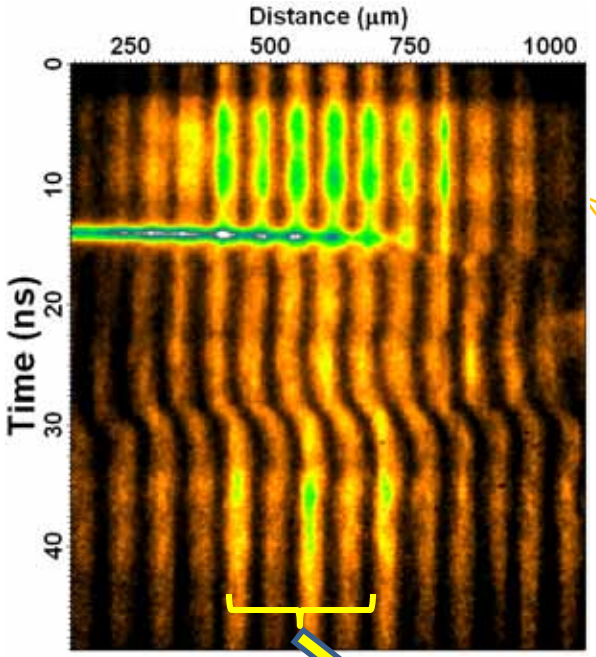

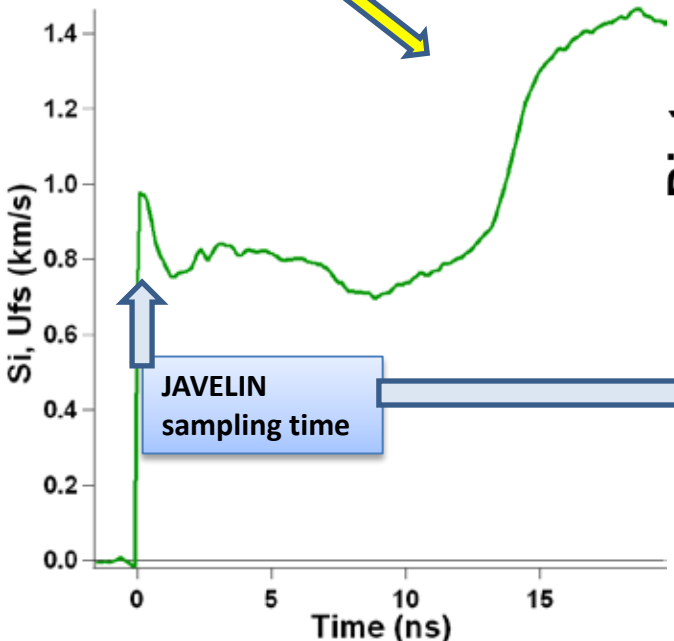

020903 – Si 111

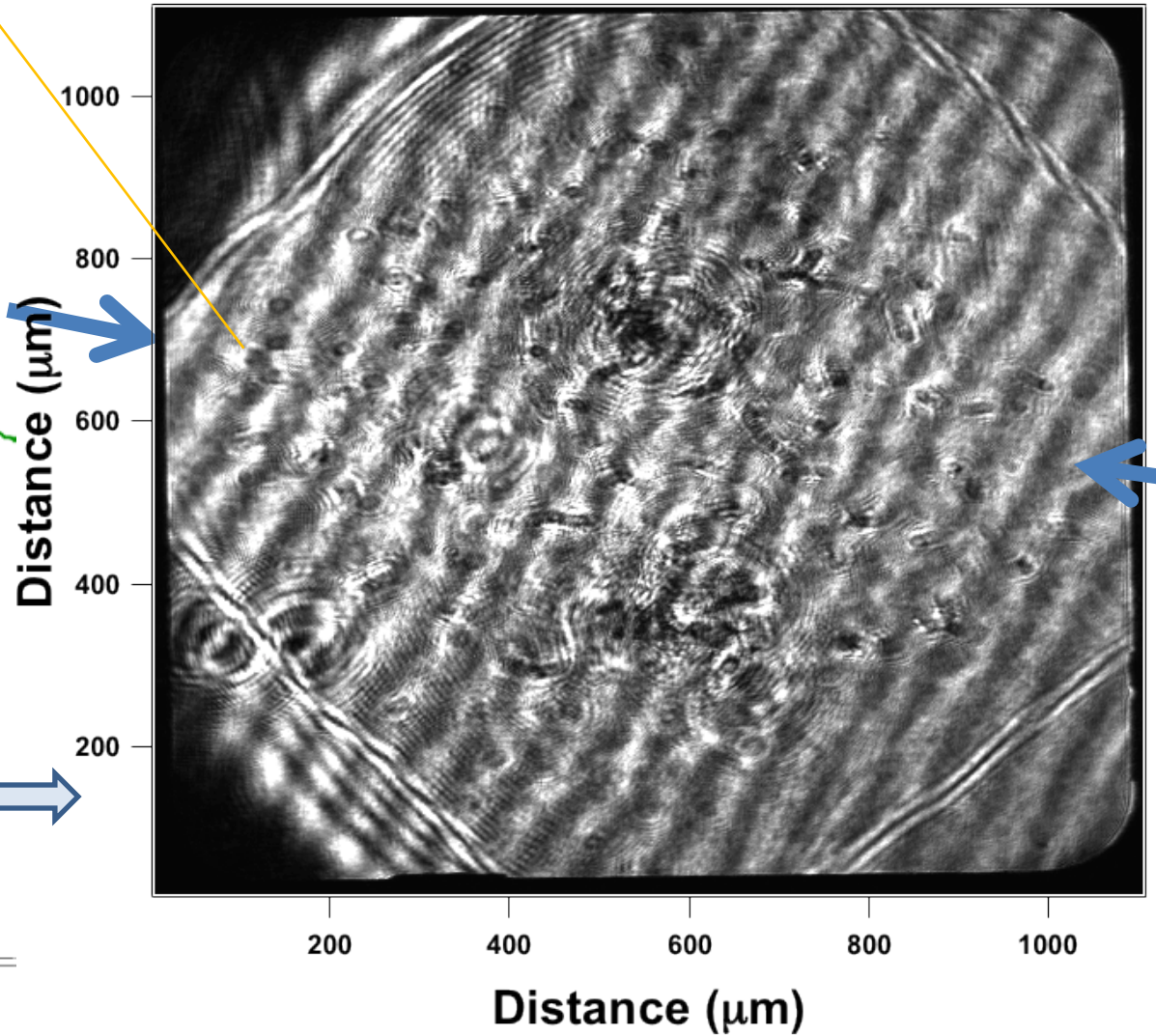

s020903 – Si 111

Velocity Map

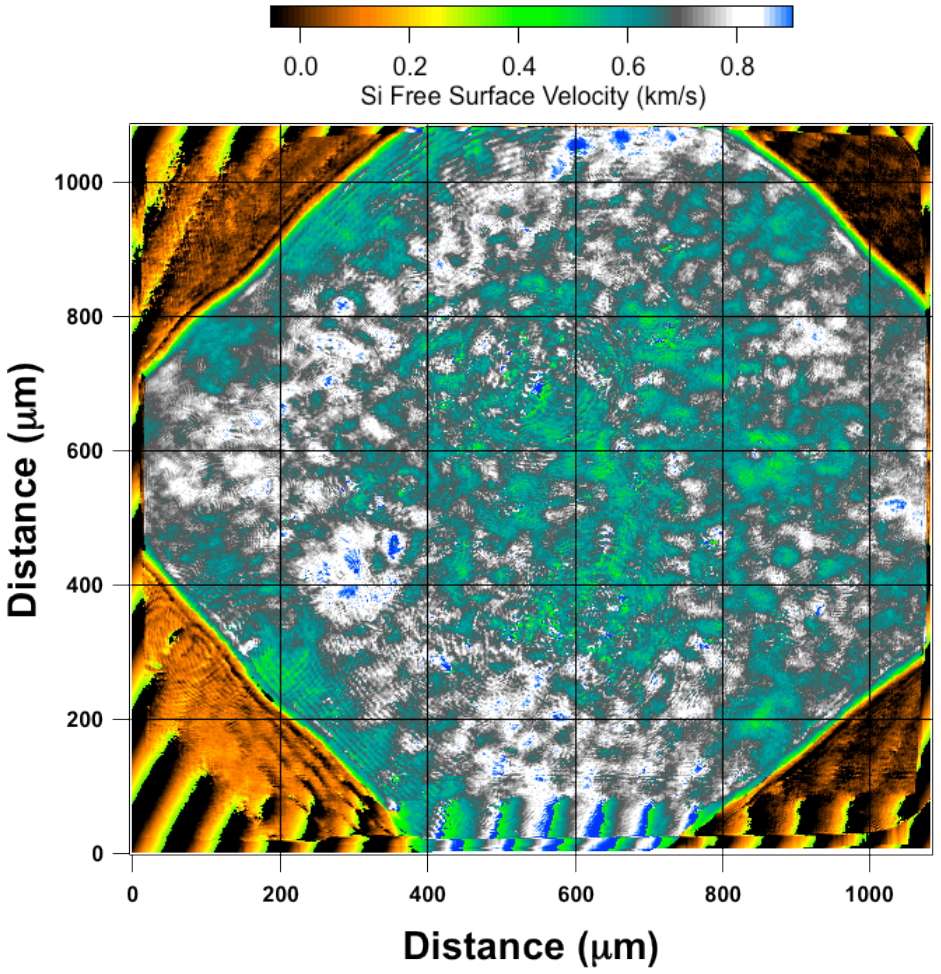

Non-fringing Image

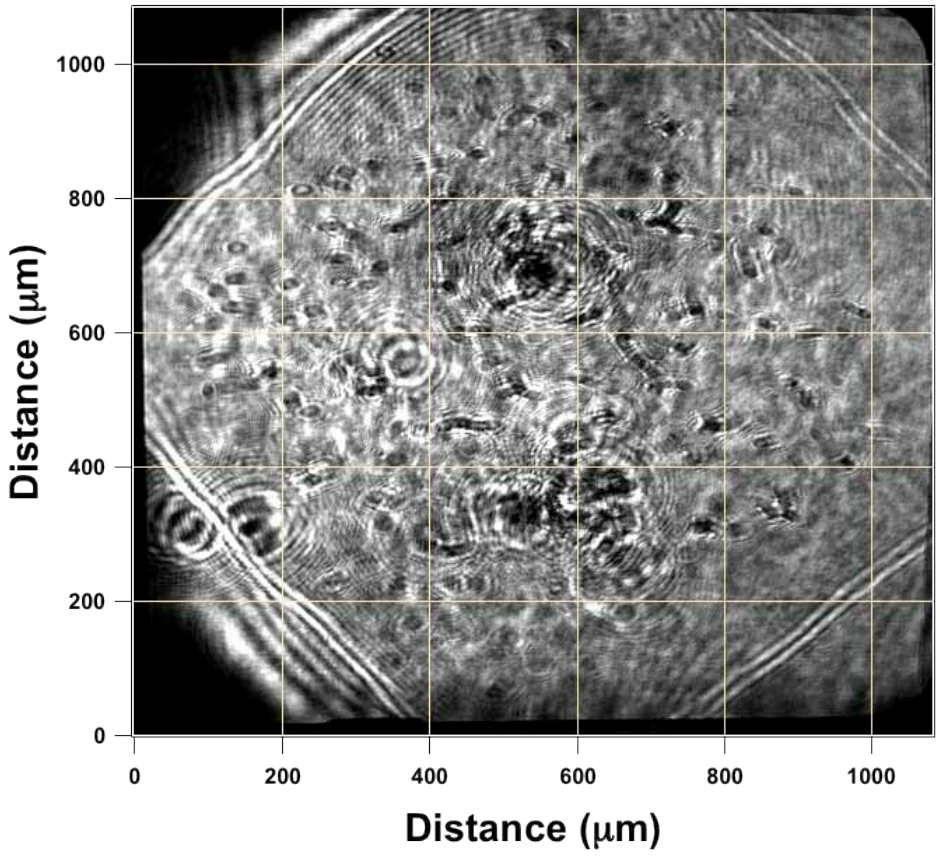

s020903

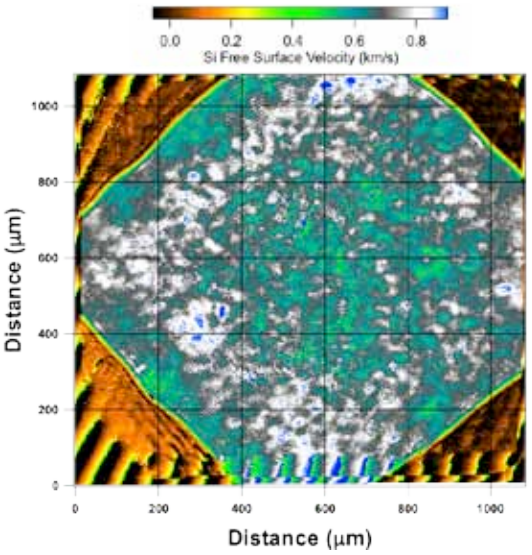

Si

U_{FS} (km/s)

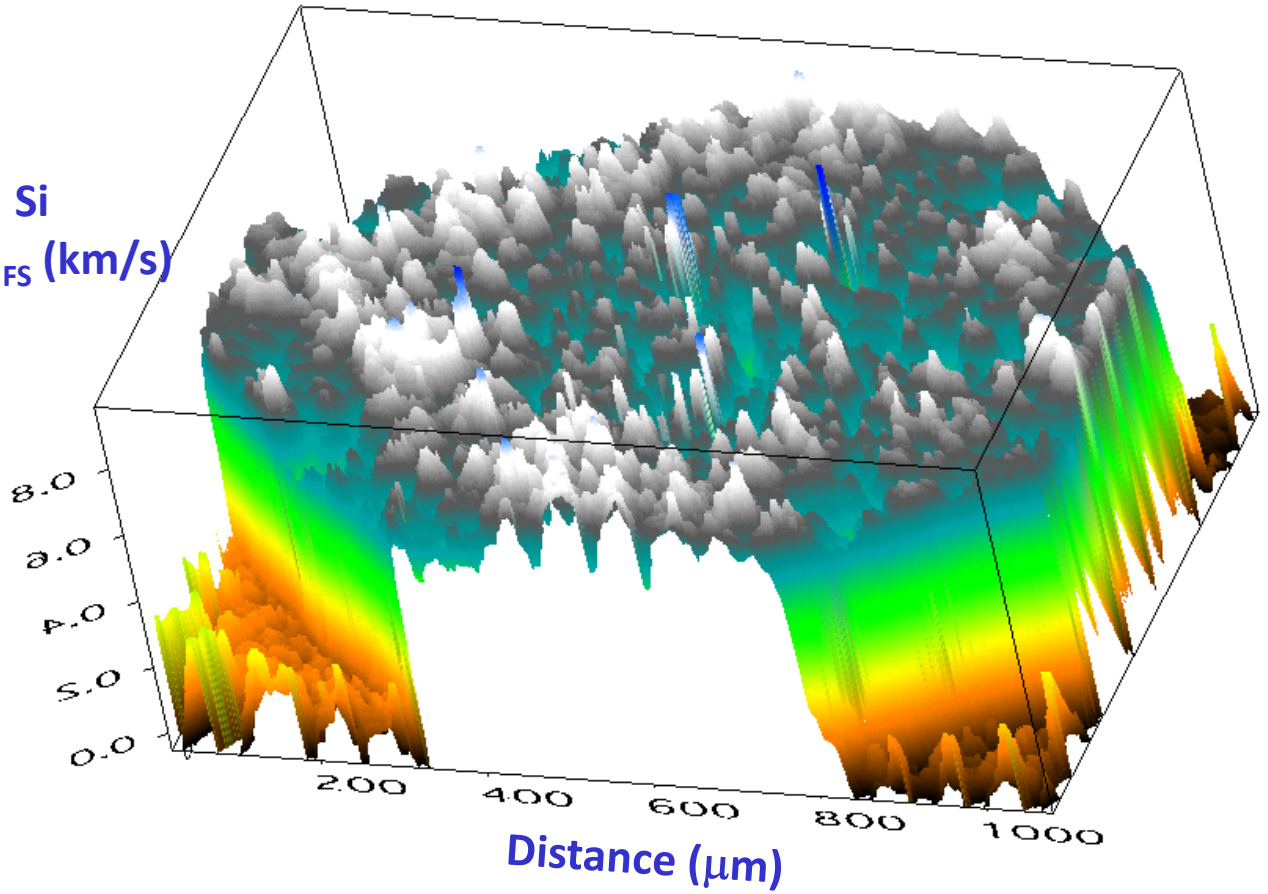

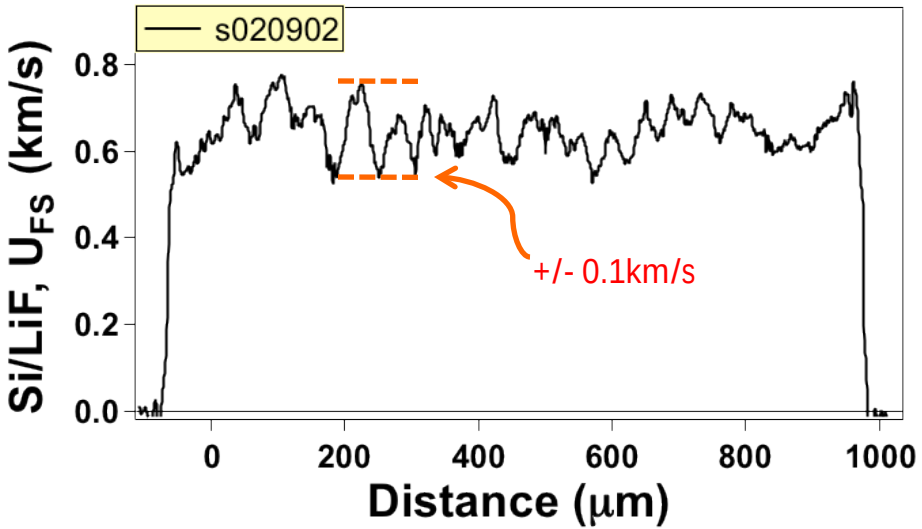

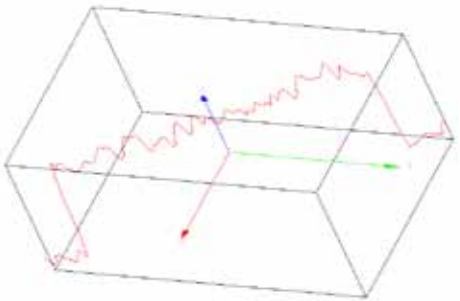

In the absence of a tamping LiF window, free-surface shows defects consistent with fracture

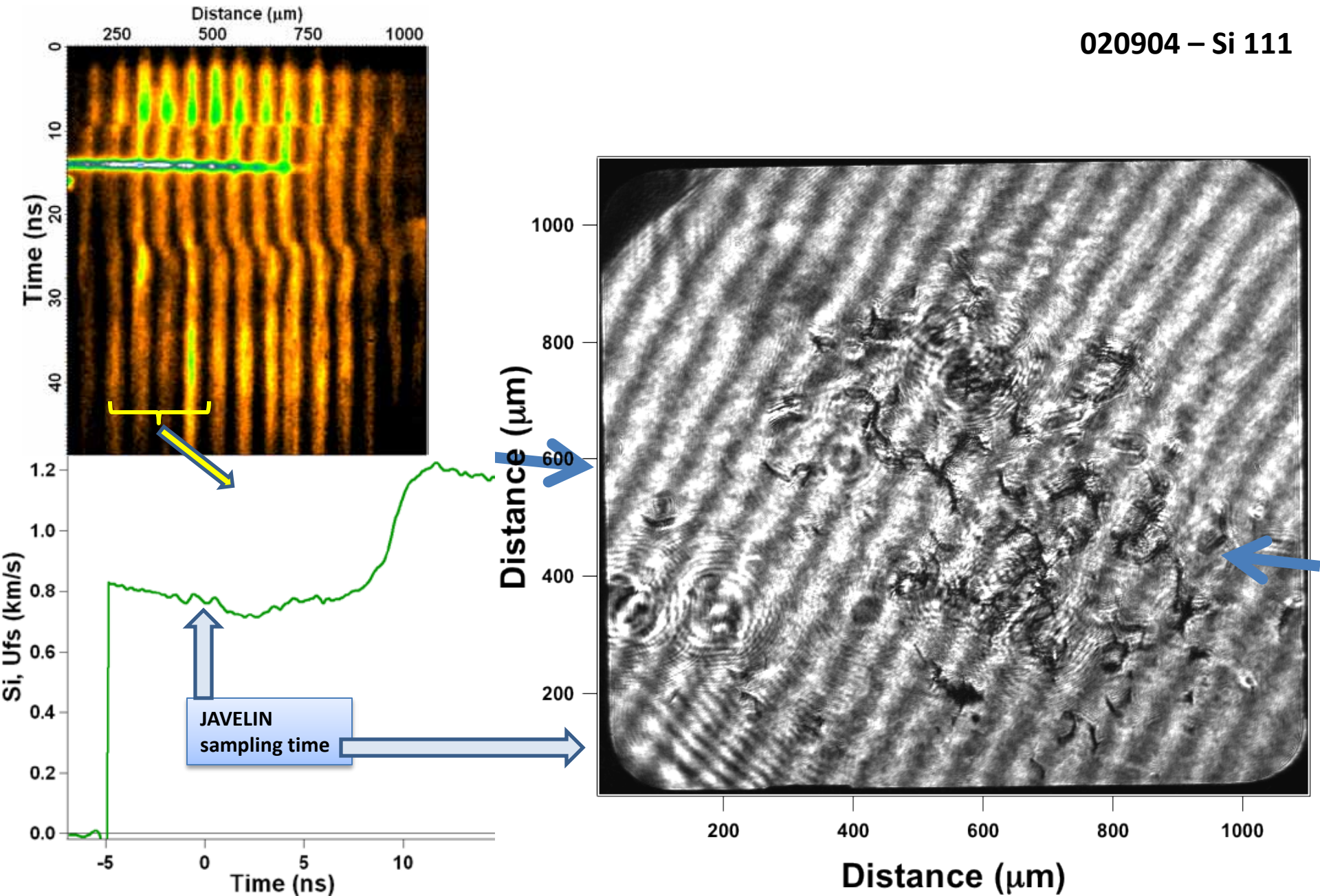

020904 – Si 111

Velocity Map

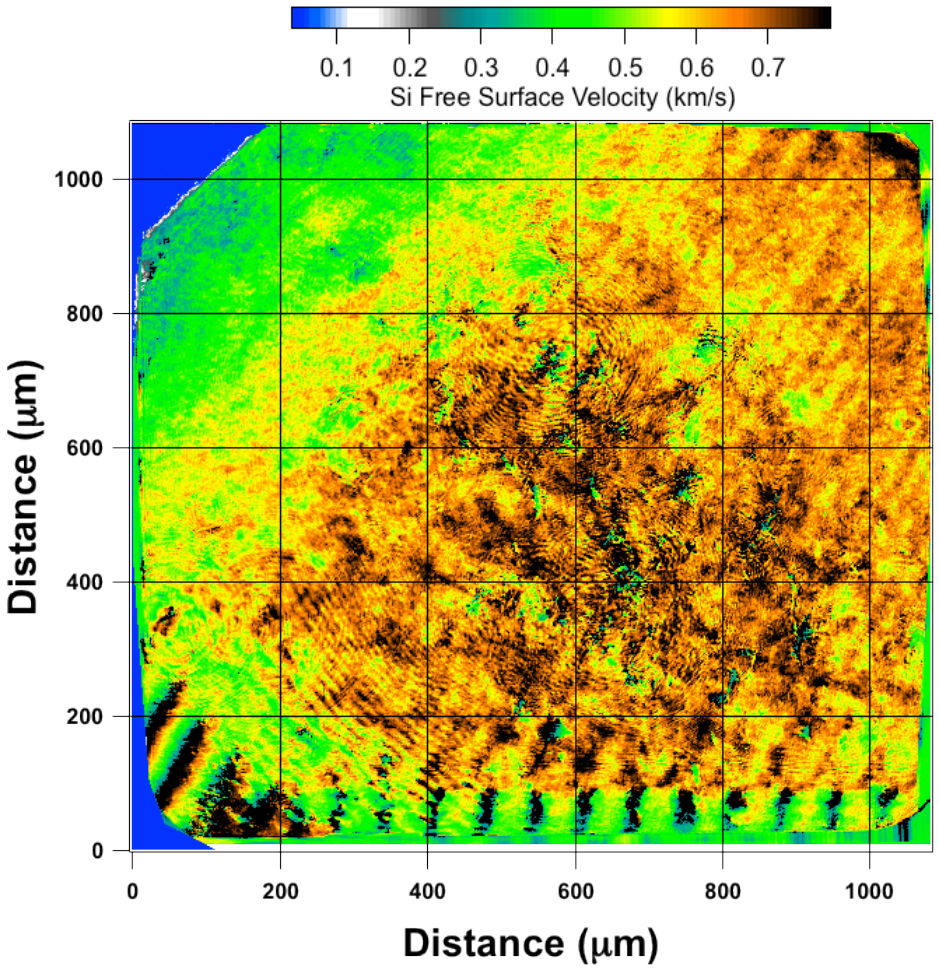

Non-fringing Image

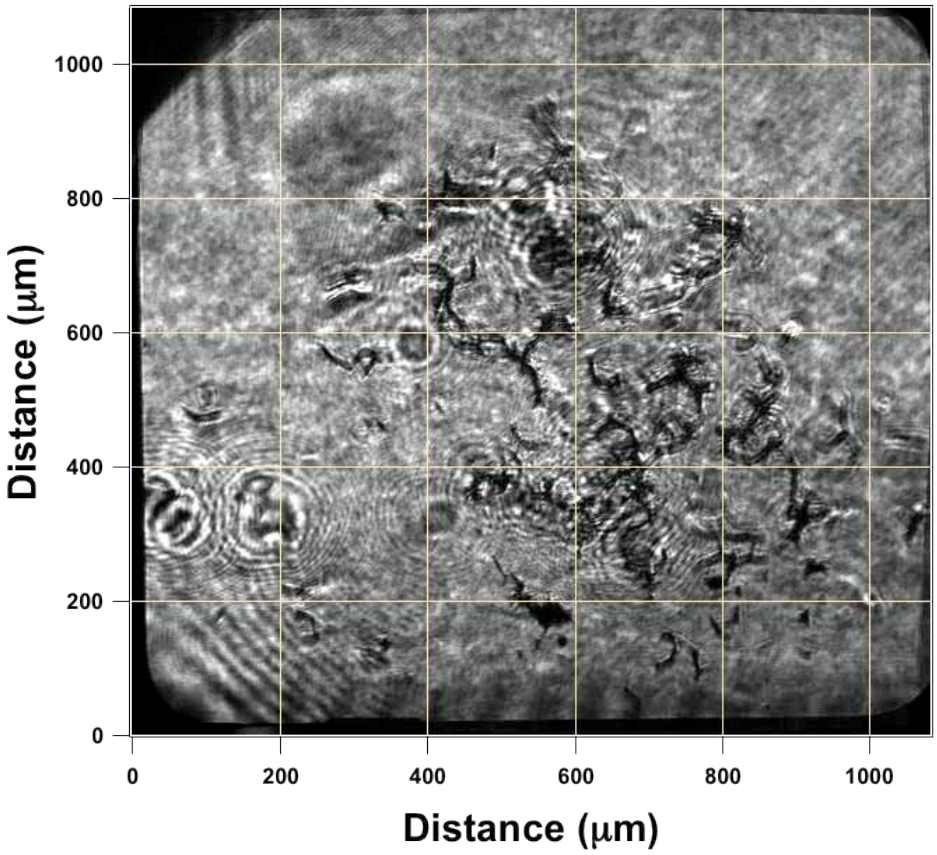

s020903

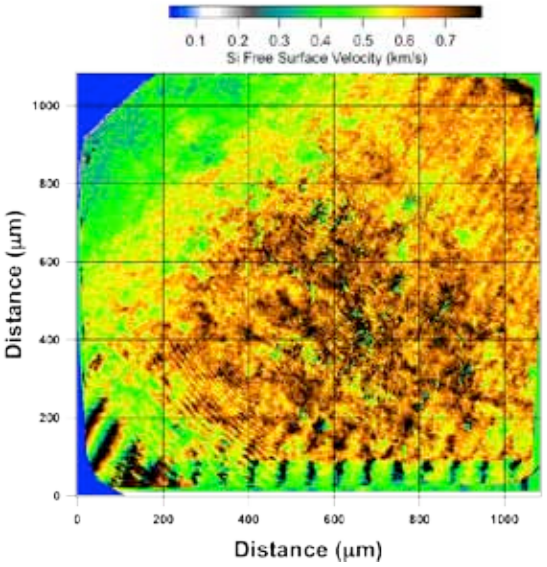
0.1 0.2 0.3 0.4 0.5 0.6 0.7
Si Free Surface Velocity (km/s)
Distance (μm)
Distance (μm)

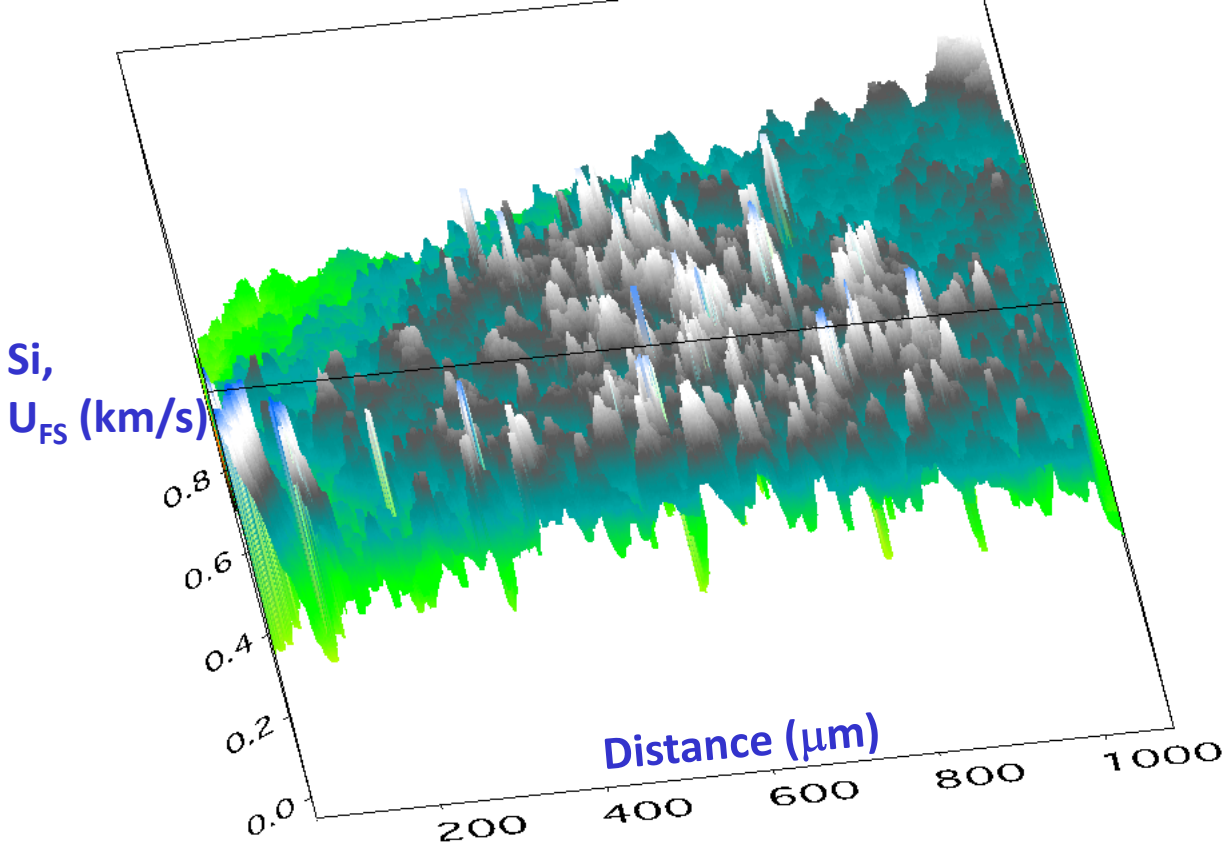
Si,
U_{FS} (km/s)
0.0
0.2
0.4
0.6
0.8
200
400
600
800
1000
Distance (μm)

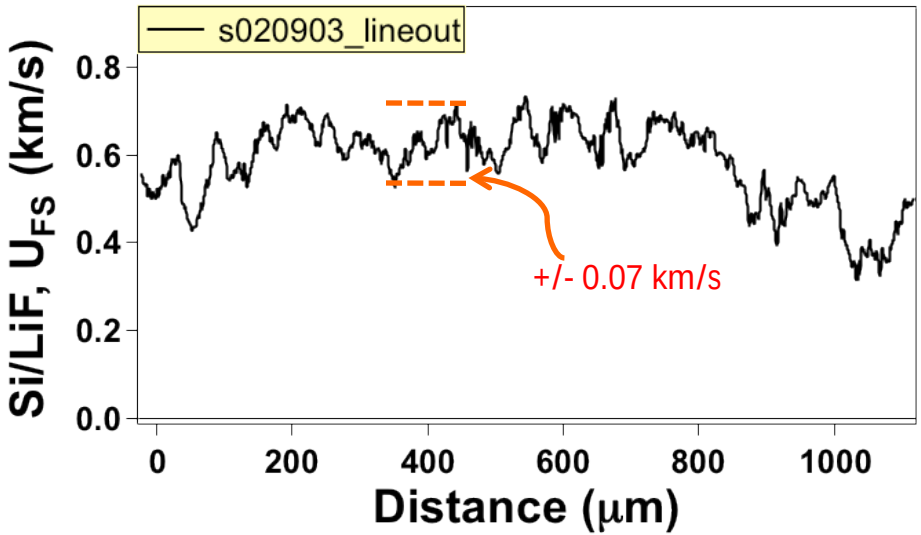
s020903_lineout
Si/LiF, U_{FS} (km/s)
0.0
0.2
0.4
0.6
0.8
+/- 0.07 km/s
0
200
400
600
800
1000
Distance (μm)

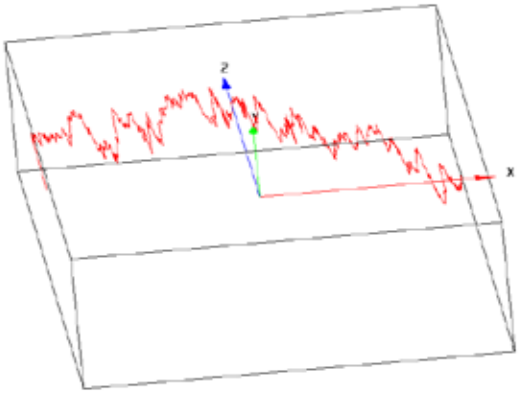

In the absence of a tamping LiF window, free-surface shows defects consistent with fracture

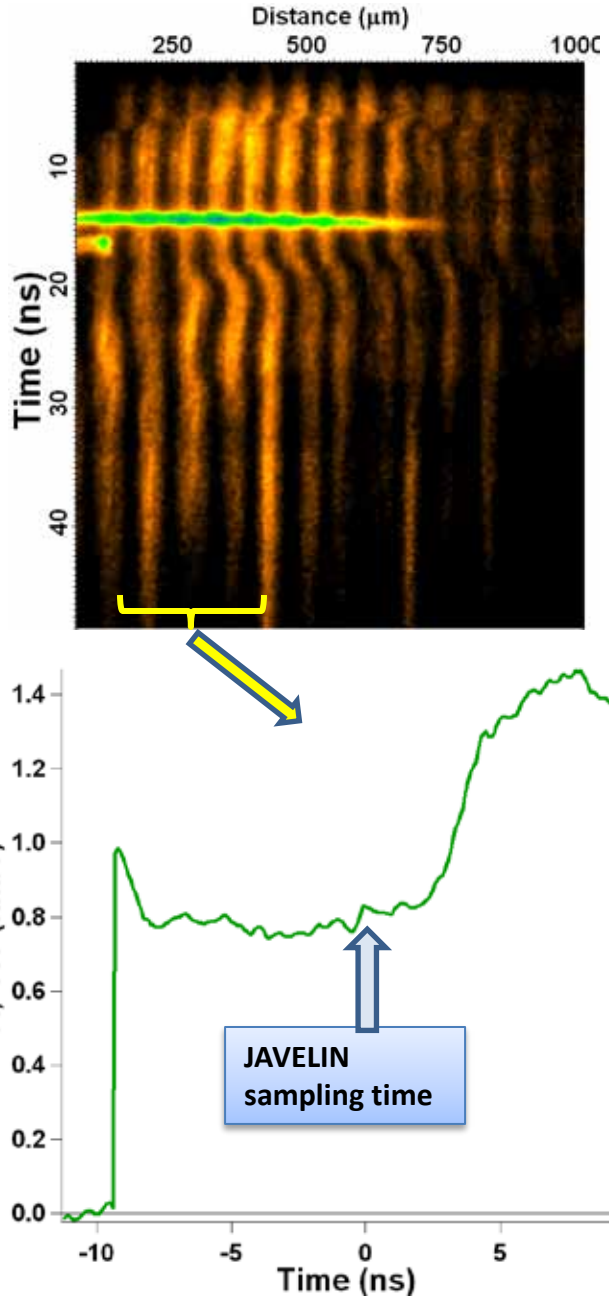

020906 – Si 111

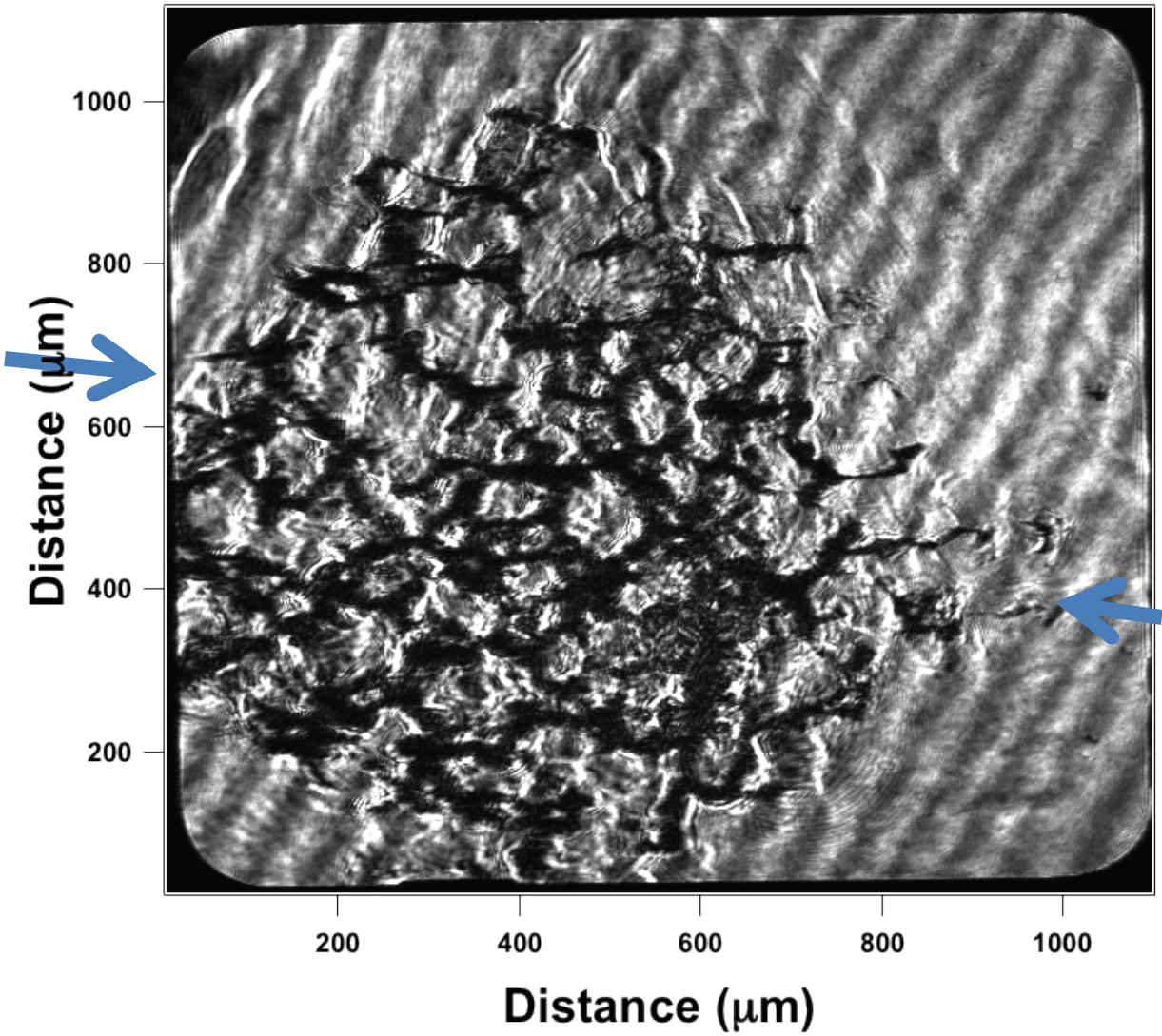

Raw Phase

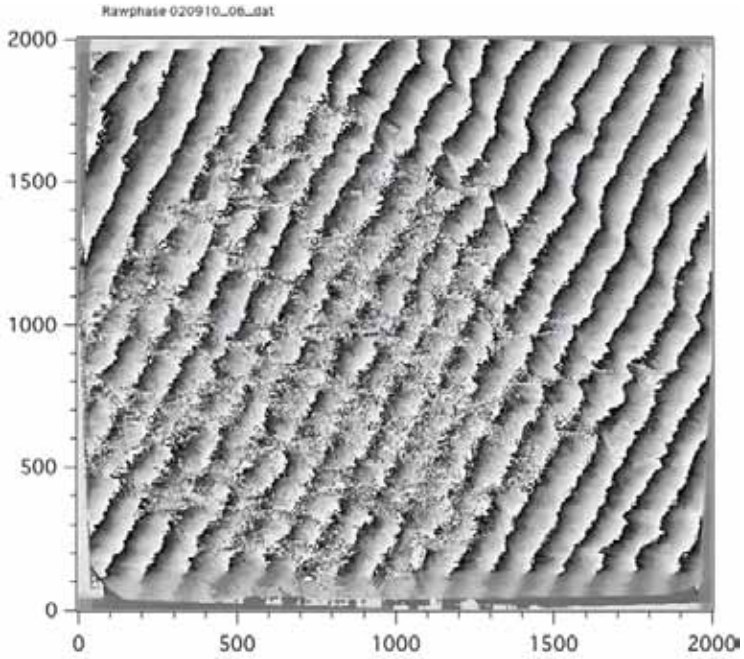

Non-fringing Image

s020910_06 – Si 111

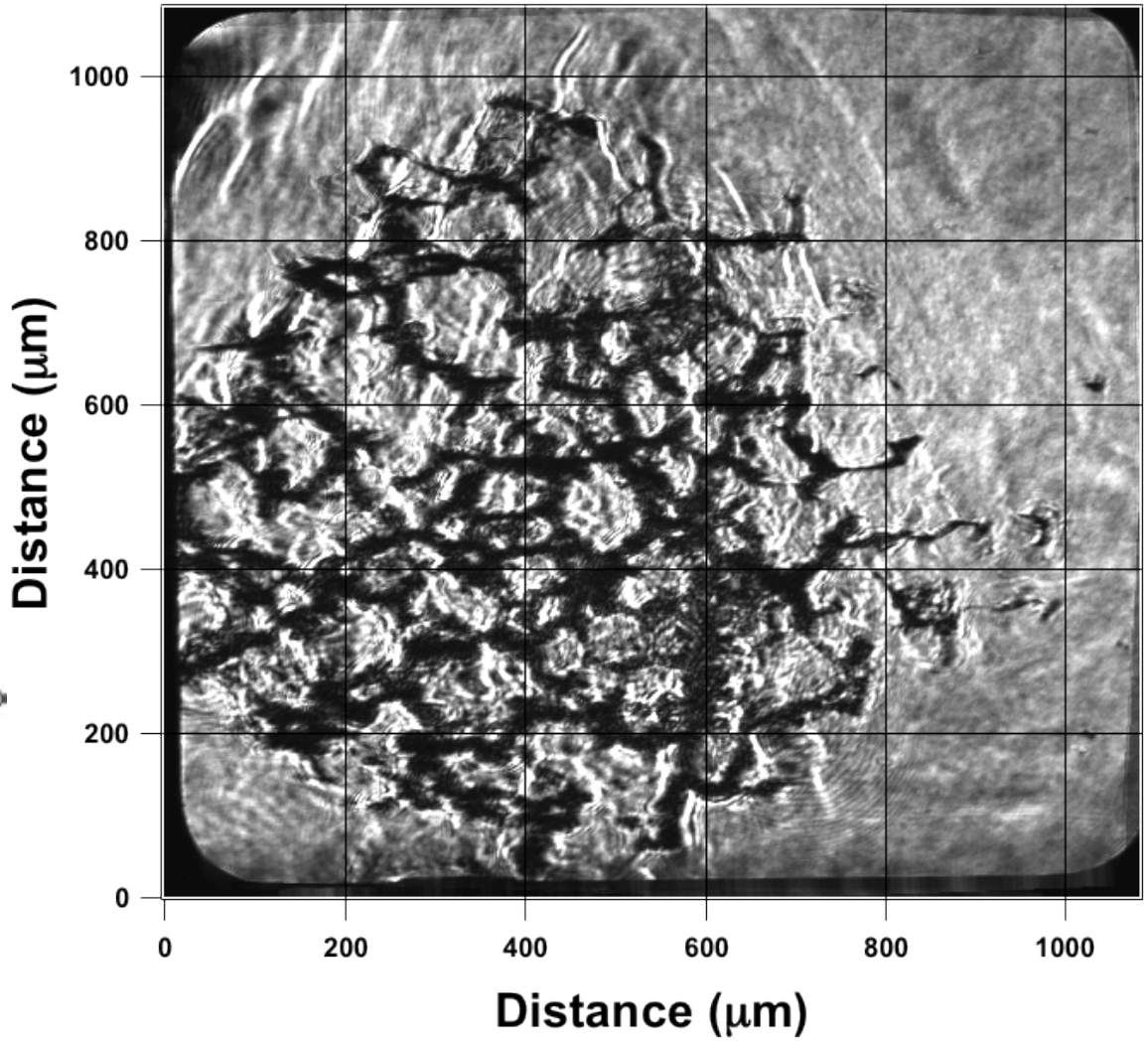

Conclusions

When does the onset of significant plasticity occur?
....a, b, c?

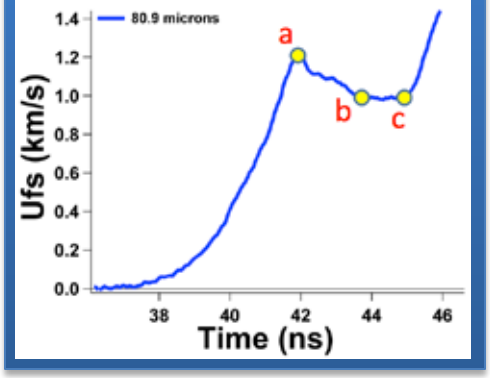

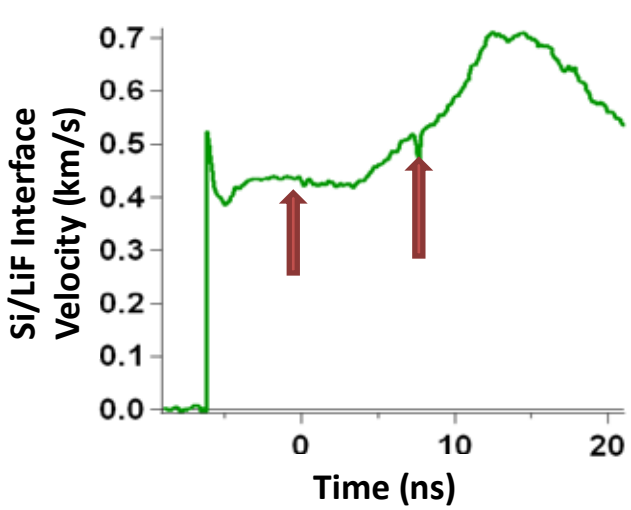

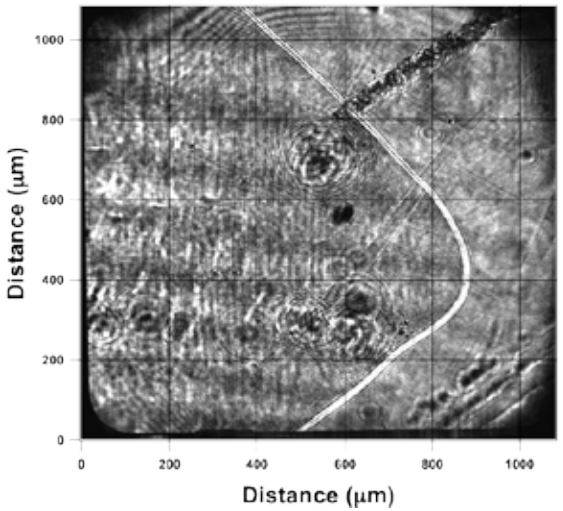

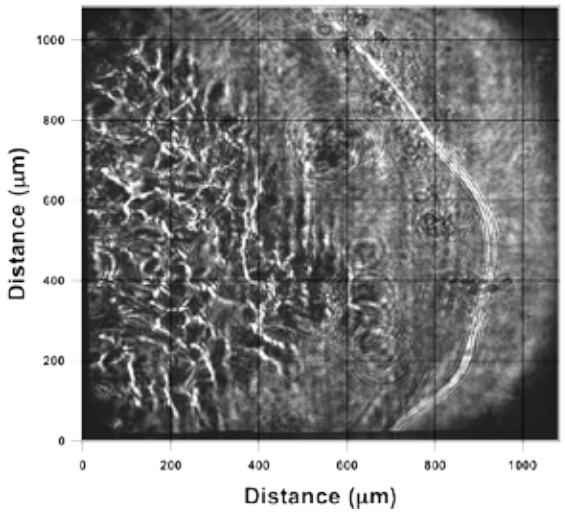

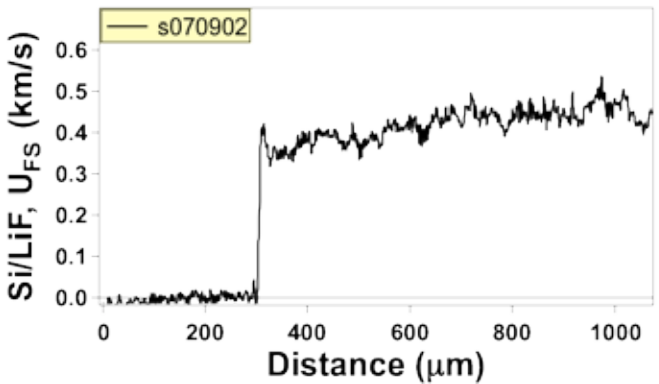

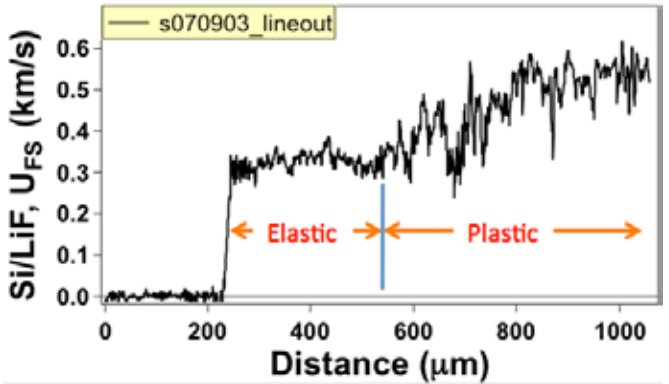

Conclusions

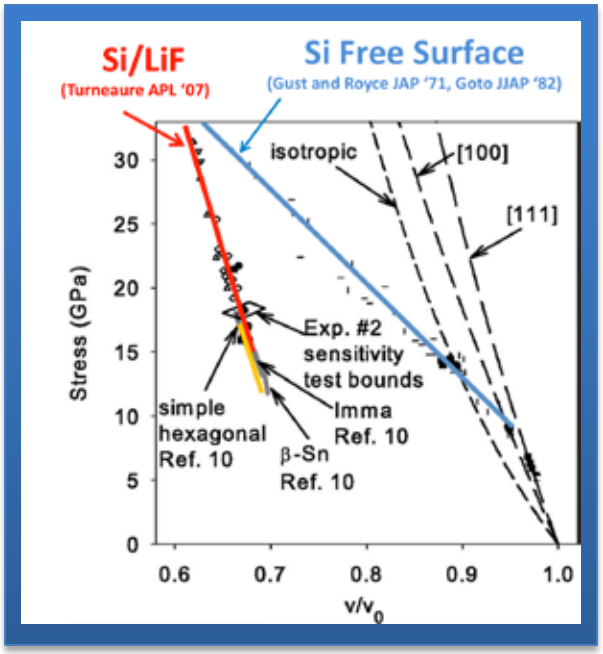

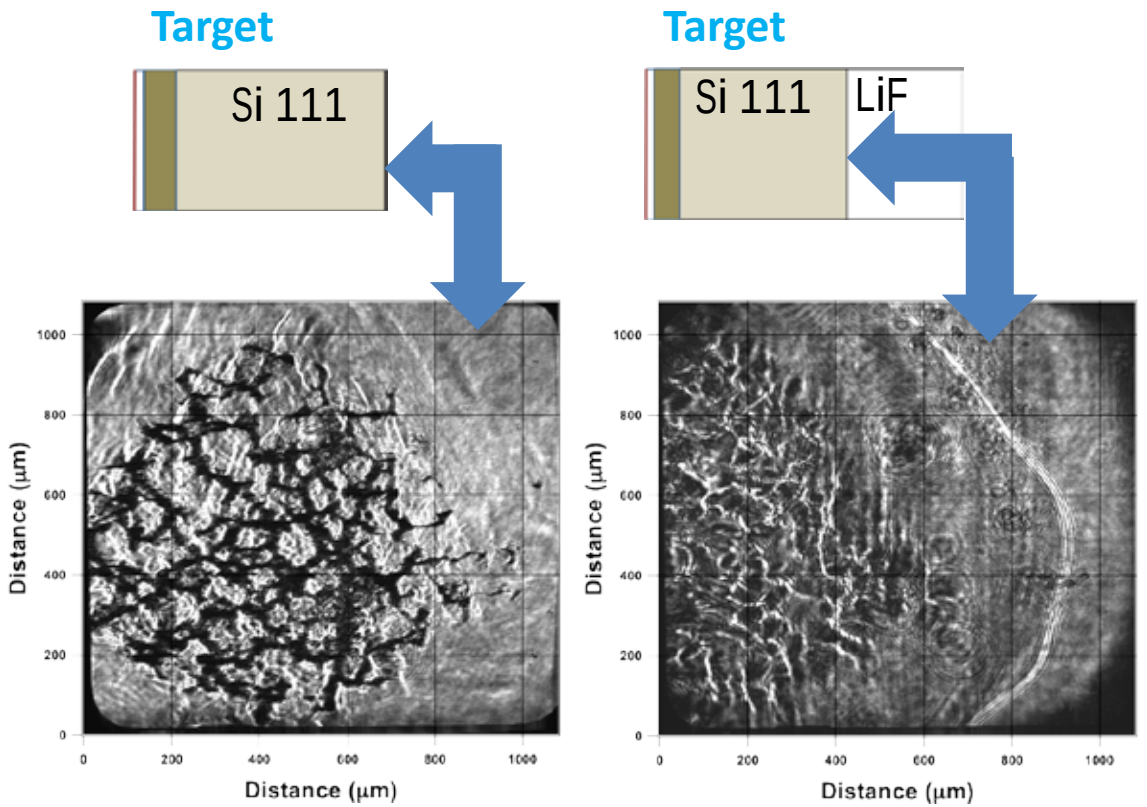

Evidence of jetting for free surface targets (due to fracture?) would contribute to differences in reported σ - rel. V response.

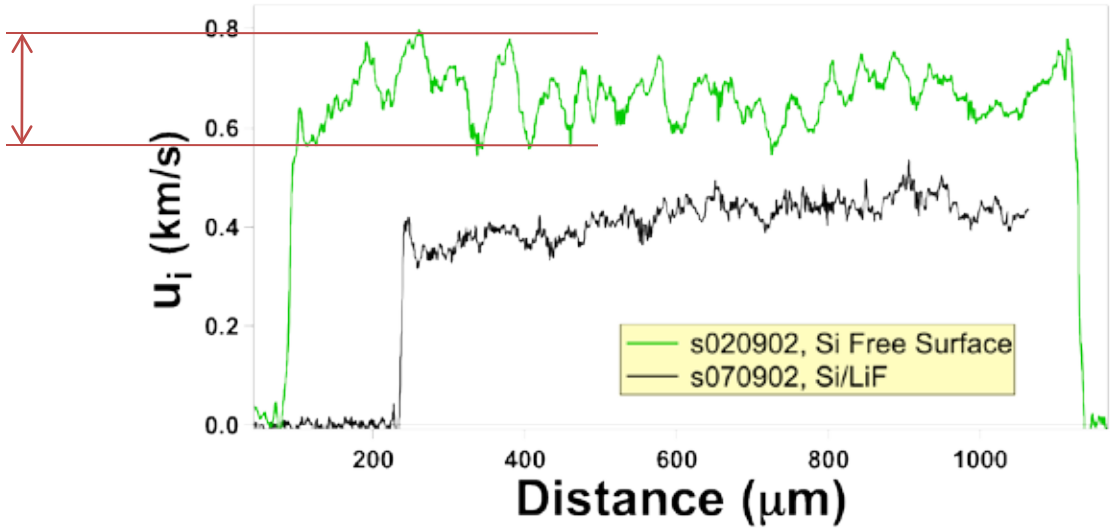

We observe very clear crystal orientation dependences

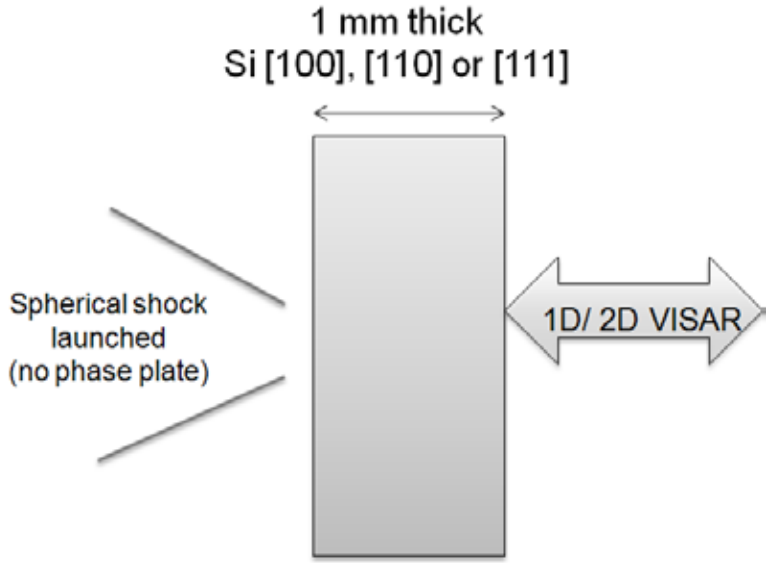

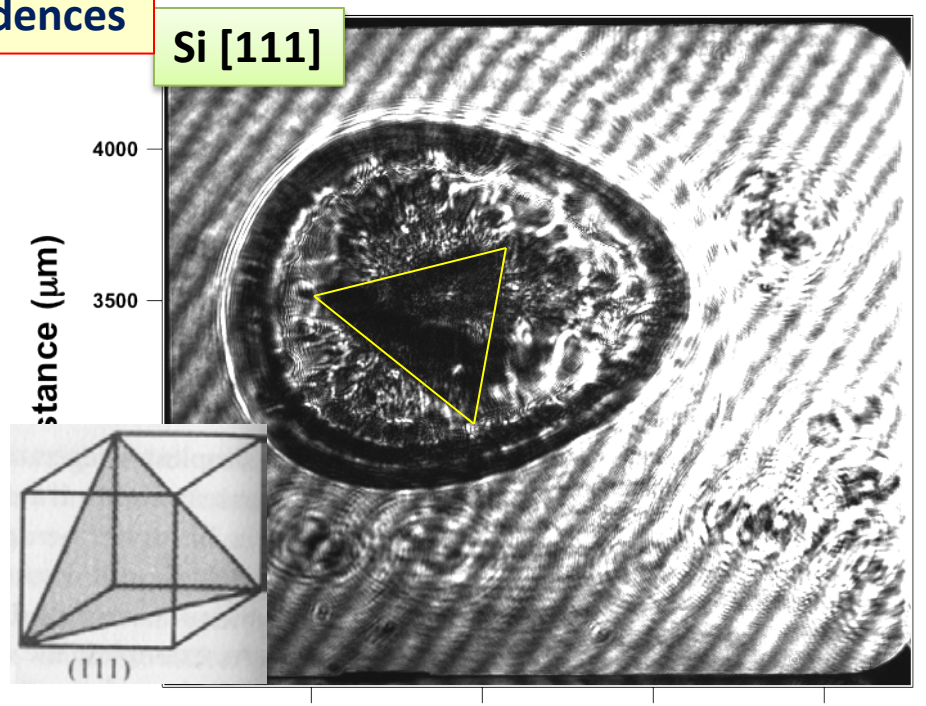

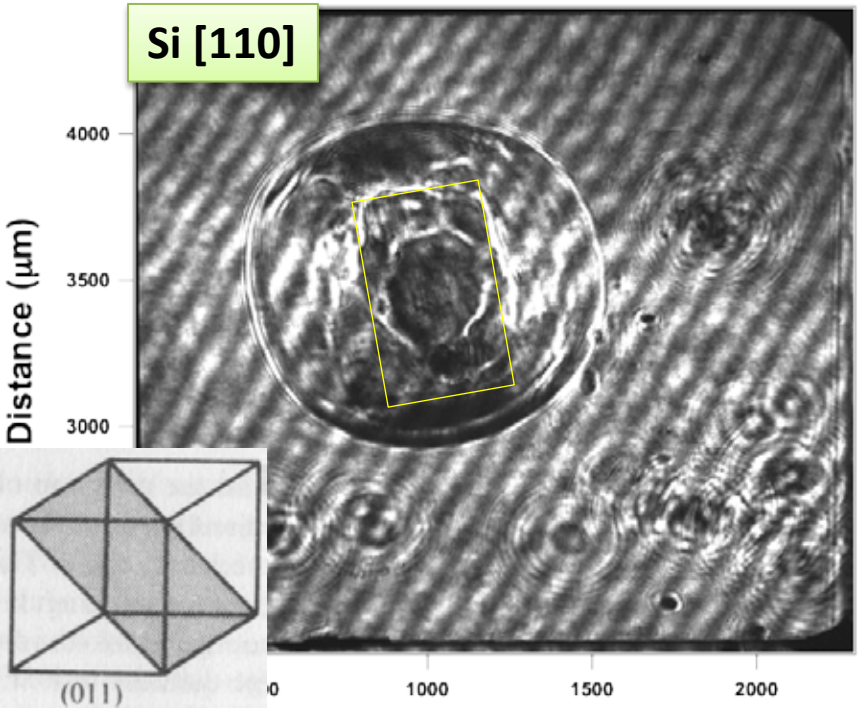

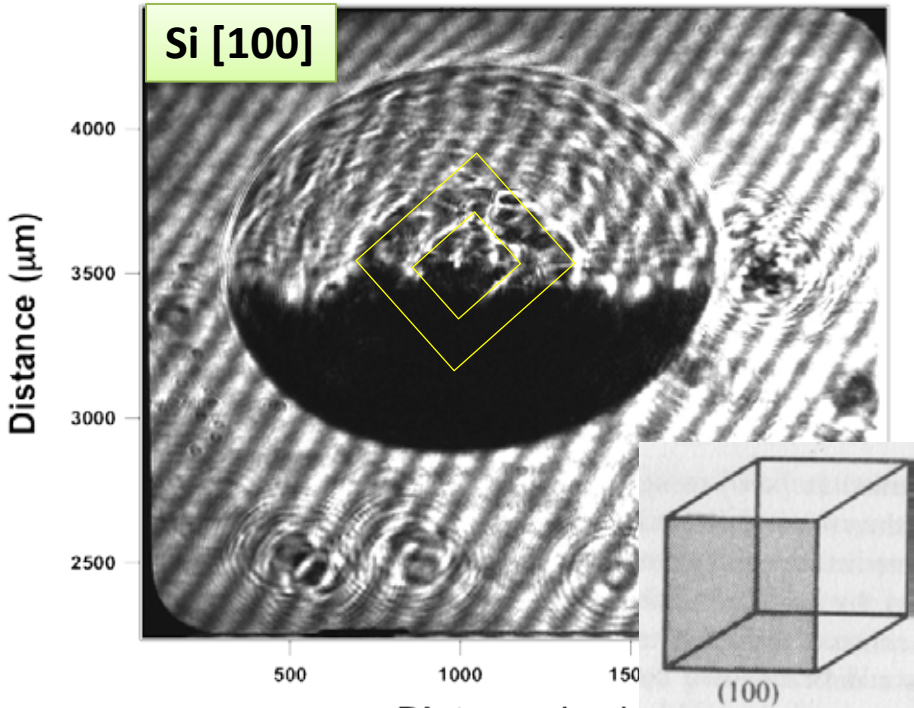

In shocked Aluminum samples, we observe what appears to be grain effects

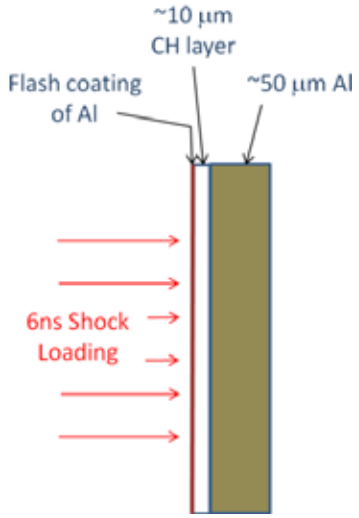

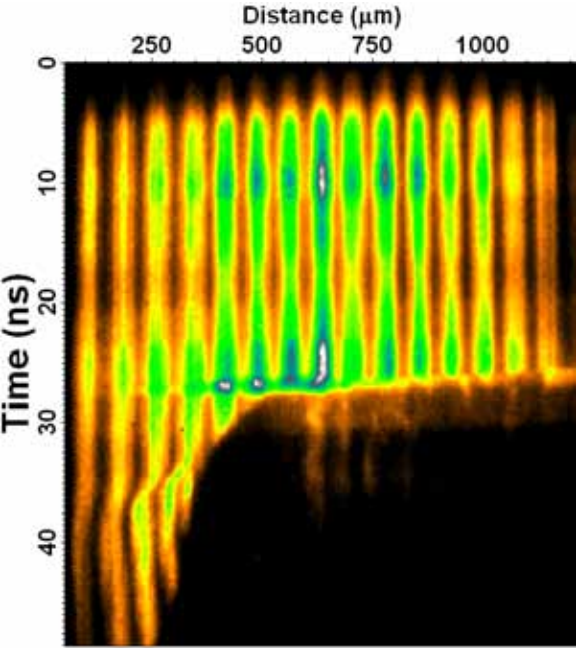

090804 – 50 microns of Al

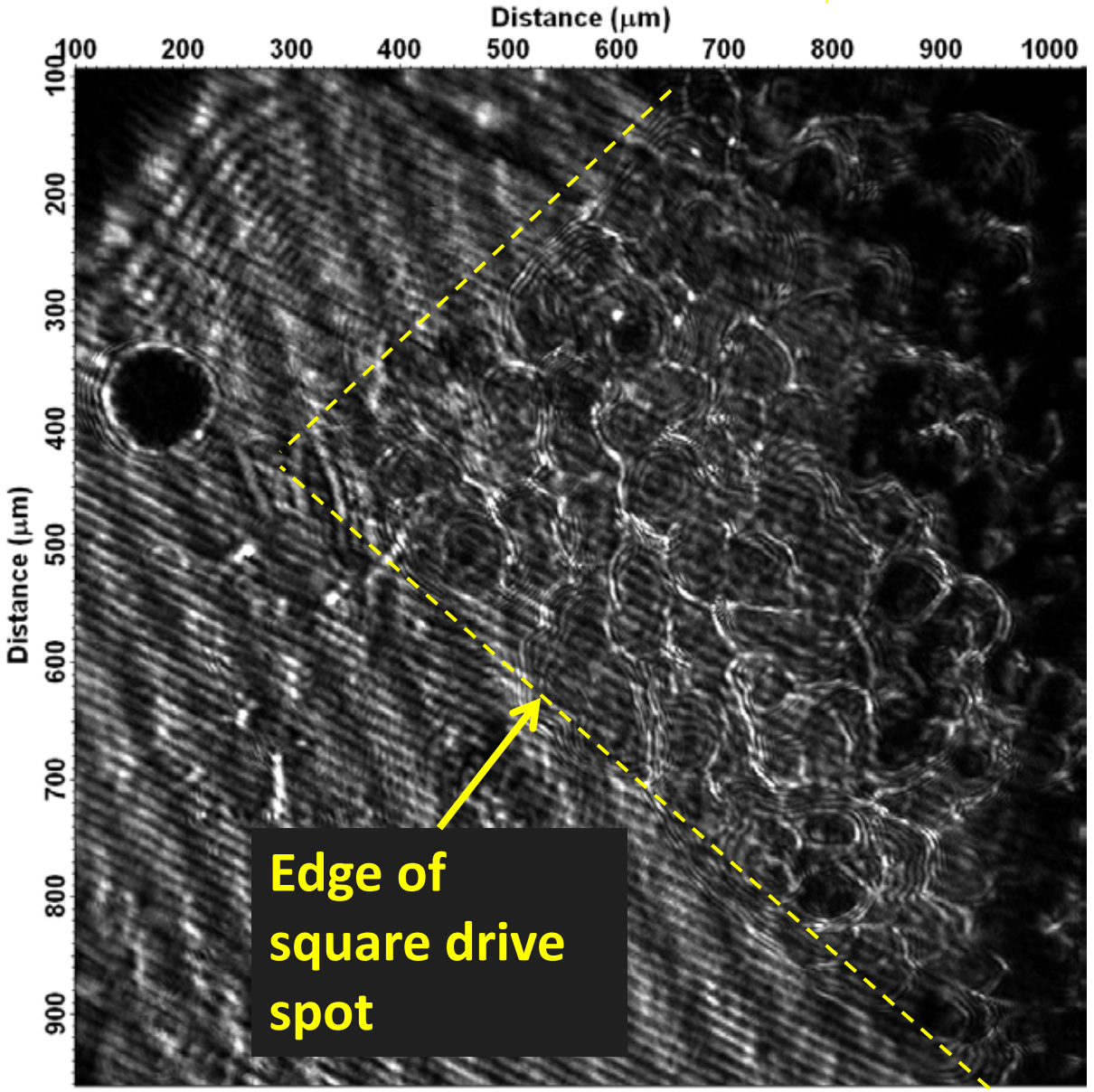

Data suggests that rich velocity distribution across grains

Raw Phase

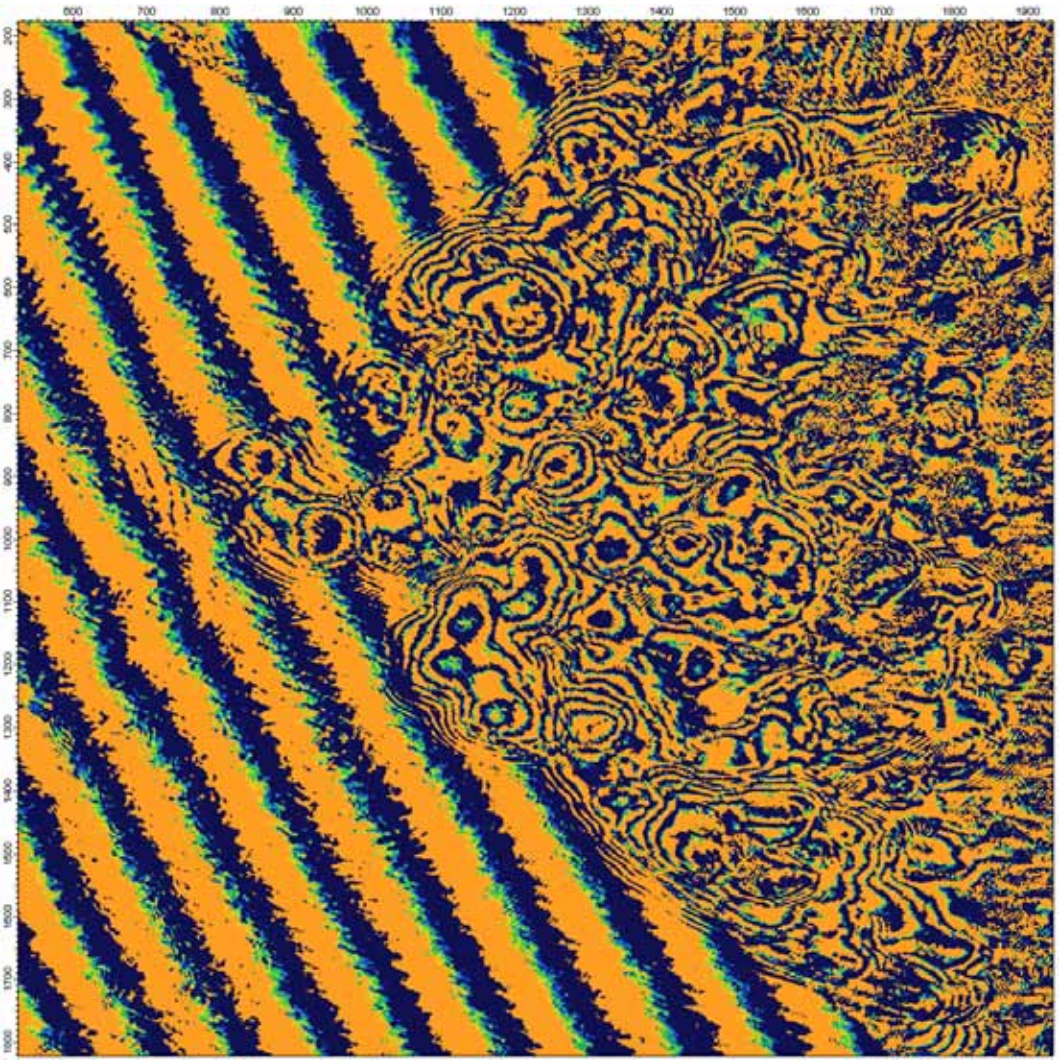

Non-fringing Image

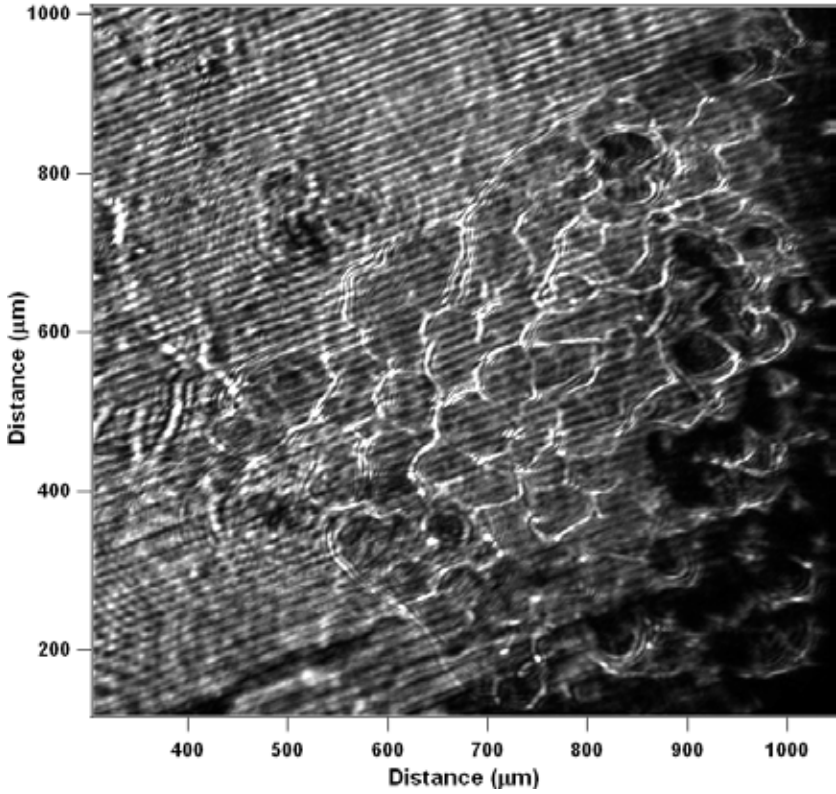

Conclusions

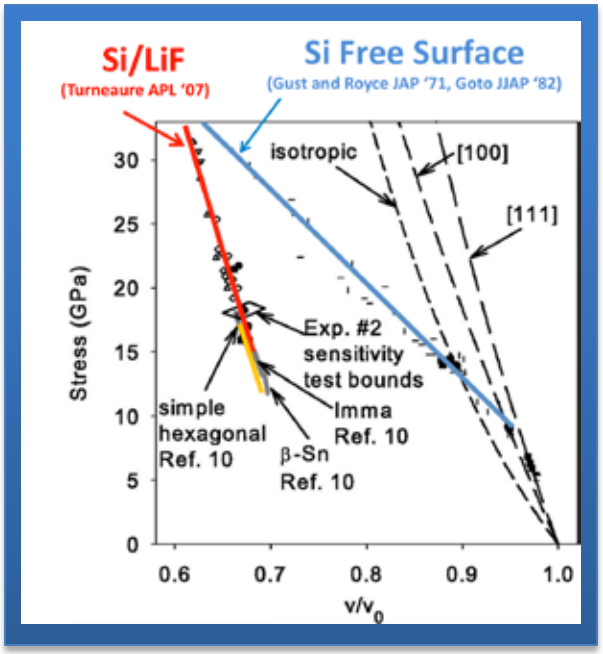

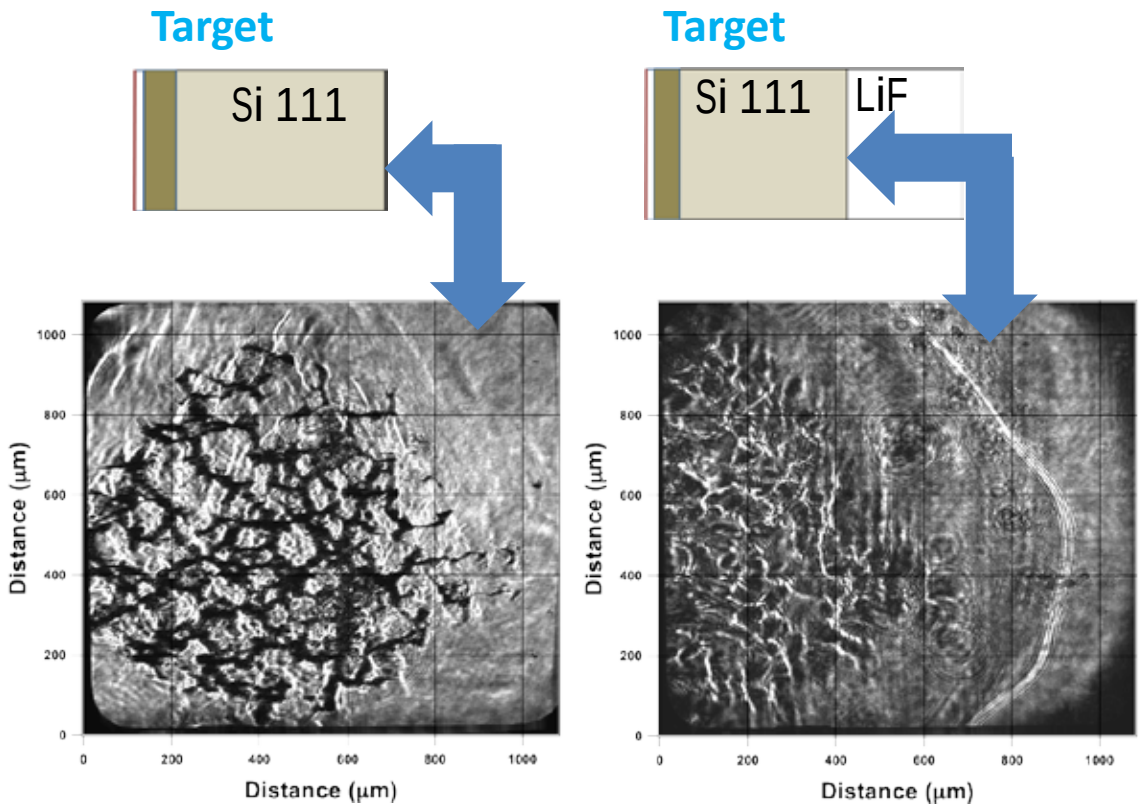

Evidence of jetting for free surface targets (due to fracture?) would contribute to differences in reported σ - rel. V response.

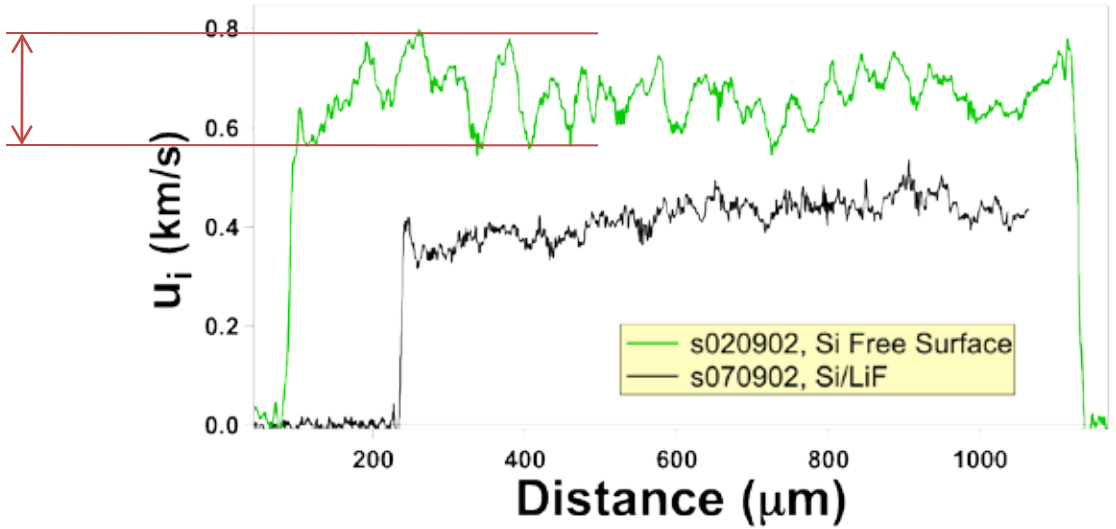

Measuring ramp compression with PDV

4th Workshop on Ramp Compression

January 18-19, 2011
Albuquerque, NM

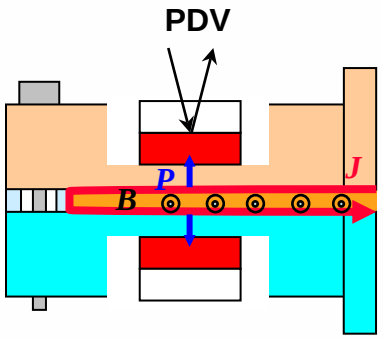

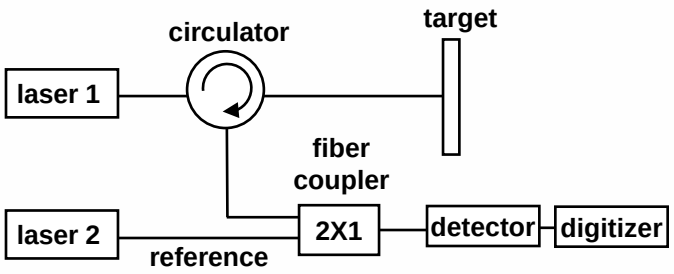

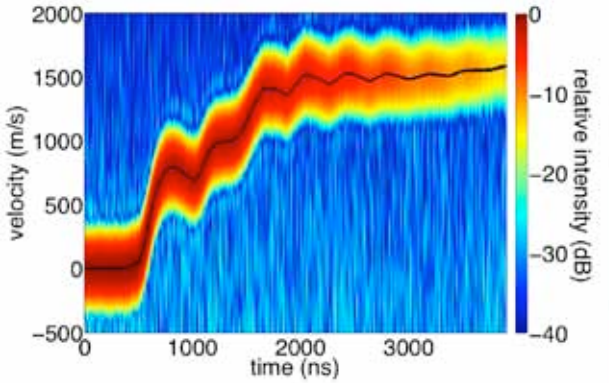

T. Ao and D.H. Dolan

1646 Dynamic Material Properties,
Sandia National Laboratories, Albuquerque, NM, USA

Sandia National Laboratories is a multi-program laboratory operated by Sandia Corporation, a wholly owned subsidiary of Lockheed Martin Corporation, for the U.S. Department of Energy's National Nuclear Security Administration under contract DE-AC04-94AL85000.

Acknowledgments

Diagnostic development of PDV

§ Sheri Payne and Rich Hacking

Operation of gas gun and Veloce machine

§ Randy Hickman and Jesse Lynch

Fabrication of targets

§ Aaron Bowers, Nicole Rivera and Andy Shay

Sandia National Laboratories

Outline

Background

- VISAR
- Photonic Doppler velocimetry (PDV)
- PDV configurations

Accuracy and precision of PDV

- Sampling rate, signal noise fraction, and analysis time duration
- PDV-VISAR validation

PDV measurements through window

- Complications due to multiple reflections

Experiments

- Shock compression using gas gun impactor
- Ramp compression using Veloce pulsed power generator

Sandia National Laboratories

Background: VISAR

Velocity Interferometer System for Any Reflector

- Doppler shifted light from a moving target split along two different paths
  - i.e. reference leg and delay leg of interferometer
- Measured signal: $s(t) = aI_A(t) + bI_B(t) + 2\sqrt{abI_A(t)I_B(t)}\cos[2\pi F(t)]$
- Fringe shift directly proportional to target velocity: $F(t) = \frac{\Phi(t) - \Phi_i(t)}{2\pi} \approx \frac{v}{K}$

Disadvantages

- Sensitive to intensity variations of reflected target light
- Requires additional system to resolve fringe jump ambiguities
- Fixed delay time

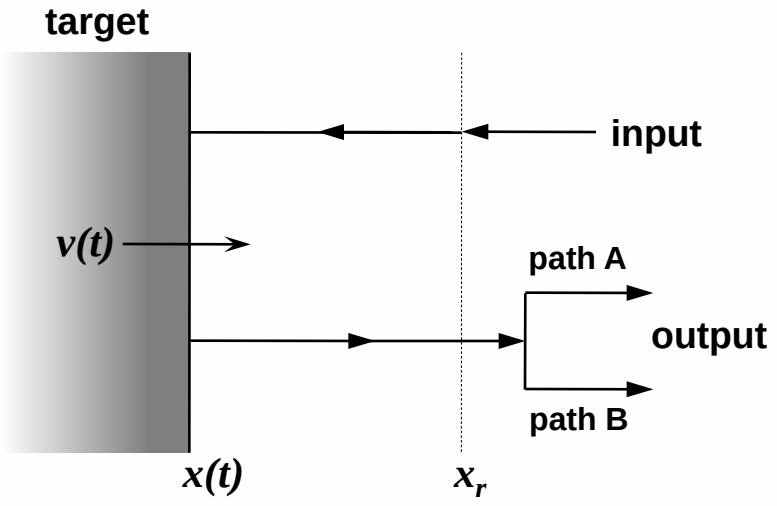

L.M. Barker and R.E. Hollenbach, J. Appl. Phys. **43**, 4669 (1972)

Sandia National Laboratories

Background: PDV

Photonic Doppler velocimetry

- Doppler shifted light from a moving target combined with unshifted light
  - "Heterodyne velocimetry"
- Measured signal: $s(t) = aI_R(t) + bI_T(t) + 2\sqrt{abI_R(t)I_C(t)}\cos\left[\Phi(t_i) + 4\pi\frac{x(t) - x(t_i)}{\lambda_0}\right]$
- Beat frequency proportional to velocity: $f = \frac{2v}{\lambda_0}$

Advantages

- Readily available components
  - Infrared fiber-based (λ_0 = 1550 nm)
  - Fast detectors; GHz digitizers
- Insensitive to intensity variations of reflected target light
- Resolve multiple velocities
- Simple assembly and operation
- Lack of intrinsic delay time

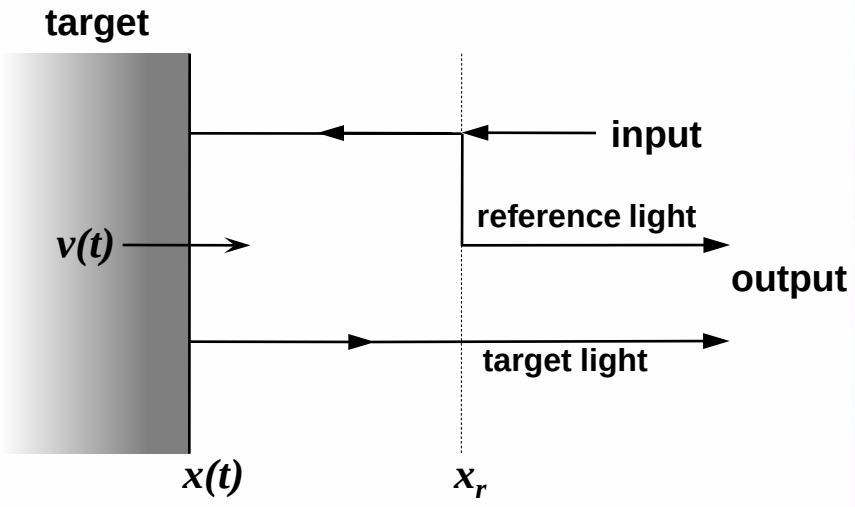

O.T. Strand, *et al.*, Rev. Sci. Instrum. **77**, 083108 (2006)

Sandia National Laboratories

Analysis of PDV data

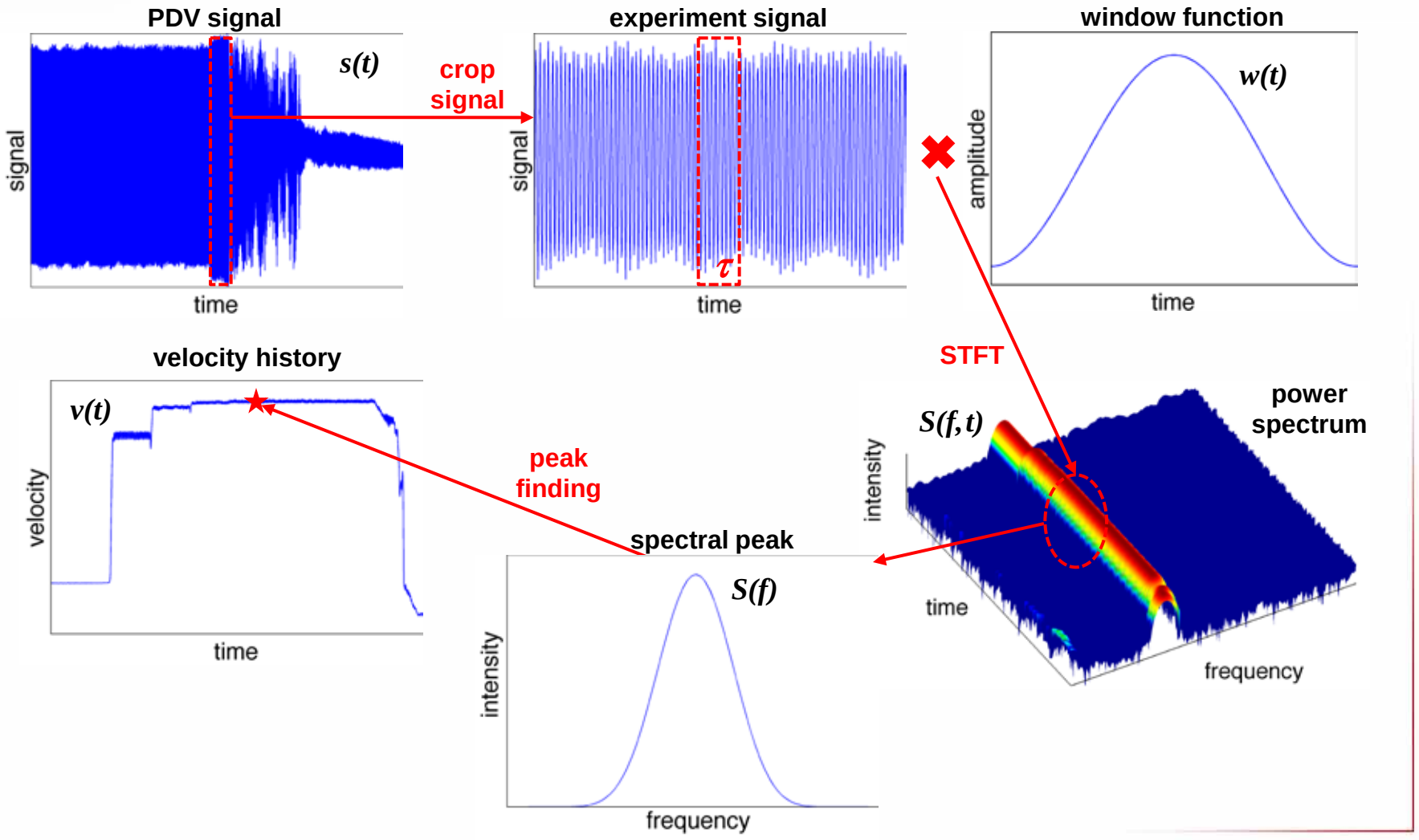

T. Ao and D.H. Dolan, SAND2010-3628, June 2010

Sandia National Laboratories

Digital window functions

Window weighting functions

- Data multiplied by window function to reduce spectral leakage associated with finite observation intervals

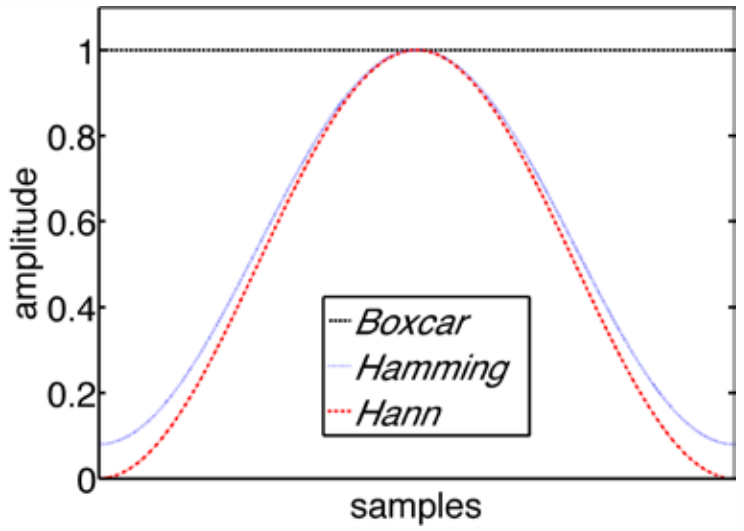

Spectral response goals

- Narrow main-lobe
- Low first-side-lobe
- Rapid fall-off of side-lobes

Boxcar

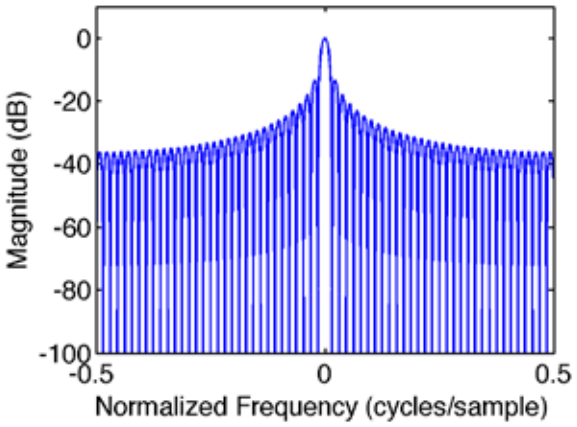

Hamming

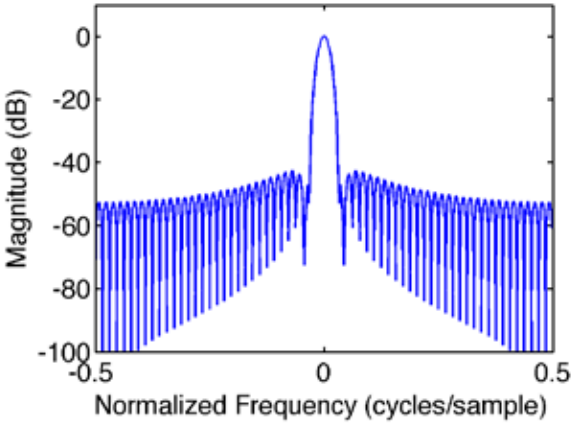

Hann

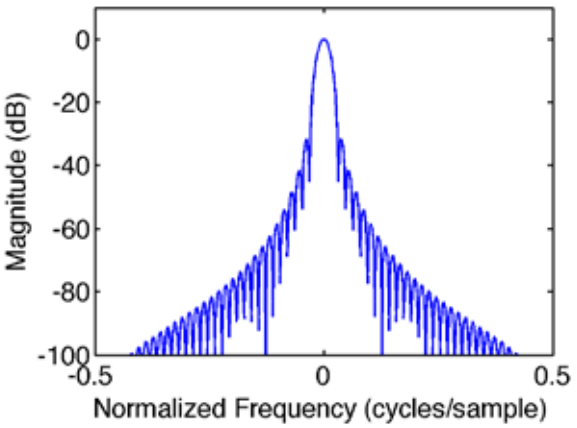

F. Harris, Proceedings of the IEEE **66**, 51 (1978)

Sandia National Laboratories

PDV configurations

Conventional PDV

- Reference light and target light initially same frequency
  - Infrared laser
  - Circulator
  - Fiber couplers
  - Infrared detector
  - GHz digitizer

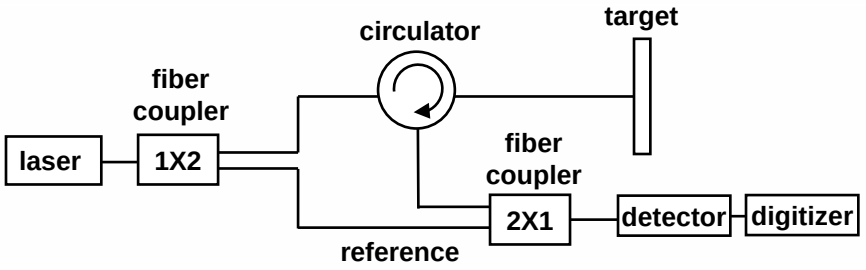

Frequency-conversion PDV

- Reference light and target light always different frequencies
  - Two tunable infrared lasers
  - Acousto-optic frequency shifter

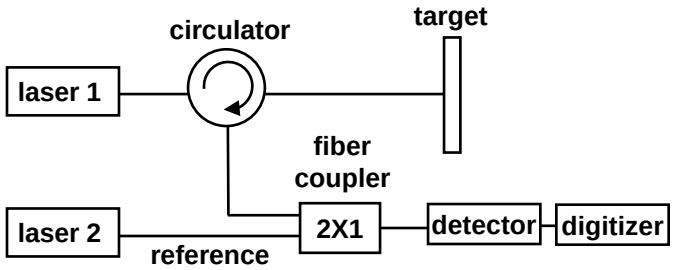

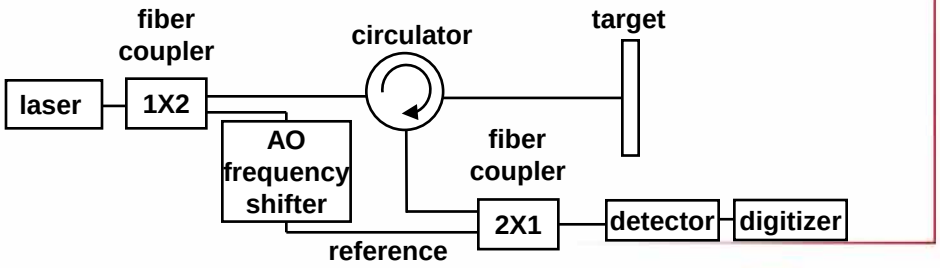

T. Ao and D.H. Dolan, SAND2010-3628, June 2010

Sandia National Laboratories

PDV signal of shock loading

E.g. velocity step

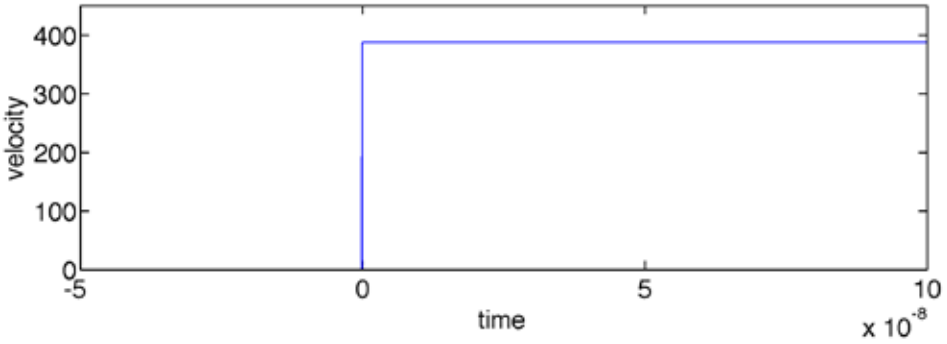

Conventional PDV

- No target motion = no beat frequency

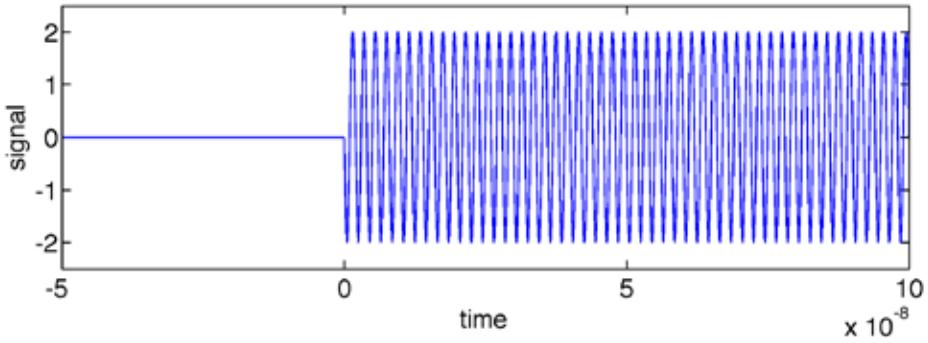

Frequency-conversion PDV

- Underlying beat frequency even with no target motion

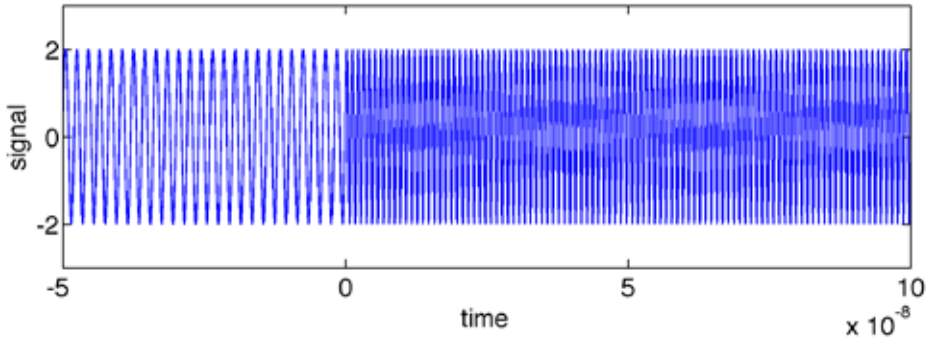

T. Ao and D.H. Dolan, SAND2010-3628, June 2010

Sandia National Laboratories

Conventional PDV issues

E.g. velocity ramp

Conventional PDV

- Inability to resolve the low velocity portion of ramp
  - At low velocities, beat period longer than analysis time duration

Frequency-conversion PDV

- Oscillations at low velocities eliminated
  - Underlying beat frequency results in the low velocity features now having a shorter beat period

"Modest" velocity (~ 100 m/s) transients

- Structured waves (ramps and multiple shocks)
  - Elastic precursor, phase transition
- Want to achieve both optimal velocity & time precision

$\tau = 15$ ns

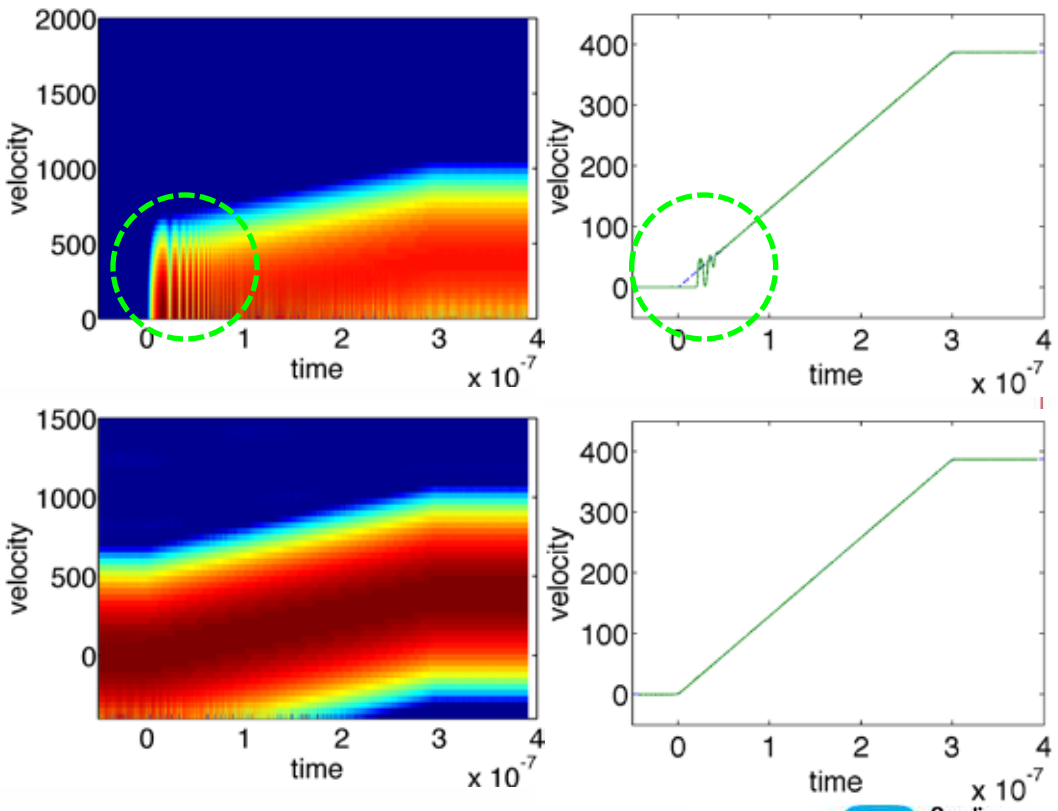

T. Ao and D.H. Dolan, SAND2010-3628, June 2010

Sandia National Laboratories

What is the performance of PDV?

Quantitatively, how good can PDV be?

- Accuracy: being right (on average)
- Precision: variability about the average
- Small numbers mean "high performance"

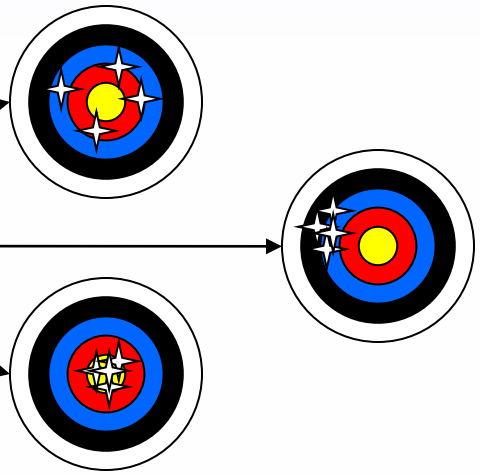

Things that are neglected

- Window corrections (0.2-1%)
- Probe effects/cosine corrections (<0.1%-?)
- Absolute wavelength errors (<10-100 ppm)
- Digitizer clock errors (<10 ppm)

Looking for an equivalent to the "1-2% of a fringe rule (VISAR)"

Sandia National Laboratories

Monte Carlo simulations

Generate discretely sampled signal

$$s_k = \cos(2\pi f_0 T k + \delta) + \sigma R_k$$

- Specified input frequency f_0
- $k = -M \ldots M$ ($2M+1$ points)
- Sampling interval T
- Noise fraction σ
- Random phase δ
- Random noise array R

One iteration

25 samples over 1 ns, 10% noise

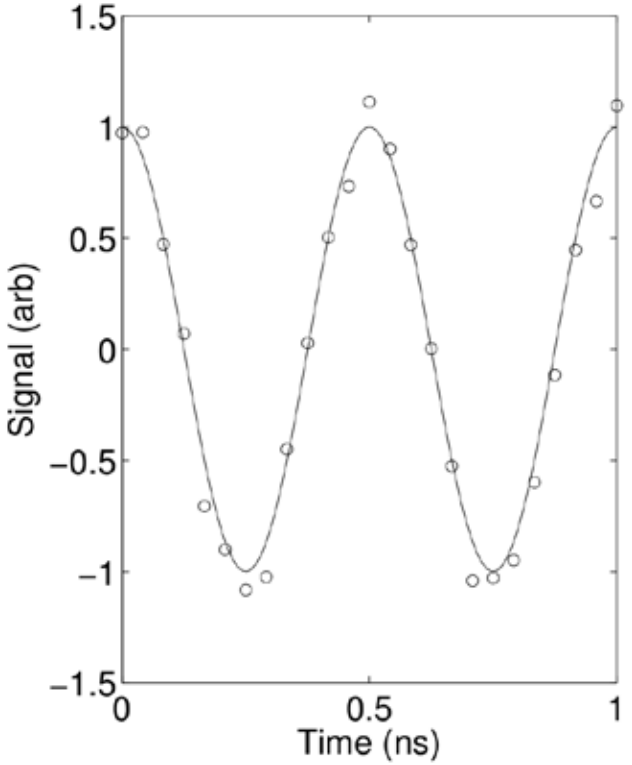

Extract frequency from signal

- FFT analysis, etc.

Compare the result to input frequency

Repeat MANY times with different phases and noise arrays

D.H. Dolan, Rev. Sci. Instrum. **8**1, 053905 (2010)

Sandia National Laboratories

Resolution example

Inputs

- 1 ns duration, 25 GS/s
- 10% noise fraction
- 0.1-6 GHz (0.02 GHz steps)
- ~590 million iterations total

Analyze many random signals

- Ensemble of frequency results from a set of inputs
- Accuracy: difference between ensemble mean and input (solid lines)
- Precision: ensemble standard deviation (dashed lines)

Poor accuracy and precision below 1 GHz (partial fringe)

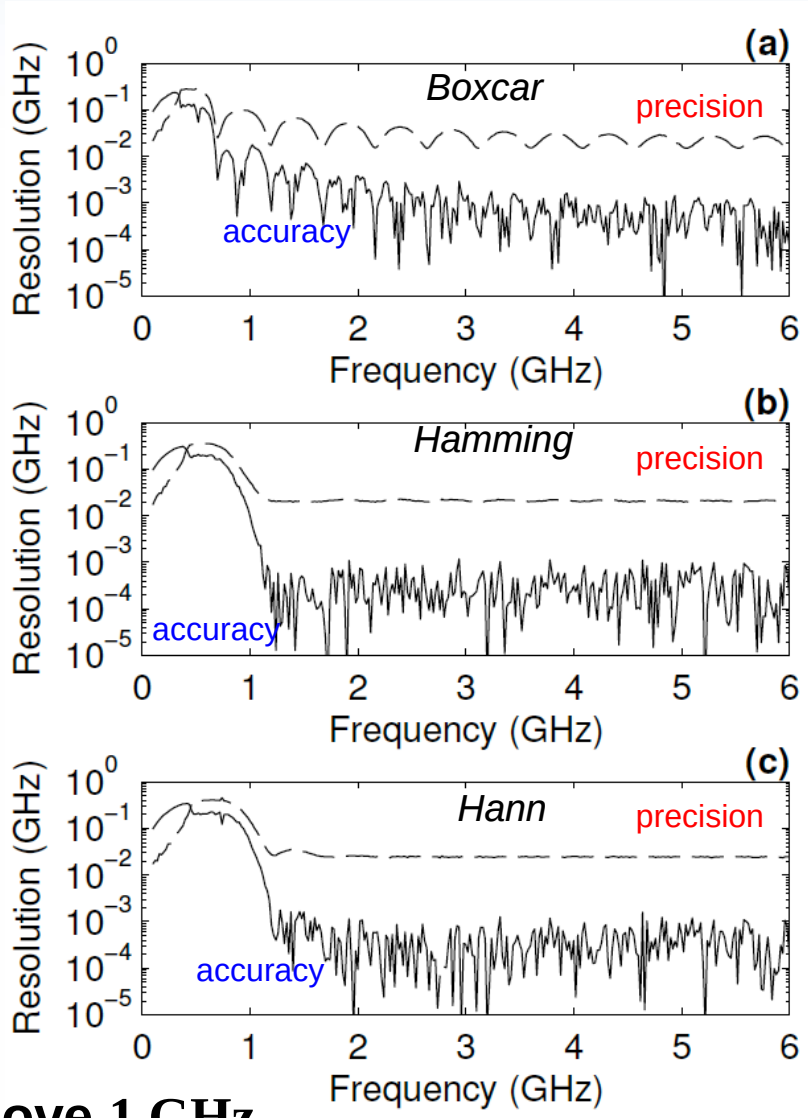

Measurements are precision-limited above 1 GHz

D.H. Dolan, Rev. Sci. Instrum. **8**1, 053905 (2010)

Sandia National Laboratories

Precision and noise

Simulations performed at various noise fractions

- Solid lines: 1%
- Dashed lines: 10%
- Dot-dash lines: 50%

Window performance

- Hann window best at low noise fractions
- Boxcar best at high noise fractions

Precision benefits are largely constant above low frequency "shoulder"

- Precision limit of PDV measurement scales with signal noise fraction σ, inversely with sampling rate f_S, and to -3/2 power with analysis time duration τ

$$\delta f = \sqrt{\frac{6}{N}}\frac{\sigma}{\pi\tau} = \left(\sqrt{\frac{6}{f_S}}\frac{\sigma}{\pi}\right)\tau^{-3/2}$$

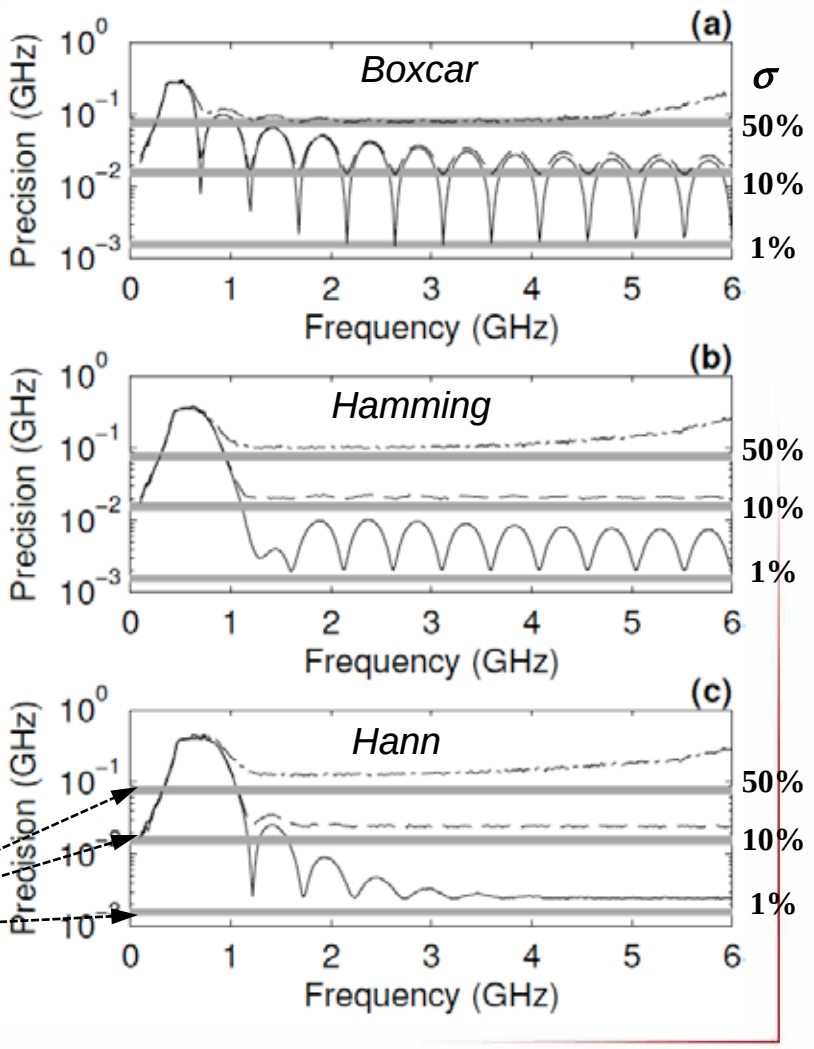

D.H. Dolan, Rev. Sci. Instrum. **8**1, 053905 (2010)

Sandia National Laboratories

PDV validation

Free surface velocity of shocked sapphire

§ Measured with shorting pins, air-delay VISAR, frequency-conversion PDV

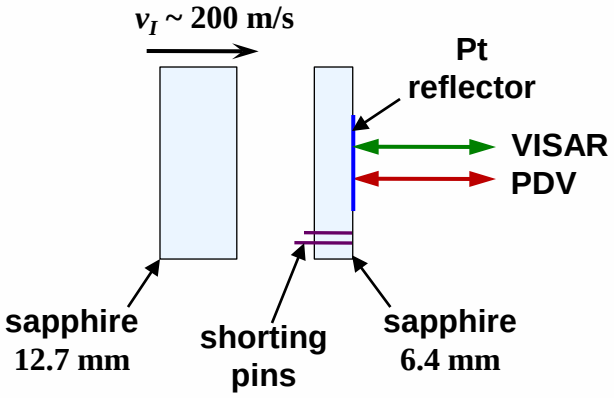

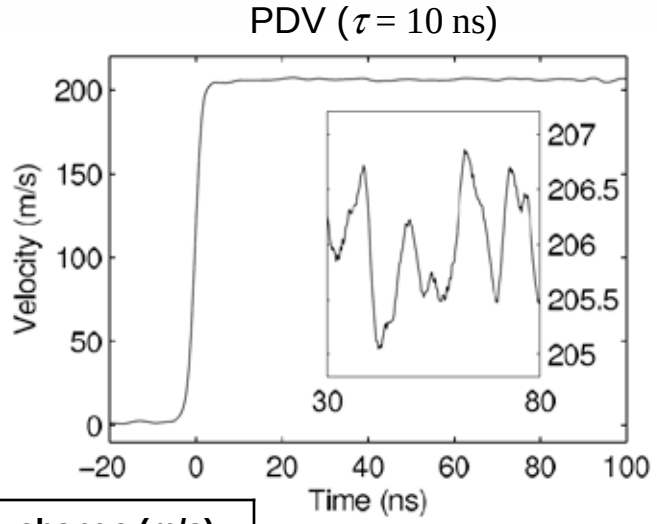

Diagnostic	Time scale (ns)	Velocity change (m/s)
Pins	>1000	206.6 ± 1.1
VISAR	19	206.11 ± 0.28
PDV	19	205.95 ± 0.32
PDV	10	205.93 ± 0.64
PDV	1	206 ± 21

D.H. Dolan, Rev. Sci. Instrum. **8**1, 053905 (2010)

Sandia National Laboratories

Risetimes of PDV and VISAR

Velocity step

- Convert velocity profile to PDV and VISAR signals
- Analyze PDV and VISAR signals to get velocity profile
- Measure 10-90% risetime

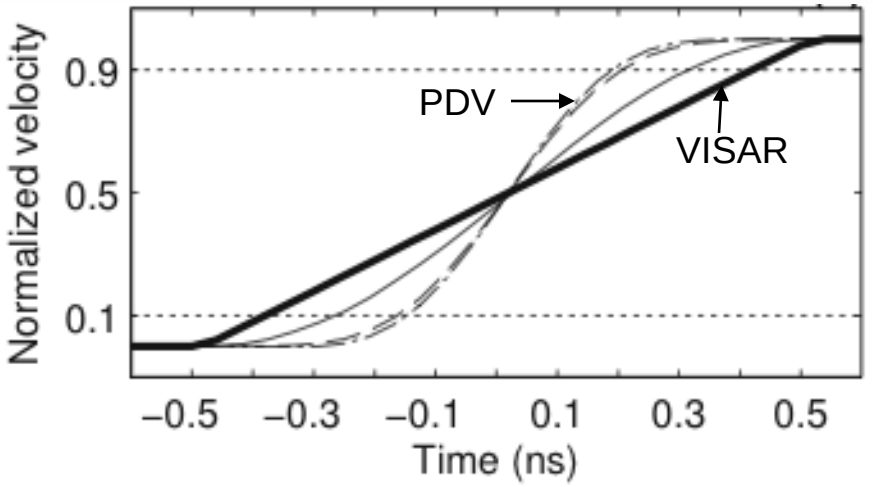

VISAR

- Time delay of 1 ns (heavy solid line)
- Linear risetime of 0.8 ns

PDV signal

- Sampled at 25 GS/s and frequency shifted to 3 GHz
- Analysis time duration $\tau = 1$ ns
- Boxcar (solid line), Hamming (dashed line), Hann (dash-dot line) digital window

PDV

Digital window	Risetime (ns)
Boxcar	0.58
Hamming	0.37
Hann	0.34

D.H. Dolan, Rev. Sci. Instrum. **8**1, 053905 (2010)

Sandia National Laboratories

Comparison with VISAR

Resolution ratio (PDV/VISAR)

- PDV noise fraction $\sigma \sim 10\%$
- VISAR fringe resolution $\varepsilon \sim 2\%$
- Common delay/analysis time

$$\rho = \frac{1550}{532}\sqrt{\frac{6}{f_s \tau}}\frac{\sigma}{\pi\varepsilon}$$

- For 1 ns analysis, ratio is 2.3: VISAR better (maybe)
- For 10 ns analysis, ratio is 0.72: PDV better
- PDV time scale is adjustable, VISAR fixed by hardware

Mitigating factors

- PDV rise faster than VISAR for common delay/analysis time (improvements depend on digital window)
- PDV uses one signal, VISAR uses 4-8 signals (2-2.8x improvement)
- VISAR requires good characterization (5-10% fringe resolution not unusual)

D.H. Dolan, Rev. Sci. Instrum. **8**1, 053905 (2010)

Sandia National Laboratories

PDV through window

Complications due to multiple reflections

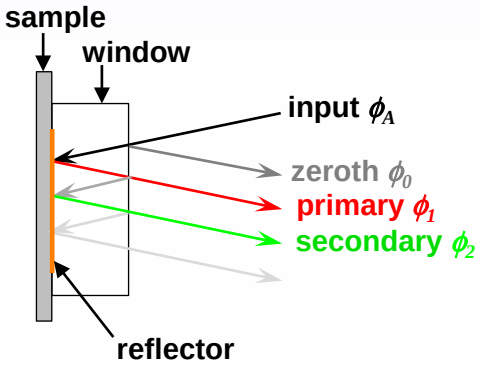

§ Detector signal: $s(t) = \sum_{k=0}^{N} A_k \cos(2\pi f_k t + \Delta_k)$

§ Optical phase of the k-th reflection:

$$\Phi_k(t) = 2\pi(f_C + kf_D)t + \Delta_k$$

§ Short-time Fourier transform (STFT) of signal to obtain power spectrum:

$$\tilde{S}(f,\bar{t}) = \int_{-\infty}^{\infty} s(t)w(t-\bar{t})e^{-i2\pi ft}dt$$

$$\tilde{S}(f,\bar{t}) = \sum_{k=0}^{N} \frac{A_k}{2}\left\{e^{+\gamma_k(\bar{t})}S_{+f_k}(f) + e^{-\gamma_k(\bar{t})}S_{-f_k}(f)\right\}$$

$$\gamma_k(\bar{t}) = 2\pi f_k \bar{t} + \Delta_k \qquad \tilde{S}_{\pm f_k}(f) = \int_{-\infty}^{\infty} w(q)e^{\pm 2\pi i(f \mp f_k)q}dq$$

T. Ao and D.H. Dolan, Rev. Sci. Instrum., in press (2011)

Sandia National Laboratories

Spectral contributions to power spectrum

$$\left|\tilde{S}(f,\bar{t})\right|^2 \propto \sum_{k=0}^{N} A_k^2 \left\{S_{+f_k}^2(f) + S_{-f_k}^2(f) + 2\cos\left[2\gamma_k(\bar{t})\right] S_{+f_k}(f) S_{-f_k}(f)\right\}$$

primary reflection f_1

$$+2\sum_{k}^{N}\sum_{j=k+1}^{N} A_k A_j \cos\left[\gamma_k(\bar{t}) - \gamma_j(\bar{t})\right]\left\{S_{+f_k}(f) S_{+f_j}(f) + S_{-f_k}(f) S_{-f_j}(f)\right\}$$

$$+2\sum_{k}^{N}\sum_{j=k+1}^{N} A_k A_j \cos\left[\gamma_k(\bar{t}) + \gamma_j(\bar{t})\right]\left\{S_{+f_k}(f) S_{-f_j}(f) + S_{+f_k}(f) S_{-f_j}(f)\right\}$$

Each signal contribute positive & negative frequency components to power spectrum

- Positive, negative, and cross-sign products of frequency peak for each component
- Same-sign cross product of different components
- Opposite-sign cross product of different components

Extraction of primary reflection frequency hindered

- Static terms affect accuracy
- Dynamic terms affect precision

T. Ao and D.H. Dolan, Rev. Sci. Instrum., in press (2011)

Sandia National Laboratories

Interactions of spectral functions

Small analysis time duration

- Conventional PDV allow for many spectral interactions

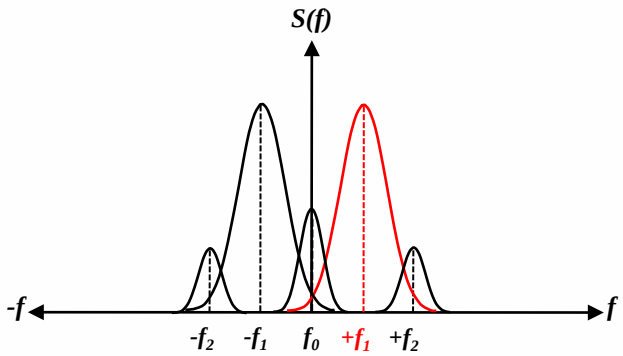

conventional PDV

- Frequency-conversion PDV separates negative and positive frequency spectral functions

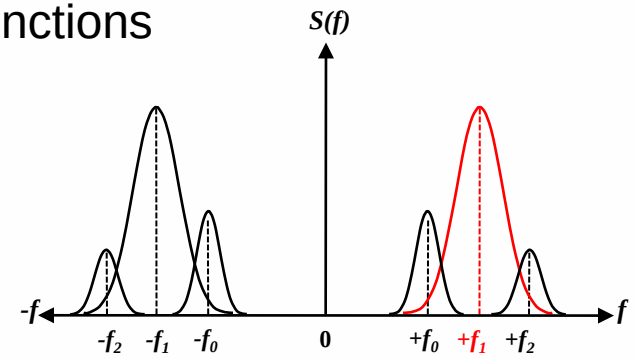

frequency-conversion PDV

Large analysis time duration

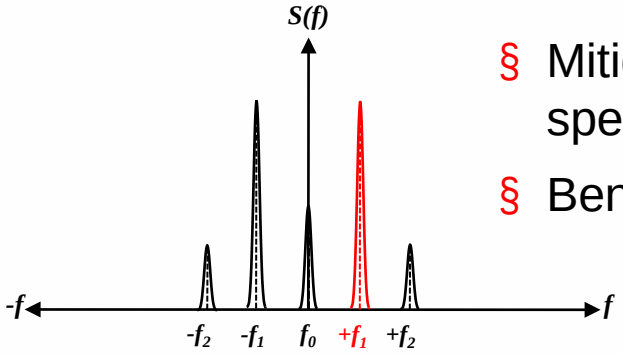

conventional PDV

- Mitigate spectral interactions by narrowing the spectral functions at the cost of time resolution
- Benefits conventional and frequency-conversion PDV

T. Ao and D.H. Dolan, Rev. Sci. Instrum., in press (2011)

Sandia National Laboratories

Shock reverberation experiment

Measurement of transient wave structure

§ Quartz sample sandwiched between sapphire impactor and sapphire window

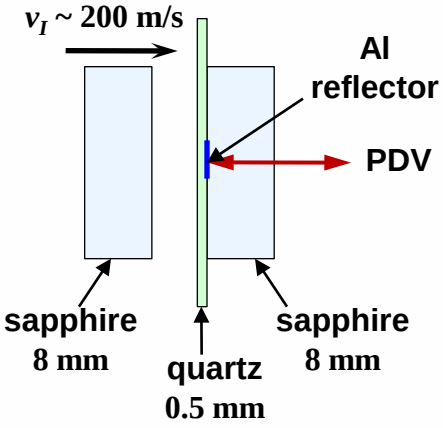

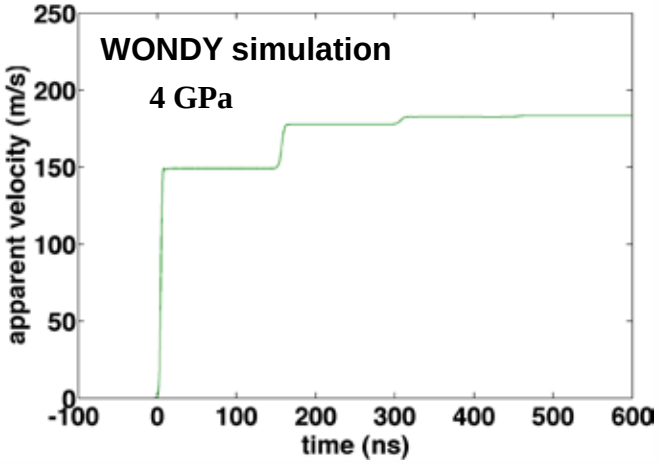

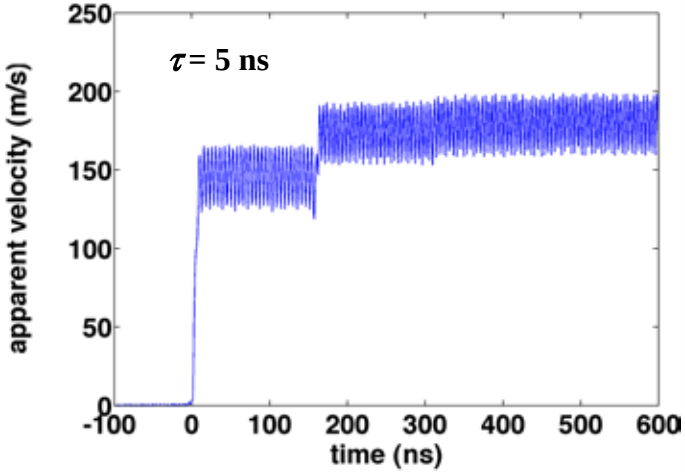

Multiple window transits due to reflections from free surface of window

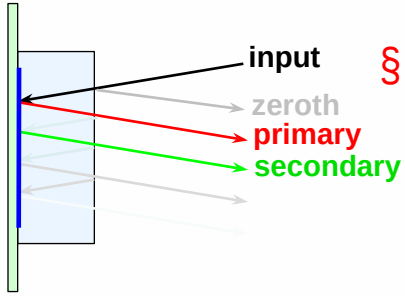

§ Oscillations within velocity profile due to other reflections perturbing primary

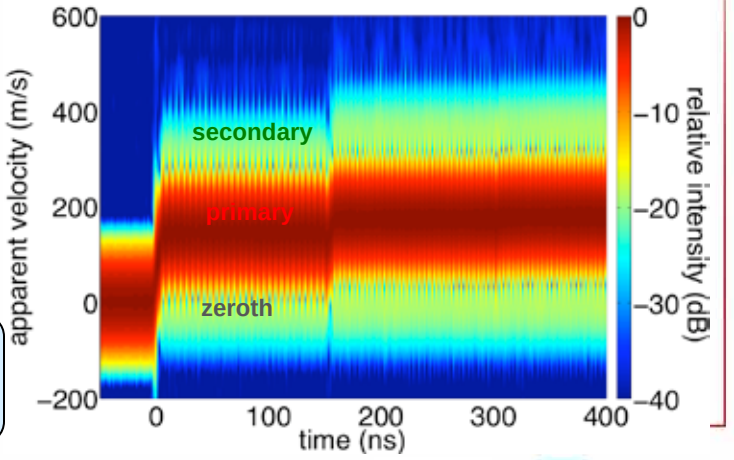

$$s(t) \propto \sqrt{I_R I_0(t)}\cos\Phi_0 + \sqrt{I_R I_1(t)}\cos\Phi_1 + \sqrt{I_R I_2(t)}\cos\Phi_2 + \mathrm{K}$$

T. Ao and D.H. Dolan, Rev. Sci. Instrum., in press (2011)

Sandia National Laboratories

Mitigating window reflections

Wedge window deflect reflections from free surface

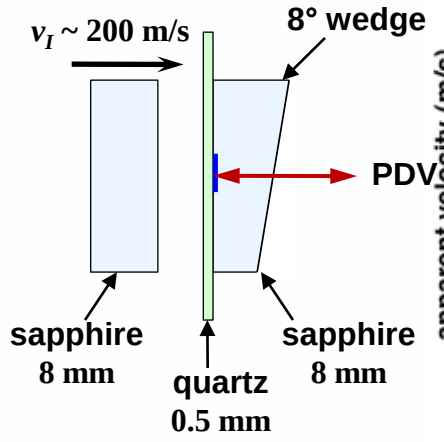

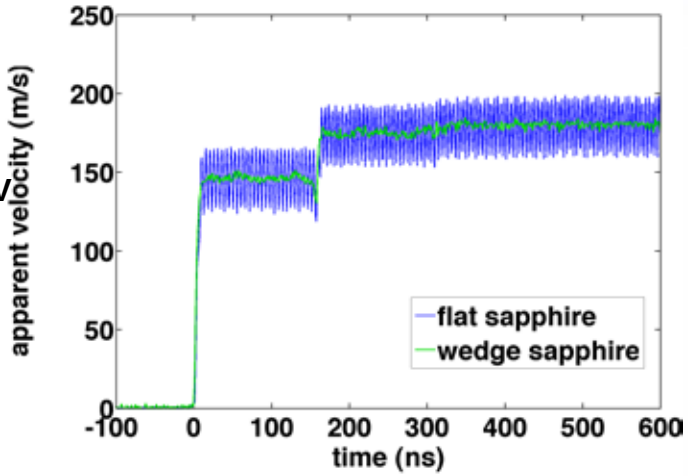

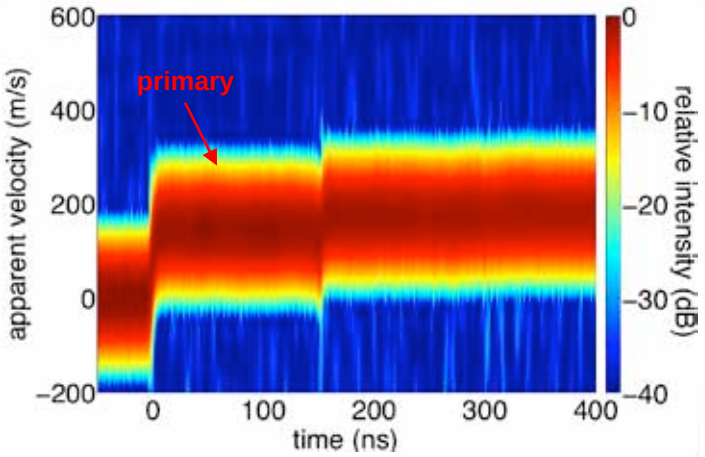

Anti-reflective coating attenuates reflections from free surface

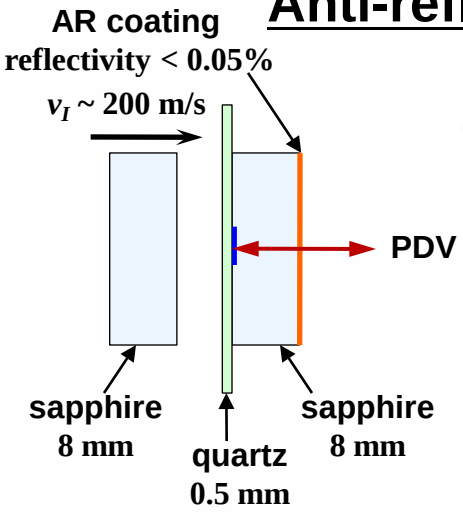

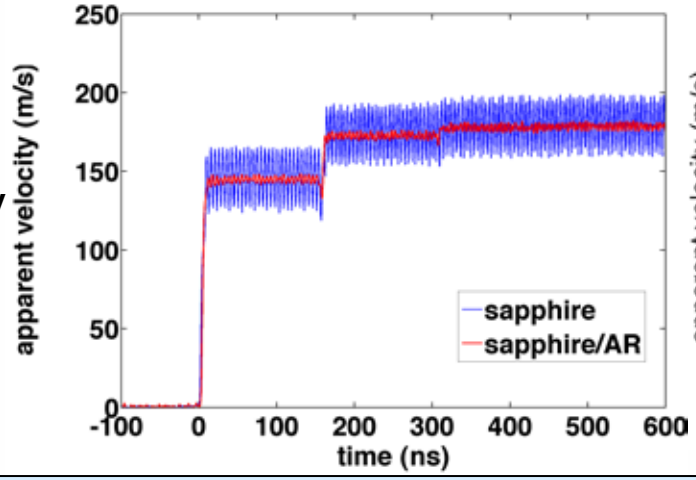

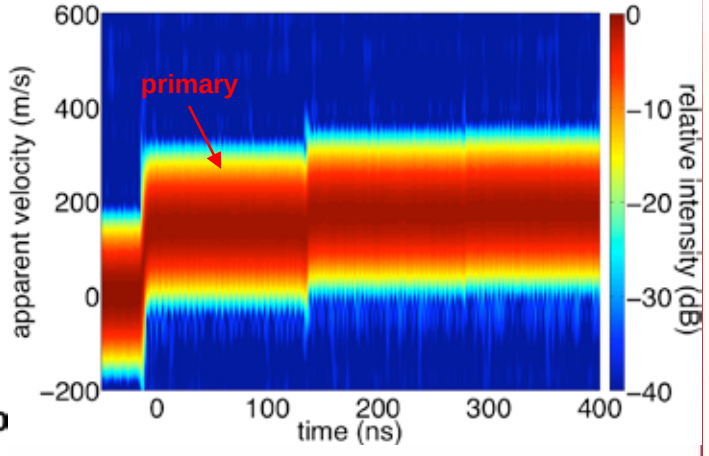

Velocity variations $\delta v/v \approx 1\%$ and analysis time duration $\tau = 5$ ns comparable to velocity and time precision of VISAR

Sandia National Laboratories

Ramp loading: free surface

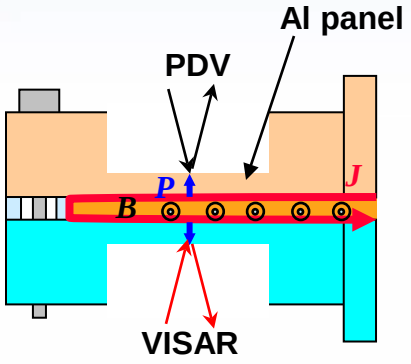

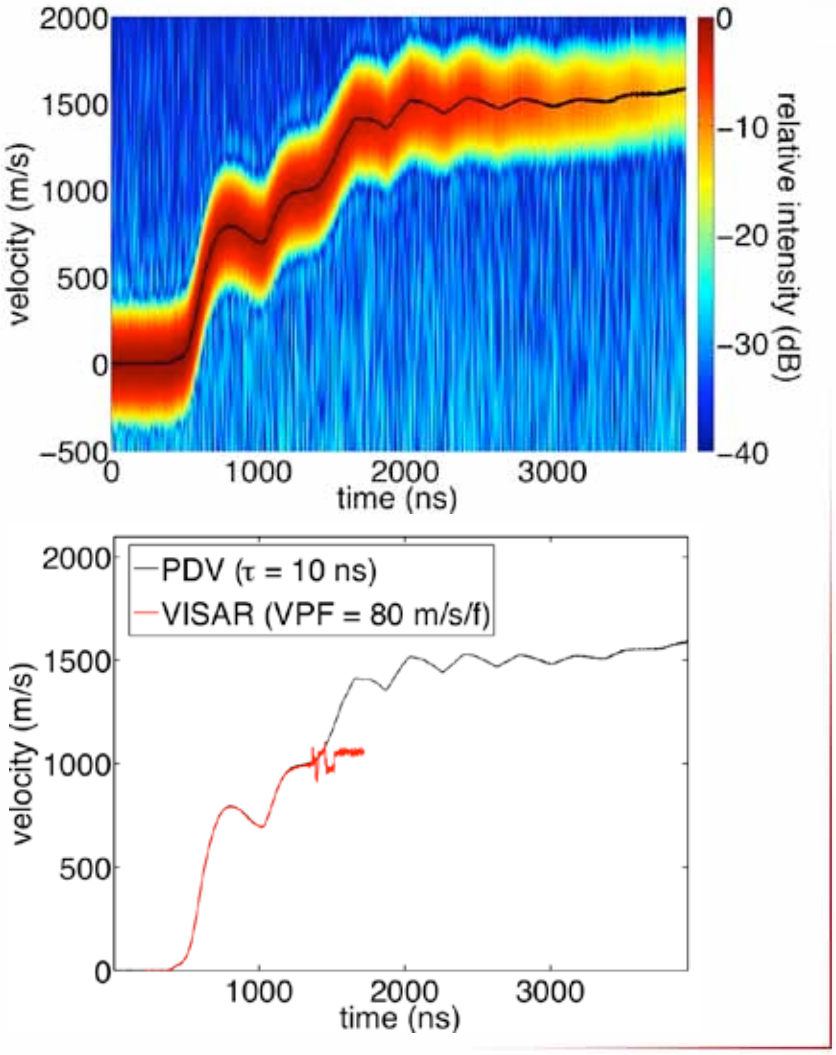

Validation between PDV and VISAR

- PDV able to track free surface over considerable distance after VISAR loses signal
- VISAR's VPF = 80 m/s/f corresponds to and ideal risetime of 2.7 ns but detector risetime needs to be accounted for
- PDV's $\tau = 10$ ns (Hamming window) corresponds to a risetime of 3.7 ns

Sandia National Laboratories

Ramp loading: sapphire window

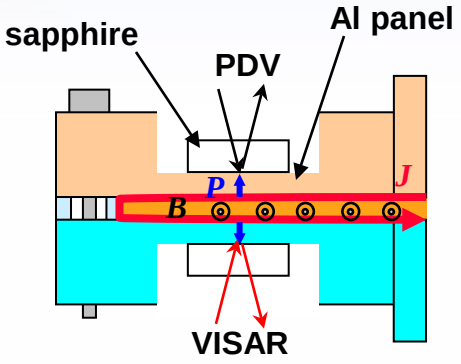

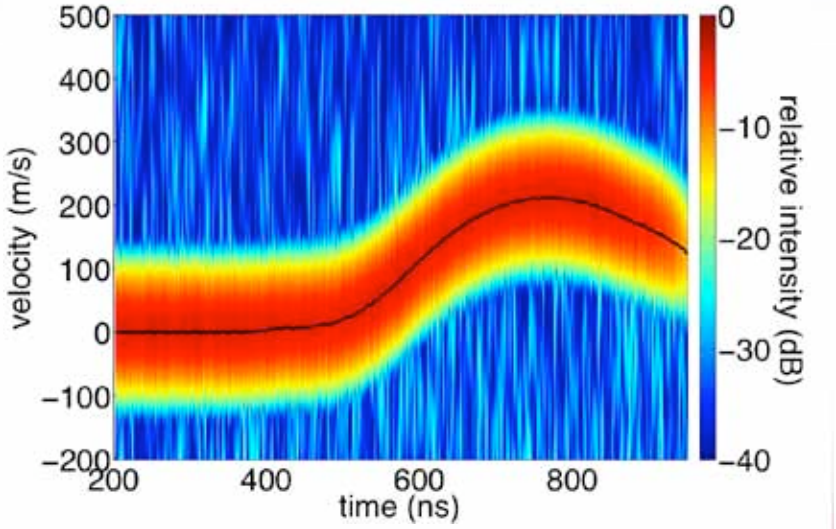

Batch variation of AR coating on sapphire window

- Velocity oscillations require larger analysis time duration

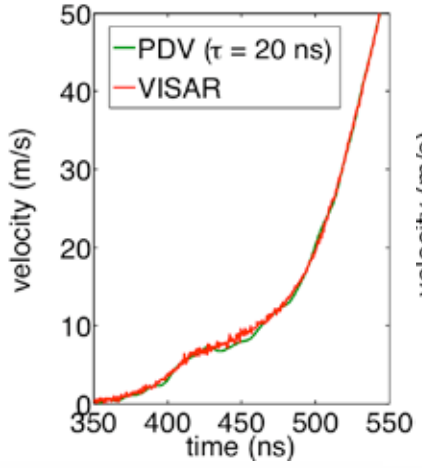

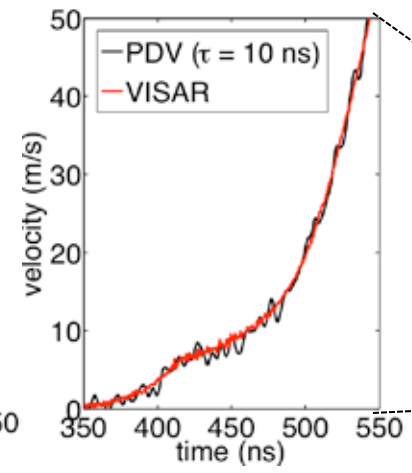

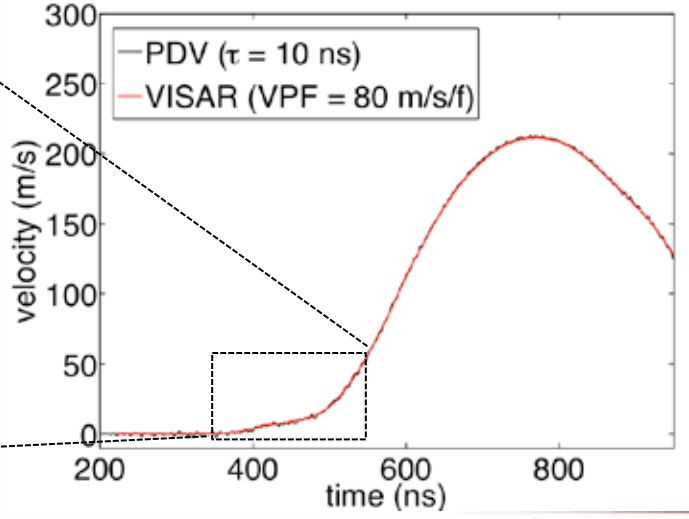

Sandia National Laboratories

Summary #1

Limiting performance of PDV is determined by power spectrum location resolutions

- The uncertainty principle overestimates error
- Peak fit confidences underestimates error

Monte Carlo simulations indicate that PDV is:

- Inaccurate and imprecise at low frequencies
- Accurate and (potentially) precise otherwise
- Limiting performance can be tied to sampling rate, noise fraction, and analysis time duration

Sandia National Laboratories

Summary #2

Frequency-conversion is a good thing!

- Underlying beat frequency resolves low velocity features while maintaining good time resolution
- Separates negative and positive frequency spectral functions

PDV validated with VISAR

- Competitive time and velocity precision with VISAR, despite wavelength difference
- PDV requires fewer signals than VISAR

PDV through window

- Windows should either be wedged or have sufficient anti-reflective coating to mitigate secondary reflections

Sandia National Laboratories

Discussion

What diagnostic risetime is required?

- What physical phenomena are we trying to measure?
  - Elastic precursor, phase transition, etc.
- We can analytically predict 10-90% rise for PDV
  - Faster events are still detectable

Is there a need for multiple point PDV?

- How many spots?
- Total velocity range?

Sandia National Laboratories

Extra slides

Peak finding methods

Frequency location of the strongest peak within power spectrum

- Maximum
  - Accuracy dependent on the number of frequency points used in STF
  - Increase accuracy with large “zero-padding” of signal; computationally intensive
  - Issues during transitions produce velocity “hopping”
- Gaussian
  - Fit spectral profile with a Gaussian curve: $S(f) = A\exp\left(-\frac{(f-\overline{f})^2}{2\sigma^2}\right) + S_0$
- Parabola
  - Fit spectral profile with a parabola: $S(f) = A(f-\overline{f})^2$
- Centroid
  - Integrate spectral profile to obtain center of mass: $\overline{f} = \frac{\int_{f_1}^{f_2} f \cdot S(f)\,df}{\int_{f_1}^{f_2} S(f)\,df}$

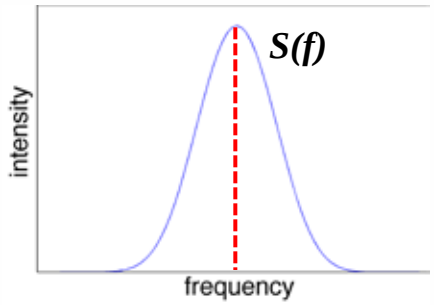

Sandia National Laboratories

Uncertainty principle

Time-velocity uncertainty product always exceeds a constant:

$$\sigma_v \sigma_t \geq \frac{\lambda_0}{8\pi}$$

- 1 m/s velocity width requires > 62 ns(!)
- This is really a separability criterion, not location uncertainty
- No reference to noise or sampling rate

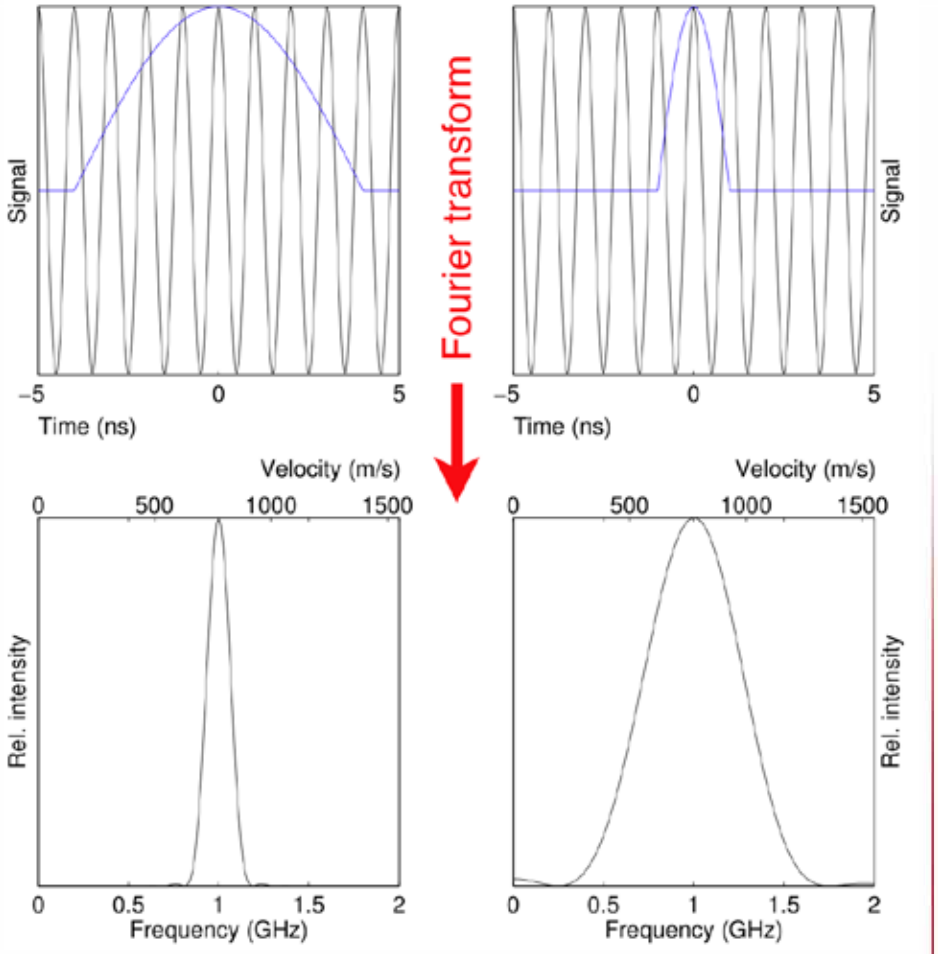

Sandia National Laboratories

Peak fitting

Fit the PDV power spectrum with curve

- Estimate resolution from how quickly residual increases away from the minimum

Peak location can be determined more narrowly than uncertainty principle bound

- However, the results may be systematically wrong!
- Error depends on many factors

Signal (1.880 GHz)
discretely sample 25 times in 1 ns

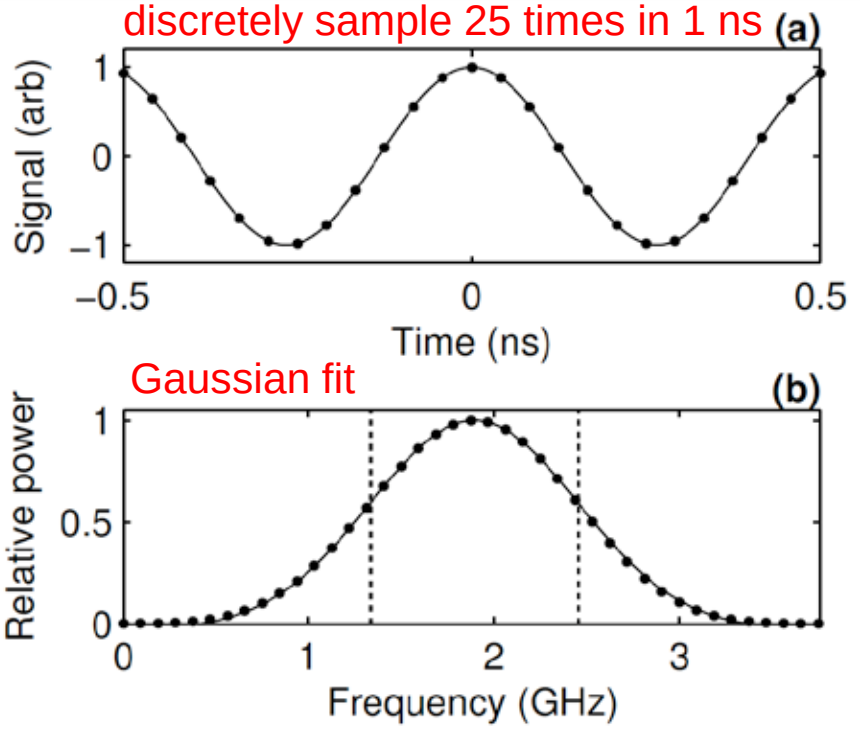

Peak location: 1.894 GHz
Peak width: 1 GHz
Fit uncertainty: 0.003 GHz (2 m/s)
Error: 0.014 GHz

D.H. Dolan, Rev. Sci. Instrum. **8**1, 053905 (2010)

Sandia National Laboratories

Power spectrum subtlety #1

$$S^2(f) \propto S_+^2(f) + S_-^2(f) + 2\cos(2\delta) S_+(f) S_-(f)$$ (real signal)

Negative frequency components affect the positive frequency domain

- Significant overlap for narrow digital windows
- Power spectrum biased away from the S_+ peak
- Reduces accuracy

Cross-term creates time variation

- Reduces precision

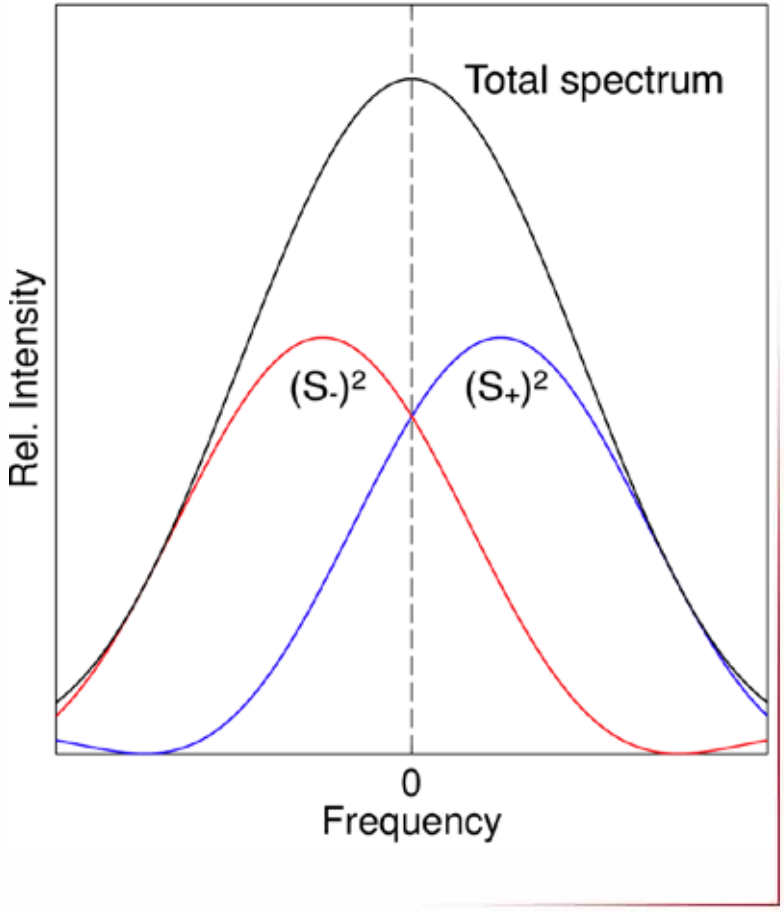

Sandia National Laboratories

Power spectrum subtlety #2

$$S^2(f) \propto S_+^2(f) + S_-^2(f) + 2\cos(2\delta) S_+(f) S_-(f)$$ (real signal)

Side lobes have an effect

- Net spectrum can be biased toward or away from DC (accuracy)
- Cross-term reduces precision (dominant effect)

Resonances due to overlap of primary peak with a side lobe

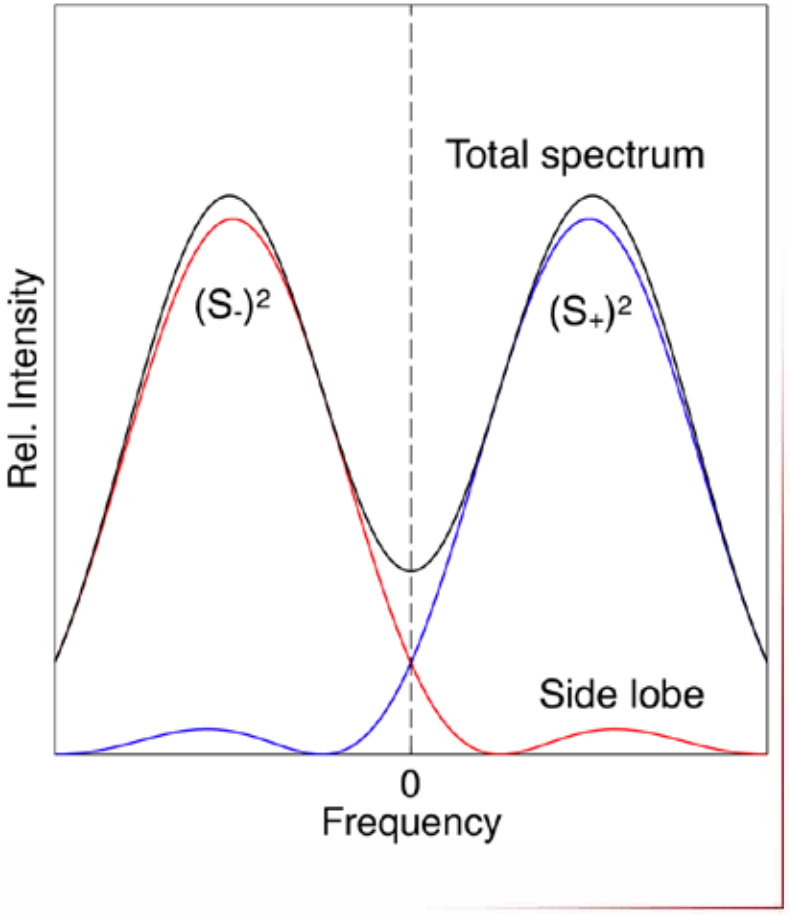

Sandia National Laboratories

Limiting performance

There is a limit to how well frequency can be determined from a discretely sample signal

$$\delta f = \sqrt{\frac{6}{N}}\frac{\sigma}{\pi\tau} = \left(\sqrt{\frac{6}{f_S}}\frac{\sigma}{\pi}\right)\tau^{-3/2}$$

Fixed parameters:

- Sampling rate
- Noise fraction (digital filtering does NOT help)

Adjustable parameters:

- Analysis time duration
- Improvement faster than uncertainty principle predicts

FFT windows alters the effective duration

- This expression assumes all data is treated equally (boxcar window)

Some typical values

1550 nm, 10% noise, boxcar window

		25 GS/s	50 GS/s
Duration (ns)	Risetime (ns)	Resolution (m/s)	Resolution (m/s)
0.1	0.06	380	270
0.5	0.29	34	24
1.0	0.58	12	8.5
5.0	2.9	1.1	0.76
10	5.8	0.38	0.27
50	29	0.034	0.024

This resolution is only attainable above low-frequency shoulder!

Sandia National Laboratories

Imperial College London

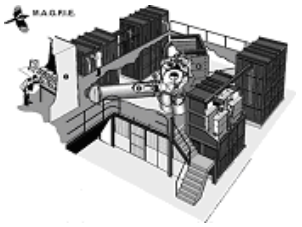

Initial Ramp Wave Experiments at Imperial College

S.N. Bland

S.V. Lebedev, J.P. Chittenden, G. Burdiak, G.N. Hall, L. Pickworth, J. Skidmore, F. Suzuki-Vidal, G. Swadling, D. Chapman, and D. Eakins
Imperial College London

A. Critchley, A. George, E. Price, S. Vickers
AWE plc Aldermaston, Reading

D.J. Ampleford, T. Ao
Sandia National Laboratories

R. Spielman and the team
Ktech Corporation

Sponsored by AWE, EPSRC, NNSA, and Sandia National Labs

Imperial College London

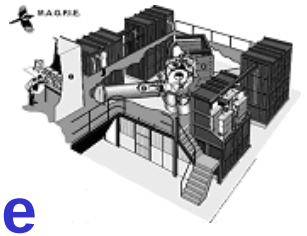

Institute of Shock Physics at Imperial College

AWE funded research and teaching institute dedicated to studying the fundamental science behind shock waves, high velocity collisions and extremes of pressure and heat

Vision

To form a UK community linked through the ISP at Imperial College delivering world-leading research and education in shock physics

Key facts

- Institute of Shock Physics (ISP) started in mid 2008
- Hub: Imperial College London
- Spokes at UCL, Cranfield University (Shrivenham), Oxford and Edinbrugh
- National and international collaborations with National Labs, Academia and Industry

Imperial College
London

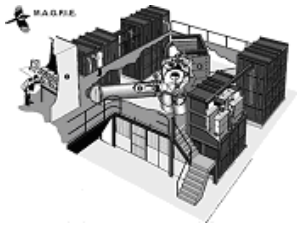

Facilities, diagnostics and capabilities

Imperial College London

Imperial College MAGPIE facility

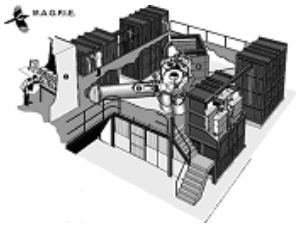

At Imperial the 1.5MA (soon 2MA) 240 ns MAGPIE generator drives HEDP experiments on a daily basis

Mega
Ampere
Generator for
Plasma
Implosion
Experiments

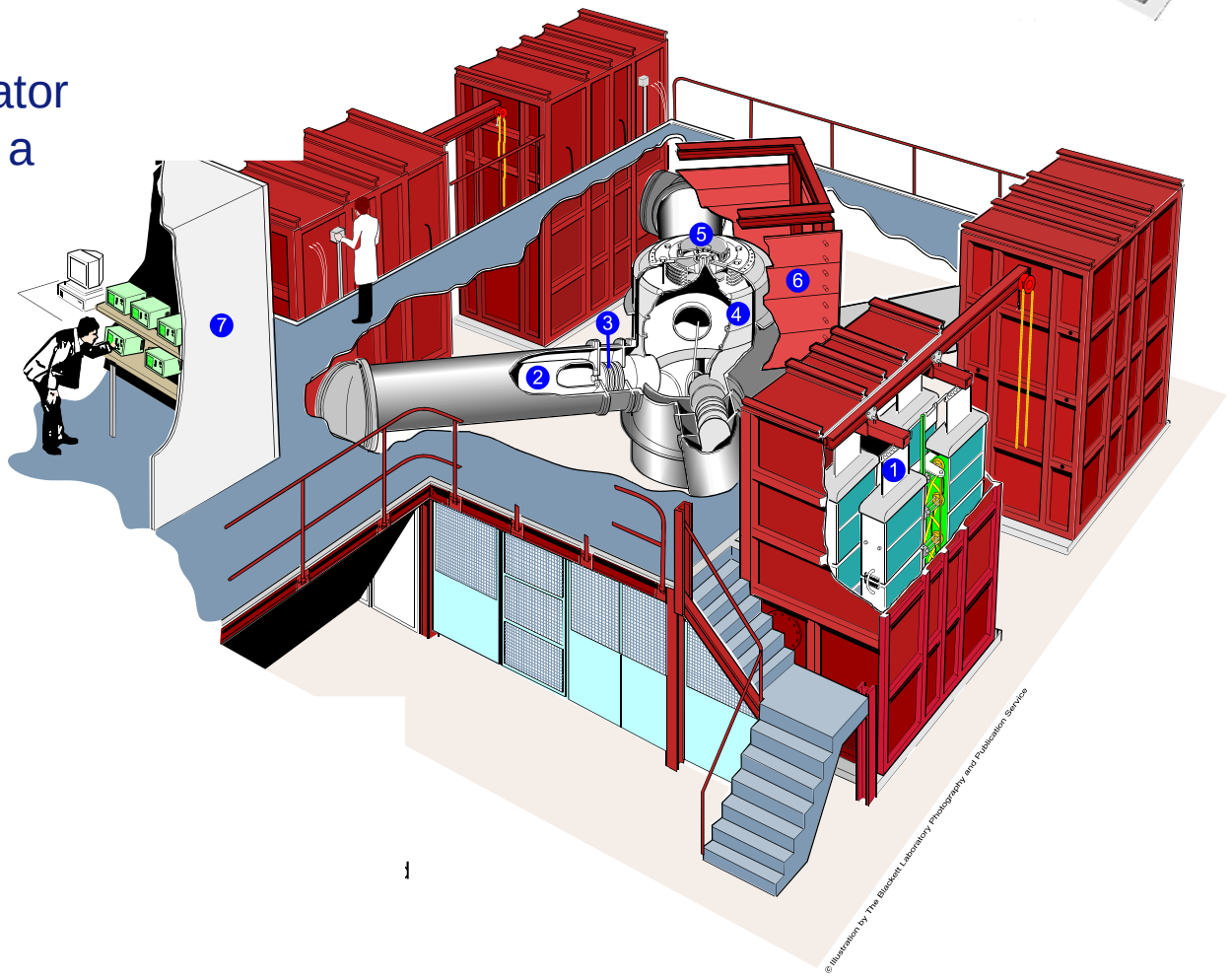

- High impedance drive – current relatively unaffected by load
- Excellent diagnostic access

Imperial College London

New facilities at Imperial College

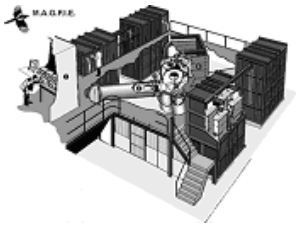

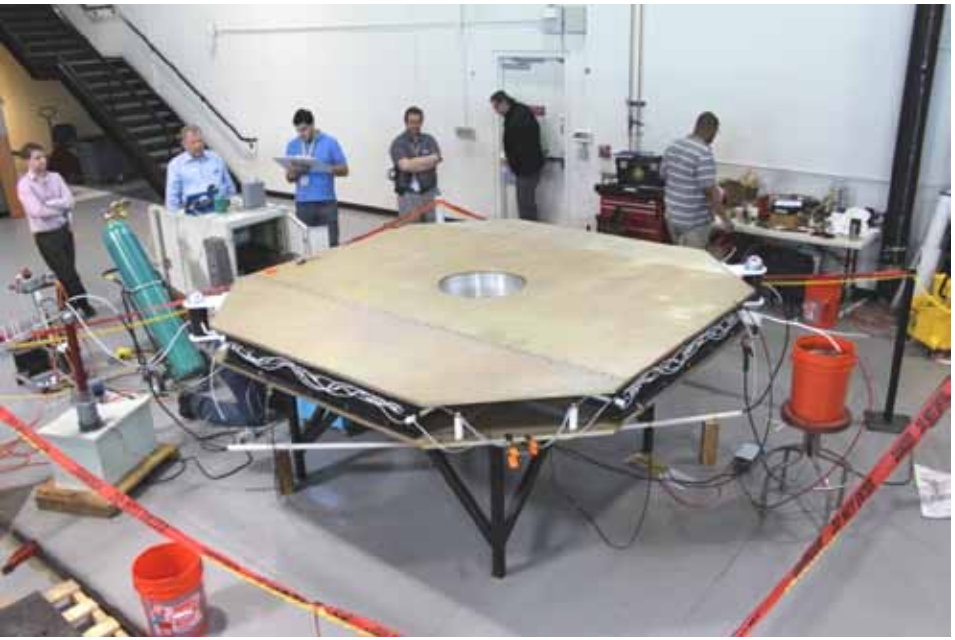

2MA LTD generator dedicated to isentropic compression experiments

Mega

Ampere

Compression &

Hydrodynamics

(more later)

100mm gas gun for large scale experiments

8kg flyer to 800ms^{-1}

Imperial College London

Diagnostics for shock physics

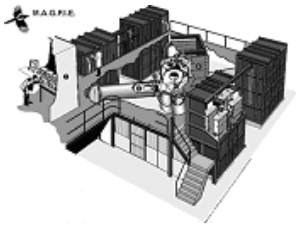

Het-V system

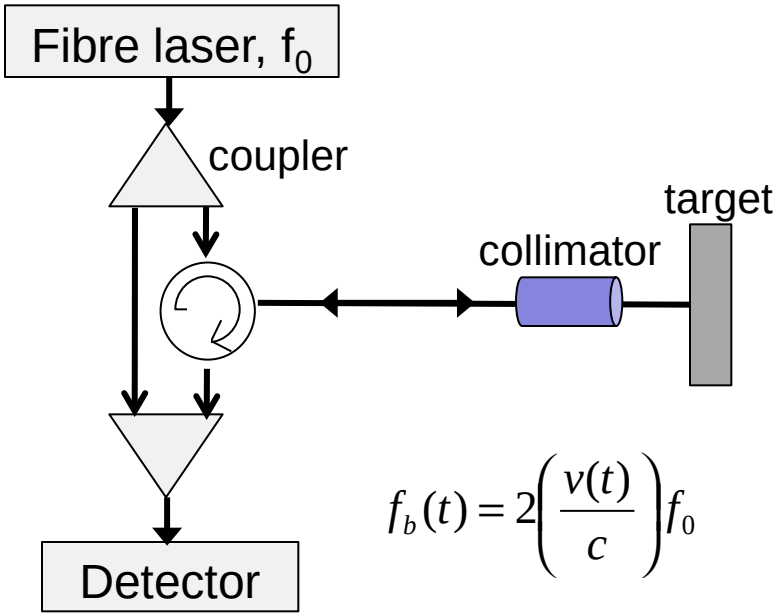

$$f_b(t) = 2\left(\frac{v(t)}{c}\right) f_0$$

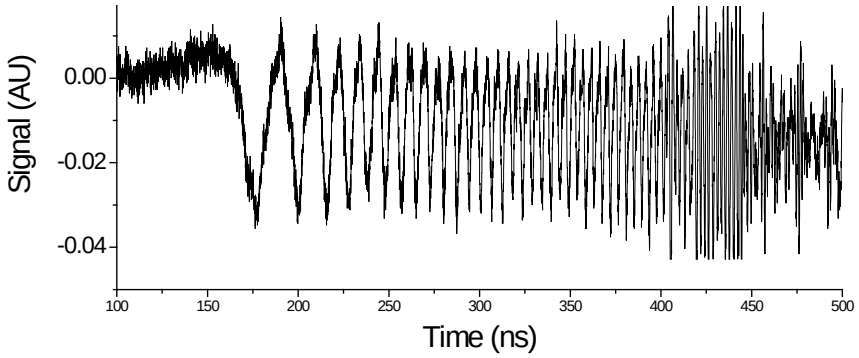

Gen 1 Het-V

Frequency shifted Het-V now in development

Interferometer

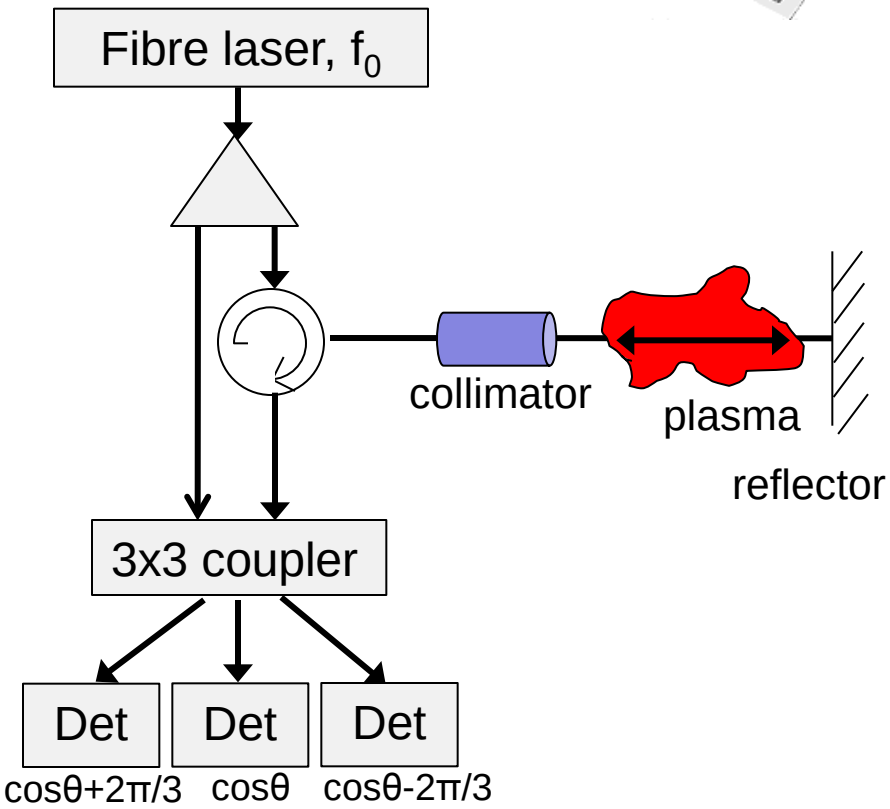

Mach-Zehnder or Michelson configuration

Monitors plasma at electrodes

Imperial College London

Diagnostics for shock physics

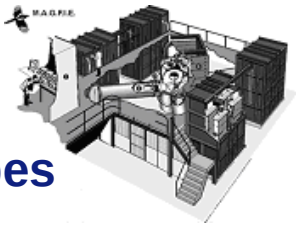

Line VISAR

2 independent VISAR channels sampling 100um wide and to 25mm long
- can examine macroscopic and mesoscopic properties
- with speeds ~ 200ms^{-1} per fringe to 25kms^{-1}

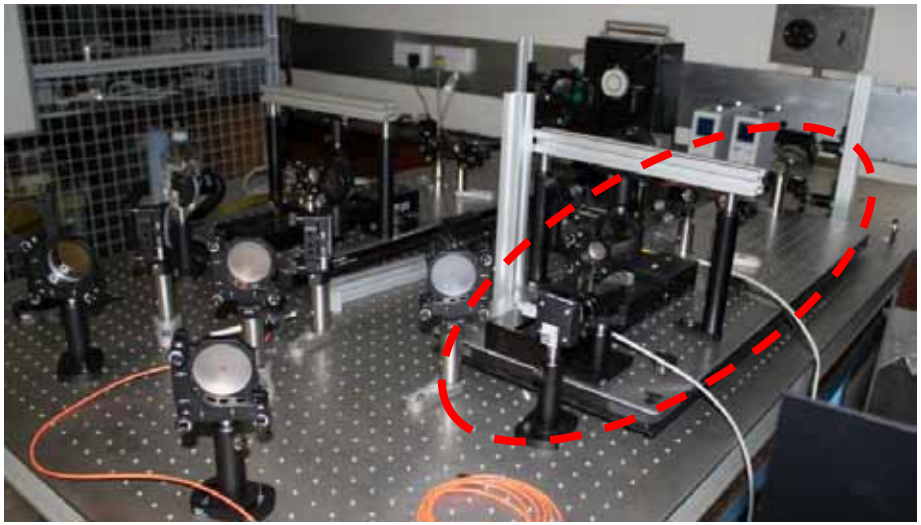

Line VISAR system showing white lights and streak cameras

Now in test on foil and radiative shock experiments on MAGPIE

Mini Magnetic Probes

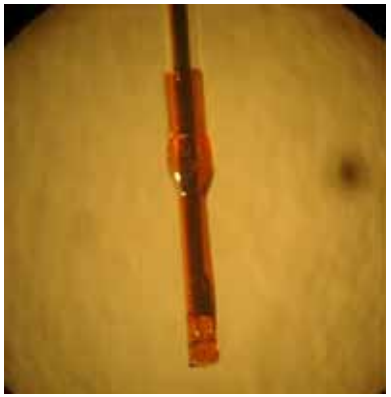

Magnetic probes only 0.75mm diameter

Fielded at different depths in targets – directly monitor current over surface of target and diffusion through target material

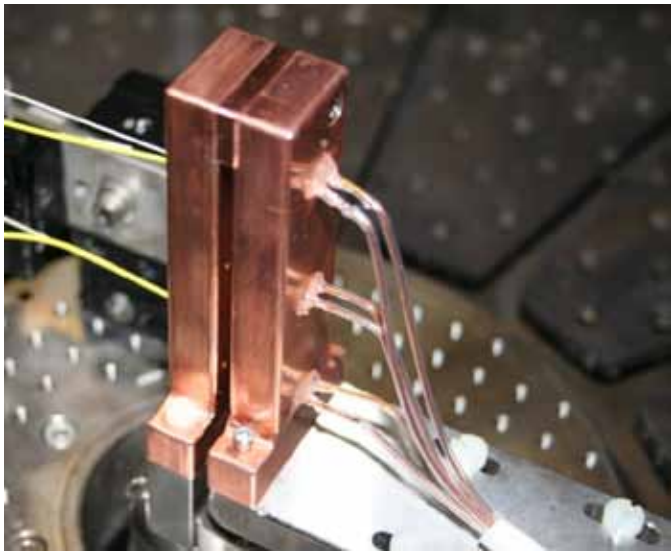

Imperial College London

Code Development

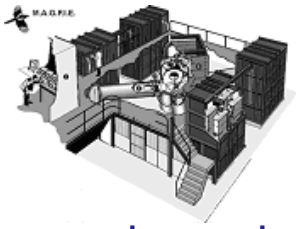

- Explore using Comsol / Autodyne to look magnetic field around electrodes and couple to simple 1 and 2D compression effects
- Condensed matter EOS and real material effects being added to GORGON code
  - in house developed 3D resistive MHD code, used for z-pinch and HEDP research
  - massively parallel code, able to handle large scale 3D structures
  - everything from electron emission at electrodes, through to ablated plasma at surface of strip lines to compressed material in electrodes

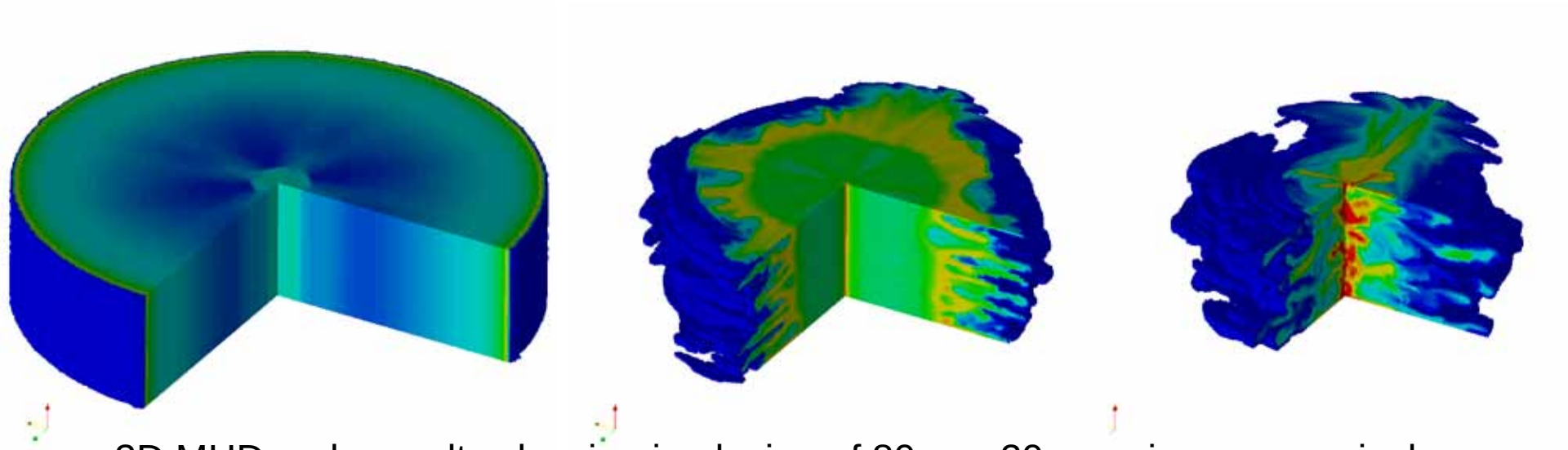

3D MHD code results showing implosion of 80mmx20mm wire array z-pinch

Imperial College
London

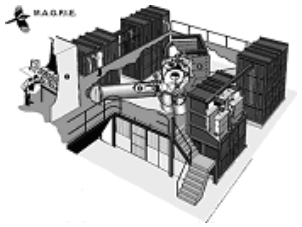

Initial Ramp experiments on MAGPIE

Imperial College London

Magnetically driven EOS experiments

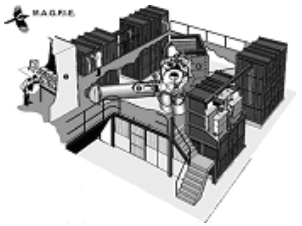

Initial experiments on MAGPIE use a strip lines setup:

- Soft material (helps prevent shock up) - Copper
- Width of electrodes 20 – 10mm - pressures from ~30-120kBar with 1.5MA drive
- Gap 2 – 1mm – hopefully magnetic insulation prevents breakdown
- Target thicknesses 1-7mm - shocks expected after ~5mm thickness
- Length of electrodes 40 – 80mm

15mm width for 60 KBar peak pressure

sample area up to 60x12mm on each side

cathode in throat of MITL

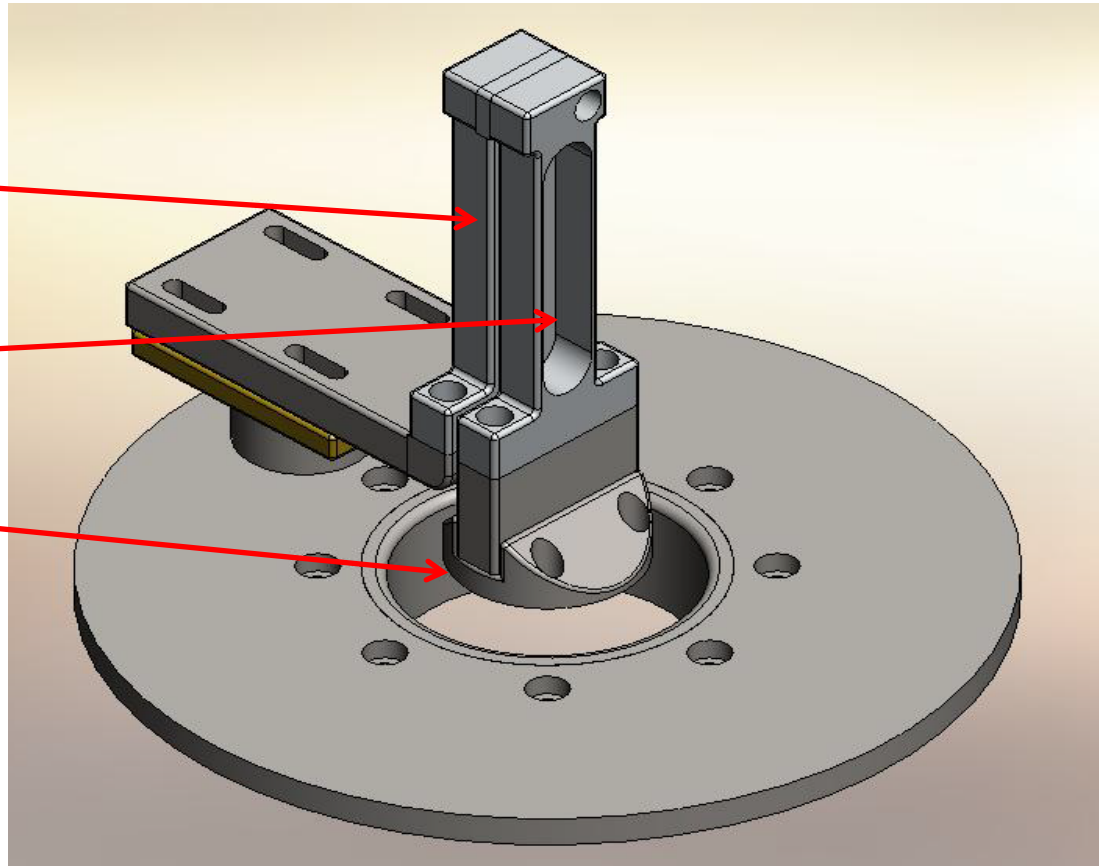

Imperial College London

Magnetically driven EOS experiments

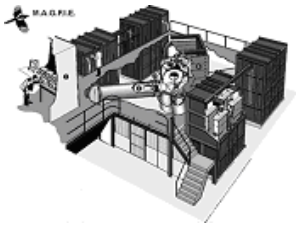

Typically for shock experiments:

flatness ~5um, roughness <um via. diamond machining

Overkill for initial experiments (and very expensive)

2 part ‘glued electrode’ electrode - target area and support

4 axis CNC mill allows fast production of blanks

Precision ground then hand polished – mirror finish ~5um

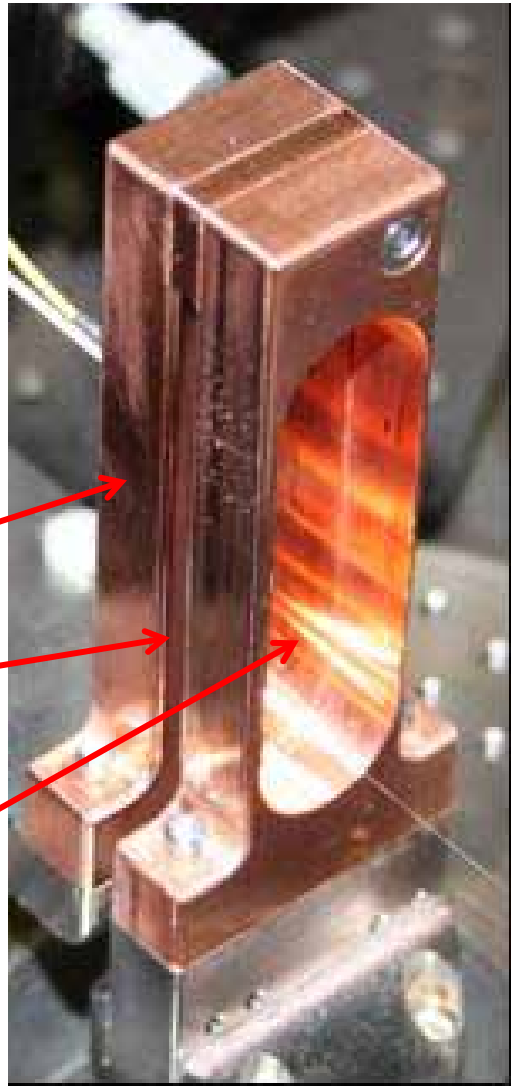

Close up of 20mm wide copper strip line in MAGPIE

Imperial College London

Magnetically driven EOS experiments

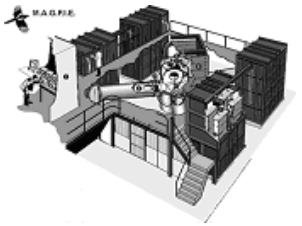

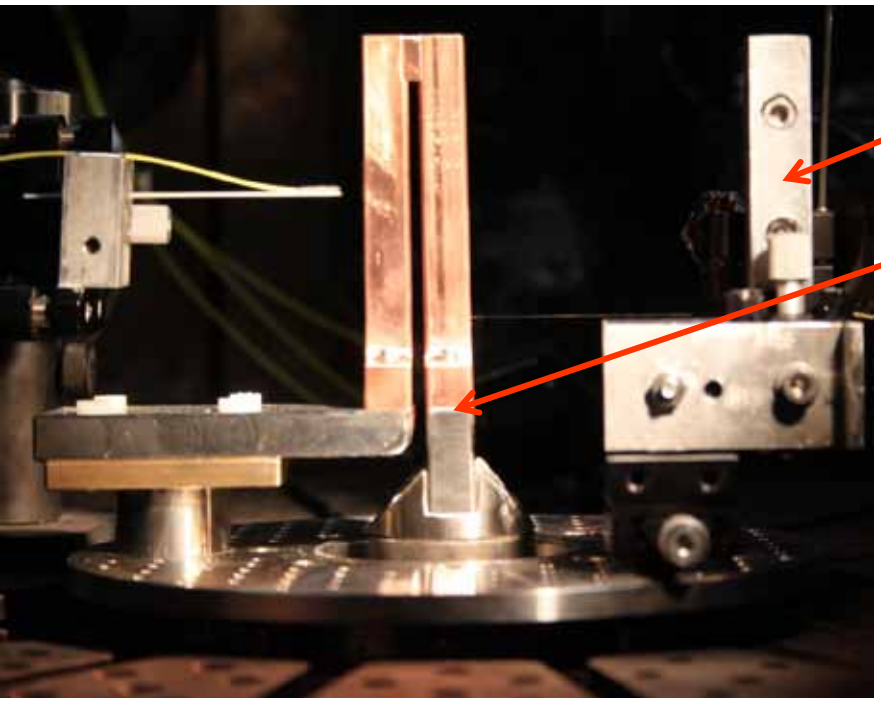

Holder for Het-V probes

Stripline mounted on break away system to prevent damage to MAGPIE

Side view of strip line

Top down view

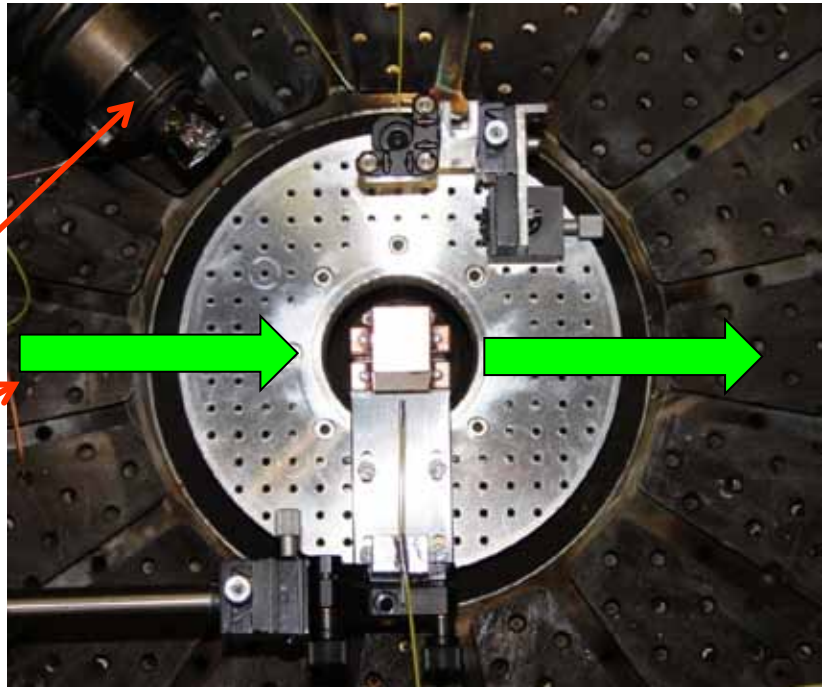

Resistive voltage probe

Path of probing laser

½ inch armoured plate top and bottom to ‘catch’ stripline (not shown)

Imperial College London

Magnetically driven EOS experiments

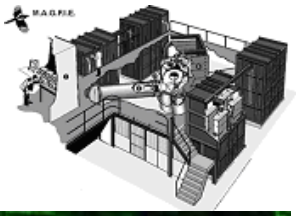

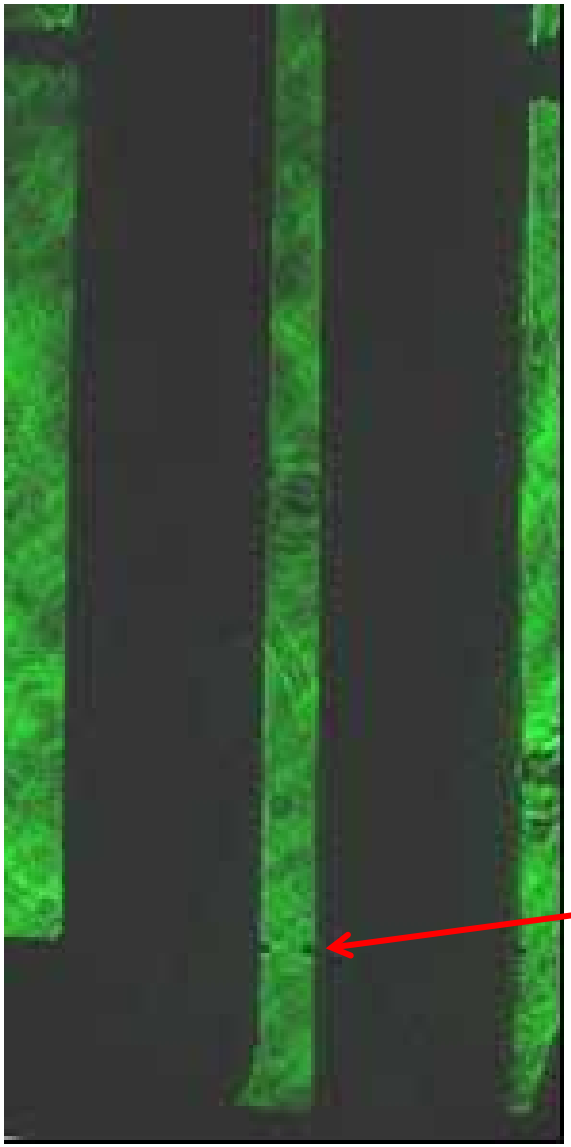

Laser probing of gap in 20mm wide stripline shows little build up of plasma J

Voltage monitored across stripline also indicates no sudden breakdowns occurring

⇒ Consistent with all current flowing through strip line (should give 20-30kBar)

Only plasma present comes from join to holder – expands ~200um into gap

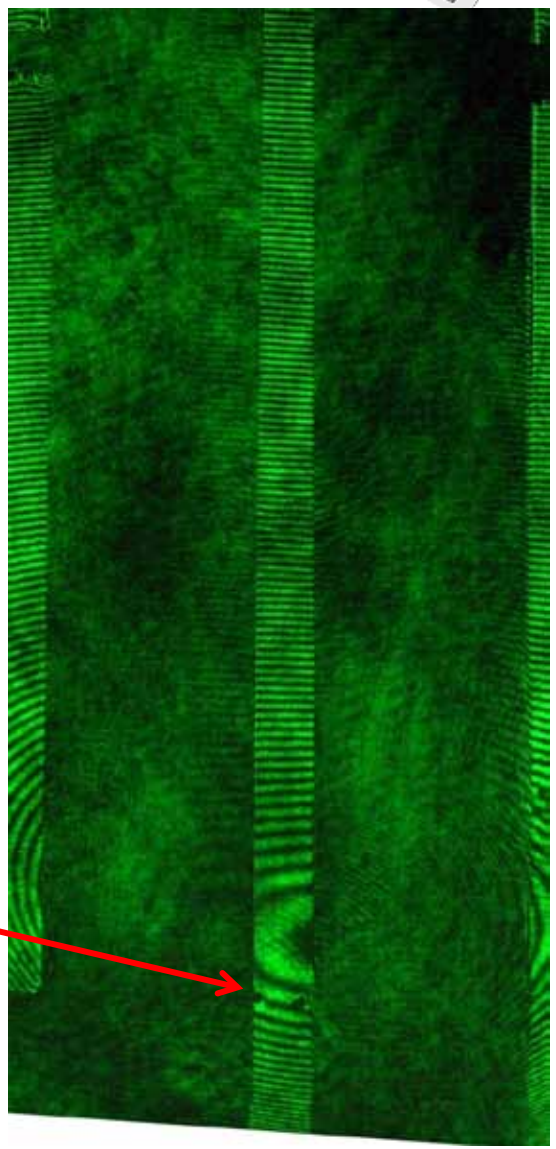

Laser shadow image @200ns

Laser interferogram @200ns

Imperial College London

Magnetically driven EOS experiments

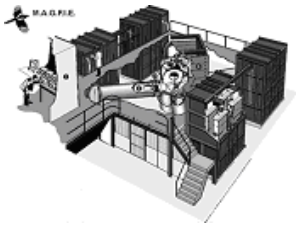

Post shot target recovery...

80x20mm electrode, with support (left) and target plate (right)

40x20mm target plate

No target plate showed any sign of spall – consistent with isentropic compression

Target plates did prove to be good flyer plates though, vaporising diagnostics and ricocheting off armour plates L

Imperial College London

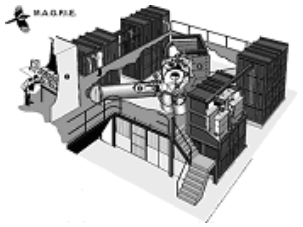

Magnetically driven EOS experiments

Unfortunately the Het-V probe indicated a laser fault...

... Hence we have no EOS information yet (but only 3 shots)

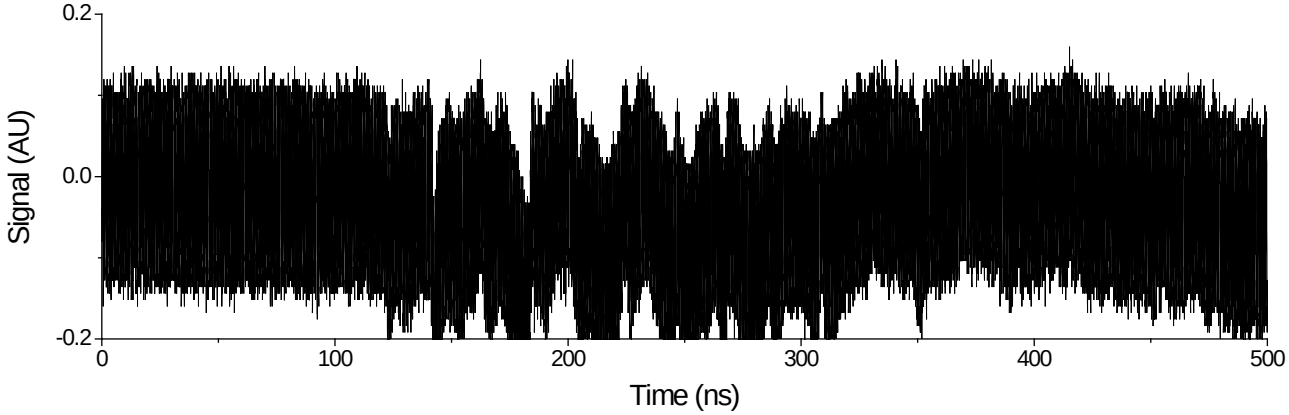

What we got

What we wish we had got

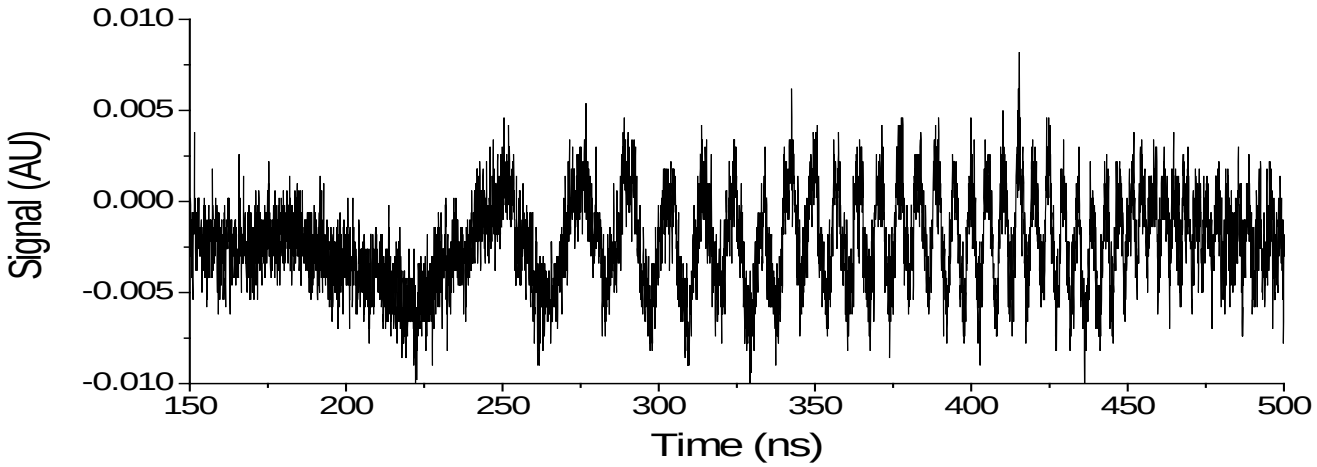

Het-V system has now been repaired ready for next shots...

... But MAGPIE is very busy... need something else...

Imperial College
London

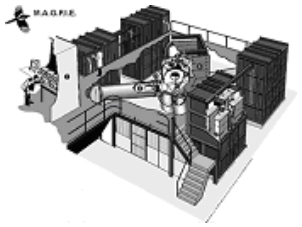

MACH

Imperial College London

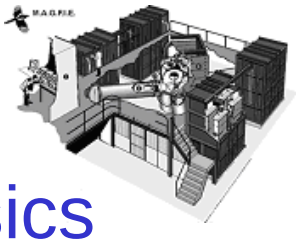

The MACH generator – A new pulsed power source for shock physics

A small, fast turn around machine for dedicated to shock physics experiments, especially when developing new ideas

Mega
Ampere
Compression **&**
Hydrodynamics

In house facility being developed by Rick Spielman of Ktech for the ISP

•Direct drive with lots of low inductance capacitors and switches

•Low maintenance – no oil, no water, no SF6 gas (light, almost portable – maybe put at end of beam lines)

• Pressure drive can be shaped

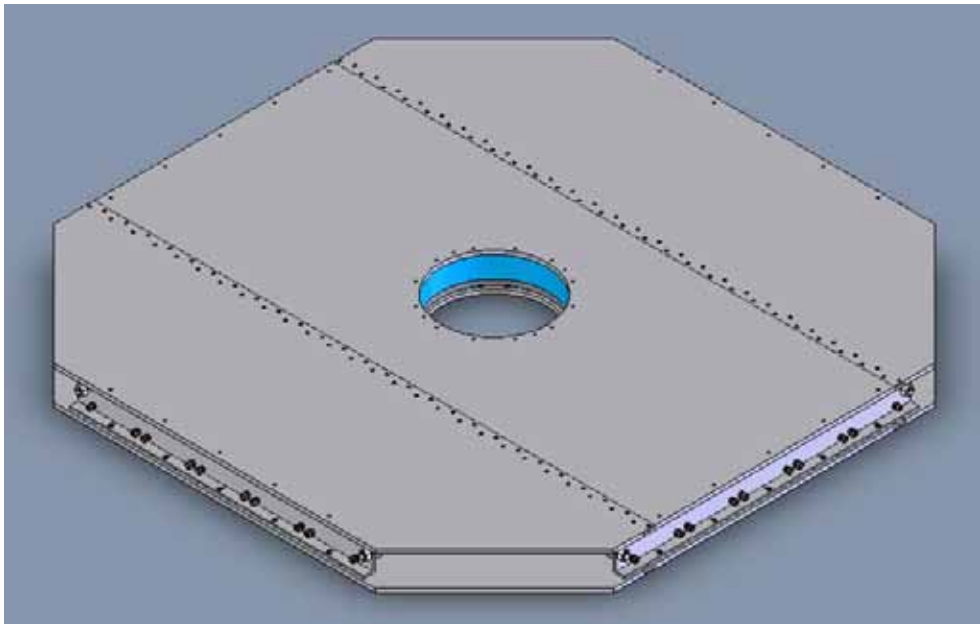

2.5m LTD cavity being built by Ktech

Imperial College London

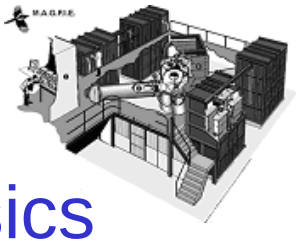

The MACH generator – A new pulsed power source for shock physics

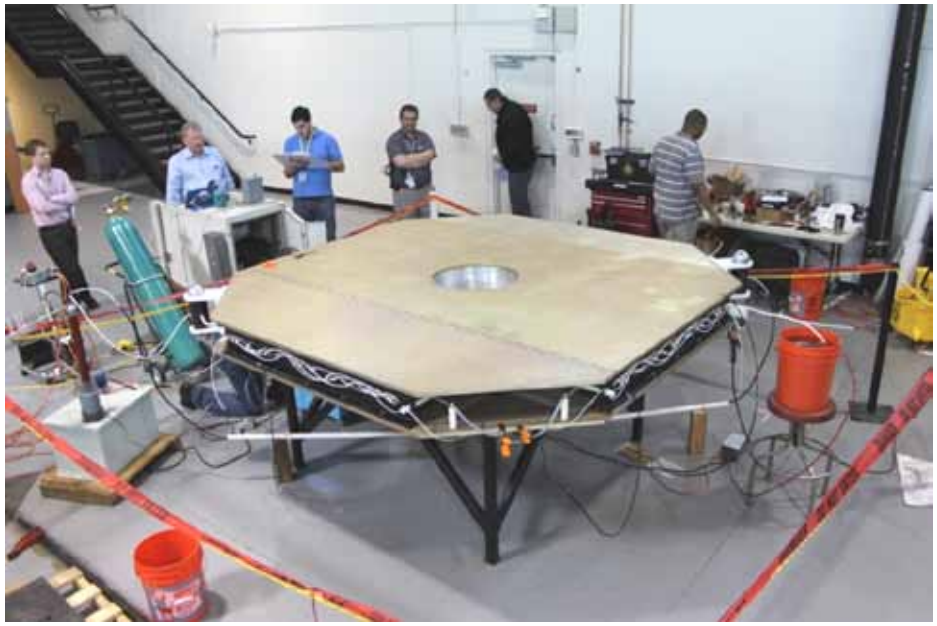

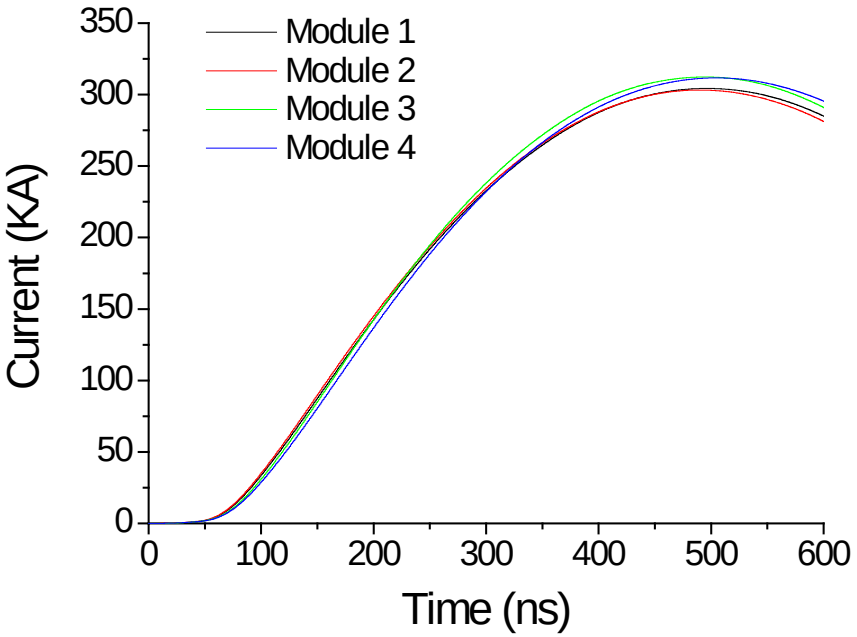

70kV charge demonstrates 1.2MA, 280ns (10-90%) pulse into resistive test load

With 100kV, and inductive load this will give 2MA ~260ns risetime expected

MACH has now been assembled and is being tested Imperial College

Generator can be stacked: Add in series for more voltage (bigger targets)

Add in parallel for more current (pressure)

Imperial College
London

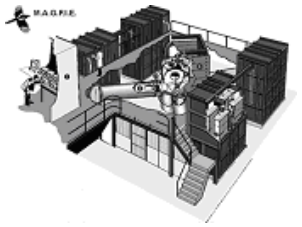

So what are we planning to do...

Imperial College London

Future magnetically driven EOS expts

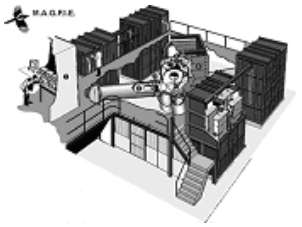

Methods to change initial conditions

- Heating systems allow exploration of EOS near phase boundaries
  - Iron found in earths core
  - EOS of tin near around melting point
- Cryogenics systems to use of gases in liquid/solid state
  - e.g. H_2, He mix in Jupiter

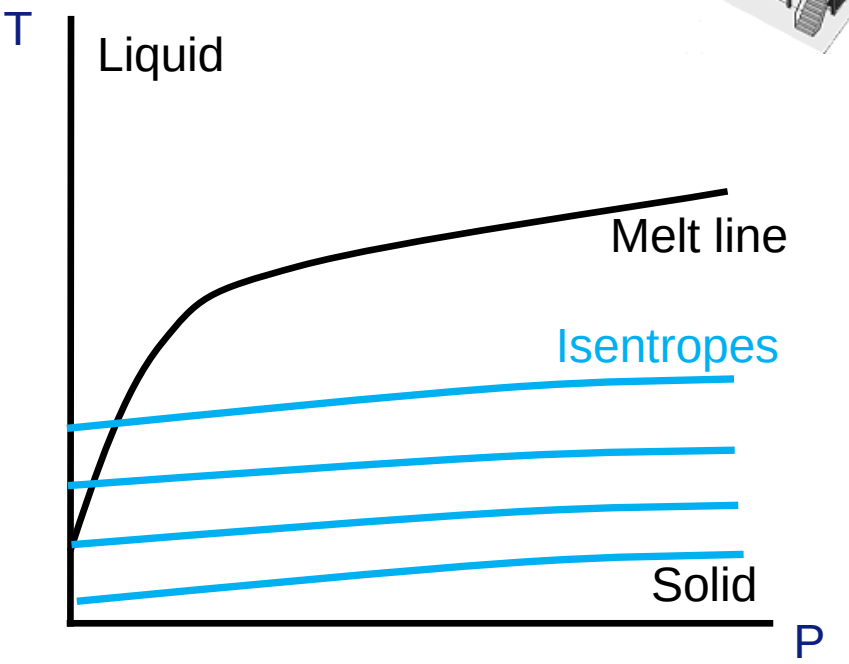

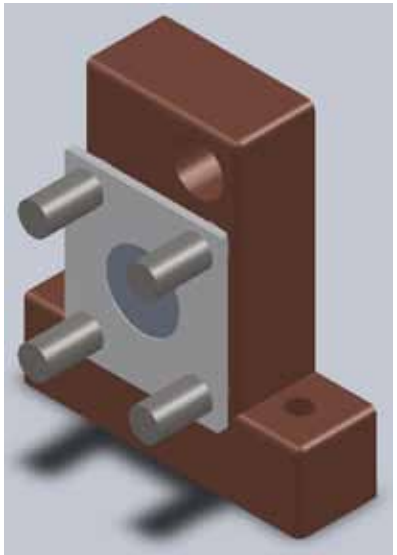

Preheating cell designed to allow 1000^0 sample temperatures

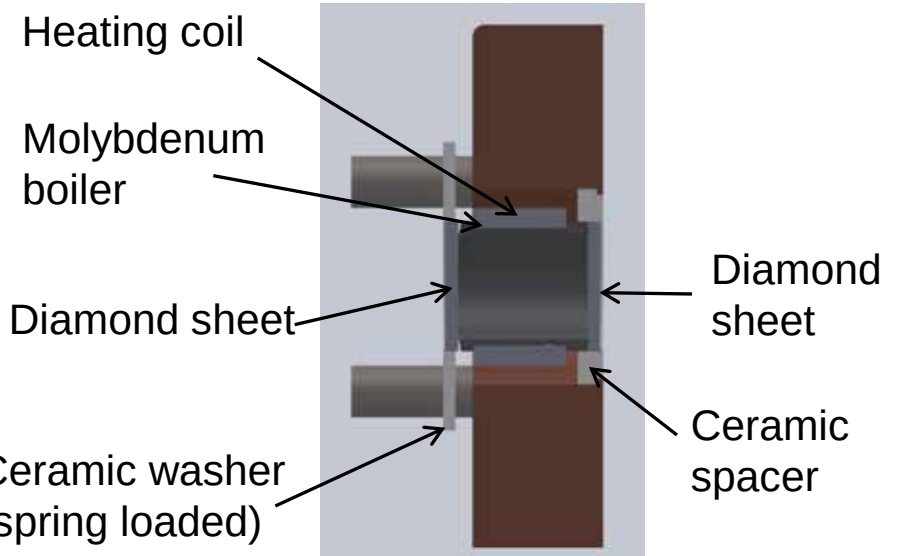

Imperial College London

Future magnetically driven EOS expts
Cerberus laser

Plasma Physics – Laser consortium project; with amplifiers from AWE

50J long pulse and short pulse beams (150fs)

- Thomson Scattering for plasma temperature
- X-ray radiography (1 and 6 KeV)
- Proton probing for field measurement in HEDP experiments

Use X-ray diffraction to probe **microscopic scale** (e.g. changes in lattice structure) in relation to **macroscopic properties** (e.g. strength)

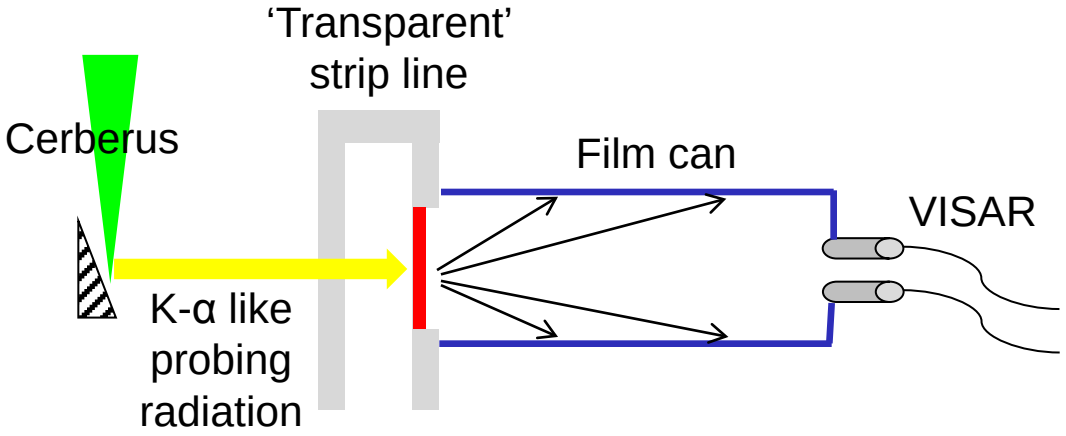

Aside... A future upgrade to ~300J would allow laser driven isentropic compression and shock experiments

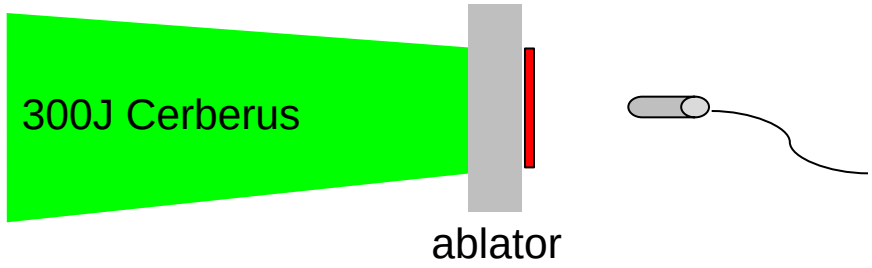

Imperial College London

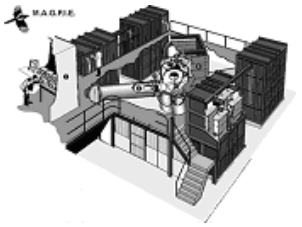

Future magnetically driven EOS expts: Getting to higher pressures – cross over

New 100mm gas gun, 8Kg slug to 800ms^{-1} velocities (multi MJ energy)

Highly versatile – exploring use of graded density targets to provide isentropic compression on gun

Rapid prototyping – 3D printing of plastics and metals – may allow graded density flyer/target to be made easily. Magnetic buffer also in examination.

Can test ideas with pulsed power, then transfer to gun for higher pressures

Imperial College
London

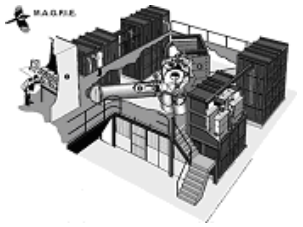

New methods of achieving higher pressures

Imperial College London

Using a plasma jet to apply high pressures

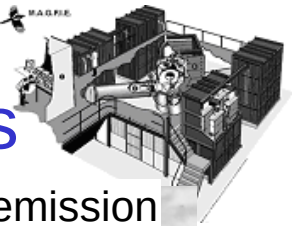

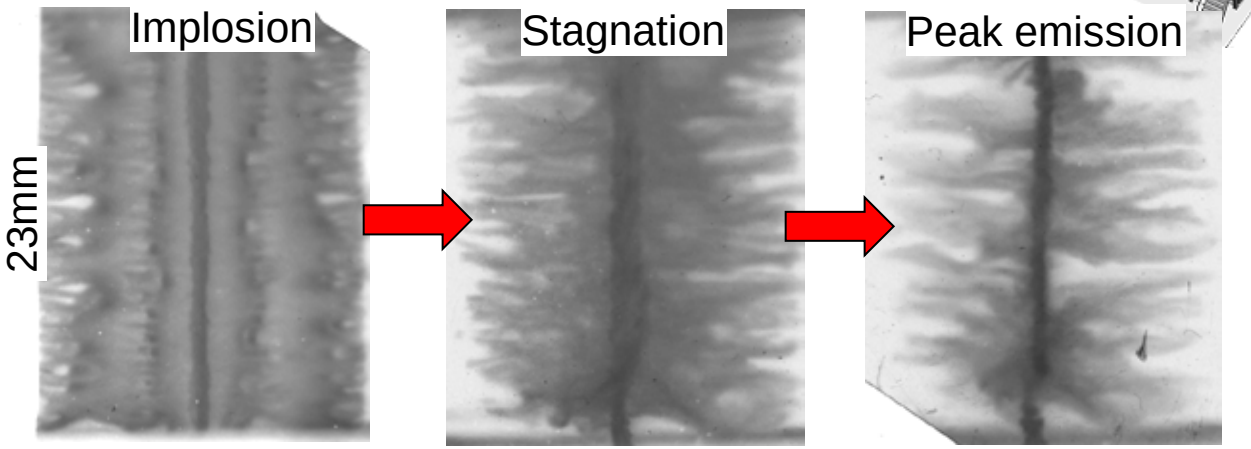

At MAGPIE we pioneered understanding of the implosion of wire array z-pinches

The majority of the evolution of a wire array is dominated by the gradual ablation of the wires into dense, warm plasma

$n_i \sim 10^{16}$ -10^{17} cm^{-3}

$T_i \sim 30eV$

velocity ~ $150kms^{-1}$

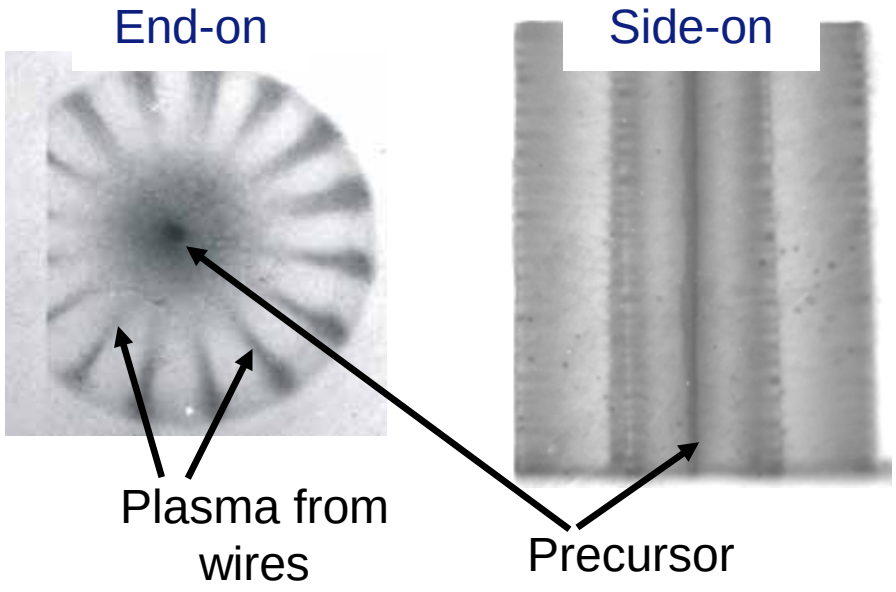

Imperial College London

Using a plasma jet to apply high pressures

Use a conical array to form a plasma jet

- It takes time for the ablating plasma to form a jet
- Before arrival of jet ablated plasma gathers on foil
- Once formed jet speed 200kms^{-1}

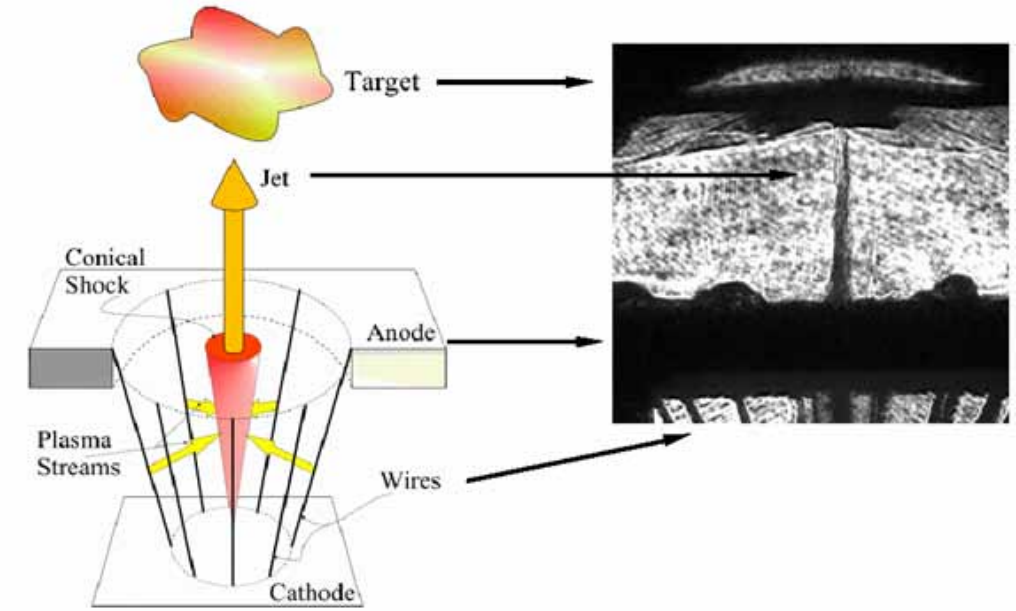

XUV images

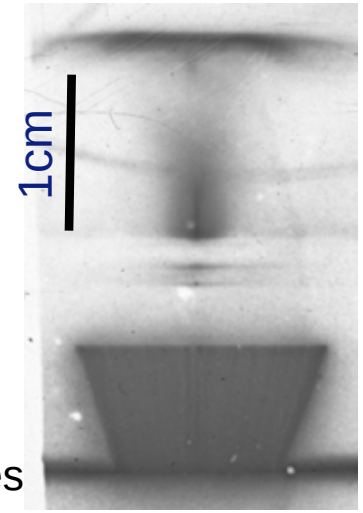

165ns

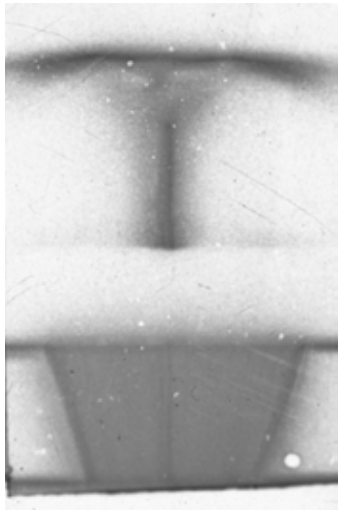

195ns

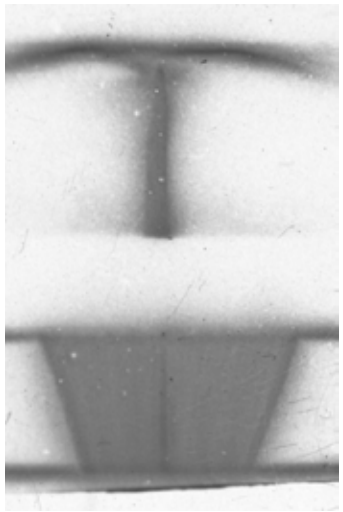

215ns

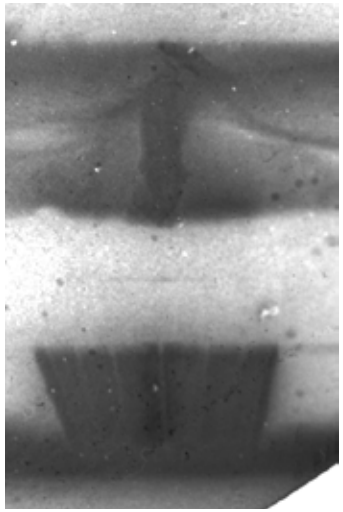

334ns

Imperial College London

Using a plasma jet to apply high pressures

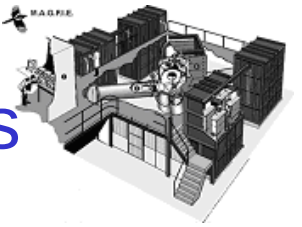

2D MHD GORGON simulations

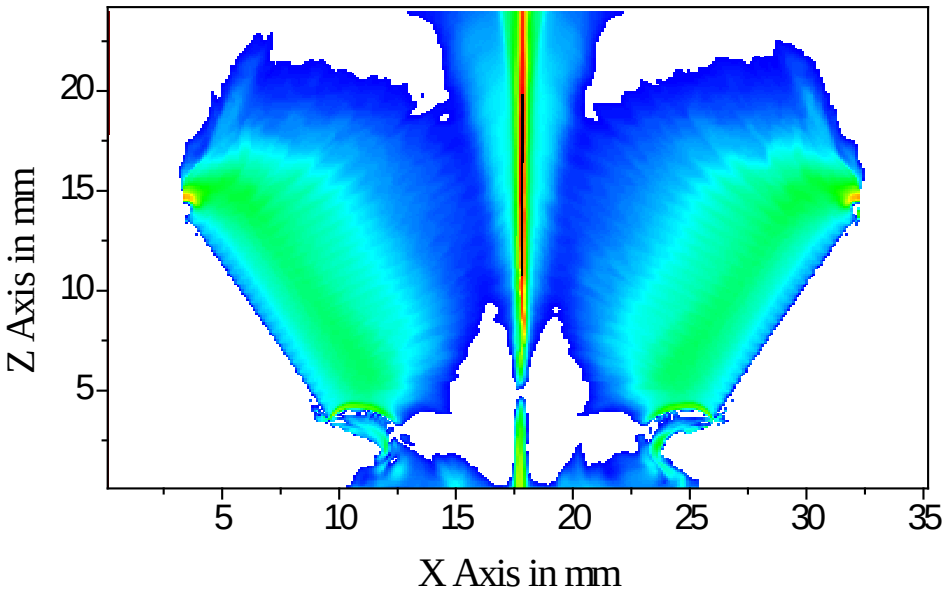

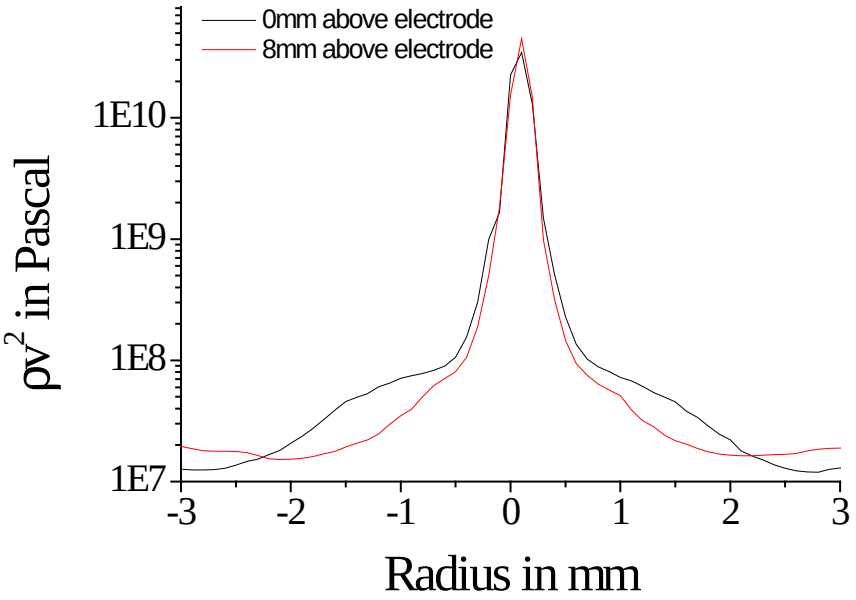

But Jet is very narrow

1mm outside jet, pressure reduced by 2 orders

'Ride-along' experiments on Z will field target and Het-V on lab-astro experiments. Probes will cover large area.

Expect 100s Kbar ablated plasma flow, MBar from jet.

Future experiments will use line and 2D imaging VISAR to examine profile of jet

Then we will examine ways to launch plasma projectile to drive shocks in targets

Imperial College London

Using cylindrically convergent loads

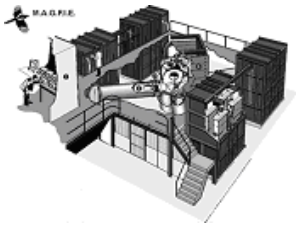

Maximum isentropic compression pressure on MAGPIE (2MA) ~ 2-400KBar

Isentrope and hugoniot only start to diverge at ~200KBar

Can upgrade MAGPIE (in 2 years) or use other methods

One possibility is to use convergent targets

1mm copper rod

2MA, 240ns rise

Simulations reach 1.5MBar

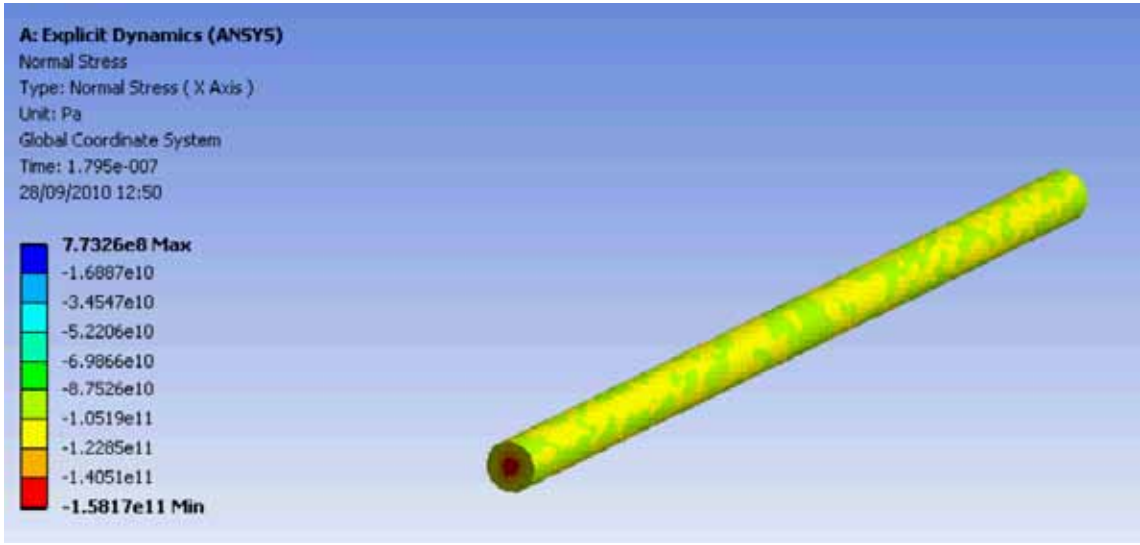

Looking at what is possible on Z

- Use cylindrical isentropic compression of hollow rod on H/He mix to examine conditions at centre of giant planets ?
- Possible new way to get high pressure fusion fuel mixes ?

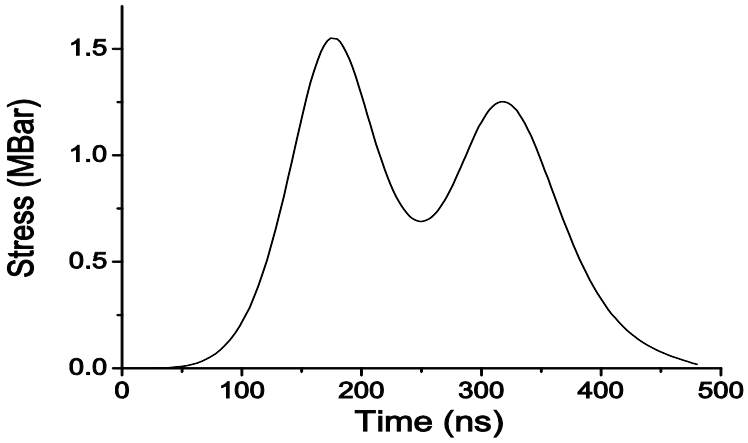

Imperial College
London

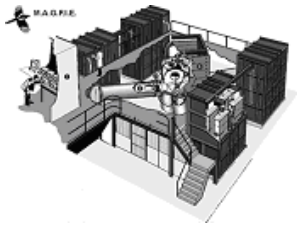

To be continued...

Imperial College London

Diagnostics for shock physics: testing velocity diagnostics

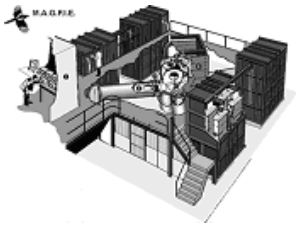

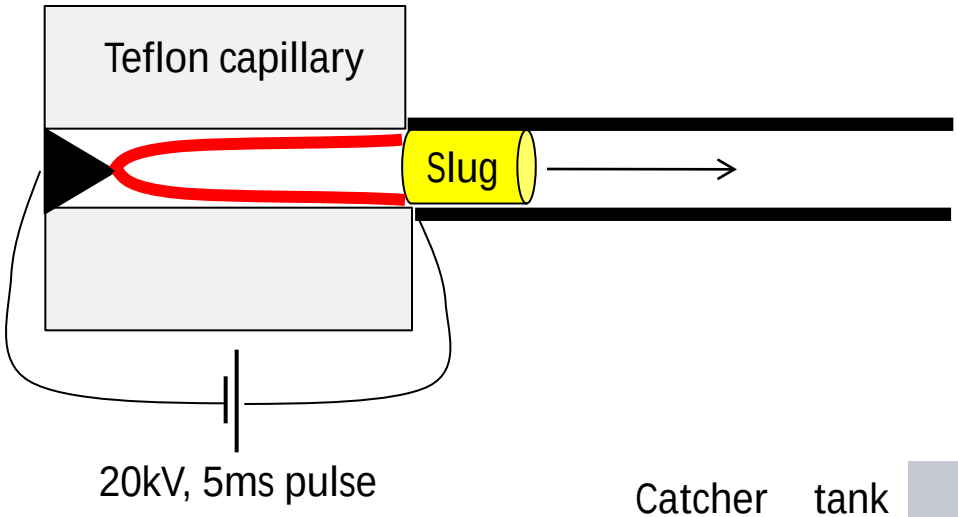

Need easy to use fast reload diagnostic development rig

Developing electro-thermal launcher

- High voltage pulse ablates teflon capillary
- Plasma pressure accelerates slug
- 10mm bore
- Speeds hopefully to 100s ms^{-1}

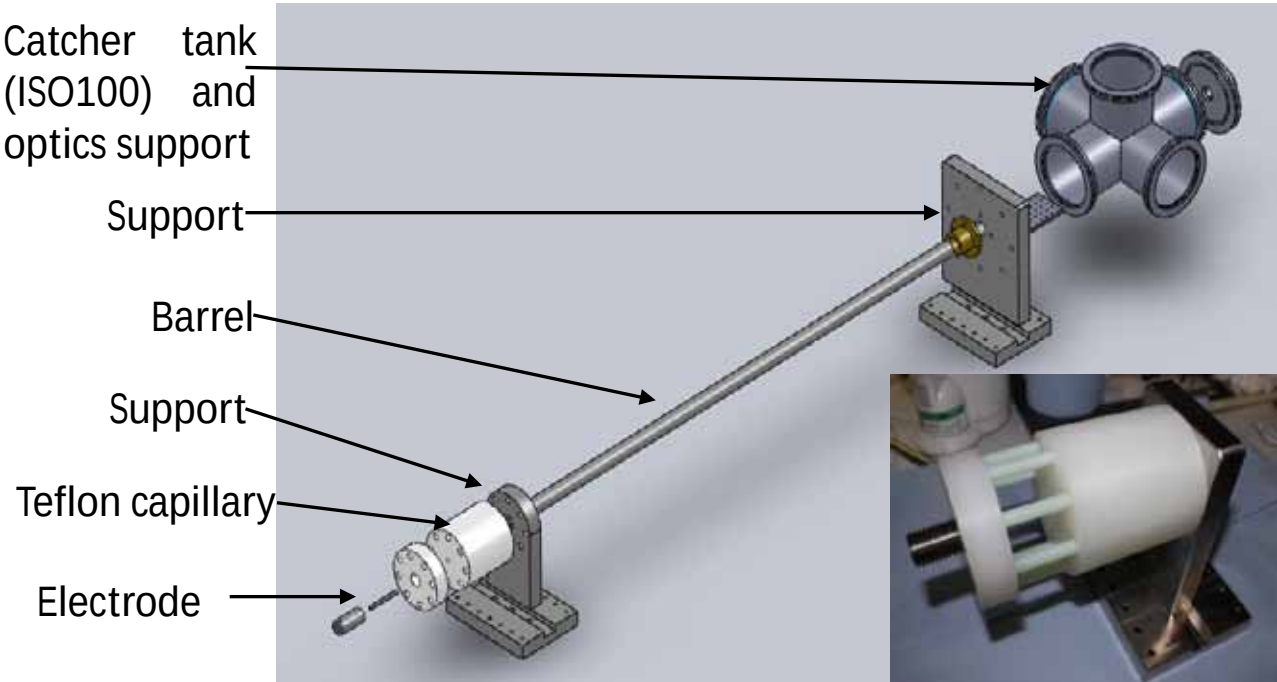

Imperial College London

Using a plasma jet to apply high pressures

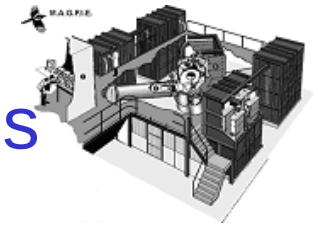

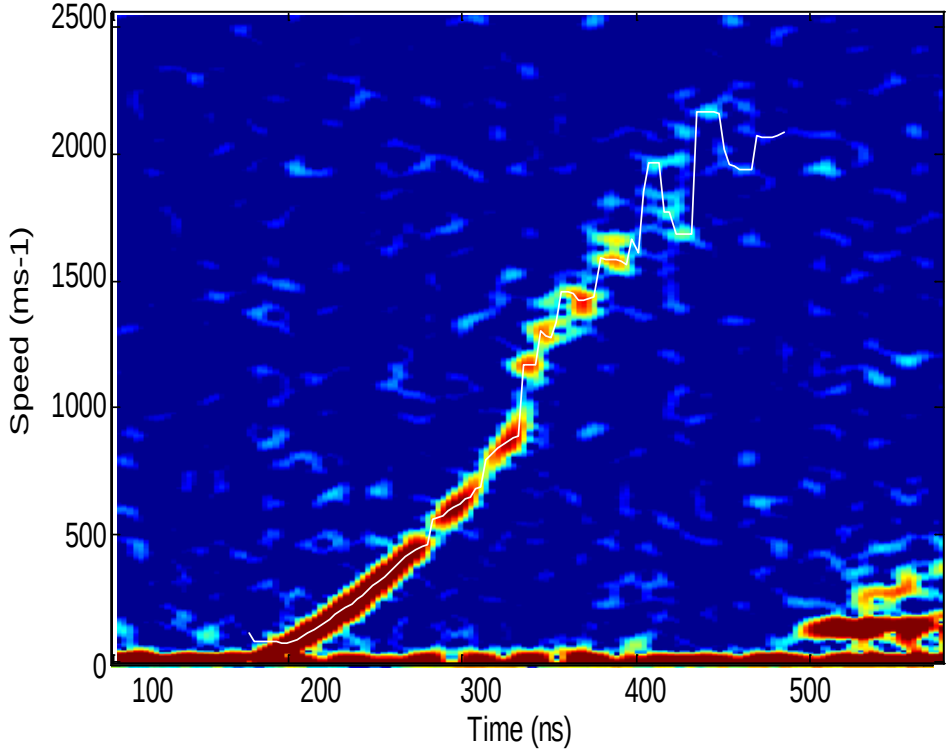

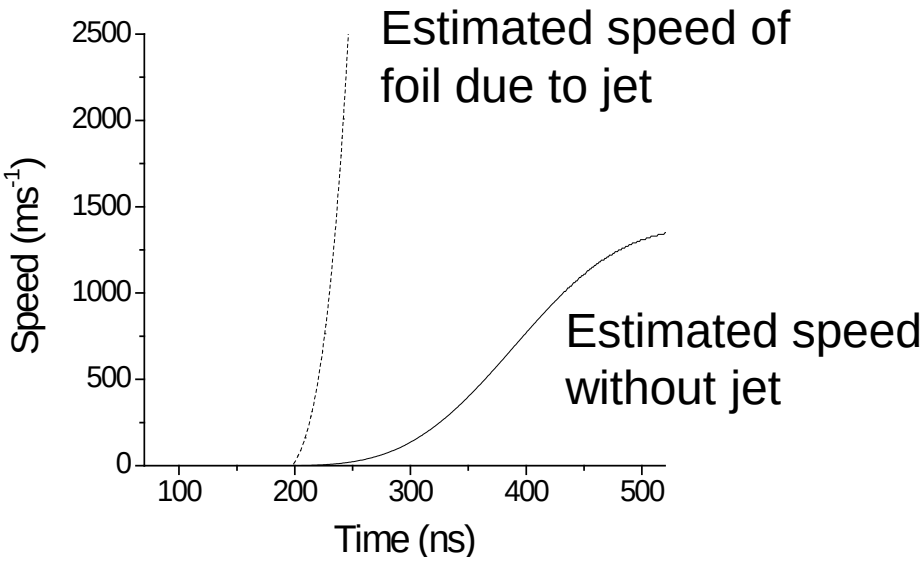

Initial acceleration is ~6x10^{9} ms^{-2} and remains constant until ~280-300ns

Corresponds to ~2KBar pressure

After 280ns, small ‘discrete’ readings of higher velocities

Initial acceleration is due to plasma ablating from array reaching target foil before jet forms

Imperial College London

Using a plasma jet to apply high pressures

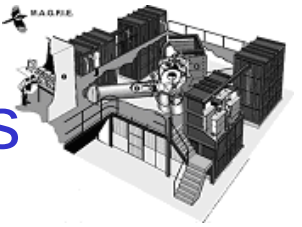

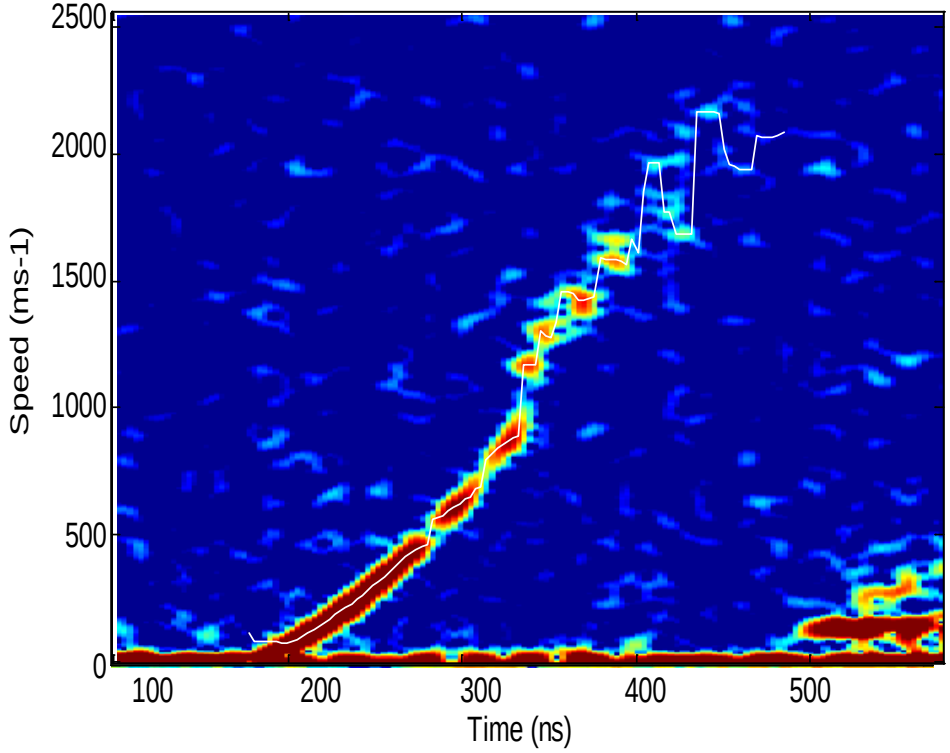

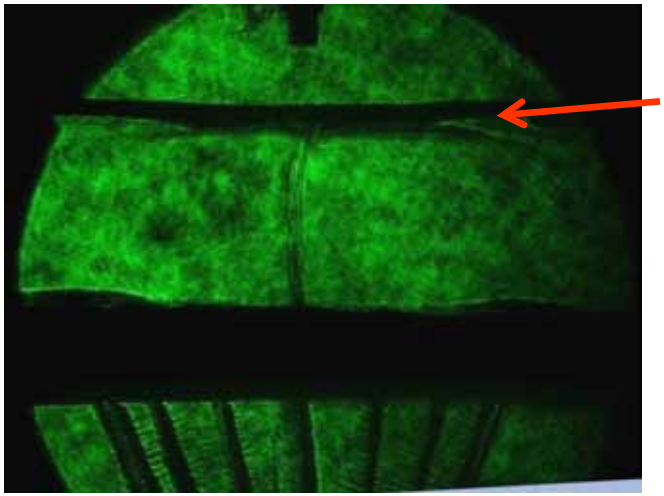

287ns after start of current

Initial acceleration is ~6x10^{9} ms^{-2} and remains constant until ~280-300ns

Corresponds to ~2KBar pressure

After 280ns, small ‘discrete’ readings of higher velocities

Initial acceleration is due to plasma ablating from array reaching target foil before jet forms

Arrival of jet launches shock through foil destroying back surface

Imperial College London

Using a plasma jet to apply high pressures

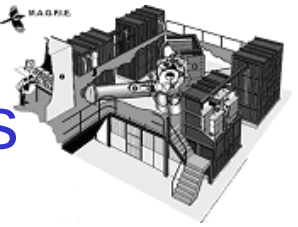

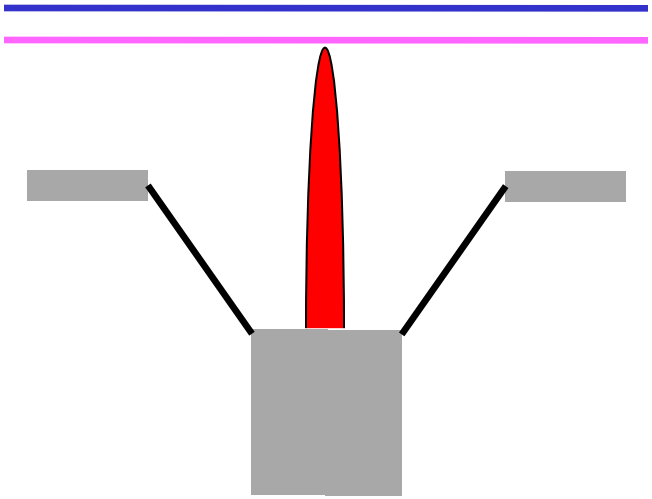

- Prevent preheat of target foil
- Prevent initial acceleration of foil
- Prevent shock from jet destroying target, possibly by acting as plasma reservoir

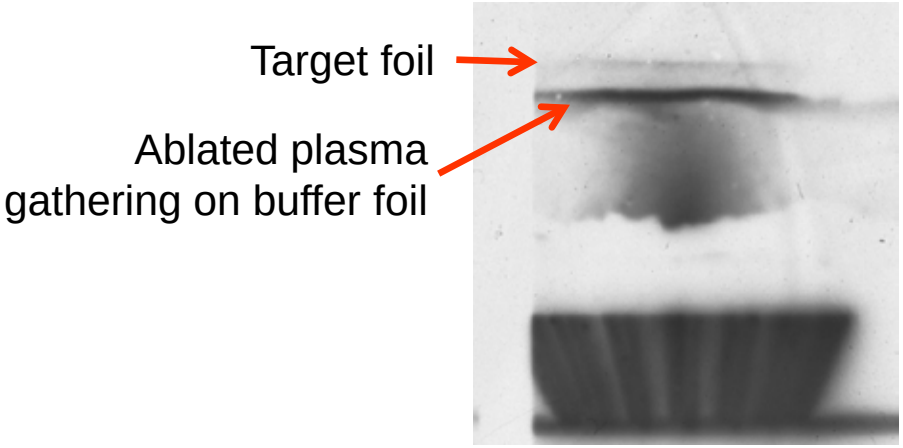

201ns

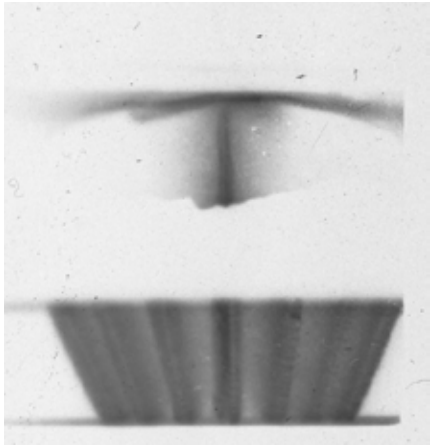

261ns

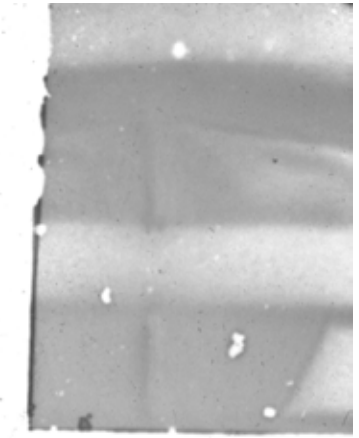

331ns

Imperial College London

Using a plasma jet to apply high pressures

Without buffer foil

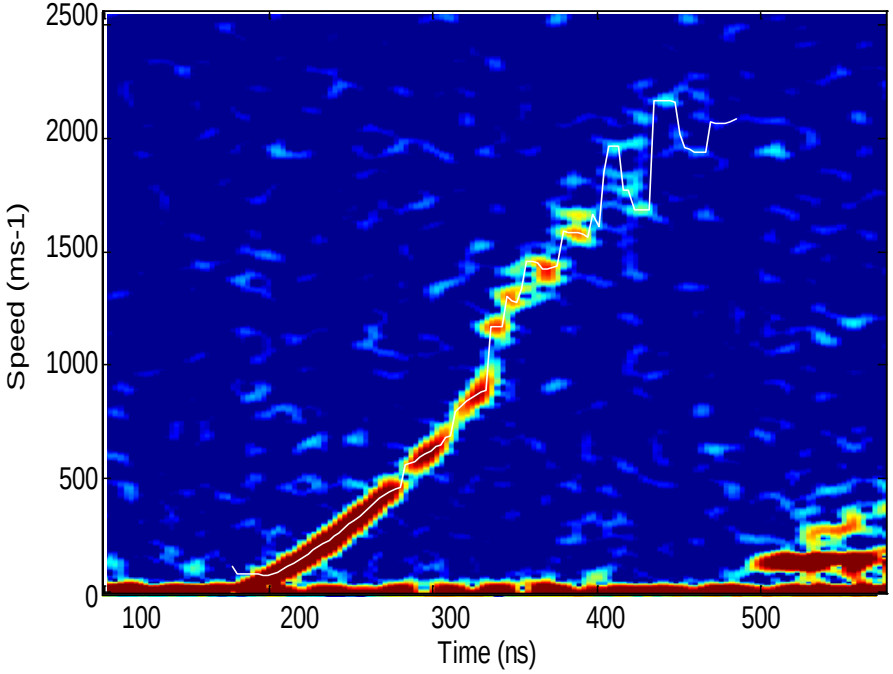

With buffer foil

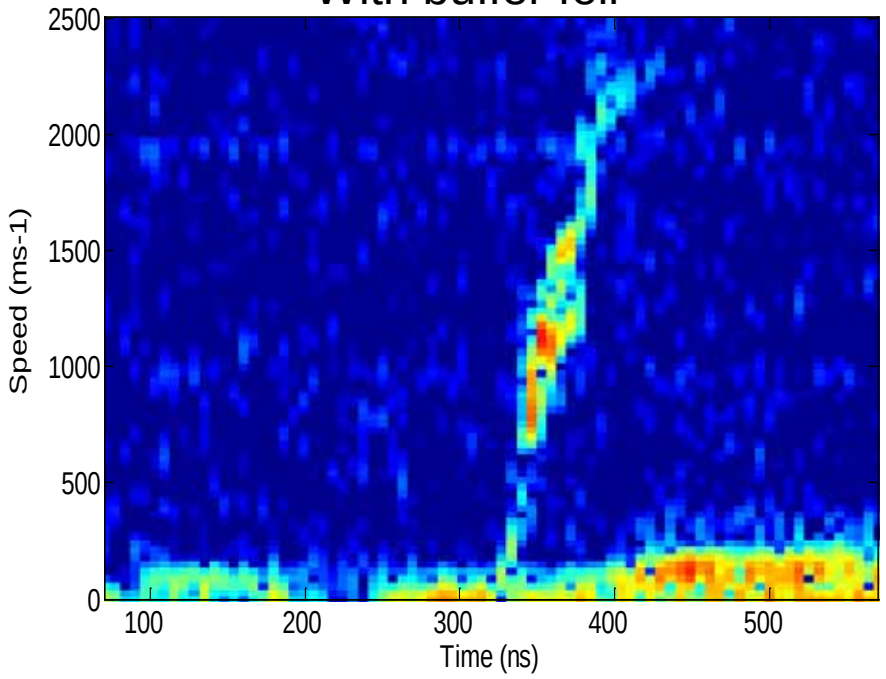

With buffer foil, no acceleration due to ablated plasma is observed

Rapid acceleration observed once jet arrived at foil

Acceleration ~ 40×10^9 ms^{-2} corresponds to 14KBar

Still somewhat lower than expected? Why?

energie atomique • energies alternatives

Isentropic compression driven by high explosive

Application to experiments on Tin and aluminum 6061-T6

Christophe VOLTZ CVA/DRMN

With the collaboration of
Patrice ANTOINE and Mickaël BOSSU

Introduction

Our goal is to evaluate the capacity of explosive driven experiment to generate ramp compression

- With first experiment on TA6V4, we demonstrated[1]
  - § the possibility to generate ramp compression up to 20 GPa with 0,8 µs rise time
  - § the measurement of material properties along the isentrope such as :
    - ü sound velocity
    - ü elastoplastic behavior

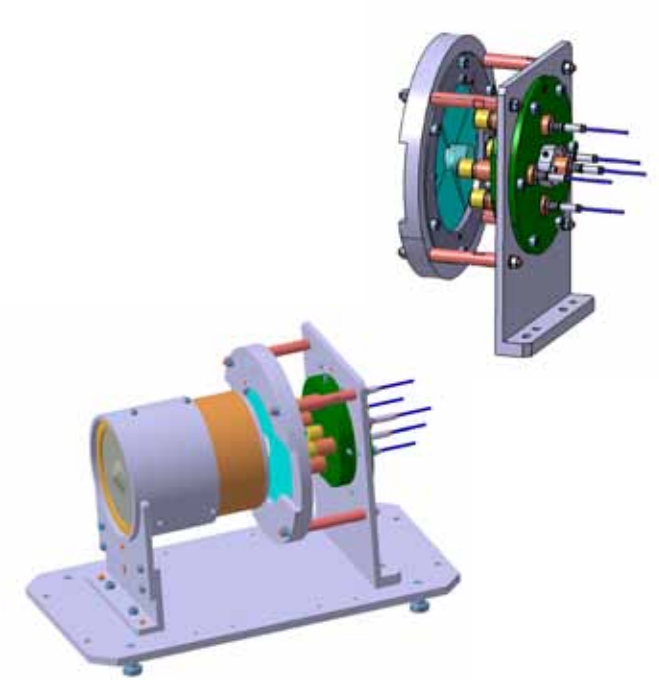

- Small scale apparatus
- Low cost experiment
- Common technologies
  - § Plane Wave Generator (CEA PWG)
  - § VISAR interferometry
  - § machining
  - § dimensional inspection

[1] C.Voltz, A.Sollier, J.-B.Maillet, and V.Bouyer – AIP conference proceedings – SCCM 2009 pp. 1143-1146

Background (1)

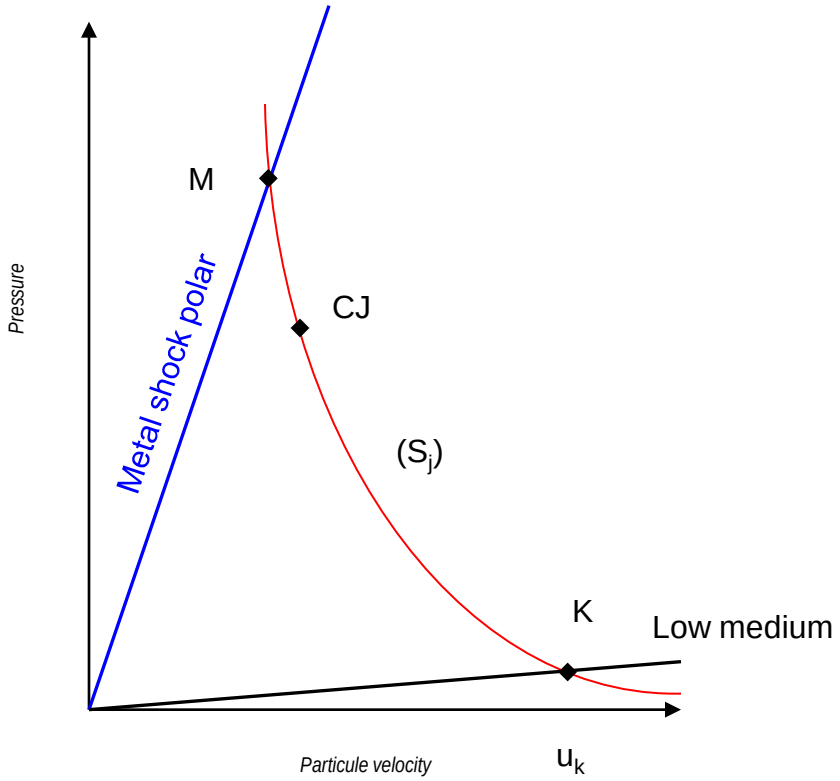

As gases act in low pressure range, it is important to have an accurate detonation products EOS in this range

- The objective is not to use detonation product from the CJ state but from a low pressure released state K
- The explosive is separated from flyer with low impedance medium (air or vacuum)
- K point is at the intersection of rarefaction isentrope (S_j) and the low medium impedance shock polar
- In this situation gases have high velocity (u_k near D_{cj}) and low density
- This process have been investigated as anti-spalling design and then as anti-entropy propeller

Background (2)

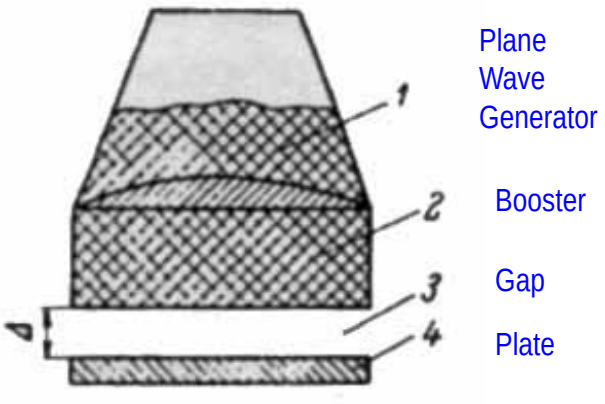

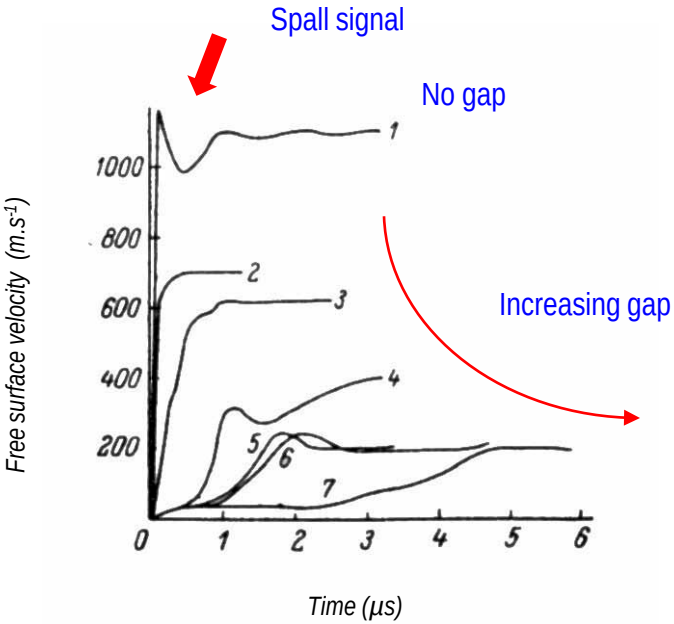

- According to Tsypkin[2] work on copper plate :
  - § ramp compression over 1µs can be achieved
  - § as gap is increased, maximum velocity decreases
  - § if gap is filled by air, a bump in the velocity profile may occur
  - § ramp compression shape is strongly dependent in the combination of PWG+booster and position from the apparatus center
  - § some material erosion can occur under air gap
  - § under vacuum the erosion is strongly reduced

[2] Tsypkin et *al*. - Zh. Tkh., 45, 624-629 (march 1975)

Technical requirement specifications

- Tin and Al target in order to compare the results with published work
- Apparatus structuring
  - § to insure precise gap and parallelism between PWG and targets
  - § by copper plate (buffer)
    - ü target are glued on buffer
- Experiment is conducted under vacuum
  - § the apparatus is set inside a cylindrical chamber with feed through
- Evaluating the input drive
  - § by measuring the buffer motion (with and without LiF window)
  - § by a measuring the particle velocity at LiF window front (facing the detonation product stream)
    - ü in order to avoid window erosion an aluminum foil is glued
- Measuring the detonation product stream symmetry
  - § by 6 special optical fibers placed at same radius
- Spatial reference
  - § the buffer front side is the spatial reference for : LiF window, fibers

Simulation scheme

- The apparatus is design by hydrocode simulation
- 1D lagrangian scheme
- JWL EOS for explosive
- Elastoplastic behavior for metallic parts

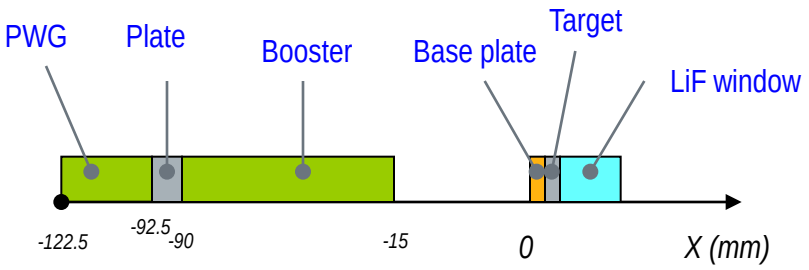

1D lagrangian diagram – Pressure chart

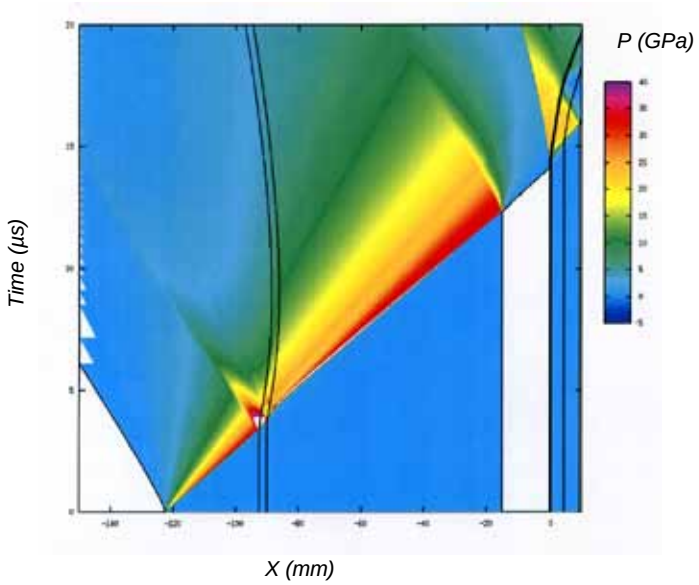

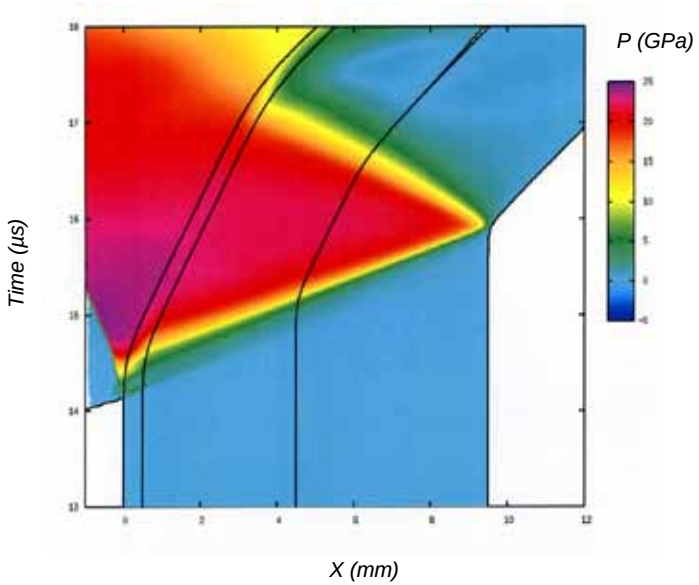

Apparatus description

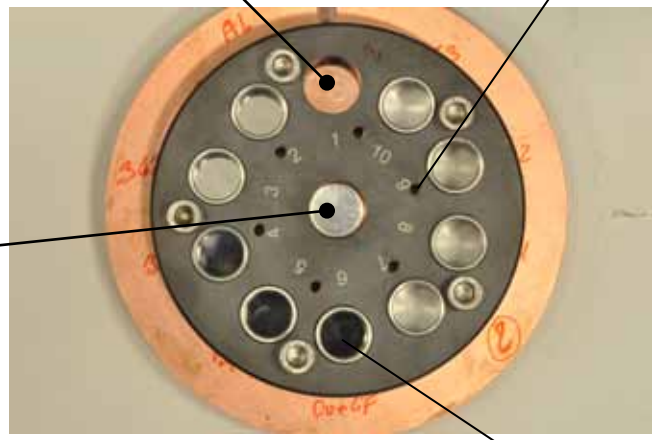

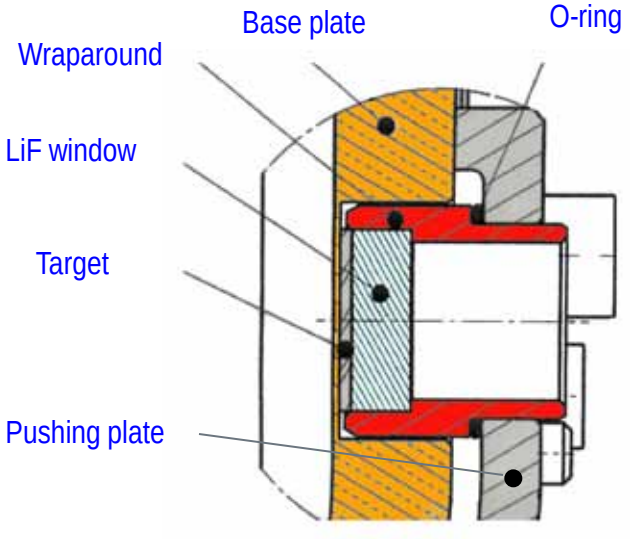

- For the target sub-assembly, we use a 10 mm copper plate for structuring
- The copper plate is hollowed in 10 places (at 35 mm radius), with a base plate thickness of 0.5 mm
- 8 targets :
  - § targets (ϕ 15 mm) are glued between base plate and window
  - § glue is RTV-1[3]
  - § target and/or LiF Windows are tacked on the base plate by a steel wraparound
  - § the O-ring acts as a spring
  - § 1, 2, 3, 4 mm with or without LiF window (ϕ 15 mm - h 5 mm)
  - § dimensional inspections to measure each thickness (base plate target, glue, LiF)

[3] CAF 730 Bluestar Silicones

Diagnostics

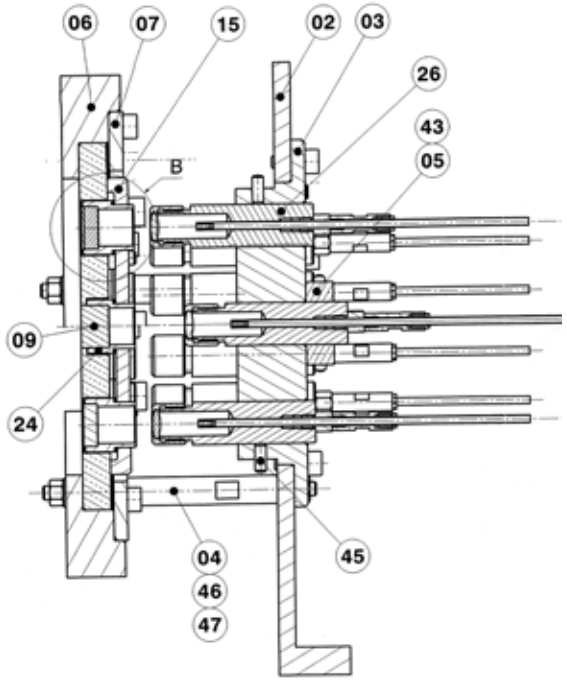

- We have 11 channels for interferometry measurements
- Base plate
  - § free surface velocity > base plate monitoring
- Base plate with LiF
  - § interface velocity > input drive
- 4 Targets
  - § free surface velocity
- 4 Targets with LiF
  - § interface velocity
- Central LiF
  - § ϕ 15 – h 10 mm
  - § with 0.1 mm al foil (glue) > detonation products stagnation

- 6 Optical fibers
  - § 600/800 silicon fiber
  - § front face is metalized with 5 µm Al
  - § light detection by Si detector > detonation products chronometry

Some pictures…

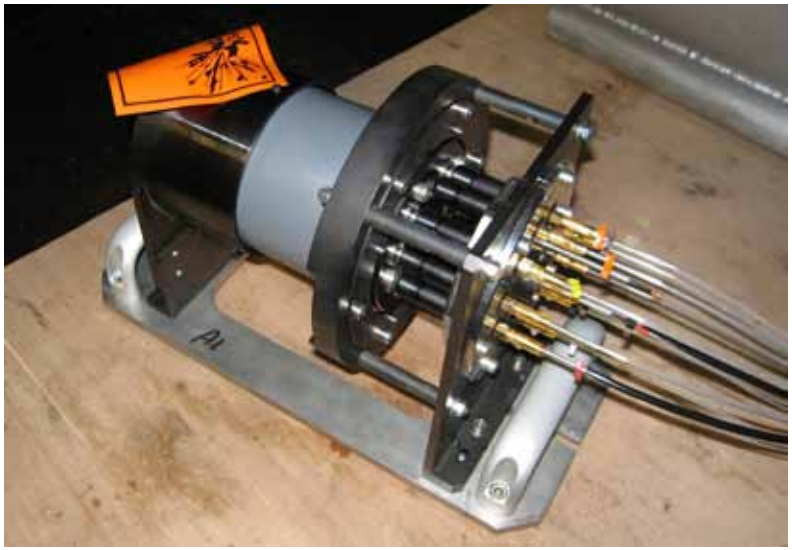

The materials

Tin

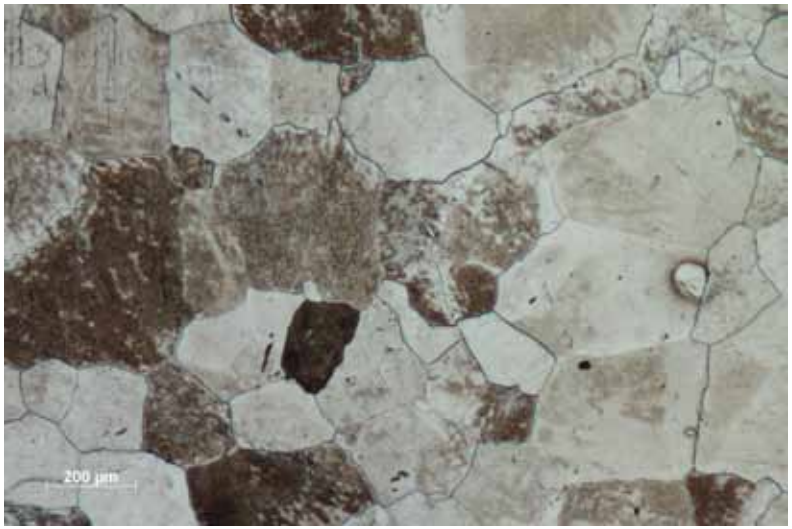

- Sn
  - § “pure Tin” Goodfellow
  - § 99.95 purity
  - § main impurity Cu, Zn and Fe
  - § quite large grain size d_0 > 150 µm
  - § hardness $Hv_{0.3}$ = 5
  - § density 7.275 σ 0.0045 g.cm^{-3}
  - § surface roughness Ra = 0.03 mm

Al 6061 T6

- Al 6061 T6
  - § metallurgical structure conform to ASTM handbook reference pictures
  - § hardness $Hv_{0.3}$ = 110 1
  - § density 2.708 σ 0.002 g.cm^{-3}
  - § surface roughness Ra = 0.03 mm

Results detonation products stagnation

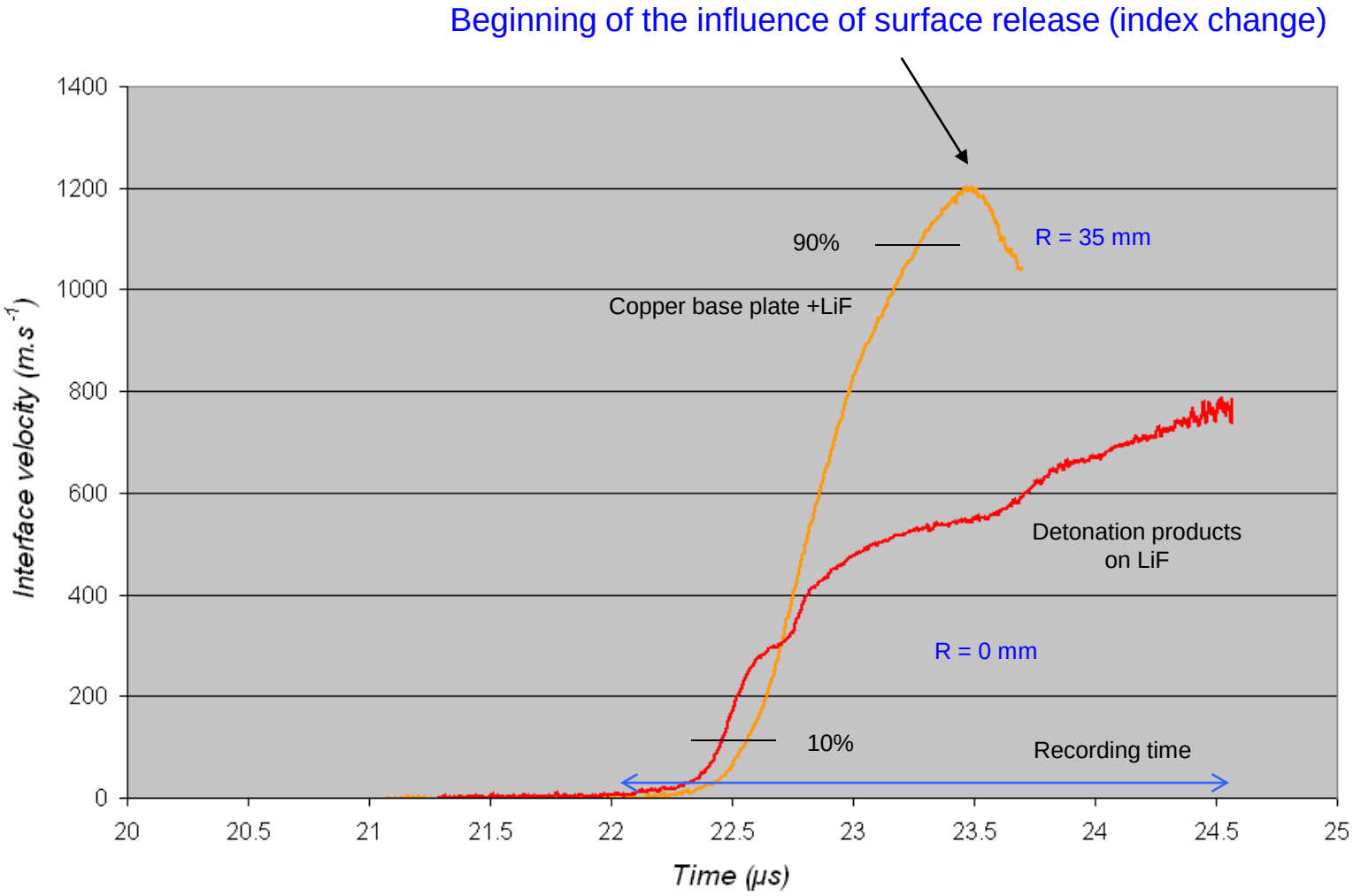

Ramp compression at Cu/LiF interface ≈ 0.69 µs rise time 10/90

Results Time correlation

Data's from optical fibers located at 30 mm radius

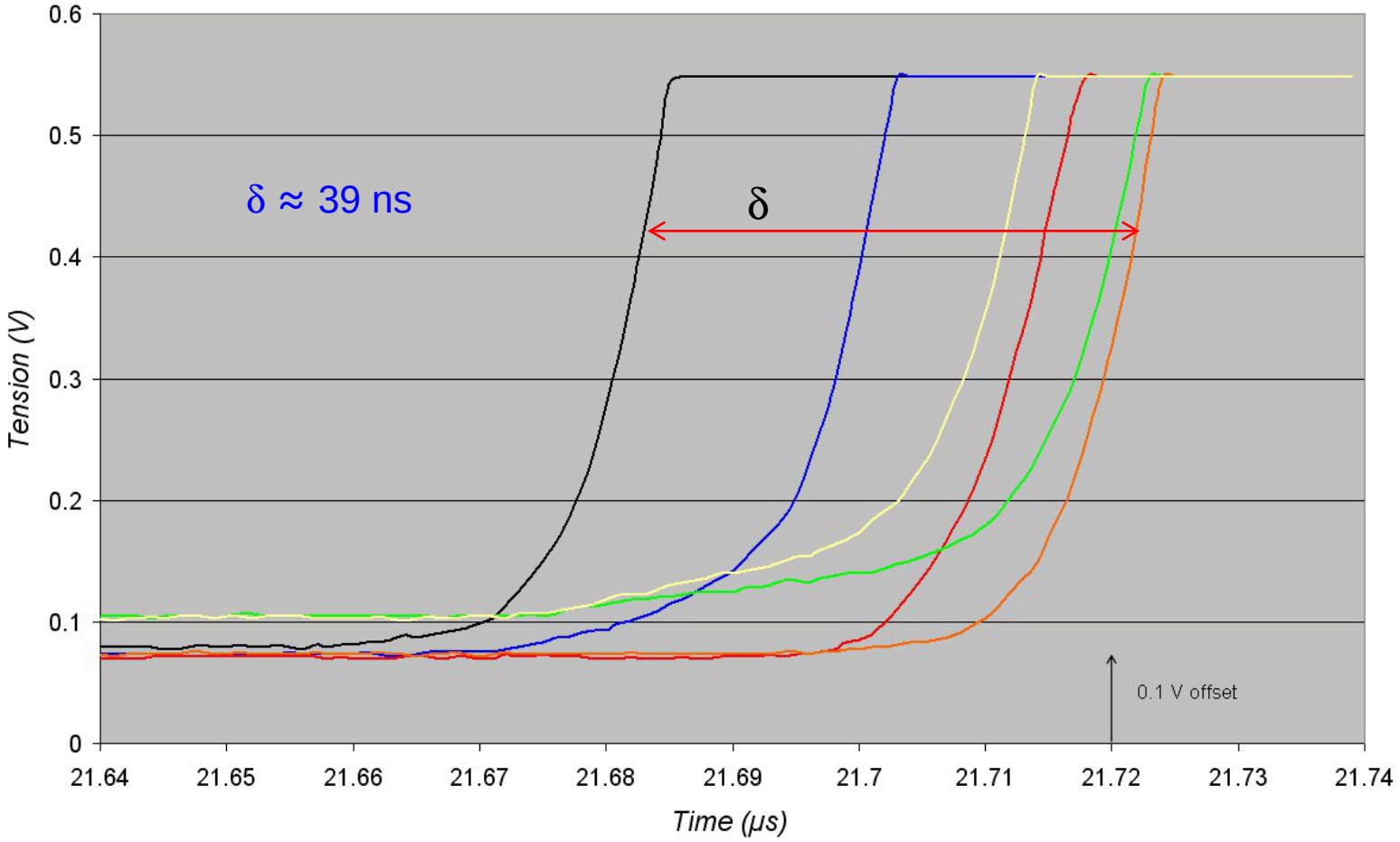

We must take into account these time shift in time base observations

Sn-LiF interface velocity

Due to “small” LiF thickness, the observation time is less than 1µs
But enough regarding to phase change time occurrence

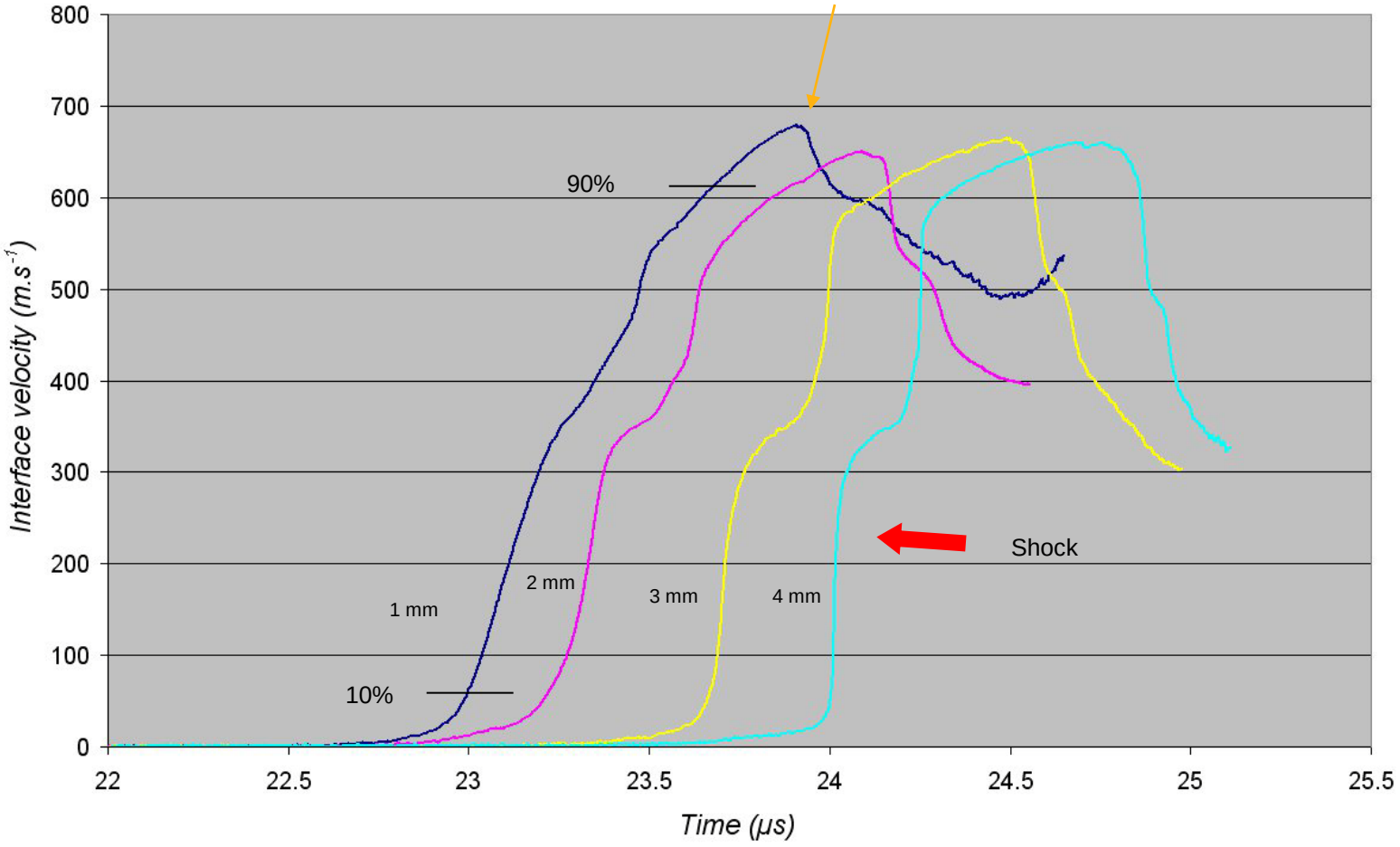

Ramp compression duration ≈ 0.67 µs rise time 10/90

Sn free surface velocity

Limitation of recording due to short VISAR stand-off

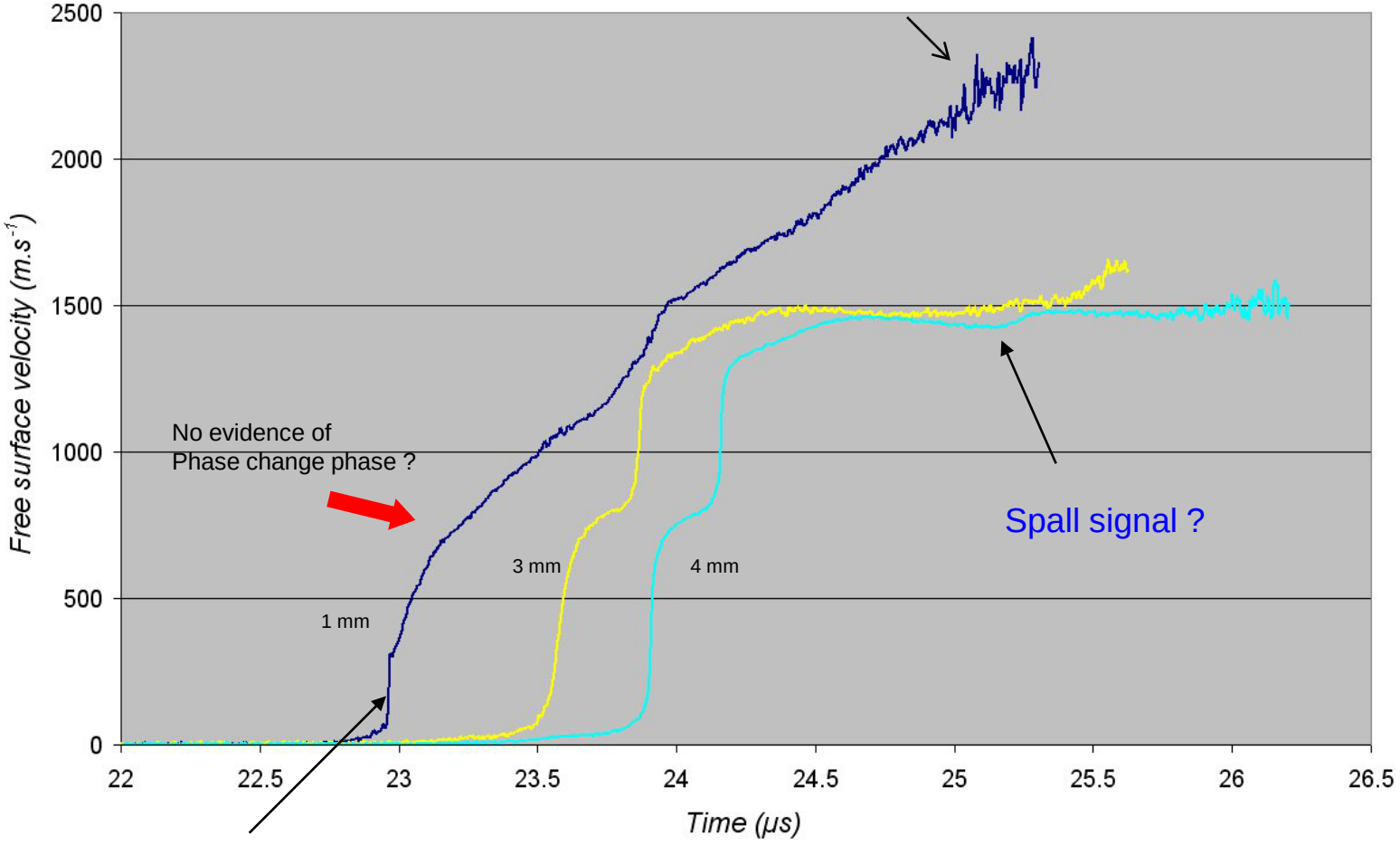

Artifact from VISAR

From certain signals we suppose that spallation occurs

Al-LiF interface velocity

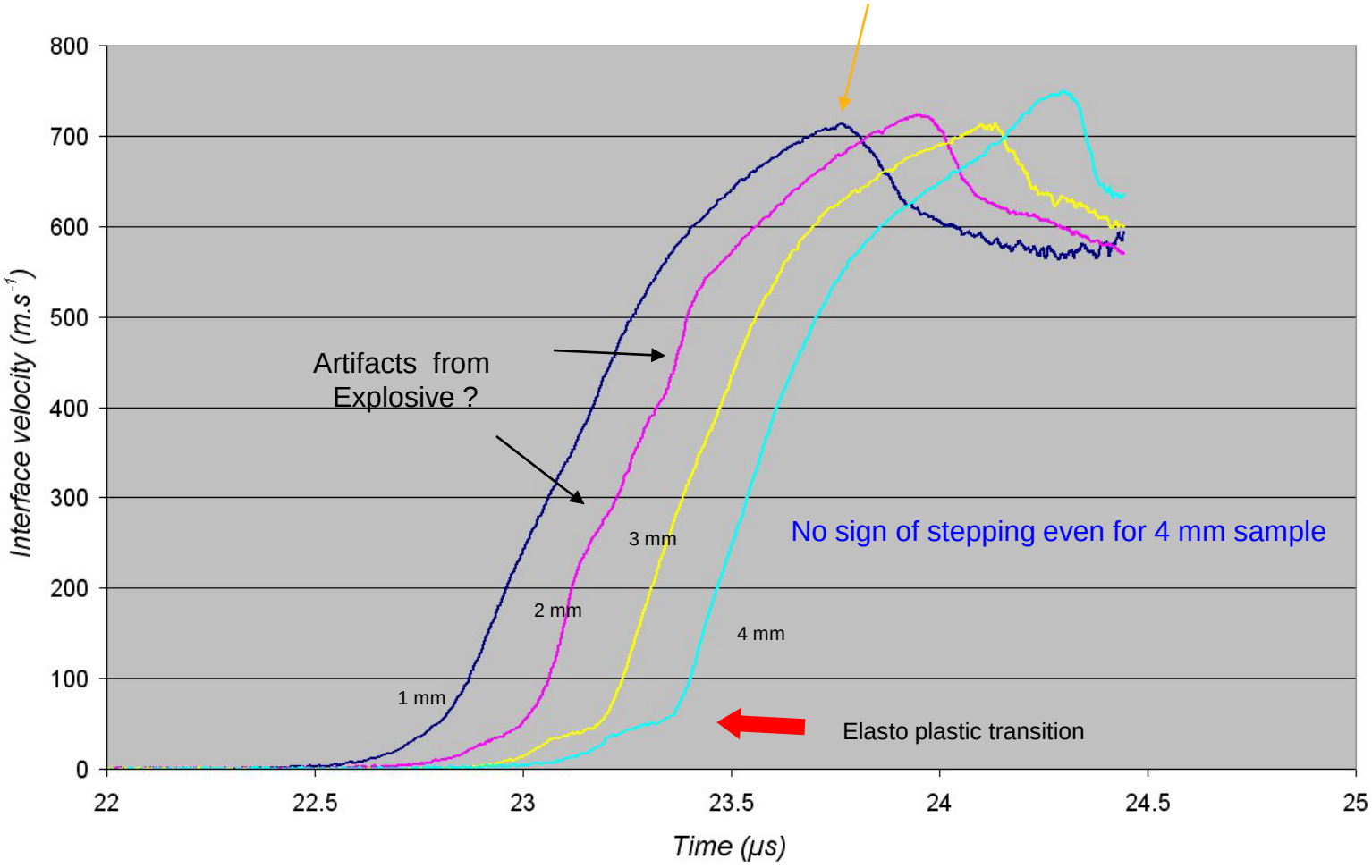

Ramp compression duration ≈ 0.65 to 0.6 µs rise time 10/90

Al free surface velocity

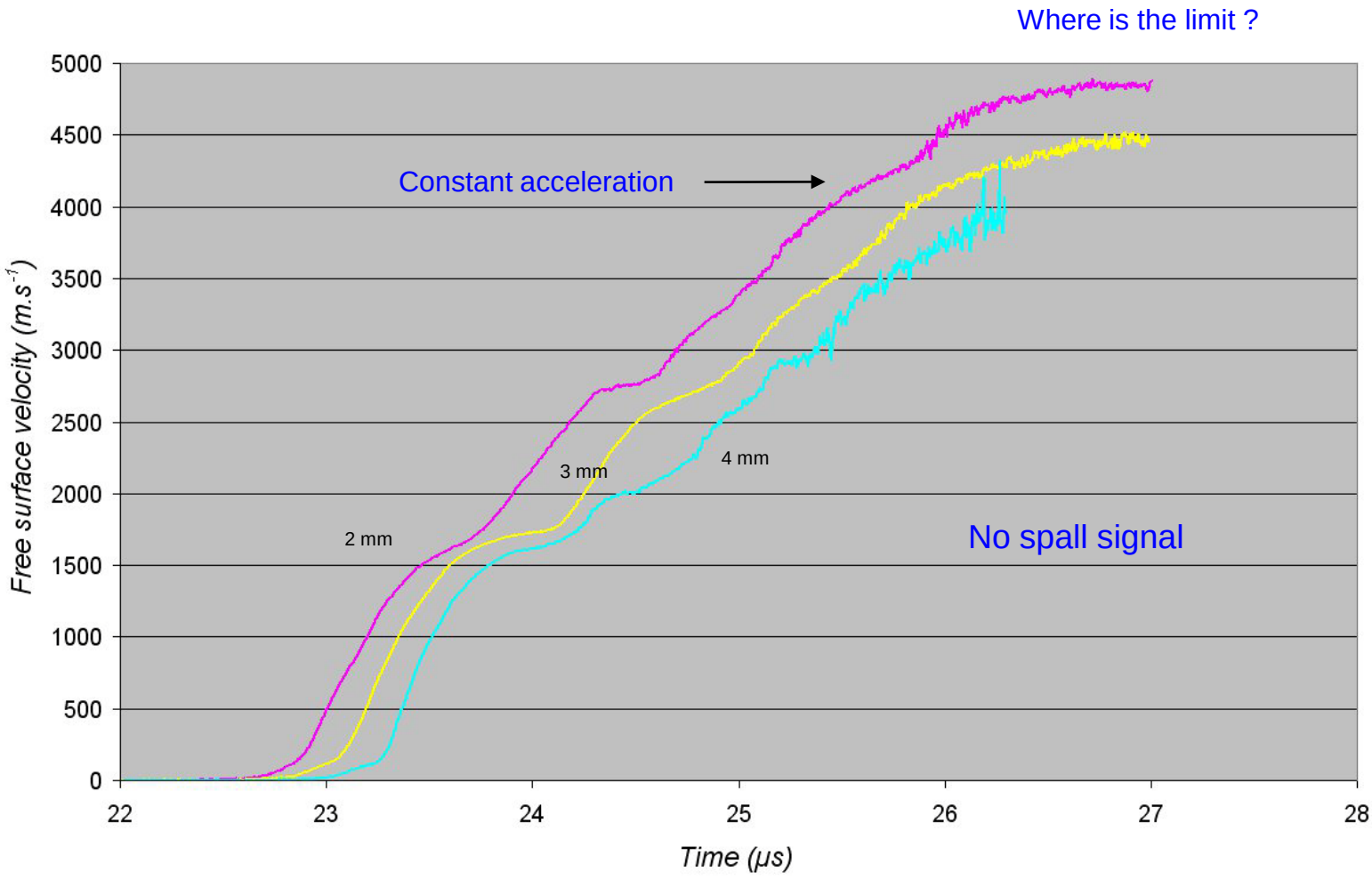

Multi reverberation inside the target
Complex interactions between forward and backward waves

Feedback

L

- Glue thickness, 20 µm
- Base plate deformation
- With the O-ring we don't know exactly the force applied on targets
  - § it's important for Tin which can undergo creep
- It is difficult to have the same spatial reference
- Final dimensional inspection is quite difficult with such complex sub-assembly
- Some discrepancy revolution symmetry for PWG+booster assembly

J

- The experiment "works" even detonation products flush away inside the vessel
- No crosstalk between interferometry channels
- Easy to operate on ground field
- Vacuum better than 3 10^{-2} mbar

Conclusions

- We are able to conduct ramp compression with explosive device
- Experimental results are exploitable and comparable with literature
- The pressure is up to 23 GPa on Sn and Al
- The rise time is near 0.6 µs (Al) and 0.69 µs (Cu base plate)
- Detonation products stagnation has been recorded for more 2 µs
- As well known time duration is limited by window size but in the experiment on tin it works
- We have good results with aluminized optical fibers

Perspectives

- Conduct 2D simulation and compare to experimental data's
  - § in order to acquire information on explosive detonation products behavior in low pressure range
  - § to have feedback on Sn and Al EOS
- Make experiment on Tin with longer time ramp loadings
  - § to see if there is an influence of kinetic on phase change
- Two stage PWG in order to achieve (?) 50 GPa – 0.5 µs ramp loading on Tin
- Target heating to modify the thermo mechanical path in (P,T) plane
  - § in order to "move" the isentrope pole
- Modify VISAR detection to achieve higher time resolution
  - by replacing PMT by fast detectors
- Test 50 mm diameter PWG (from 2 to 4 measurements location)

Many fields of development …

Adaptation of Existing Facilities to Isentropic Compression Experiments

Douglas G. Tasker, WX-6

Charles Mielke, MPA-CMMS

George Rodriguez, MPA-CINT

Dwight Rickel, MPA-CMMS

4th Workshop on Ramp Compression

18-19 January 2011 at Sandia National Laboratories

Abstract

- **Magnetic isentropic compression experiments (ICE) provide the accurate shock free compression data for materials at megabar pressures.**
- **QUESTION: can we adapt NHMFL single-turn to ICE experiments? YES**
- **We show the NHMFL can offer a less complex ICE experiment at relatively high pressures (~½ Mbar) with a high sample throughput at a relatively low cost.**
- **We will:**
  - discuss the physics of the NHMFL-ICE experiments
  - predict the likely performance space
  - present data from the first proof-of-principle experiments.

NHMFL single-turn magnet circuit

- **Simple low voltage circuit**
  - Capacitors typically charged to 35 kV but capable of 60 kV
- **Electronic closing switches deliver current to load via coaxial cables**
  - Rise time ~2 μs
  - No water lines, magnetic insulation, etc.
- **Only the load is expended**
- **Typical fields 50 T**

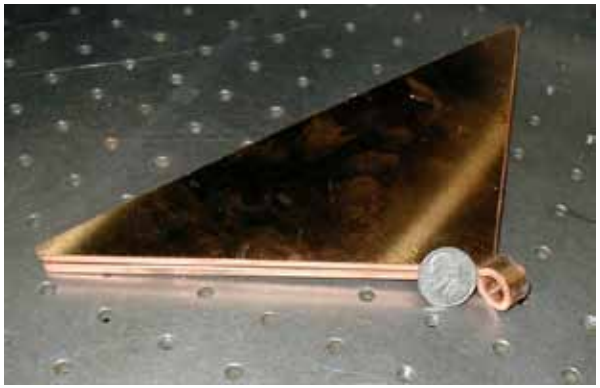

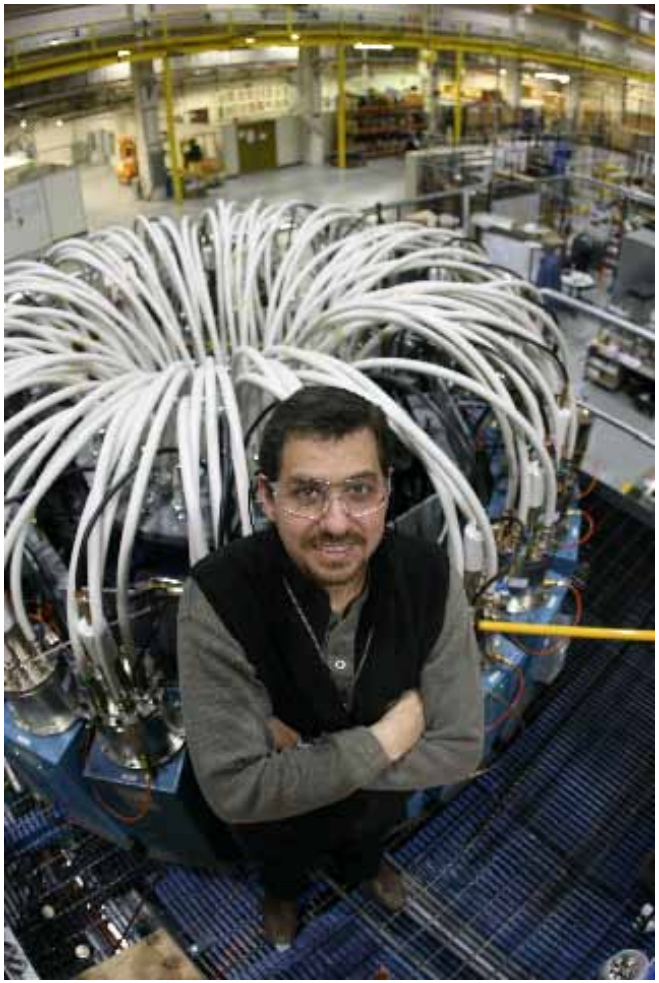

The Single Turn Magnet Setup

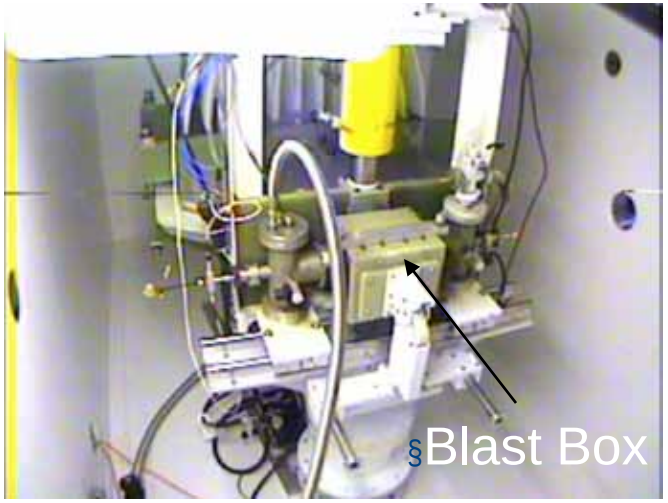

Simple NHMFL-ICE POP experiments

- Triangular plate and load "coil" pressed to shape as parallel plate load
  - Not ideal design, but OK for proof-of-principle experiments
    - In future will need better design/metrology to obtain conductor and sample thicknesses, parallelism, densities, etc.
  - Connected directly to capacitor bank
- With $50K from C2 (Rick Martineau) we performed 6 proof-of principle experiments in Sept 2010

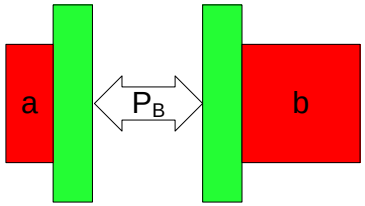

spICE analysis of circuit

- **For experimental design and subsequent data analysis it is important to have good predictive models of the system performance.**
  - We chose to use the SPICE circuit code to simulate all aspects of the experiment, electrical AND physical
- **For the NHMFL-ICE circuit this is not straightforward.**
  - The capacitor bank and closing switches may be modeled by simple circuit parameters
  - The load is a complex system dominated by the material dynamics (shock physics) of the materials
- **The load is *time dependent* and *current dependent***
  - Accurate dynamic load models had to be developed to simulate the compression and expansion of the load from shock physics principles

spICE circuit simulation for NHMFL

- **Predictive tool – not used for data analysis**
- **Dynamic components (in yellow): Xup is the load simulation circuit**
- **Static components:**
  - C, Lb and Rbnk are the capacitance (144 µF) inductance and resistance of the capacitor bank, its cables and connections between the bank. Ltpr is the inductance of the load taper
    - At 60 kV, energy = 260 kJ (equivalent to ~40 g explosive)
- **Output values:**
  - U_{p1} and U_{p2} are the interior particle velocities, U_{fs1} and U_{fs2} are the surface velocities
  - P_{mag} is the magnetic stress common to both samples
- **Have models for both parallel plate and coaxial loads**

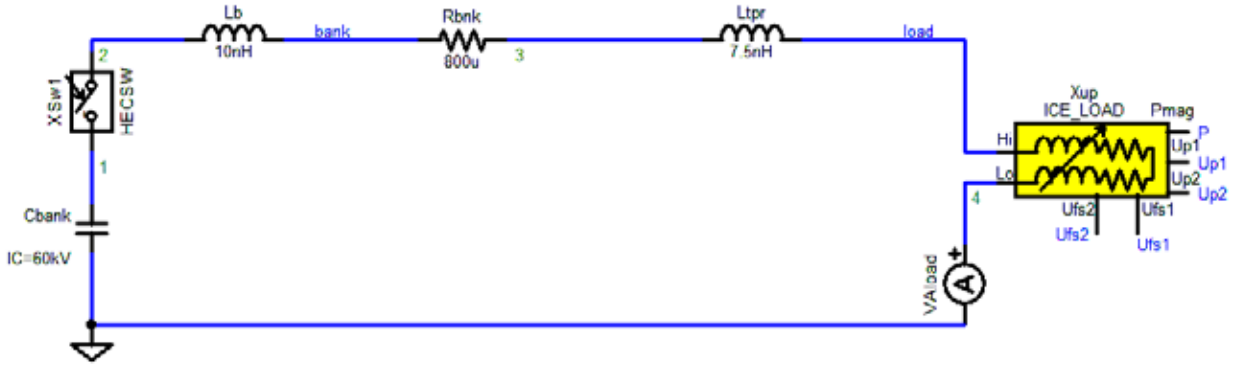

Parallel plate load compression

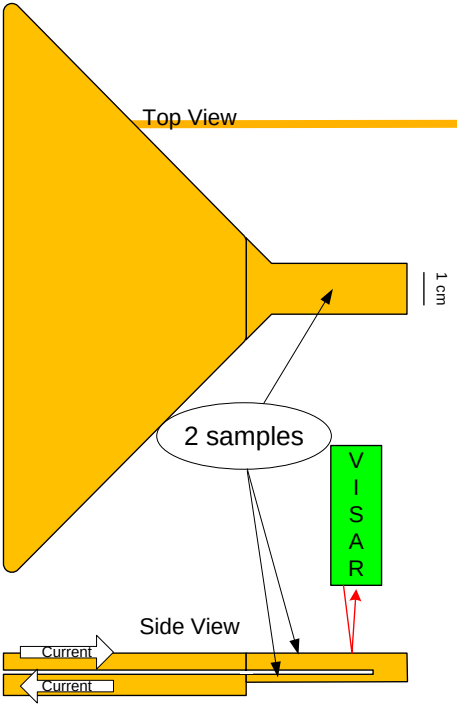

- **Inner plate separation *d(t)* increases with time**
  - So must calculate velocities of inner surfaces (Up)
- **Inductance increases with *d(t)***
- **Rarefactions from outer surfaces accelerate separation when they return to inner surfaces**
  - Diffusion effects not modeled yet

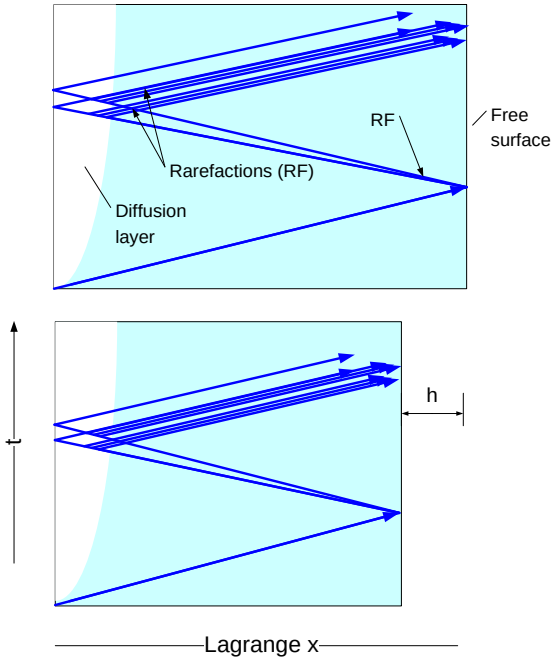

Load model transmission line analog

- **Wave propagation and reflection in the expanding electrodes were modeled in an electromechanical analog**
  - Mechanical particle velocity = electrical current
  - Mechanical pressure = electrical voltage
- **Load with free surface treated as a short-circuited transmission line**
  - Cannot yet handle effects of diffusion layer
  - Windows accommodated by adding a second transmission line, etc.
- **Electrical *Z* = acoustic wave impedance of the load = $\rho_0 c_L$**
  - Lagrangian wave speed, c_L ; initial density, ρ_0
  - Delay time = l / c_L where l is length
  - As the wave velocity $c_L = c_L(P)$ - function of pressure
    - c_L increases with time during the ICE experiment
    - *spICE* uses equivalent to SESAME tables
- ***Dynamic transmission line has voltage dependent velocity***
  - Difficult to model - can be numerically unstable
  - Stable solution with a 16-staged lumped RCL circuit model for the transmission line
    - capacitance per stage $C = C(V)$, *i.e.,* a function of V (≡ pressure)
- **Load inductance *L(t) of parallel plates solved analytically***

$$L(t) = \mu_0 K l \times \left(d(t) / W \right)$$

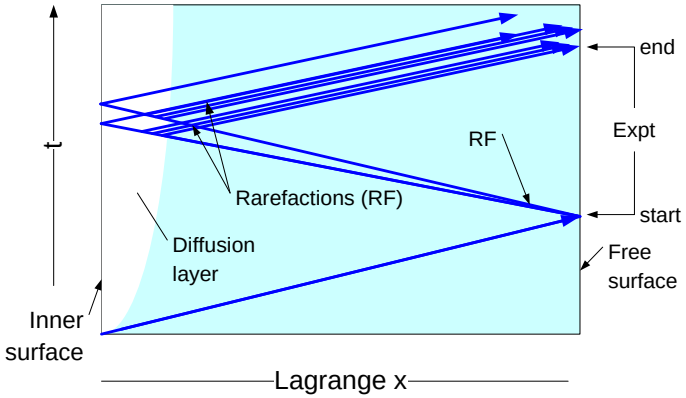

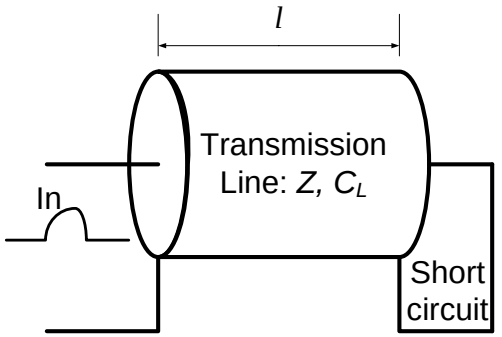

Highly uniform pressure distribution on load

- **Load modeled to solve for the magnetic field, current distributions and pressure vs. time**

- **Field calculations were first performed for fixed positions of the electrodes**
  - Movement of electrodes was obtained from the *spICE* calculations described below, then the PDE calculations were by repeated for the different load separations.
  - Assumed that the conductivity of the conductors was constant

- **Calculations showed that the magnetic pressures in the central flat region normal to the surface, P_y, could be fitted to within 5% with a simple logarithmic function,**

$$P_y = \tfrac{1}{2}\mu_0\left(0.11853 - 0.21641 \times \ln \overline{h/W}\right) J^2$$

  - where J is the linear current density.

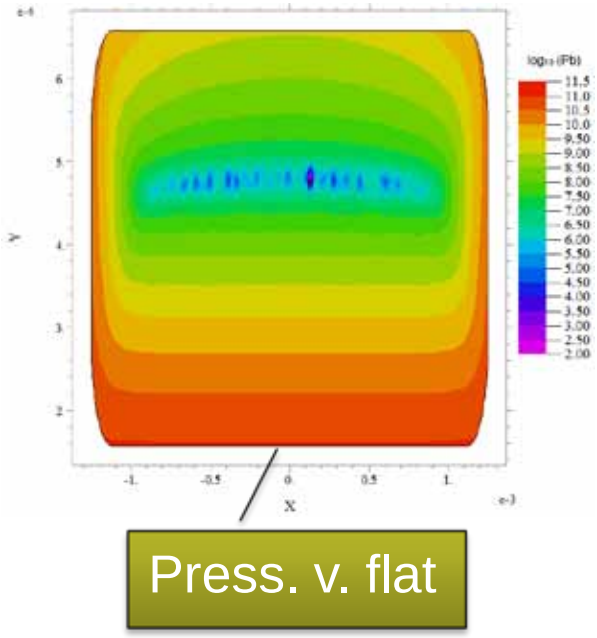

- **Equation was incorporated into *spICE* load model**
  - Calculated peak pressures are always close to experimental values obtained in ICE experiments.

Recent experiments

1	Copper	One VISAR	Proof-of-principle	Good data
2	Copper	One VISAR	Proof-of-principle	Good data
3	Copper	Two PDV	EOS demo	Good data
4	Tantalum	Two PDV	EOS demo	Single-can misfire
5	Tungsten	Two PDV	EOS demo	Good data

splCE calculation of NHMFL-ICE Cu load

- **Copper samples 77 and 125 mil**
- **Bank 35 kV**
- **PDV data**
- **Effective end of the experiment is the time when first relief waves arrive back at the surface of the thinner sample**
- **We will see the experimental results in a moment**

Load voltages, kV

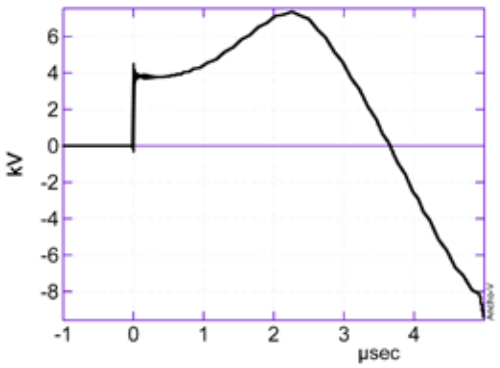

Load stress, GPa

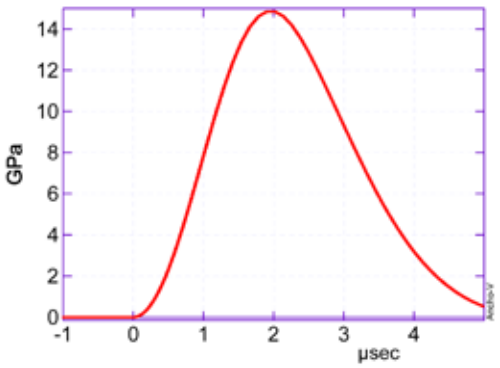

Surface velocities, km/s

End of expt

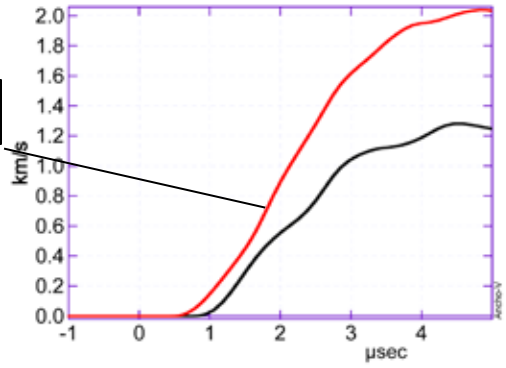

Load current, MA

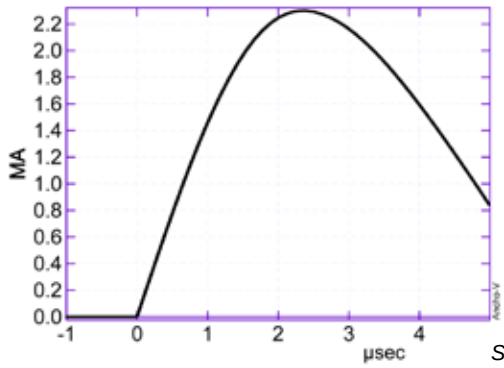

Recent experiment – before and after

- **PDV gauges situated above and below the load**
  - Detected velocities of the two tungsten samples

Shot 1 – nominally 125 mil copper

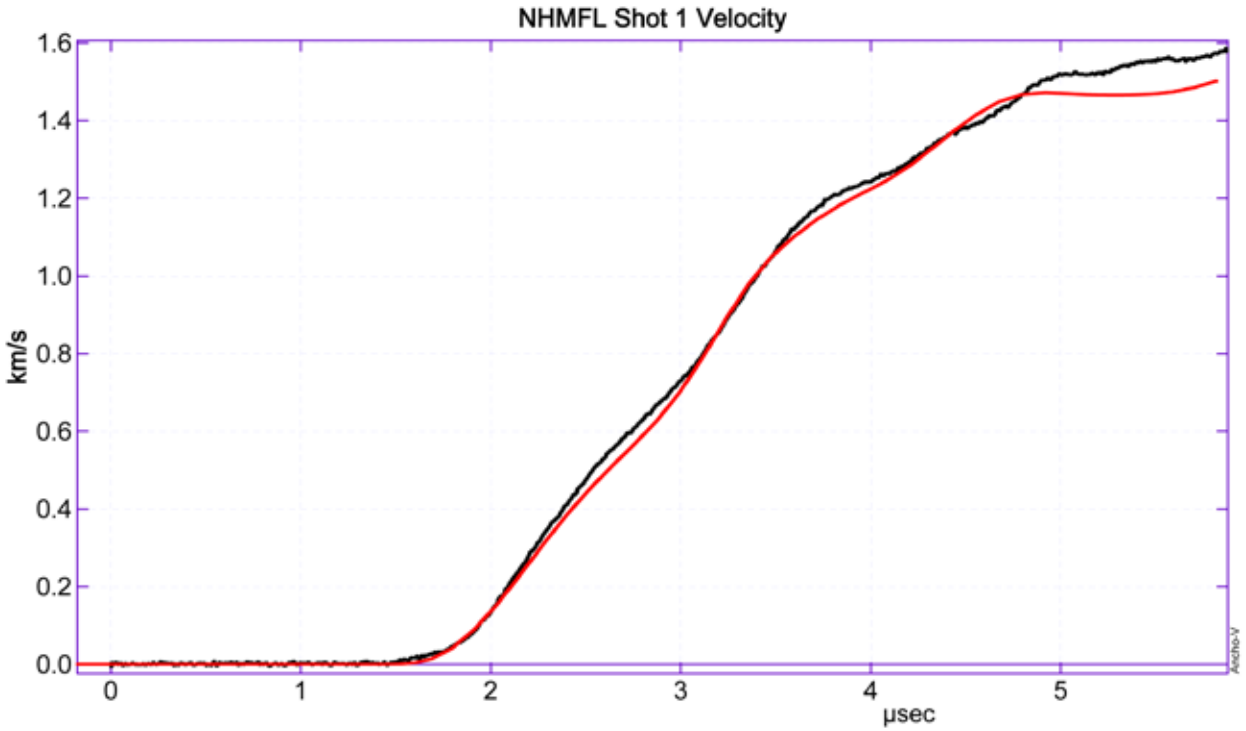

- **VISAR velocity from one of two copper samples, both 125 mil**
  - *spICE* model (red) appears to under-predict surface velocity
  - But exact dimensions and material properties not known

Experiments performed on copper

- **Samples, 77 and 125 mil, PDV diagnostics**
  - PDV data for 77-mil sample data exceed Nyquist limit (~3 GHz)
  - *Upper right- spICE* model velocities

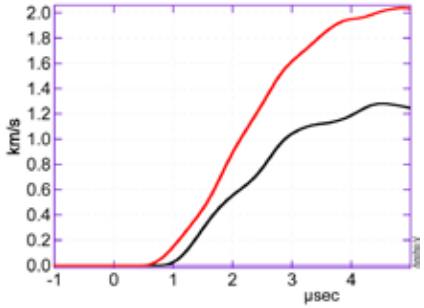

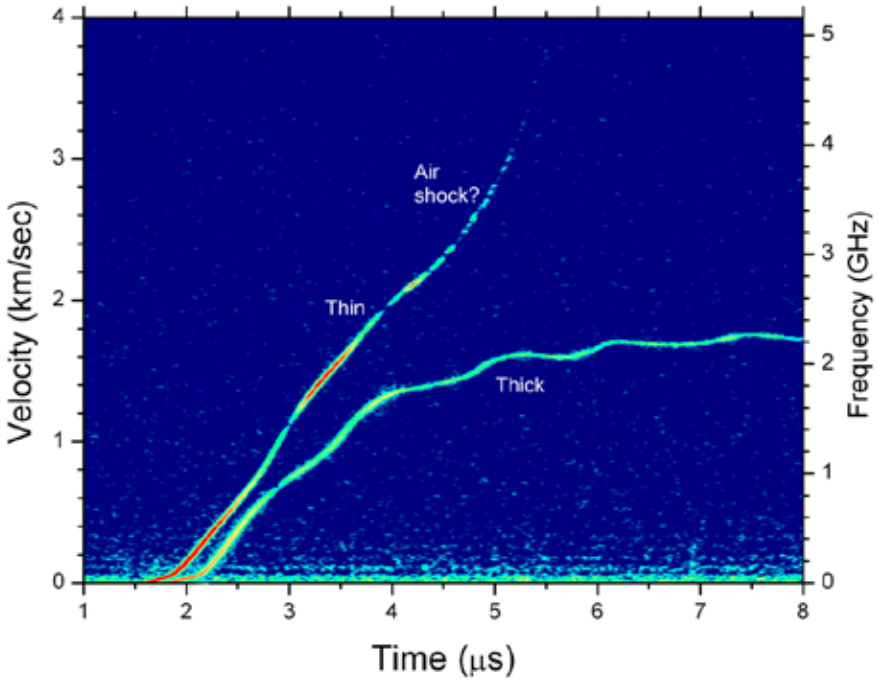

Conclusions

- **The feasibility of NHMFL-ICE experiments has been demonstrated**
- **Modeled successfully with a hybrid electromechanical simulation using SESAME equivalent EOS**
- **Sample dimensions determine the required rise time of the stress in the load which was shown to be approximately 2 μs**
  - Good for larger samples
- **NHMFL-ICE technique would be an excellent complement to ongoing studies with gas guns**

Extras

NHMFL phase changes diagnostics - 1

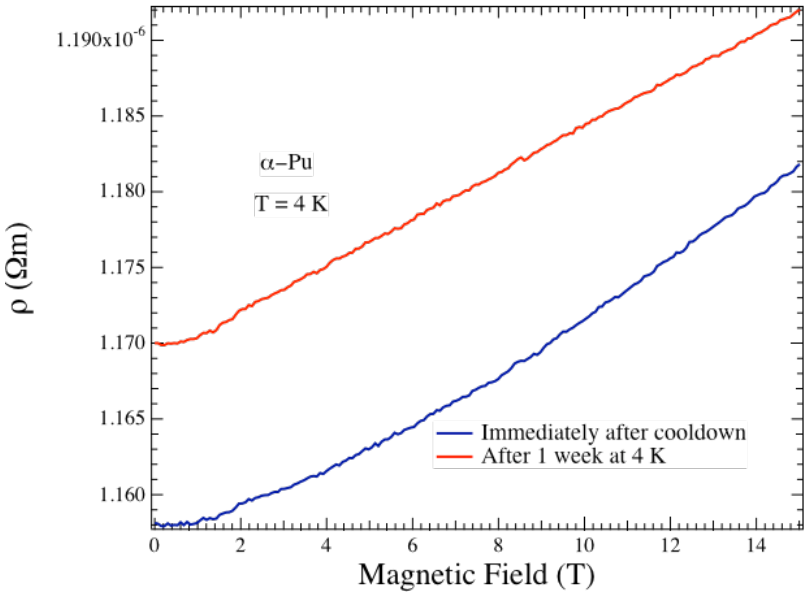

Contactless conductivity of α-Pu

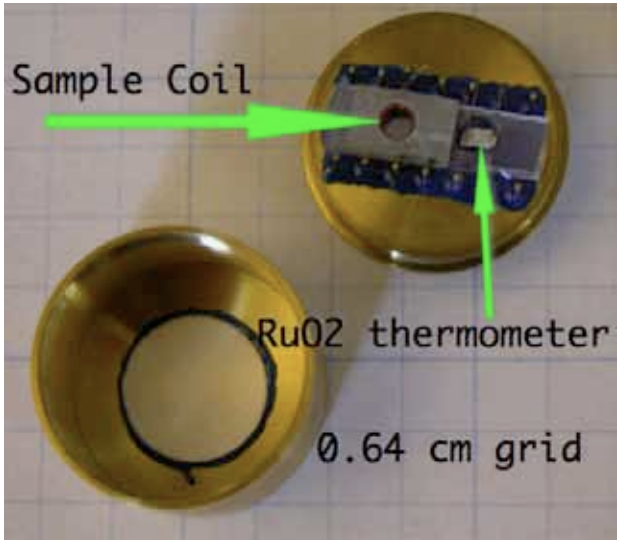

NHMFL phase changes diagnostics - 2

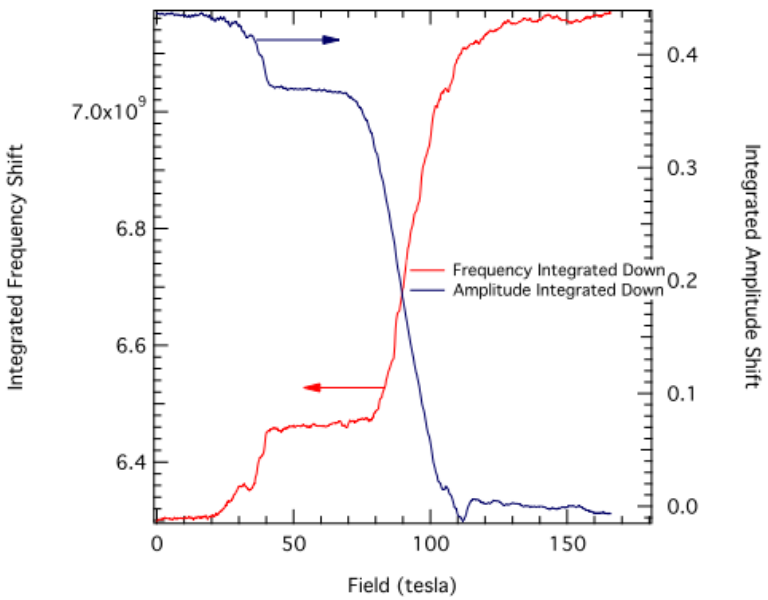

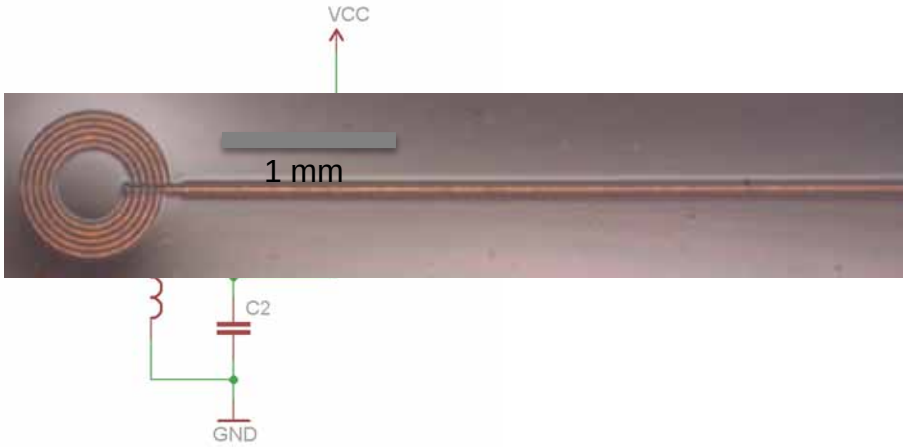

- New Contactless technique can be applied to materials in dynamic pressure experiments: Track Phase Changes
- Superconducting to normal state transition detected with new technique
- Colpitts Oscillator, tracks Frequency and Amplitude

Direction forward for ICE at NHMFL

- **Potential users**
  - Geologists
    - complete description of material properties in *P, T, ρ* space, off-Hugoniot
  - Metallurgists
    - study phase transitions off-Hugoniot
  - Weapons designers
  - …
- **NHMFL-ICE is economical**
  - Complete EOS from 0 to peak pressure in ONE shot
  - Can fire many shots per day

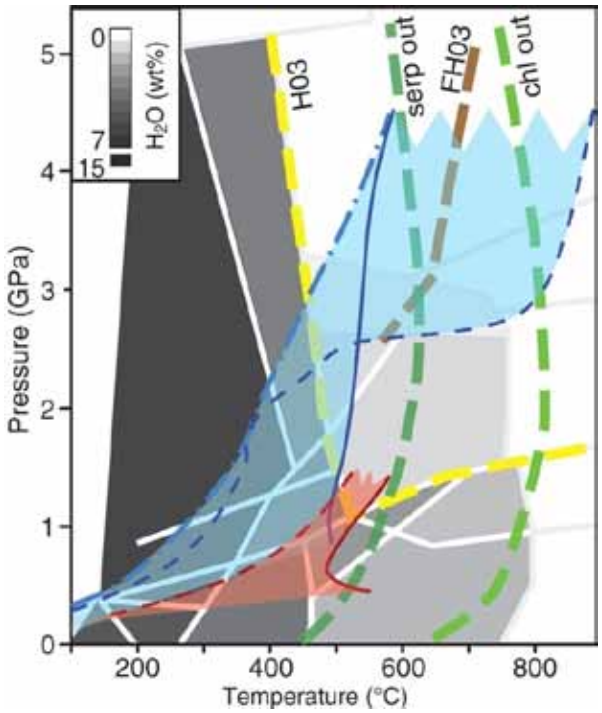

Predicted *P-T* paths for the subducted crust beneath central Alaska (blue shading) and Cascadia (red shading), over phase diagram for hydrated metabasalts of Hacker et al. (2003)

Acknowledgement

The authors are indebted to

C. Barnes

T. Taylor

D. Watkins

R. Martineau (C2)

energie atomique • energies alternatives

Recent Developments on the GEPI facility for isentropic compression experiments

Pierre-Yves CHANAL (CEG/DEA/SDMT/LMSA)

GEPI : Electric Generator for Intense Pressure

energie atomique • energies alternatives

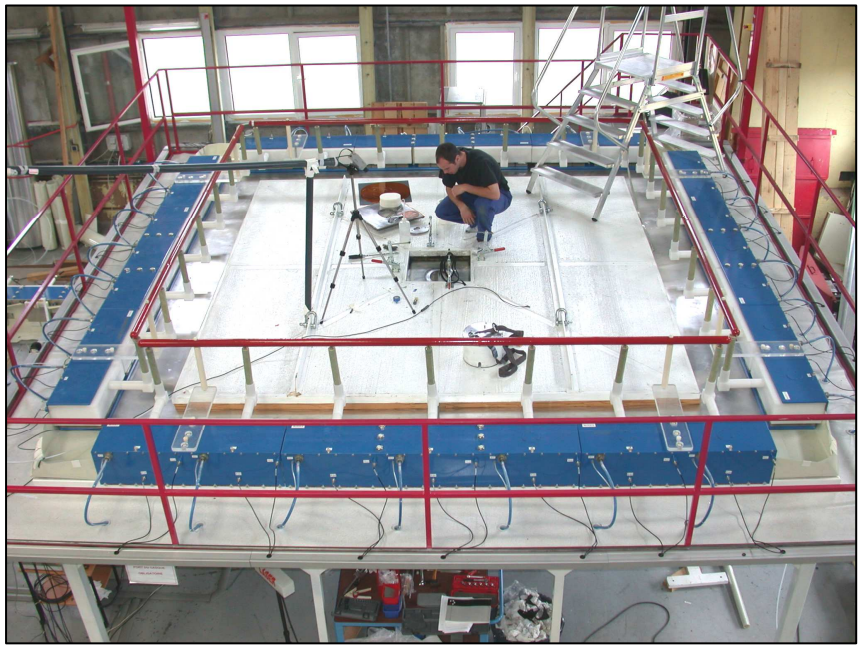

GEPI is a pulsed power generator mainly devoted to Isentropic Compression Experiments (ICE)

Objectives

- Analysis of material behavior under quasi-isentropic compression
  *pressure range : **0.1 GPa** to **80 GPa** (0.8 Mbar)*
- Launch of non-shocked flyer plates
  *velocitiy range : **1 km/s** to **> 8 km/s***

GEPI : strip line concept

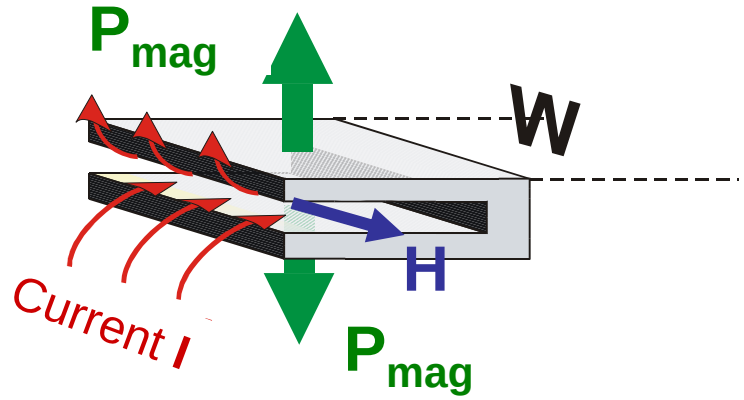

100 GPa = 1 000

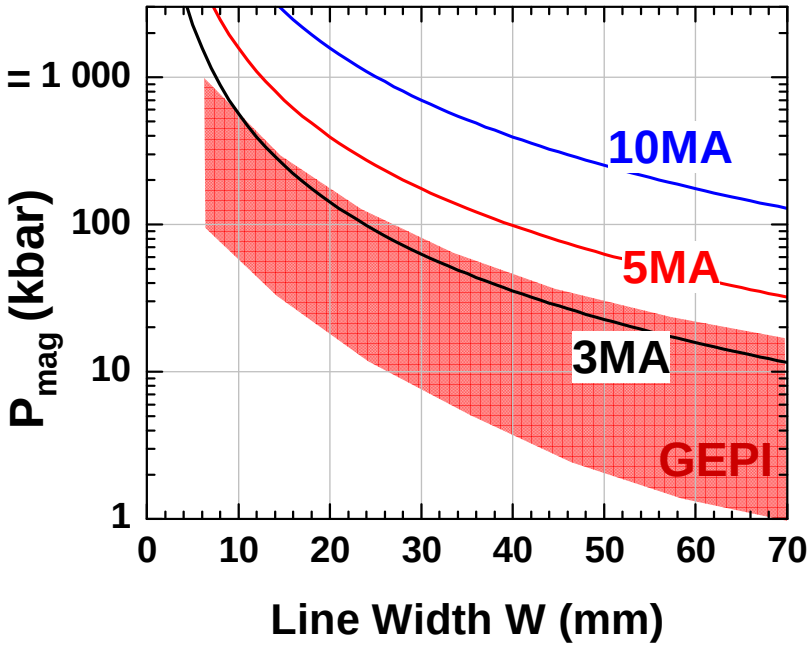

Theoretical magnetic pressure in the strip line :

$$P_{mag[kbar]} = k_p . \frac{1}{2} . \mu_o . H^2 = k_p . \frac{1}{2} . \mu_o . \left(\frac{I}{W} \right)^2$$

with
- k_p : edge effect coefficient
- μ_0 : free space magnetic permeability
- H : magnetic field
- W : strip line width

GEPI : general arrangement

energie atomique • energies alternatives

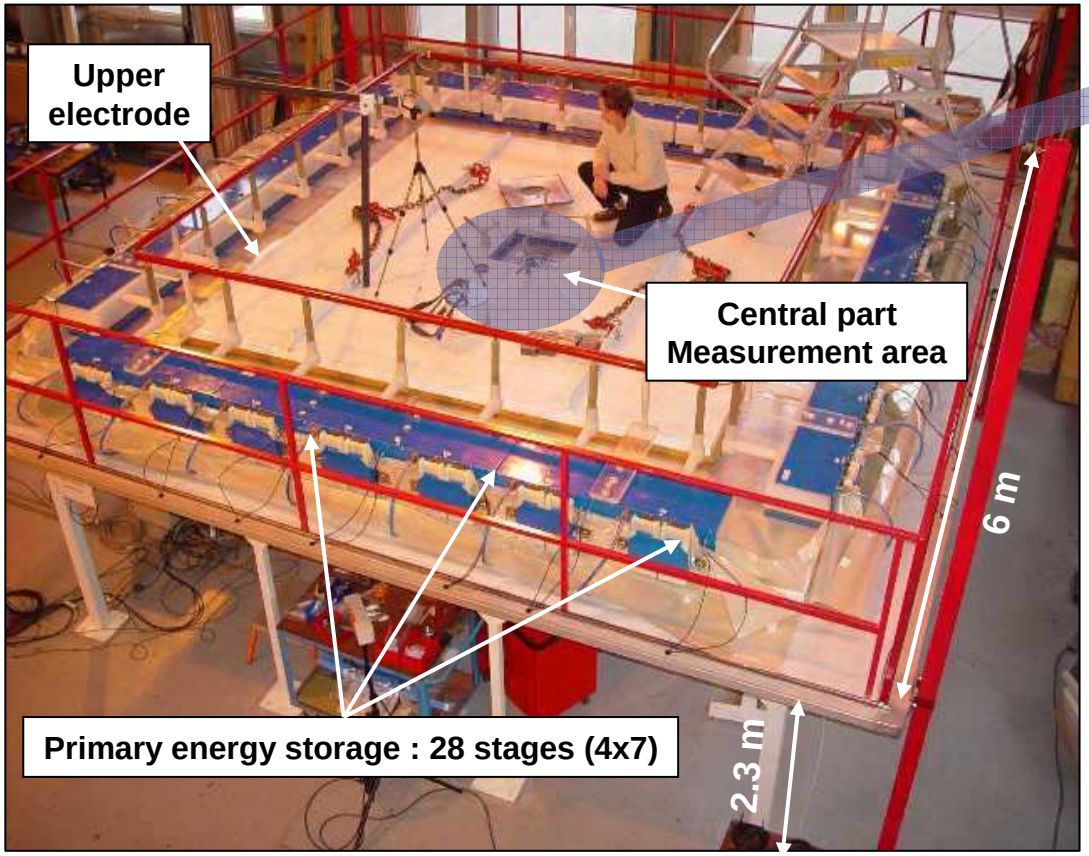

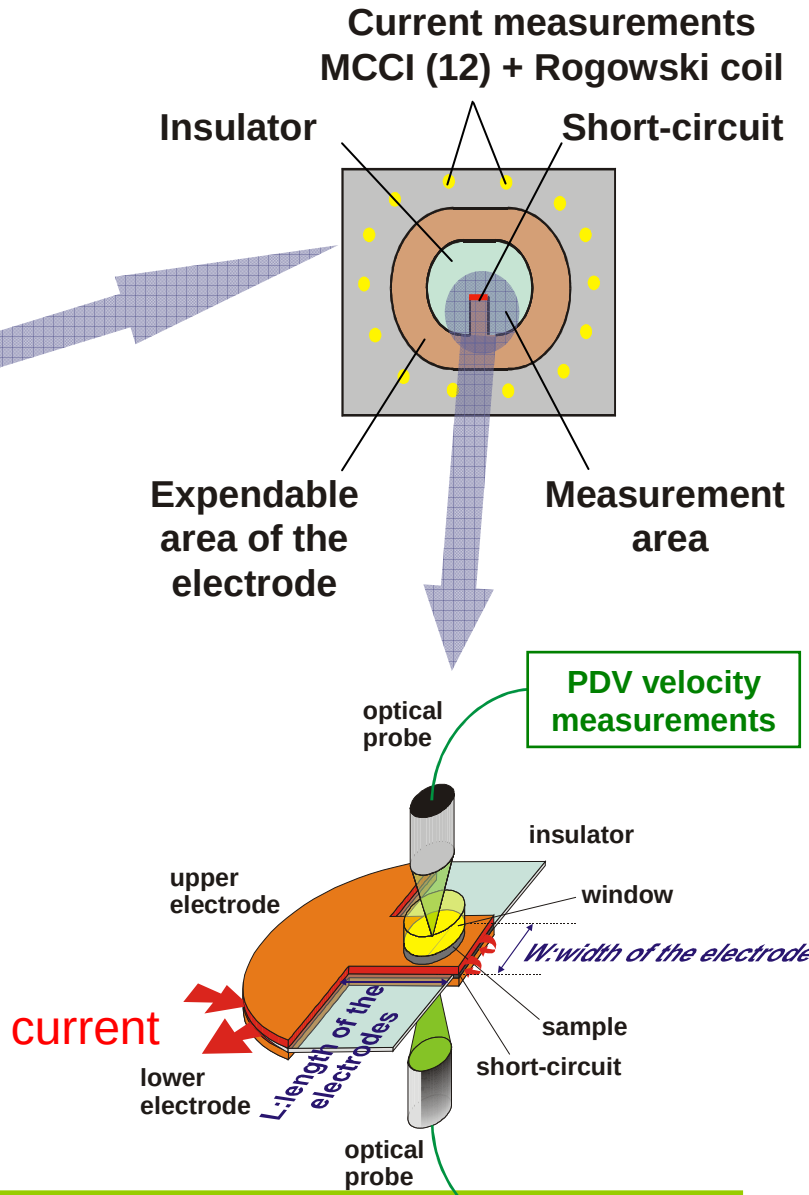

GEPI : technology & characteristics

energie atomique • energies alternatives

- **28** stages in parallel (may be disconnected 1 by 1)
- voltage : **70 to 85 kV**
- total stored energy : **70 kJ** (at 85 kV)
- dielectric insulation made with mylar & kapton films (low inductance)
- peak current : from <**1 to 3.3 MA** (depending of generator configuration) with **500-600 ns** risetime
- **peaking** capacitors (to « flatten » current ramp)

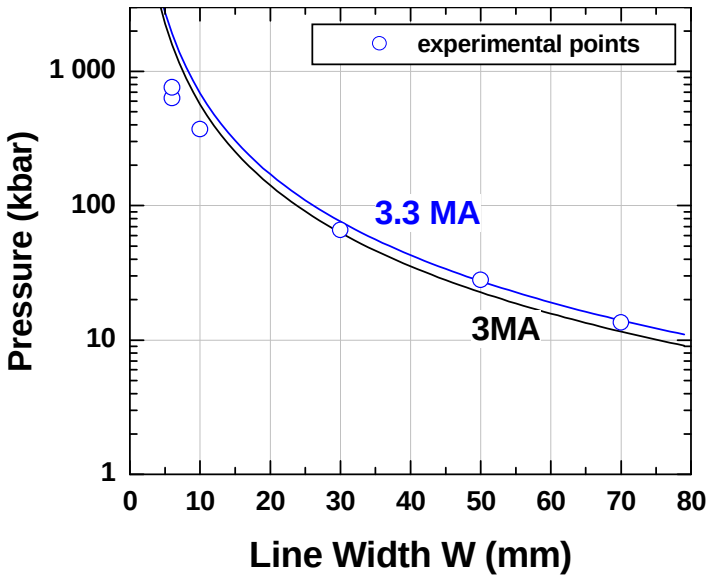

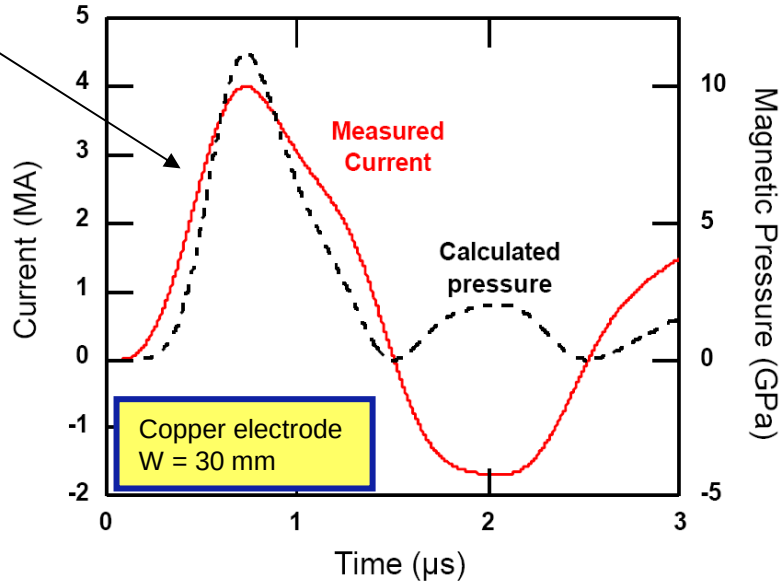

Edge effect and magnetic field diffusion in the strip line → **Decrease of the pressure compared to the ideal case**

GEPI : material behavior example

Isentropic loading of BPR300

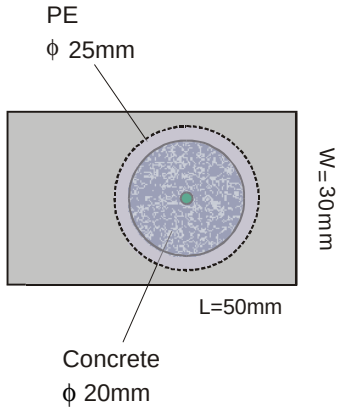

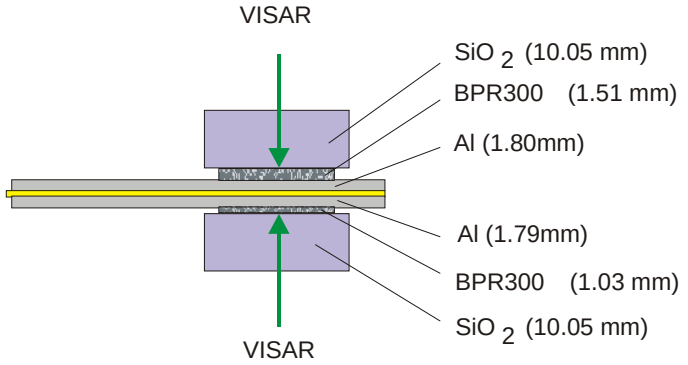

VISAR measurements

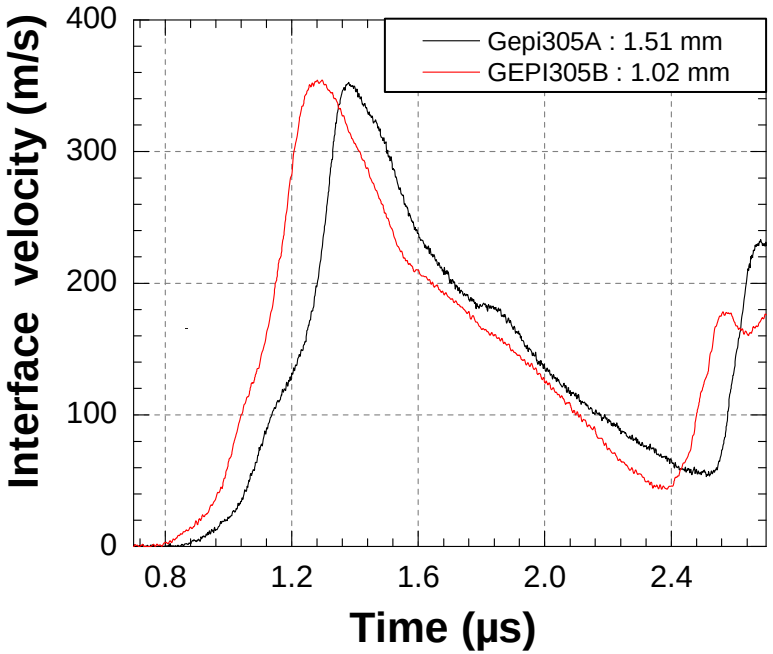

Lagrangian analysis

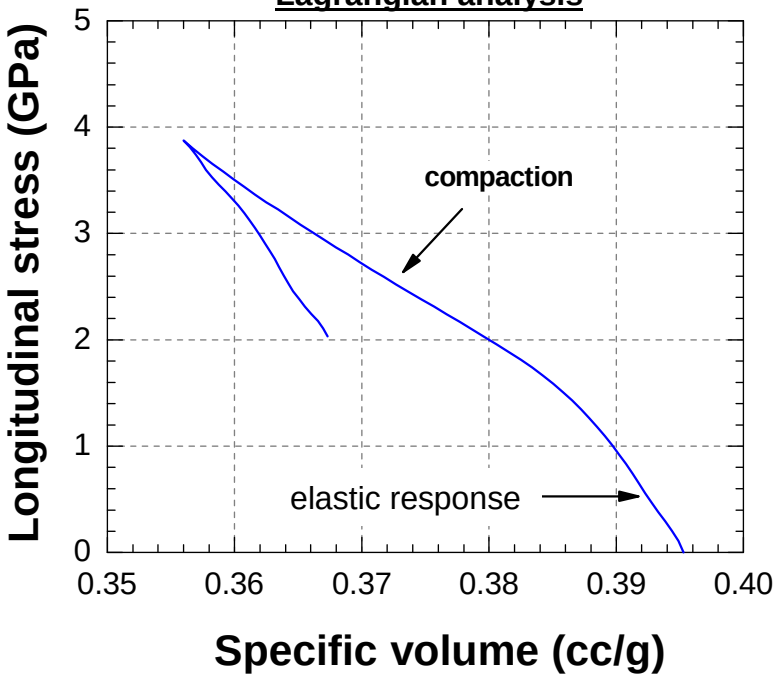

GEPI : material behavior example

energie atomique • energies alternatives

13 GPa polymorphic transition in Iron

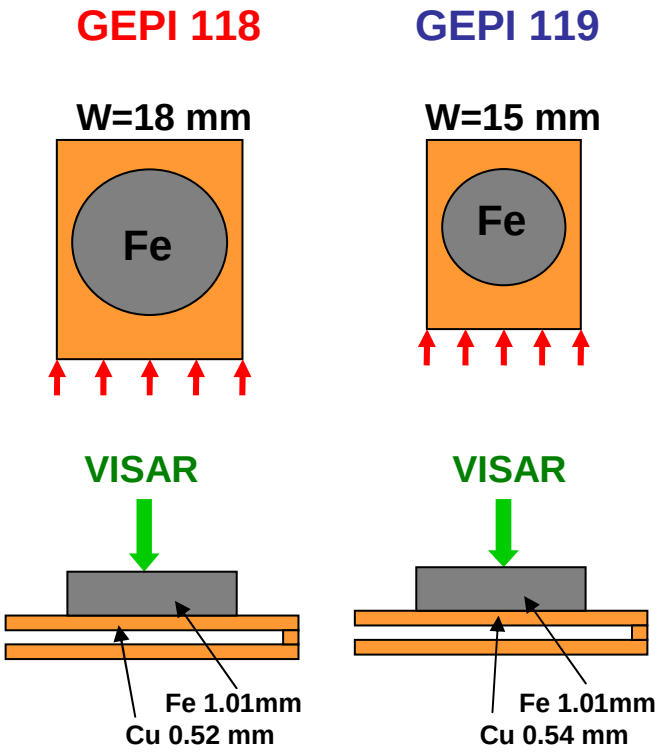

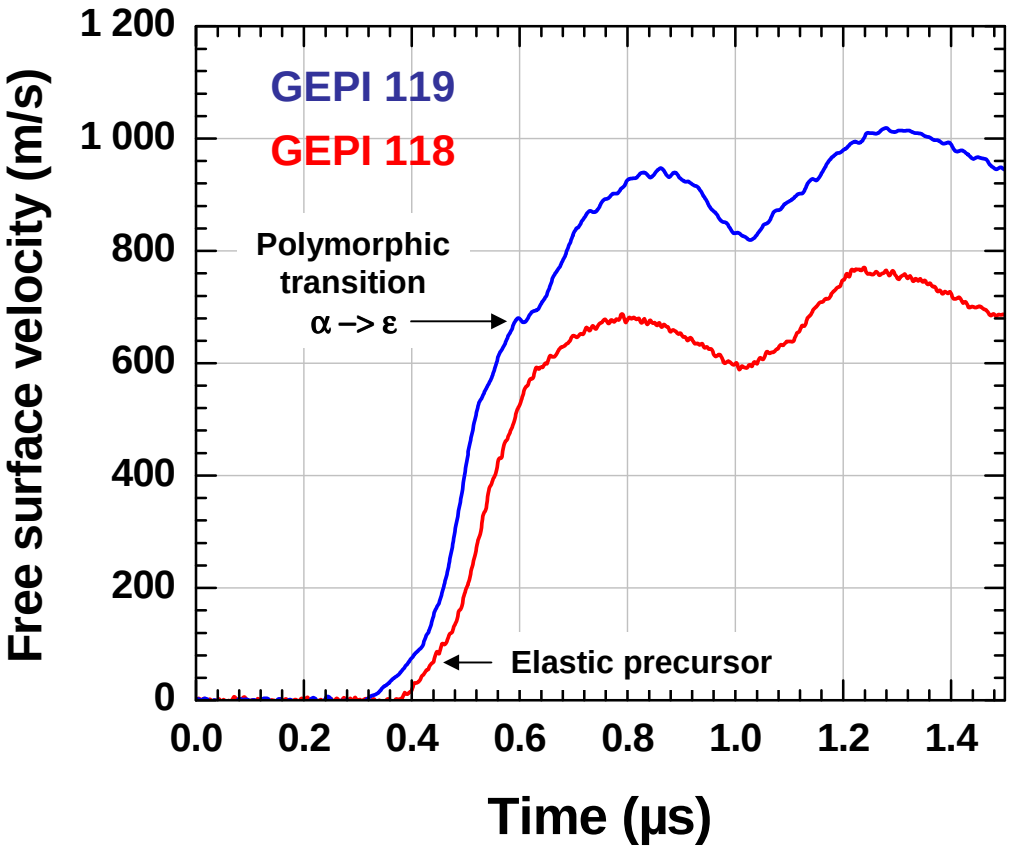

GEPI : recovered sample after spalling experiment

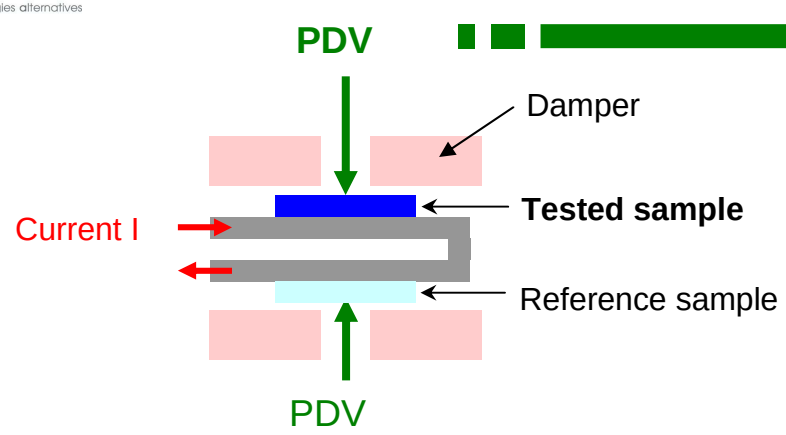

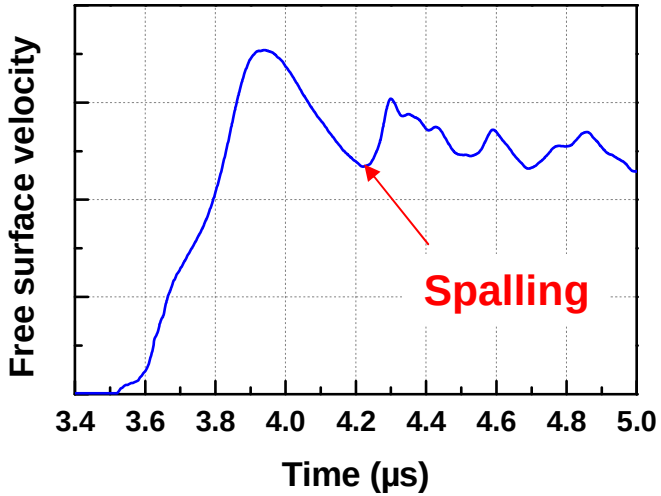

Crossed sections of the recovered **tested sample** after stress of several GPa (Xray µ-tomography)

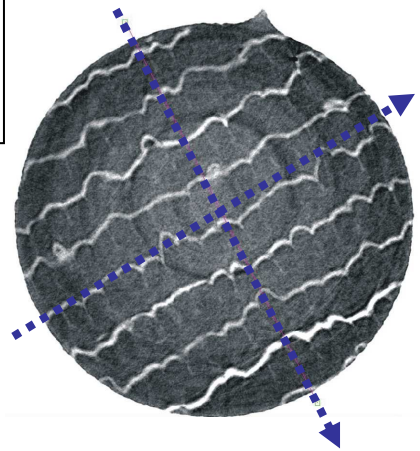

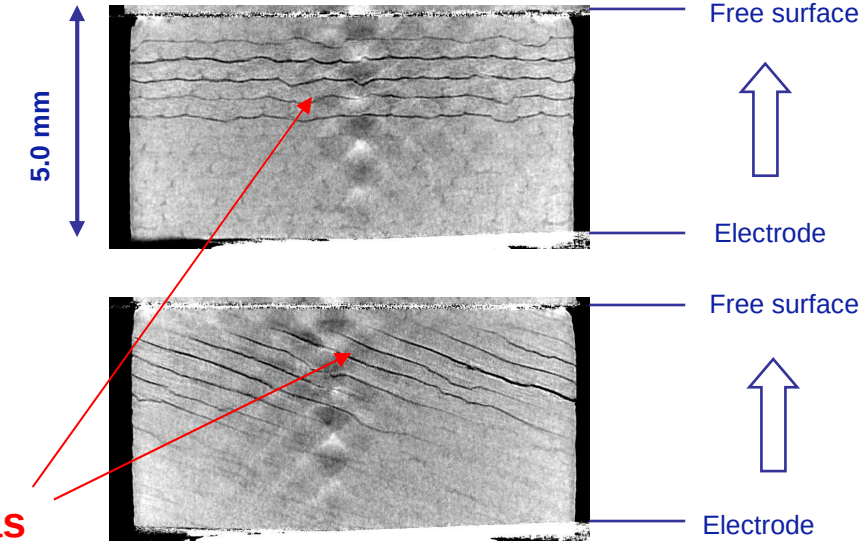

GEPI : non-shocked flyer plates potentialities

energie atomique • energies alternatives

GEPI 248

W=6 mm

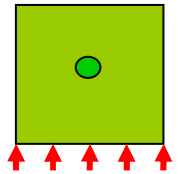

VISAR

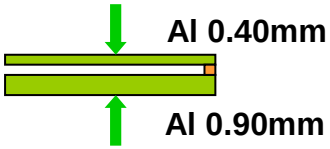

VISAR

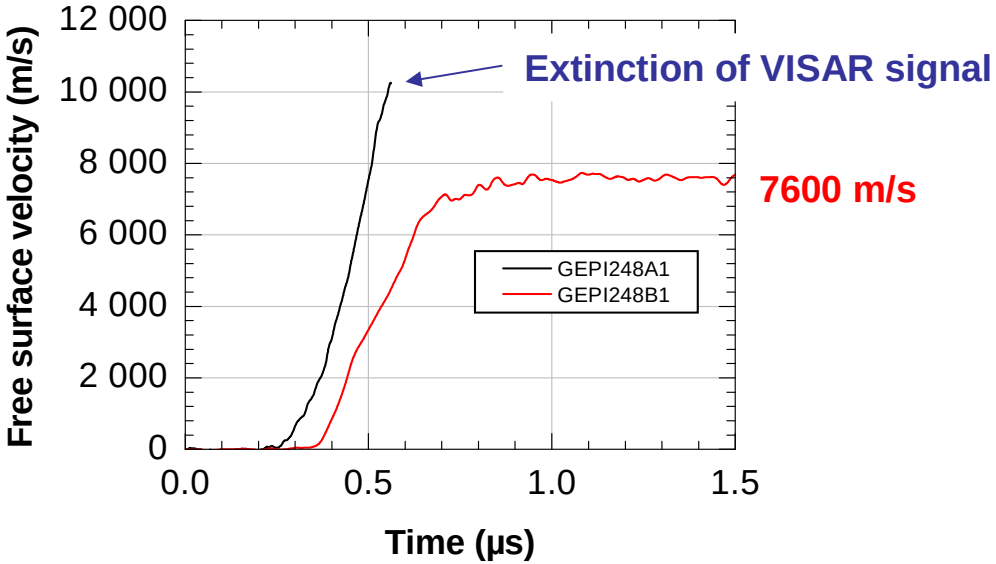

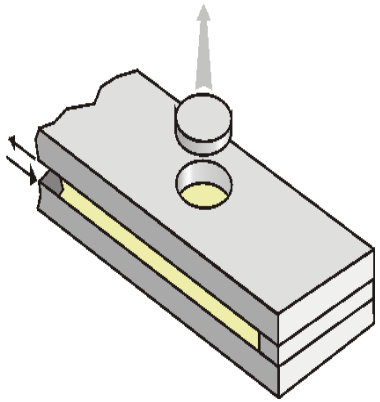

CEPAGE

Developed specifically for micro-detonic experiments

GEPI : load improvements

Strip line history

Type 1 (2001-2005)

Special features :
- Machined from a metal sheet
- Short circuit with 2 wires in parallel
- Compression of the 2 loads with PE blocks

Advantages :
- Good electrical contacts
- Length optimized

Drawbacks :
- Poor surfaces planarities and loads parallelism

Type 2 (2006-2007)

Special features :
- Machined from a plate
- Strip line screwed on an hexagonal plate (Veloce like)
- Short circuit with flashing (very good parallelism)

Advantages :
- Control of planarity and parallelism

Drawbacks :
- Electrical contacts not controlled
- Length not optimized

Type 3 (2008-2011)

Special features :
- Machined from a plate
- Circular upstream contact
- Short circuit with 2 linear pegs (Veloce like)
- 1mm step on the sides

Advantages :
- Control of planarity
- Good electrical contacts
- Length optimized
-Low current on the edges

Drawbacks : ?

GEPI : load improvements

Results with type 3 strip lines

energie atomique • energies alternatives

Free Surface Velocities for load types #1, #2 and #3

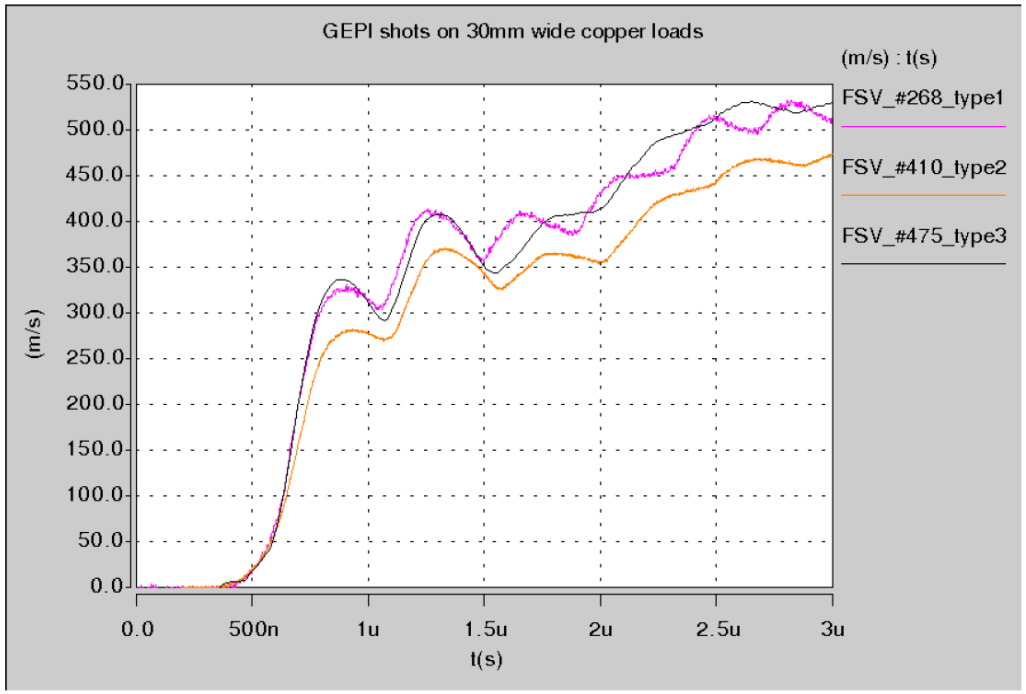

20% FSV improvement over type II due to:

- Decrease of the current on the sides
- Contacts improvement (upstream and downstream)
- Optimization of the length (slightly)

GEPI : load improvements

Type 3 strip lines : pressure homogeneity

energie atomique • energies alternatives

Along lateral axis
GEPI 475

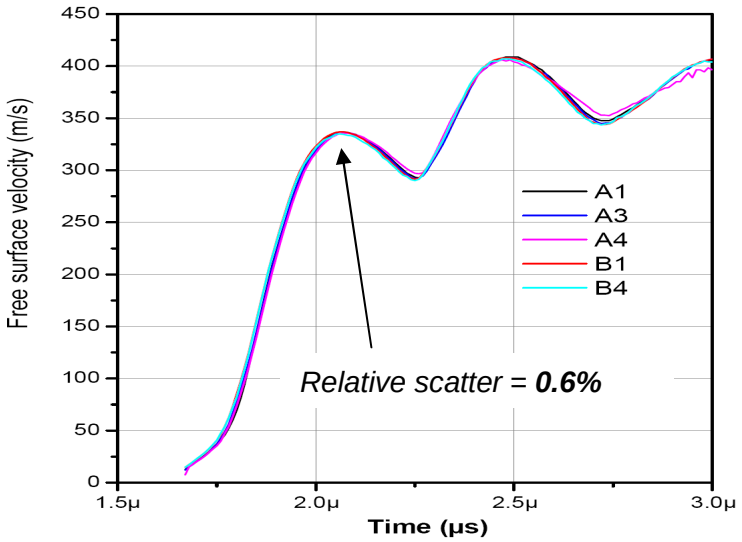

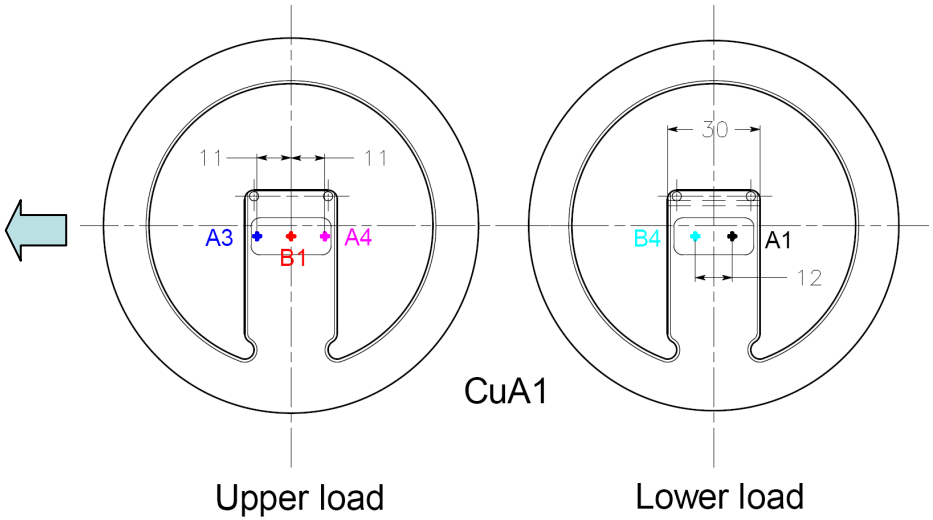

Along longitudinal axis
GEPI 476

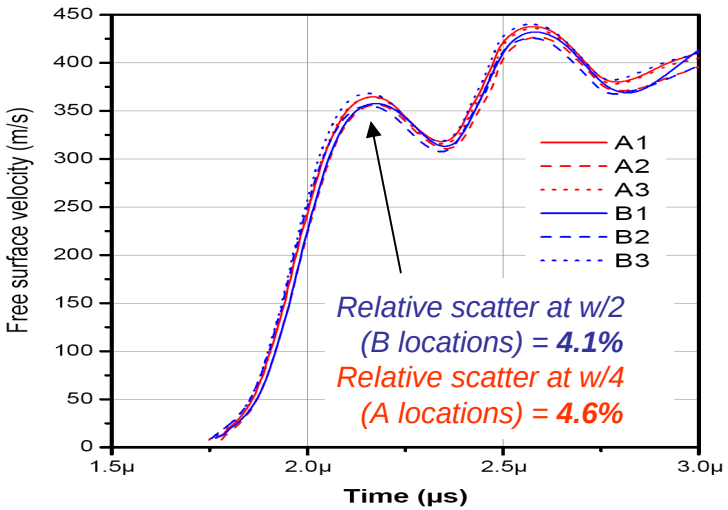

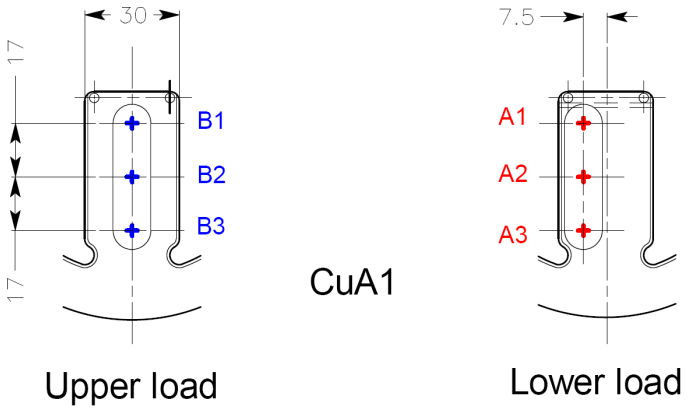

GEPI : load improvements

3D MHD simulations on LS-DYNA

energie atomique • energies alternatives

Development in LSDYNA by LSTC using the boundary elements method.

- **No air meshing.**

- **Actual limitations :**

- **Run on multi-processors**
- **Injection of an homogeneous current**
- **Lagrangian only**
- **1 phase only**

185 592 3D elements
114 572 brick (Emag)
23 592 BEM faces

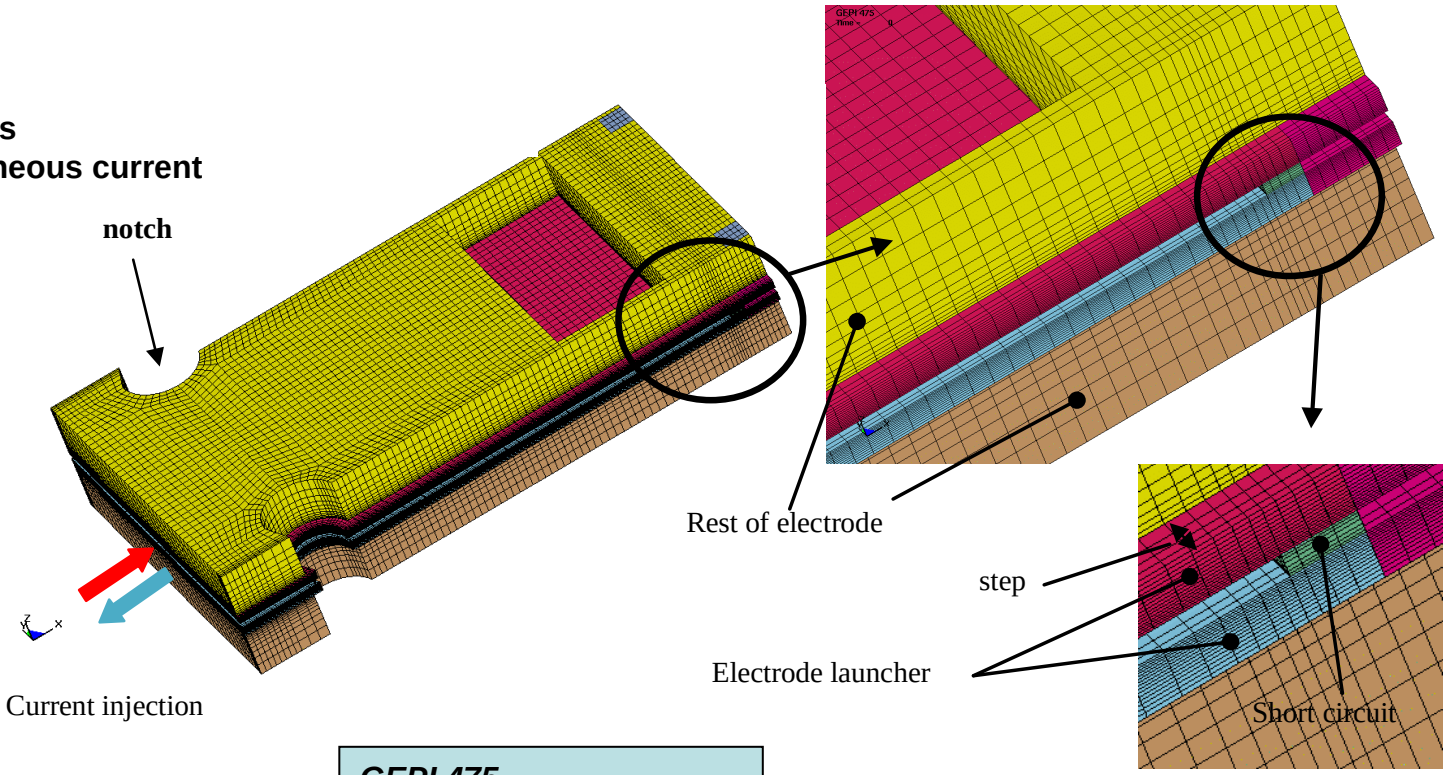

GEPI 475
Copper load
W = 30mm
Thickness = 1mm / 5mm

GEPI : load improvements

3D MHD simulations on LS-DYNA

energie atomique • energies alternatives

- **GEPI 475: free surface velocity (FSV) at different locations using the experimental current as input.**
- **Rather good agreement in term of peak FSV (no tunable parameters used)**

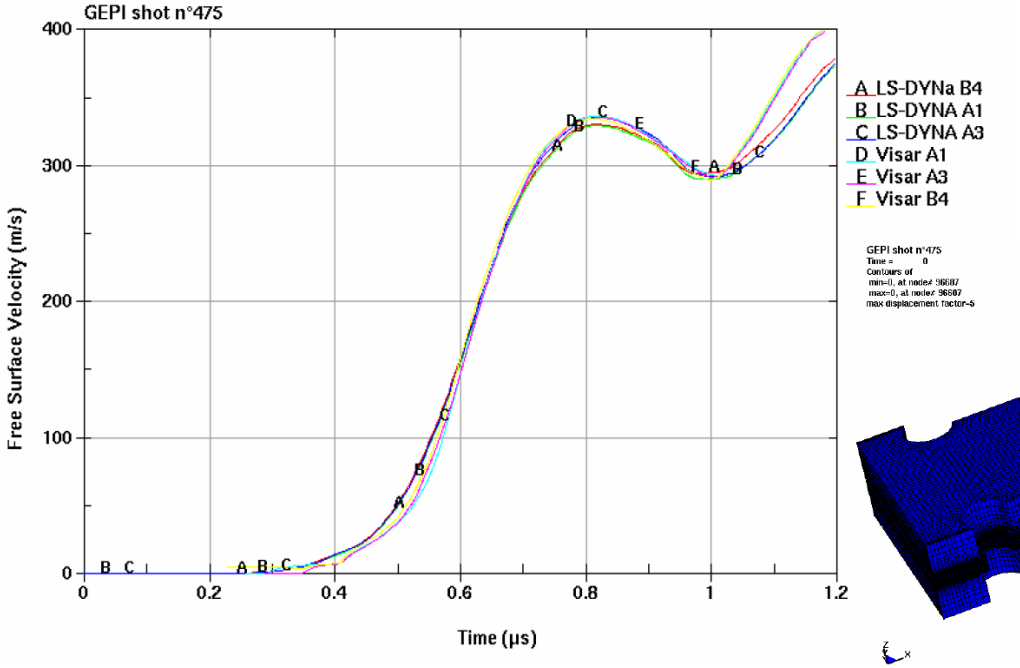

GEPI 475
Copper load
W = 30mm
Thickness = 1mm / 5mm

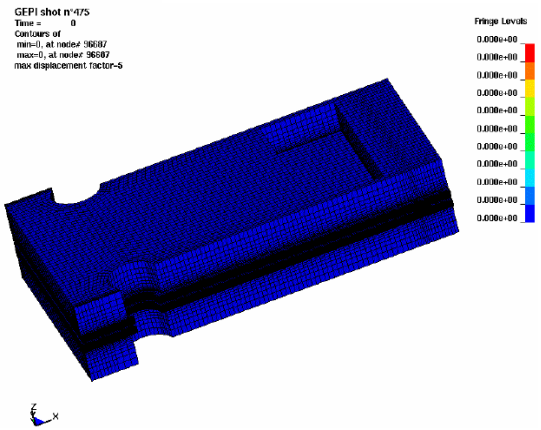

- *Le Blanc G., Petit J., Chanal P.-Y., L'Eplattenier P. and Avrillaud G., Modelling the Dynamic Magneto thermomechanical Behaviour of Materials using a Multi-phase EOS, 7th European LS-DYNA® Conference, Salzburg, Austria, May 14-15th, 2009.*
- *Le Blanc G., Chanal P.-Y., Héreil P.-L., Laporte P., Avrillaud G., Vincent P. and L'Eplattenier P., Ramp Wave Compression in a Copper Strip Line : Comparison Between MHD Numerical Simulations (LS-DYNA®) and Experimental Results (GEPI device), 10th International LS-DYNA® Users Conference, Dearborn, MI, USA, June 8-10th, 2008.*

P_{mag} homogeneity - Experimental results

Reproducibility tests

energie atomique • energies alternatives

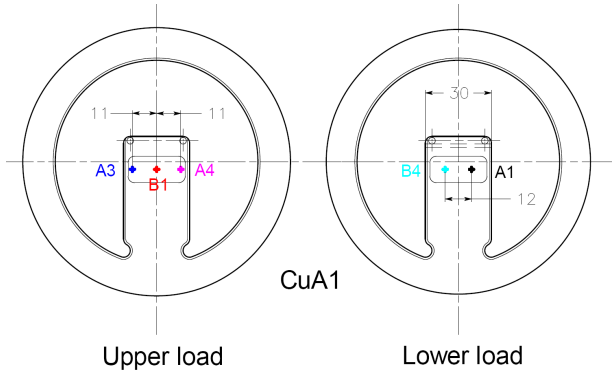

Type 3 stripe lines - CuA1 - W30
80 kV - 28 generators

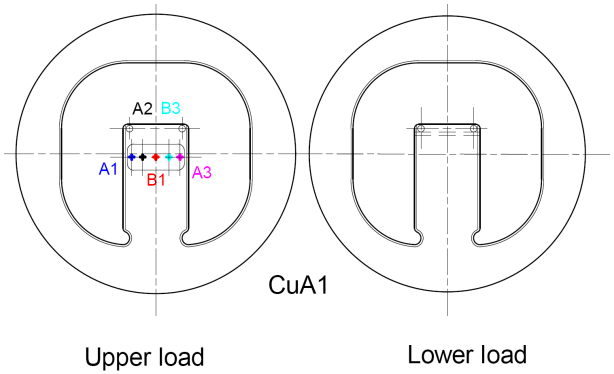

GEPI 475
($I_{mcci\ max}$ = 3.20 MA)

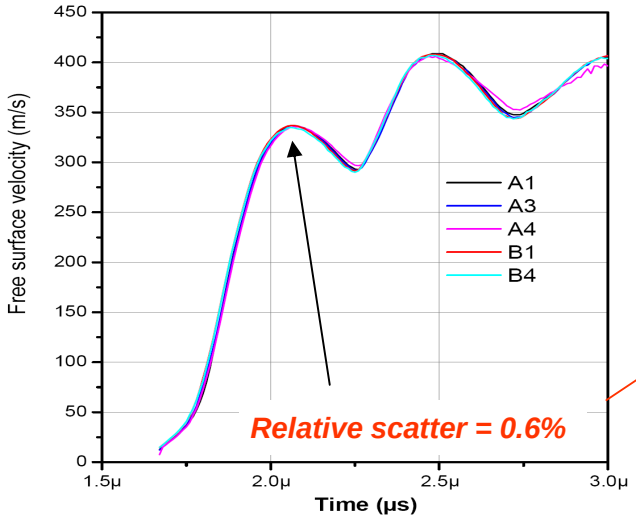

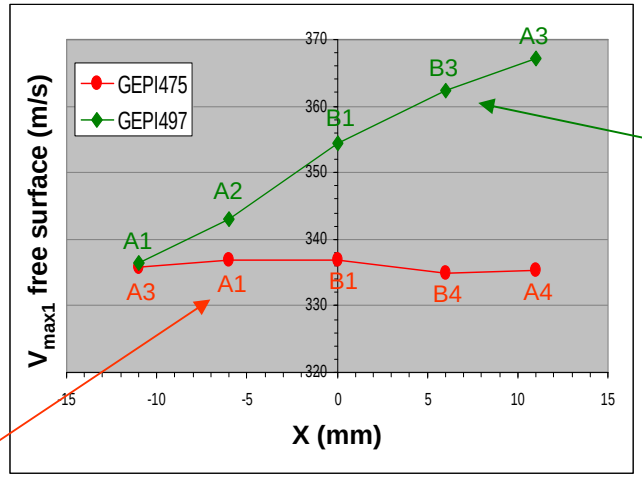

GEPI 497
($I_{mcci\ max}$ = 3.32 MA)

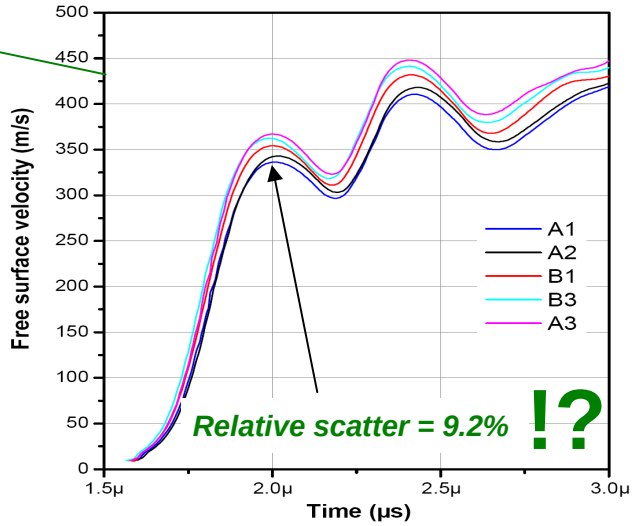

P_{mag} homogeneity – LS-DYNA® simulations

energie atomique • energies alternatives

Angular variation around center

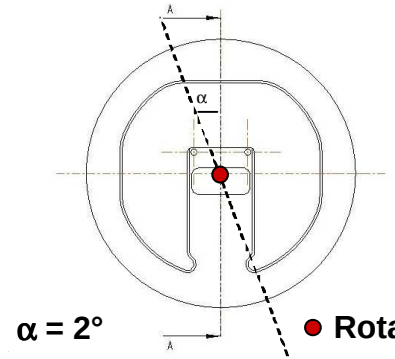

α = 2° Rotation center

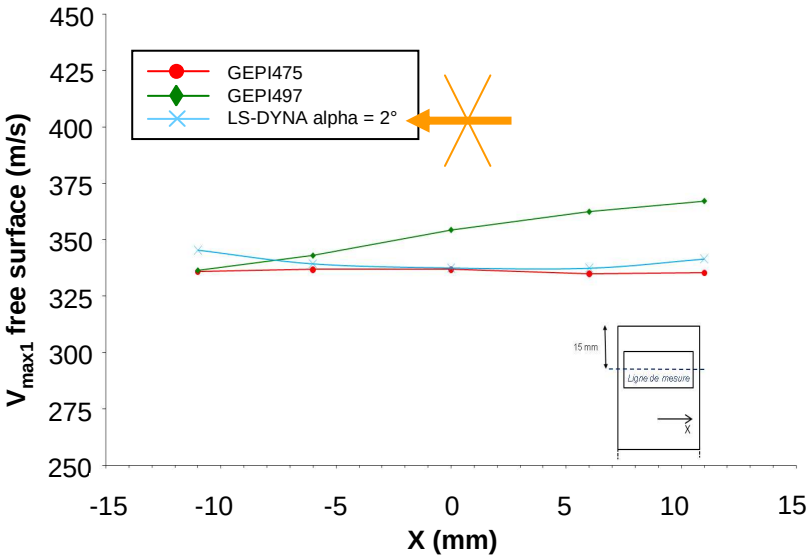

Angular variation around longitudinal axis

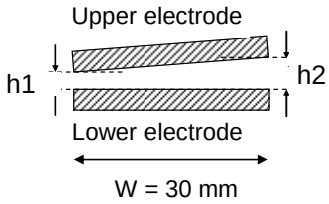

Delta gap = h2 – h1
with h1 = 0.5 mm

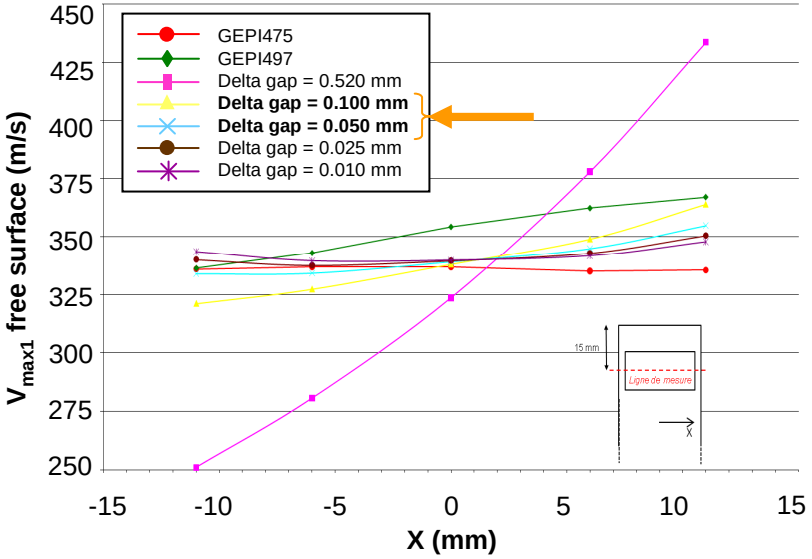

Optimisation of
- **assembly process**
- **strip line's machining process for surfaces planarities and parallelisms improvement (short-circuit, strip lines lower faces, ...)**

Diagnostics

energie atomique • energies alternatives

PDV-IDF interferometers

- Routinely used on GEPI since 2007 ~~(VISAR)~~
- Velocity error : << 1%
- Developments for V > 8000 m/s
- Miniaturisation
- 12 systems in January 2011

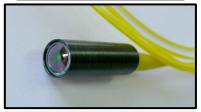

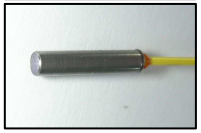

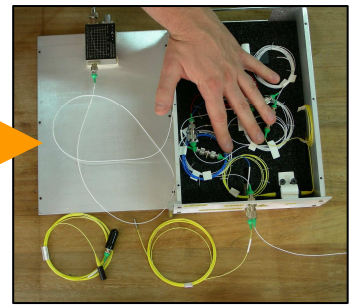

Ex. : multipoint measurements on a flyer experiment (GEPI 575)

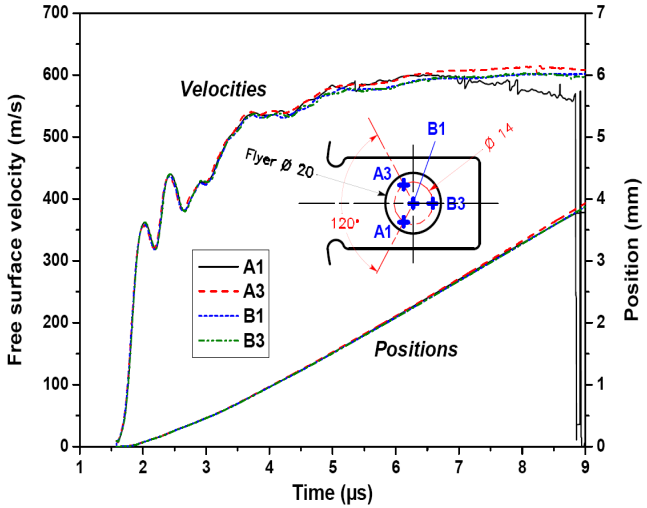

« Low temperature » pyrometry integration

- Electromagnetic noises problems resolved in July 2009
- **Optical noises problems still to be adressed**

- *Lefrançois A., Chanal P.-Y., Le Blanc G., Petit J., Avrillaud G. and Delchambre M., Flyer Plate Developments on Two High Pulsed Power Generators Based on a Strip Line Design (GEPI and CEPAGE), 15th International Symposium on Electromagnetic Launch Technology, Paper No. 277, Brussels, Belgium, May 17-20th, 2010., IEEE Trans. Plasma. Sci., Special Issue Jan. 2011.*
- *Chanal P.-Y. and Luc. J., Development of Fibered Velocity Interferometers for Dynamical Material Behaviour Studies, 60th Aero Ballistic Range Association Meeting, Baltimore, MD, USA, September 20-25th, 2009.*

Polymorphic transitions

energie atomique • energies alternatives

- Study of kinetics of phase transitions … to test the available multiphasic EOS models

- GEPI to access thermodynamics fields non explored with shock experiments
- Sn as a model material

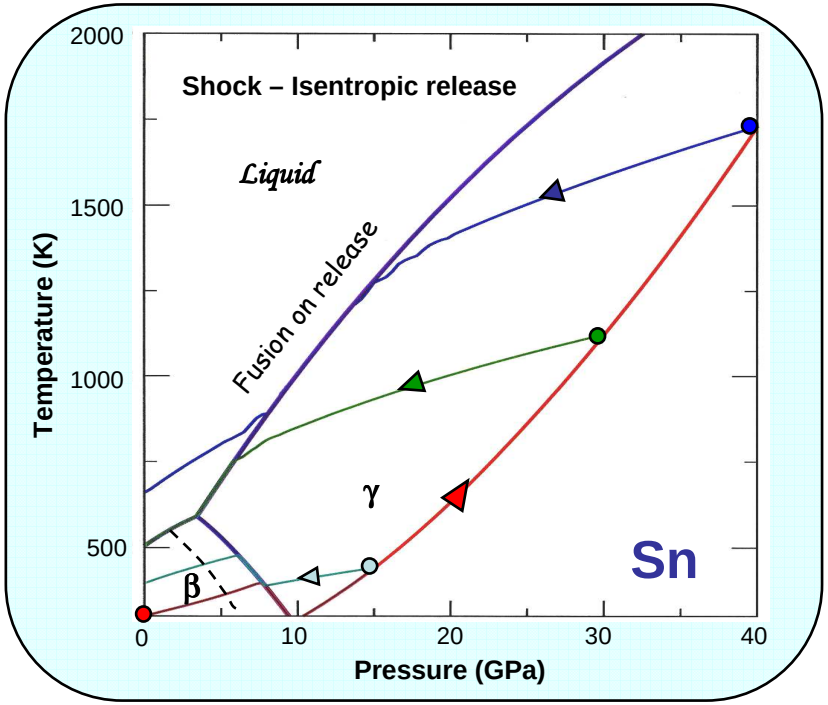

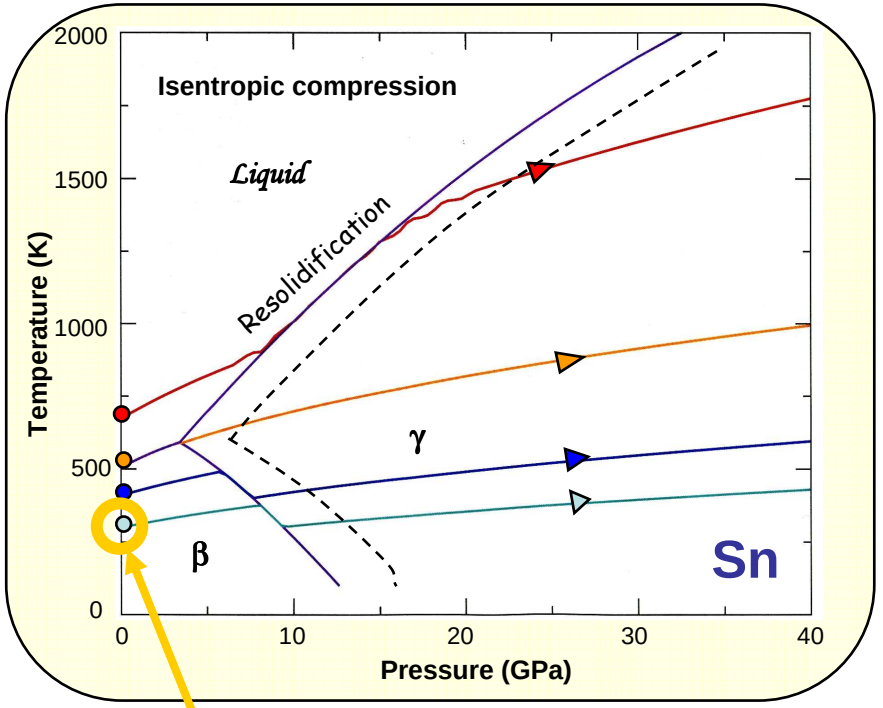

Preliminary experiments with different Sn grades

Sn polymorphic transitions

Examples with initial pole at T_{amb}

energie atomique • energies alternatives

GEPI 548

80 kV, 28 generators

Al2017 strip line, W20 mm

$I_{mcci\ max}$ = 2.91 MA

Sn 9N4 (99.99%)

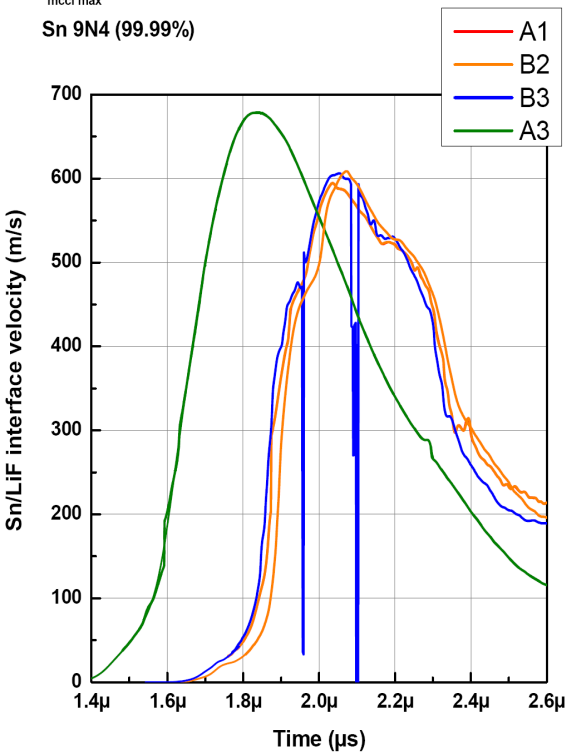

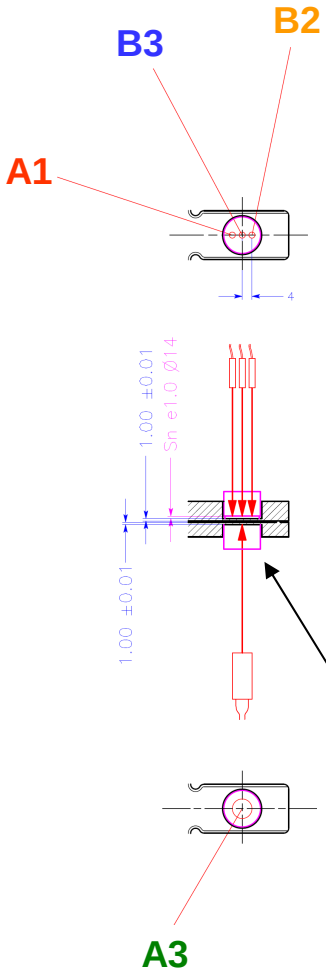

LiF(100) windows without (GEPI548) or **with (GEPI570)** reflective coating

GEPI 570

80 kV, 28 generators

Al2017 strip line, W20 mm

$I_{mcci\ max}$ = 2.85 MA

Sn 9N3 (99.93%)

Polymorphic transition β-γ (at ~ 9 GPa)

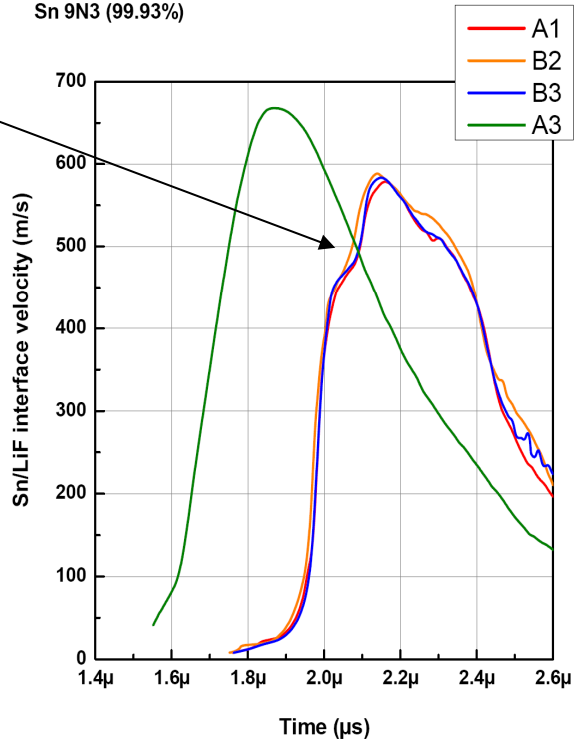

Pre-heating system development

Some specifications

- Metallic samples (Cu, Fe, Sn)
- $T_{sample\ max.}$ minimal : 800 K (527 °C)
- $T_{sample\ max.}$ nominal : 1200 K (927 °C)
- T_{sample} homogeneity : ± 10 K
- Regulation of T_{sample} at ± 20 K around specified temperature
- T_{sample} known at ± 5 K before shot
- Material interfaces < 10 µm
- Integration of velocimetric (PDV-IDF) and « low temperature » pyrometric diagnostics
- Low cost of consumable parts
- Limited modifications of central parts of GEPI

Pre-heating system development

Inductive heating system : design & optimization

- **Magneto-dynamic / thermic coupling with ANSYS**
- **Optimization of sample / induction coil coupling**
- **Study of multispires solutions**

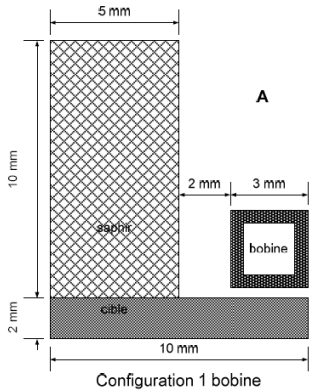

Configuration 1 bobine
Diamètre cible = 20 mm

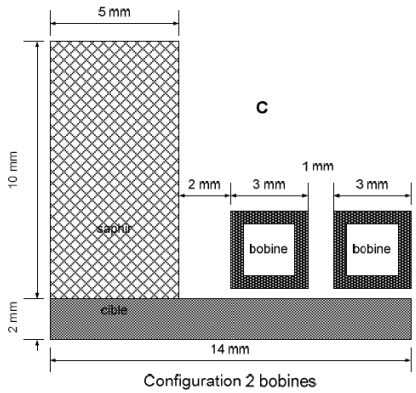

Configuration 2 bobines
Diamètre cible = 28 mm

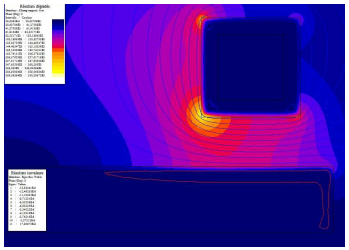

Cu sample
Gap 1,5mm
200kHz

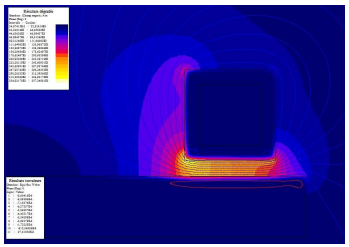

Cu sample
Gap 0,5mm
200kHz

Strip lines

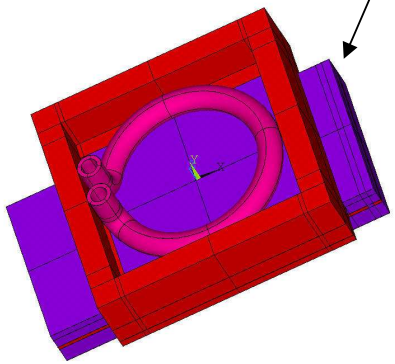

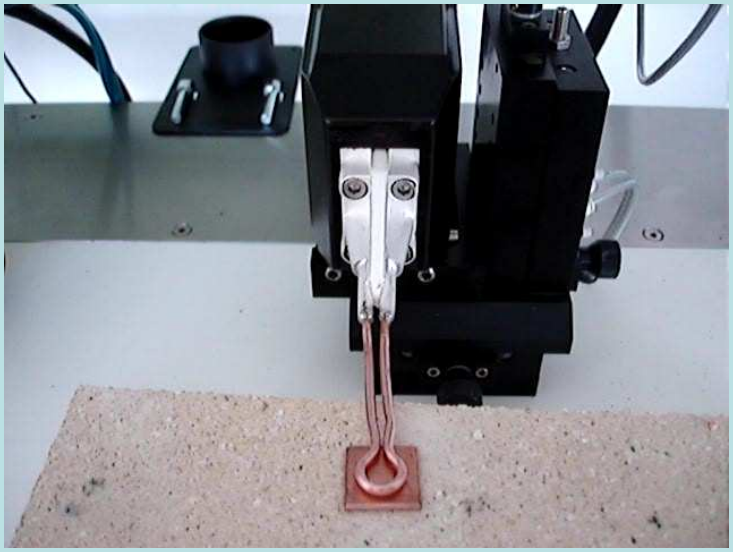

Test of a 6 kW generator

-Cu sample

- 20 x 20 x 2 mm^3
- Monospire coil
- Frequency 900kHz

T_{sample} ~ 1200K in 15s

Pre-heating system development

Optimization of heating cycle

energie atomique • energies alternatives

- **3D thermic modelling example :**

- W40 mm Al strip line
- Fe sample 40 x 40 x 3 mm^3
- Kapton & ceramic dielectric/ thermic insulator between strip lines
- Ceramic thermic insulator between sample & strip line

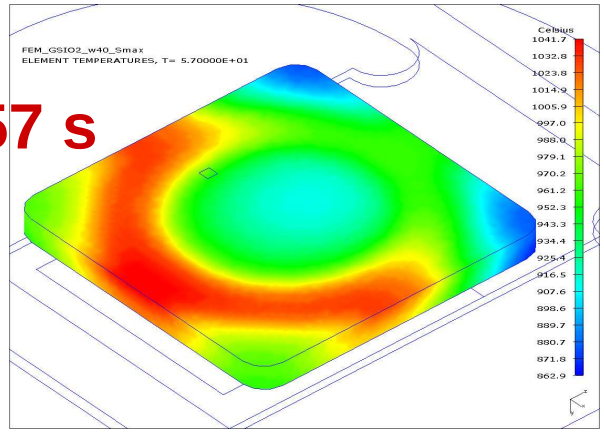

Sample upper face temperature

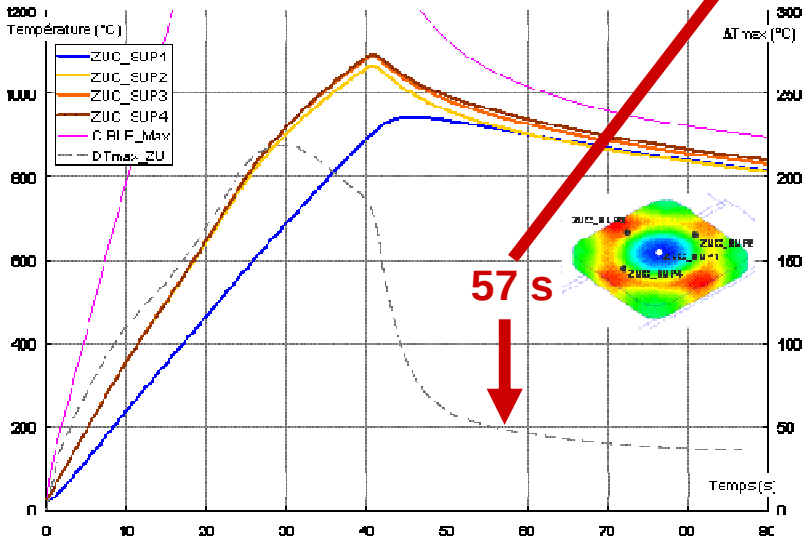

Sample lower face temperature

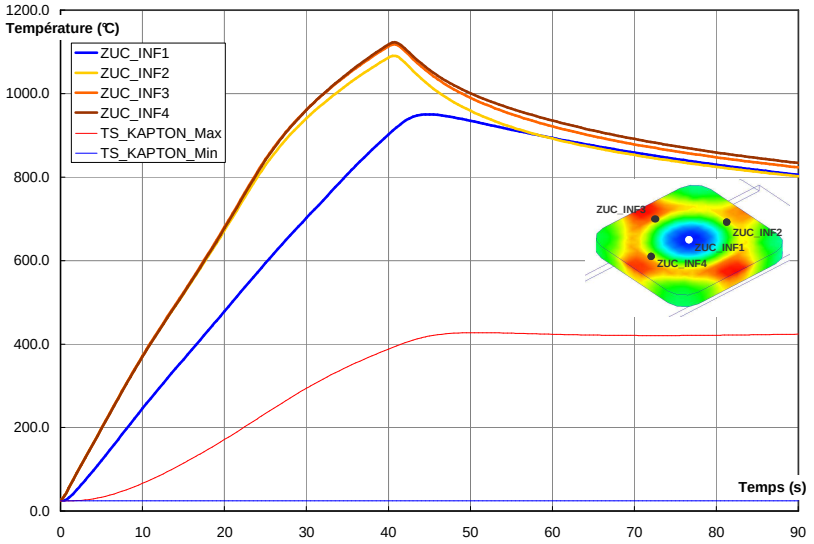

Pre-heating system development

Ceramic choice : thermal and dynamical properties

- **Material for thermal insulation between sample and strip line**

• Lowest thermal conductivity
• Highest elastic limit
• « Simple » dynamical behaviour for ease of numerical simulations
• Resistance to thermal shock

Zircone (ZrO_2) → **Pyroceram 9606** → **Alumine (Al_2O_3) [Coors AD995]**

Good thermal properties …
… but a complex phases diagram

Poorest thermal properties …
… but a much more simple phases diagram

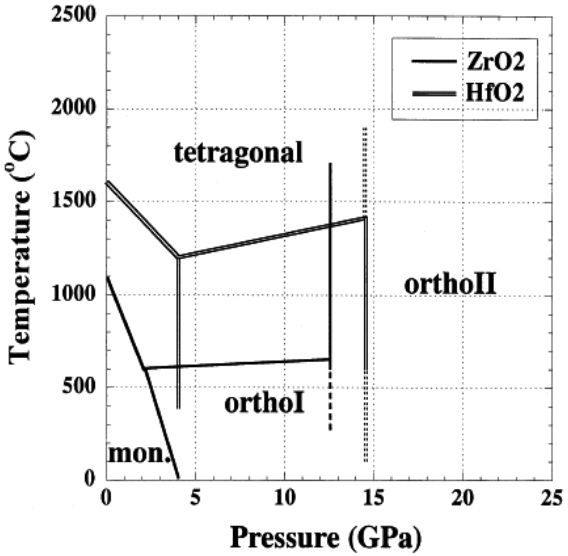

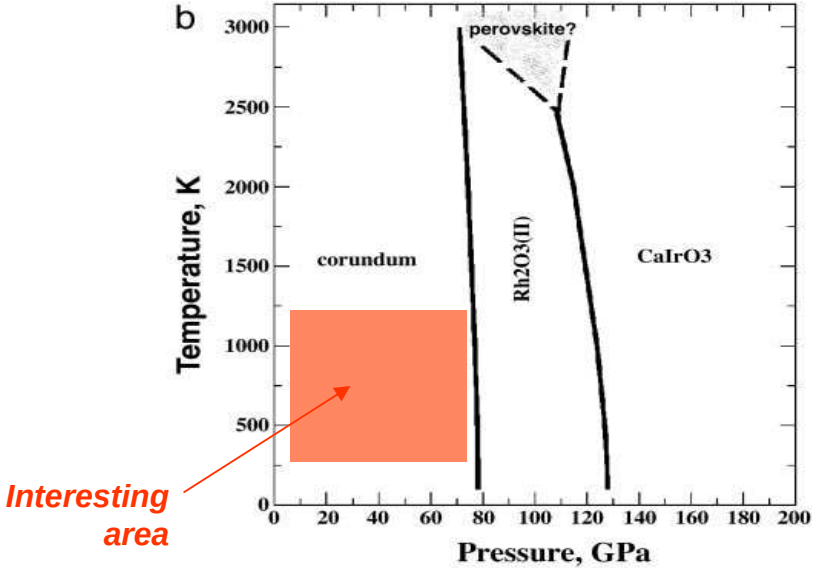

Interesting area

Pre-heating system development

Ceramics choice : dynamical properties

energie atomique • energies alternatives

- **Example of 1D-MHD numerical simulations (UNIDIM lagrangian code)**

• Influence of ceramic and sample thicknesses on sample/Lif interface velocity (shock formation ?)
• Observation of Al_2O_3 « special » behaviour
• Al2017 strip line, W 20mm, T_{amb} = 300K
• Current from GEPI tests at W 20mm

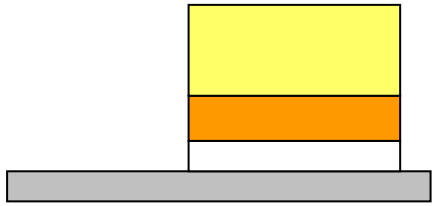

LiF (window)

Cu (sample)

Al_2O_3 (thermal insulation)

Al2017 (strip line)

LiF	**e = 10 mm**
Cu	**e = 1, 3 or 5 mm**
Al_2O_3	**e = 1 mm**
Al2017	**e = 1 mm**

AFvarepCu_vinterCuep1
AFvarepCu_vinterCuep3
AFvarepCu_vinterCuep5

AFvarepAl3_vinterAlOep1
AFvarepAl3_vinterAlOep3
AFvarepAl3_vinterAlOep5

LiF	**e = 10 mm**
Cu	**e = 1 mm**
Al_2O_3	**e = 1, 3 or 5 mm**
Al2017	**e = 1 mm**

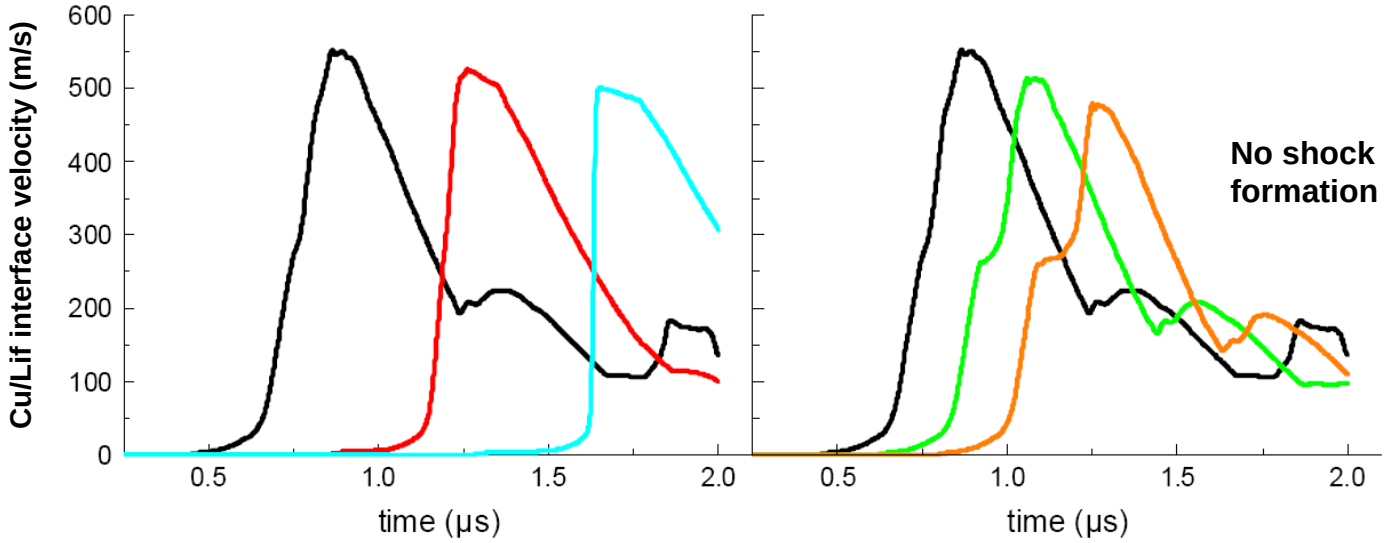

Pre-heating system development

Diagnostics integration

energie atomique • energies alternatives

Sample temperature measurement before shot with IMPAC IPE140-MB10 pyrometer

Velocity interferometric diagnostic (PDV-IDF)

« Low temperature » pyrometric diagnostic (C. Chauvin)

Not the actual pre-heating system configuration

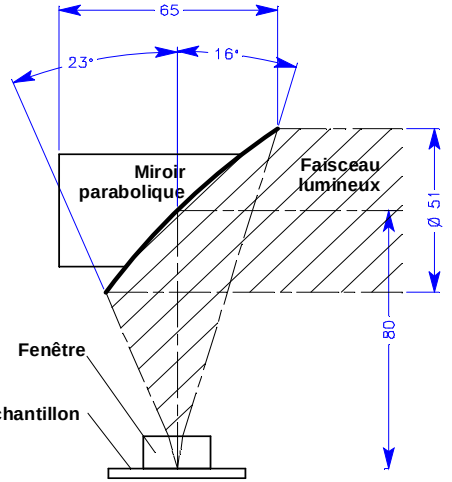

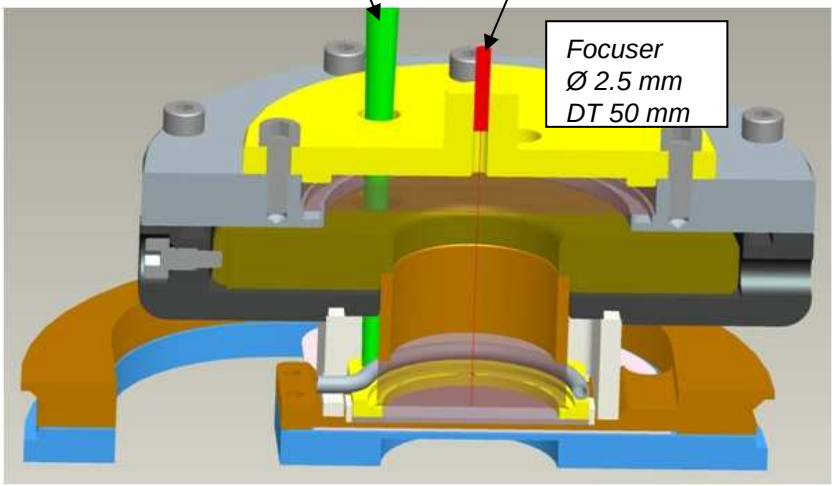

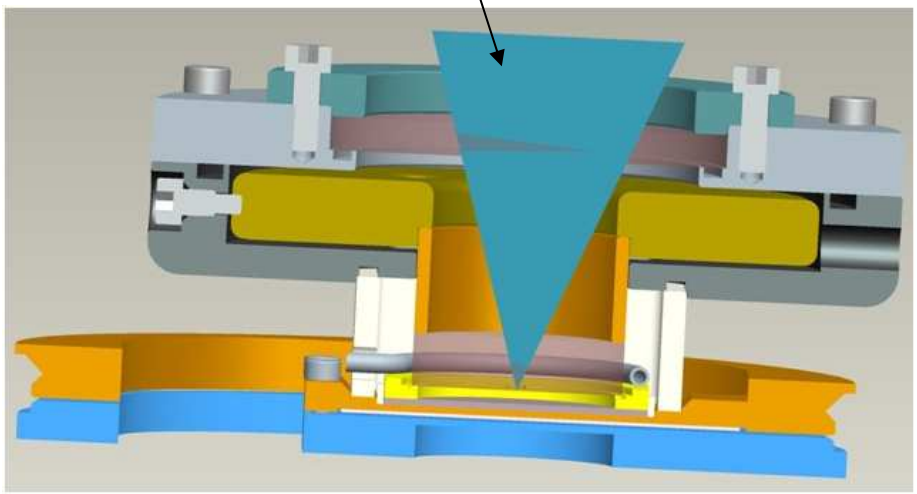

Pre-heating system development

To conclude …

- A prototype is available for static tests
- Integration to GEPI will be done in 2011
  - Modification of central terminal parts
  - Upgrading of generator's command & control systems
- To test, verify ….and resolve
  - T_{sample} max,
  - T_{sample} homogeneity
  - Configuration for liquid samples (Sn)

and also …

- Thermal dilatations between materials
- Thermal shocks in window's materials (LiF, …)
- Velocimetric and pyrometric diagnostics on high temperature samples
- PDV-IDF for material's dilatation measurement (?)
- Material interfacing solutions
- Bonding solutions
- Ceramic materials choices (thermal & dynamical behaviour)
- etc.

Lawrence Livermore National Laboratory

Estimating the Energy Dissipation and Entropy in a Ramp Wave

Roger W. Minich and Daniel Orlikowski

4th Workshop on Ramp Compression

January 18-19, 2011

Albuquerque, NM

Lawrence Livermore National Laboratory, P. O. Box 808, Livermore, CA 94551

This work performed under the auspices of the U.S. Department of Energy by Lawrence Livermore National Laboratory under Contract DE-AC52-07NA27344

UCRL-XXXX-12345

Introduction: The evolution of tailored stress waves.

I. **Motivation: Why study ramp waves?**

II. **Characterizing a ramp wave: Is it a simple wave?**

III. **Experimental Observations: Scaling laws.**

IV. **Theory: Scaling laws point to symmetries and constraints of dynamical system. Geometrical interpretation.**

Symmetry is a powerful constraint for modeling and simulating dynamical systems

Why study ramp waves?

- Question: can stress waves be tailored (e.g. slow ramp) in order to determine the equation of state (EOS) arbitrarily close to an isentrope?

- There is interest in extending quasi-static EOS measurements(e.g. Diamond Anvil Cell) to pressures > 100 GPa (1 Mbar), without generating a dissipative shock.

- Current experimental platforms for producing tailored stress waves:
  * Graded Density Impactor (Gas-gun)
  * Z-Ramp (magnetic flux compression)
  * High power laser (OMEGA, JANUS)

New Frontier: **Generate nonlinear stress waves to probe thermodynamic paths between an isentrope (ΔS=0) and the Hugoniot (ΔS>0) (shock).**

Nonlinear wave propagation: Simple wave (isentrope)

Ray Smith Aluminum – Omega Laser compared to calculation

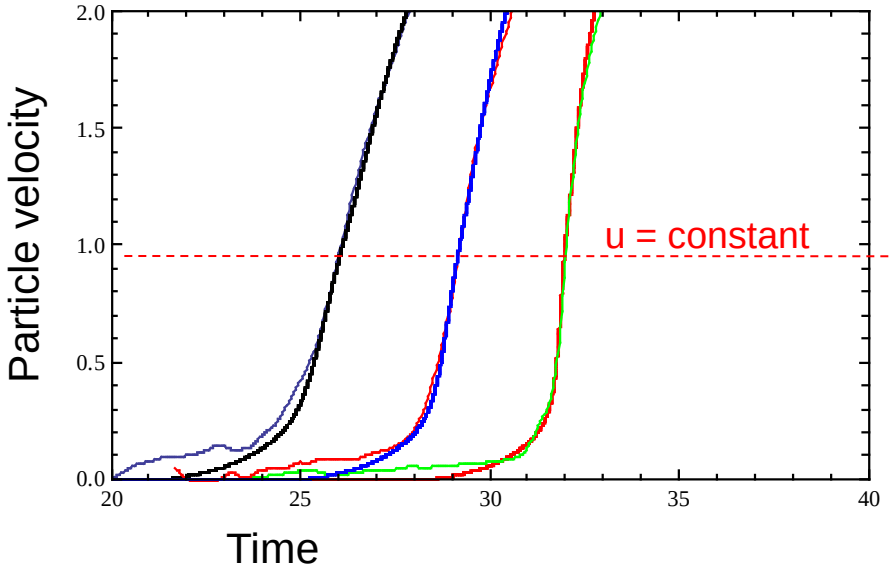

Lines of constant u with slope: $c_L^{-1}(u)$

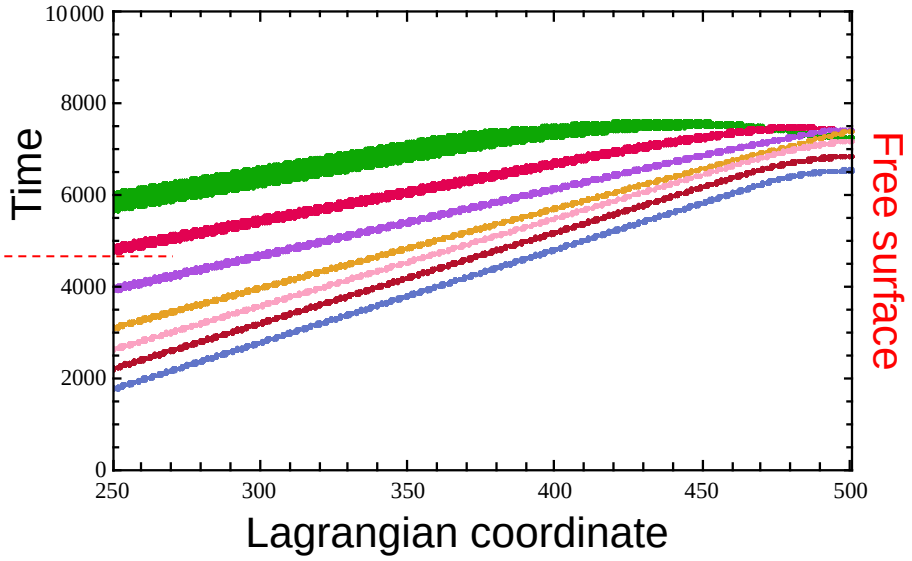

Riemann Characteristics: **The Lagrangian velocity, $C_L(u)$ contains all of the information necessary to determine the EOS.**

Two Empirical Laws : Clues to estimating energy dissipation in structured and stationary waves.

I. Energy dissipated over time of dissipation appears to be a shock invariant – "Fourth Power Law" (*see D. Grady, J. of Applied Phys.*)

$$\Delta E_D \tau \approx \text{constant}$$ Stationary wave

$$\int \Delta E_D d\tau \approx \text{constant}$$ Structured wave

II. Stationary waves tend to exhibit a linear $u_s - u_p$ relationship.

Empirical Laws can be understood in terms of the stress-energy tensor.

Nonlinear wave propagation: Simple wave (isentrope)

A simple wave may be constructed at a new position, $x+\Delta x$, with only knowledge of $c_L(u)$

$c_L(u)$ - Lagrangian sound speed

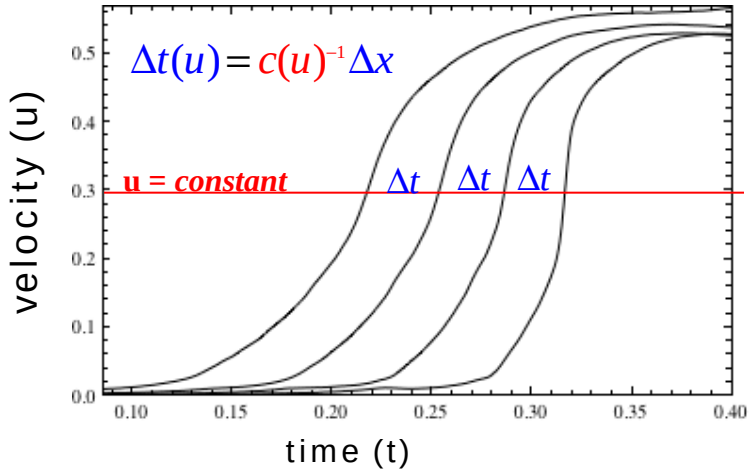

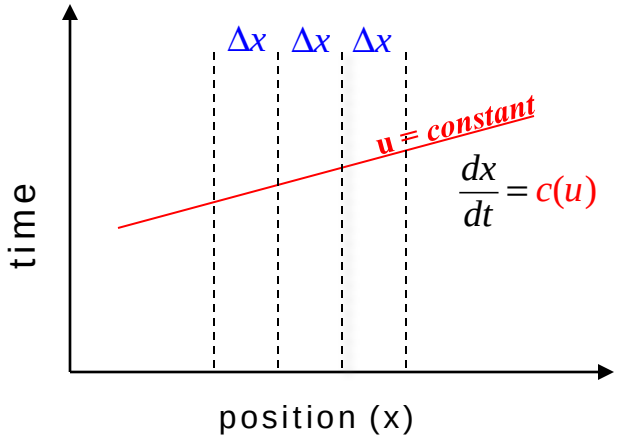

Stress vs. strain: $\sigma(\varepsilon)$

$$c_L(u) = \frac{1}{\rho_0}\frac{d\sigma}{du} = \left(\frac{d\varepsilon}{du}\right)^{-1}$$

A simple wave is reversible, isentropic, and has no explicit dependence on the local velocity gradient.

Departures from the simple wave as material response times shrink.

Material response to velocity gradient can result in dispersion and dissipation

$$\frac{\partial u}{\partial t}(x,t)+\alpha\, u(x,t)\frac{\partial u}{\partial x}(x,t)+\int_{-\infty}^{+\infty} K(x-\xi)\frac{\partial u}{\partial \xi}(\xi,t)\,d\xi = 0$$

$$c(k) = \frac{\omega}{k} = \int_{-\infty}^{+\infty} e^{-ik\xi} K(\xi)\,d\xi \qquad c(k) = a_0 + a_2 k^2 + \ldots + a_{2m} k^{2m}$$

$$\frac{\partial u}{\partial t} + \alpha\, u \frac{\partial u}{\partial x} + a_0 \frac{\partial u}{\partial x} - a_2 \frac{\partial^3 u}{\partial x^3} + \ldots + (-1)^m a_{2m} \frac{\partial u^{2m+1}}{\partial x^{2m+1}} = 0$$

Phase portraits of $u(x,t)$ versus $\frac{\partial u(x,t)}{\partial x}$ reveal presence of higher order derivatives.

Typical phase portraits of nonlinear wave with dispersion and dissipation.

$$\frac{\partial u}{\partial t} + a_1 u \frac{\partial u}{\partial x} + a_0 \frac{\partial u}{\partial x} - a_2 \frac{\partial^2 u}{\partial x^2} + a_3 \frac{\partial^3 u}{\partial x^3} = 0$$

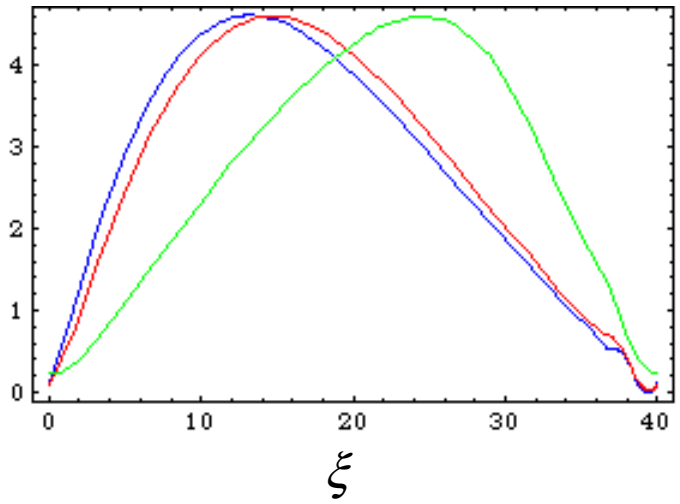

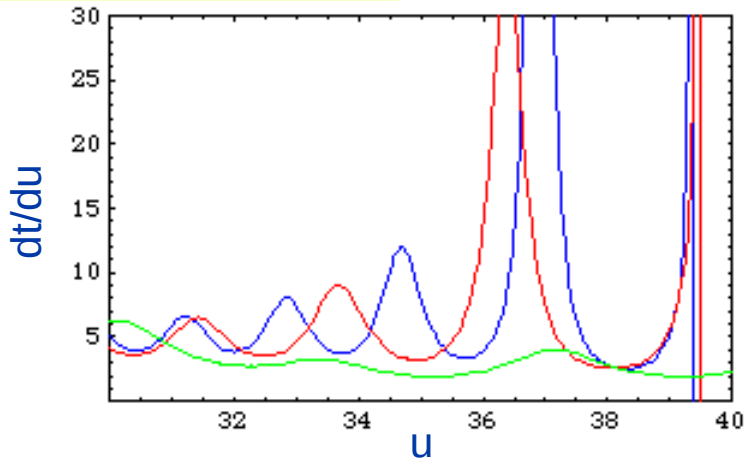

$$u(\xi) = \frac{v_0}{a_1} + \frac{3 a_2^{\,2}}{25 a_3}\left(Sech^2(\xi) - 2 Tanh(\xi)\right)$$

$$\xi = \frac{a_2}{10 a_3}\left(x - t\, v_0\right)$$

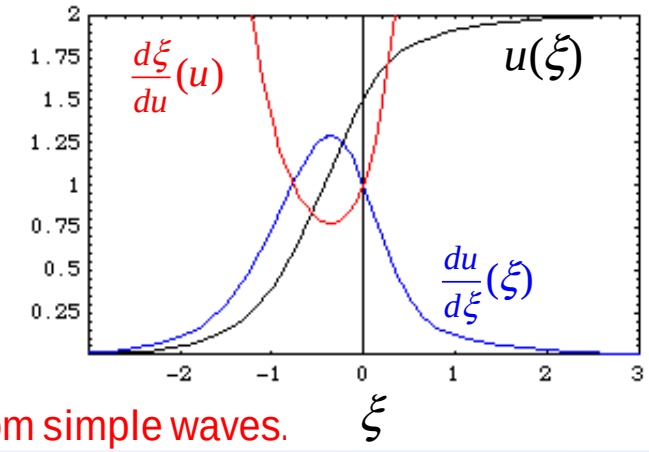

Phase portraits are a valuable tool for testing departures from simple waves.

Use tailored pressure waves to study entropy production as nonlinear wave (ΔS~0) steepens to a stationary wave (ΔS>0)

Thermodynamic estimate of entropy jump in a stationary wave (Hans Bethe).

Stationary wave:

$$\Delta E(V,S) = -\frac{1}{2}P(V,S)\Delta V$$

Taylor expansion:

$$\left(\frac{\partial \Delta E}{\partial V}\right)_S \Delta V + \frac{1}{2!}\left(\frac{\partial^2 \Delta E}{\partial V^2}\right)_S \Delta V^2 + \frac{1}{3!}\left(\frac{\partial^3 \Delta E}{\partial V^3}\right)_S \Delta V^3 + \left(\frac{\partial \Delta E}{\partial S}\right)_V \Delta S + \ldots = \frac{-1}{2}\left[\left(\frac{\partial p}{\partial V}\right)_S \Delta V^2 + \frac{1}{2!}\left(\frac{\partial^2 p}{\partial V^2}\right)_S \Delta V^3\right] + \ldots$$

$$p = -\left(\frac{\partial \Delta E}{\partial V}\right)_S$$

$$T = \left(\frac{\partial \Delta E}{\partial S}\right)_V$$

The net entropy produced in a stationary wave is proportional to the third order jump in a given state variable, (e.g. ΔV, Δu).

$$\Delta S \approx -\frac{1}{12}\left(\frac{\partial^2 p}{\partial V^2}\right)_S \Delta V^3$$

Experimental observations : Range of peak acceleration in scaling study

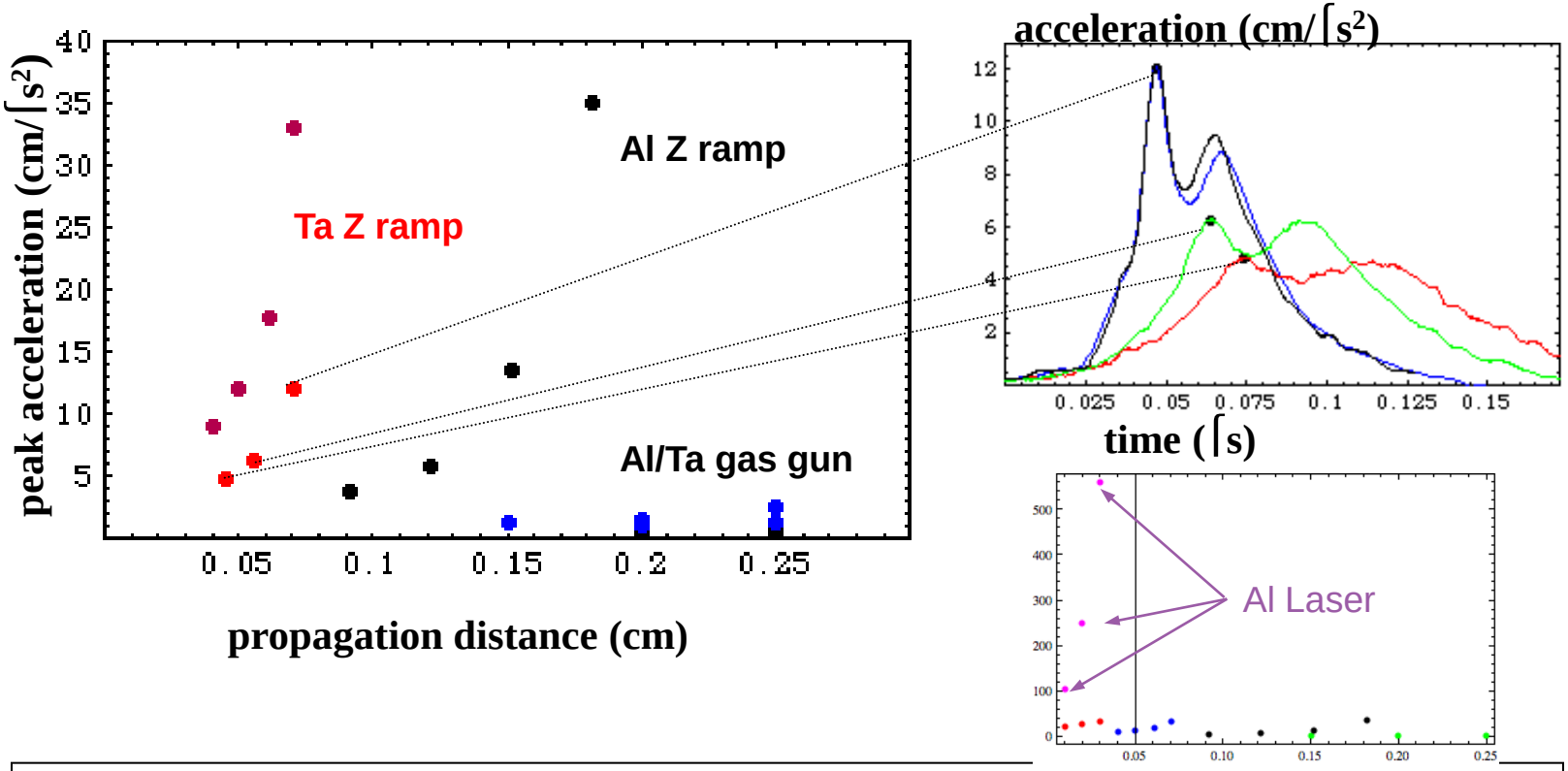

The experimental data (strain rate) spans nearly two orders of magnitude.

Experimental observations I : "sech^2" structures in acceleration time histories

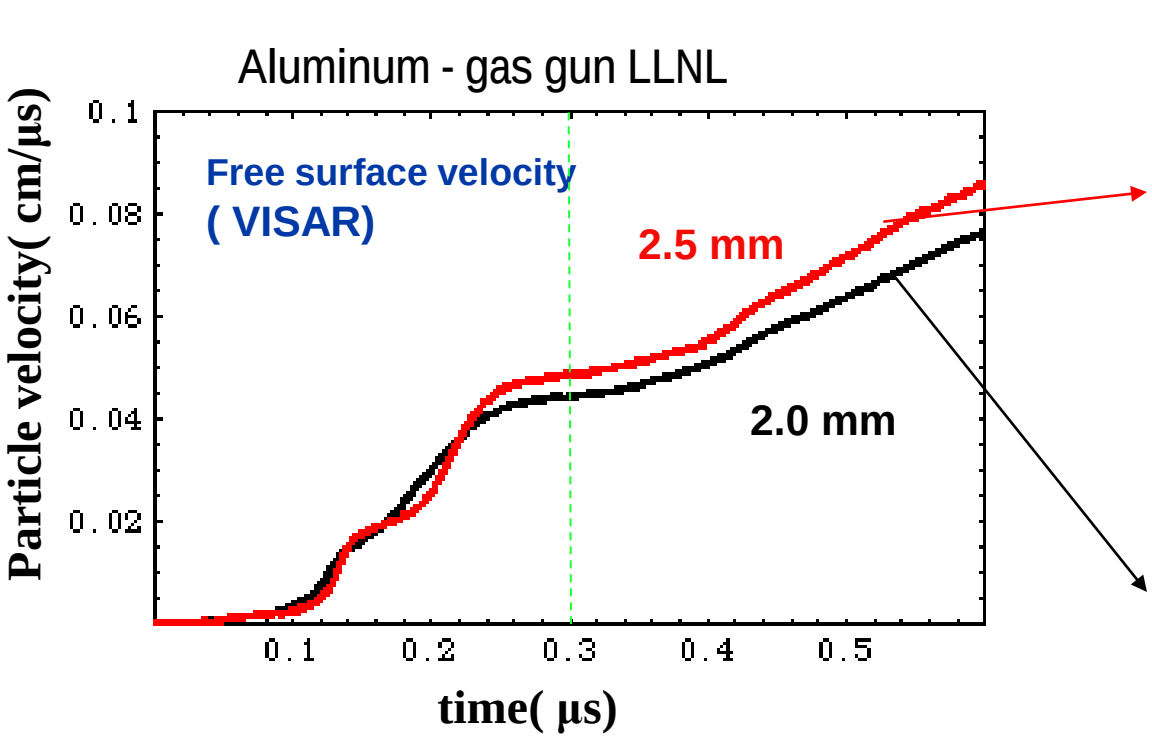

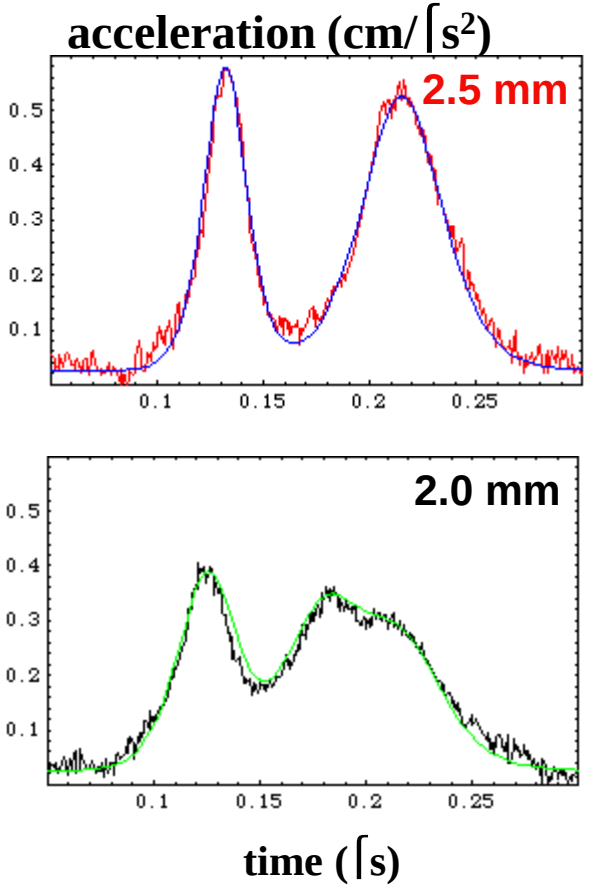

$$\frac{du}{dt} = const. + \sum_{j=1}^{N} a_j \, \mathrm{sech}^2\left[b_j\left(t - t_j\right)\right]$$

Experimental observations I (cont.): "sech^2" structures in acceleration time histories

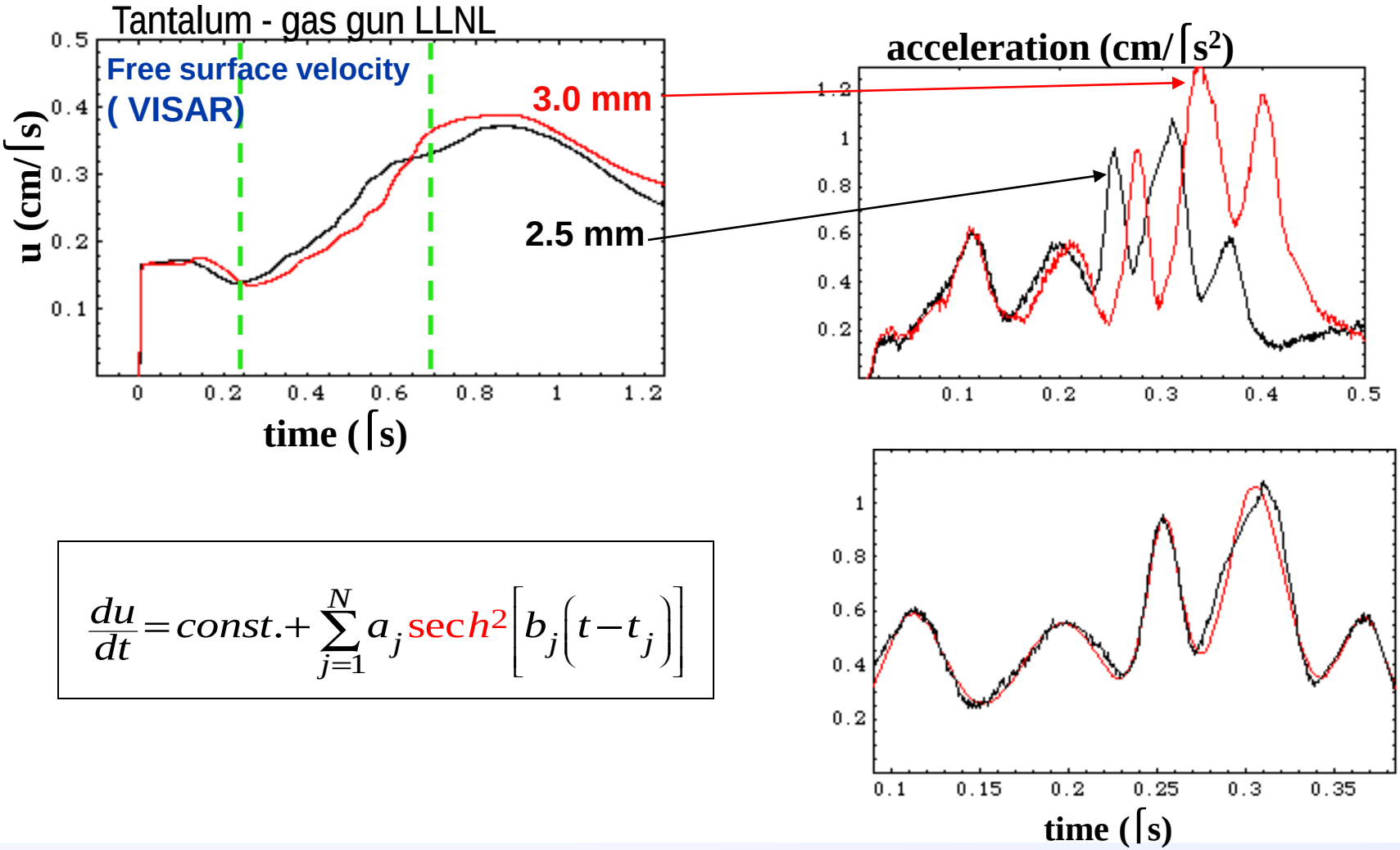

$$\frac{du}{dt} = const. + \sum_{j=1}^{N} a_j \, \mathrm{sech}^2\left[b_j \left(t - t_j \right) \right]$$

Experimental observations I (cont.): "sech^2" structures in acceleration time histories

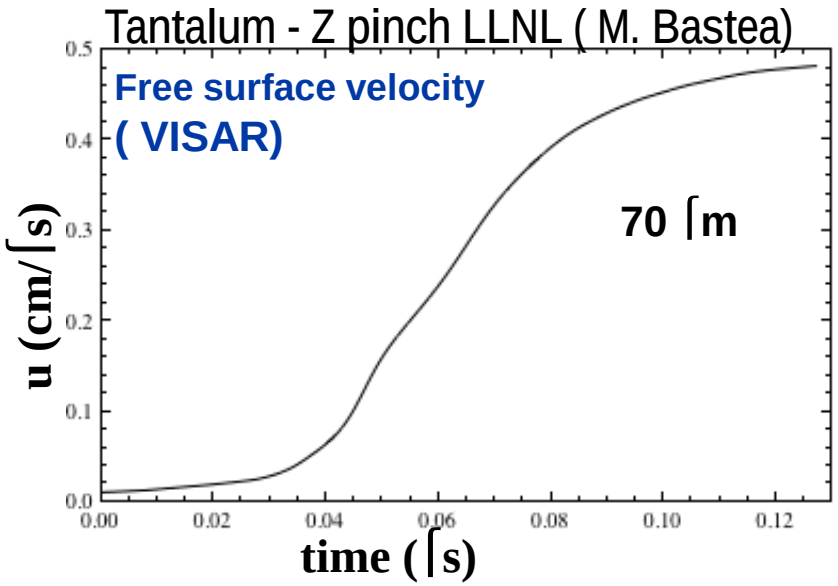

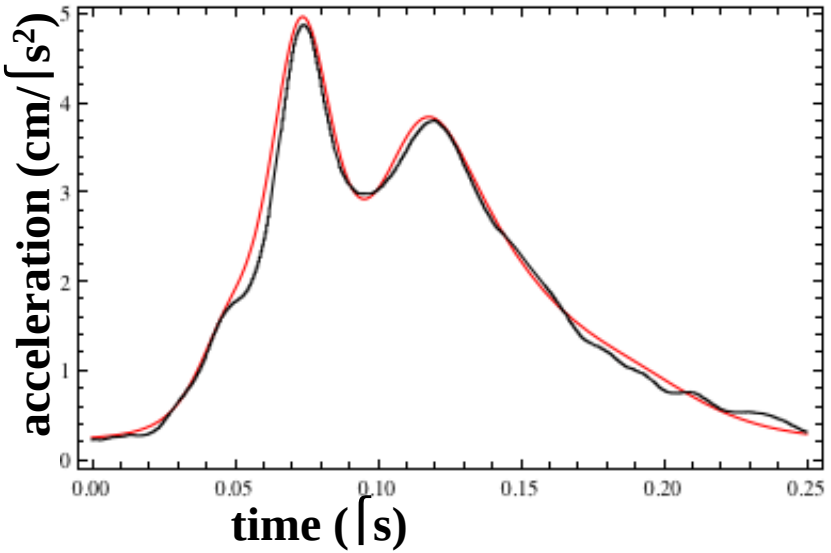

$$\frac{du}{dt} = const. + \sum_{j=1}^{N} a_j \, \mathrm{sech}^2\left[b_j\left(t - t_j\right)\right]$$

Experimental observations II:
Possible scaling over two orders of magnitude

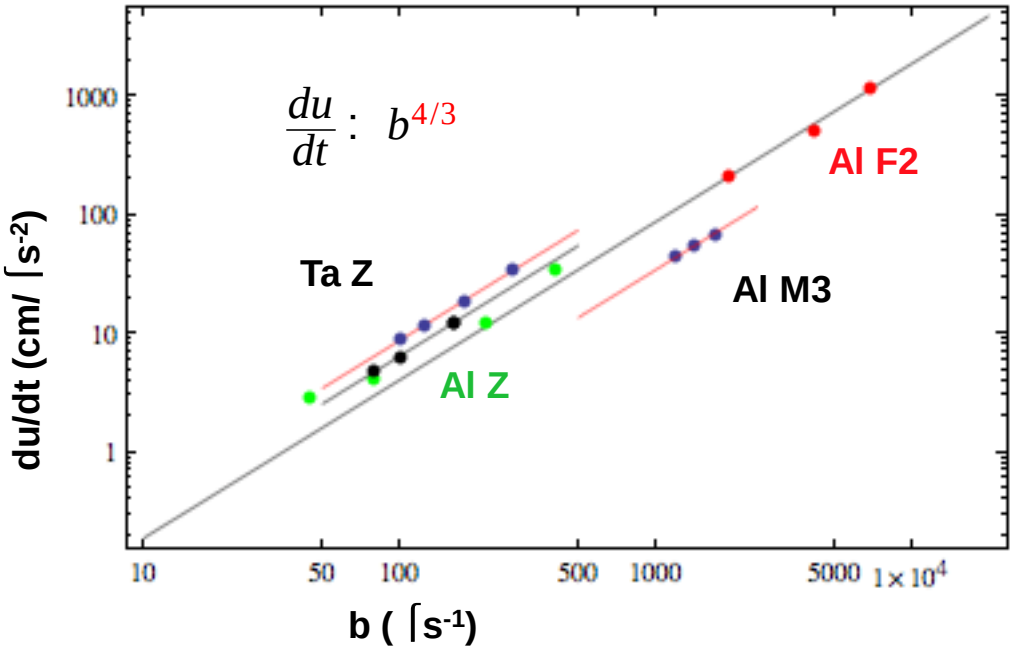

Scaling of typical local structure

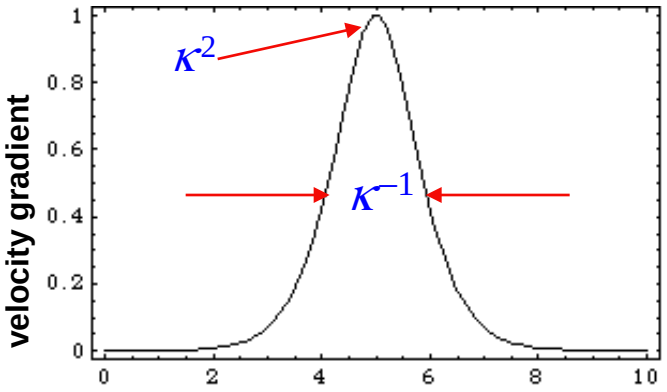

$$\xi = \kappa\left(x - \kappa^2 t\right)$$

$$\frac{du}{dt} = const. + \sum_{j=1}^{N} a_j \, \mathrm{sech}^2\left[b_j\left(t - t_j\right)\right]$$

$$\tau: b^{-1}: \kappa^{-3}$$
$$\frac{du}{dt}: b^{4/3}: \kappa^4$$
$$u: \kappa$$

$$\rightarrow \quad \frac{du}{dt}: u^4$$

Experimental observations III:
Scaling of peak acceleration and time scale (propagation distance)

$$t = -\frac{1}{\alpha}\left(\frac{1}{S} - 1 + \beta Log\left[\frac{S-\beta}{1-\beta}\right]\right)$$

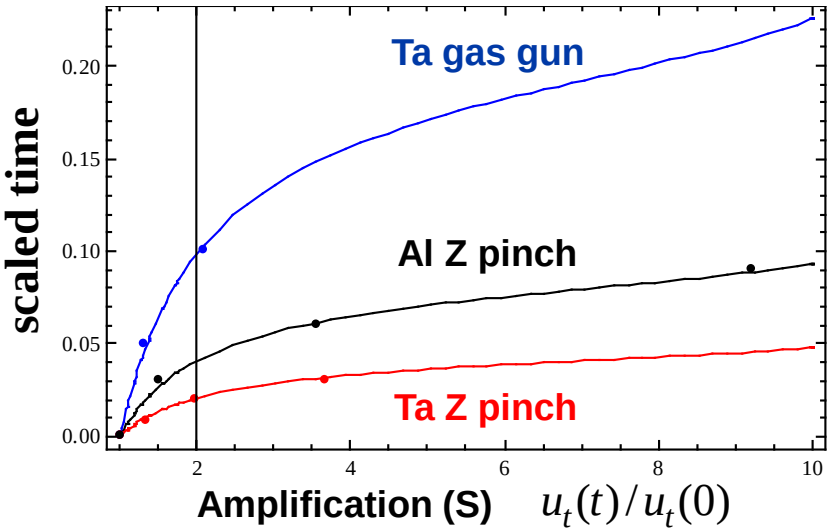

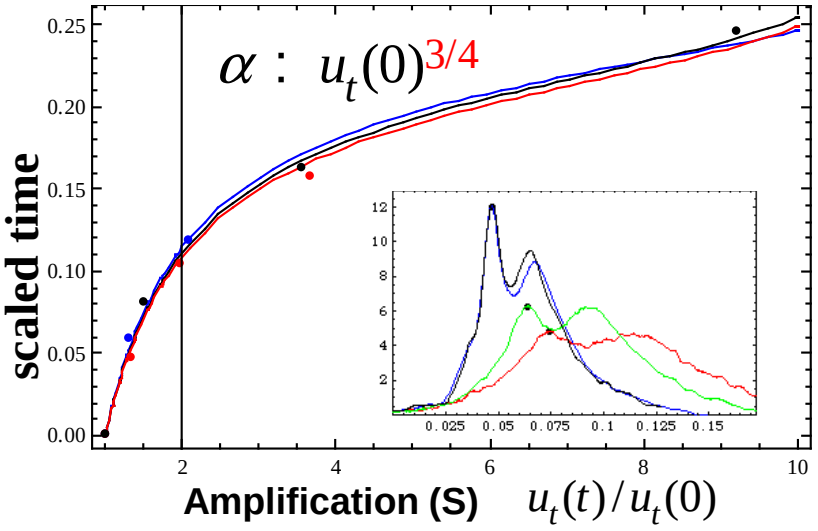

Time scale, α^{-1} , and strain rate $u_t(0)$, are related by exponent of 3/4

Experimental observations IV: Approaching a stationary wave
Saturation of amplification in Al

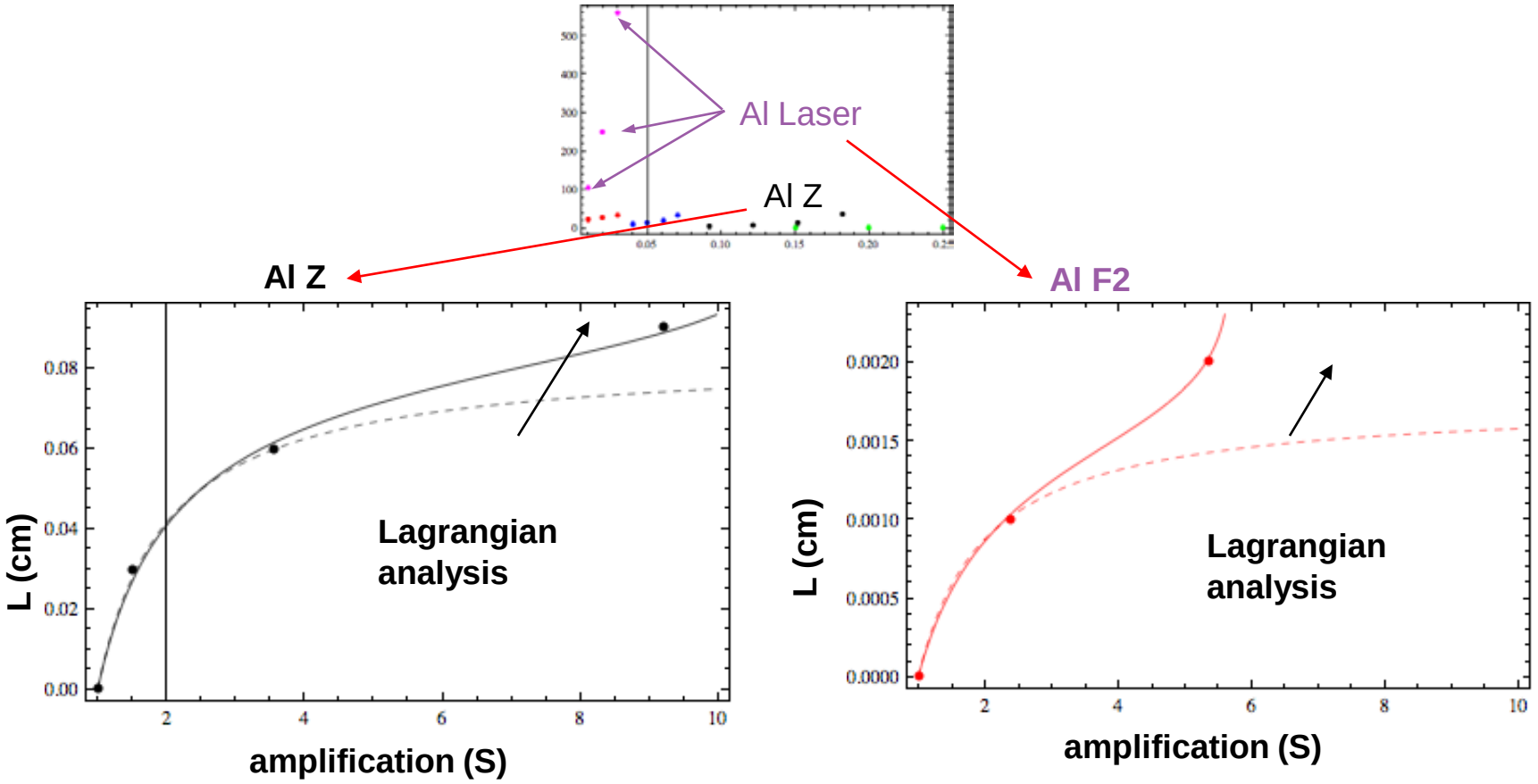

Experimental observations summary: Scaling and "sech^2" structure suggest Korteweg- deVries equation for the velocity gradient ,Ω

I : Traveling wave solution with distinct aspect ratio

$$\Omega(x,t) \equiv u_x(x,t) \propto \kappa^2 \sec h^2(\kappa(x-\kappa^2 t)$$

II : Scaling

$$\Omega(x,t) = u_x(x,t) \propto t^{-2/3}\Phi\left(\frac{x}{t^{1/3}}\right)$$

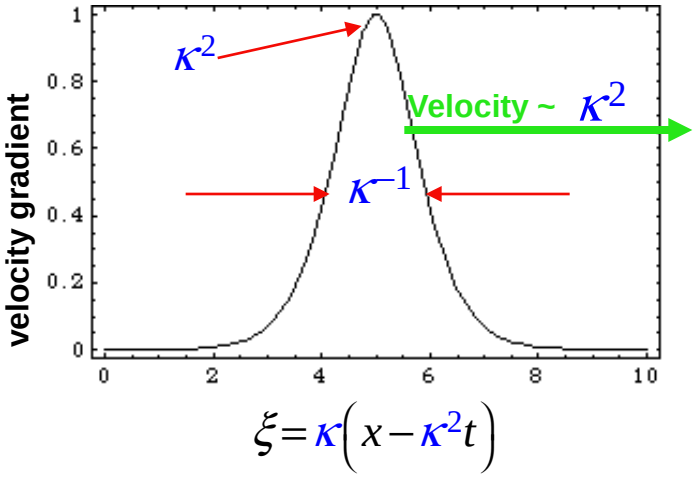

$$\Omega_t + \alpha\Omega\Omega_x + \beta\Omega_{xxx} = 0$$

Korteweg-deVries Equation

Puzzle: What is the unusual origin of a third order equation for the velocity gradient?

Experimental observations V:
The KdV equation is consistent with evolution of acceleration profiles

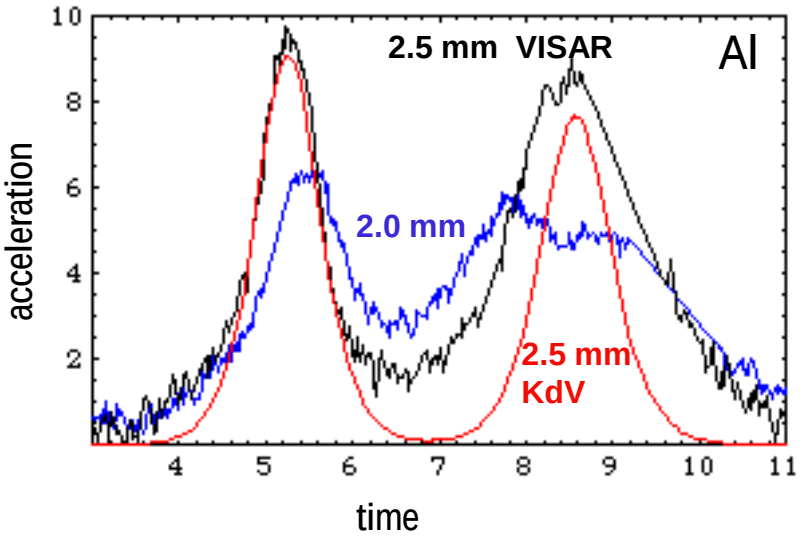

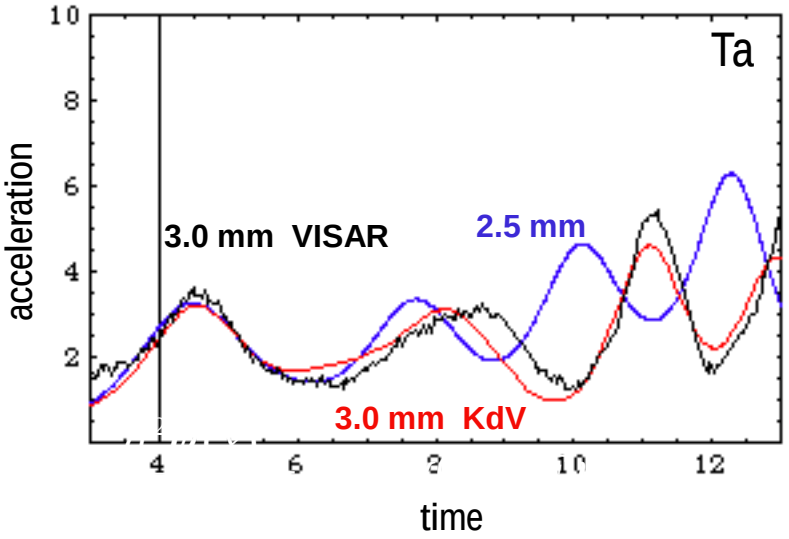

Inverse Scattering Transform solves KdV exactly

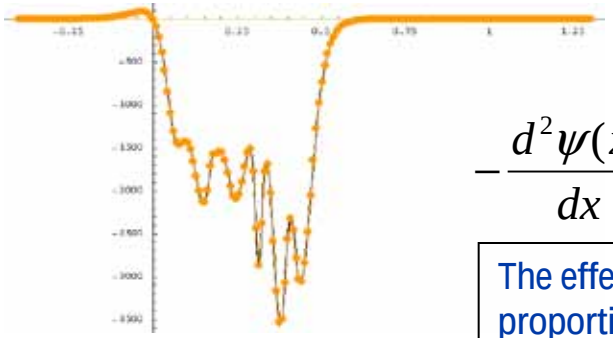

$$-\frac{d^2\psi(x)}{dx} + U(x)\,\psi(x) = E\,\psi(x)$$

The effective potential U(x) is proportional to the acceleration profile

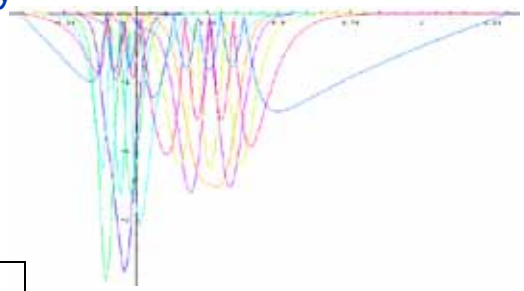

Experimental observations VI: The KdV equation predicts “Fourth Power Law”

Stationary dissipative structure (stationary wave) obeys “Fourth Power Law”

Korteweg-deVries Equation: $\Omega_t + \alpha\Omega\Omega_x + \beta\Omega_{xxx} = 0$

Traveling wave solution: $u(x,t) = \Delta u \tanh\left[\kappa\left(x - 4\kappa^2 t\right)\right]$

Acceleration: $u_t(x,t) = \frac{\alpha^3}{432\beta^2}\Delta u^4 \operatorname{sech}^2\left[\kappa(x-\kappa^2 t)\right]$

$$\Delta u = \frac{12\kappa\beta}{\alpha}$$

Alternative statement of scaling law:

(Energy dissipated) (characteristic time) = constant

Δu^3 Δu^{-3} Δu^0

Experimental observations V: "Fourth Power Law"

Grady-Swegle Scaling:
{Al,Be,Bi,Cu,Fe,U,MgO,SiO_2}

J. Appl. Phys. 58(2),1985.

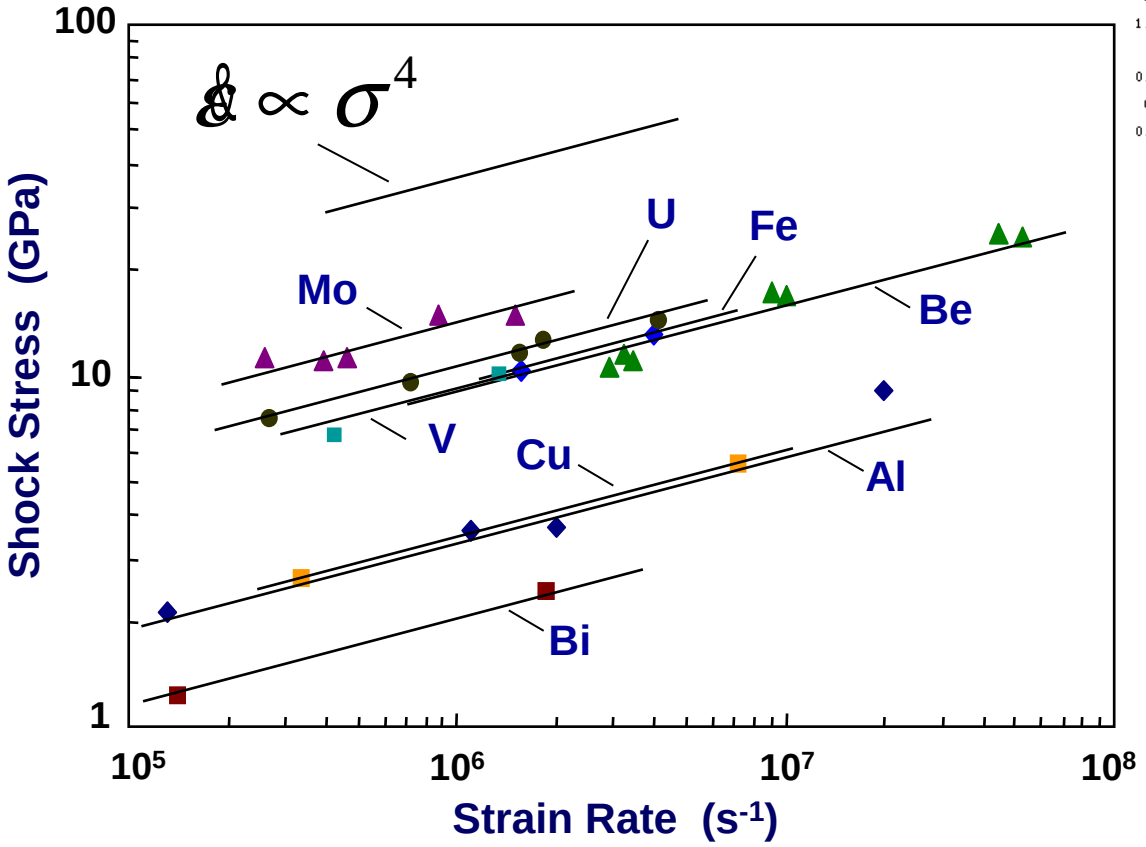

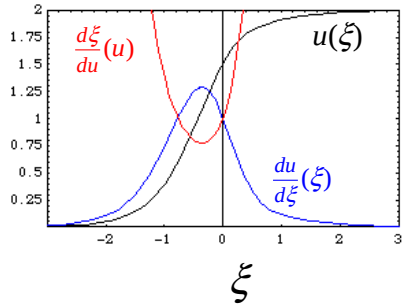

Experimental observations V (cont.): "Fourth Power Law"

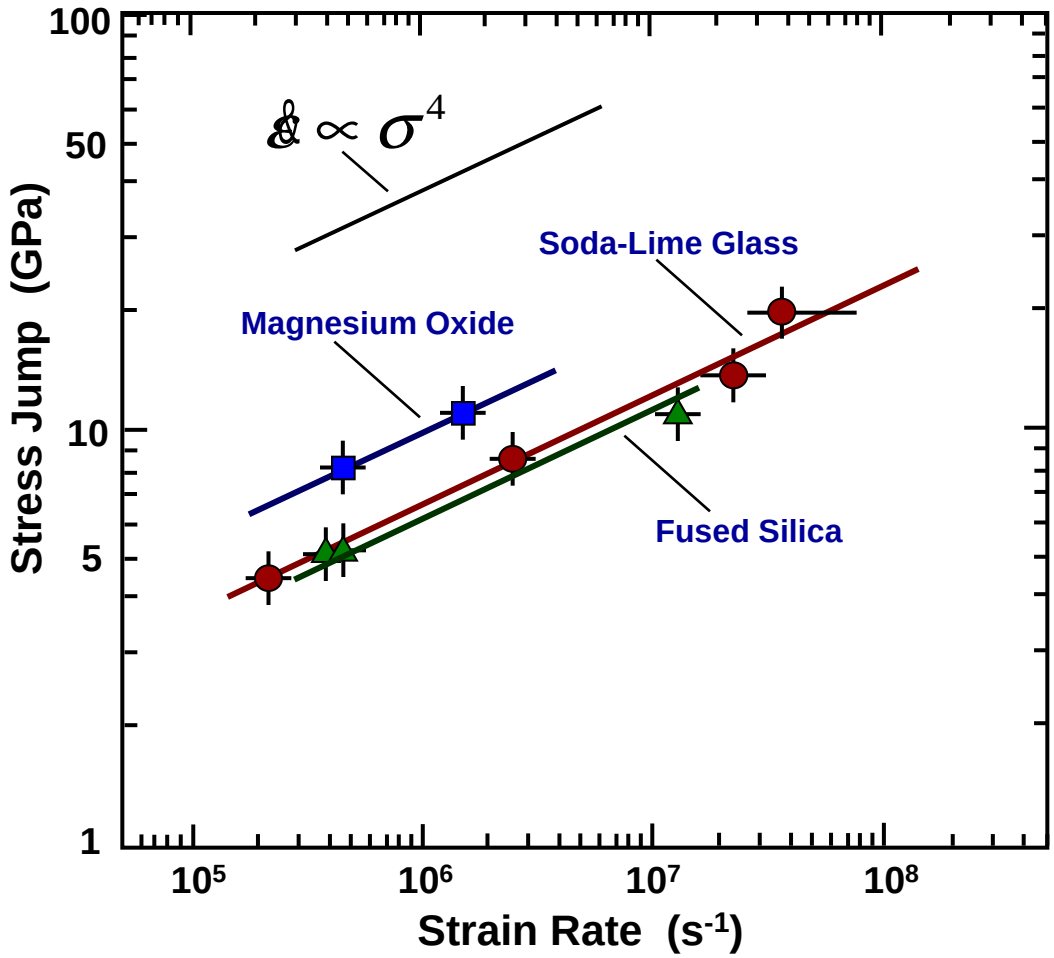

Energy-momentum tensor: Simple wave (ΔS = 0)

$$\partial_\beta T^{\alpha\beta} = 0 \qquad T^\alpha_\alpha = 0$$ *Scale invariance in 2d*

$$\partial_0 T^{10} + \partial_1 T^{11} = 0$$ *Conservation of momentum*

$$\partial_0 T^{00} + \partial_1 T^{01} = 0$$ *Conservation of energy*

Simple wave/perfect fluid (reversible transfer of momentum)

$$T^{\alpha\beta} = P\eta^{\alpha\beta} + (P+\varepsilon)U^\alpha U\beta$$

$$TdS = Pd\left(\frac{1}{n}\right) + d\left(\frac{\varepsilon}{n}\right) = 0$$

The energy-momentum tensor provides nice theoretical framework for studying symmetries and constraints on a dynamical system.

Energy-momentum tensor: Dissipation-irreversible momentum transfer

$$\partial_\beta T^{\alpha\beta} = 0 \qquad T^\alpha_\alpha = -3\zeta\,\partial_\alpha U^\alpha \neq 0$$

Broken scale invariance in 2d

Imperfect fluid

$$T^{\alpha\beta} = P\,\eta^{\alpha\beta} + (P+\varepsilon)U^\alpha U\beta + \Delta T^{\alpha\beta}$$

Thermodynamics requires linear dependence on velocity gradient

Entropy production

$$\partial_\alpha S^\alpha = \frac{\eta}{2T}\left(\partial_j U^i + \partial_i U^j - \frac{2}{3}\delta_{ij}\vec{\nabla}\cdot\vec{U}\right)^2 + \frac{\zeta}{T}\left(\vec{\nabla}\cdot\vec{U}\right)^2$$

The energy-momentum tensor provides nice theoretical framework for studying symmetries and constraints on a dynamical system. The introduction of dissipation introduces a length scale and a finite trace. This reduces the symmetry in a well defined way in 2d.

Theory of surfaces:
The origin of the KdV equation for the velocity gradient (Ω)

Velocity gradient breaks scale invariance proportional to trace of energy-momentum tensor and induces length scale through induced curvature K.

Gaussian curvature, K, defines local curvature of 2d surface.

Curvature, K, is described by KdV equation for K_0 time independent.

Since, velocity gradient, Ω, is proportional to the Gaussian curvature, K, the KdV for the velocity gradient, Ω , results.

$$T^{\mu}_{\mu} = -\frac{c}{12}K = -\zeta \partial_{\gamma} u^{\gamma} \equiv -\zeta \Omega$$

$$ds^2 = dx^2 + c(x,t)dt^2$$

$$\partial_x^2 c(x,t) + (K + K_0)c(x,t) = 0$$

$$\partial_t K + a K \partial_x K + K_0 \partial_x K + b \partial_x^3 K = 0$$

$$\partial_t \Omega + \bar{a} \Omega \partial_x \Omega + \Omega_0 \partial_x \Omega + \bar{b} \partial_x^3 \Omega = 0$$

The intercept of the “Fourth Power Law”

Energy dissipation (thermodynamics) Energy dissipation (velocity gradient)

$$\frac{1}{12}\left(\frac{\partial^2 P}{\partial u^2}\right)_S \frac{\Delta u^3}{c_L(u)} \approx \frac{\beta}{c_L(u)} \int dx \left(\partial_x u\right)^2$$

Stress-Energy Tensor: $T(u) = \alpha u^2 + \beta \partial_x u = T_0$ Stationary wave

Theory allows possible extraction of β from Grady-Swegle law for a given material.

$$P \approx \frac{\rho_0 c_0 \beta}{\alpha^{3/4}} \dot{\varepsilon}^{1/4} \qquad \alpha = \frac{1}{12}\left(\frac{\partial^2 \sigma}{\partial u^2}\right)_S$$

Intercept of “Fourth Power Law” is linearly proportional to viscosity coefficient, β

Experimental observations IV: "Fourth Power Law"

Grady-Swegle Scaling:
{Al,Be,Bi,Cu,Fe,U,MgO,SiO_2}

J. Appl. Phys. 58(2),1985.

$$P \approx \frac{\rho_0 c_0 \beta}{\alpha^{3/4}} \dot{\varepsilon}^{1/4} \qquad \alpha = \frac{1}{12}\left(\frac{\partial^2 \sigma}{\partial u^2}\right)_S$$

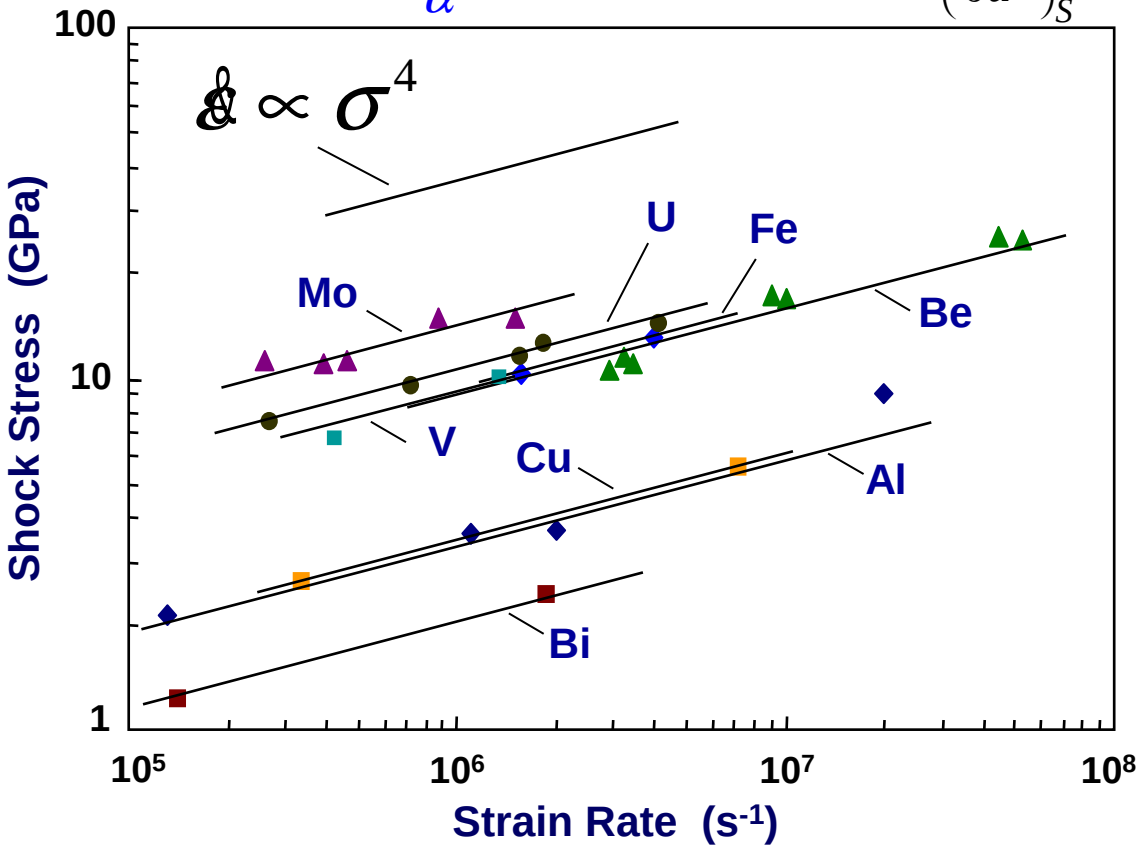

Estimate of deviation from isentrope

$$\mathrm{E}_{disipation} = \frac{\beta}{c_0}\int \partial_x^2 u \, dx \qquad \Delta P \approx \rho_0 \gamma_0 \mathrm{E}_{dissipation}$$

$$\mathrm{E}_{dissipation} = \frac{\beta^3}{c_0 \alpha^2}\sum_j \kappa_j^3 \qquad \kappa_j = \frac{\alpha}{\beta}\Delta u_j$$

$\kappa_j \equiv$ *eigenvalues of Schrodinger equation*

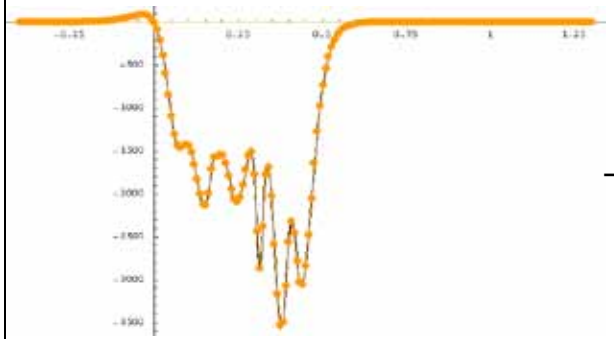

$$-\frac{d^2\psi(x)}{dx} + U(x)\psi(x) = E\,\psi(x)$$

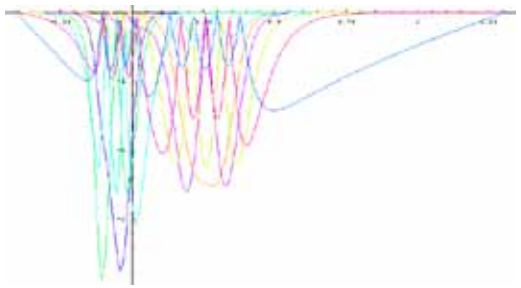

Summary and Conclusions

- Nonlinear compression waves manifest common features over a wide range of pressures and strain rates (velocity gradients).
- The dependence on velocity gradient suggests departures from simple wave Lagrangian analysis.
- A common partial differential equation(KdV) for the acceleration describes the main features of the flow and in the stationary, traveling wave limit reproduces the "Fourth Power Law" and linear u_s-u_p curves.
- The origin of the KdV equation for the velocity gradient can be attributed to the breaking of scale invariance in the energy-momentum tensor for two dimensional flow.
- The dynamical evolution of the KdV surface may be described by a self consistent Hamiltonian with constraints.
- The current formalism allows an estimate of the entropy production at different stages in the flow.

Relationship to other fields of research: a common mathematical framework

- Relativistic heavy ions: breaking of conformal invariance of energy momentum tensor is observed and related to a bulk viscosity and entropy production. It was a surprising discovery that relativistic heavy ion collisions behave like a viscous fluid.

- Two dimensional models of gravity: Two dimensional models of gravity, exhibit similar conformal symmetry breaking. This allows an estimate of the density of states and corresponding entropy, which gives the correct Hawking temperature.

Symmetries are a very powerful way to characterize a physical system.

Experimental observations VI:
The KdV equation predicts shock invariant

Energy dissipated due to velocity gradient:

$$\varepsilon_D = \nu \int_{-\infty}^{\infty} u_x^2(x,t)\,dx = \nu \int_{-\infty}^{\infty} \mathrm{sech}^4(y)dy = \frac{\nu\alpha}{9\beta}\Delta u^3$$

Entropy T⊗S generated for stationary wave with velocity jump ⊗u:

$$T\Delta S = \frac{1}{12}\left(\frac{\partial^2\sigma}{\partial\varepsilon^2}\right)_S \Delta\varepsilon^3 = 2\rho_0 \frac{d\ln\left[c_L(u)\right]}{du}\Delta u^3$$

Alternative statement of scaling law:

(Energy dissipated) (characteristic time) = constant

Δu^3 Δu^{-3} Δu^0

Experimental observations V:
Length scaling consistent with Ray Smith et.al. data

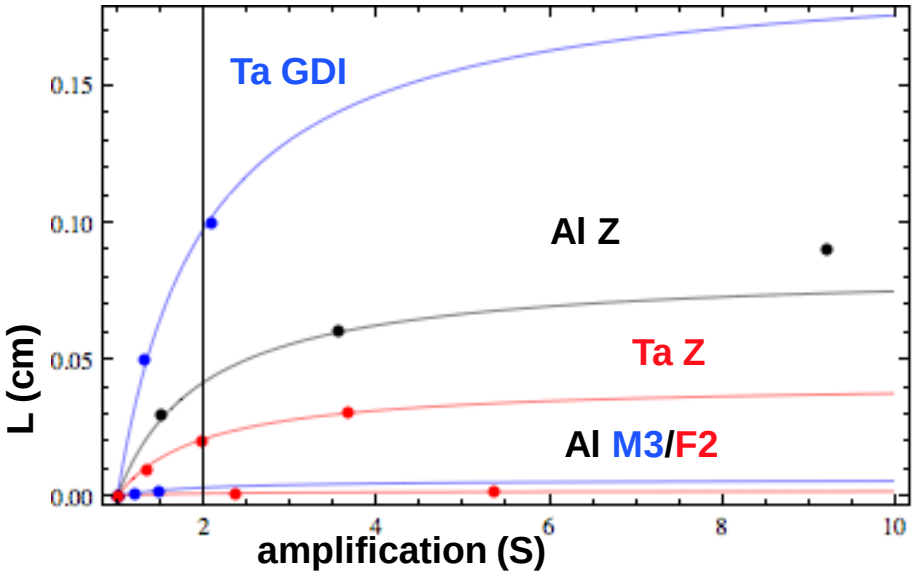

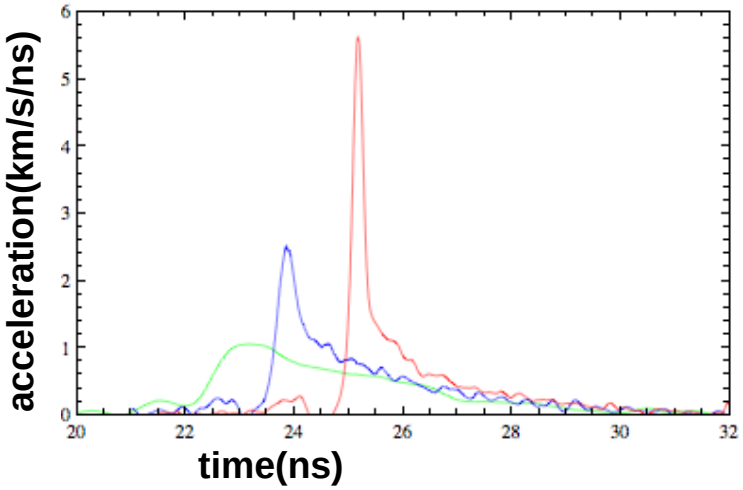

$L / (du/dt)^{z}$

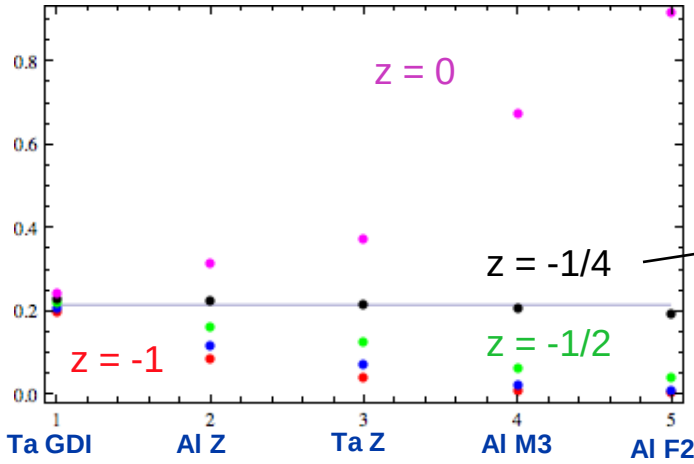

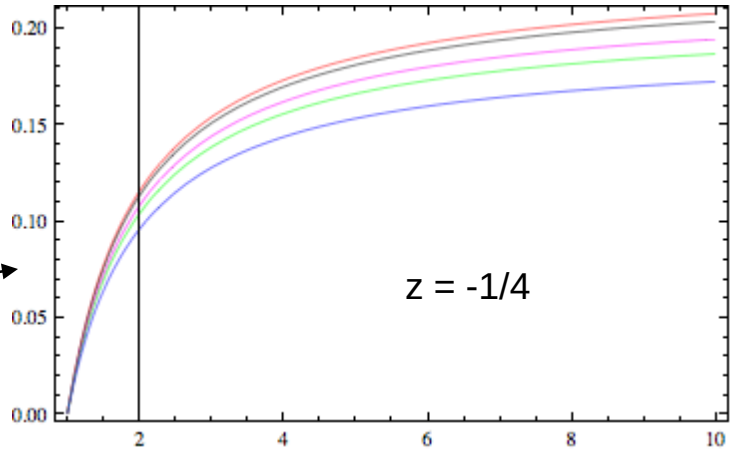

Experimental observations VI: Saturaturation of amplification in Al

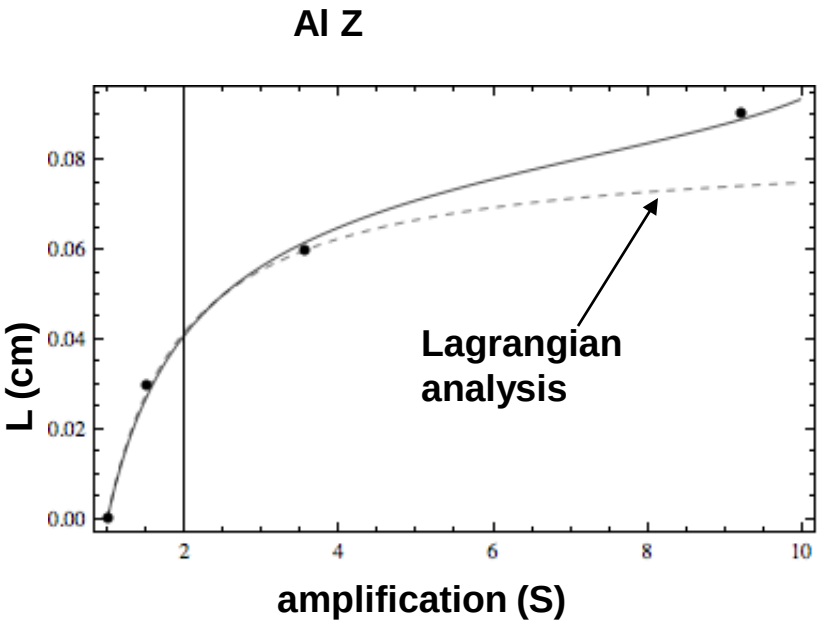

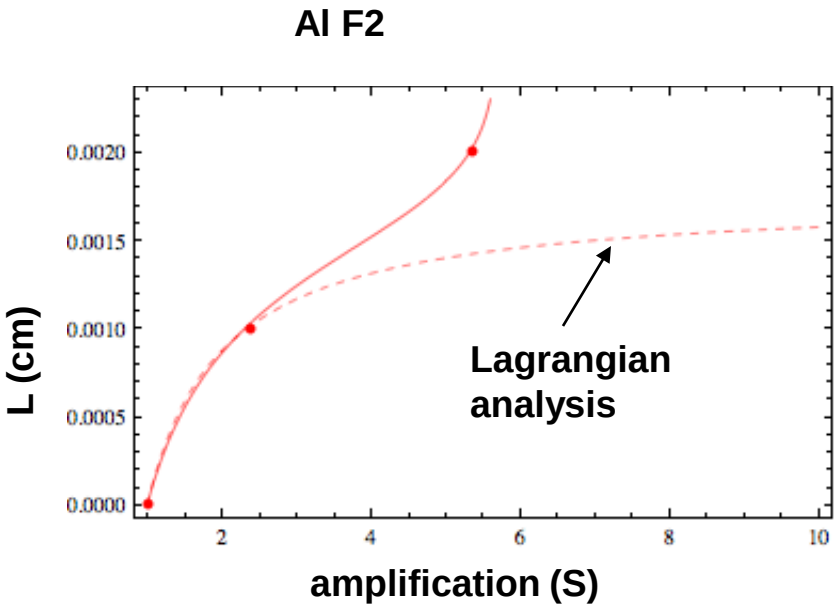

Experimental observations III (cont.): Length scaling consistent with Ray Smith et.al. data

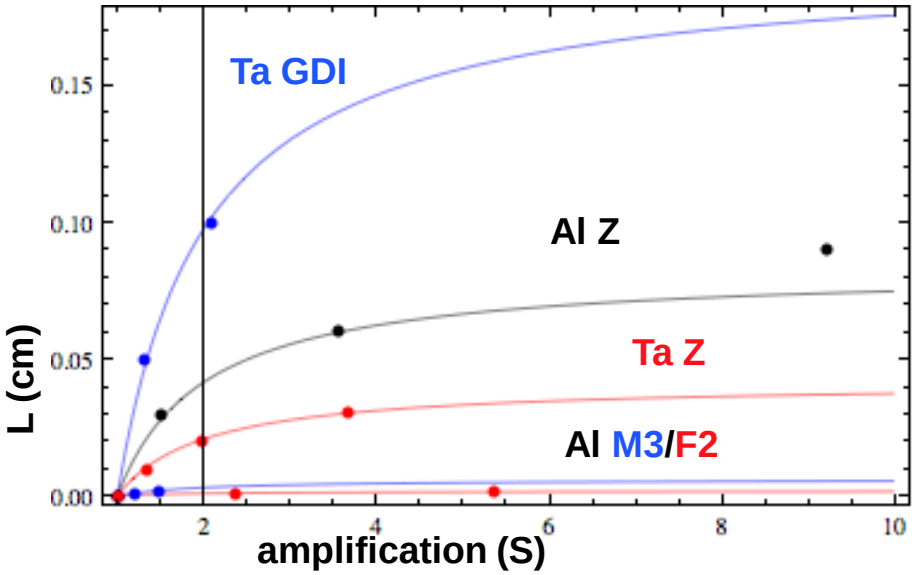

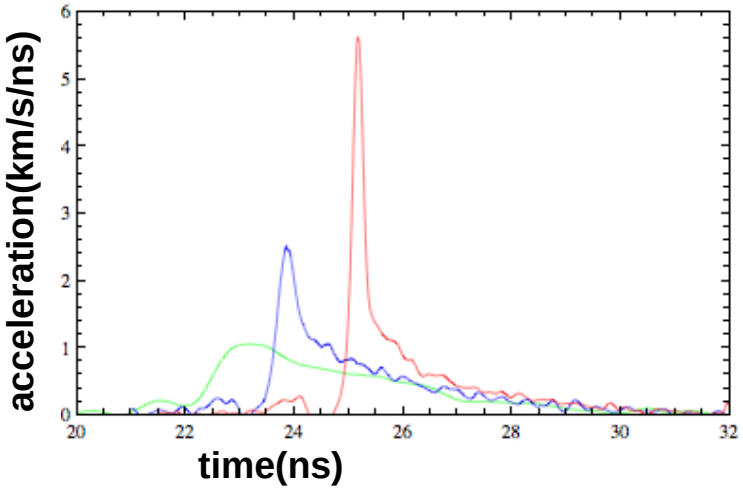

$L / (du/dt)^{z}$

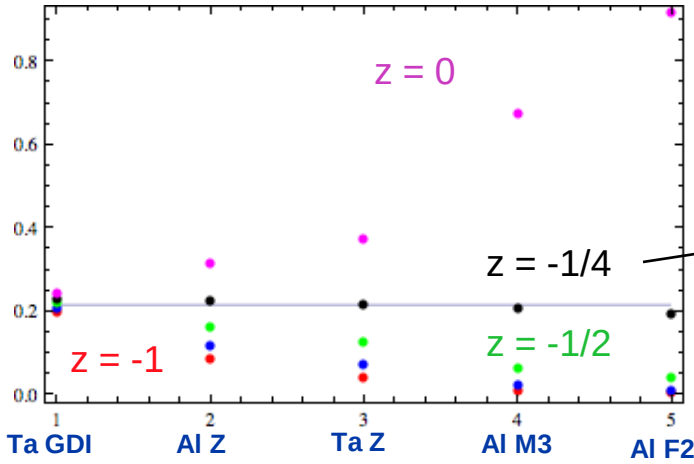

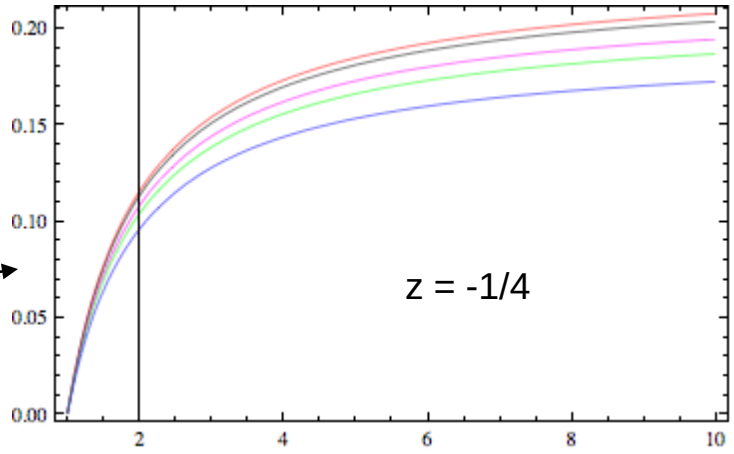

Experimental observations III (cont.): Scaling of peak acceleration and time scale (propagation distance)

$$u_t(t) = a\,\mathrm{sech}^2\left[b(t-t_0)\right]$$

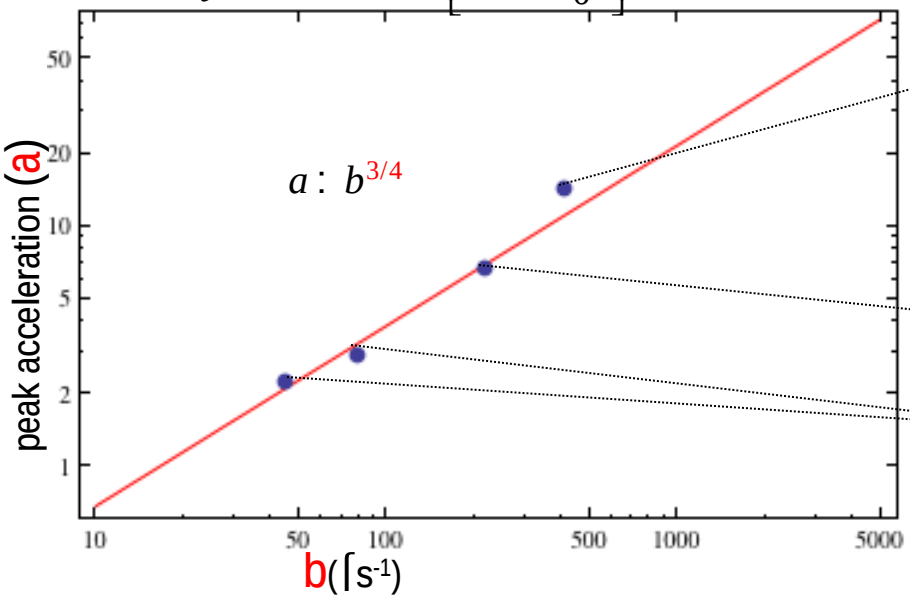

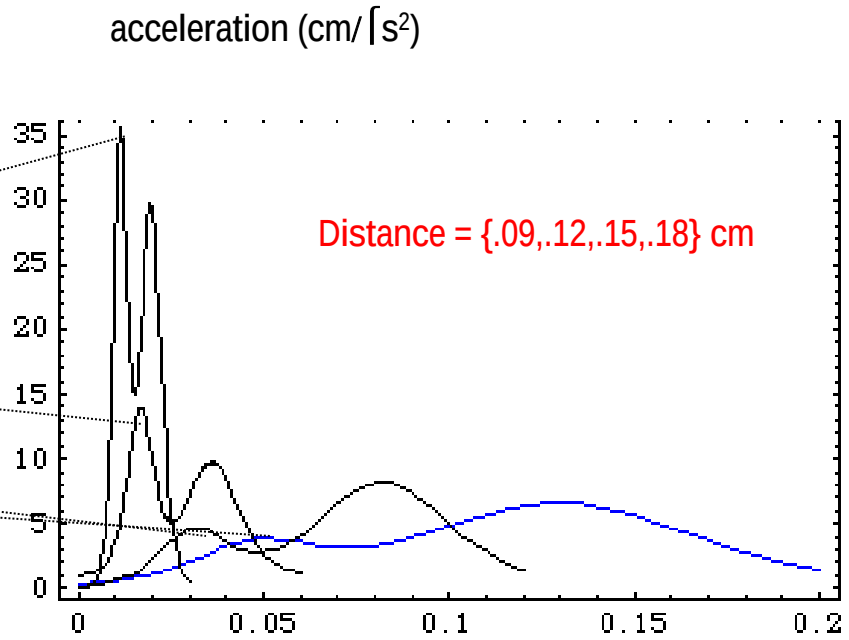

Time scale, b^{-1} , and strain rate a are also related by exponent of 3/4

Dissecting Lagrangian Velocities and Ramp Waves

Roger W. Minich and Daniel Orlikowski

Lawrence Livermore National Laboratory

Ramp Compression Workshop
19 January 2011

Lawrence Livermore National Laboratory, P. O. Box 808, Livermore, CA 94551
This work performed under the auspices of the U.S. Department of Energy by
Lawrence Livermore National Laboratory under Contract DE-AC52-07NA27344

LLNL-PRES-465263

Nonlinear wave propagation: Simple wave (isentrope)

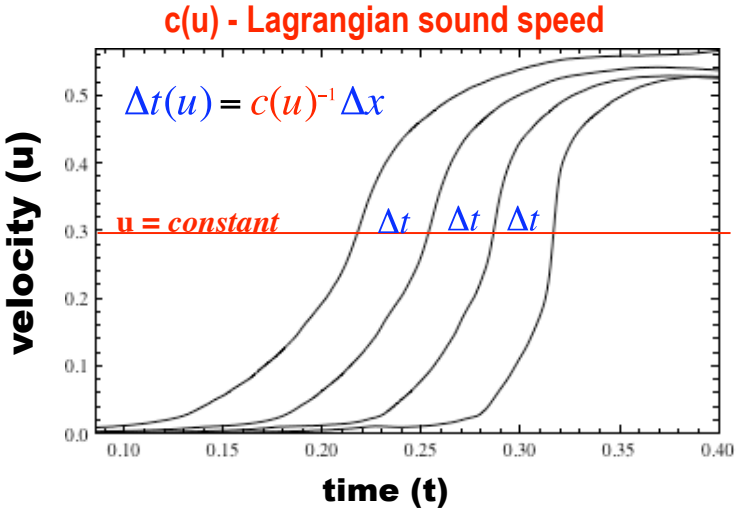

Stress vs. strain: $\sigma(\varepsilon)$

$$c(u) = \frac{1}{\rho_0}\frac{d\sigma}{du} = \left|\frac{d\varepsilon}{du}\right|^{-1}$$

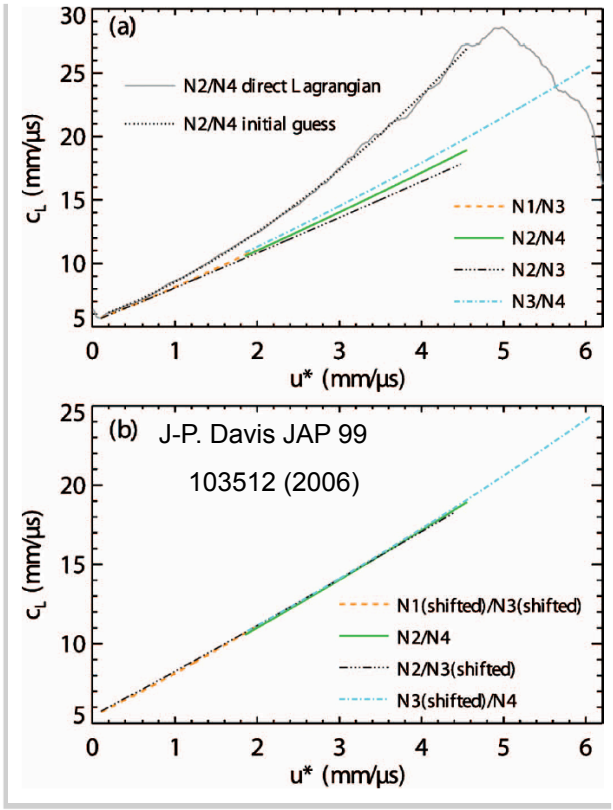

A simple wave may be constructed at a new position $x + \Delta x$ with only knowledge of c(u)

A simple wave is reversible, isentropic, and has no explicit dependence on the local velocity gradient.

Some XT views …

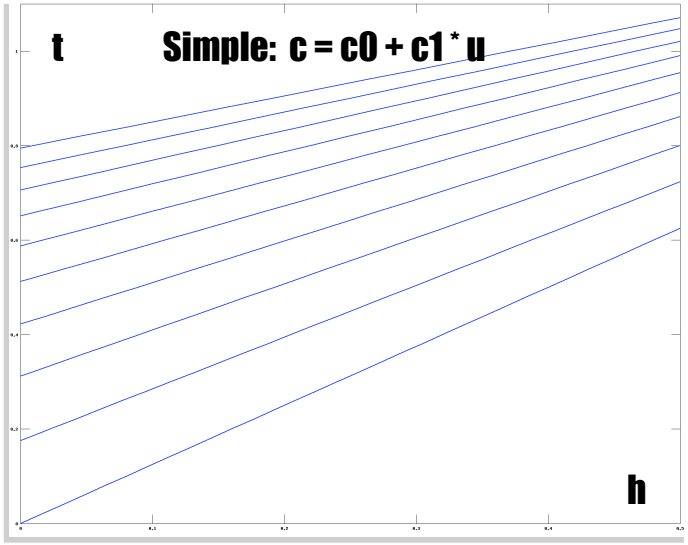

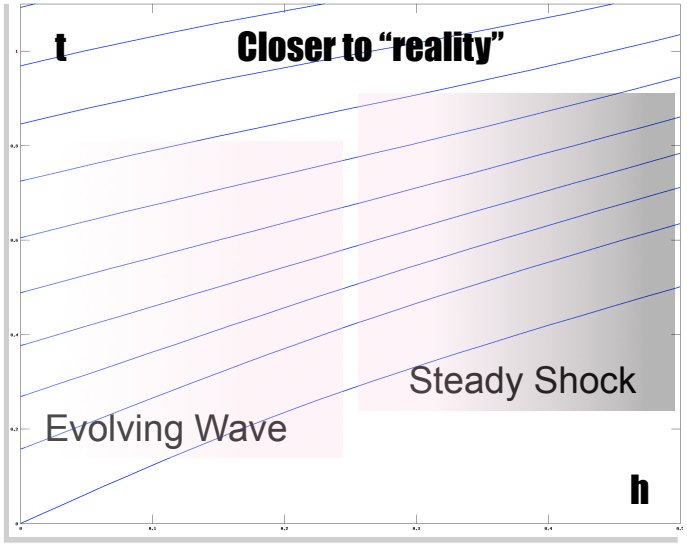

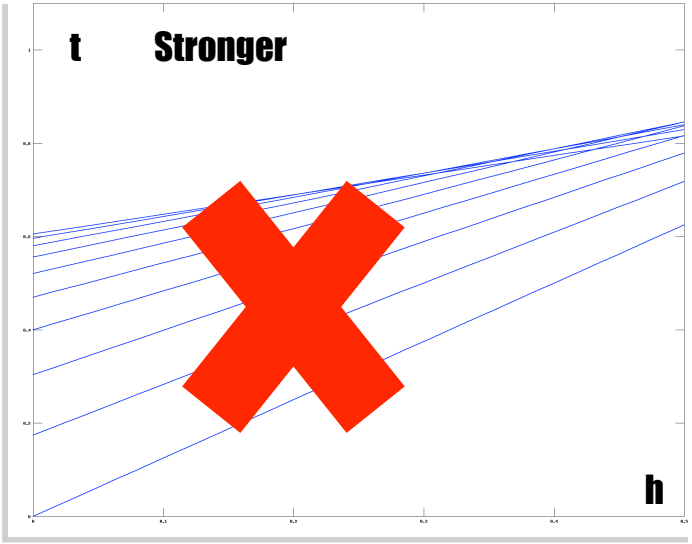

Entropy generation:

Strength, phase transitions,

constrained micro-cracking, etc.

=> C ~ c0 + c1* u + F(u,t)

Nonlinear wave propagation: Simple wave (isentrope) (cont.)

$$t_{k+1}(u) - t_k(u) \;=\; \tau(u) \;=\; \left(x_{k+1} - x_k\right) c_{Lag}^{-1}(u)$$

Differentiate: $$\Gamma_{k+1}^{-1}(u) - \Gamma_k^{-1}(u) \;=\; (x_{k+1} - x_k) \frac{d}{du} c_{Lag}^{-1}(u)$$

Acceleration: $$\Gamma_k(u) \;\equiv\; \left[\frac{du}{dt}\right]_k$$

No explicit time dependence.

Proportional to difference in Lagrangian coordinate.

Depends on nonlinearity of $\sigma - \varepsilon$

Reciprocal acceleration analysis: A quantitative test to identify regions of the flow that are amenable to Lagrangian analysis.

- Linearly proportional to step size.
- Proportional to nonlinear elasticity.
- Vanishes in limit of any stationary wave, including linear acoustical waves and dissipative structures.
- Emphasizes slowest strain rates in flow, where the Lagrangian velocity is least dissipative and well behaved.
- Probes derivative of Lagrangian velocity with respect to particle velocity, allowing a unique perspective to characterize deviations from reversible flow (experimental noise, dissipative/dispersive processes).

Current techniques presume reversibility and define an arbitrary consistency condition. e.g. backward integration involves two characteristics, whereas three are needed to account for the curvature of constant velocity characteristics.

Nonlinear wave propagation: Simple wave (isentrope)

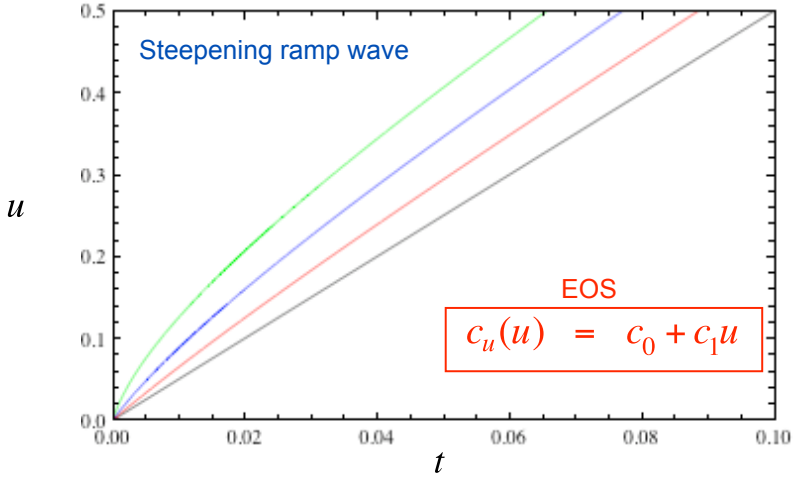

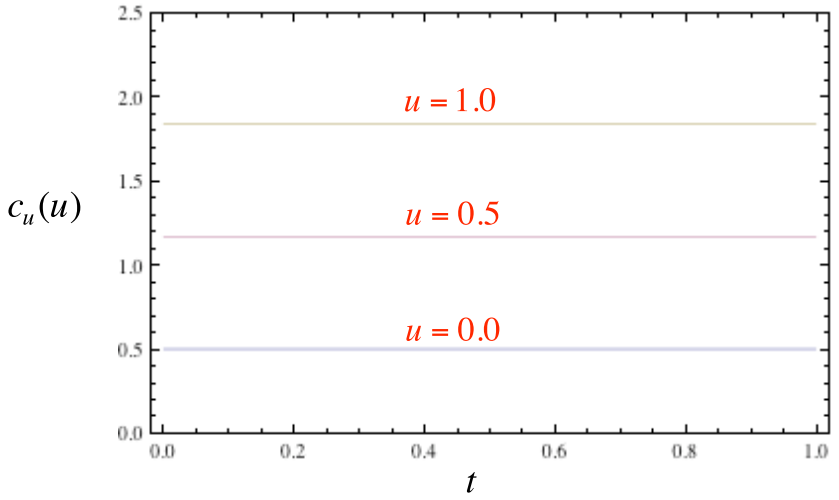

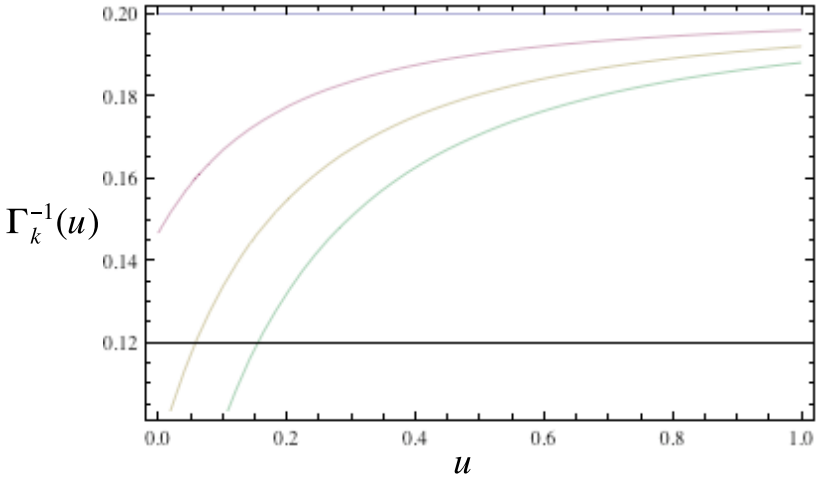

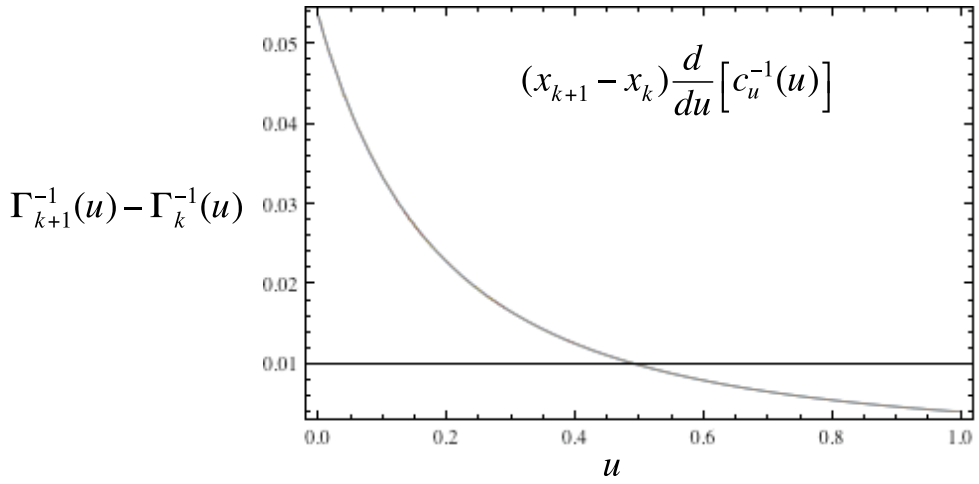

Summary: Simple wave (isentrope) (cont.)

Proportional to step size for a fixed u.

Decreases monotonically with u.

Proportional to nonlinearity in EOS.

$$\Gamma_{k+1}^{-1}(u) - \Gamma_k^{-1}(u) = (x_{k+1} - x_k)\frac{d}{du}c_{Lag}^{-1}(u)$$

Experiments should be designed to isolate reciprocal profiles from uncorrelated noise, e.g. sufficiently large step size and range of particle velocities.

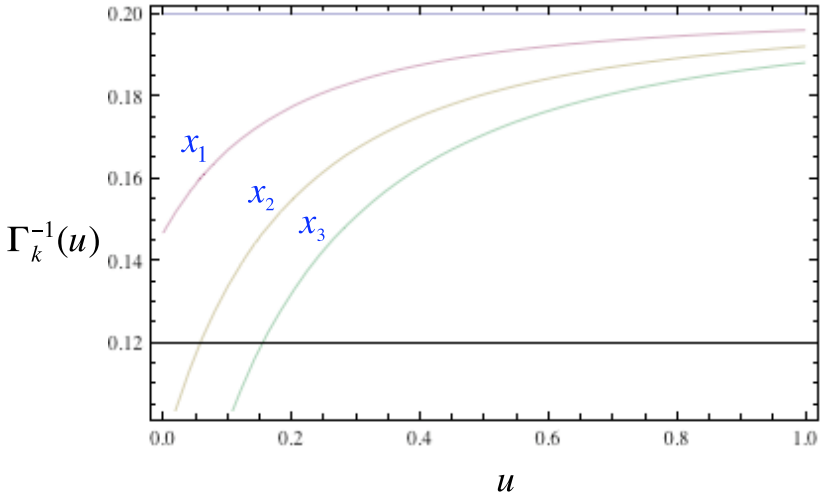

Aluminum

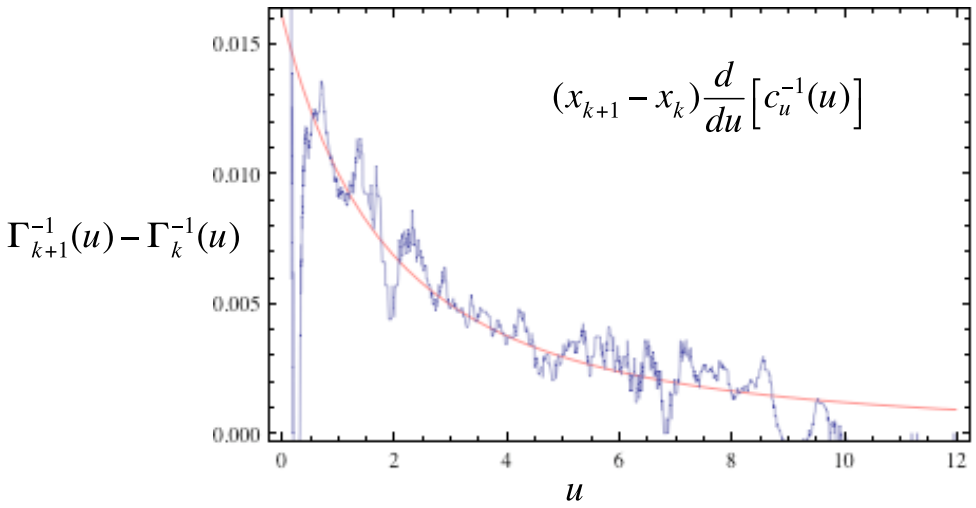

Experimental aluminum data: Z-ramp (J. P. Davis)

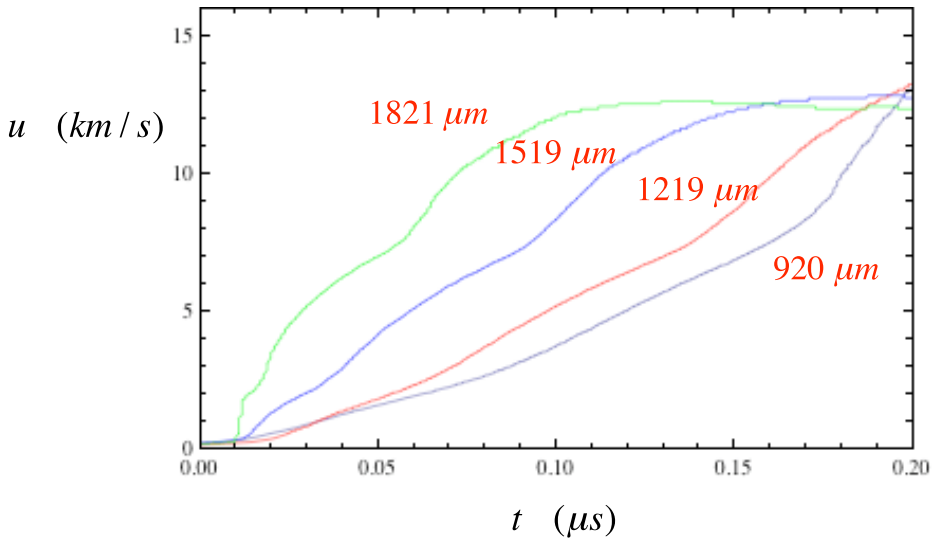

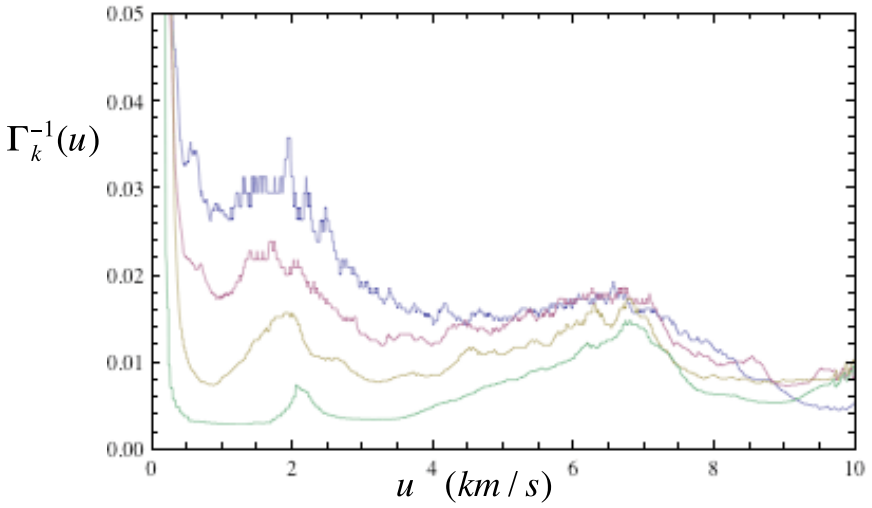

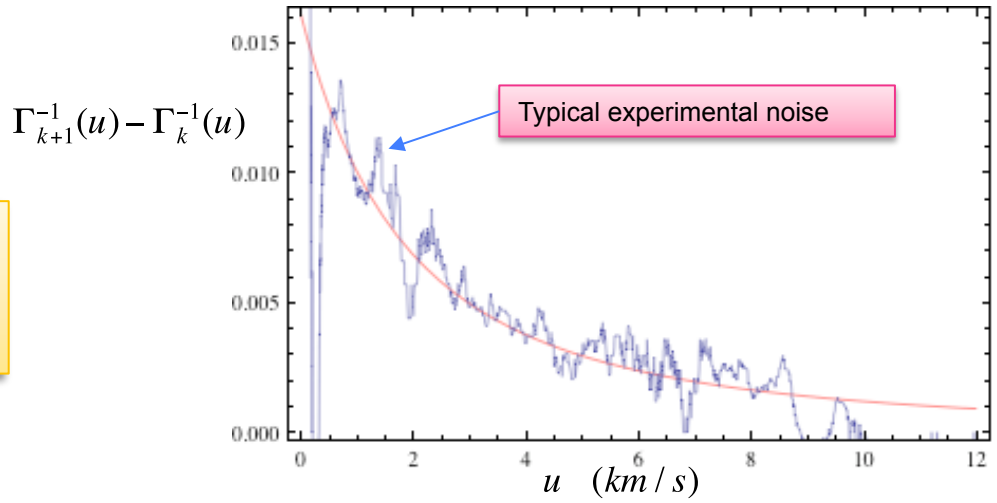

The formation of a dissipative structure is followed by approximate simple wave behavior.

Experimental aluminum data: Z-ramp (J. P. Davis)

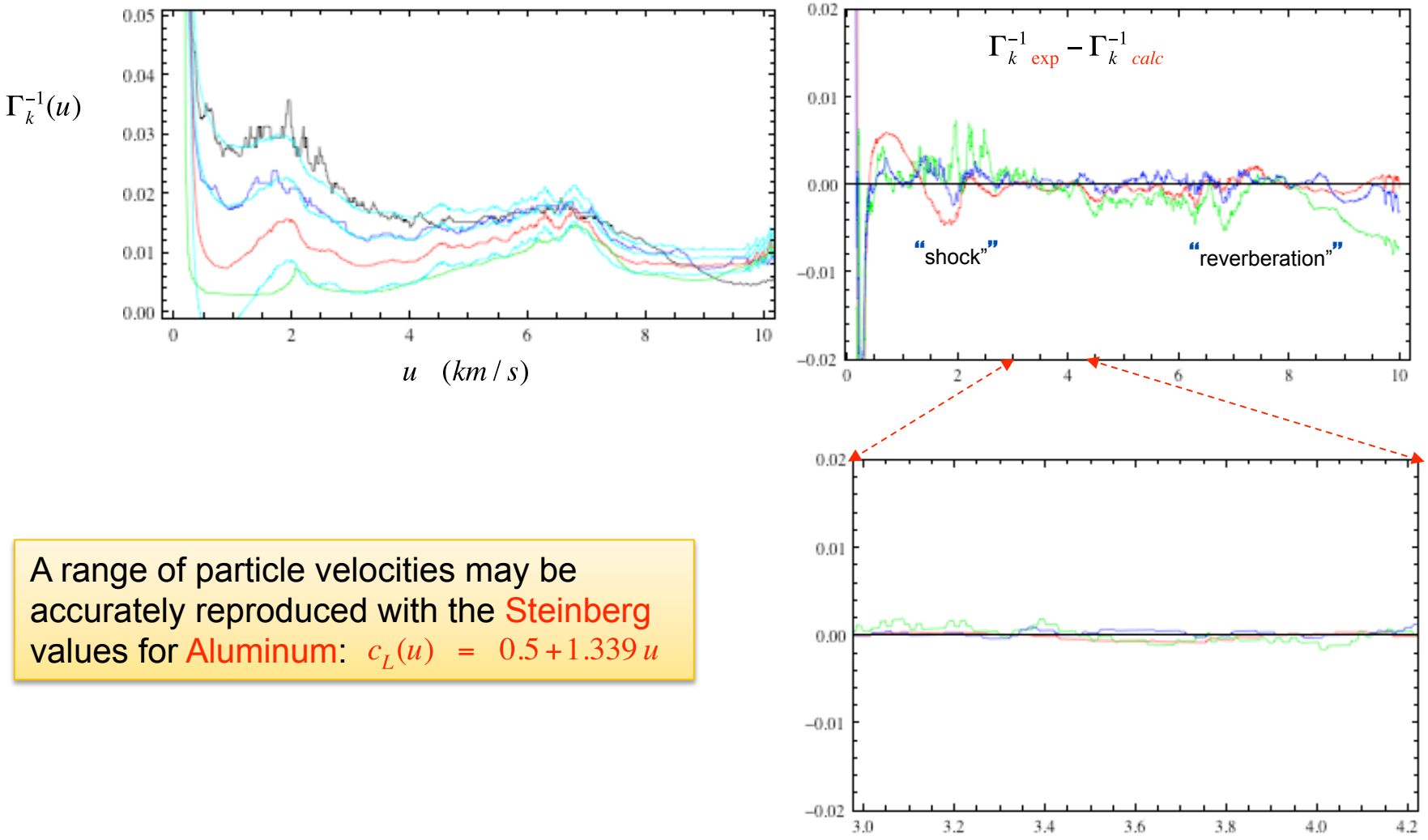

A range of particle velocities may be accurately reproduced with the Steinberg values for Aluminum: $c_L(u) = 0.5 + 1.339\,u$

Nonsimple wave : Curved characteristics

$$x(u,t) = c_u(u)\,t + F(u,t)$$

$$c_L(u,t) = c_u(u) + \frac{\partial F(u,t)}{\partial t}$$

$$c_\sigma(u) = c_L(u,t) + \left(\frac{\partial u}{\partial t}\right)_x^{-1} \int du \frac{\partial^2 F(u,t)}{\partial t^2} \qquad \sigma(u) = \rho_0 \int du\, c_\sigma(u)$$

$$\Gamma_{k+1}^{-1}(u) - \Gamma_k^{-1}(u) = \left(x_{k+1} - x_k\right)\frac{dc_u^{-1}(u)}{du} + \left(x_{k+1} - x_k\right)\frac{\partial}{\partial u}\left[\left(\frac{\partial F(u,t)}{\partial t}\right)^{-1}\right]$$

Curved characteristics introduce explicit time dependence. In principle, F(u,t) may be inferred from the reciprocal acceleration profiles and used to estimate corrections to the stress (σ).

Nonlinear wave propagation: Curved characteristics introduce explicit time dependence and split degeneracy for equal step sizes.

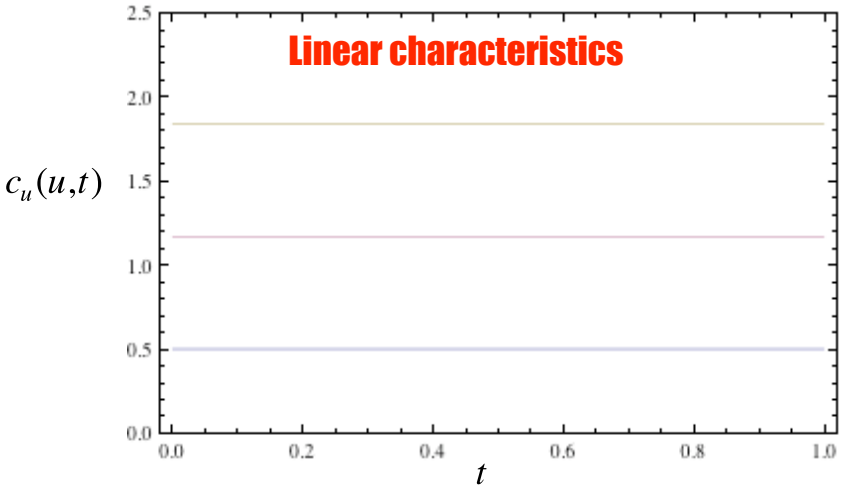

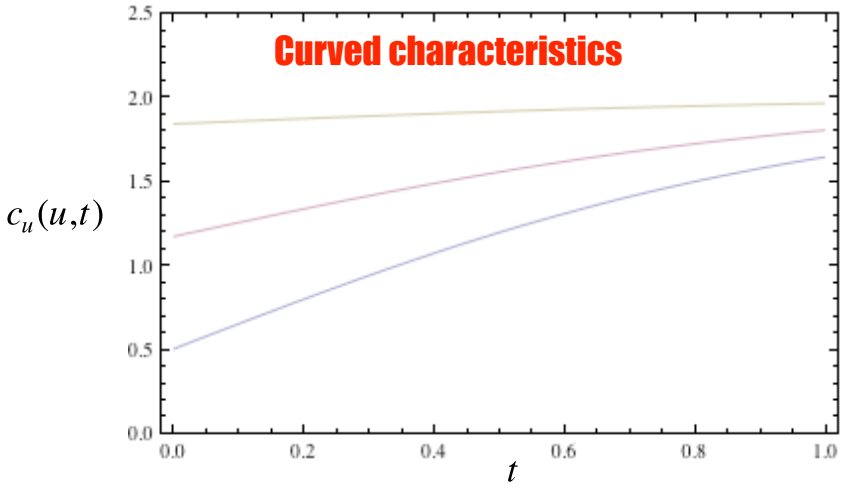

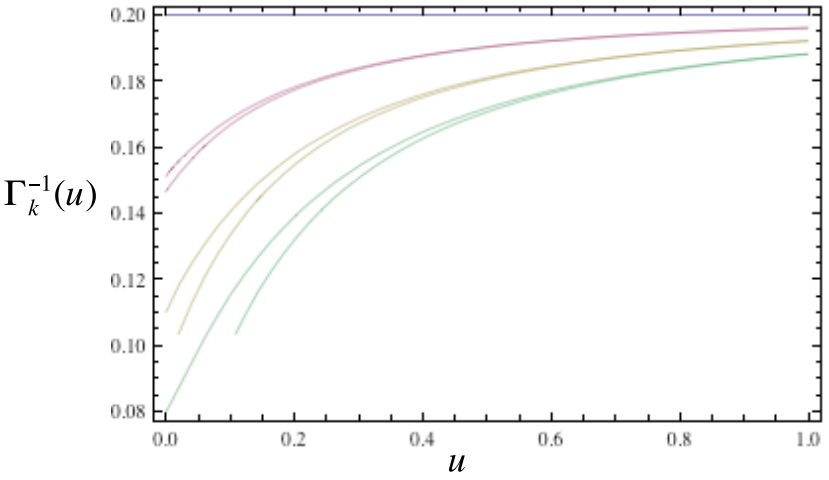

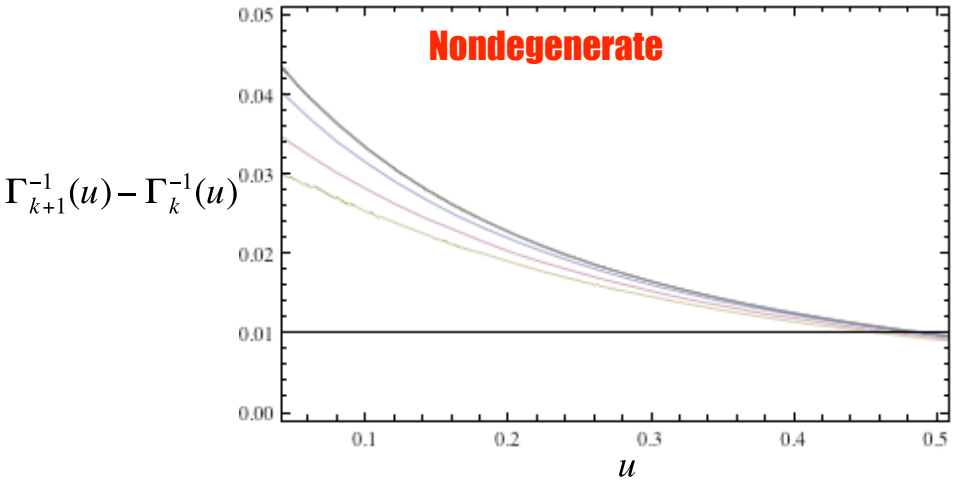

Beryllium Z-ramp data (Knudson)

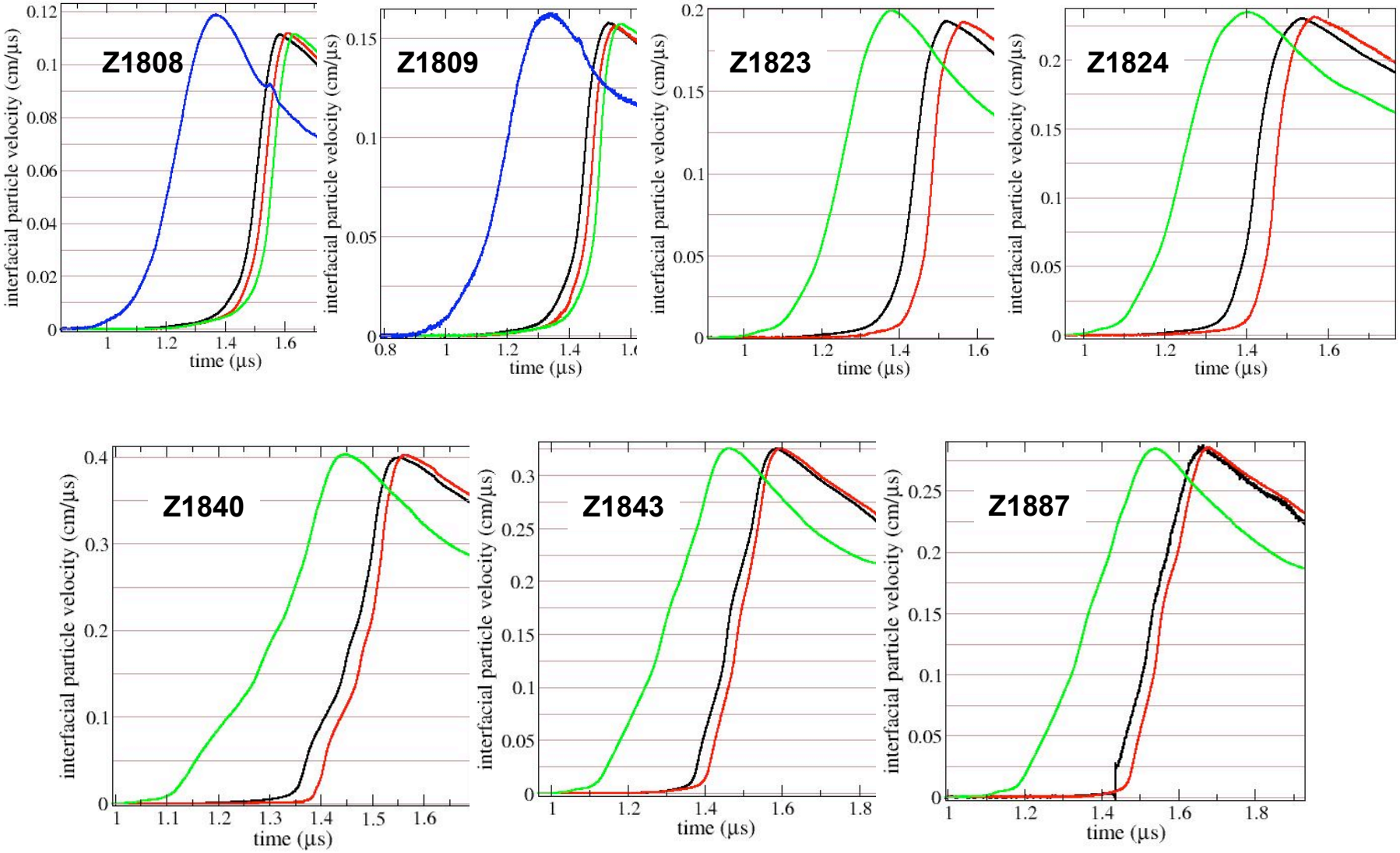

Typical Be data for this set

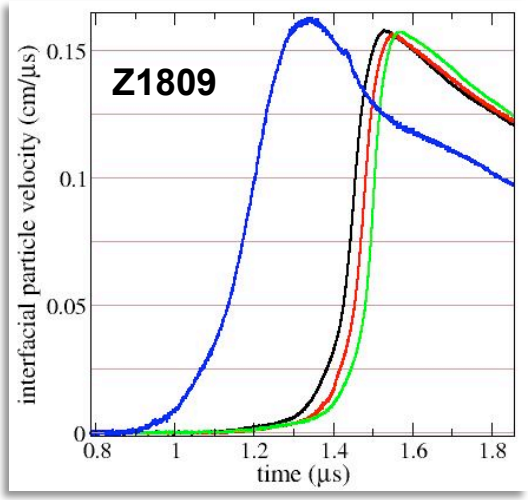

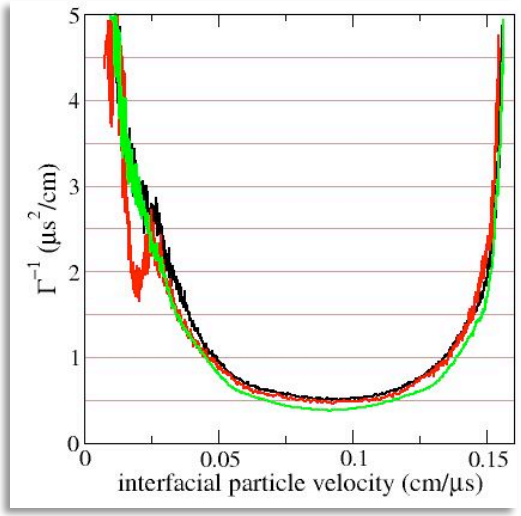

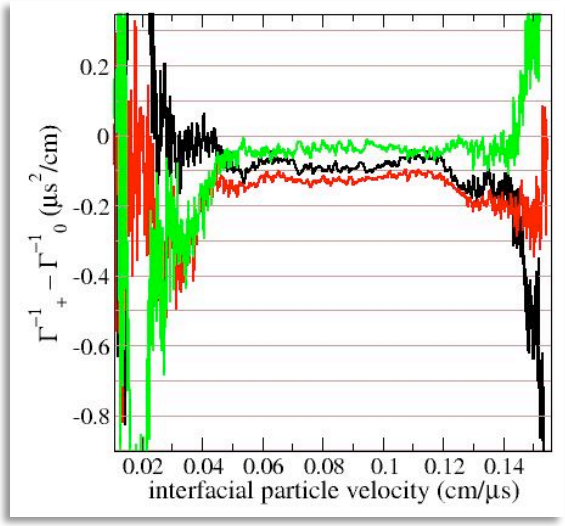

$$(x_{k+1} - x_k)\frac{d}{du}\left[c_u^{-1}(u)\right]$$

- **Most data from this set indicates a mostly flat U dependence for $\Delta\,\Gamma^{-1}$**
- **Flat Up suggests C(u) ~ 1/Up**

Z1808 and Z1824 are different

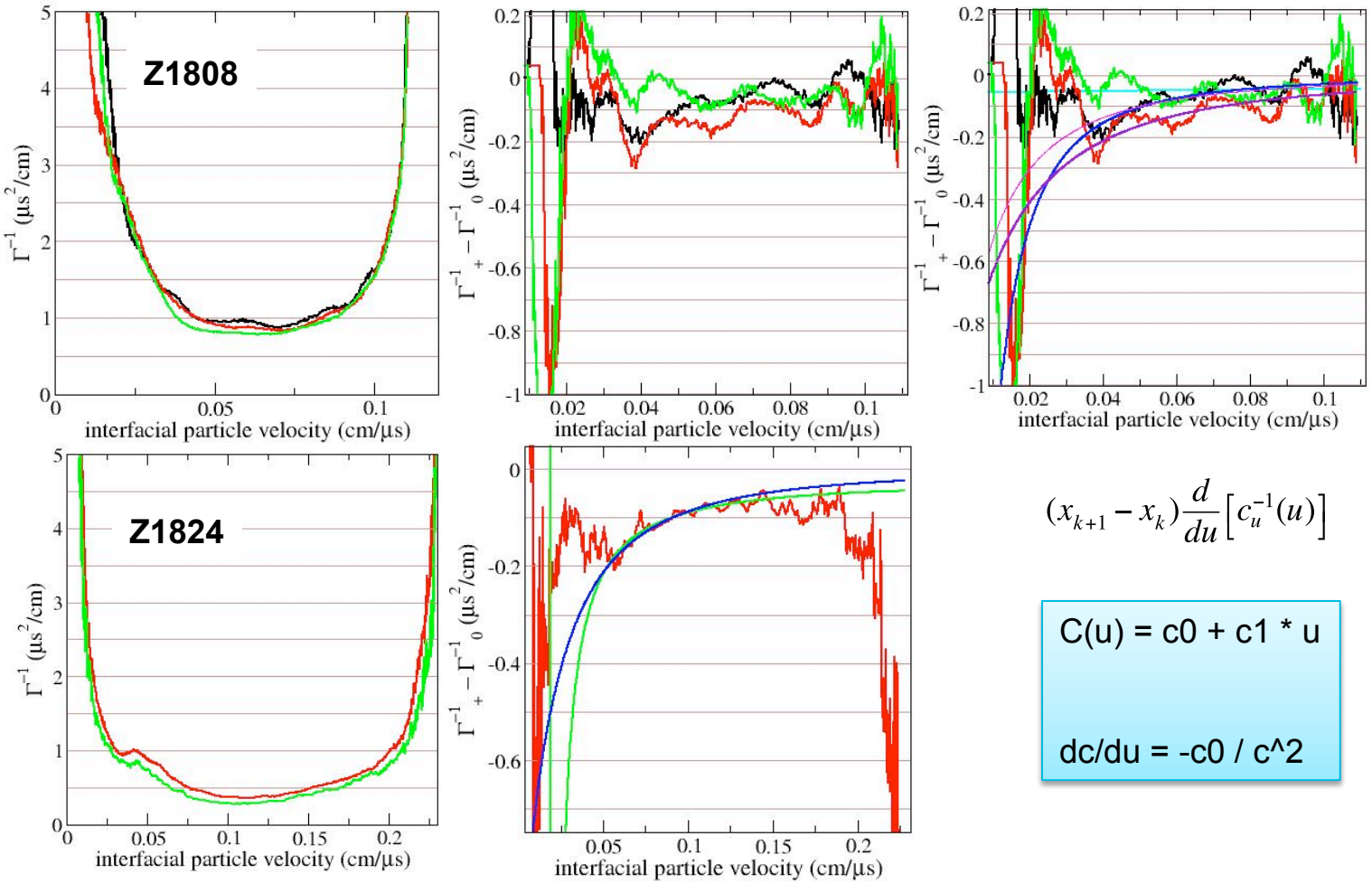

$$(x_{k+1} - x_k)\frac{d}{du}\left[c_u^{-1}(u)\right]$$

C(u) = c0 + c1 * u

dc/du = -c0 / c^2

- **Fitting the results yields very different c0 and c1 values.**
- **Overall, unusual material behavior is suggested**

Be

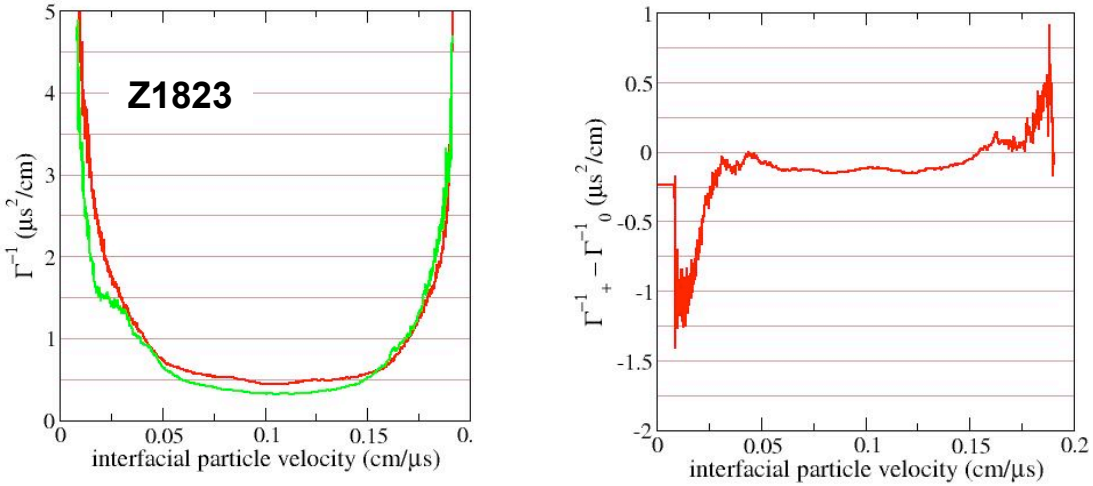
Z1823
Γ^{-1} (μs^2/cm)
interfacial particle velocity (cm/μs)
$\Gamma^{-1}_+ - \Gamma^{-1}_0$ (μs^2/cm)
interfacial particle velocity (cm/μs)

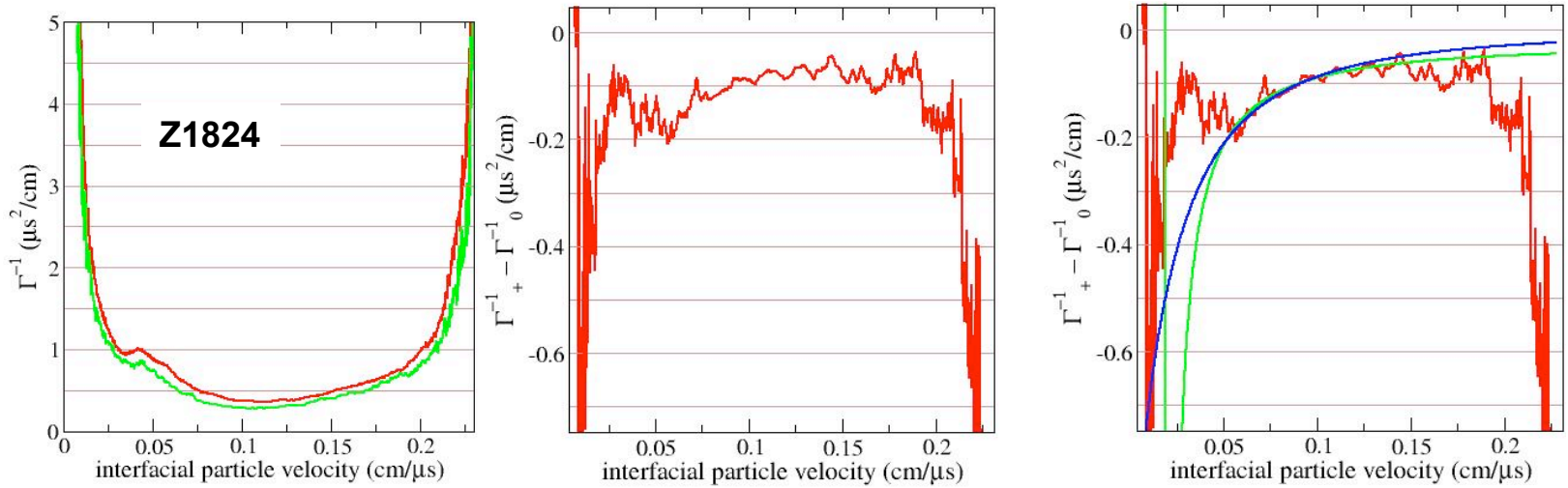
Z1824
Γ^{-1} (μs^2/cm)
interfacial particle velocity (cm/μs)
$\Gamma^{-1}_+ - \Gamma^{-1}_0$ (μs^2/cm)
interfacial particle velocity (cm/μs)
$\Gamma^{-1}_+ - \Gamma^{-1}_0$ (μs^2/cm)
interfacial particle velocity (cm/μs)

Be

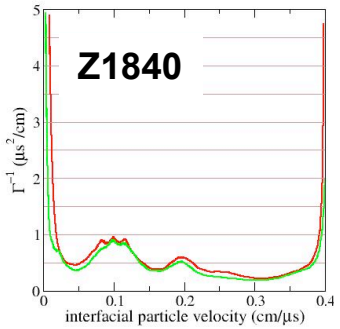
Z1840
Γ^{-1} (μs^2/cm)
interfacial particle velocity (cm/μs)

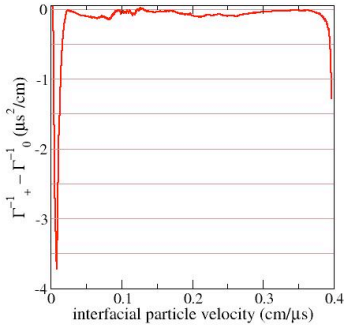
$\Gamma^{-1}_+ - \Gamma^{-1}_0$ (μs^2/cm)
interfacial particle velocity (cm/μs)

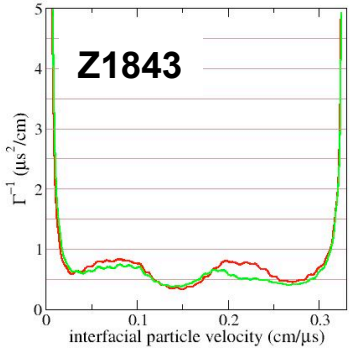
Z1843
Γ^{-1} (μs^2/cm)
interfacial particle velocity (cm/μs)

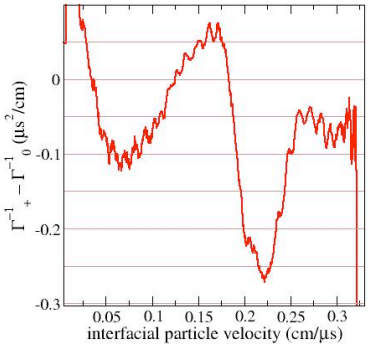
$\Gamma^{-1}_+ - \Gamma^{-1}_0$ (μs^2/cm)
interfacial particle velocity (cm/μs)

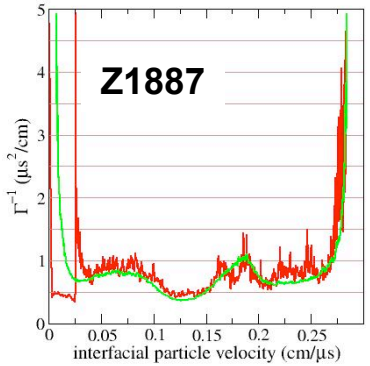
Z1887
Γ^{-1} (μs^2/cm)
interfacial particle velocity (cm/μs)

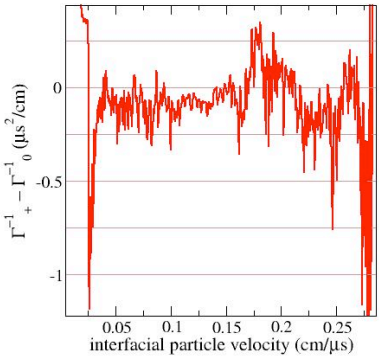
$\Gamma^{-1}_+ - \Gamma^{-1}_0$ (μs^2/cm)
interfacial particle velocity (cm/μs)

Reciprocal acceleration analysis: A quantitative test to identify regions of the flow that are amenable to Lagrangian analysis.

- Linearly proportional to step size.
- Proportional to nonlinear elasticity.
- Vanishes in limit of any stationary wave, including linear acoustical waves and dissipative structures.
- Emphasizes slowest strain rates in flow, where the Lagrangian velocity is least dissipative and well behaved.
- Probes derivative of Lagrangian velocity with respect to particle velocity, allowing a unique perspective to characterize deviations from reversible flow (experimental noise, dissipative/dispersive processes).

Current techniques presume reversibility and define an arbitrary consistency condition. e.g. backward integration involves two characteristics, whereas three are needed to account for the curvature of constant velocity characteristics.

Summary

- Reciprocal acceleration analysis was used to investigate beryllium data from Z-ramp.
- Non-linear Lagrangian Sound Speed wrt particle velocity is evident.
  - Fits to restricted regions of particle velocity suggest abnormal values for linear sound speed.
  - Most data gives $\Delta\,\Gamma^{-1}$ as a constant wrt particle velocity.
- Such material response might be the result of brittle behavior---a constrained fracture?
- We would like more experiments with minimum of 3 step sizes to better understand the phase character in the sound speed.

Experimental data: Marina Bastea Tantalum Z-ramp

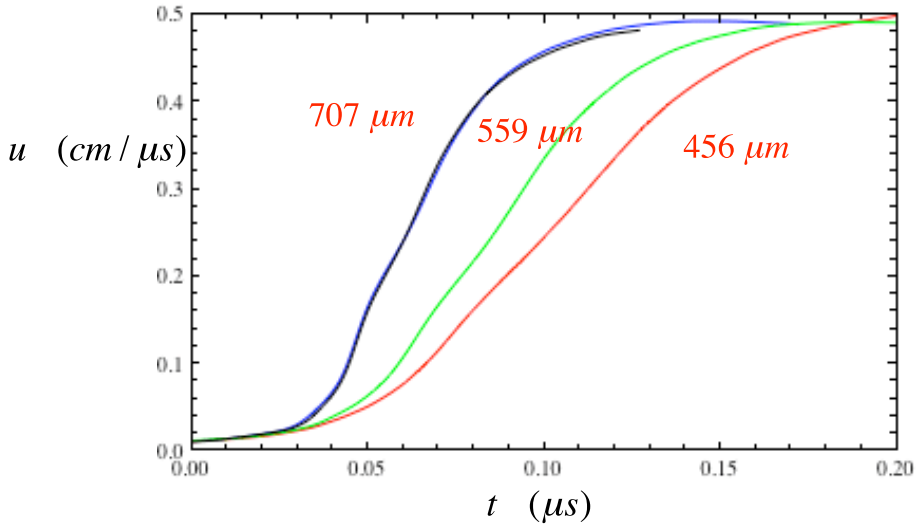

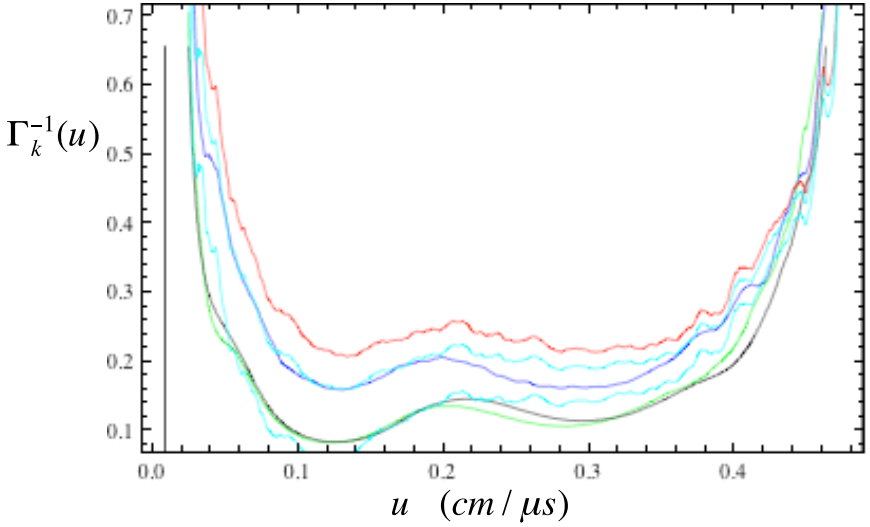

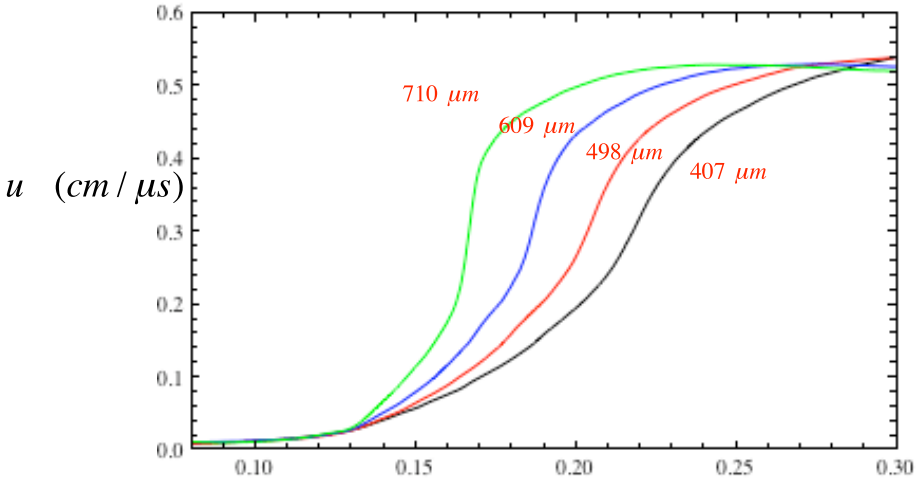

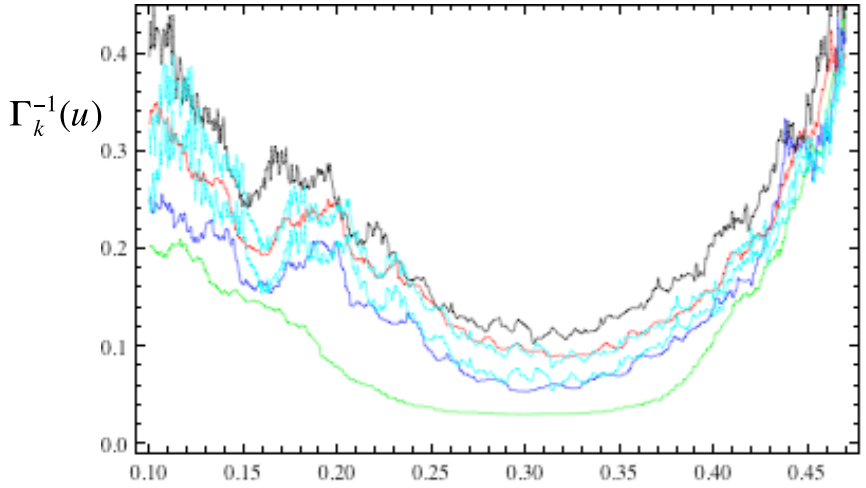

Experimental data: Marina Bastea Tantalum

$\Gamma_k^{-1}(u)$

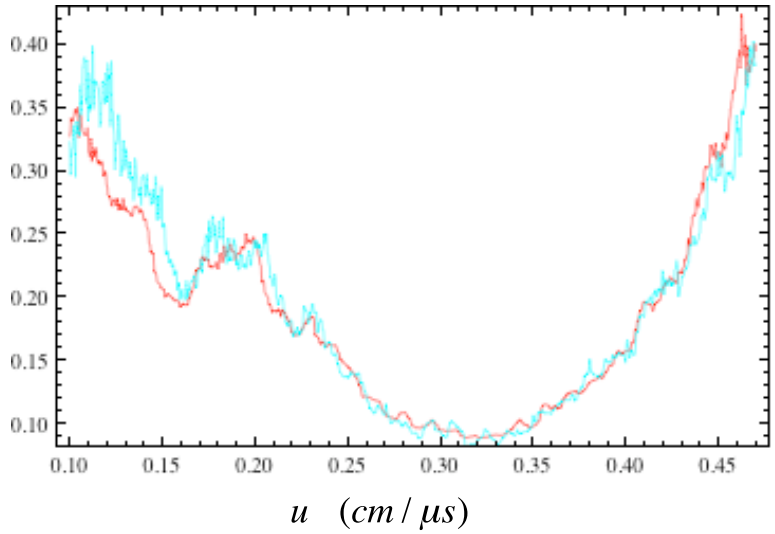

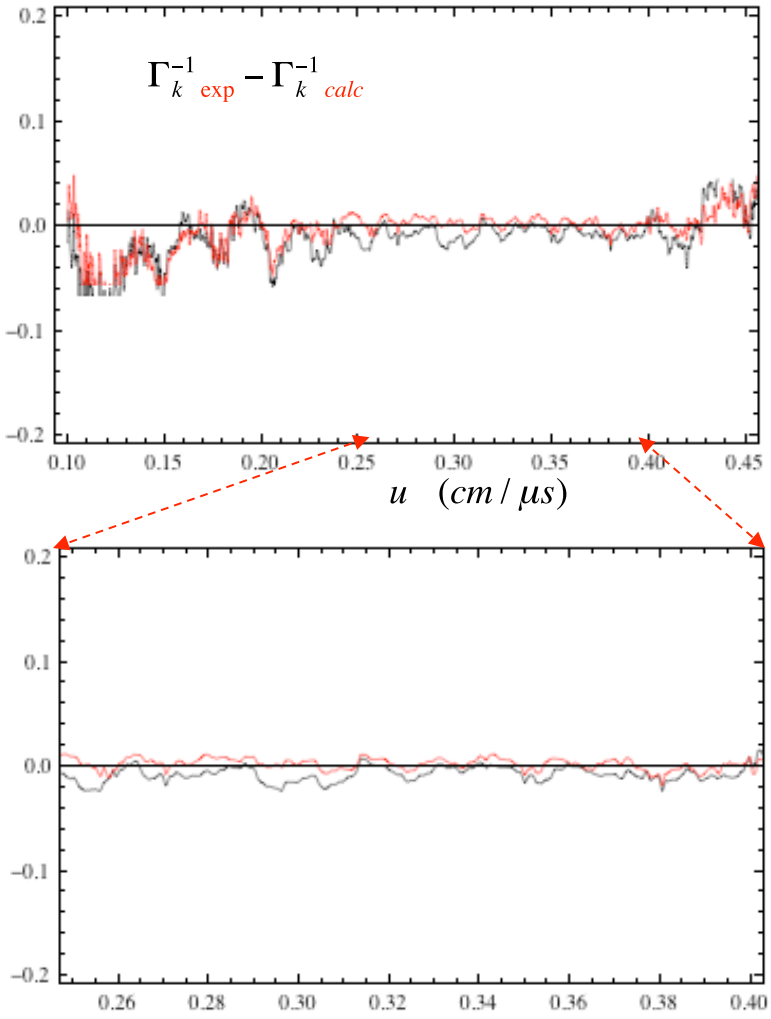

A range of particle velocities may be accurately reproduced with the Steinberg values for Tantalum: $c_L(u) = 0.348 + 1.20\,u$

Dissipation: Burgers equation as a model of dissipation (cont.)

$$\partial_t u + \left(c_0 + c_1 u\right)\partial_x u = \beta \partial_x^2 u$$

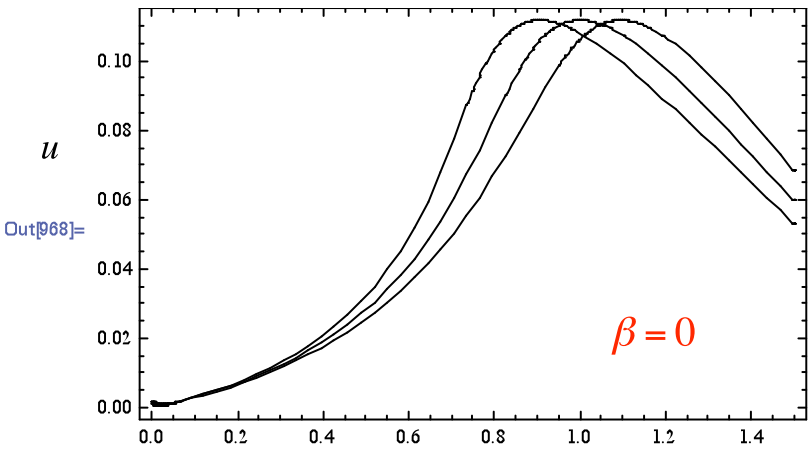

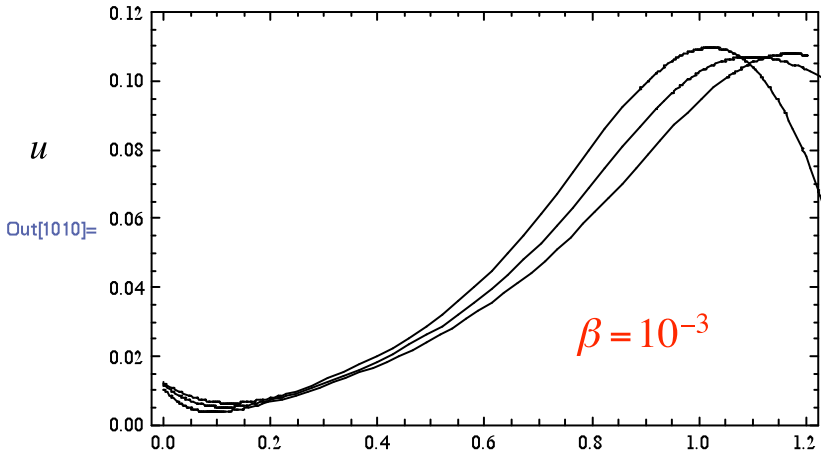

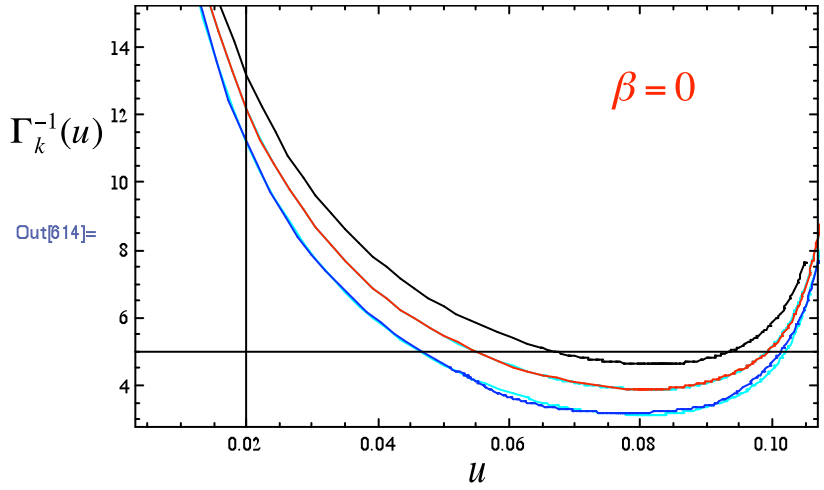

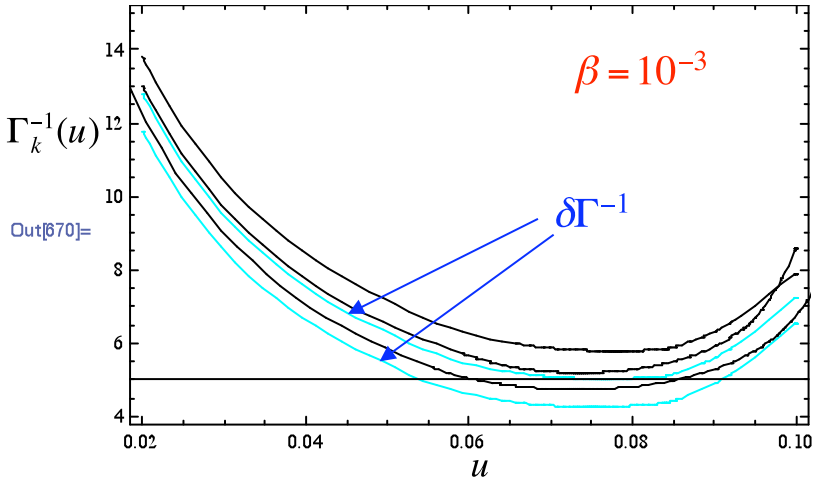

Sensitivity Analysis and Parameter Optimization Using 1-D MHD Simulations of Magnetic Drive Experiments

Ramp Compression Workshop

January 19, 2010

Joshua Robbins

Sandia National Laboratories is a multi-program laboratory operated by Sandia Corporation, a wholly owned subsidiary of Lockheed Martin company, for the U.S. Department of Energy's National Nuclear Security Administration under contract DE-AC04-94AL85000.

Outline

- Intro to Laslo
- Short description of MAPS
- Model equations of MHD in 1D with static applied field
- Sensitivity analysis
- Optimization problems
- Summary / conclusions

Sandia National Laboratories

Laslo: Lagrangian Analysis and Simulation of Loading in One dimension

Objective is to simplify:

- material model development / implementation
- development / implementation of new kinematics, model equations, etc.
- parameter study / optimization

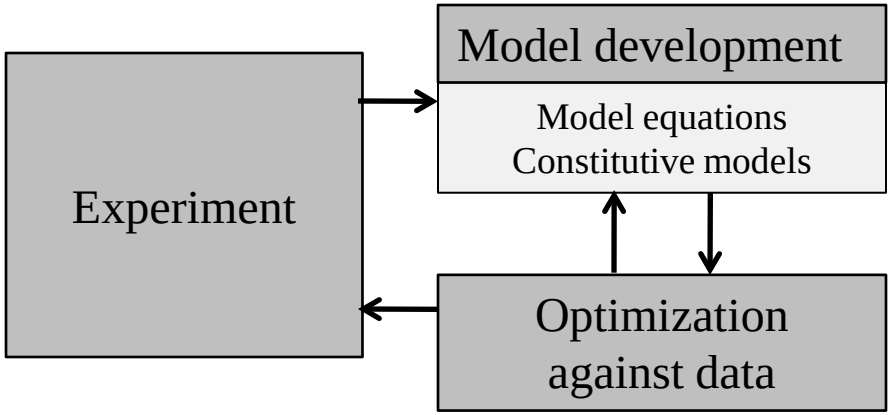

Approach:

- Python interface / virtual base class
- Integrated optimization kernel (Opt++)
- Modular: re-implement functions

- Updated Lagrangian formulation
- General 1D: velocity is 3D but varies only in x
- Central difference vs. Predictor-multicorrector (G. Scovazzi)
- 1D MHD
- Micro-inertia
- *Perturbation method, UQ, etc*

Sandia National Laboratories

Laslo: Lagrangian Analysis and Simulation of Loading in One dimension

Material model interface:

- C / C++ / Fortran: implementation is more involved. Fast.
- Python: implementation is fairly trivial. Slow.

Input file:

```
material 1 {
  density = 2785.0
  models = {1, 2}
}
python_model 1 {
  file = "plasticity_model"
  function = "plasticity_model”
  constant {
    name = "bulk_modulus"
    value = 4.324e10
  }
constants {
   names = {”hardening_modulus”, "initial_yield"}
   values = {0.0, 7.5e7}
  }
  input_variables = {"strain”,"strain increment”,"density”}
  output_variables = {"deviatoric stressxx”,
                      "deviatoric stresszz",
                      "pressure”, "soundspeed”}
  state_variables = {"back stress",
                     "plastic strain”, "yield stress",
                     "effective stress”, "alpha"}
}
mie_gruneisen 2 {
  gruneisen_parameter = 2.1
  slope = 1.345
  soundspeed = 5008.0
}
```

plasticity_model.py:

```
def plasticity_model(data, constants, numElements):

        ### boilerplate for loading math functions ###
        import math

        #### setup constants ###
        bulk_modulus = constants["bulk_modulus”]
.
.
        ### unpack arrays from data dictionary ###
        strain     = data["strain"]
        strain_inc = data["strain increment"]
        density    = data["density"]

        dev_stressxx = data["deviatoric stressxx”]
        dev_stresszz = data["deviatoric stresszz"]
        pressure     = data["pressure"]
        sound_speed  = data["soundspeed"]
        yield_stress = data["yield stress"]
        effective_stress = data["effective stress"]

        plastic_strain = data["plastic strain"]
        back_stress = data["back stress"]
        alpha = data["alpha"]

        ### for each element ###
        # see Simo, Hughes, (1998), Computational Inelasticity
        for ielem in range(numElements):
```

Magnetically Applied Pressure-Shear

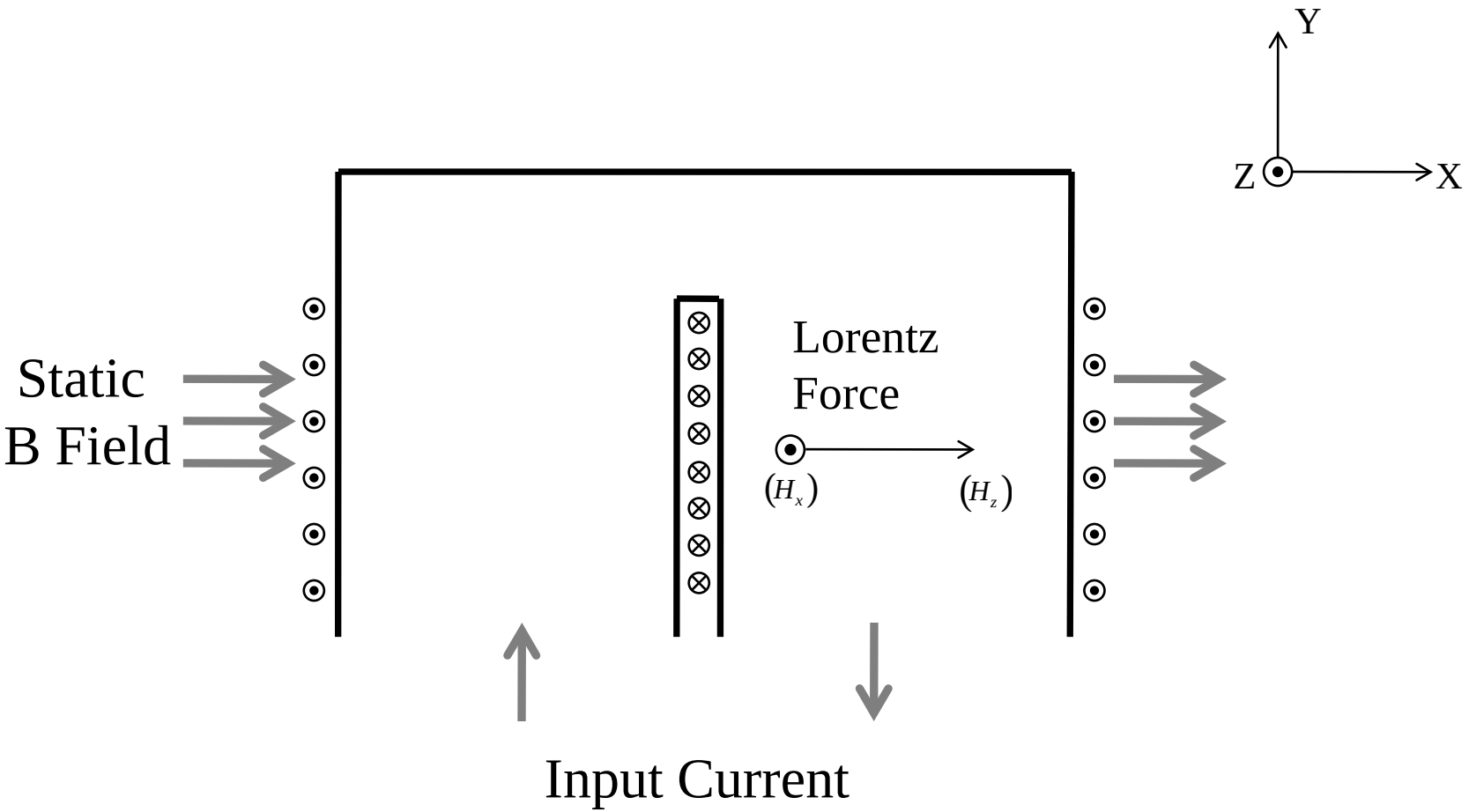

Sandia National Laboratories

Model Equations

Maxwell-Faraday: $\nabla \times \mathbf{E} = -\mu \frac{\partial \mathbf{H}}{\partial t}$

Ampere: $\nabla \times \mathbf{H} = \mathbf{J}$

Ohm: $\eta \mathbf{J} = \mathbf{E} + \mathbf{v} \times \mu \mathbf{H}$

Combine

$$\mu \frac{D\mathbf{H}}{Dt} = -\nabla \times \eta(\nabla \times \mathbf{H}) - \mu \mathbf{H}(\nabla \cdot \mathbf{v}) + \mu(\mathbf{H} \cdot \nabla)\mathbf{v}$$

Reducing to one dimension: Magnetizing field, H, and velocity, v, generally can have three non-zero components, but only vary in x:

$$\mu \frac{DH_x}{Dt} = \eta \frac{\partial^2 H_x}{\partial x^2}$$

$$\mu \frac{DH_y}{Dt} = \eta \frac{\partial^2 H_y}{\partial x^2} - \mu \left(H_y \frac{\partial v_x}{\partial x} - H_x \frac{\partial v_y}{\partial x} \right)$$

$$\boxed{\mu \frac{DH_z}{Dt} = \eta \frac{\partial^2 H_z}{\partial x^2} - \mu \left(H_z \frac{\partial v_x}{\partial x} - H_x \frac{\partial v_z}{\partial x} \right)}$$

With initial conditions:

$$\begin{matrix} H_x(x,t_o) = H_x^o \\ H_y(x,t_o) = 0 \end{matrix} \Rightarrow \begin{matrix} H_x(x,t) = H_x^o \\ H_y(x,t) = 0 \end{matrix}$$

the problem reduces to solving for the z component of H.

Sandia National Laboratories

Discrete Form

Using the Galerkin approximation for H and v in the weak form of the model equation results in the discrete form:

$$\mathbf{H}^{n+1} = \mathbf{K}^{-1}\frac{1}{\Delta t}\mathbf{M}\mathbf{H}^{n} + \mathbf{F} \qquad \mathbf{M} = \sum_{el}\int_{\Omega_{el}} N^{T}\mu N\frac{dx}{d\xi}d\Omega_{\xi}$$

$$\mathbf{K} = \frac{1}{\Delta t}\mathbf{M} + \mathbf{L} + \mathbf{S} \qquad \mathbf{L} = \sum_{el}\int_{\Omega_{el}} B^{T}\eta B\frac{dx}{d\xi}d\Omega_{\xi}$$

$$\mathbf{F} = \sum_{el}\int_{\Omega_{el}} N^{T}\mu H_{x}Bv_{z}^{n+1/2}\frac{dx}{d\xi}d\Omega_{\xi} \qquad \mathbf{S} = \sum_{el}\int_{\Omega_{el}} N^{T}\mu Bv_{x}^{n+1/2}N\frac{dx}{d\xi}d\Omega_{\xi}$$

The linear system is solved using AztecOO. Lorentz forces and Joule heating are computed by:

$$\mathbf{f}^{l} = \mu\begin{Bmatrix} -H_{z}\dfrac{\partial H_{z}}{\partial x} \\ 0 \\ H_{x}\dfrac{\partial H_{z}}{\partial x} \end{Bmatrix} \qquad \dot{E}_{j}^{Y} = \eta\rho J_{y}J_{y}$$

Sandia National Laboratories

Alegra Comparison

Models: MG Us-Up, elastic plastic, LMD

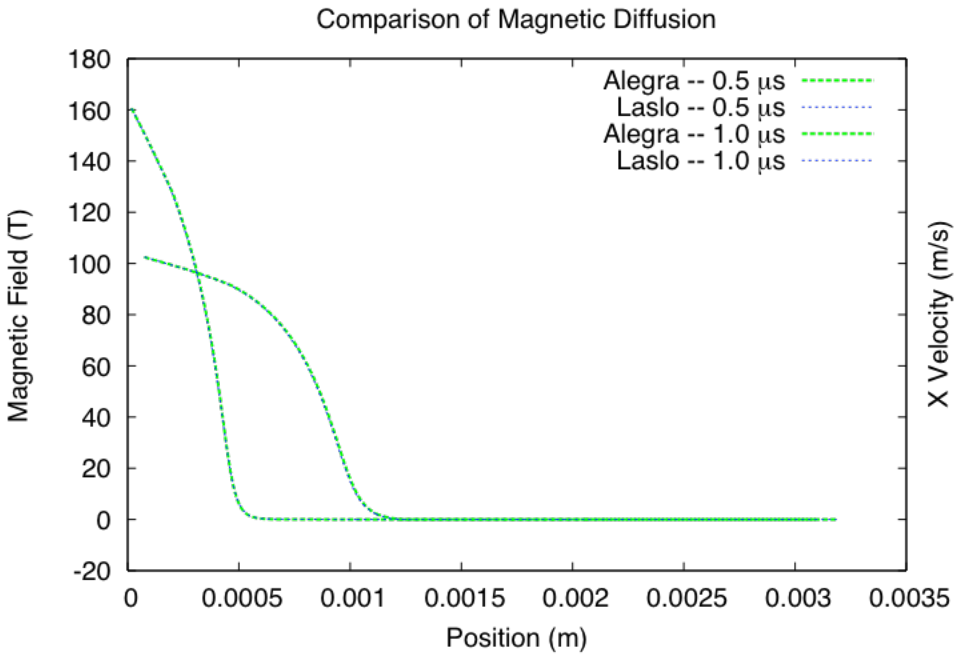

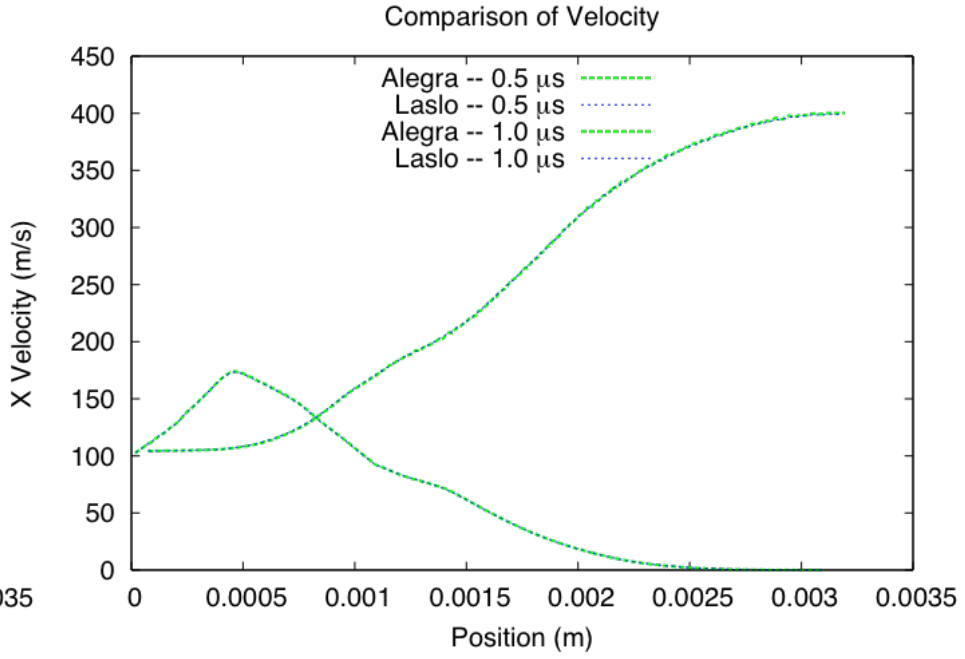

Sandia National Laboratories

Sensitivity Study

```
parameter_study {
  variable 1 {
    variable = "elastic_plastic(11)|yield_stress"
    range = {8e8, 24e8}
    intervals = 4
  }
}
```

```
.
.
elastic_plastic 11 {
  youngs_modulus = 1.86e11
  poissons_ratio = 0.38
  yield_stress = 16e8
}
.
.
```

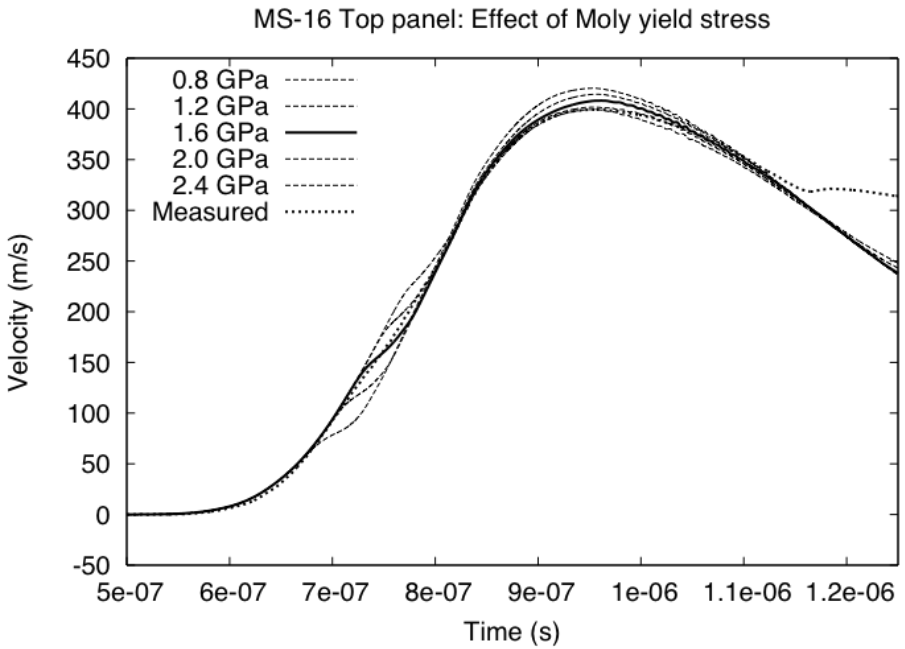

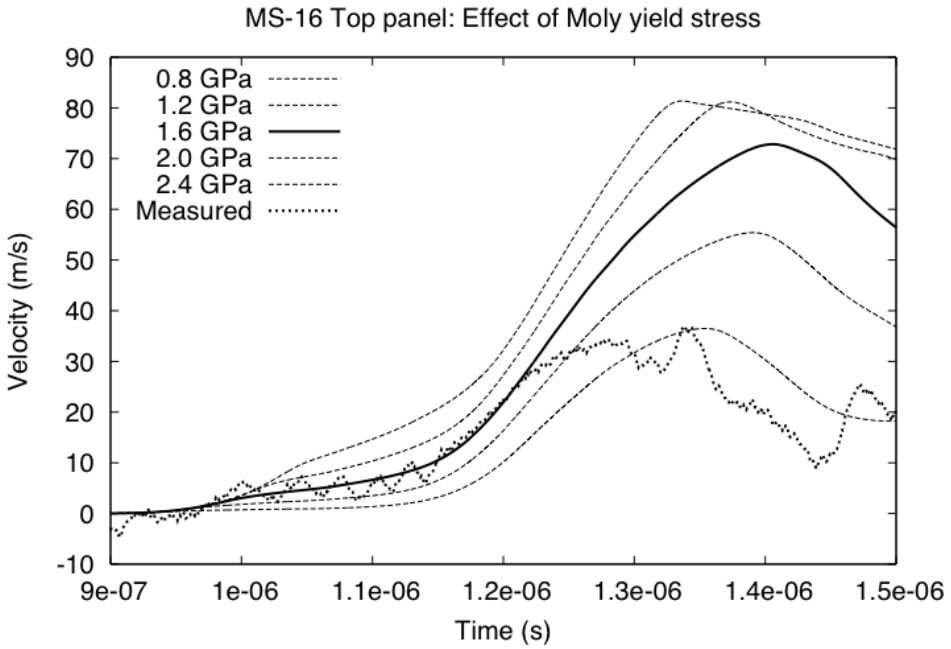

Sandia National Laboratories

Sensitivity Study

```
parameter_study {
  variable 1 {
    variable = "mesh|block(1)|length"
    range = {1.0413e-3, 1.2413e3}
    intervals = 4
  }
}
```

```
.
.
mesh {
  block {
    length = 1.1413e-3
    .
    .
  }
}
.
.
```

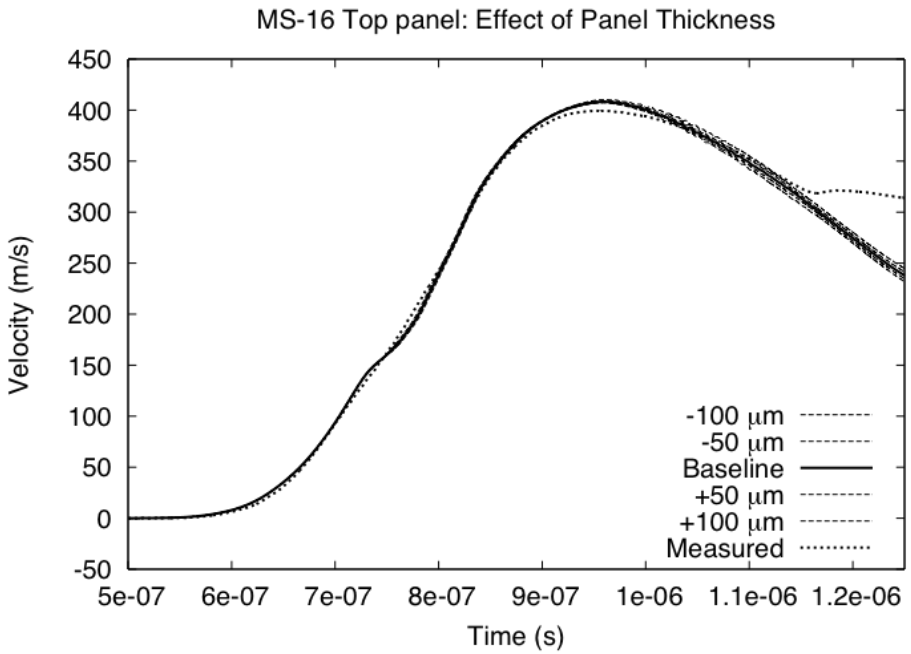

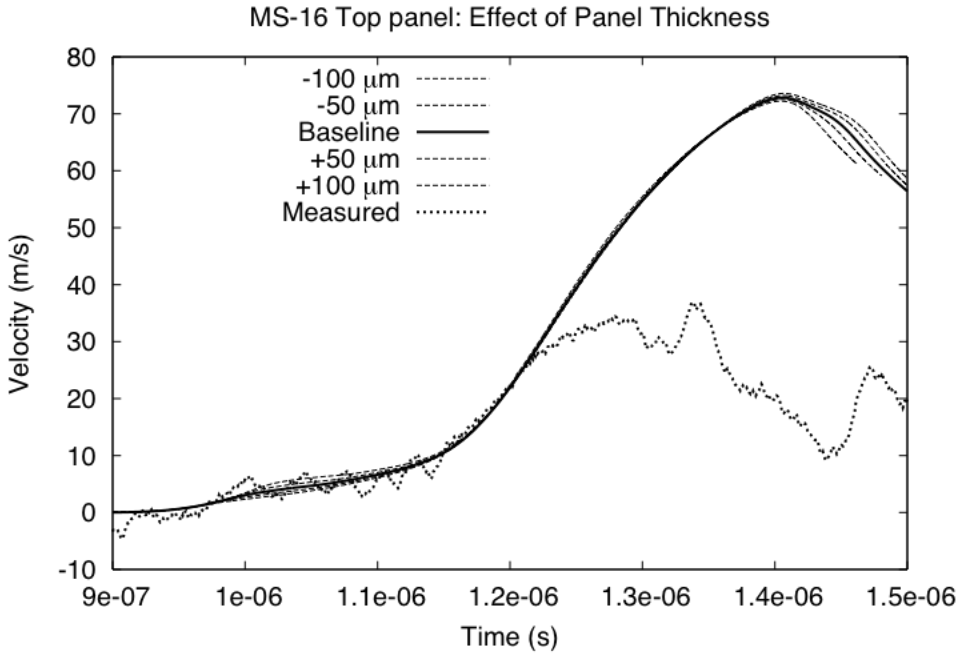

Sandia National Laboratories

Optimization

```
optimization {
  relative_tolerance = 1e-6
  variable 1 {
    variable = "boundary_conditions|tabular_magnetic_field|scale"
    range = {56.33333, 57.0}
  }
  variable 2 {
    variable = "elastic_plastic(11)|yield_stress"
    range = {8e8, 24e8}
  }
  variable 3 {
    variable = "elastic_plastic(11)|hardening_modulus"
    range = {-3.1e10, 3.1e10}
  }
  variable 4 {
    variable = "initial_conditions|uniform|values[0]"
    range = {6.0e6, 6.2e6}
  }
  objective {
    square_difference {
      variable_alias = "optimize_x"
      target = "vx_target.dat"
      domain = {5e-7, 1.15e-6}
    }
    square_difference {
      variable_alias = "optimize_z"
      target = "vy_target.dat"
      domain = {9e-7, 1.7e-6}
    }
  }
}
```

	OTS	Optimized 1	Optimized 2
Yield stress (GPa)	1.6	1.35	1.72
Hardening Modulus (GPa)	0.0	-27.2	9.2
Peak Current	1.0	0.994	--
Static Field	1.0	0.982	0.33

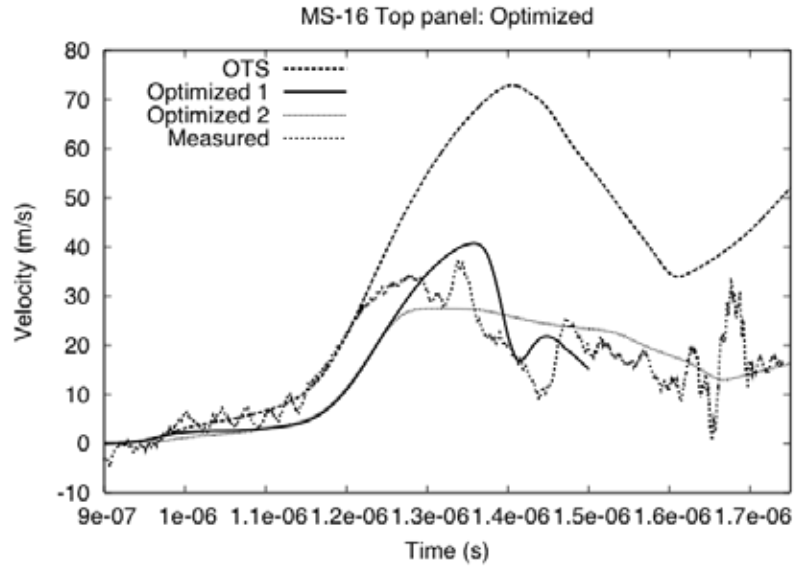

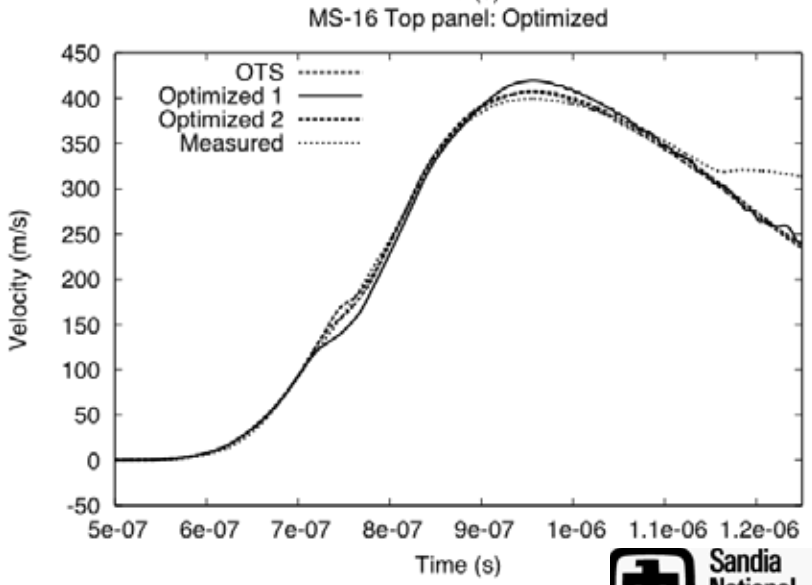

Sandia National Laboratories

Summary

Laslo is a simple and lightweight transient dynamics code that is intended to simplify:

- **development and implementation of model equations (e.g., MHD)**
- **development and implementation of material models**
- **sensitivity study / optimization**

Modeling of the dynamic inelasticity of poly- and single crystal tantalum under ramp wave loading*

Jow Ding[1] & Jim Asay[2]

[1]Washington State University
[2] Sandia National Labs

*** Work sponsored by Sandia National Labs**

Presented at the 4th Workshop on Ramp Compression

Sandia is a multi-program laboratory operated by Sandia Corporation, a Lockheed Martin Company for the United States Department of Energy's National Nuclear Security Administration under contract DE-AC04-94AL85000.

Outline

- Experimental observations of poly- and single crystal tantalum behavior under ramp wave loading.
- Objectives and approach.
- Dislocation-mechanics based continuum material model for polycrystal.
- Simulation of the single crystal experiments and insights gained from the simulation.
- Extension of the polycrystal model to single crystals.
- Simulation of the single crystal experiments and insights gained from the simulation.
- Conclusion.

Configuration Of The Ramp Wave Experiments On Veloce

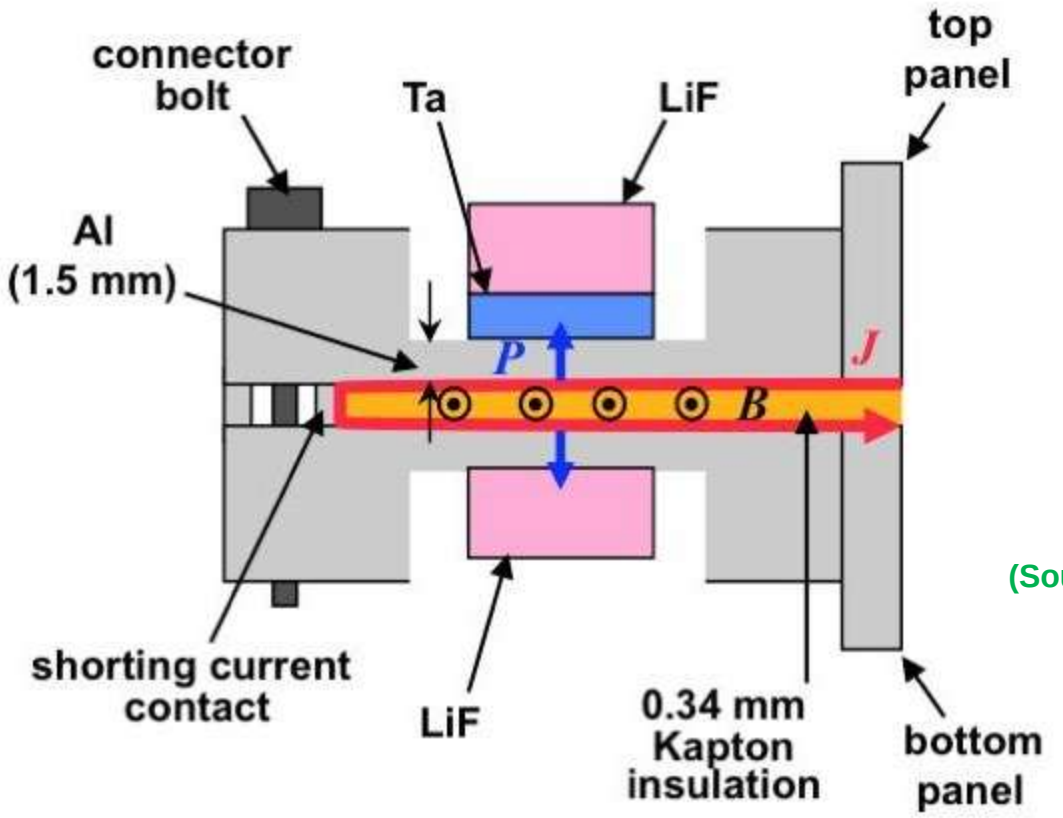

(Source: Ao et al. Rev. Sci. Instr. 2008)

generate a structured wave with finite risetime in the very high stress regime

Polycrystal Tantalum Under Ramp Wave Loading

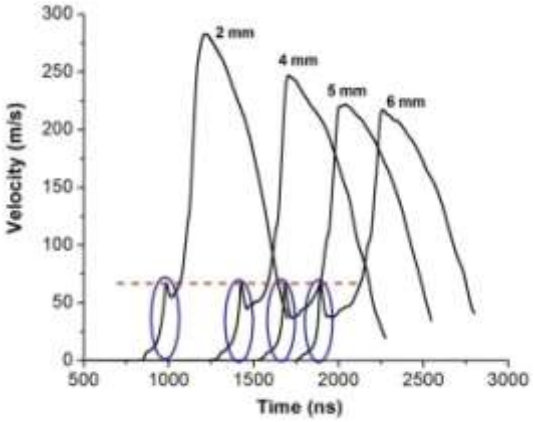

Annealed

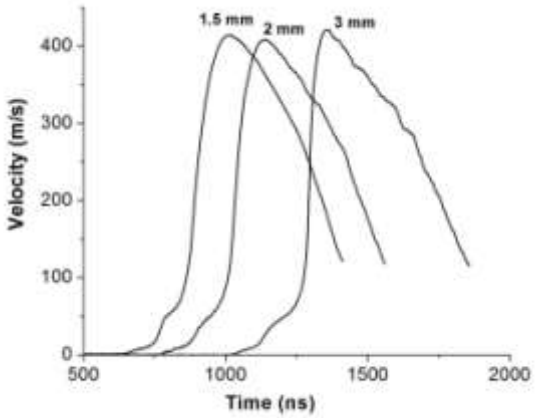

Cold-Rolled (26%)

- **Annealed samples**:

  - **Elastic precursor showed a pronounced overshoot followed by a significant velocity drop or stress relaxation**

  - **The extent of the velocity drop increased with the sample thickness.**

  - **precursor amplitude showed very little attenuation, even with the significant stress relaxation behind the precursor**

- **Cold-Rolled**:

  - **More dispersed elastic precursor.**

  - **no rapid velocity drop or stress relaxation was observed behind the precursor**

Single Crystal Tantalum Under Ramp Wave Loading

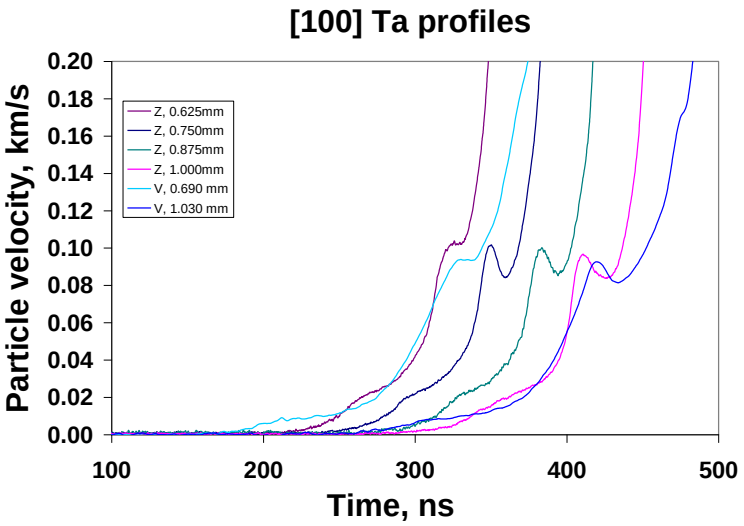

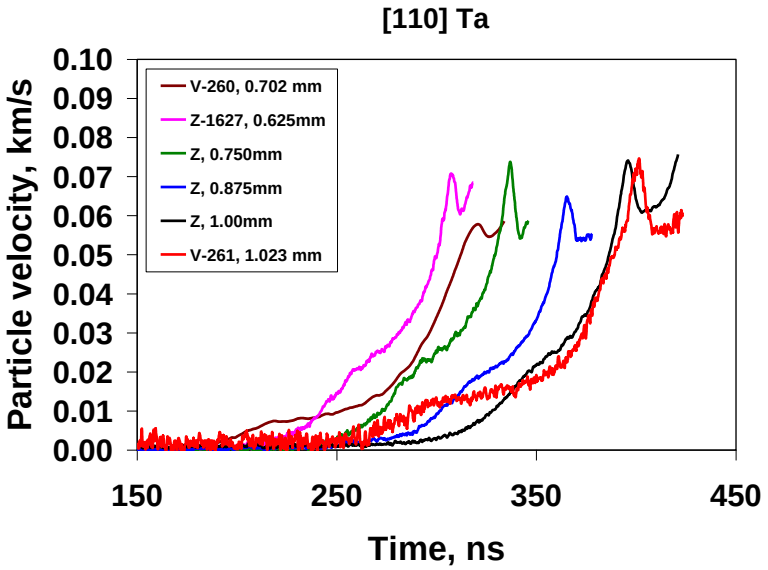

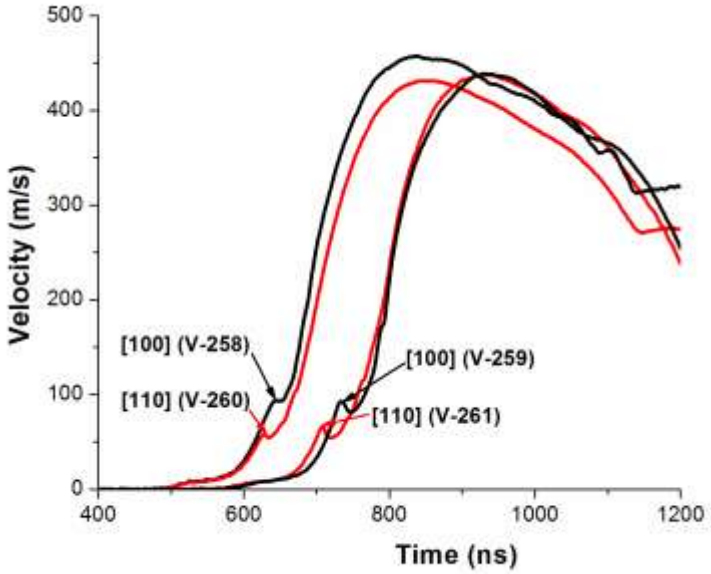

- **Similar elastic precursor behavior as polycrystal.**
- **Strong orientation dependence**
- **[100] orientation showed slight decay of the precursor , but no apparent trend for [110] orientation.**
- **[100] orientation is more rate sensitive than [110].**

Comparison of Annealed Polycrystal With Some Existing Models

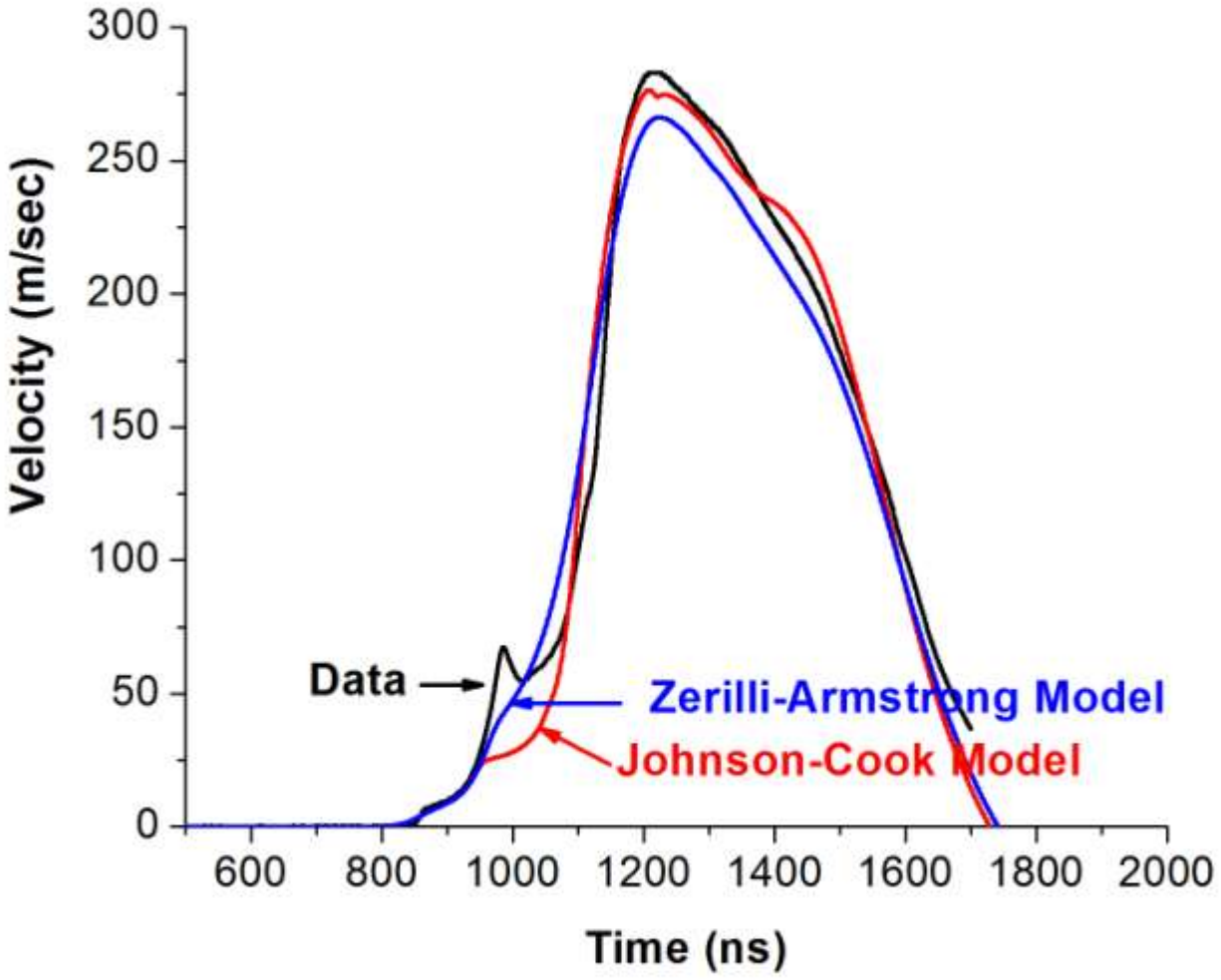

Objectives and Approach

Objectives:

- To gain insights into the mechanical behavior of tantalum, particularly the elastic precursor behavior, and their implication on the deformation mechanisms for tantalum.

- To gain an understanding of the dynamic inelasticity of poly- and single crystal tantalum, including the material strength and its evolution.

Approach:

- Develop a constitutive model that captures the material features observed experimentally.

- Use numerical simulation to gain additional insight into the inelastic behavior of tantalum.

Thermomechanical Constitutive Relation

$$\dot{\sigma}_{ij}^{e} = B_{ijkl}\dot{\varepsilon}_{kl}^{e} - \rho\Gamma_{ij}\theta\dot{s} = B_{ijkl}(\dot{\varepsilon}_{kl} - \dot{\varepsilon}_{kl}^{p}) - \rho\Gamma_{ij}\theta\dot{s}$$

$$\left(B_{ijkl} = \left.\frac{\partial\sigma_{ij}}{\partial\varepsilon_{kl}^{e}}\right|_{s} , \quad \Gamma_{ij} = -\frac{1}{\rho\theta}\left.\frac{\partial\sigma_{ij}}{\partial s}\right|_{\varepsilon_{ij}^{e}} \right)$$

$$\dot{\theta} = -\theta\Gamma_{ij}\dot{\varepsilon}_{ij}^{e} + (\theta / C_{v})\dot{s} = -\theta\Gamma_{ij}(\dot{\varepsilon}_{ij} - \dot{\varepsilon}_{ij}^{p}) + (\theta / C_{v})\dot{s}$$

$$\dot{s} = \frac{1}{\rho\theta}(\sigma_{ij}^{'e}\dot{\varepsilon}_{ij}^{p} - q_{i,i})$$

$$q_{i} = -k\theta_{,i}$$

$$\dot{\gamma} = \dot{\gamma}_{mech} + \dot{\gamma}_{con}$$

$$\dot{\gamma}_{mech} = \frac{ds}{dt} - (-\frac{1}{\rho\theta}q_{i,i}) = \frac{\sigma_{ij}^{e'}\dot{\varepsilon}_{ij}^{p}}{\rho\theta} \geq 0$$

$$\dot{\gamma}_{con} = -\frac{1}{\rho\theta^{2}}q_{i}\theta_{,i} \geq 0$$

Strength Model

$$\dot{\sigma}'_{ij} = 2G\dot{\varepsilon}^{e}{}'_{ij} = 2G(\dot{\varepsilon}'_{ij} - \dot{\varepsilon}^{p}_{ij})$$

$$\dot{\varepsilon}^{p}_{ij} = \dot{\bar{\varepsilon}}^{p}(\sigma'_{ij} / \left|\sigma'_{ij}\right|) \quad \textbf{and} \quad \dot{\bar{\varepsilon}}^{p} = A[\left|\sigma'_{ij}\right| - \sigma_{th})]^{1.5}$$

$\dot{\bar{\varepsilon}}^{p} = (\frac{2}{3}\dot{\varepsilon}^{p}_{ij}\dot{\varepsilon}^{p}_{ij})^{1/2}$: effective plastic strain rate

$\left|\sigma'_{ij}\right| = (\frac{3}{2}\sigma'_{ij}\sigma'_{ij})^{1/2}$: effective stress, a measure of material strength

$$G = G_0[1 + (\frac{G'_P}{G_0})\frac{P}{\eta^{1/3}} + (\frac{G'_T}{G_0})(T - T_0)]$$

$$\sigma_{th} = \sigma_{th_0}[1 + \beta(\bar{\varepsilon}^{p} + \bar{\varepsilon}^{p}_{i})]^{n}[1 + (\frac{G'_P}{G_0})\frac{P}{\eta^{1/3}} + (\frac{G'_T}{G_0})(T - T_0)]$$

(Steinberg, Cochran, and Guinan, JAP, 1980)

Association of The Rate Eqn. with Dislocation Motion

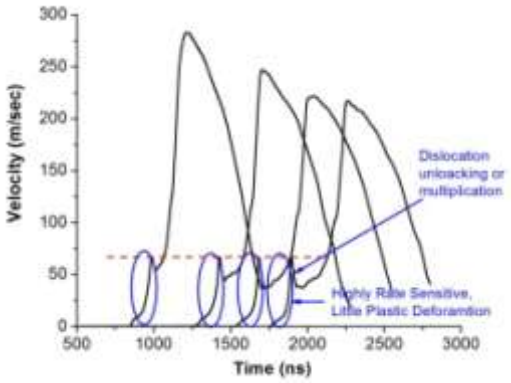

- **Little decay of precursor implies little plastic deformation during precursor loading**
- **Dislocation unlocking or multiplication at the precursor tip.**

Dislocation model (Orowan Eqn.):

$\dot{\gamma}^p = b\rho_m v$ where $\dot{\gamma}^p$: plastic strain rate;

b : Burgers vector;

ρ_m : mobile dislocation density;

v : stress dependent dislocation velocity

$$\dot{\bar{\varepsilon}}^p = A[\left|\sigma'_{ij}\right| - \sigma_{th})]^{1.5} = b\rho_m\{c[\left|\sigma'_{ij}\right| - \sigma_{th})]^{1.5}\}$$

where

$\rho_m = f\rho_t$ with ρ_t being the total dislocation density

$\rho_t = \rho_0 + C(\bar{\varepsilon}^p)^a$ (Hahn, Acta Met. 1962)

$f = f_i + (f_f - f_i)(1 - e^{-\lambda\bar{\varepsilon}^p})$ (Yoshida et. al., IJP, 2008)

Simulated Polycrystal Velocity Histories

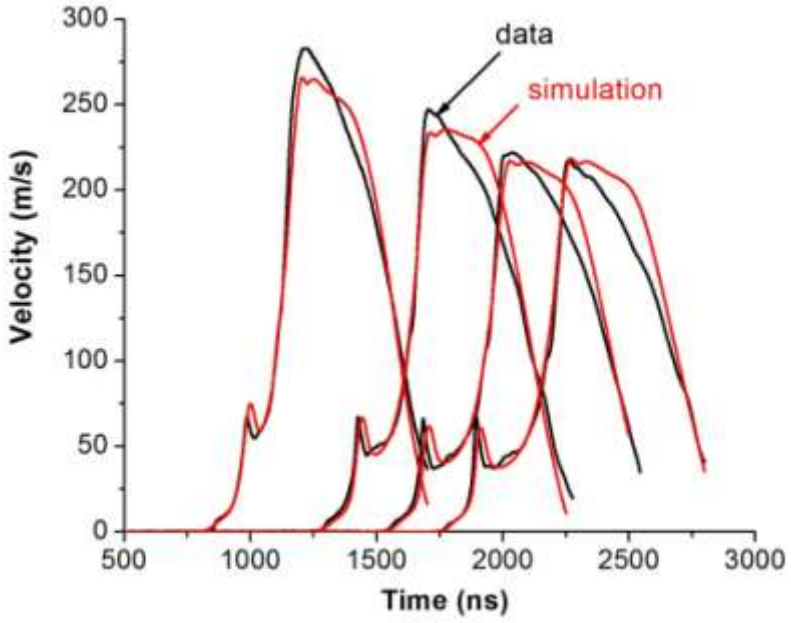

Annealed

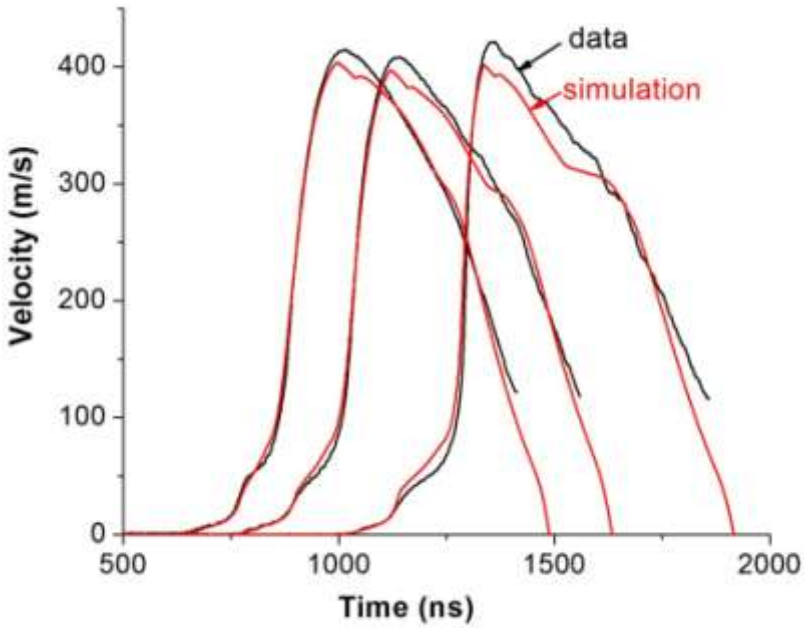

Cold-Rolled (26%)

Annealed vs Cold Rolled

Annealed

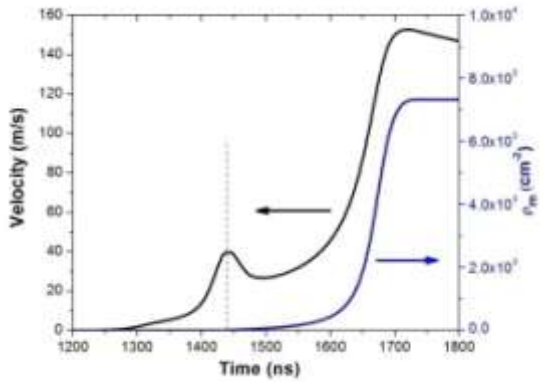

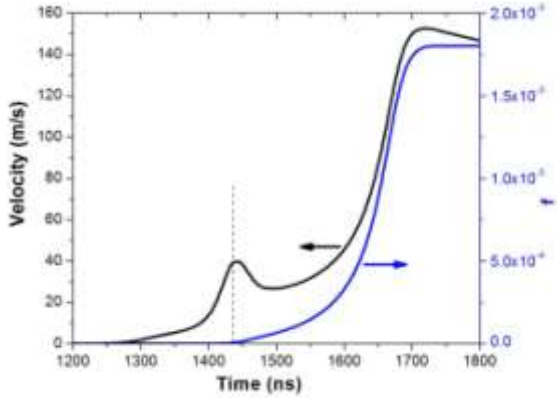

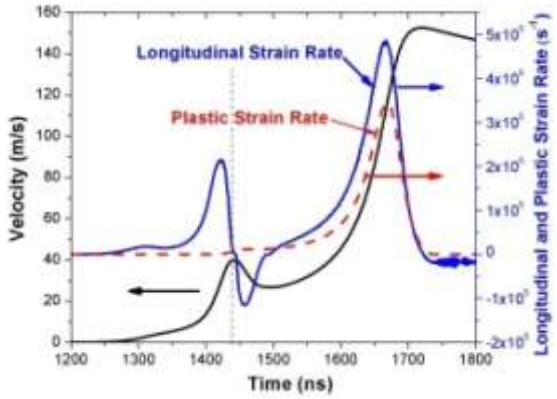

Cold-Rolled

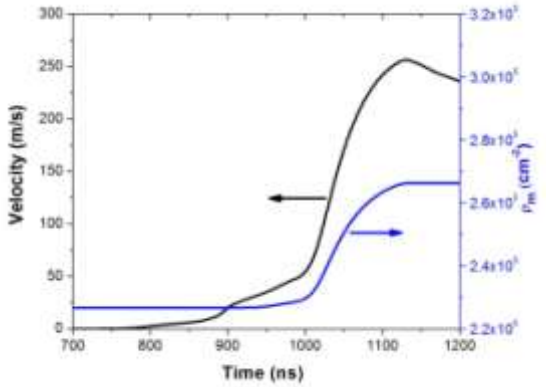

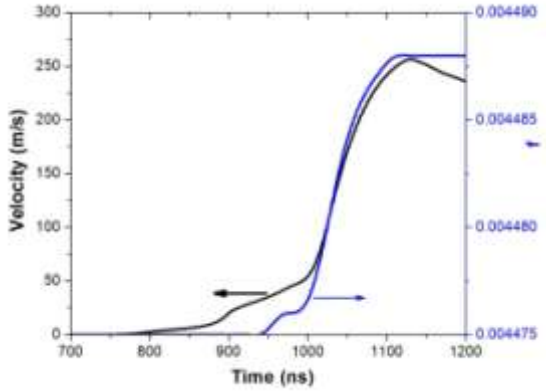

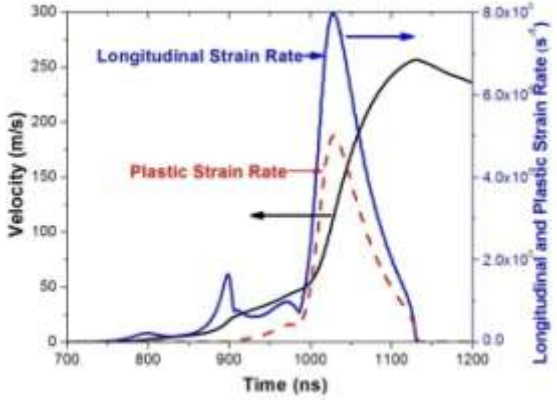

Annealed vs Cold Rolled

Annealed

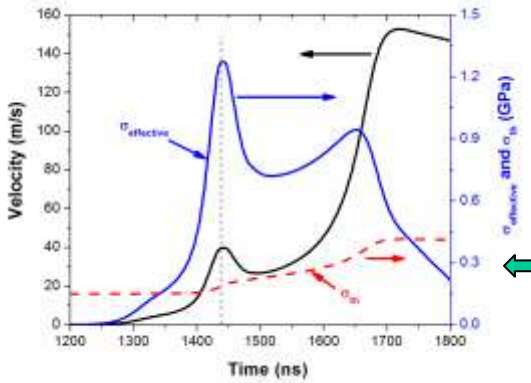

highly rate sensitive response

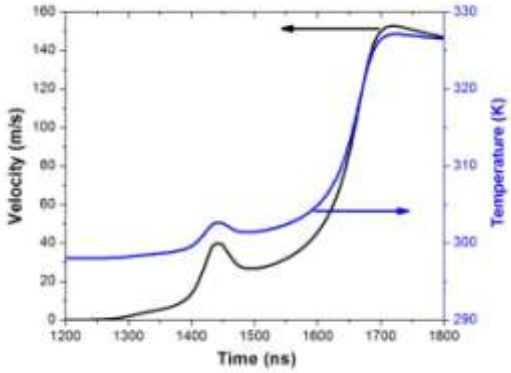

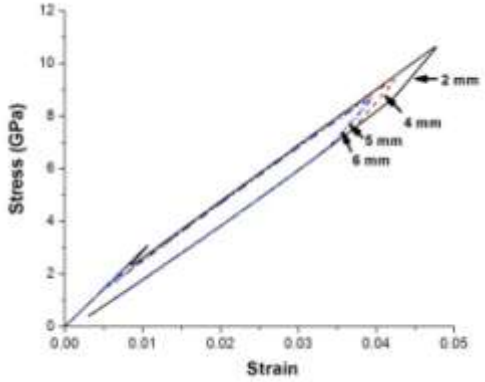

Cold-Rolled

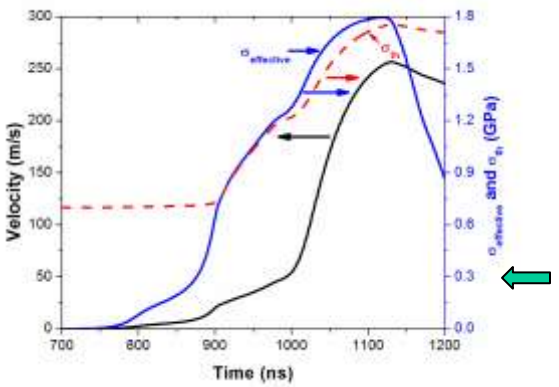

less rate sensitive response

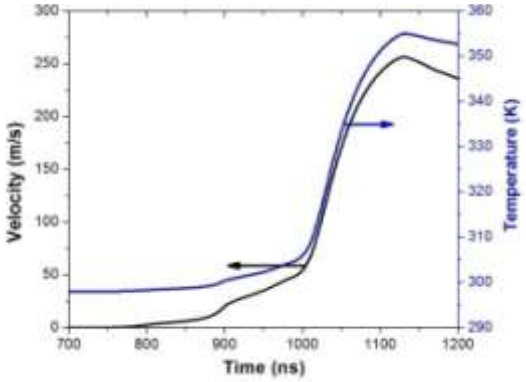

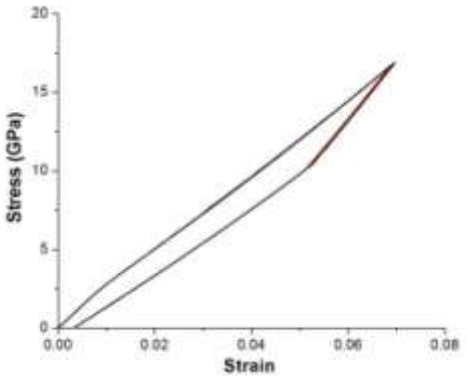

Simulation of Single Crystal Tantalum With Polycrystal Model

- **Use continuum model with different material constants for different orientations to describe the single crystal behavior.**

- **The model is used as a data analysis tool to estimate the material properties and their evolution.**

$$\dot{\bar{\varepsilon}}^p = A[|\sigma'_{ij}| - \sigma_{th})]^{1.5} = b\rho_m\{c[|\sigma'_{ij}| - \sigma_{th})]^2\} \quad (\dot{\gamma}^p = b\rho_m v)$$

where $\rho_m = f\rho_t$ with ρ_t being the total dislocation density

$$\rho_t = \rho_0 + C(\bar{\varepsilon}^p)^a \quad \text{(Hahn, Acta Met. 1962)}$$

$$f = f_i + (f_f - f_i)(1 - e^{-\lambda\bar{\varepsilon}^p}) \quad \text{(Yoshida et. al., IJP, 2008)}$$

- **All the material constants are kept the same as for polycrystal except for λ**

- $\lambda = 25$ **for [100]; and** $\lambda = 60$ **for [110] orientation**

- **Smaller λ results in a more rate sensitive behavior**

Simulation of Single Crystal Tantalum With Polycrystal Model

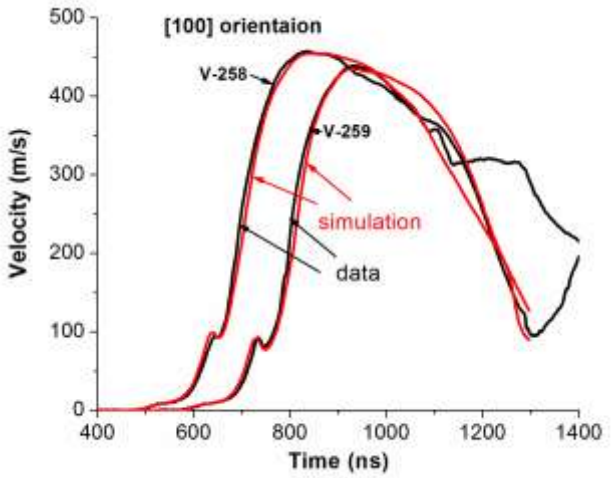

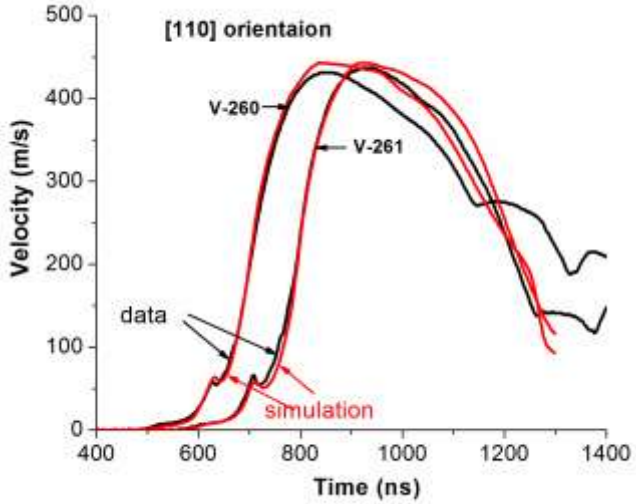

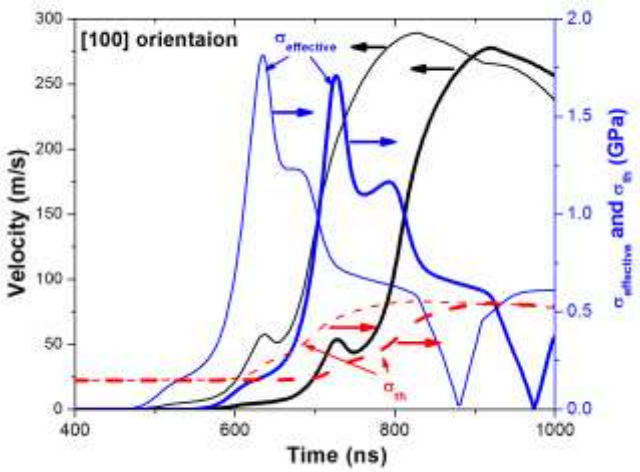

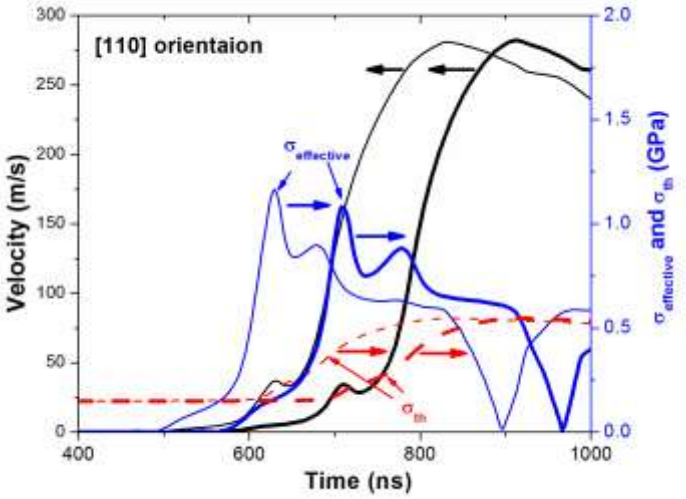

What is the physical justification for different rate sensitivity for different orientations?

Single Crystal Model - Kinematics

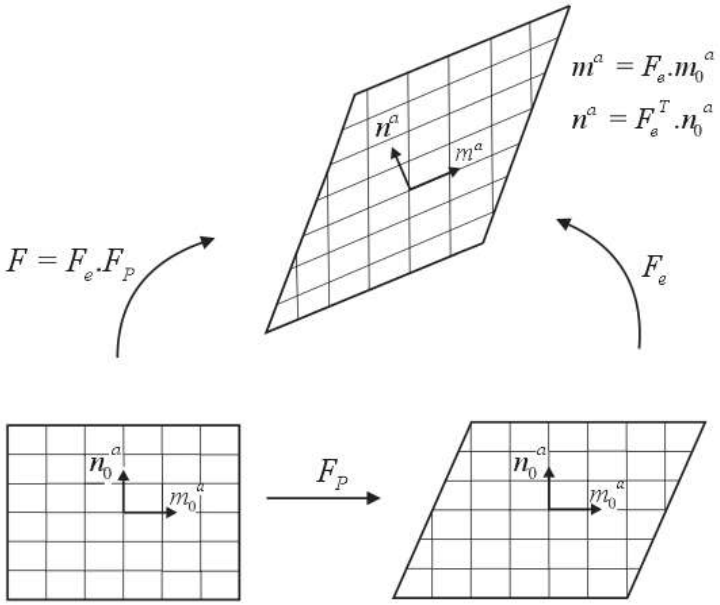

$$\tau^{\alpha} = \underline{\mathrm{m}}_0^{\alpha} \cdot \underset{\sim}{C}^{e} \cdot \underset{\sim}{S} \cdot \underline{\mathrm{n}}_0^{\alpha}$$

$$\underset{\sim}{\bar{L}}^{p} = \sum_{\alpha} \dot{\gamma}^{\alpha} \underline{\mathrm{m}}_0^{\alpha} \otimes \underline{\mathrm{n}}_0^{\alpha}$$

Single Crystal Model – Constitutive Relation

$$\dot{\gamma}^{\alpha} = b\rho_m^{\alpha}\bar{v}^{\alpha} = b\rho_m^{\alpha}\{\beta[(\left|\tau^{\alpha}\right| - \tau_{th}^{\alpha}) / \tau_{th}^{\alpha}]^{\mu}\}$$

$$\rho_m^{\alpha} = f^{\alpha}\rho_t^{\alpha}$$

$$f^{\alpha} = f_0^{\alpha} + (f_s^{\alpha} - f_0^{\alpha})(1 - e^{-\lambda^{\alpha}\gamma^{\alpha}})$$

$$\rho_t^{\alpha} = \rho_{t0}^{\alpha} + \kappa(\gamma^{\alpha})^{\eta}$$

$$\tau_{th}^{\alpha} = \tau_0^{\alpha}(1 + \omega\gamma)^{\zeta}$$

Single Crystal Model – Slip Systems

Slip System Considered: {110}<111> and {112}<111>

{112}<111> possesses twinning/anti-twinning asymmetry

1	$(0\bar{1}1)[111]$	**13**	$(1\bar{2}1)[111]$
2	$(1\bar{1}0)[111]$	**14**	$(\bar{2}11)[111]$
3	$(10\bar{1})[111]$	**15**	$(11\bar{2})[111]$
4	$(01\bar{1})[\bar{1}11]$	**16**	$(\bar{1}1\bar{2})[\bar{1}11]$
5	$(\bar{1}0\bar{1})[\bar{1}11]$	**17**	$(211)[\bar{1}11]$
6	$(1\bar{1}0)[\bar{1}11]$	**18**	$(\bar{1}\bar{2}1)[\bar{1}11]$
7	$(011)[\bar{1}\bar{1}1]$	**19**	$(\bar{1}21)[\bar{1}\bar{1}1]$
8	$(\bar{1}10)[\bar{1}\bar{1}1]$	**20**	$(2\bar{1}1)[\bar{1}\bar{1}1]$
9	$(\bar{1}0\bar{1})[\bar{1}\bar{1}1]$	**21**	$(\bar{1}\bar{1}2)[\bar{1}\bar{1}1]$
10	$(0\bar{1}\bar{1})[1\bar{1}1]$	**22**	$(1\bar{1}2)[1\bar{1}1]$
11	$(10\bar{1})[1\bar{1}1]$	**23**	$(\bar{2}\bar{1}1)[1\bar{1}1]$
12	$(110)[1\bar{1}1]$	**24**	$(121)[1\bar{1}1]$

$\lambda = 15$ **for the above slip systems**

$\lambda = 50$ **for the {112}<111> system along the twinning direction**

Simulation of Single Crystal Tantalum

[100]

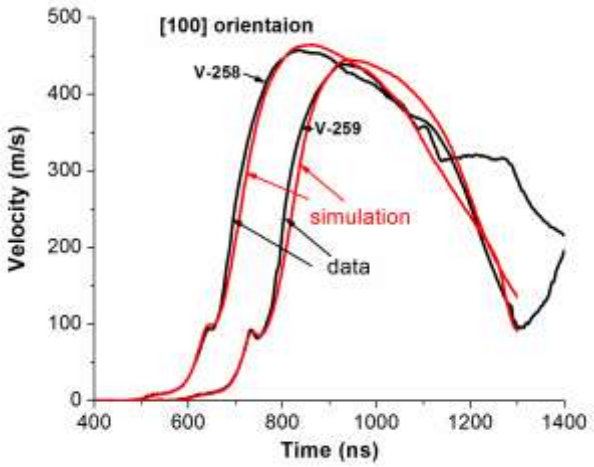

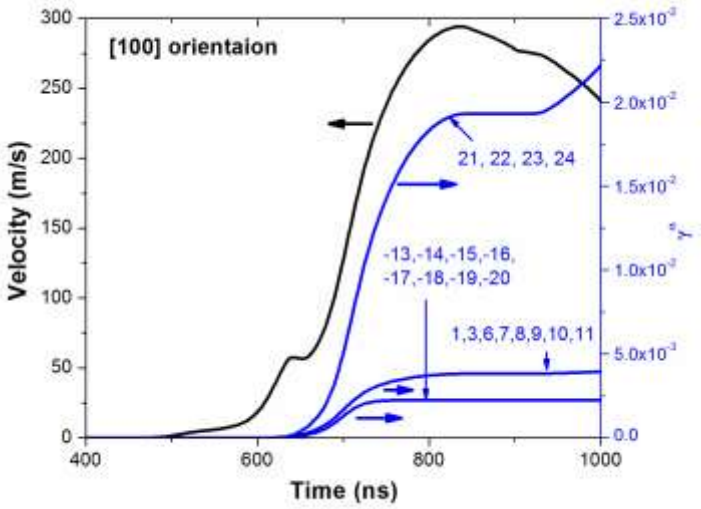

[110]

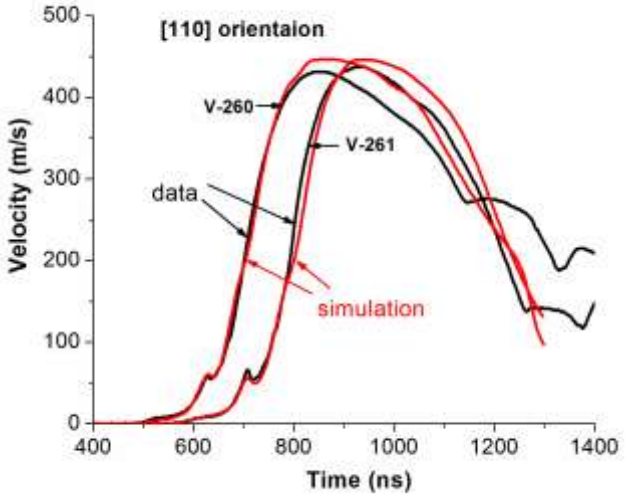

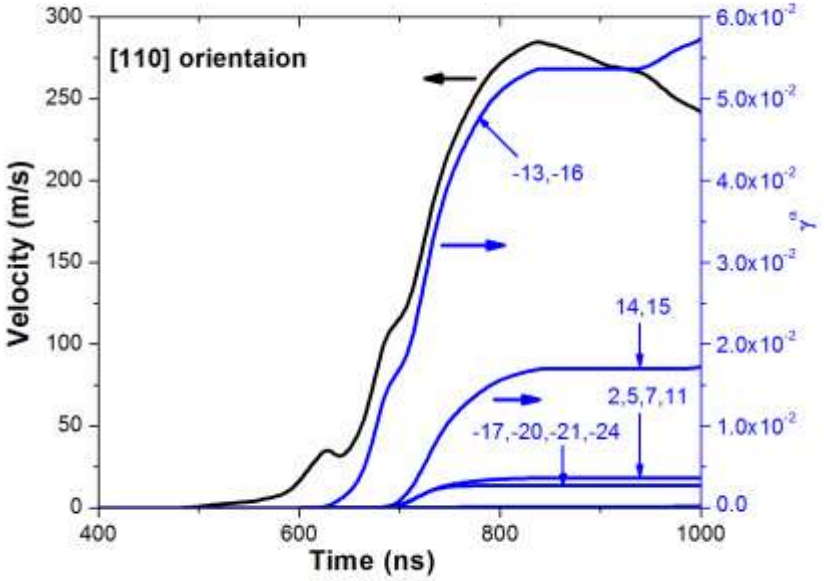

Simulation of Single Crystal Tantalum

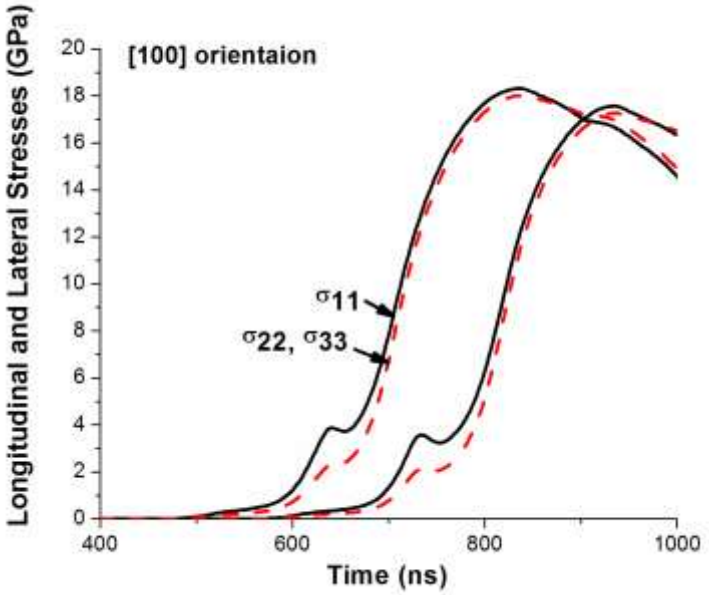

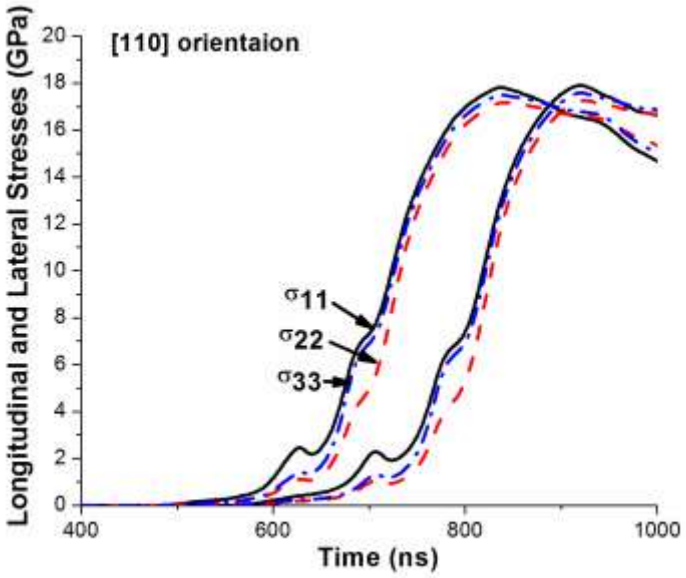

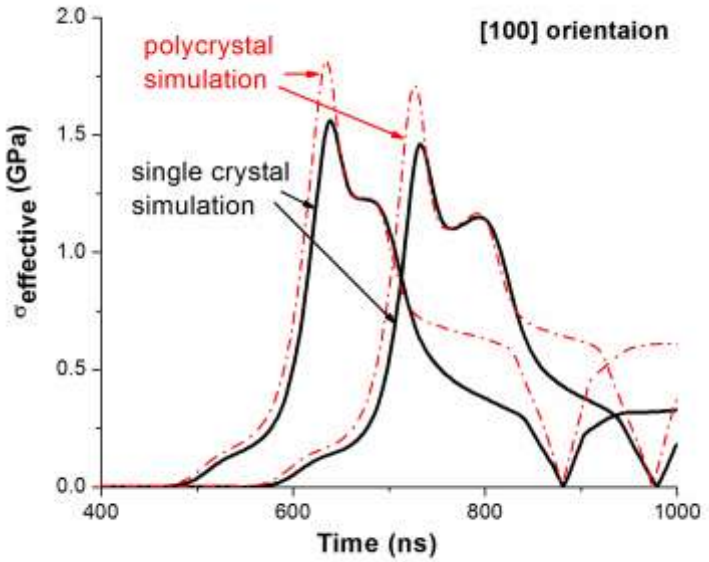

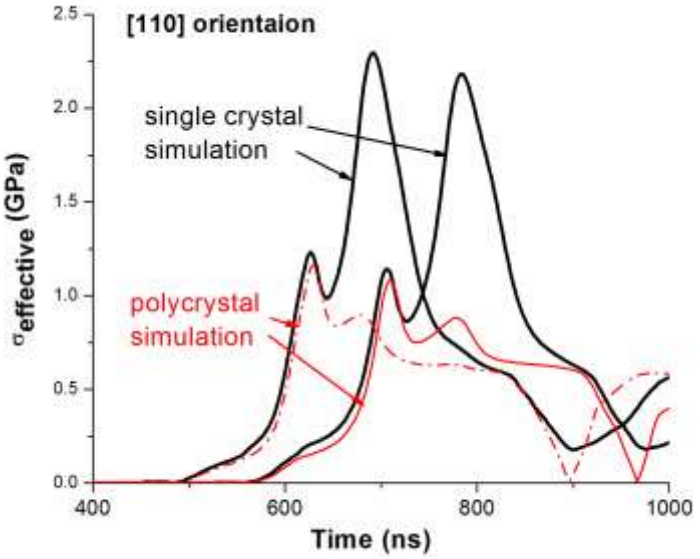

Simulation of Single Crystal Tantalum

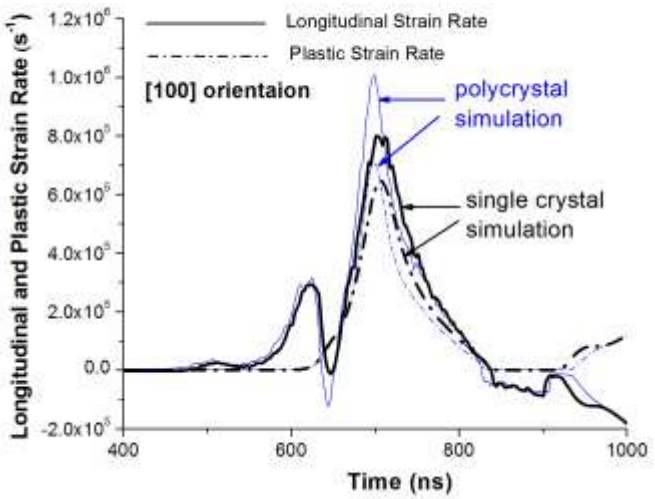

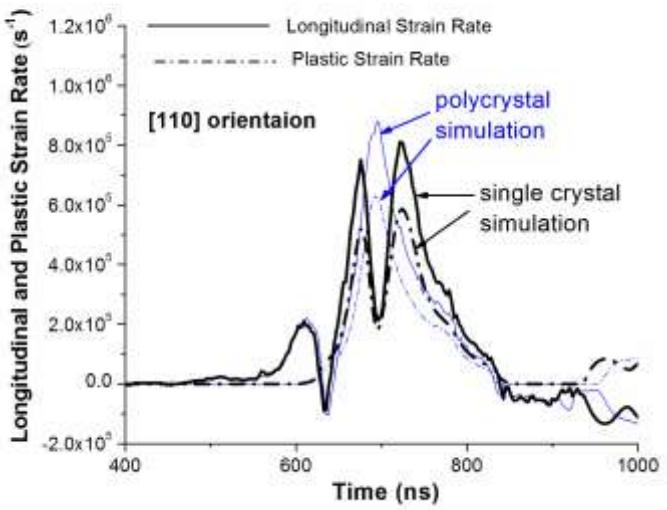

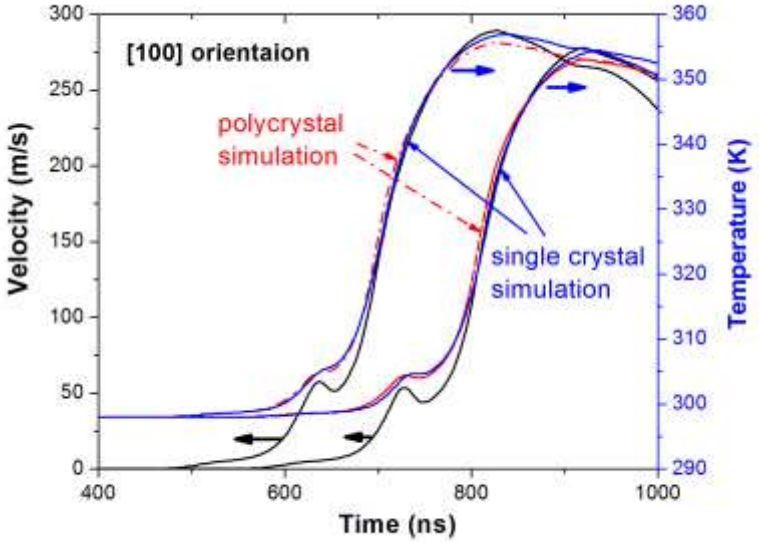

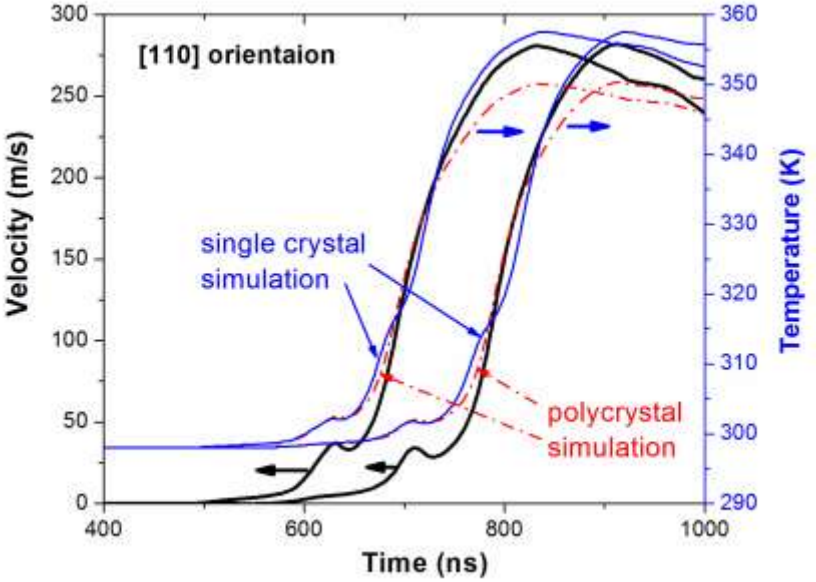

Conclusions

- A dislocation-density based model yields consistent description of the behavior of both the poly- and single crystal tantalum under ramp wave loading.

- The various features of the observed tantalum behavior are attributed to the rate effect.

- The rate effect is attributed mainly to dislocation density.

- Strong orientation dependence is attributed to anisotropy of dislocation nucleation.

- On the microscopic level, the anisotropy of dislocation nucleation is attributed to the twinning/antitwinning asymmetry of the BCC crystals.

Review of Tailored Loading Effort at LLNL Gas Gun Facility

UCRL-PRES-XXXX

Jeffrey H Nguyen

D. Orlikowski, R. Krone, P. Martin, R. Patterson, N. Holmes

LLNL

Presented at 4th Workshop on Ramp Compression

January 18, 2011

This work was performed under the auspices of the U.S. Department of Energy by Lawrence Livermore National Laboratory in part under Contract W-7405-Eng-48 and in part under Contract DE-AC52-07NA27344.

physical and life sciences

We are ramping up our experimental effort this year

- **Extend the pressure range of experiments**
- **EOS**
- **Strength experiments on warm quasi-isentropes using triangular waves**
- **Phase Transitions and kinetics**

physical and life sciences

Summary of techniques

- **Our focus is on warm quasi-isentropes. A principal quasi-isentrope can also be achieved**
  - **Low impedance materials are less controllable and are more expensive to make**
- **Cu-Mg range has been consistently demonstrated in many experiments**
- **Ta-Mg range requires processing at much higher pressures and temperatures**

Why GDI is a necessary tool in getting materials properties on complex paths

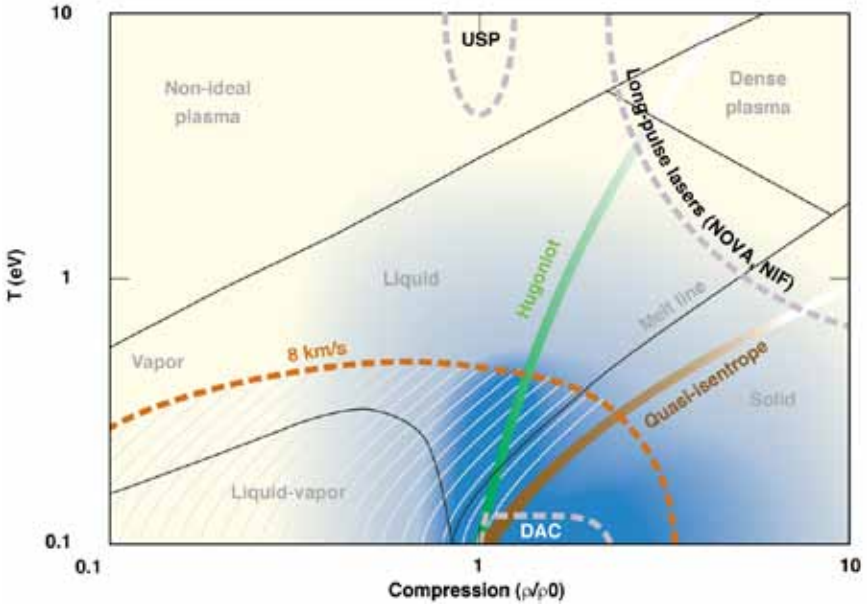

- **User can define compression path, i.e., obtain materials properties where we want to know them**
- **Direct measurements of materials strength on quasi-isentrope with triangular waves**
- **Observation of kinetics of phase transitions**

We are measuring material properties in previously inaccessible regions for dynamic experiments

physical and life sciences

We developed GDI to explore previously inaccessible regions of the phase space (P, ⟩, T)

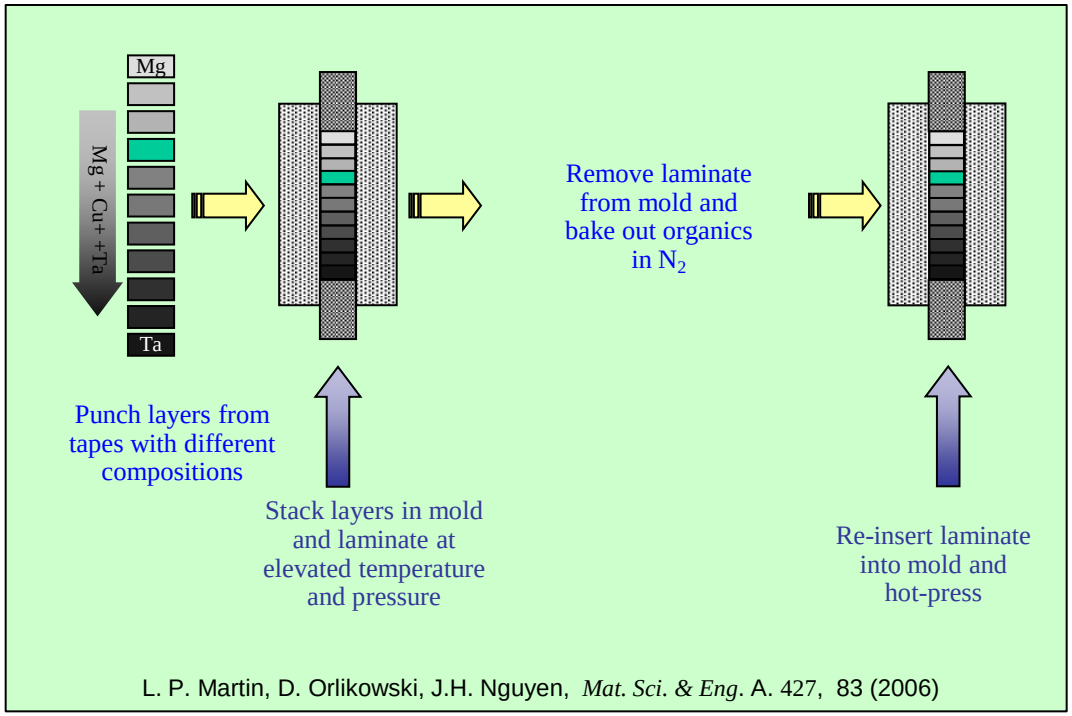

L. P. Martin, D. Orlikowski, J.H. Nguyen, *Mat. Sci. & Eng.* A. 427, 83 (2006)

We can access a broad range of P, ⟩, T, and t

- Complex paths, including release rate, are defined by the experimenter
- Compression path not necessarily monotonic
- 50 to 100 individually controlled layers
- Tape-casting technique employed in the manufacturing process
- We used hydrocode simulations to refine impactor profile for each thermodynamic path
- Experimental pressure up to 5 Mbars
- Strain rate 10^5 to 10^6

physical and life sciences

Ta data on a warm loading path

Particle Velocities at Ta/LiF interfaces

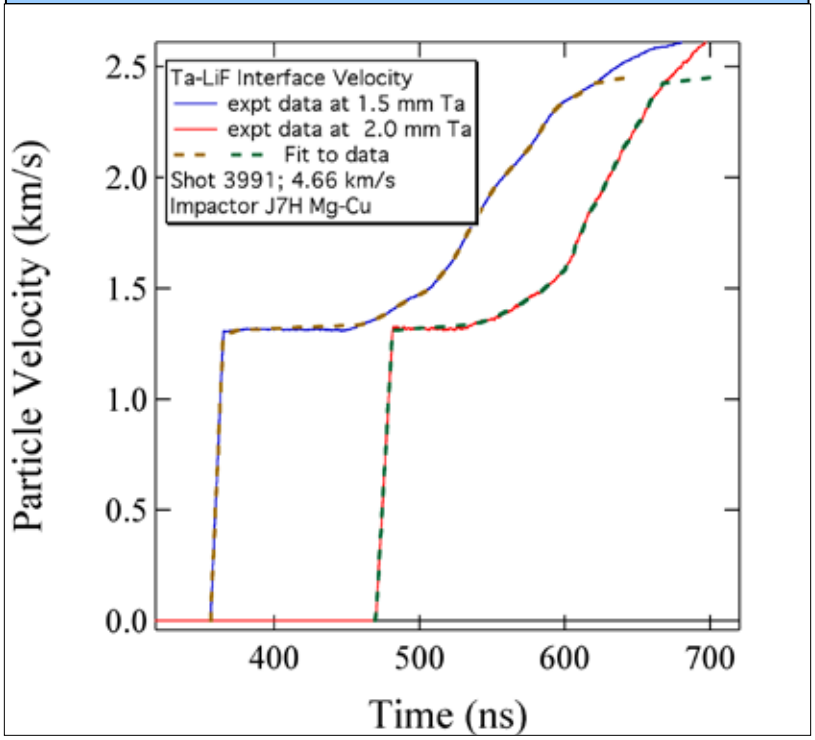

Dynamic EOS data on quasi-isentropes

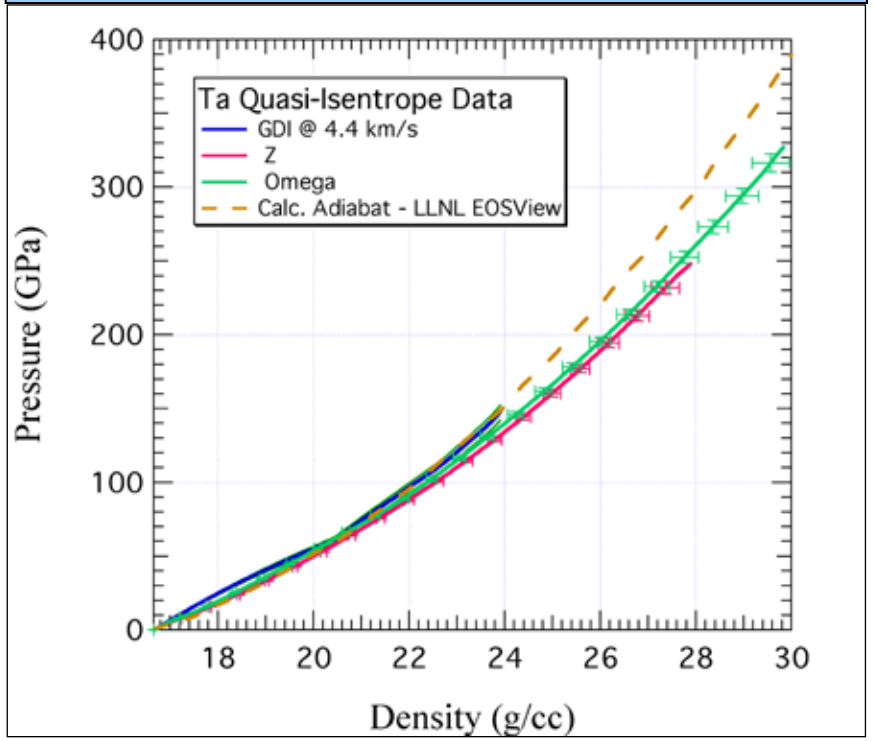

- **Uncertainty is a conservative estimate dominated by density uncertainty**

physical and life sciences

Advanced impactor manufacturing technique enhances quality of data on unique loading paths

Hand-made impactors

Quasi-Isentropic Compression

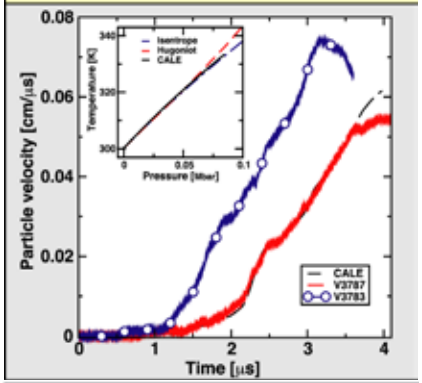

More Complicated Paths

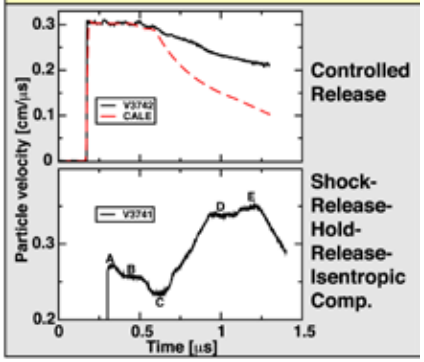

Controlled Release

Shock-Release-Hold-Release-Isentropic Comp.

Recent manufacturing techniques improved quality of data significantly

Smooth compression for EOS studies

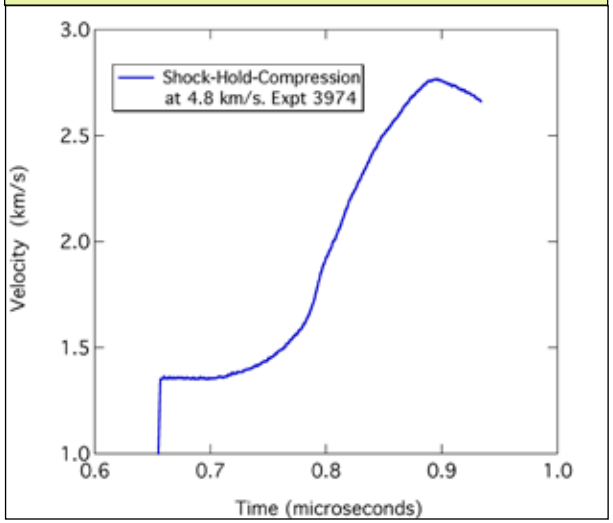

Triangular wave: strength and phase transition

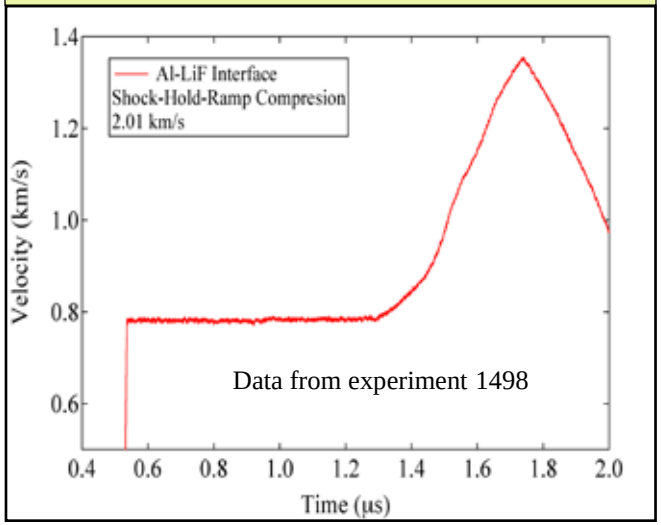

- **Hundreds of layers facilitate a smooth, user-defined and reproducible compression path**
- **Allows a unique method to measure strength or study phase transitions from loading and unloading path.**

physical and life sciences

We generated triangular loading path and measured strength of materials on hot quasi-isentropes

Triangular Loading-Unloading Curve

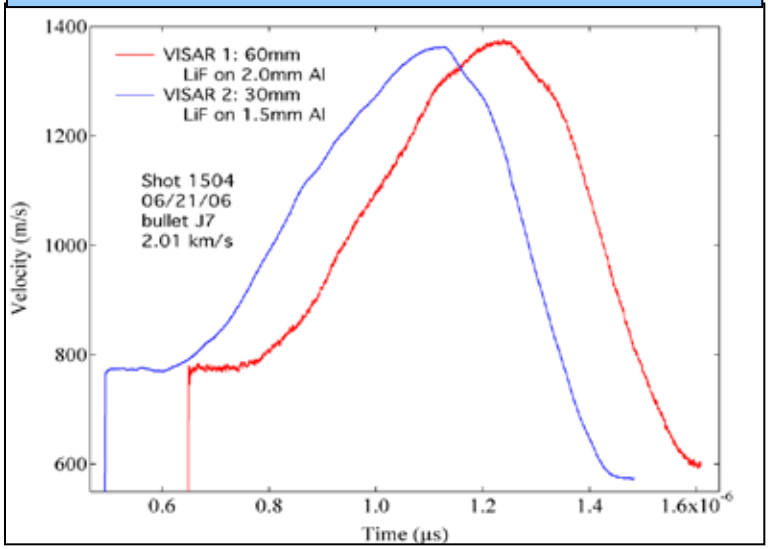

Strength meas. on a quasi-isentrope

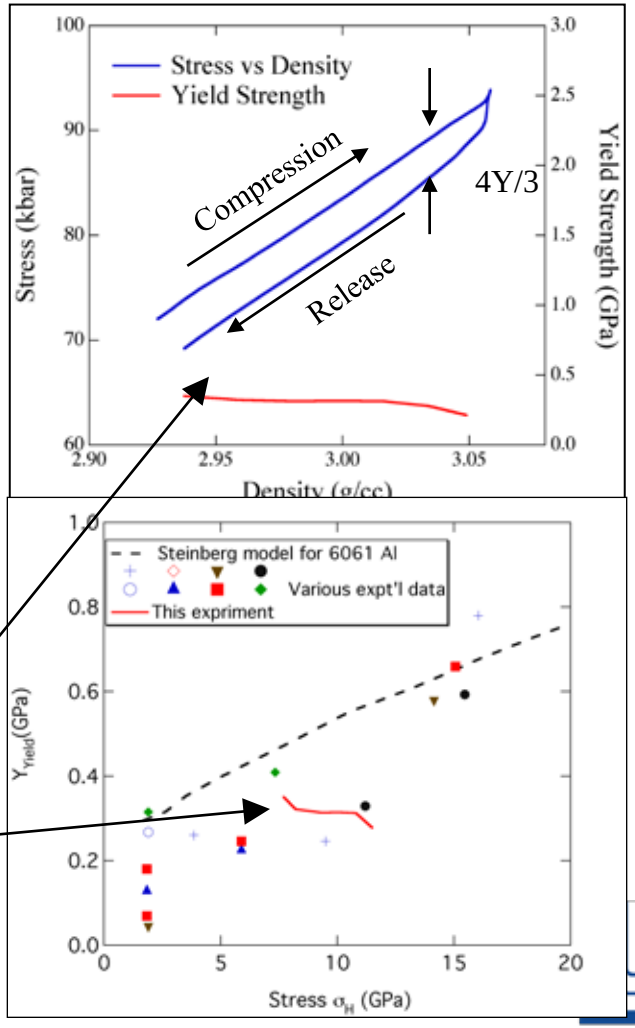

- **A plateau in the compression drive insures that all samples are at the same state prior to further compression**
- **Loading and unloading rates are nearly the same to reduce rate effects**
- **Strength data on a "hot" quasi-isentrope, not a Hugoniot point**

physical and life sciences

An example of Phase Transition

- **We observed optical signature of solidification of water on ramp compression**

Thermodynamic path of experiment

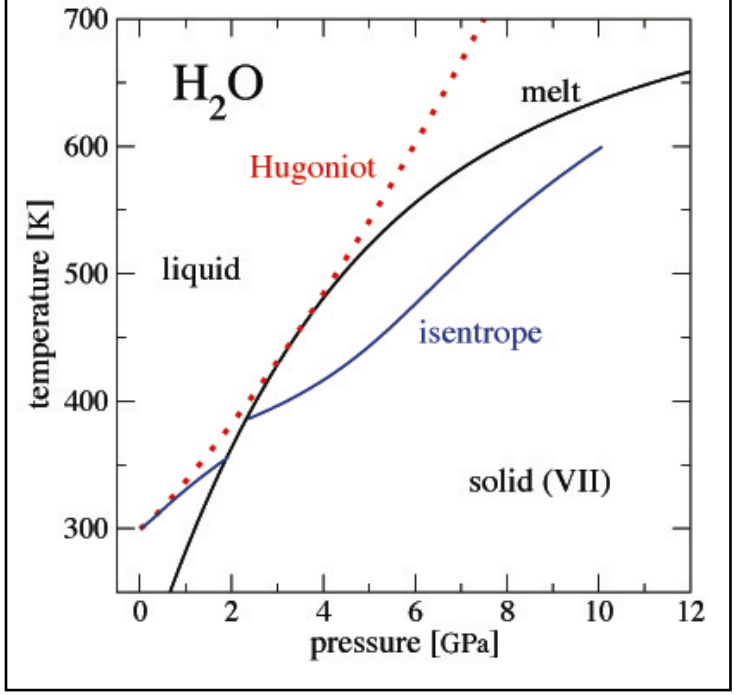

Optical observation of solidification

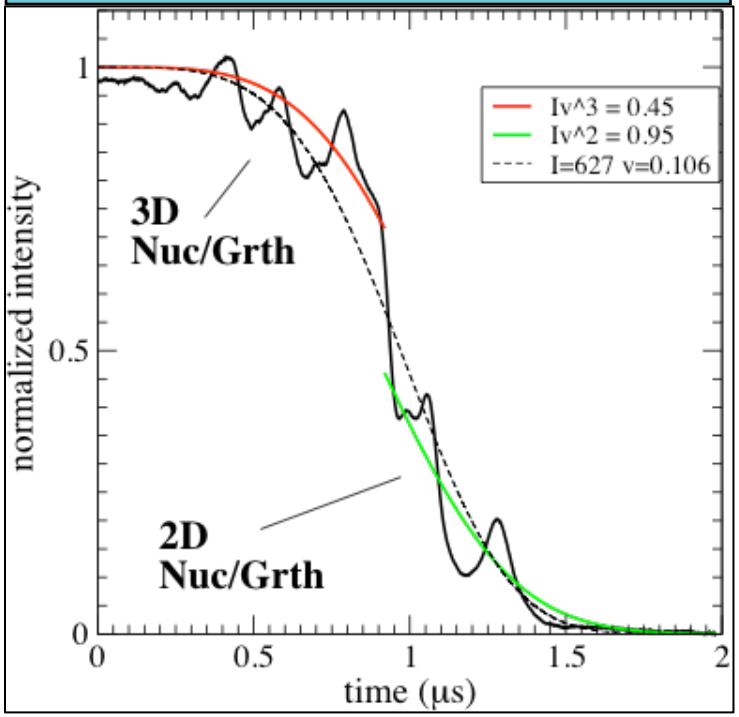

physical and life sciences

Potential warm isentrope experiments

- **Various compression paths can be be explored**

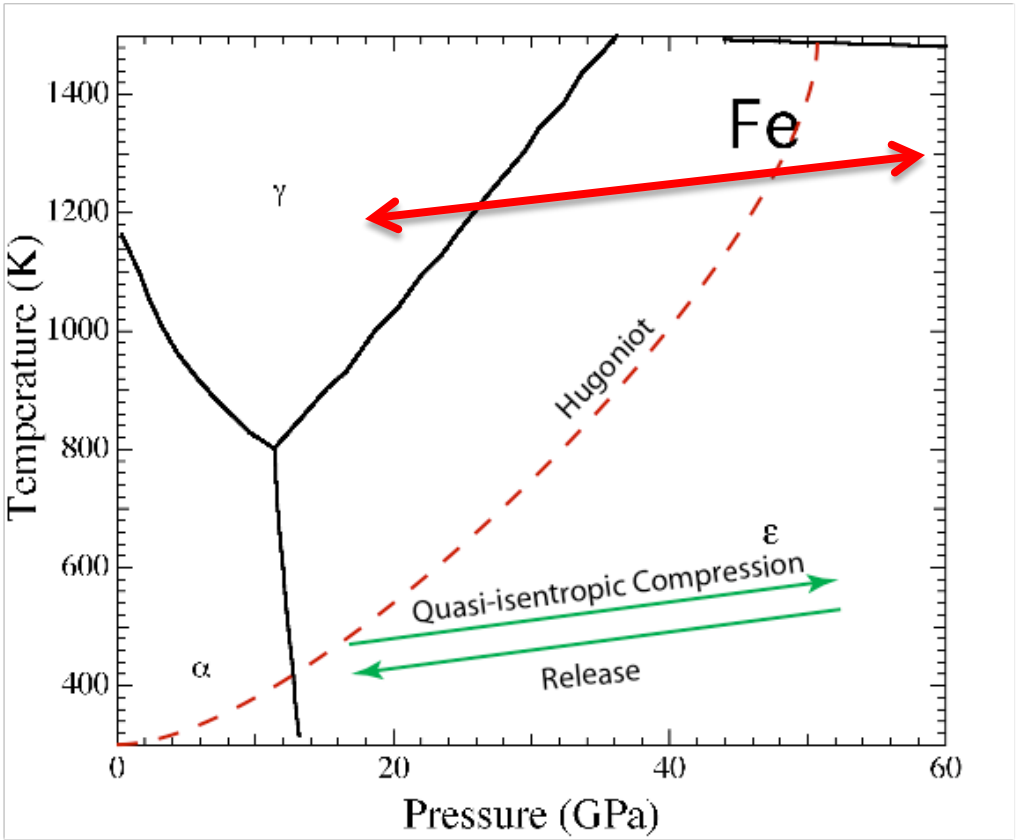

physical and life sciences

Summary and path forward

- **Our primary focus is on warm isentrope experiments**
  - **Experiments beyond phase transitions**
- **Strength measurements of Al and Ta**
- **Solidification of pre-heated materials**
- **Phase transitions and kinetics**

Lawrence Livermore National Laboratory

Fundamental Thermodynamic Approaches to Extracting Strength from Velocimetry

Bryan W. Reed, Roger W. Minich, James S. Stolken, and Mukul Kumar

Lawrence Livermore National Laboratory, P. O. Box 808, Livermore, CA 94551

This work performed under the auspices of the U.S. Department of Energy by Lawrence Livermore National Laboratory under Contract DE-AC52-07NA27344

LLNL-PRES-465264

Strength is part of a general tensor equation of state

	Zero Strength/Viscosity	More General
Energy Conservation	$dU = TdS - PdV$	$dU = TdS + \sigma_{ij} d\varepsilon_{ij}$
		$\sigma_{ij} = P\delta_{ij} + \tau_{ij}$
		$\varepsilon_{ij} = \varepsilon_{ij}^{elastic} + \psi_{ij}$
EOS	$U(S,V) \rightarrow P(T,V)$	$U(S,\varepsilon_{ij}^{elastic}) \rightarrow \sigma_{ij}(T,\varepsilon_{ij}^{elastic})$
		$\dot{\psi}_{ij}(T, P, \tau_{ij}, \psi_{ij}, \rho^{mobile}, \ldots)$

. . . plus terms for microstructural DOF, pressure/shear interaction, phase changes, etc.

For full development, see:
D. C. Wallace, PRB 22, 1477 (1980)

Stress-strain curves illustrate the wide range of behavior relevant to strength

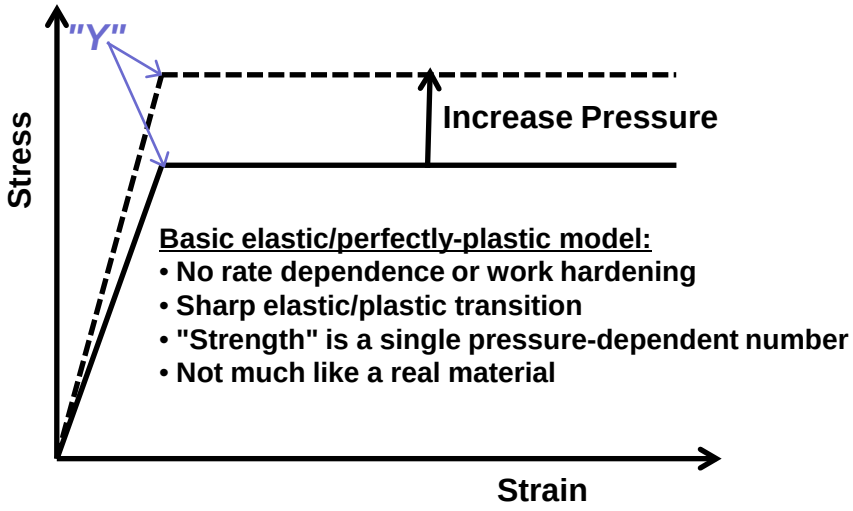

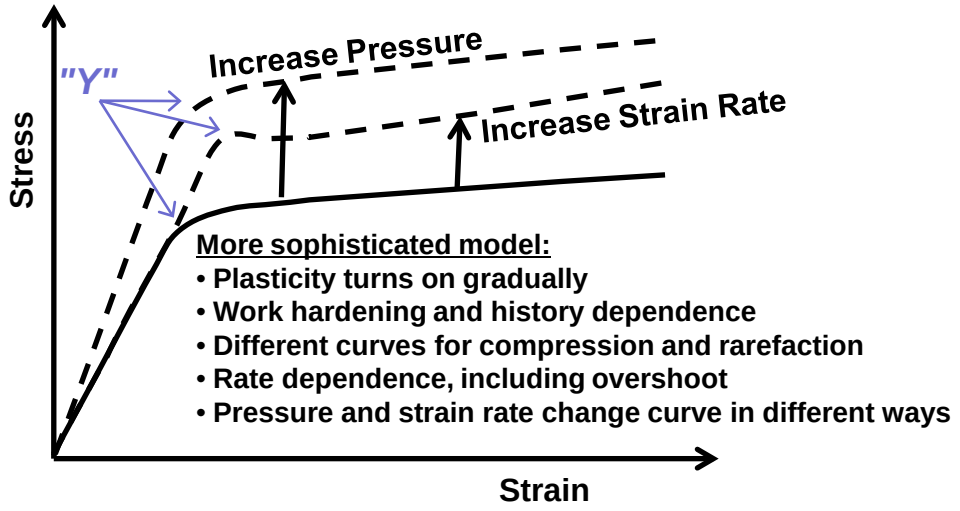

These curves are not invariant properties of a material!
They are particular deformation paths obtained under specific conditions.

"Yield strength" is twice the deviatoric stress at one arbitrary point on such a curve.

1D symmetry greatly simplifies the tensor quantities

$$\sigma_{ij} = \begin{bmatrix} \sigma & 0 & 0 \\ 0 & \sigma-2\tau & 0 \\ 0 & 0 & \sigma-2\tau \end{bmatrix}$$

$$\sigma_{ij}^{deviatoric} = \begin{bmatrix} 4\tau/3 & 0 & 0 \\ 0 & -2\tau/3 & 0 \\ 0 & 0 & -2\tau/3 \end{bmatrix}$$

$$P = \sigma - 4\tau/3$$

$$\varepsilon_{ij} = \begin{bmatrix} \ln\frac{V_0}{V} & 0 & 0 \\ 0 & 0 & 0 \\ 0 & 0 & 0 \end{bmatrix}$$

$$= \varepsilon_{elastic}^{isotropic} + \varepsilon_{elastic}^{deviatoric} + \varepsilon_{plastic}^{deviatoric}$$

$$= \begin{bmatrix} \frac{1}{3}\ln\frac{V_0}{V} & 0 & 0 \\ 0 & \frac{1}{3}\ln\frac{V_0}{V} & 0 \\ 0 & 0 & \frac{1}{3}\ln\frac{V_0}{V} \end{bmatrix} + \begin{bmatrix} \frac{2}{3}\ln\frac{V_0}{V}-\psi & 0 & 0 \\ 0 & -\frac{1}{3}\ln\frac{V_0}{V}+\psi/2 & 0 \\ 0 & 0 & -\frac{1}{3}\ln\frac{V_0}{V}+\psi/2 \end{bmatrix} + \begin{bmatrix} \psi & 0 & 0 \\ 0 & -\psi/2 & 0 \\ 0 & 0 & -\psi/2 \end{bmatrix}$$

Only 4 quantities needed:

- Normal stress σ
- Deviatoric stress parameter τ
- Volumetric strain $\varepsilon = 1\text{-}V/V_0$
- Plastic strain parameter ψ

Two of our four quantities can be integrated directly from the particle velocity (assuming it's known!)

Conserve Momentum: $\frac{\partial \sigma}{\partial h} = -\rho_0 \frac{\partial u}{\partial t}$

Conserve Mass: $\frac{\partial \varepsilon}{\partial t} = -\frac{\partial u}{\partial h}$

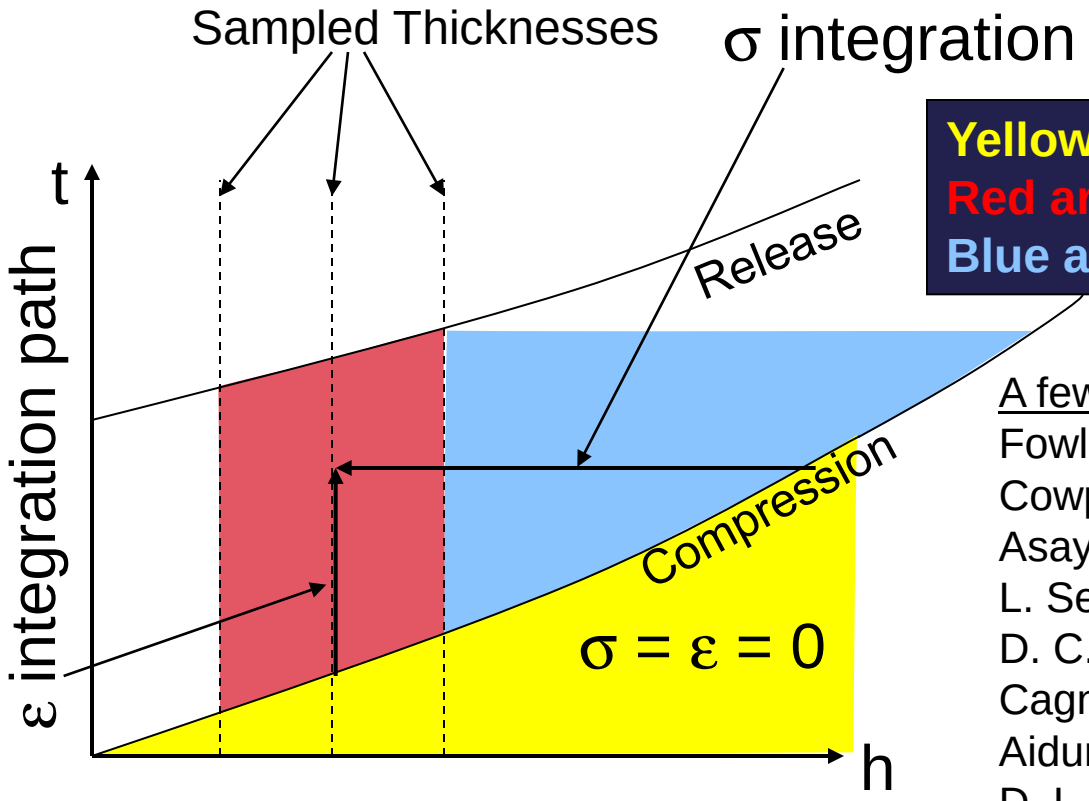

Yellow areas have known conditions
Red areas are interpolated
Blue areas are extrapolated

A few of *many* references:
Fowles & Williams, JAP 41, 360 (1970)
Cowperthwaite & Williams, JAP 42, 456 (1971)
Asay, Fowles, & Gupta, JAP 43, 744 (1972)
L. Seaman, JAP 45, 4303 (1974)
D. C. Wallace, PRB 22, 1487 (1980)
Cagnoux et al., Ann. Phys. Fr. 12, 451 (1987)
Aidun & Gupta, JAP 69, 6998 (1991)
D. L. Tonks, "DataShoP," LA-12068-MS
D. Hayes et al., LA-13830-MS

The other two quantities require some kind of EOS information, as shown on a stress-volume plot

Scalar EOS with isentrope and plastic work term: $P = P_0(\varepsilon) + 2\int \gamma\tau d\psi$

Linear isotropic elastic shear response approximation: $\sigma^{deviatoric} = 2\mu(P)\varepsilon^{deviatoric}_{elastic}$

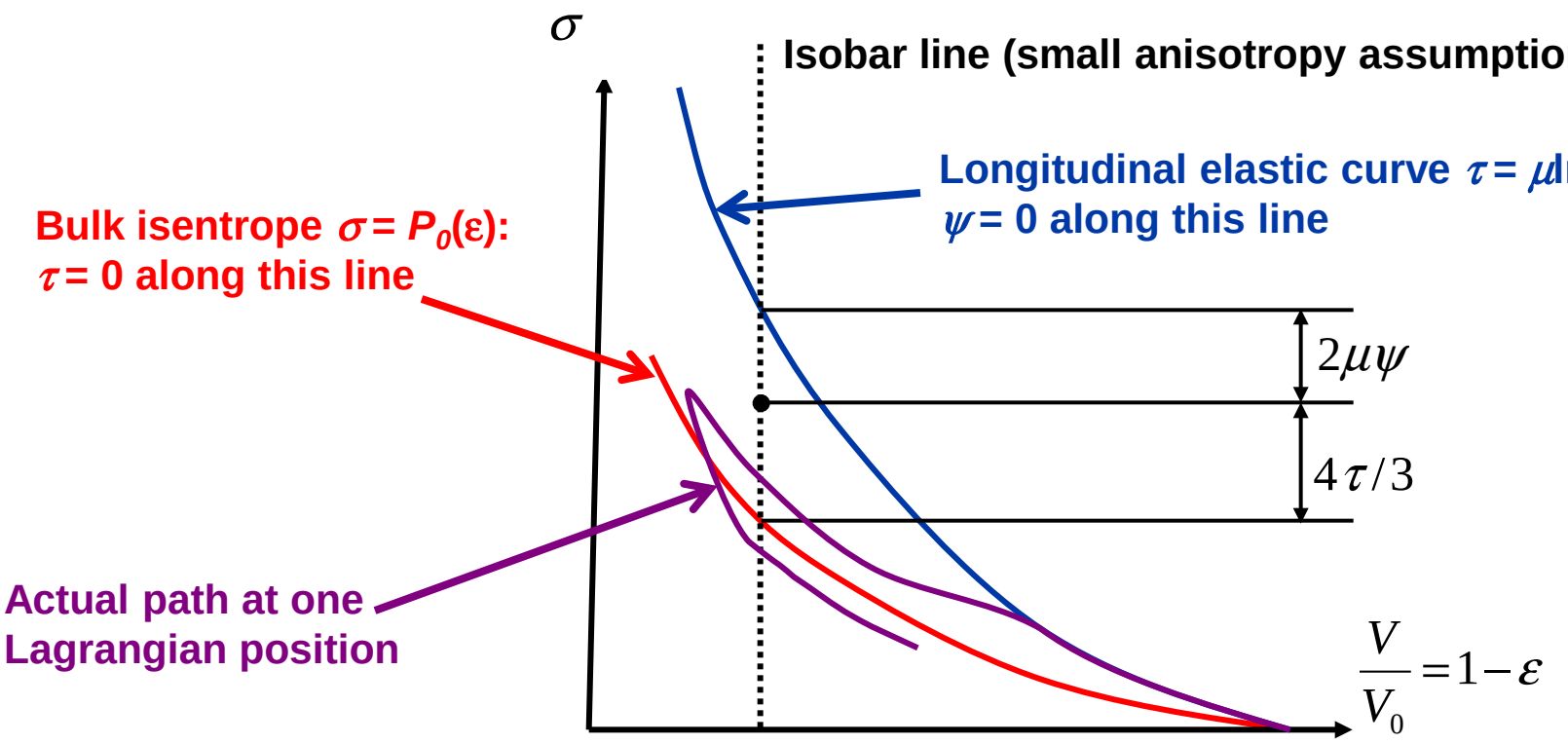

Summarizing the logic so far

IF we know

- The in situ particle velocity $u(h,t)$
- The thermoelastic properties

THEN we can calculate, for all (h,t),

- The full stress tensor
- The full elastic strain tensor
- The plastic strain
- The equivalent plastic strain $\int |d\psi|$
- The irreversible work

This scheme generalizes previous methods to include in a single formalism:

Nonsteady/simple waves

Full extraction of tensor stresses and elastic/plastic strains

Improved convergence at higher pressures

So in essence, the problem is reduced to determining $u(h,t)$.

Wave propagation is described by a number of different wave speeds

- Lagrangian phase velocities c_u associated with each state variable e.g. c_ε, c_u, c_σ
- Longitudinal elastic and bulk wave velocities c_L, c_B
- On σ-V/V_0 plots, slope = $-\rho_0 c^2$ for some c

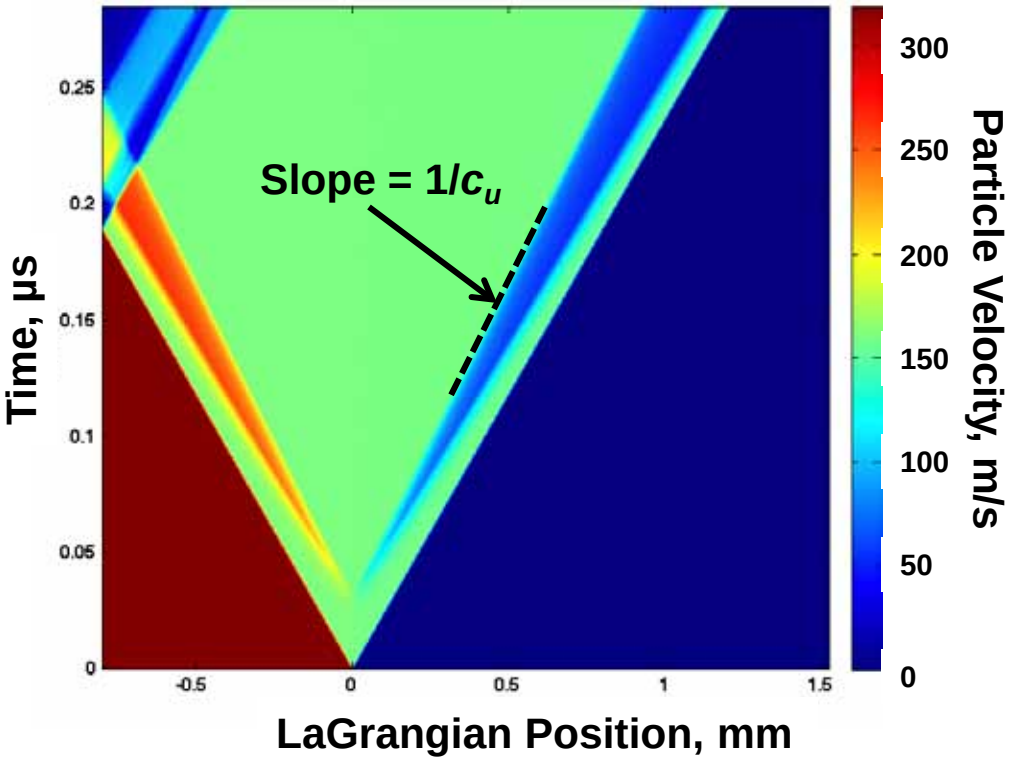

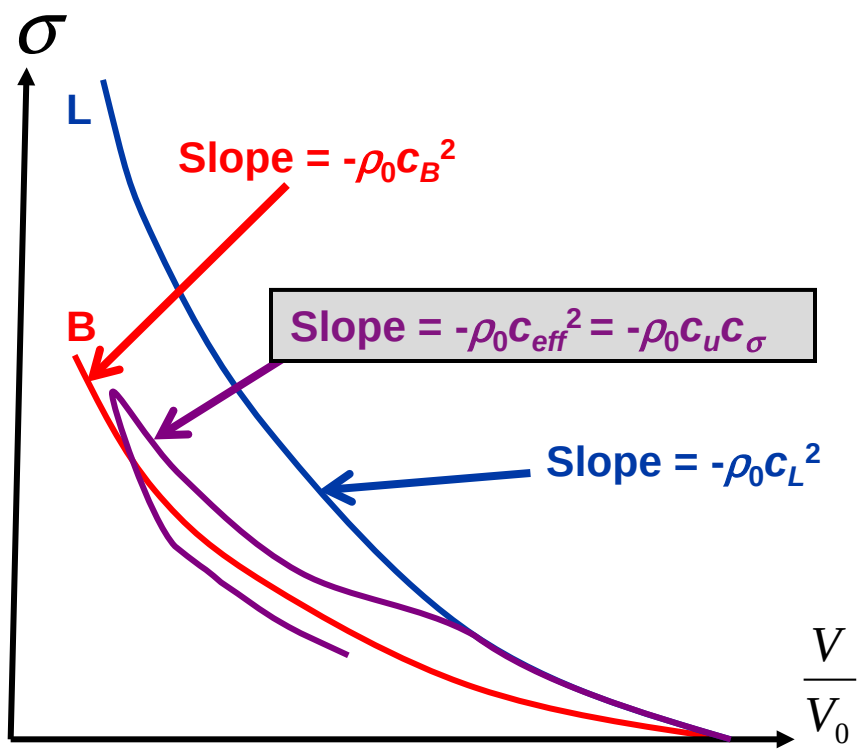

The effective wave speed is a resultant of left-traveling, right-traveling, and local effects

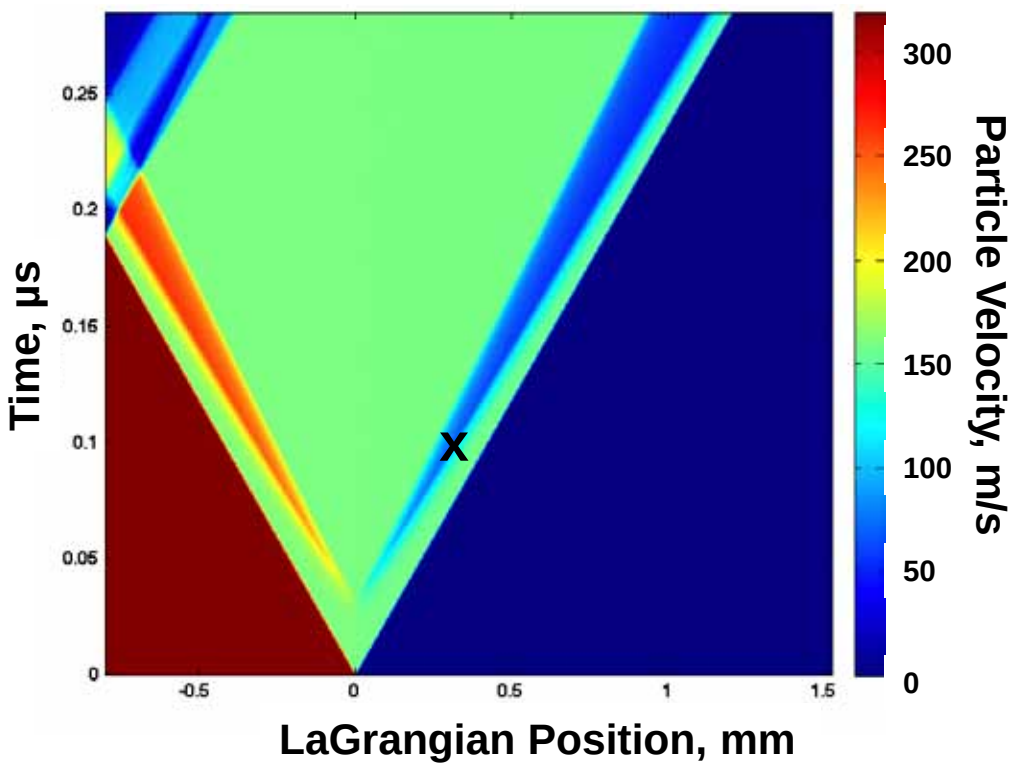

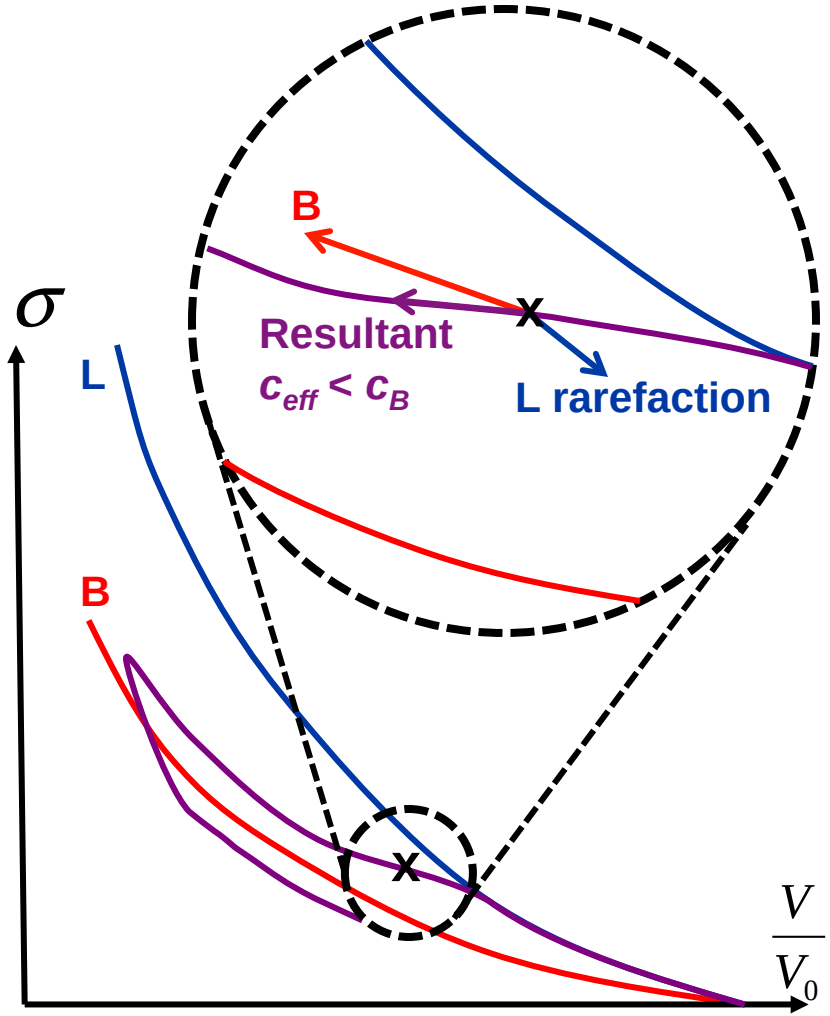

The most common integration scheme assumes simple waves

- All "characteristics" are straight and identical for different state variables
- $c_u = c_\sigma = c_\varepsilon = c_\tau = c_\psi = c(u)$
- Hysteresis associated with strength is implicitly disallowed
- $O(\tau)$ EOS terms neglected
- Equations for all state variables are easy to integrate

$$\left(\frac{\partial \varepsilon}{\partial u}\right)_h = \frac{1}{c} \qquad \left(\frac{\partial \sigma}{\partial u}\right)_h = \rho_0 c$$

$$2\mu\left(\frac{\partial \psi}{\partial \varepsilon}\right)_h = \rho_0\left(c_L^2 - c^2\right) \qquad c_L^2 = \left(B + \frac{4}{3}\mu\right)\frac{\rho}{\rho_0^2}$$

$$\frac{4}{3}\left(\frac{\partial \tau}{\partial \varepsilon}\right)_h = \rho_0\left(c^2 - c_B^2\right) \qquad c_B^2 = \frac{B\rho}{\rho_0^2}$$

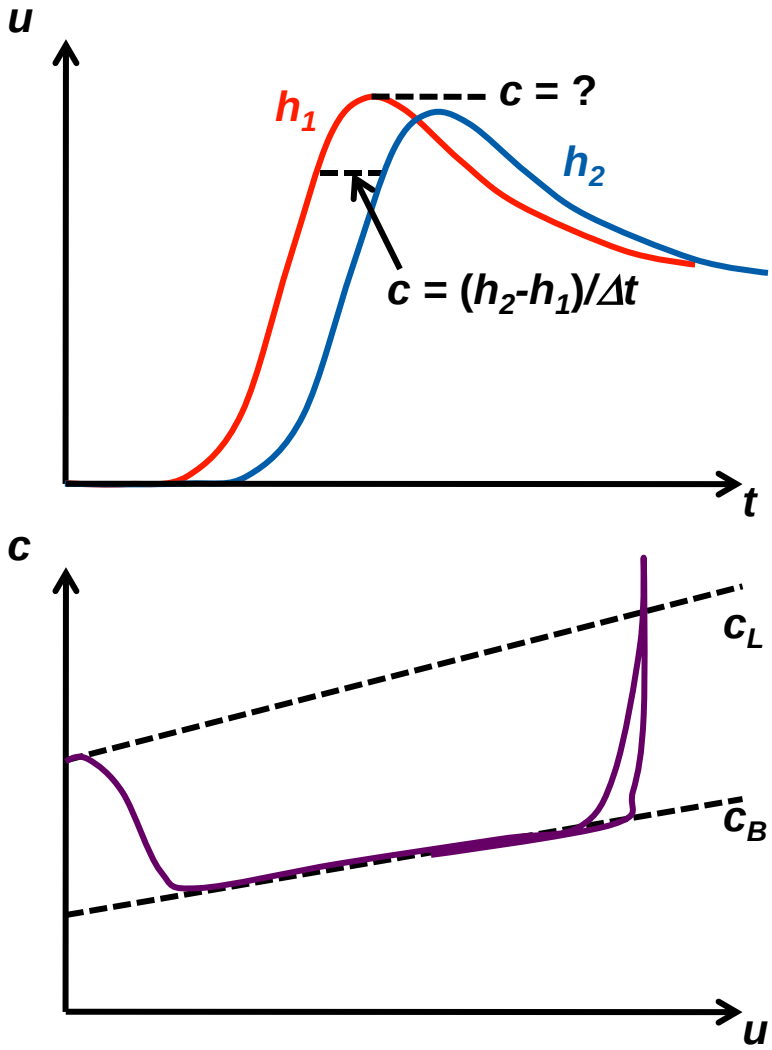

Nonsimple/nonsteady waves make the equations more complicated

- The relevant wave speed for tracking thermodynamic paths is $c_{eff} = (c_u c_\sigma)^{1/2}$

$$\left(\frac{\partial \varepsilon}{\partial u}\right)_h = \frac{1}{c_u} \qquad \left(\frac{\partial \sigma}{\partial u}\right)_h = \rho_0 c_\sigma$$

$$\left(\frac{\partial \sigma}{\partial \varepsilon}\right)_h = \rho_0 c_u c_\sigma = \rho_0 c_{eff}^2$$

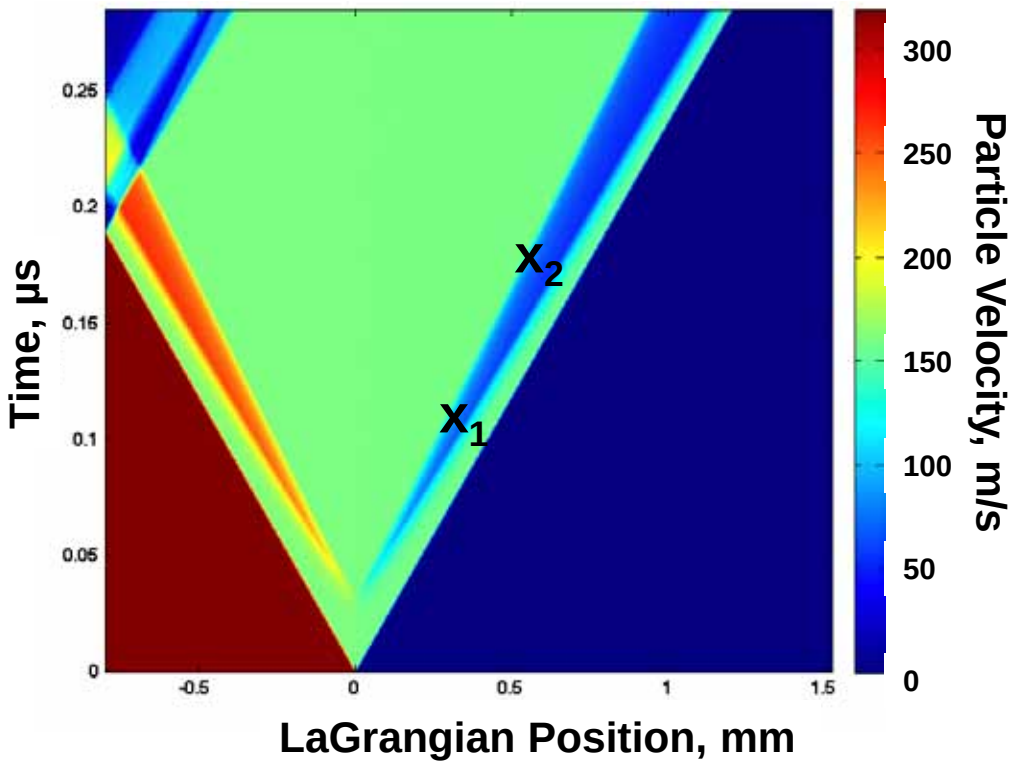

If we include all of the terms when strength is present, the τ and ψ equations get very messy

Simple Waves, Zero Strength

$$2\mu\left(\frac{\partial\psi}{\partial\varepsilon}\right)_h = \rho_0\left(c_L^2 - c^2\right)$$

$$\frac{4}{3}\left(\frac{\partial\tau}{\partial\varepsilon}\right)_h = \rho_0\left(c^2 - c_B^2\right)$$

$$c_L^2 = \left(B + \frac{4}{3}\mu\right)\frac{\rho}{\rho_0^2}$$

$$c_B^2 = \frac{B\rho}{\rho_0^2}$$

Corrected Model

$$2\mu\left(\frac{\partial\psi}{\partial\varepsilon}\right)_h = \rho_0\frac{c_L^2 - c_{eff}^2}{1 - \frac{\gamma\tau}{\mu}\left(1 + \frac{4}{3}\theta\right)} \qquad \theta = \frac{\tau}{\mu}\frac{d\mu}{dP}$$

$$\frac{4}{3}\left(\frac{\partial(\tau/\mu)}{\partial\varepsilon}\right)_h = \rho_0\frac{c_{eff}^2 - c_{B1}^2}{1 - \frac{\gamma\tau}{\mu}\left(1 + \frac{4}{3}\theta\right)}$$

$$\frac{4}{3}\left(\frac{\partial\tau}{\partial\varepsilon}\right)_h = \rho_0\frac{c_{eff}^2 - c_{B2}^2}{1 - \frac{\gamma\tau}{\mu}\left(1 + \frac{4}{3}\theta\right)}\left(1 - \frac{4}{3}\frac{\theta\gamma\tau}{\mu}\right)$$

$$c_L^2 = \left(B + \frac{4}{3}(\mu + B\theta)\right)\frac{\rho}{\rho_0^2}$$

$$c_{B1}^2 = \left(B + \frac{4}{3}\gamma\tau\right)\left(1 + \frac{4}{3}\theta\right)\frac{\rho}{\rho_0^2}$$

$$c_{B2}^2 = \left(B + \frac{4}{3}\gamma\tau\right)\frac{\rho}{\rho_0^2}\Big/\left(1 - \frac{4}{3}\frac{\theta\gamma\tau}{\mu}\right)$$

A word on entropy generation

- **Basic shock theory:**
  - $\Delta S \sim \Delta P^3$ for sudden jumps
  - Dissipation governed by linear viscosity and/or thermal conduction
  - ΔS è 0 and c è c_{B0} for slow enough ramp loading
- **In the presence of strength, none of these are true in general**
  - $\Delta S \sim \Delta P$ even at low ΔP, once it starts yielding
  - Rate-independent model cannot account for ΔP^3 term
  - Pressure-hardening and plastic work modify c_B by $O(\tau)$:

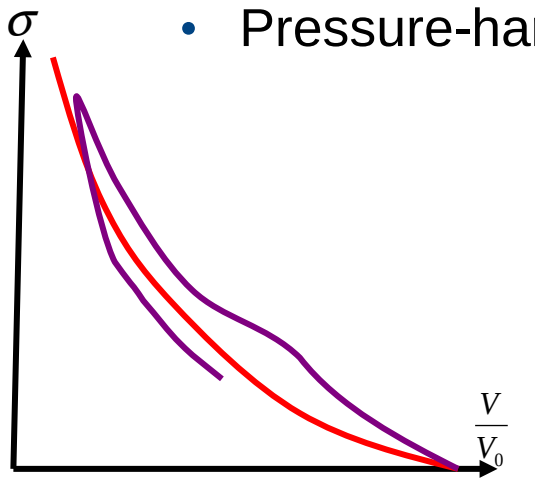

$$\left(\frac{c_{B1}}{c_{B0}}\right)^2 = \left(1+\frac{4}{3}\frac{\gamma\tau}{B}\right)\left(1+\frac{4}{3}\frac{\tau}{\mu}\frac{d\mu}{dP}\right)$$

Plug in typical values for Ta

$$\approx \left(1+\frac{4}{3}\frac{1.64*1\ \text{GPa}}{190\ \text{GPa}}\right)\left(1+\frac{4}{3}\frac{1\ \text{GPa}}{64\ \text{GPa}}*0.75\right) = (1+1.2\%)(1+1.5\%)$$

Second law of thermodynamics provides a consistency check that can be calibrated with static measurements

How can you use thermodynamics to know when τ crosses zero?

- $\tau\dot{\psi} \geq 0$ implies that τ and $\dot{\psi}$ pass through zero simultaneously when the loading reverses, if both are smooth curves
- This occurs when $c_{eff} = c_L(\tau = 0) = ((B + 4\mu/3)\rho/\rho_0^2)^{1/2}$
- Bauschinger effect is a problem

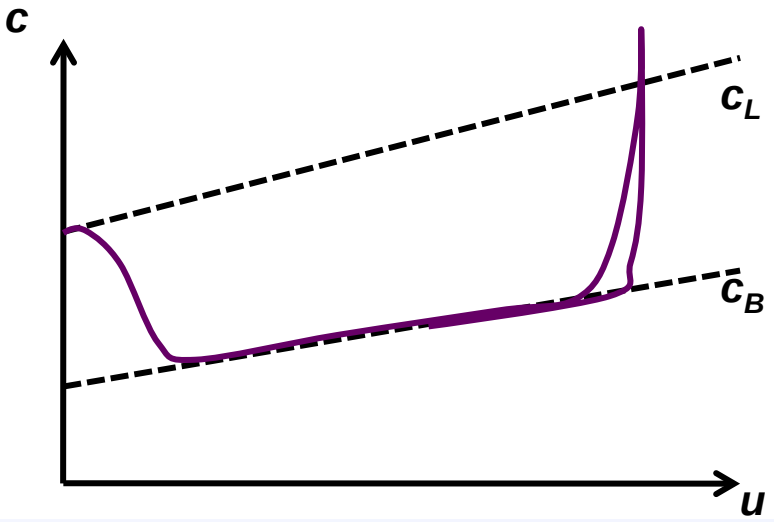

A simple wave formalism may or may not have the precision to do this

Example: Extracting flow curves from multi-step shock experiments

Ta-on-Ta and Ta-on-LiF gas gun shots to 10, 25, 45, and 60 GPa

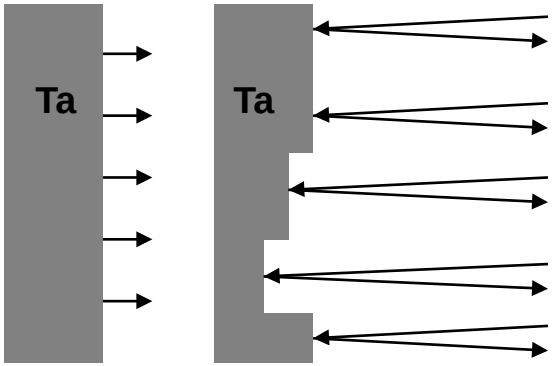

PDV 2.0 mm thickness

PDV 1.5 mm thickness

PDV 1.0 mm thickness

7 extra PDV channels for tilt/flatness correction

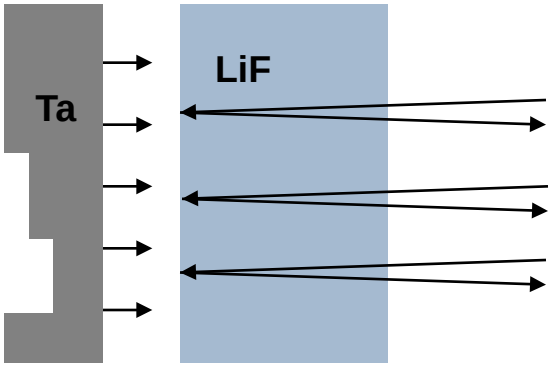

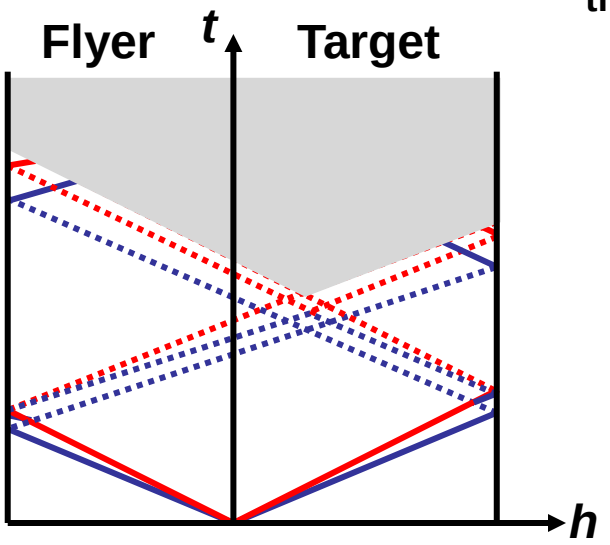

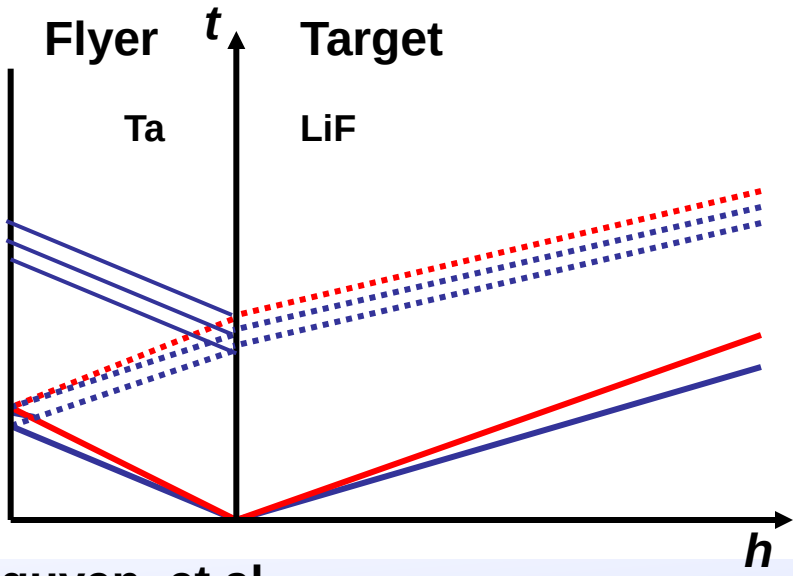

Collaboration with R. Patterson, J. H. Nguyen, et al.

We perform integrals piecewise analytically using a second order interpolation/extrapolation function

$$u = \frac{(t_{i+1} - t)u_i^+ + (t - t_i)u_{i+1}^-}{t_{i+1} - t_i} + 4\beta_i \frac{(t - t_i)(t_{i+1} - t)}{(t_{i+1} - t_i)^2}, t_i < t < t_{i+1}$$

$$t_i(h) = t_{i,2}h^2 + t_{i,1}h + t_{i,0}$$

$$u_i^a(h) = u_{i,1}^a h + u_{i,0}^a$$

$$\beta_i(h) = \beta_{i,0}$$

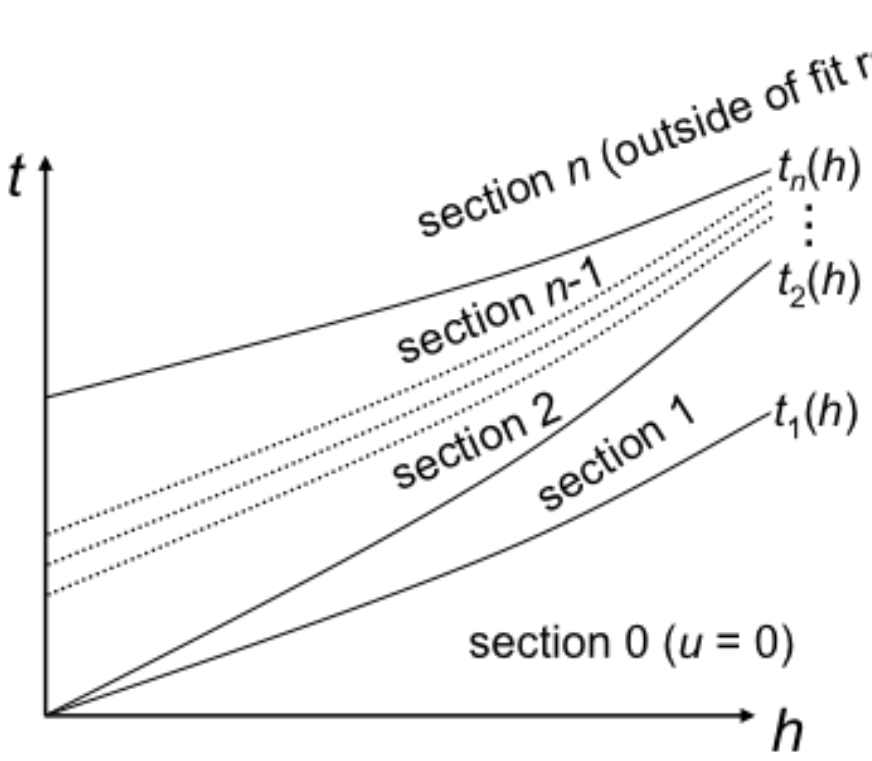

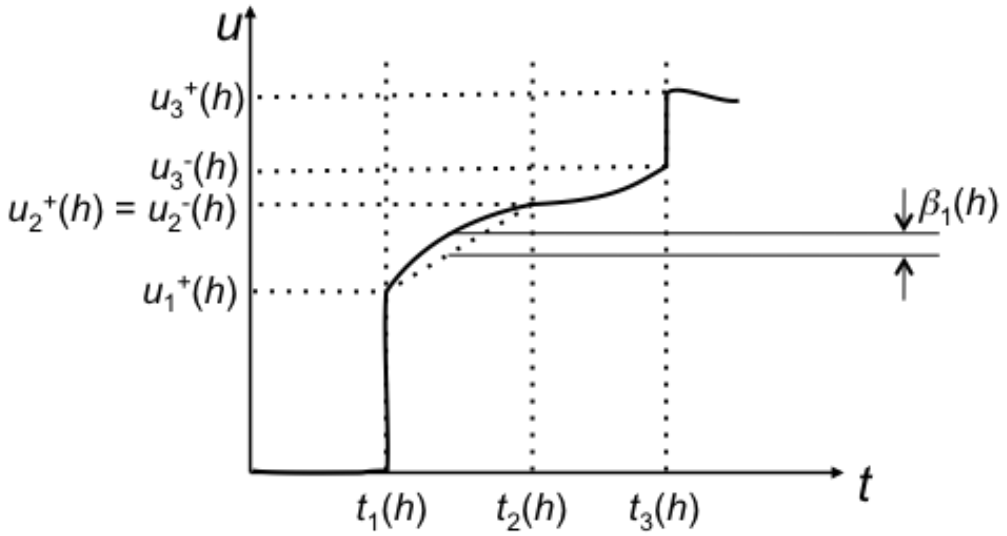

Free surface effects can be identified and corrected

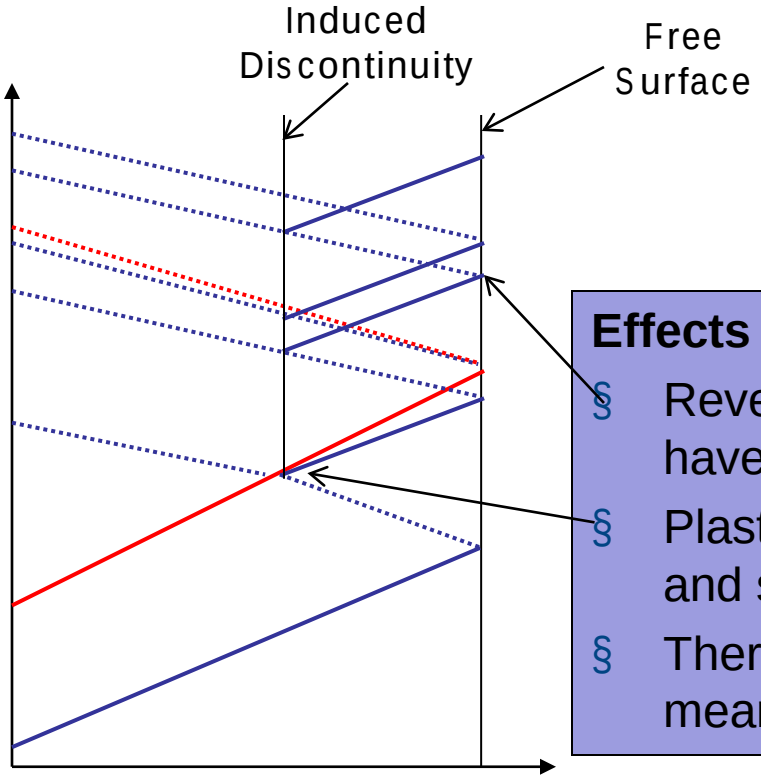

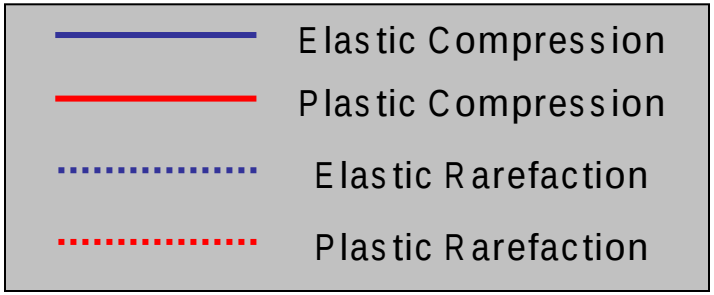

Effects to correct for:

- Reverberations are artificial; would not have happened in infinite material
- Plastic load is split, partially reflected, and slightly delayed
- Thermodynamic path hysteresis means velocity doubling is not exact

These are all few-percent systematic errors for shocks ~10-30 GPa.

Even a rough estimate is enough to reduce residual systematic error to less than 1% (as validated through simulation including rate-dependent effects).

Analysis example: Ta 3-step shock experiment
Part 1: Velocity modeling with reliability diagnostics

Free surface corrections and curve fits

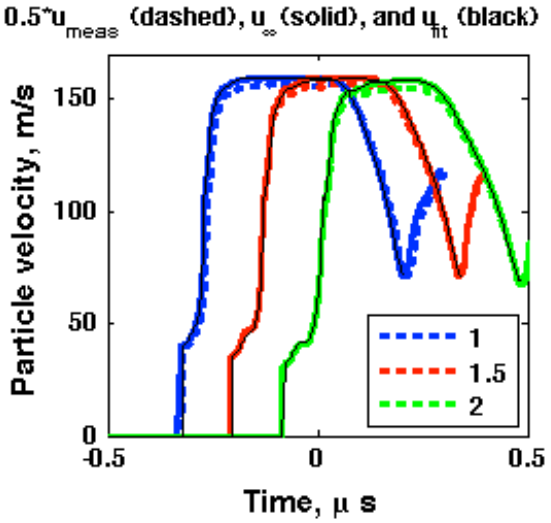

User-defined interpolation zones

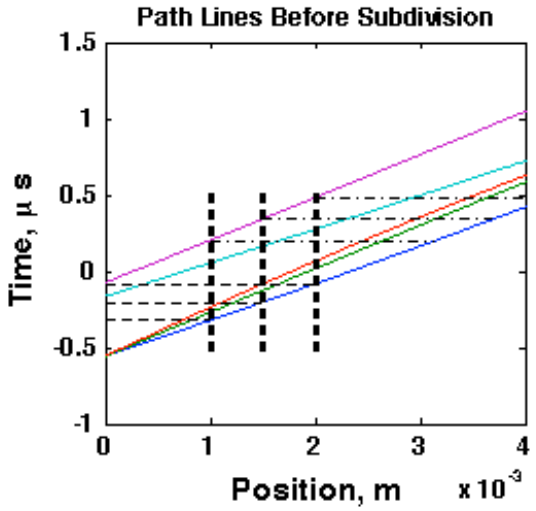

Extrapolation to drive surface

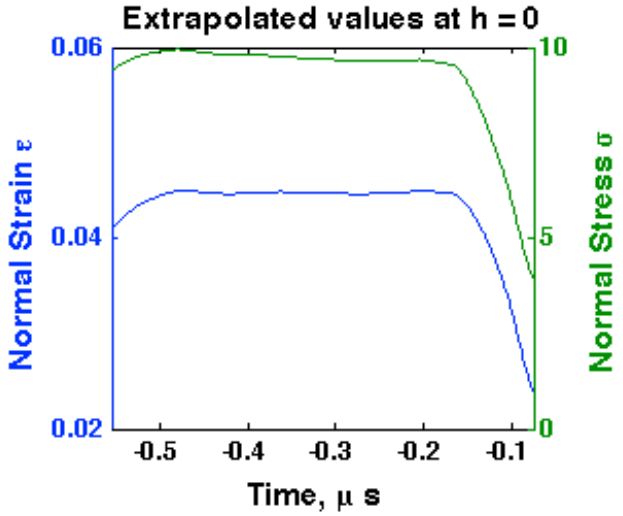

Analysis example: Ta 3-step shock experiment
Part 2: Lagrangian analysis with plastic work iteration

Calculated normal stress for all steps

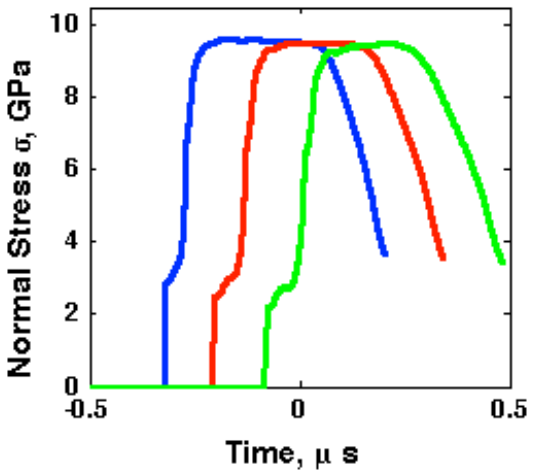

Calculated normal strain for all steps

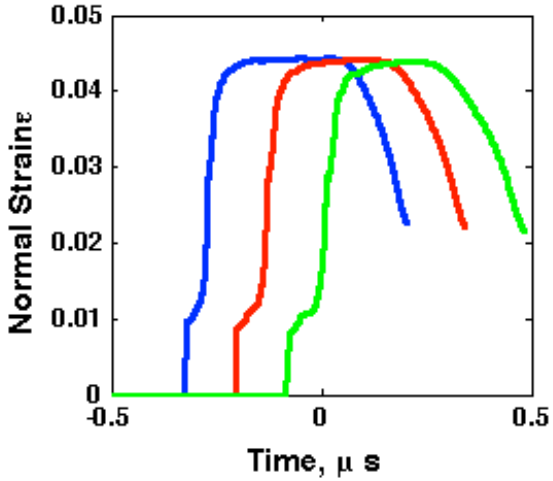

Thermodynamic path, with superposed EOS

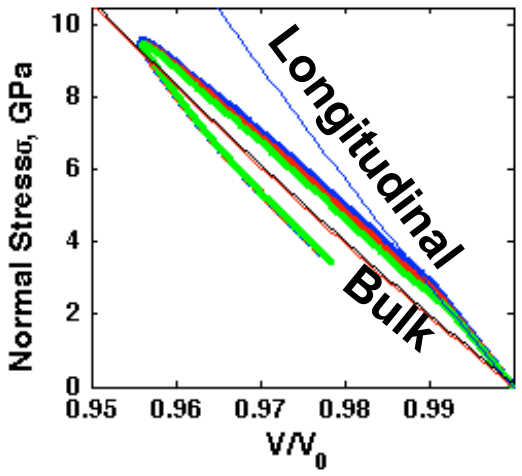

Analysis example: Ta 3-step shock experiment
Part 3: Deviatoric stress and plastic strain

Calculated deviatoric stress for all steps

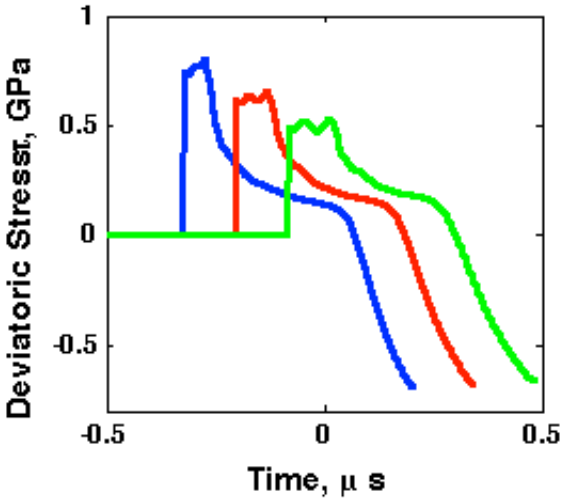

Calculated plastic strain for all steps

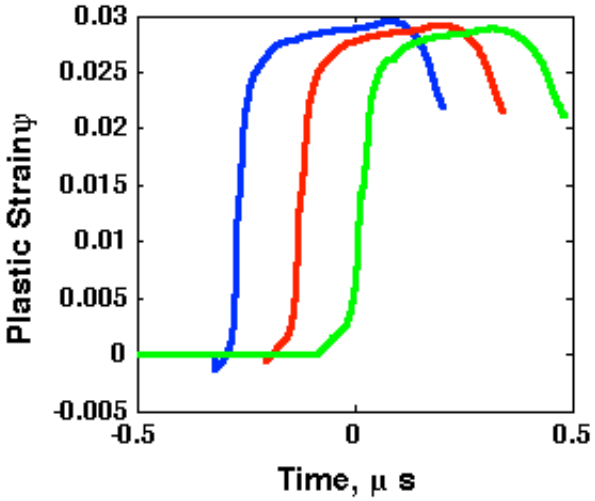

Plastic part of the stress-strain relation

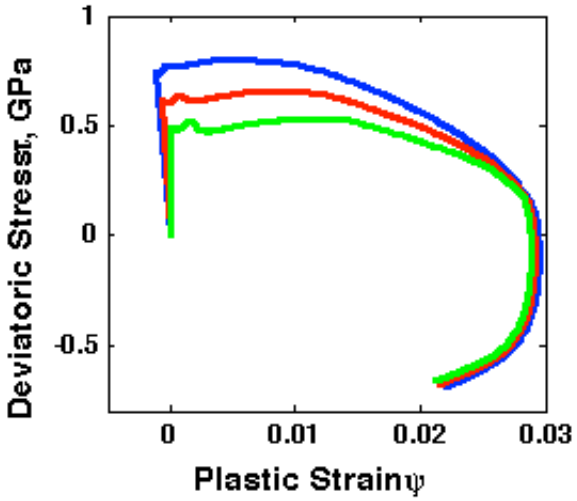

Once the analysis is done, we can plot the data any way we like, e.g. looking at strain rate and history effects on strength

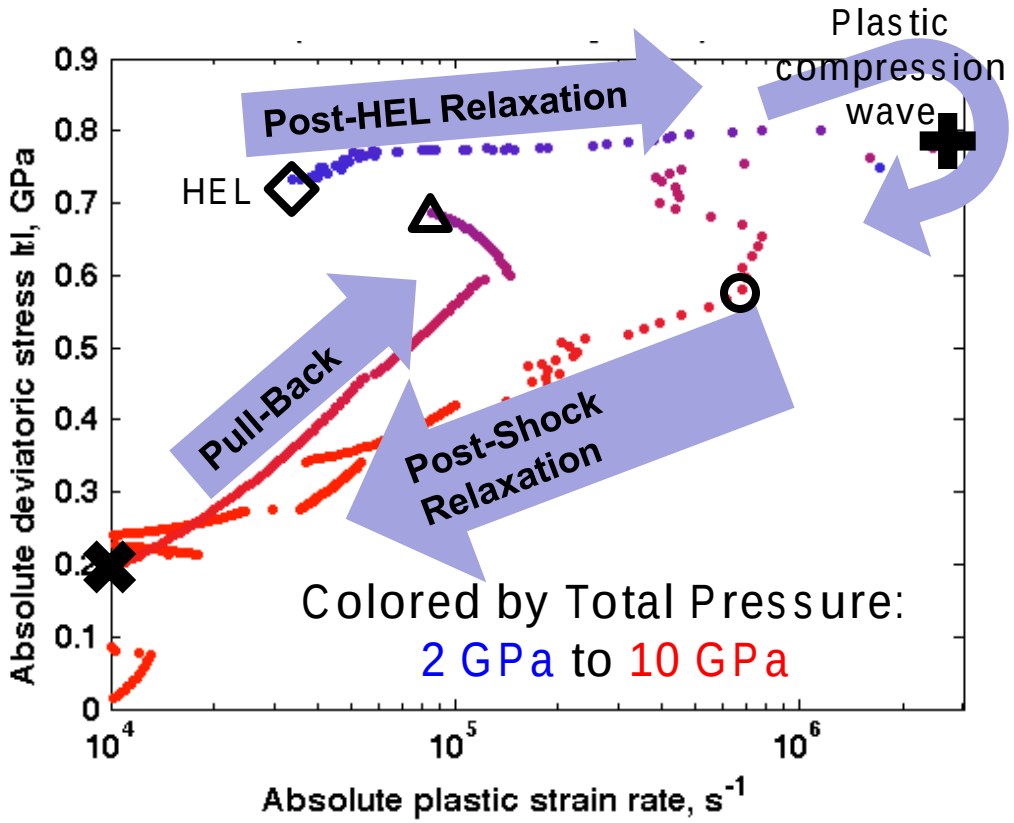

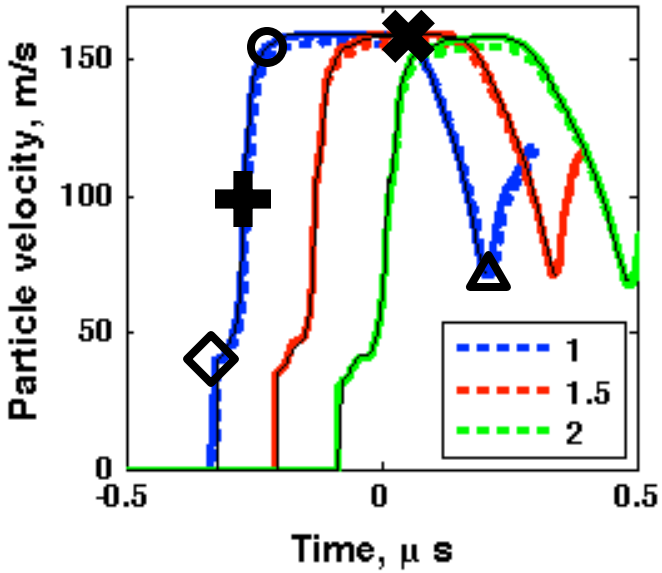

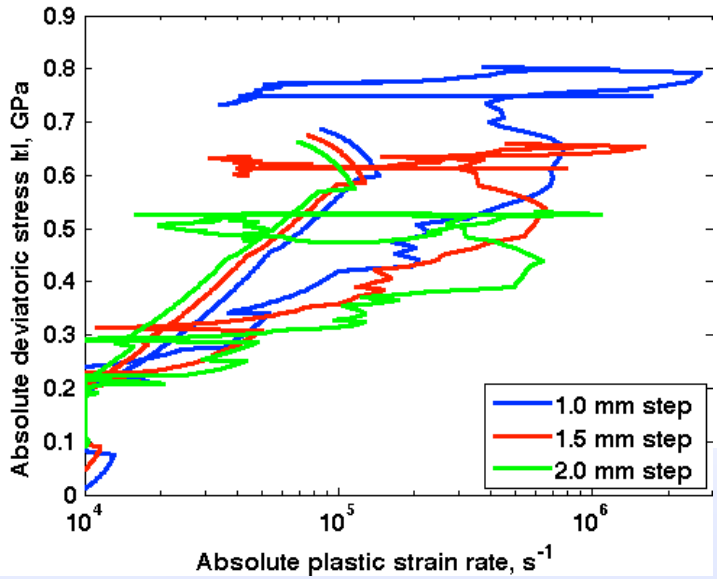

Summary

- Going back to fundamental thermodynamics shows standard wave analysis to be a special case of a more general theory
- Strength is much more than just a pressure-dependent number
- Rate dependence and nonsimple/nonsteady wave behavior can complicate the analysis
- Generalized formalism can analyze waves for complete flow curves and bracket strength behavior with minimal assumptions
- Consistency checks, especially those based on the second law of thermodynamics, offer hope for improving the stability of the inverse problem
- Free-surface/window corrections and applications to higher pressures remain very challenging

Additional features and work in progress

- We calculate the full parameter sensitivity matrix linking *all* input parameters to *all* calculated values
  - ~25000 x ~5000 matrix
  - Facilitates full error propagation
  - Also facilitates experimental design

- Preliminary tests on ramp waves are very promising
  - Drive was estimated based on surface velocities
  - Very close match even with rate-dependent plasticity

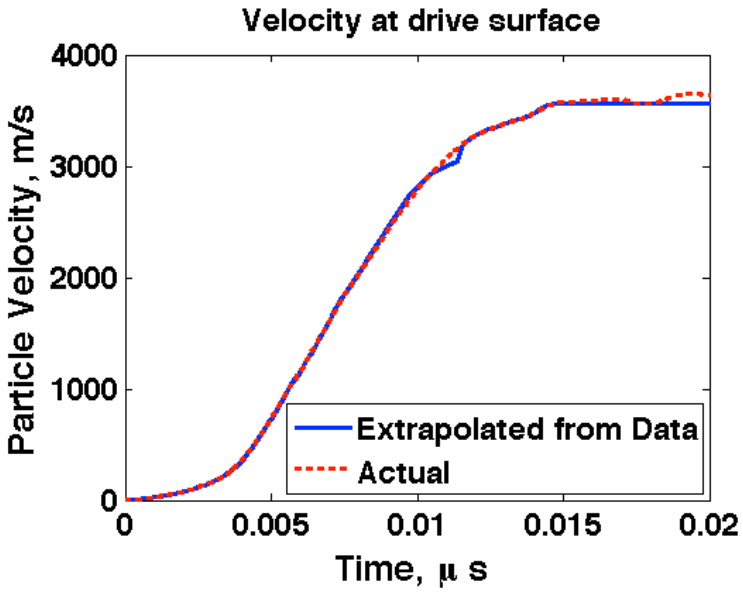

Characteristic curves and dynamic scaling in shockless compression using molecular dynamics

J Matthew D Lane

Aidan Thompson

Sandia National Laboratories

Albuquerque, NM

19 January 2011

4th Workshop on Ramp Compression

Albuquerque, NM

Sandia is a multiprogram laboratory operated by Sandia Corporation, a Lockheed Martin Company,
for the United States Department of Energy's National Nuclear Security Administration
under contract DE-AC04-94AL85000.
This work supported by the Laboratory Directed Research and Development program at Sandia National Laboratories.

Motivation for ramp waves

Z-machine at Sandia National Labs

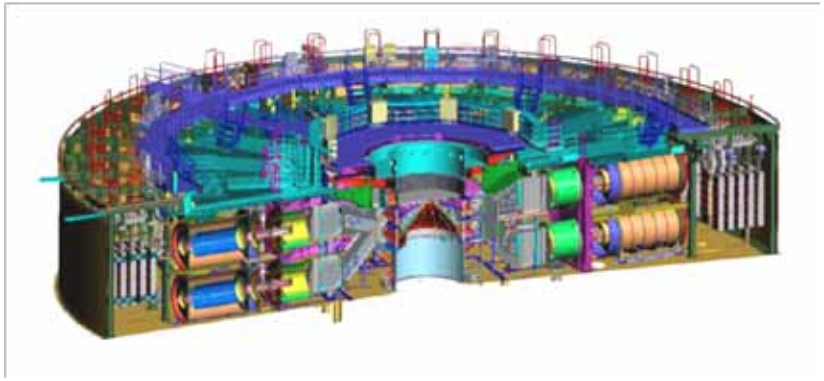

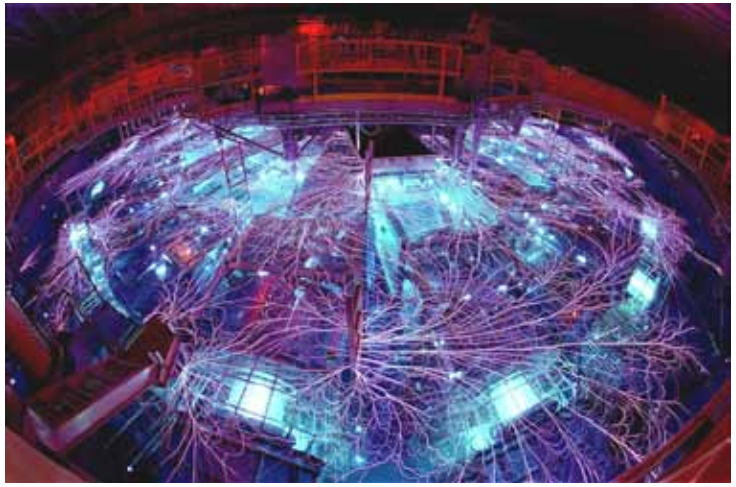

Z-machine experiments allow:

- Ramp waves to explore off-Hugoniot EOS
- Continuous data vs single shock points

- MD may offer atom-scale mechanisms for effects observed in experiments

Plot results from Knudson, SNL

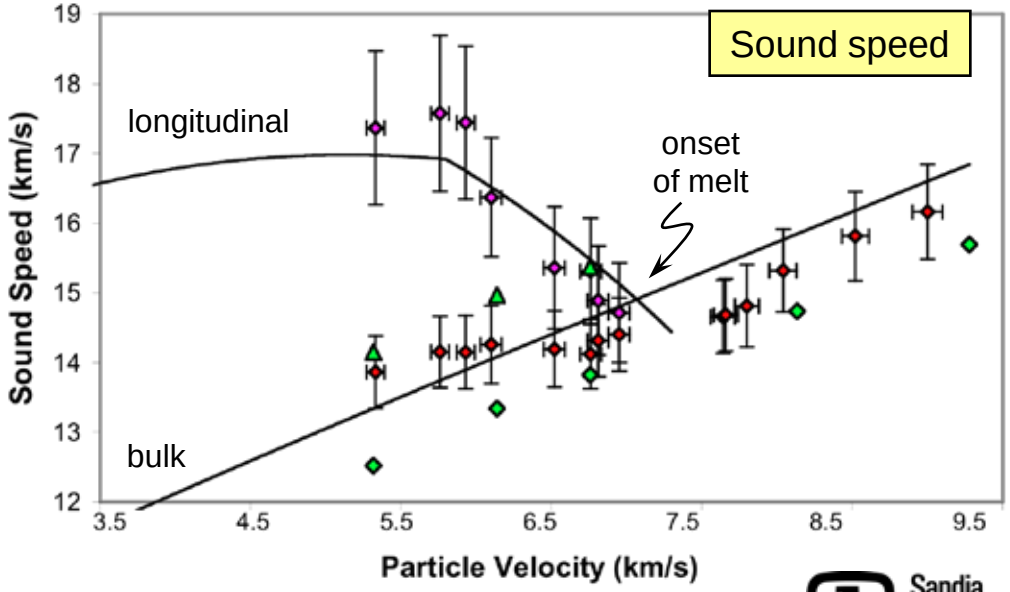

Matthew Lane - jlane@sandia.gov

Sandia National Laboratories

Hierarchy of modeling approaches

Role of atomistic (molecular dynamics) approach:

- Probe the structure and dynamics on a length scale that cannot be resolved with experiment or continuum
- Bridges gap between quantum and continuum descriptions through a hierarchical model

Continuum scale

μs times & nm-mm lengths

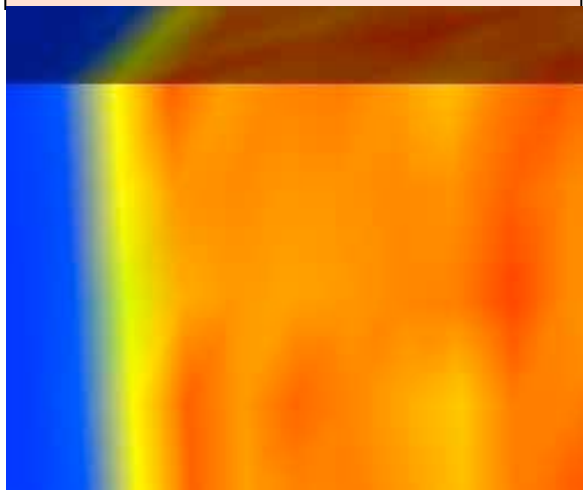

Molecular scale

ns times & 10s nm lengths

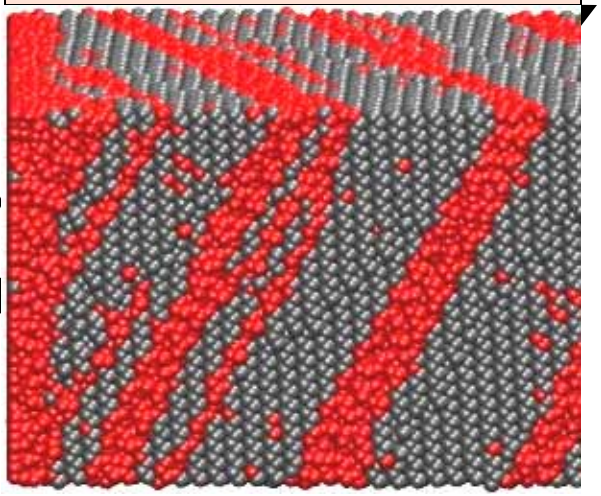

Quantum scale

fs times & Å lengths

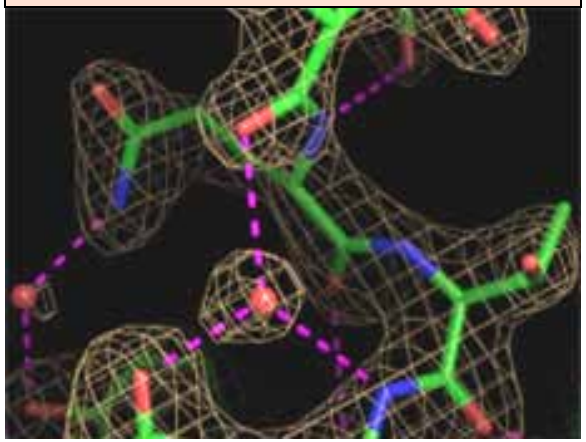

- Provides detailed picture of emergent phenomena both qualitatively and (in some cases) quantitatively

Molecular Dynamics (MD) simulations

- Solve Newton's equation…

$$m_i \frac{d^2 \mathbf{r}_i}{dt^2} = \mathbf{F}_i$$

$$\mathbf{F}_i = -\nabla V_i$$

6*N* coupled ODEs

$$\begin{aligned}
\mathbf{v}_i^{(l+\frac{1}{2})} &= \mathbf{v}_i^l - \frac{\mathbf{F}_i^l}{2m_i}\Delta t \\
\mathbf{r}_i^{(l+1)} &= \mathbf{r}_i^l + \mathbf{v}_i^{(l+\frac{1}{2})}\Delta t \\
\mathbf{v}_i^{(l+1)} &= \mathbf{v}_i^{(l+\frac{1}{2})} - \frac{\mathbf{F}_i^{(l+1)}}{2m_i}\Delta t
\end{aligned}$$

Mathematical Formulation

Classical Mechanics

Atoms are Point Masses: $\boldsymbol{r}_1$, $\boldsymbol{r}_2$, ... $\boldsymbol{r}_N$

Positions, Velocities, Forces: $\boldsymbol{r}_i$, $\boldsymbol{v}_i$, $\boldsymbol{F}_i$

Potential Energy Function = $V_i(\boldsymbol{r}^N)$

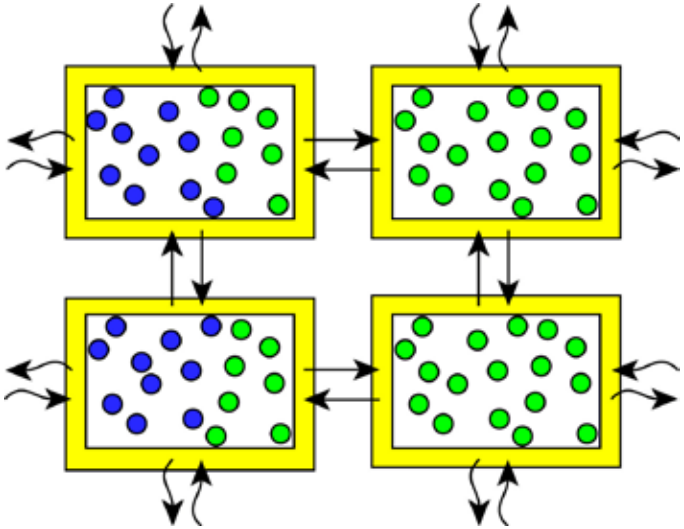

Sandia's LAMMPS code is spatially parallel

Large-scale **A**tomic/**M**olecular **M**assively **P**arallel **S**imulator

Problem: Δt tied to the fastest atomic motion t is the timescale of physical interest

$nsteps = t / \Delta t = 10^6 \ldots 10^{15}$

Two difficulties using MD for ramp waves

1. **Quantitative results require effective potentials which are accurate at high pressure and temperatures**
   - **Potentials are most often fit to ambient conditions**
   - **Historically, molecular dynamics has emphasized qualitative results using simple model potentials**

1. Computation effort is quadratic in time. Similar to issue with steady-state shock propagation, but much worse
   - Ramp waves are slow (long) ~ 100 ns rise times
   - Slow rise times require large system sizes

MEAM Potential for Beryllium

Hydrostatic Compression

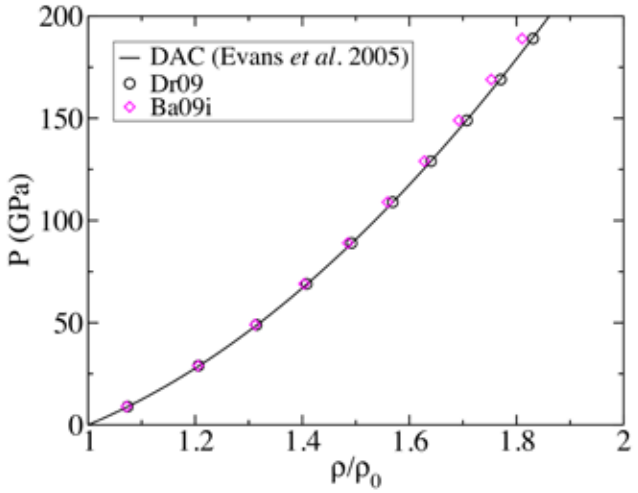

Quantity	Units	Expt.	Dr09	Ba09i
B	GPa	117	113	115
C11	GPa	294	331	259
C33	GPa	357	309	329
C12	GPa	27	-11	77
C13	GPa	14	18	9
C44	GPa	162	197	65
C66	GPa	133	171	91
a	A	2.286	2.259	2.259
(c/a)*	-	0.96	0.98	0.99
M.P.	K	1550	-	1390

MEAM - Modified Embedded Atom Method

$$\phi(R) = \frac{2}{Z}\left\{E^u(R) - F(\bar{\rho}^0(R))\right\}S$$

$$F(\bar{\rho}) = AE_c\bar{\rho}\ln\bar{\rho}$$

$$\rho_k^{(l)2} = \sum_i \rho_l(R_{ik})\sum_j \rho_l(R_{kj})P_l^0(\cos(\theta_{ikj}))$$

Shock Compression c-axis

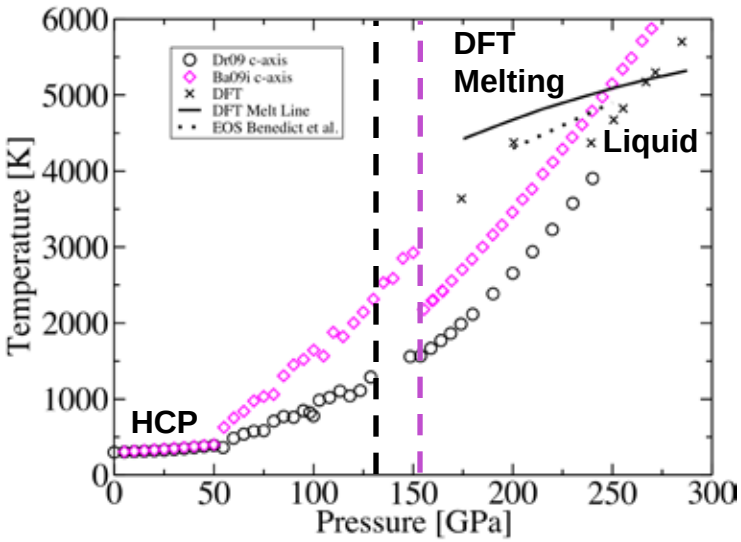

DFT data from Desjarlais, SNL

Matthew Lane - jlane@sandia.gov

GAP Potential for Beryllium

GAP Potential

Local density around each atom written as 4D spherical harmonics series, analogous to Fourier transform

GAP is an interpolation of DFT energies to bispectrum of lowest-order coefficients in series

No detailed assumptions about chemical interactions

Preserves universal symmetries: rotational & translational invariance

Shock Compression c-axis

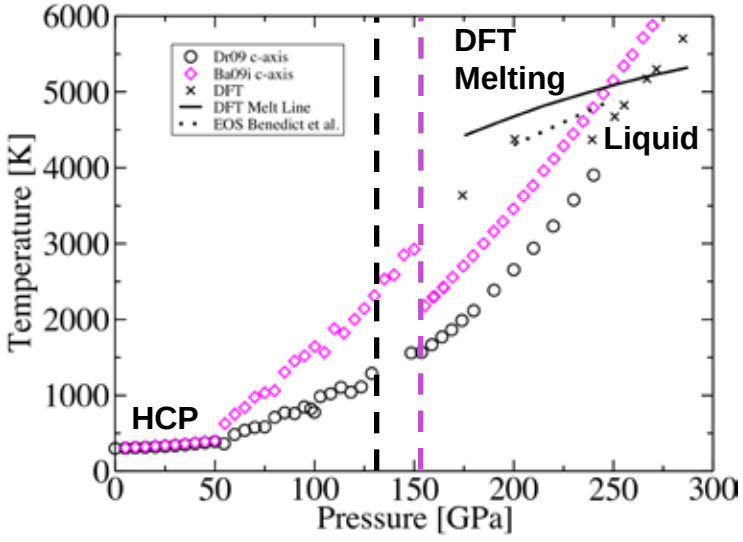

Diamond: Force errors for GAP fitted to DFT
Adding higher-order GAP coefficients systematically increases accuracy
Bartok et al., PRL 104, 136403 (2010)

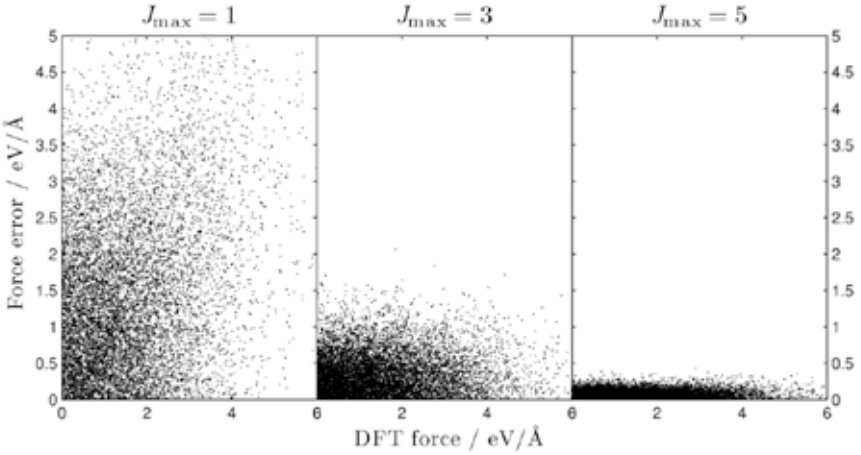

Beryllium

GAP potential now implemented in LAMMPS

Working with GAP developers, fitting directly to forces and energies from high-temperature DFT MD simulations of small systems (from Mike Desjarlais)

Initial results are promising. Large scale simulations of Beryllium are planned in the coming months.

Sandia National Laboratories

Two difficulties using MD for ramp waves

1. Quantitative results require effective potentials which are accurate at high pressure and temperatures
   - Potentials are most often fit to ambient conditions
   - Historically, molecular dynamics has emphasized qualitative results using simple model potentials

1. **Computation effort is quadratic in time. Similar to issue with steady-state shock propagation, but much worse**
   - **Ramp waves are slow (long) ~ 100 ns rise times**
   - **Slow rise times require large system sizes**

Difficulty with MD modeling ramp waves

- We'd like to apply a scaling argument (dynamic similarity) to reduce the computational expense of large-long simulations:

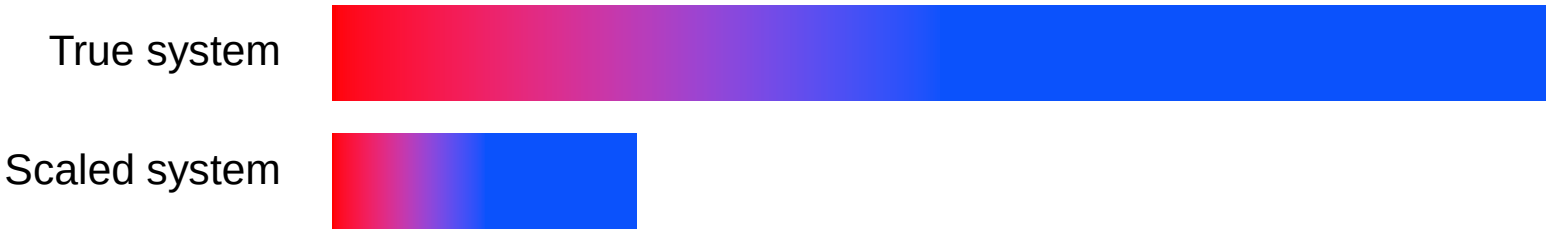

- We'll need to develop two tools first:
  - A method for extracting continuum variable fields from MD
  - A method for extracting characteristic curves from atomistics

Atomistic-Continuum formulation of Hardy

R.J. Hardy (*Journal of Chemical Physics*, 1982) -

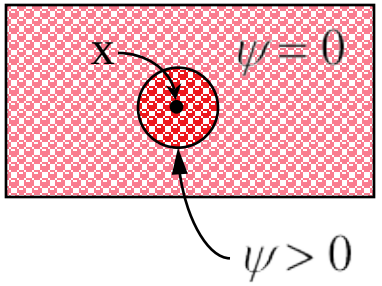

$$\rho(\mathbf{x},t) = \sum_{\alpha=1}^{N} m^{\alpha}\psi\left(\mathbf{x}^{\alpha}-\mathbf{x}\right) \qquad \mathbf{p}(\mathbf{x},t) = \sum_{\alpha=1}^{N} m^{\alpha}\mathbf{v}^{\alpha}\psi\left(\mathbf{x}^{\alpha}-\mathbf{x}\right)$$

$$E^{0}(\mathbf{x},t) = \sum_{\alpha=1}^{N}\left\{\frac{1}{2}m^{\alpha}\mathbf{v}^{\alpha}\cdot\mathbf{v}^{\alpha}+\phi^{\alpha}\right\}\psi\left(\mathbf{x}^{\alpha}-\mathbf{x}\right) \qquad [\psi] \sim \frac{1}{V_c}$$

Applying to the balance laws, *e.g.*

$$\frac{\partial \mathbf{p}}{\partial t} = \frac{\partial}{\partial \mathbf{x}}\cdot\left(\boldsymbol{\sigma} - \rho\mathbf{v}\otimes\mathbf{v}\right)$$

and separating continuum-scale momentum flux from atomic motion,

$$\hat{\mathbf{v}}^{\alpha}(\mathbf{x},t) = \mathbf{v}^{\alpha}(t) - \mathbf{v}(\mathbf{x},t) \longleftarrow \mathbf{v} \equiv \mathbf{p}/\rho$$

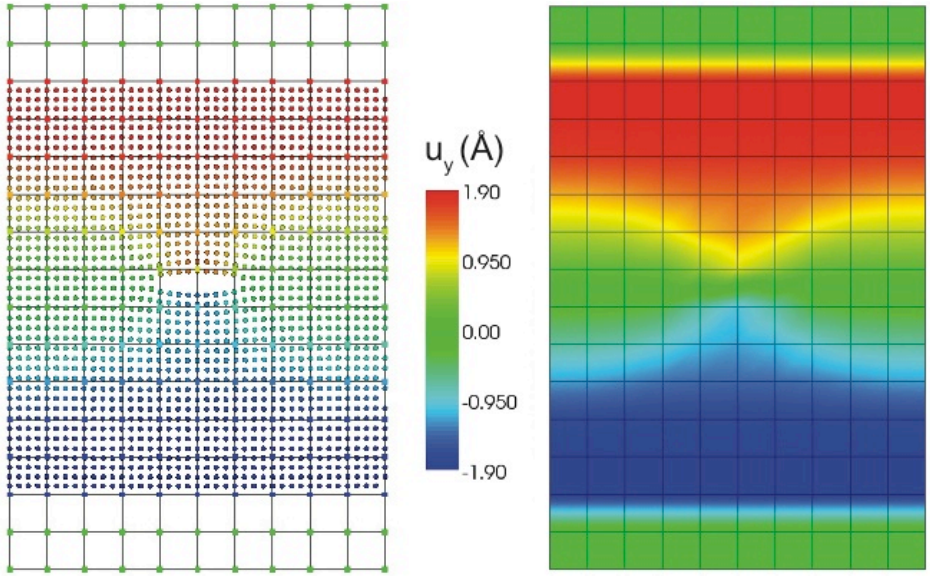

Yields the Cauchy stress tensor:

$$\boldsymbol{\sigma}(\mathbf{x},t) = -\left\{\frac{1}{2}\sum_{\alpha=1}^{N}\sum_{\beta\neq\alpha}^{N}\mathbf{x}^{\alpha\beta}\otimes\mathbf{f}^{\alpha\beta}B^{\alpha\beta}(\mathbf{x}) + \sum_{\alpha=1}^{N} m^{\alpha}\hat{\mathbf{v}}^{\alpha}\otimes\hat{\mathbf{v}}^{\alpha}\psi\left(\mathbf{x}^{\alpha}-\mathbf{x}\right)\right\}$$

Sandia National Laboratories

Characteristic curves background

- Plotted in x-t space
- Show the entire evolution of the solution
- Inverse slope of dx/dt = v+C for nonlinear wave
- Method of characteristics to evolve solutions

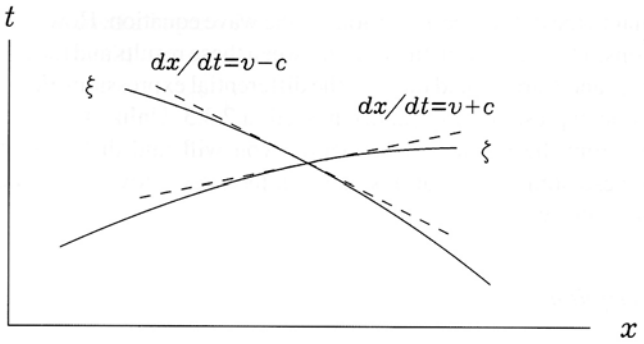

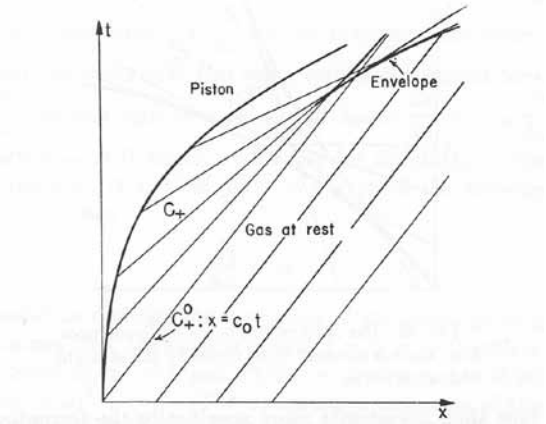

FIG. 27. Envelope with cusp formed by the straight characteristics of a compression wave produced by an accelerated piston.

Figures from Courant & Friedrichs

Characteristic curves from wave speed

- Construction from slope definition
  - Run simulation extracting continuum state variables
  - Calculate wave speeds over the range of states for load path
  - Characteristics have inverse slope, dx/dt = v ± c, where c is the wave speed
  - Starting at the piston (x_1, t_1), integrate to find (x_2, t_2), etc.

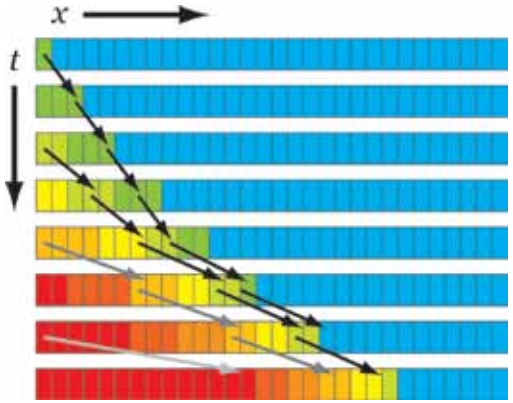

- Requires wave-speed as function of local state
  - Method 1: Gao (J. Mech. Phys Solids, 44, 1452) still in process

$$V_1 = \sqrt{B_{1111}/\rho}$$

$$B_{1111} = S_{11} + F_{1I}C_{I1K1}F_{1K}$$

    - S is the second Piola-Kirchoff stress tensor
    - F is the deformation gradient tensor
    - C is the material tangent modulus

  - Method 2: Time-of-flight was used, instead

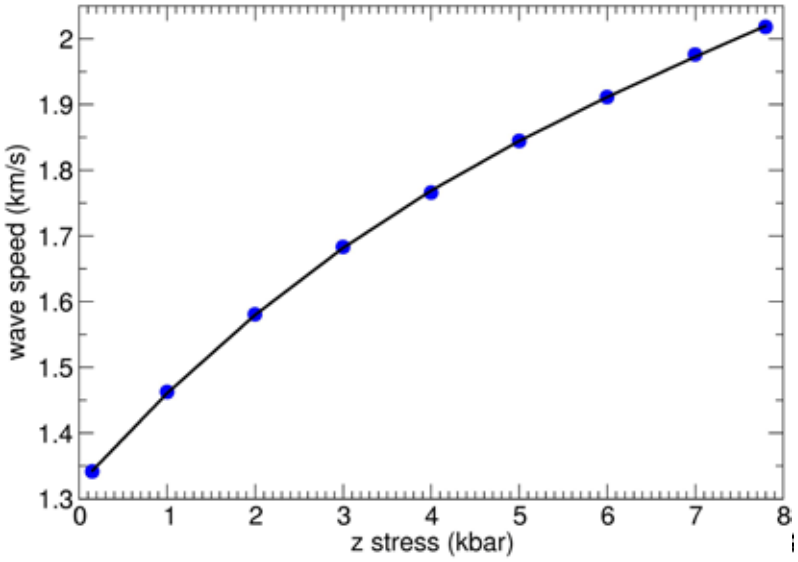

Application to Lennard-Jonesium

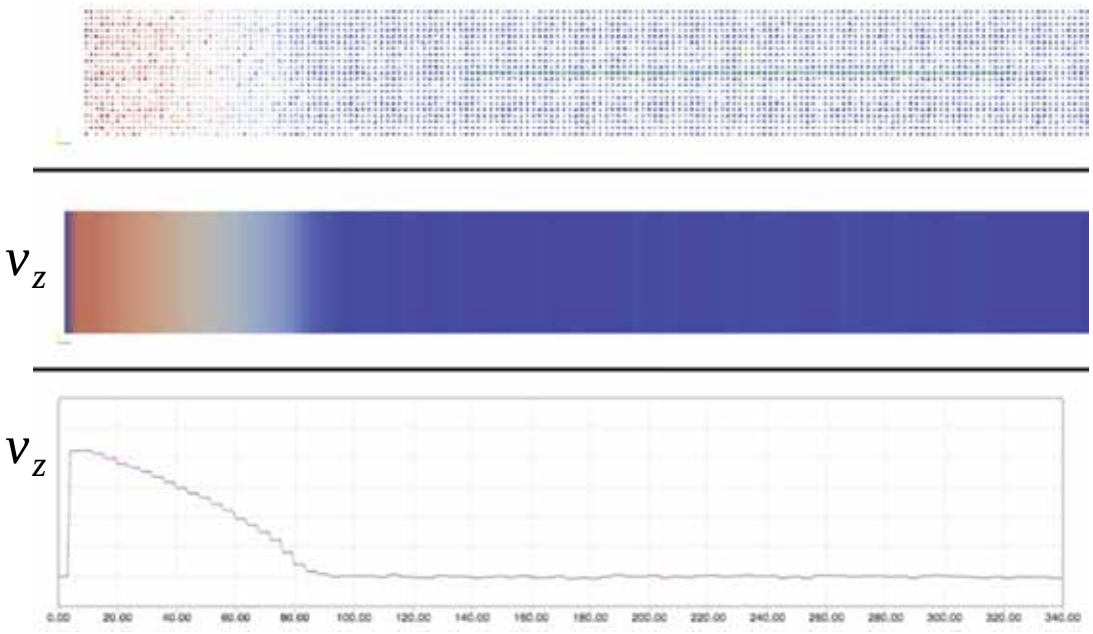

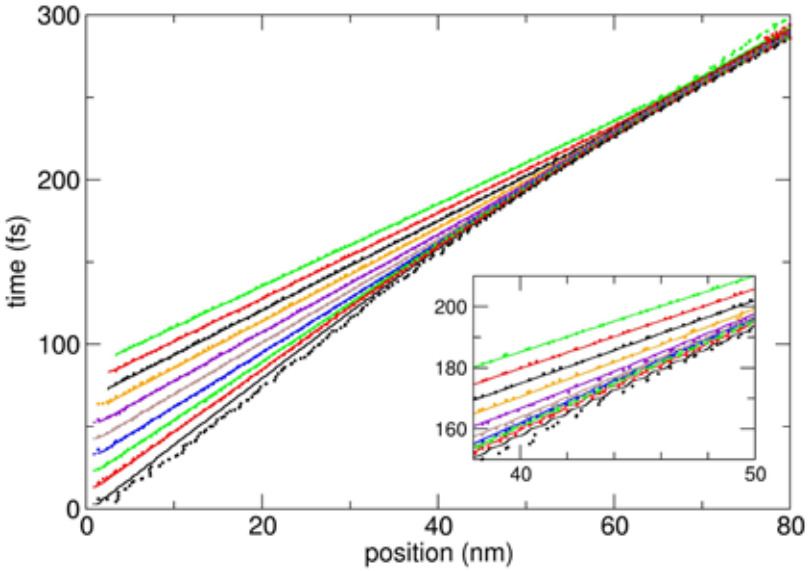

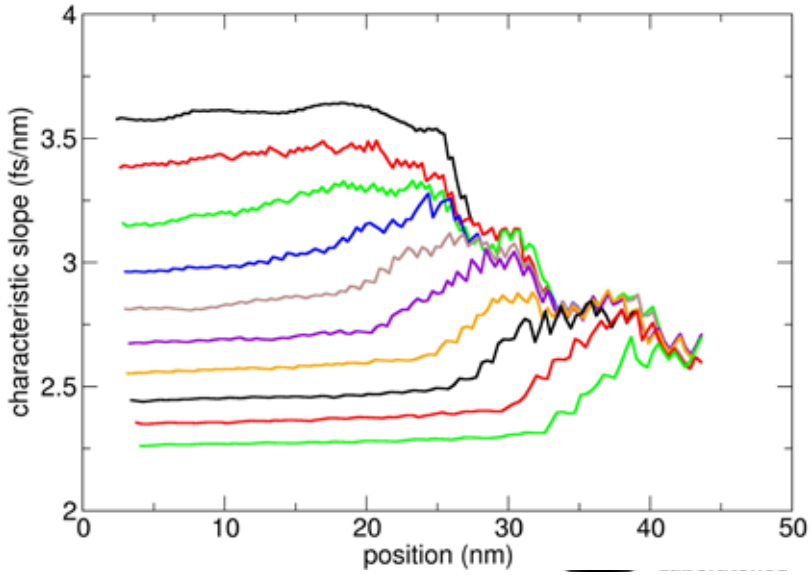

Application to Lennard-Jonesium

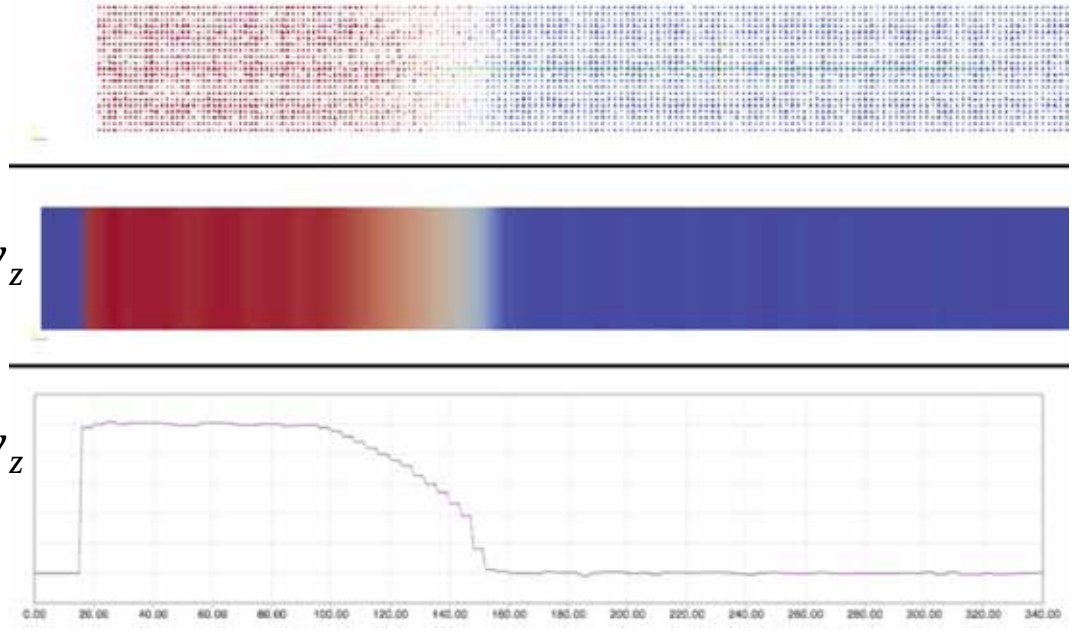

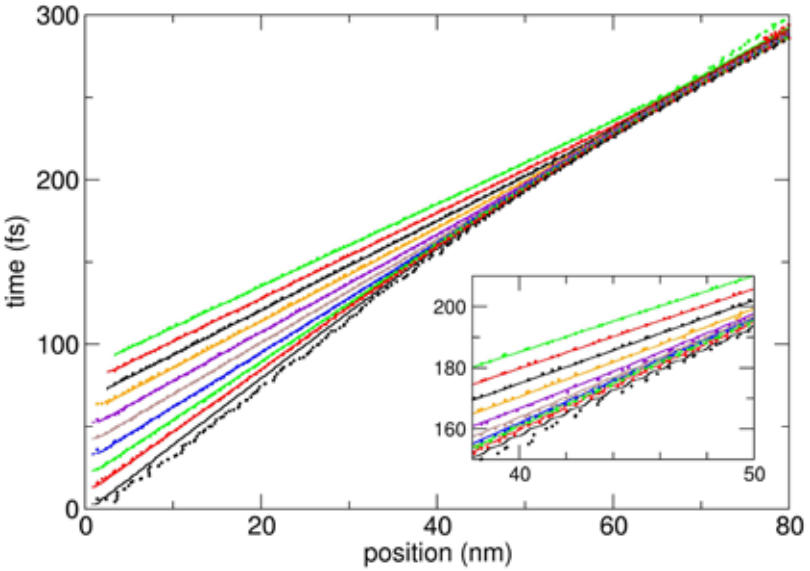

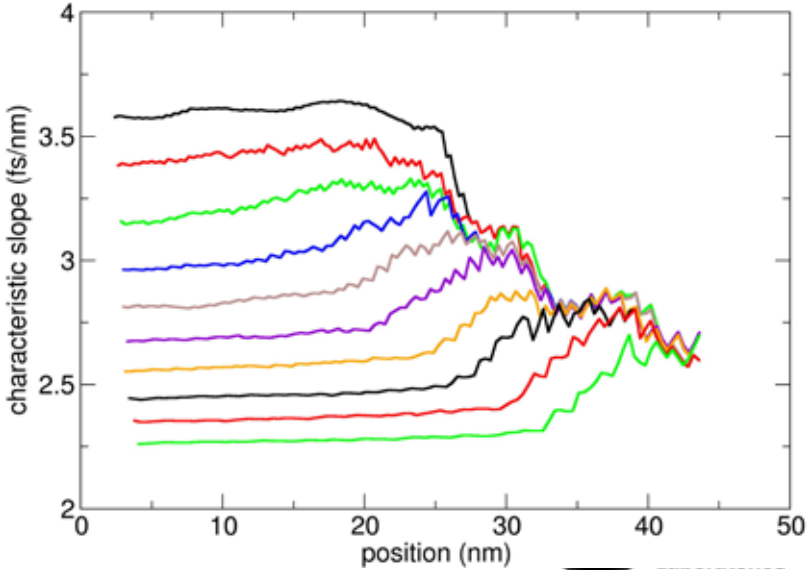

Application to Lennard-Jonesium

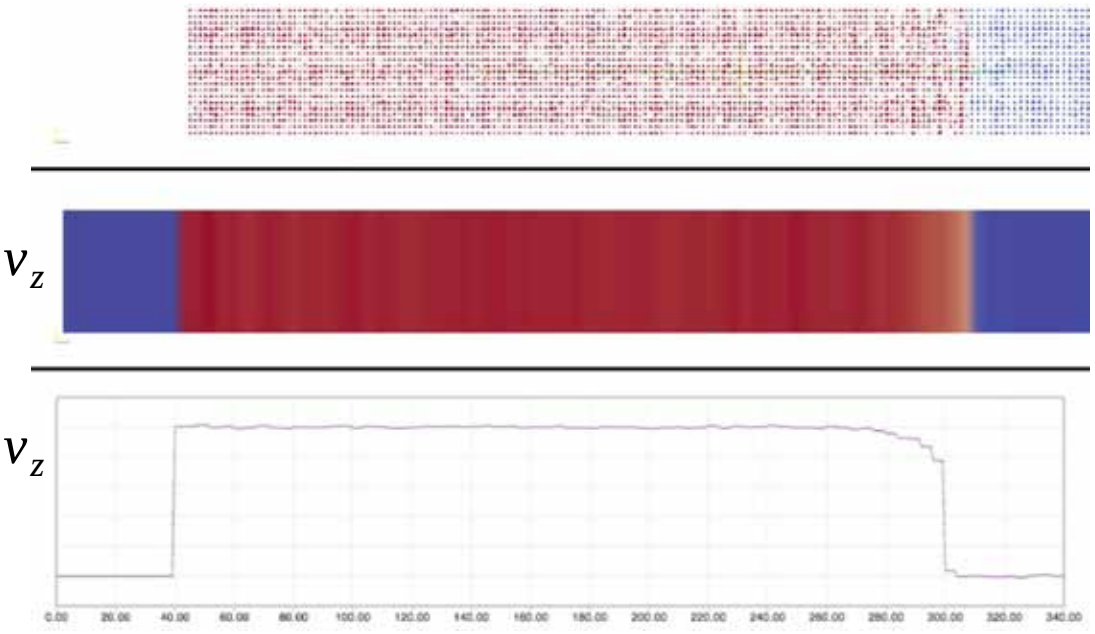

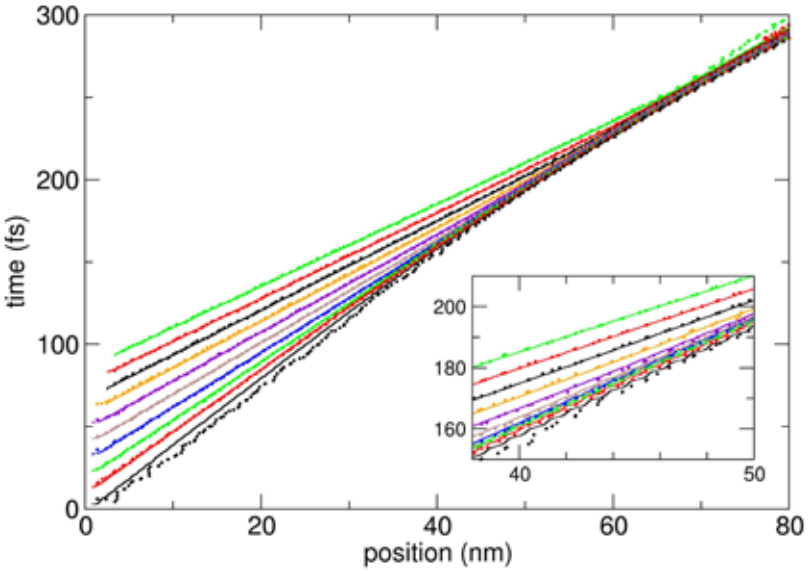

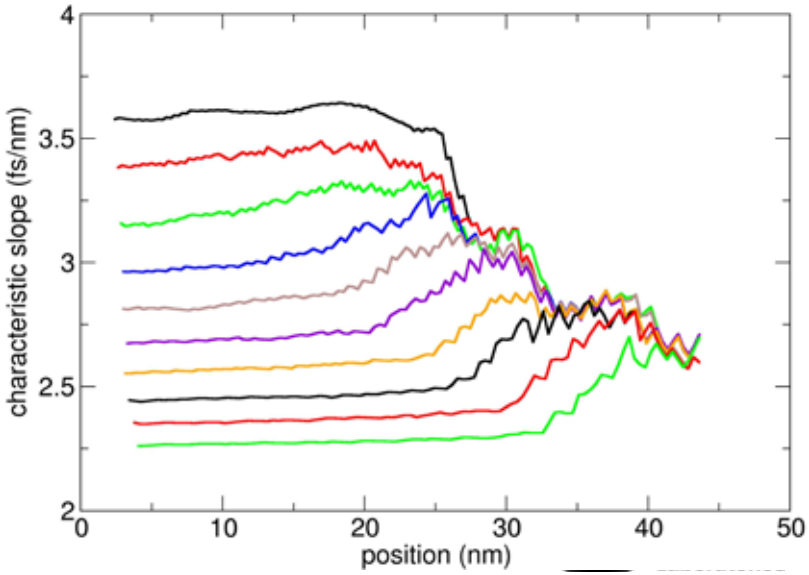

Application to Aluminum

- EAM Al with Voter-Chen parameters at 300 K
- 10 x 10 x 140 unit cells
- Characteristics reflect details sounds speed

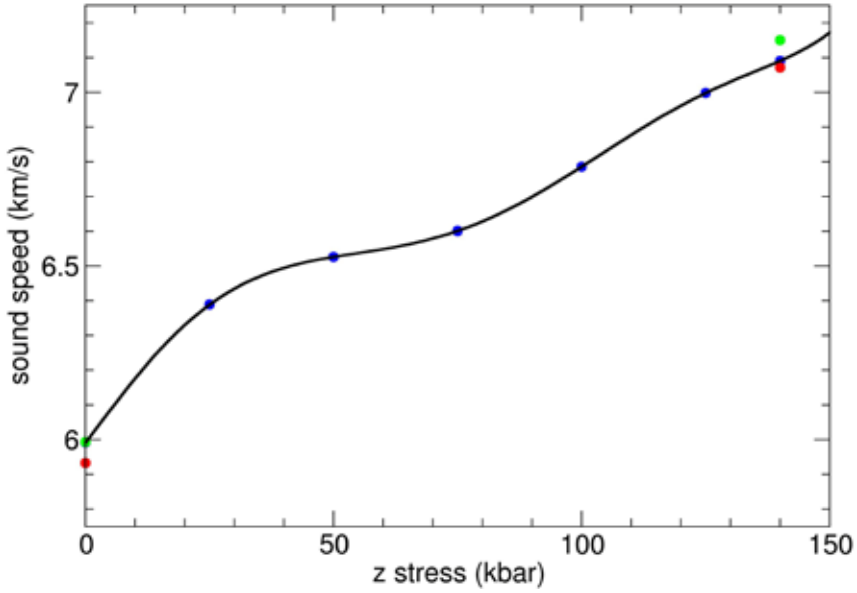

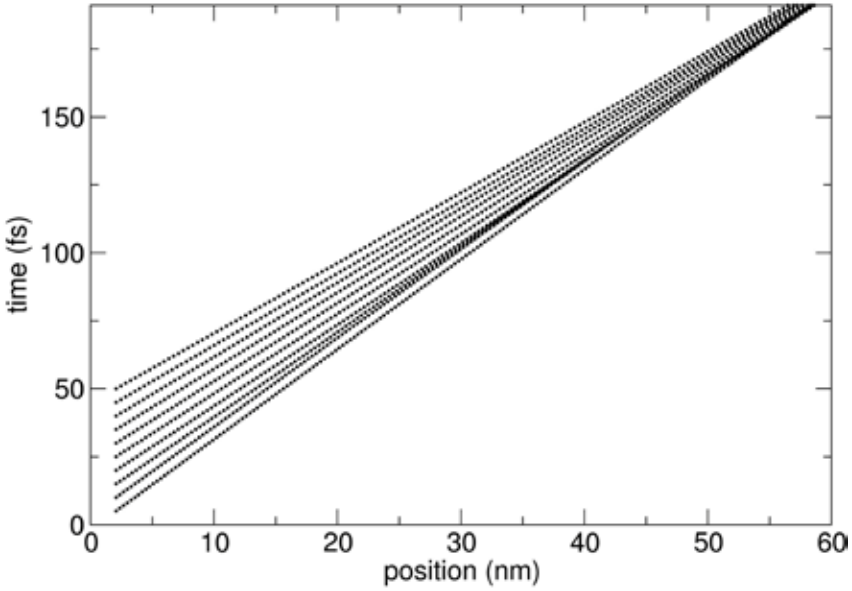

Sandia National Laboratories

Scaling and dynamic similarity theory

Driving piston velocity and position:

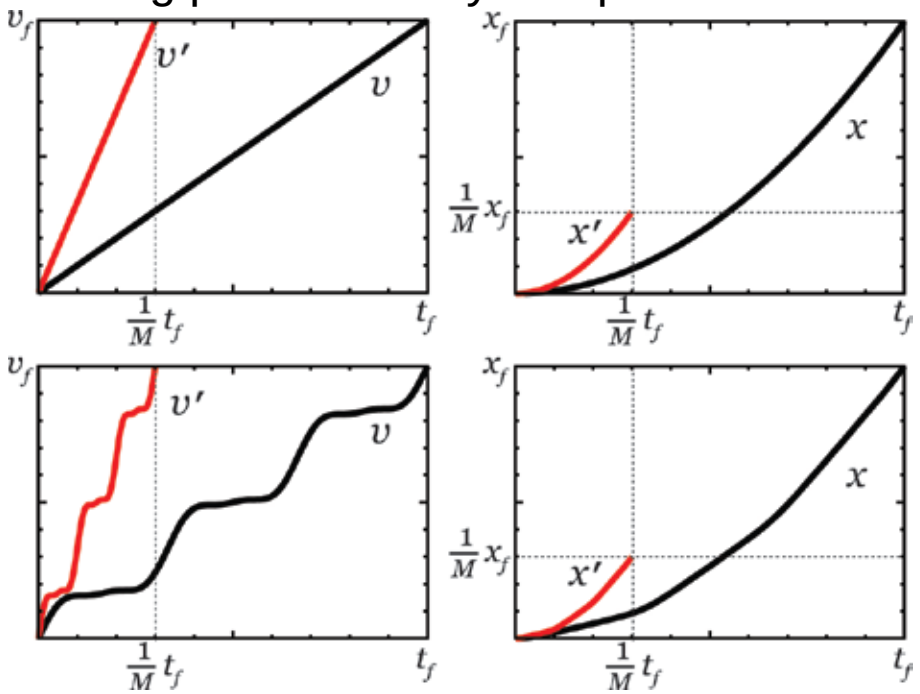

Scaling conditions for loading:

$$v(t) = v'(t') \quad \& \quad t' = \frac{1}{M}t$$

$$x'\left(\frac{1}{M}t\right) = \frac{1}{M}x(t)$$

$$v'\left(\frac{1}{M}t\right) = v(t)$$

Dynamic similarity:

$$\frac{F_{\text{model}}}{F_{\text{actual}}} = \frac{M_{\text{m}}\frac{L_{\text{m}}}{T_{\text{m}}^2}}{M_{\text{a}}\frac{L_{\text{a}}}{T_{\text{a}}^2}} = \frac{\rho_{\text{m}} A \frac{L_{\text{m}}^2}{T_{\text{m}}^2}}{\rho_{\text{a}} A \frac{L_{\text{a}}^2}{T_{\text{a}}^2}}$$

$$= \lambda_\rho \left(\frac{\lambda_L}{\lambda_T}\right)^2 = 1$$

Invariant to scaling:

Velocity	Stress
Strain	Temperature*
Forces	Density

Not invariant:

Strain rates
Accelerations
Times and distances
any extensive variable…

Matthew Lane - jlane@sandia.gov

Case of elastic compression in LJ

Matthew Lane - jlane@sandia.gov

Sandia National Laboratories

Case of elastic compression in LJ

Matthew Lane - jlane@sandia.gov

Sandia National Laboratories

Case of elastic compression in LJ

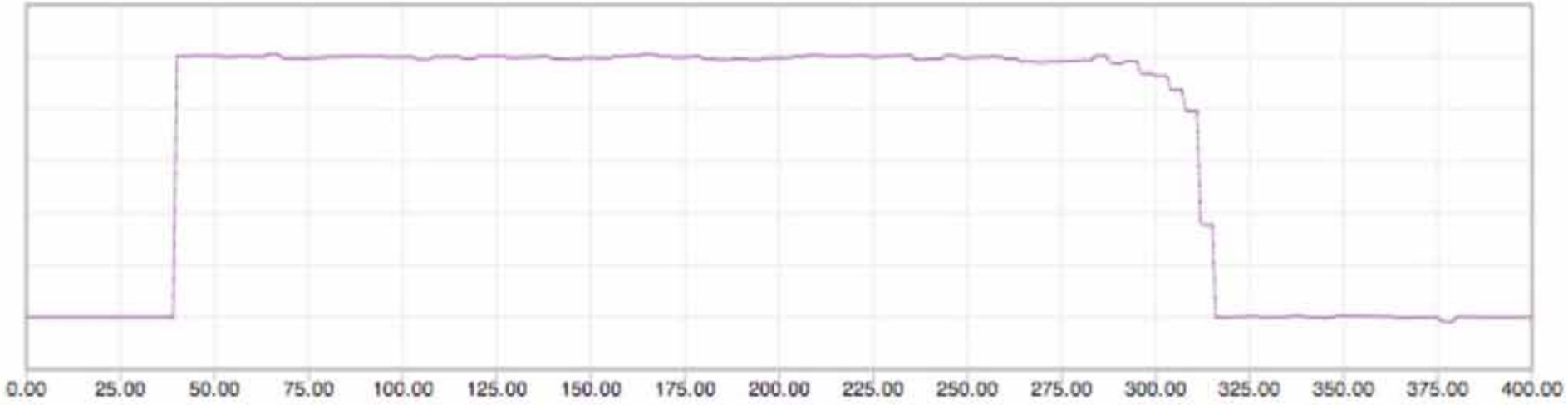

Matthew Lane - jlane@sandia.gov

Case of elastic compression in LJ

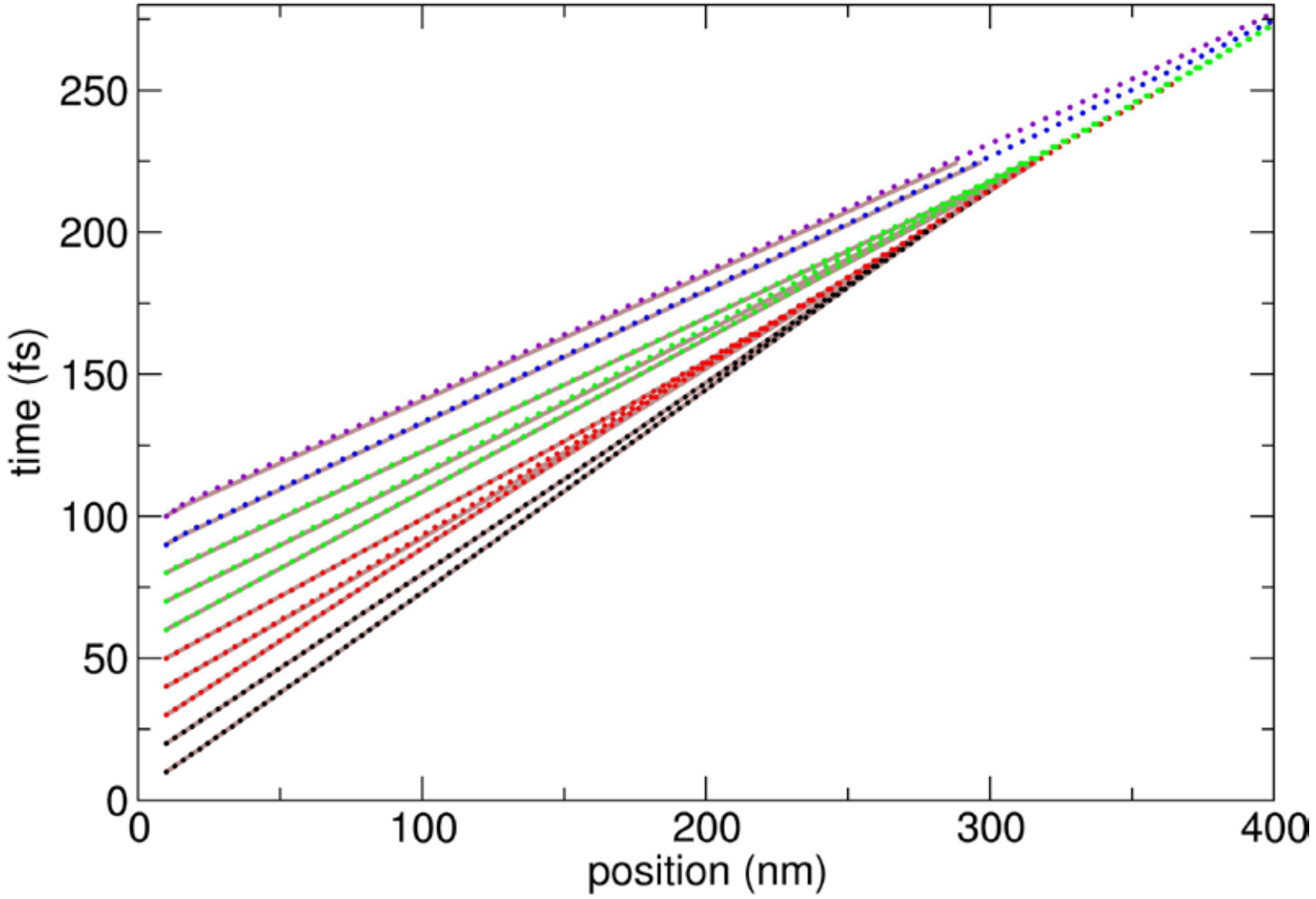

Matthew Lane - jlane@sandia.gov

Sandia National Laboratories

Case of plasticity

- Loading $v(t) = v_f\, t^3$
- Scaling factor of 10. Overall computational scaling of 100.
- Good agreement for velocity and stress. Temperature needs more careful analysis

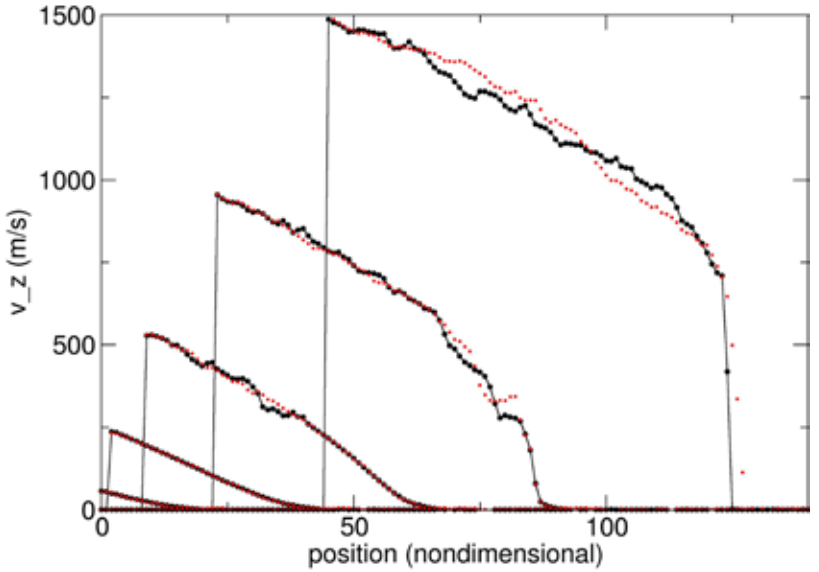

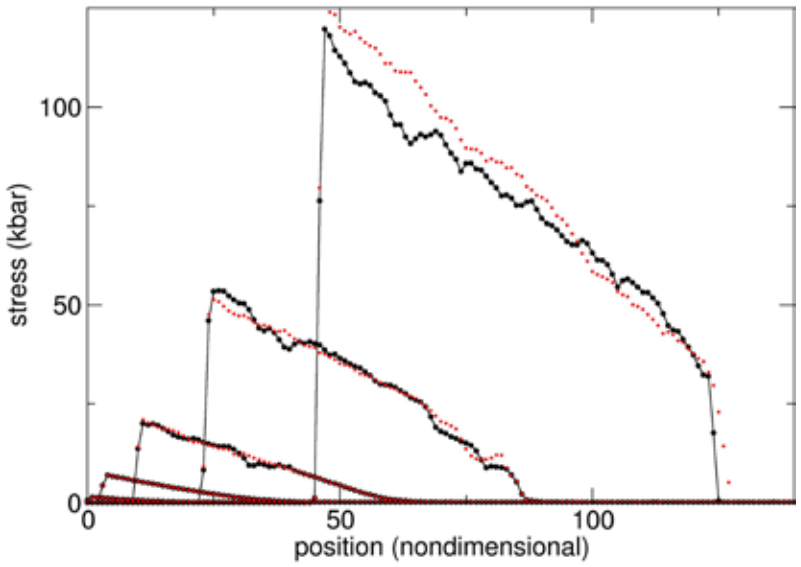

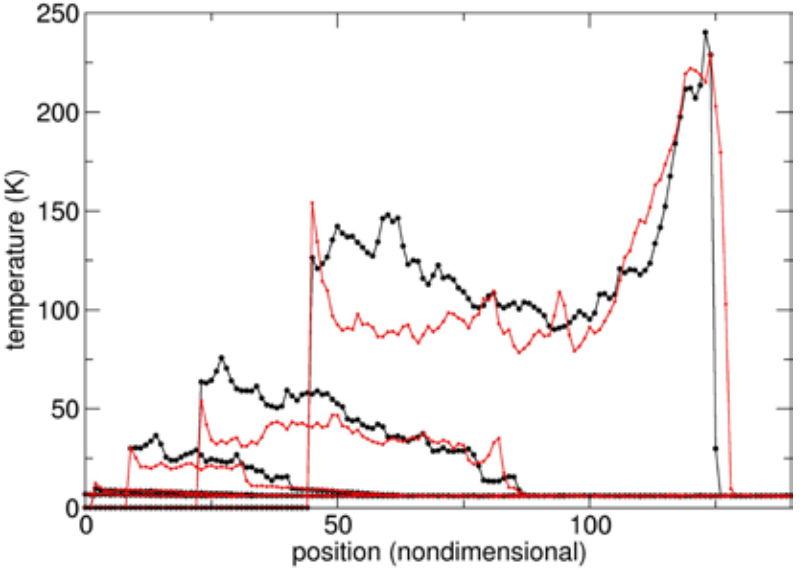

Conclusions

- Developed a method for characteristics extraction which allows comparison of ramp wave development
- Proposed a scaling method with dynamic similarity to study development of ramp waves and demonstrated it for nonlinear elastic & plastic ramps in solid LJ.
- Future: Directly address strain rate effects and examine mechanisms

GAP Potential for Beryllium

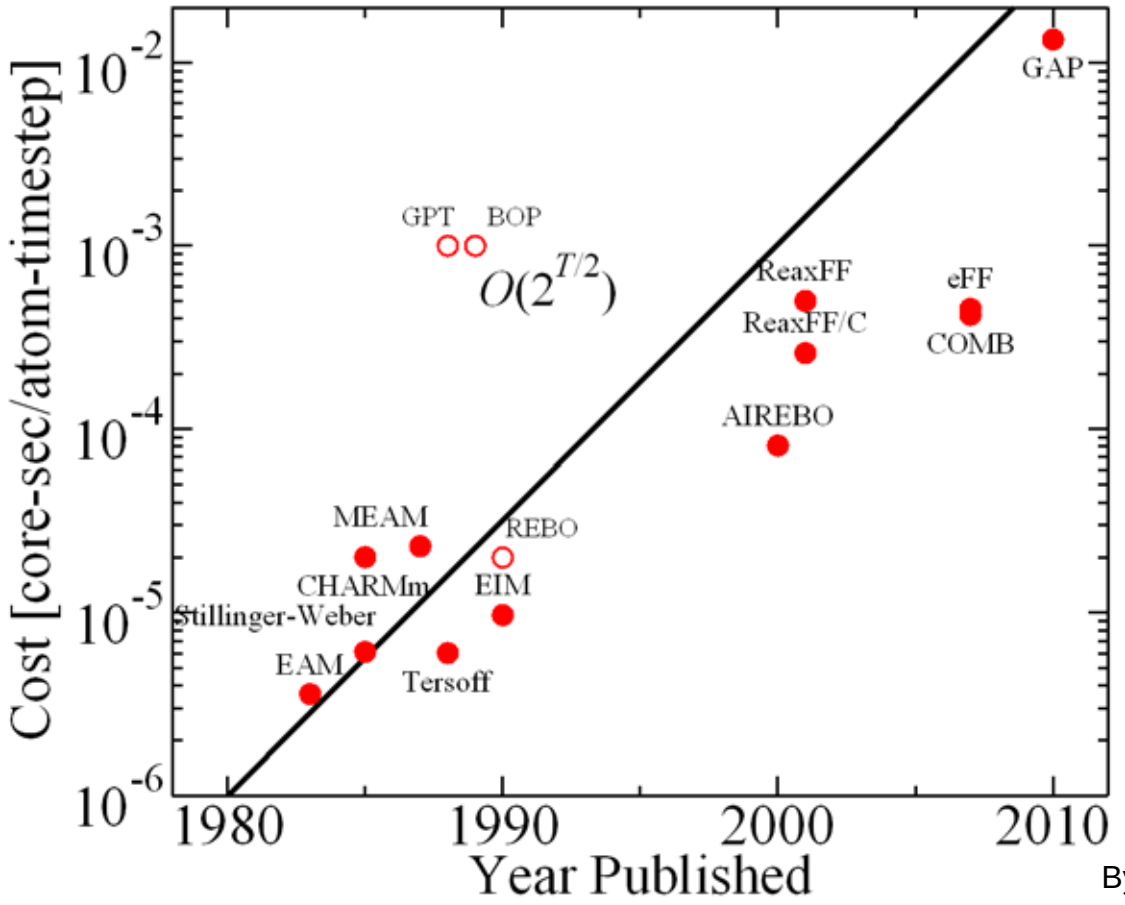

By Aidan Thompson, SNL

Sandia National Laboratories

Scaling and dynamic similarity theory

Dynamic similarity:

$$\frac{F_{\text{model}}}{F_{\text{actual}}} = \frac{M_{\text{m}}\frac{L_{\text{m}}}{T_{\text{m}}^2}}{M_{\text{a}}\frac{L_{\text{a}}}{T_{\text{a}}^2}} = \frac{\rho_{\text{m}} A \frac{L_{\text{m}}^2}{T_{\text{m}}^2}}{\rho_{\text{a}} A \frac{L_{\text{a}}^2}{T_{\text{a}}^2}}$$

$$= \lambda_\rho \left(\frac{\lambda_L}{\lambda_T}\right)^2 = 1$$

Driving piston velocity and position:

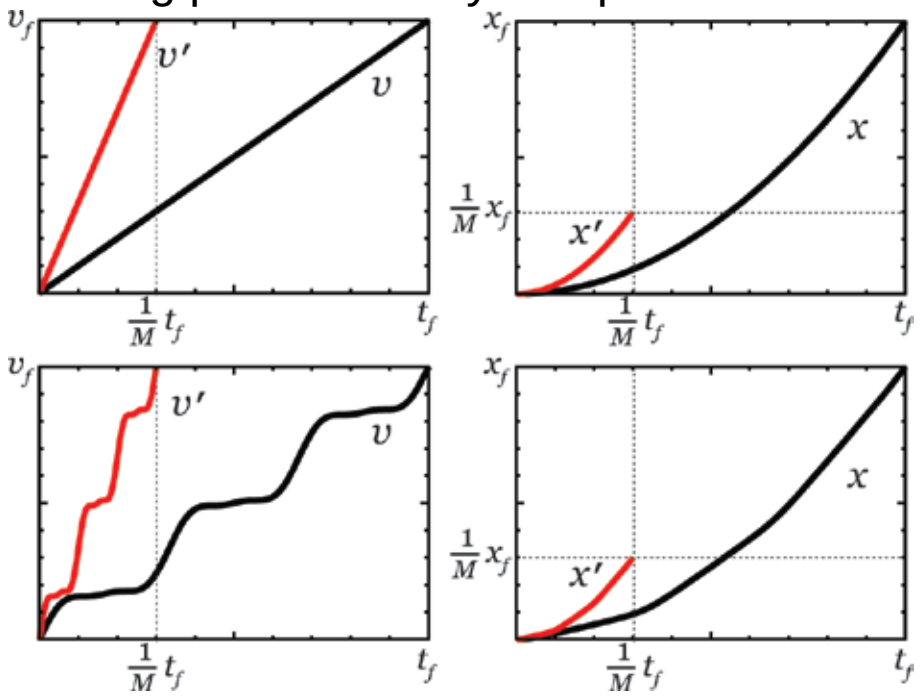

Invariant to scaling:

Velocity	Stress
Strain	Temperature*
Forces	Density

Subject to scaling:

Strain rates
Accelerations
Times and distances
and any extensive variable…

Matthew Lane - jlane@sandia.gov

Recent ALEGRA-MHD Developments Applicable to Magnetically Driven Ramp Compression

Allen C. Robinson
Richard R. Drake
Computational Shock and Multiphysics, 1443

Ramp Compression Workshop
January 18-19, 2011
Sandia National Laboratories

Sandia is a multiprogram laboratory operated by Sandia Corporation, a Lockheed Martin Company, for the United States Department of Energy's National Nuclear Security Administration under Contract DE-AC04-94AL84000.

Sandia National Laboratories

ALEGRA 2D, MHD code provides predictive capability for flyer plate experiments (Ray Lemke)

Two-sided Strip-line Flyer Plate Experiment

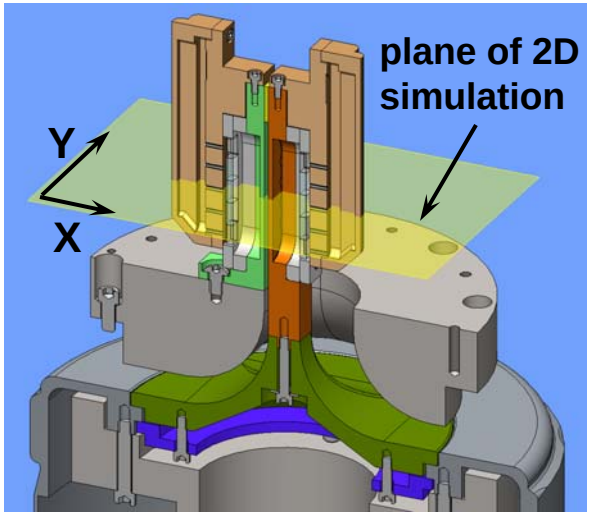

2D Simulation Plane of Two-sided Strip-line

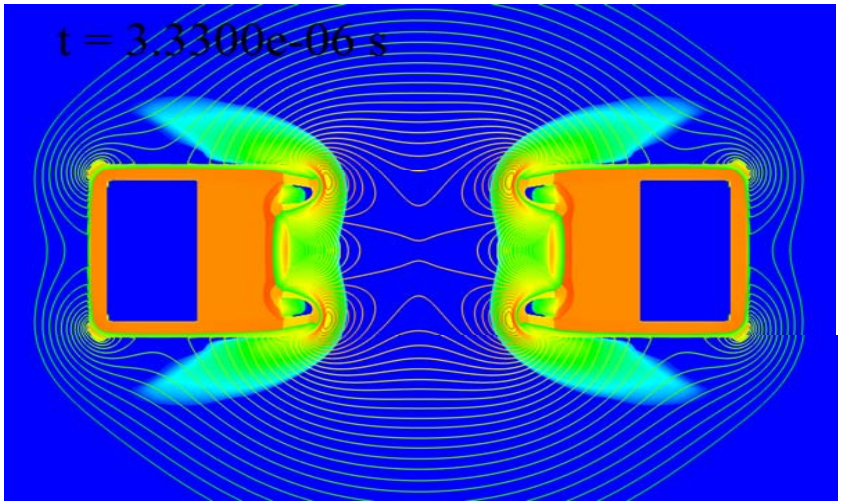

- **Resistive MHD**
- **Accurate electrical conductivities (Desjarlais QMD/LMD).**
- **Sesame EOS for materials.**
- **Circuit model for self-consistent coupling.**
- **Dakota optimization loops**

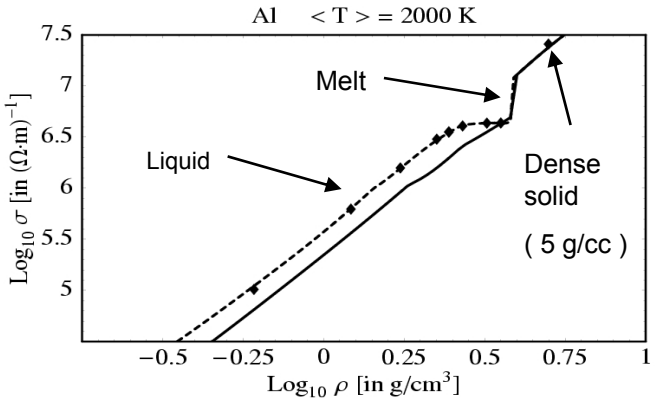

Balance laws for Resistive MHD

$$\dot{\rho} + \rho \nabla \cdot \mathbf{v} = 0$$

Balance of mass

$$\rho \dot{\mathbf{v}} = \nabla \cdot \left(\mathbf{T} + \mathbf{T}^M \right) + \mathbf{f}$$

Balance of momentum including JxB forces

$$\rho \dot{e} = \rho s + \mathbf{T} : \mathbf{L} - \nabla \cdot \mathbf{q} + \frac{1}{\sigma} \mathbf{J} \cdot \mathbf{J}$$

Balance of internal energy including Joule heating

$$\overset{*}{\mathbf{B}} = \frac{\partial \mathbf{B}}{\partial t} + \nabla \times (\mathbf{B} \times \mathbf{v}) + \mathbf{v}(\nabla \cdot \mathbf{B}) = -\nabla \times \frac{1}{\mu_0 \sigma} (\nabla \times \mathbf{B})$$

Balance of magnetic flux Including resistive diffusion

$$\nabla \cdot \mathbf{B} = 0 \qquad \mathbf{T}^M = \frac{1}{\mu_0} \left(\mathbf{B}\mathbf{B}^T - \frac{1}{2} \mathbf{B}^2 \mathbf{I} \right)$$

In addition, closure relations for the stress, electrical conductivity and heat flux are required.

ALEGRA-MHD Algorithm

The strategy used in ALEGRA for MHD is a time operator-split algorithm for ideal and resistive MHD with 3 distinguishing phases:

1. Ideal MHD step: integration of equations of motion in moving (Lagrangian) frame.
   - Compatible node/edge/face centering of magnetic quantities
   - Central difference time integrator (time-staggered)
   - Artificial viscosity for shocks
   - Maxwell stress tensor for magnetic forces
   - Magnetic flux conservation.

$$\frac{d}{dt}\int_{S_t} \mathbf{B}\cdot d\mathbf{a} = \int_{S_t} \overset{*}{\mathbf{B}}\cdot d\mathbf{a} = 0$$

2. Optional remesh/remap operation which respects the div **B** constraint for magnetic flux. (Constrained transport)

3. Magnetic diffusion at the new coordinates: transient magnetics solution for resistive component of field evolution.

Ideal MHD wave propagation

The equations of ideal MHD are hyperbolic and have seven real eigenvalues, corresponding to seven characteristics or modes:

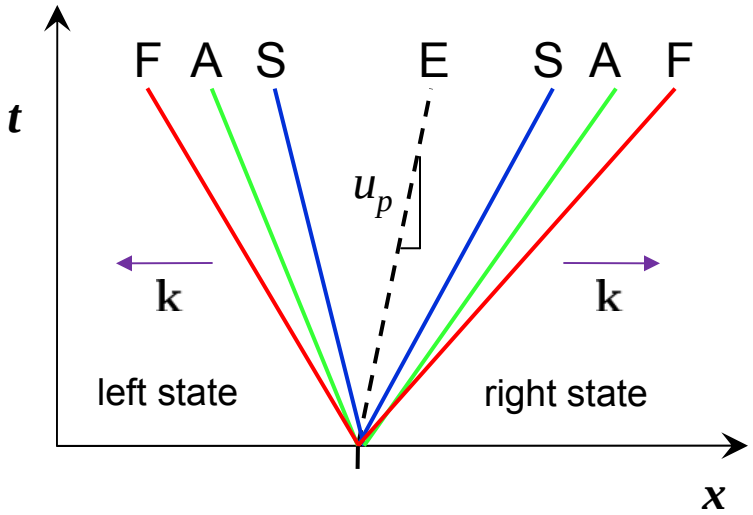

- 2 "fast" magnetosonic modes
- 2 Alfvén modes
- 2 "slow" magnetosonic modes
- 1 contact or "entropy" mode
- [In pure gas dynamics: only 3 real eigenvalues → only 3 modes.]

Magnetosonic waves:

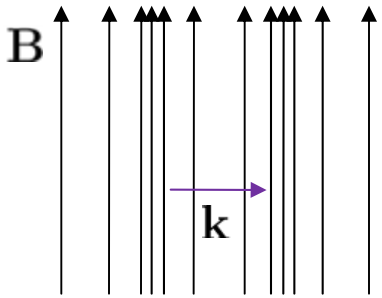

Alfvén waves:

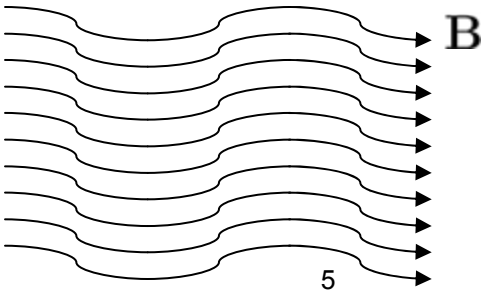

Features of ideal MHD

The wave speeds are dependent on the wave front normal relative to the magnetic field (example with Alfven speed=.9 * sound speed)

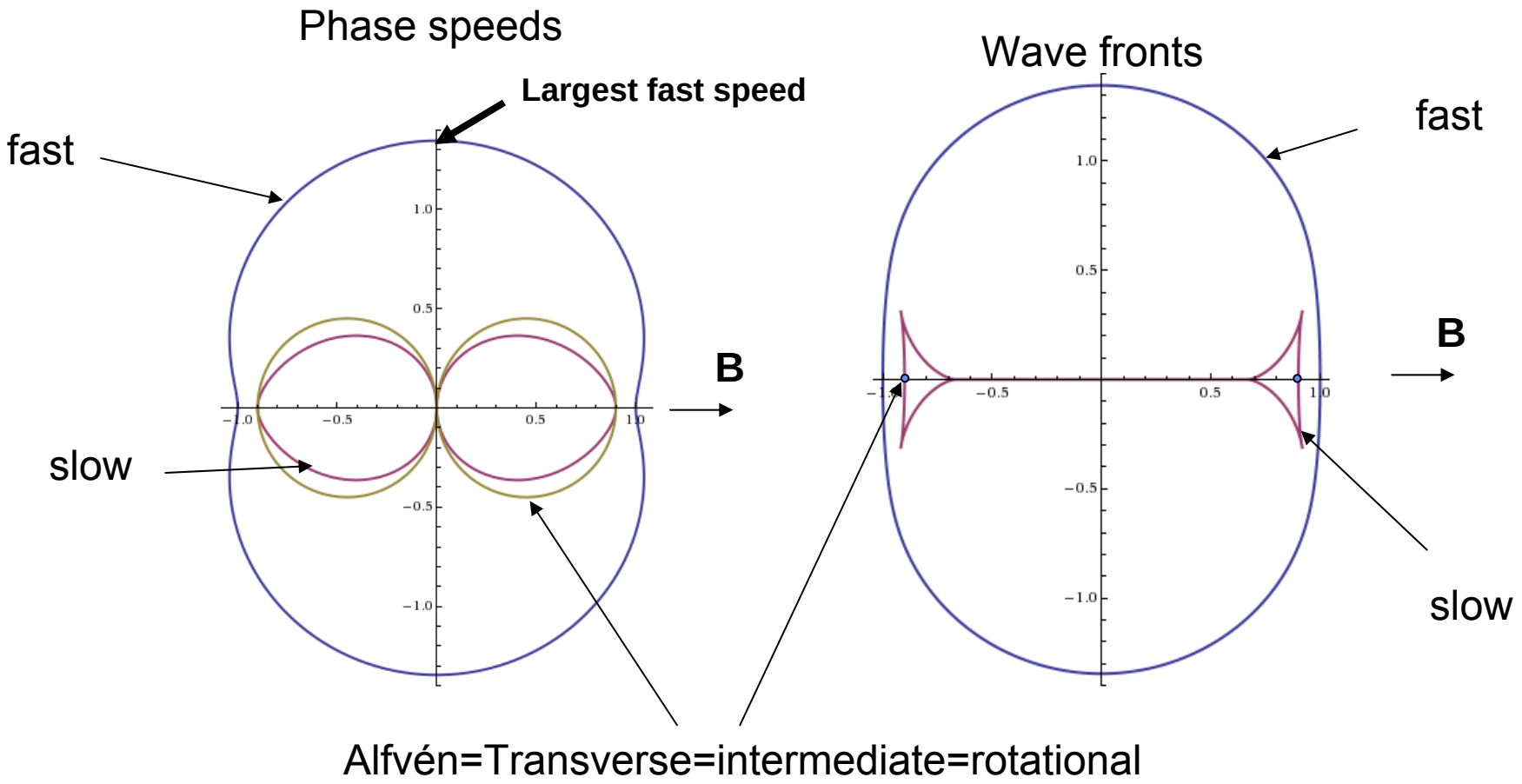

The fastest “fast” wave speed controls time step

For MHD, the CFL-based time step control used in solid dynamics and hydrodynamics is modified slightly to account for magnetoacoustic wave propagation

$$\Delta t \leq \frac{h}{\sqrt{a^2 + v_A^2}} \qquad v_A = \frac{B}{\sqrt{\mu_0 \rho}}$$

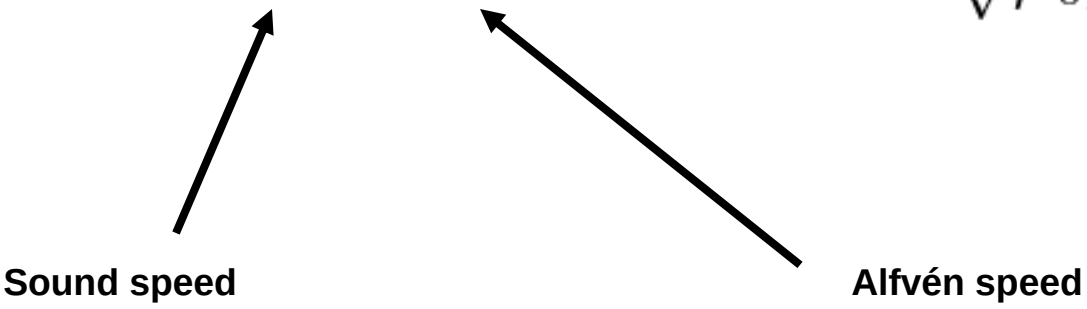

Sound speed **Alfvén speed**

The explicit hydro step must drop the time step if the sound speed or the Alfven speed increases. What if the density goes to zero where the field is large? We will be spending resources tracking waves in regions which can have little mechanical effect.

Boris's Semi-relativistic Correction

Boris, J. P., "A physically Motivated Solution of the Alfven Problem," NRL Memorandum Report 2167, 1970.

Boris proposed keeping the displacement current terms in the momentum equation to allow a user to manage the effect of the Alfven speed increasing beyond bounds.

This is termed a "semi-relativistic correction" and effectively results in a modified mass term in the momentum equation.

The user has the option of artificially reducing the speed-of-light value in the modified mass term.

Equations

$$\frac{\partial}{\partial t}\left(\rho\mathbf{v}+\epsilon_0\mathbf{E}\times\mathbf{B}\right)+\nabla\cdot\left(\rho\mathbf{v}\otimes\mathbf{v}+\epsilon_0\mathbf{E}\times\mathbf{B}\otimes\mathbf{v}\right)$$

$$=\quad\nabla\cdot(-p\mathbf{I})+\nabla\cdot\left(\frac{1}{\mu_0}\mathbf{B}\otimes\mathbf{B}-\frac{1}{2\mu_0}B^2\mathbf{I}\right)$$

$$+\quad\nabla\cdot\left(\epsilon_0\mathbf{E}\otimes\mathbf{E}-\frac{1}{2}\epsilon_0E^2\mathbf{I}\right)+\nabla\cdot\left(\epsilon_0\mathbf{E}\times\mathbf{B}\otimes\mathbf{v}\right)$$

Ideal MHD: $\mathbf{E}=-\mathbf{v}\times\mathbf{B}$ $\qquad c=\left(\epsilon_0\mu_0\right)^{-1/2}$

$$\frac{d}{dt}\int(\rho\mathbf{I}+\frac{1}{c^2\mu_0}(B^2\mathbf{I}-\mathbf{B}\otimes\mathbf{B}))\mathbf{v}dv=$$

$$=\quad\int\nabla\cdot(-p\mathbf{I})+\nabla\cdot\left(\frac{1}{\mu_0}\mathbf{B}\otimes\mathbf{B}-\frac{1}{2\mu_0}B^2\mathbf{I}\right)dv$$

0

ALEGRA OPTIONS: BORIS **SBORIS**

Full semirelativistic momentum equation (Kovetz, p 223)

Boris suggested dropping RHS displacement current terms of $O(v^2/c^2)$

The advection terms associated with the Lagrangian form are of the same order

The LHS tensor mass term is kept.

Implementation

SEMIRELATIVISTIC, {OFF | BORIS | SBORIS}, LIGHT SPEED={real(3.e8)}

Compute a tensor electromagnetic mass coefficient at each node using least squares with the neighboring element centered flux density values as data.

SBORIS stand for Simplified Boris. Boris suggested this simplification to the tensor mass term and it changes the wave velocity characteristics slightly.

Mass tensor has an exact inverse:

$$[\mathbf{I} + (v_A/c)^2(\mathbf{I} - \mathbf{b} \otimes \mathbf{b})]^{-1} = \frac{\mathbf{I} + \mathbf{b} \otimes \mathbf{b}}{1 + (v_A/c)^2}$$

Time Step Modifications for Semi-relativistic Mass

A linearized wave speed analysis (non-trivial) yields the following wave speed bounds:

$$v_f^2 \leq \begin{cases} \frac{a^2+v_A^2}{1+(v_A/c)^2} & \text{if} \quad c^2 > a^2 \\ a^2 & \text{if} \quad c^2 < a^2 \end{cases}$$

BORIS

$$v_f^2 \leq \frac{a^2+v_A^2}{1+(v_A/c)^2}$$

SBORIS

AL 1D Eulerian flyer Example using 3D code (Off,boris,sboris all shown; c=40 km/s)

Early time

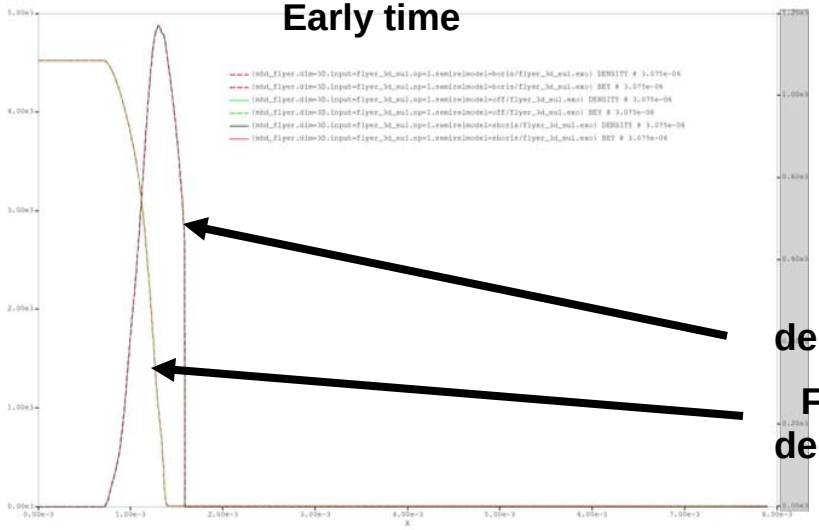

density

Flux density

Late time

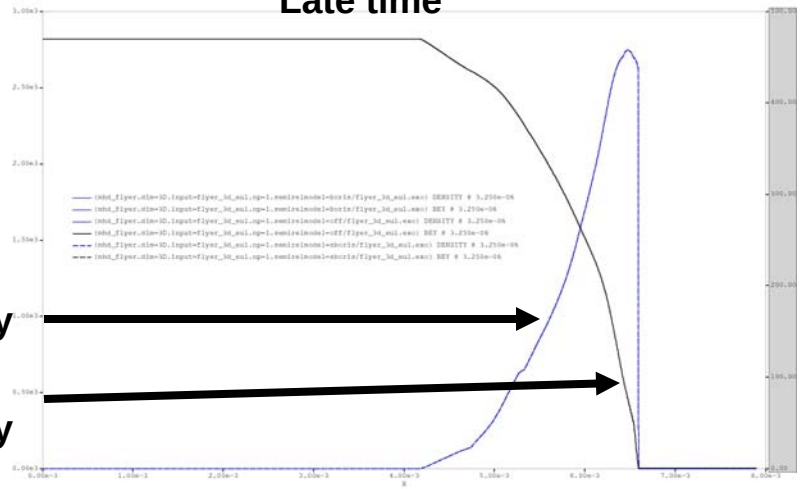

CPU

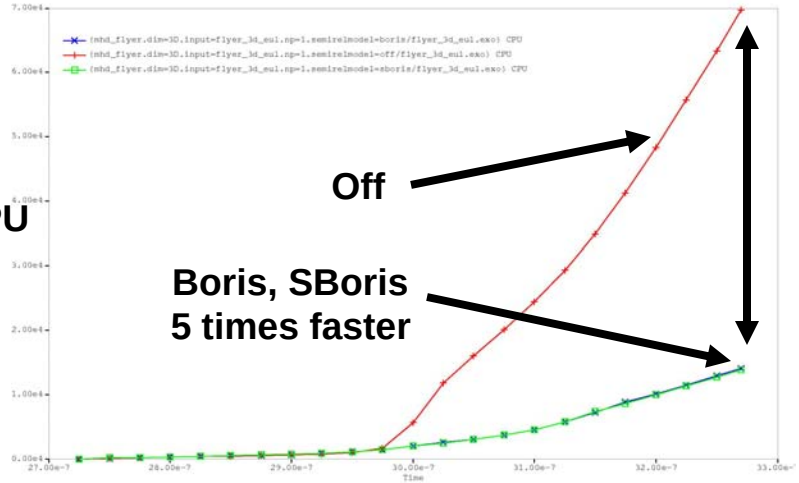

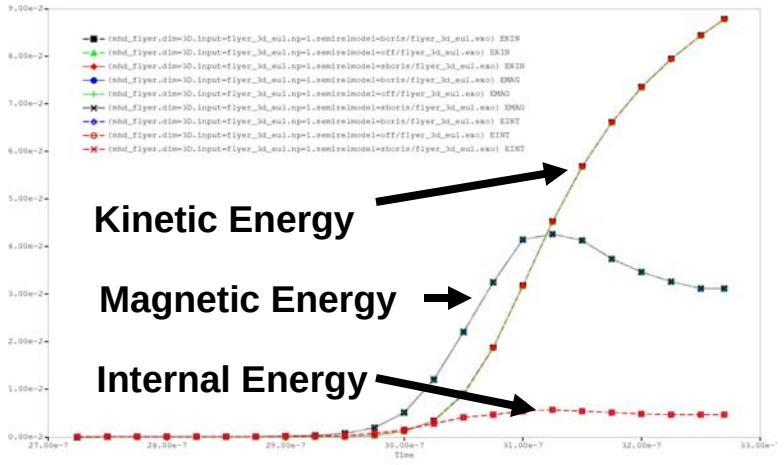

AL 1D Eulerian flyer using 3D code (Off, boris, sboris all shown; c=40 km/s)

Low density blow off region is controlling the time step

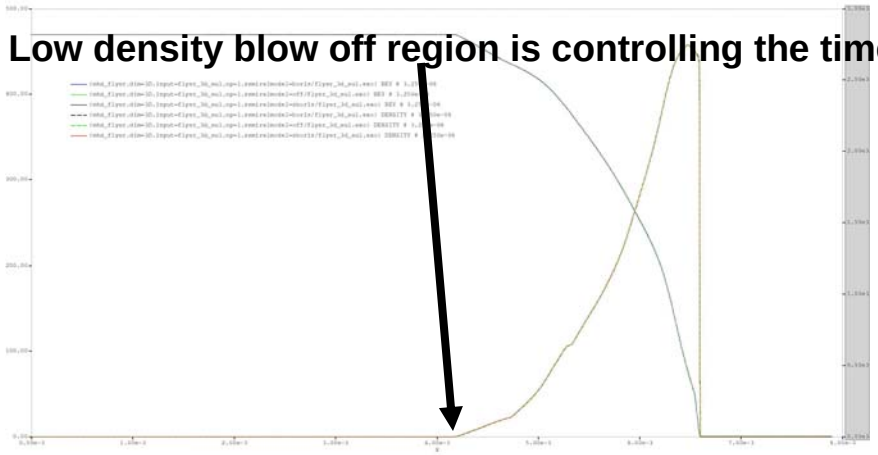

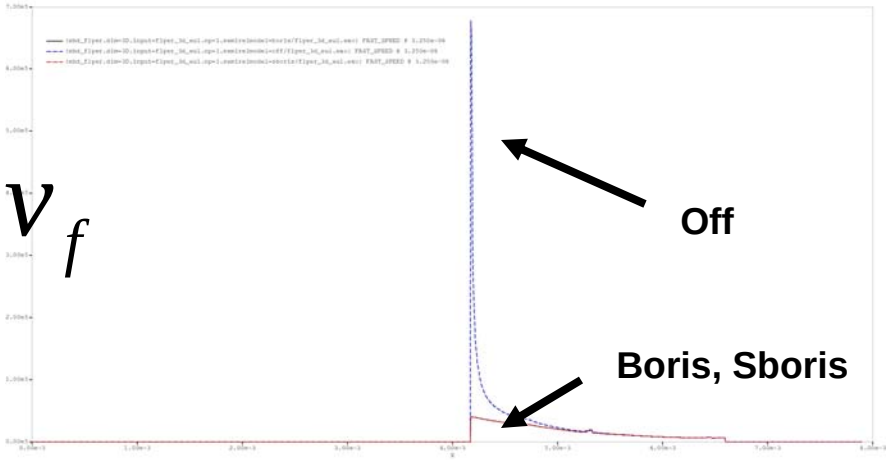

c=40 km/s	~speedup
3D Eul	5.0
3D Lag	1.5
2D Y Eul	3.5
2D Y Lag	1.3
2D Z Eul	4.3
2d Z Lag	1.2

Dakota

Dakota is a general toolkit for black box large scale engineering optimization and uncertainty analysis which has been developed and distributed by Sandia.

The historical interface between Dakota and ALEGRA is based on specialized file based communication interfaces based on scripting.

This interface permits usage by analysts with scripting skills.

Can we make the “user energy barrier” even smaller?

Simplifying ALEGRA/Dakota Usage

Can we make usage of Dakota as easy as building an ALEGRA input deck with a Dakota input section?

What response functions (quantities of interest (QOI) or figures of merit) can be provided as easy-to-use production features?

Can specialized response function scripts be easily implemented in the simplified framework?

Does overall robustness improve?

Embedding DAKOTA in ALEGRA

Script interface:

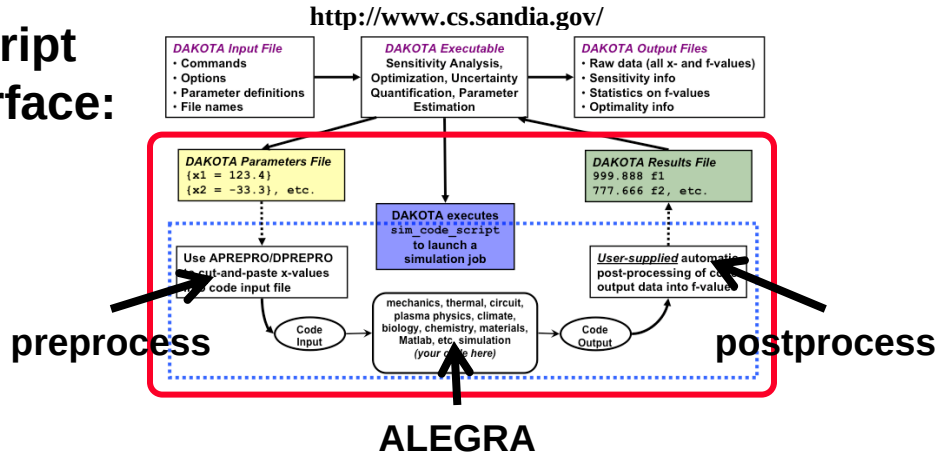

Embedded interface:

```
DAKOTA INPUT "
    method, nond_sampling, samples = 10
    variables, normal_uncertain = 2
        means           =   1.076e+12   0.355
        std_deviations =   0.01e+12    0.1
        descriptors          '_YMOD_'   '_POIS_'
    responses, num_response_functions = 1
        no_gradients, no_hessians
    interface,direct,
       analysis driver='alegra'
       processors_per_analysis=2
"
termination time 3.5e-05

... (normal ALEGRA input) ...

model 100 elastic plastic
  youngs modulus     _YMOD_
  poissons ratio     _POIS_
  yield stress       6.0e+9
  hardening modulus 2.0e+9
  beta               0.5
end
```

samples

Implementation Challenges:

- Make ALEGRA and some TPL's re-entrant
- MPI communicator cannot be hardcoded.
- Establish a transparent Dakota interface
- Place Dakota as TPL in build system.

Response Functions:

Tracers implemented so far

```
transient magnetics

  ... (physics input) ...

  tracer points
    lagrangian tracer 20, x=0.0 y=0.0 z=4.0
  end

  response functions
    tracer 20, variable = COORDINATES, z, end
  end

end
```

Response Function Interfaces

An implicit ordering of response function variables is assumed in the response function block:

```
response functions
   # currently supported
   tracer <int>, variable = <name> [, {X,Y,Z,MAG}], end
   #possible future built-in response functions ?
   norm, L2, variable = <name>, table = <id>, tmin=<real>, tmax=<real>
   norm, L2, tracer <int>, variable = <name>, table = <id>, tmin=<real>, tmax=<real>
   process (“scriptname”, <number of return variables>)
   locate, material = <id>, {xmax, xmin, ymax,ymin,zmax,zmin}
end
```

Output file handling (e.g. exodus, hisplt, spy) still needs to be improved to avoid overwriting.

We may choose to implement a variety of flexible interfaces:

- **Run Time Compiler (RTC) language**
- **Slang (SPY Language)**
- **General Subprocess Interface (Python script, etc.) – This has the same usability issues as the classic script interfaces but should still be an improvement. We will try to match the current Dakota syntax.**

Unclear how to deal with response function metrics that could (for efficiency) feed back to stop calculations when the required information is available.

Example - 3D AL Lagrangian Flyer

Assume the current profile "scale" input value is normally distributed with mean 1 and standard deviation .01. What are the statistics on the free surface velocity (X velocity of Tracer 225) at a specified time? The nominal velocity for "scale=1" is 35,191.

Polynomial Chaos (PC) representation with 3 term quadrature.

- **Result: 3 PC coefficients, Mean = 35,173., std dev = 695.**

Polynomial Chaos representation with 5 term quadrature.

- **Result: 5 PC coefficients, Mean = 35,168., std dev = 694.**

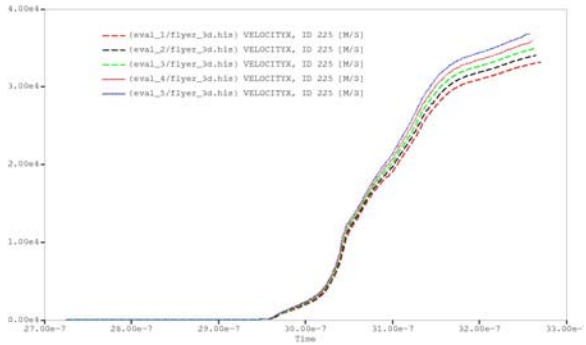

The mean velocity is slightly less than the nominal velocity.

The standard deviation is ~2 percent of the mean velocity.

Summary

Boris style generalized mass term in momentum equation for MHD computations can be a useful feature to reduce overall computational cost.

Embedding Dakota in ALEGRA is beginning to reduce the "user energy barrier" for UQ/optimization studies.

These capabilities should be useful for improving user experience with design analysis of magnetically driven ramp compression experiments using ALEGRA.

Approved for Unlimited Release
SAND2011-0153C

Visualizing Material Model Data Using PRISM

4th Workshop on Ramp Compression

19 January 2011

V. Gregory Weirs
Optimization and Uncertainty Quantification
Sandia National Laboratories

Sandia National Laboratories is a multi-program laboratory managed and operated by Sandia Corporation, a wholly owned subsidiary of Lockheed Martin Corporation, for the U.S. Department of Energy's National Nuclear Security Administration under contract DE-AC04-94AL85000.

What is PRISM?

- PRISM is a plugin to ParaView
- The SESAME reader displays material model surfaces, generally equations-of-state and scalar properties
- The PRISM filter displays experimental or simulation data on the material model surface
- Intended for analysts and code developers

SAND2011-0153C

Display surfaces, contours, phase changes

Example:

- Pressure surface vs. Density and Temperature
- Contours of Energy
- Solid Melt, Liquid Melt, and Vaporization Curves

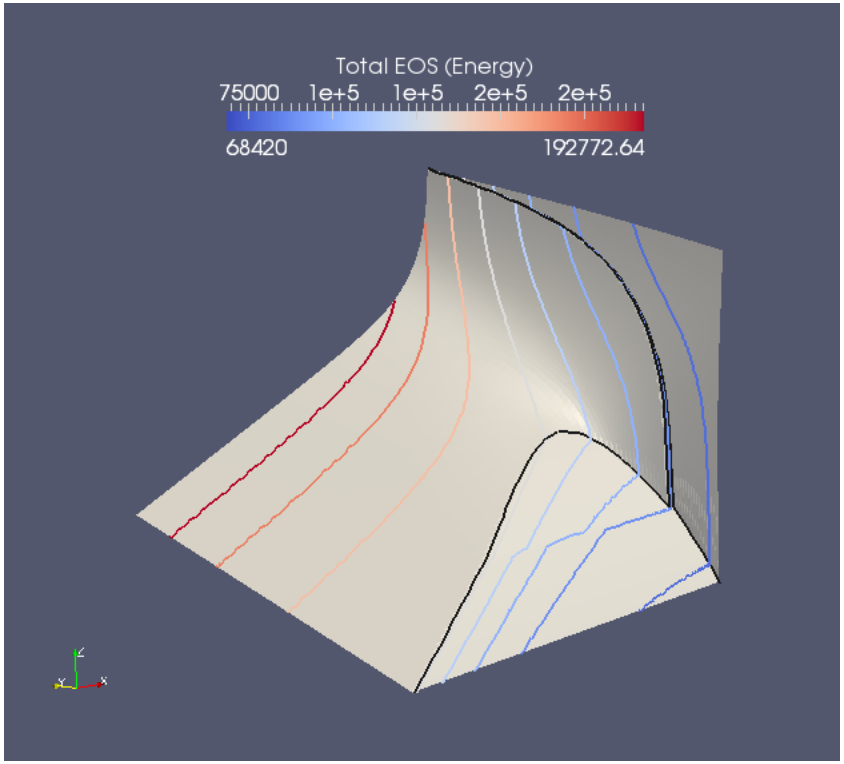

SAND2011-0153C

Sandia National Laboratories

Flexible Unit Conversion

- Default conversions file includes cgs and SI. Users can add their own conversions to the file.

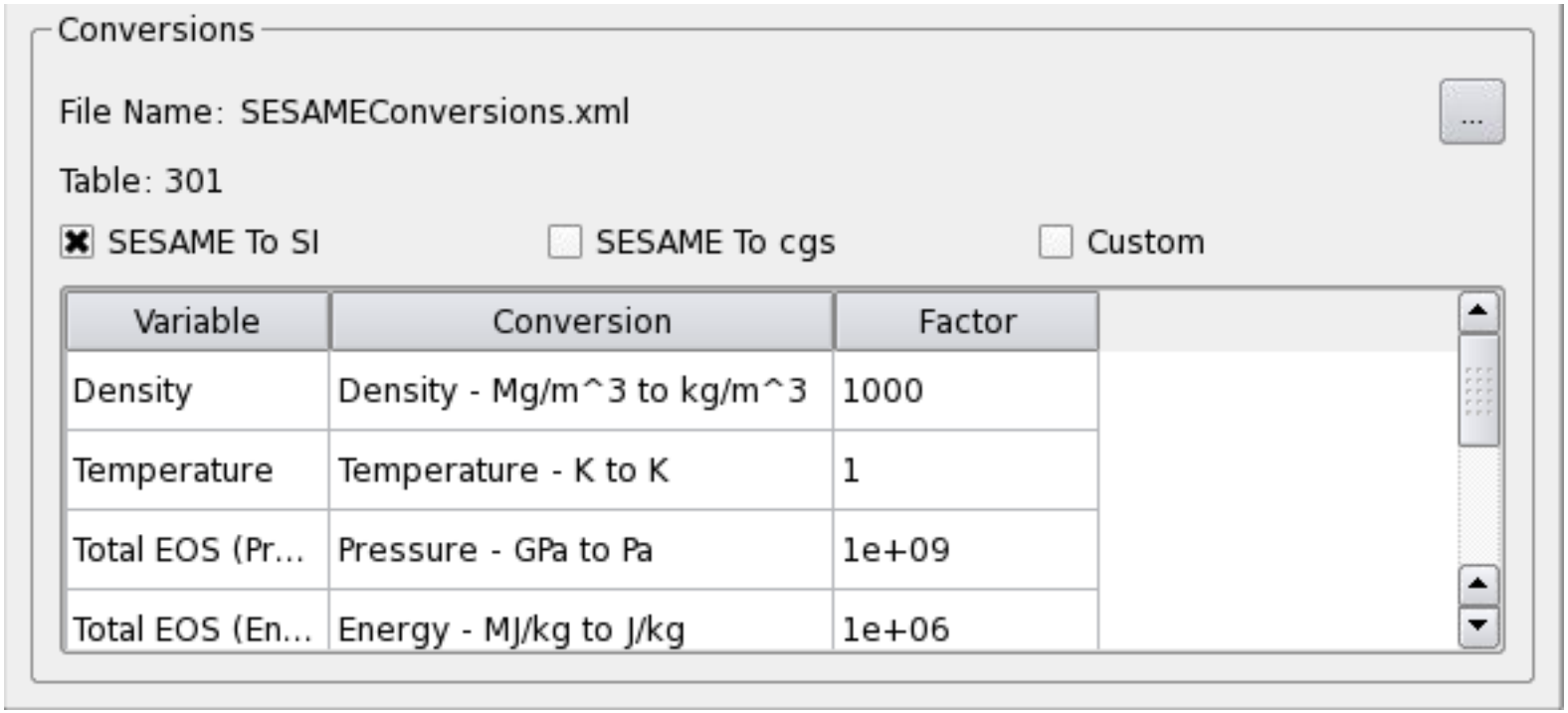

Display Simulation Data on Material Surfaces

- Element data
- Tracers in csv format (hscth format)
  - Should work for CTH and ALEGRA users
  - Others may need to reformat their data
- Linked selection: still buggy but fixes are in progress

SAND2011-0153C

Material Models Accepted

PRISM reads the complete SESAME specification (as described in LA-UR-92-3407)

- All table numbers (next slide)
- SESAME units
- ASCII format only, one material per file
  - LANL SESAME “ship” format
  - SNL “Kerley” format
- Additional variables beyond those defined by the format

PRISM works with SESAME *files*, not libraries

SESAME format is just a convenient file format; PRISM is not restricted to material models in the SESAME library

SAND2011-0153C

Types of SESAME Data Records

- Table 101 Comments
- Table 102 Comments
- Table 201 Atomic Number, Atomic Mass, Normal Density
- Table 301 Total EOS (304 + 305 + 306)
- Table 303 Ion EOS Plus Cold Curve (305 + 306)
- Table 304 Electron EOS
- Table 305 Ion EOS (Including Zero Point)
- Table 306 Cold Curve (No Zero Point)
- Table 401 Vaporization Table
- Table 411 Solid Melt Table
- Table 412 Liquid Melt Table
- Table 431 Shear Modulus Table
- Table 501 Opacity Grid Boundary: Calculated vs. Interpolated
- Table 502 Rosseland Mean Opacity
- Table 503 Electron Conductive Opacity1
- Table 504 Mean Ion Charge1
- Table 505 Planck Mean Opacity
- Table 601 Mean Ion Charge2
- Table 602 Electrical Conductivity
- Table 603 Thermal Conductivity
- Table 604 Thermoelectric Coefficient
- Table 605 Electron Conductive Opacity2

SAND2011-0153C

Future Work

- Bug fixes. As you find them, please report them – no one will try to fix a bug they don't know about.
- Solid mechanics models
- Visualizing material model uncertainties

SAND2011-0153C

Live Demonstration

Two plates in a symmetric impact

- ALEGRA Eulerian simulation, essentially 1-D
- No strength
- Fake material “proxium”
- Conditions chosen to be interesting in EOS space

SAND2011-0153C

Sandia National Laboratories